IC
10-15-91 JSO (1)

Nuclear Science Division

LBL-30798
UC-413

1989-1990 ANNUAL REPORT

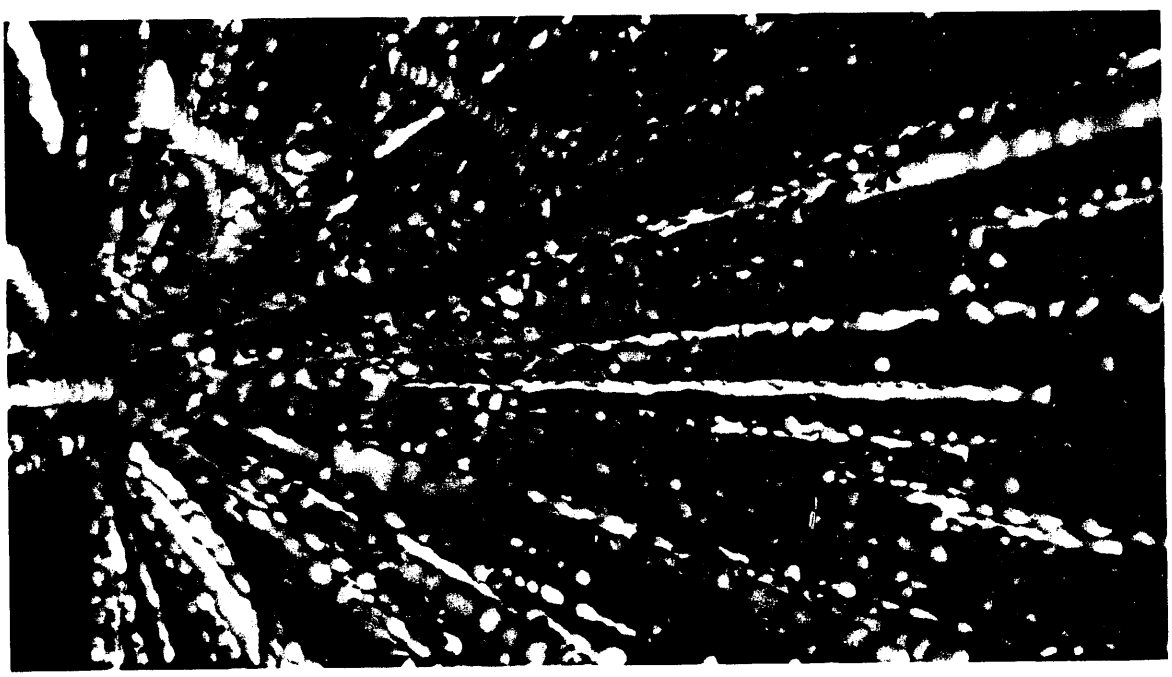

Lawrence Berkeley Laboratory
University of California

April 1991

Prepared for the U.S. Department of Energy under Contract DE-AC03-76SF00098

On the Cover

On the cover is an image of what is expected for an EOS time projection chamber event. It was generated from a FRESCO simulated collision of a one GeV/nucleon gold projectile nucleus colliding head on with a gold target nucleus. Ionizing particles radiating from the collision, mostly protons, leave trails of electrons in the TPC gas volume which are shown in this perspective view.

LBL--30798

DE92 000695

NUCLEAR SCIENCE DIVISION

Annual Report for the Period
October 1, 1988 - December 31, 1990

Division Director
T. J. M. Symons

Editor
A. M. Poskanzer

Assistant Editors
M. A. Deleplanque
R. B. Firestone
J. B. Lofdahl

Lawrence Berkeley Laboratory
1 Cyclotron Road
Berkeley, California 94720, USA

This work was supported by the Director, Office of Energy Reserach, Office of High Energy and Nuclear Physics, Division of Nuclear Physics and by the Office of Basic Energy Sciences, Division of Nuclear Sciences, of the U.S. Department of Energy under Contract No. DE-AC03-76SF00098

Table of Contents

Introduction and Overviews

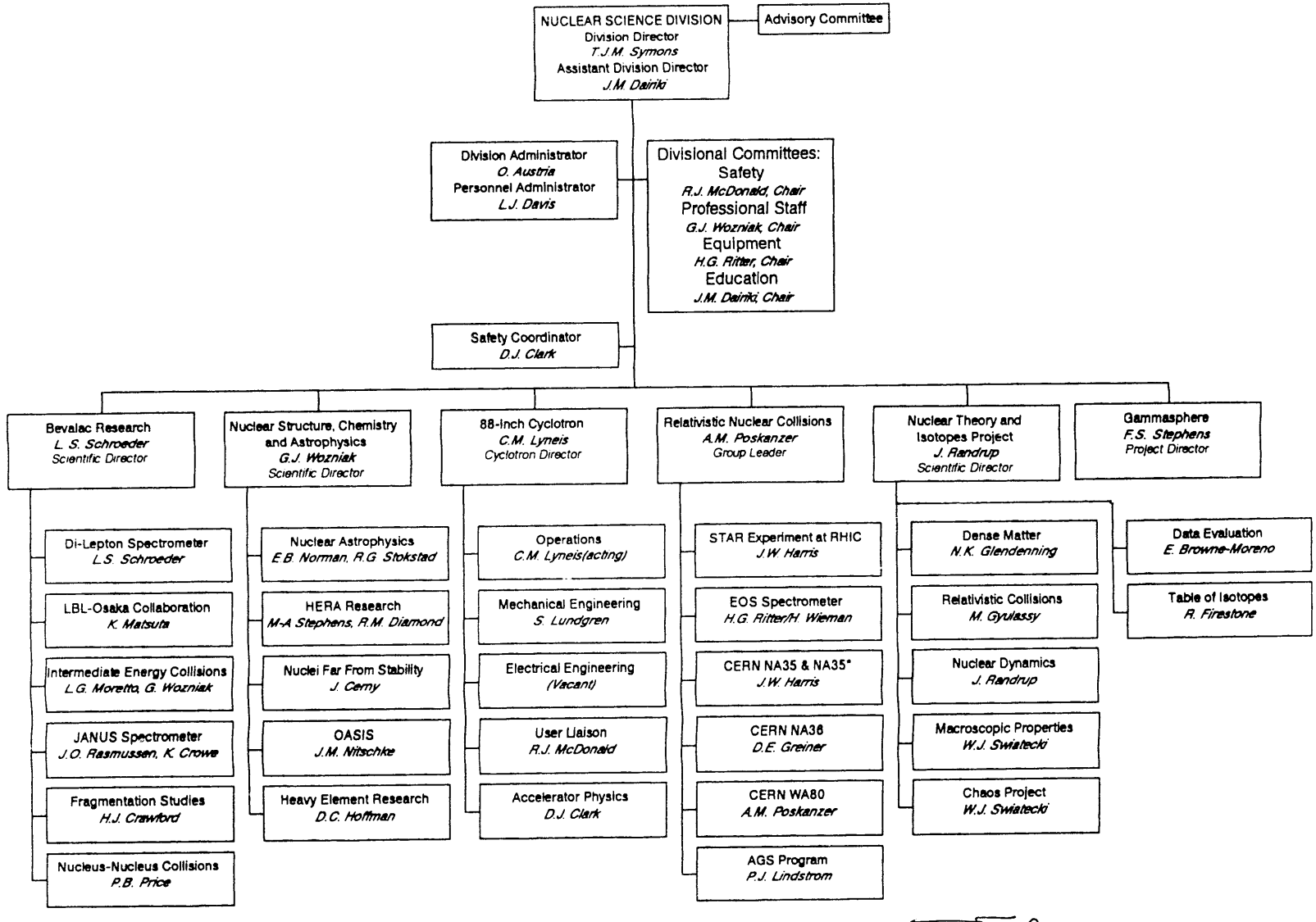
NUCLEAR SCIENCE DIVISION
Division Director
T.J.M. Symons
Assistant Division Director
J.M. Dairiki
Advisory Committee
Division Administrator
O. Austria
Personnel Administrator
L.J. Davis
Divisional Committees:
Safety
R.J. McDonald, Chair
Professional Staff
G.J. Wozniak, Chair
Equipment
H.G. Ritter, Chair
Education
J.M. Dairiki, Chair
Safety Coordinator
D.J. Clark
Bevalac Research
L. S. Schroeder
Scientific Director
Nuclear Structure, Chemistry and Astrophysics
G.J. Wozniak
Scientific Director
88-Inch Cyclotron
C.M. Lyneis
Cyclotron Director
Relativistic Nuclear Collisions
A.M. Poskanzer
Group Leader
Nuclear Theory and Isotopes Project
J. Randrup
Scientific Director
Gammasphere
F.S. Stephens
Project Director
Di-Lepton Spectrometer
L.S. Schroeder
LBL-Osaka Collaboration
K. Matsuta
Intermediate Energy Collisions
L.G. Moretto, G. Wozniak
JANUS Spectrometer
J.O. Rasmussen, K. Crowe
Fragmentation Studies
H.J. Crawford
Nucleus-Nucleus Collisions
P.B. Price
Nuclear Astrophysics
E.B. Norman, R.G. Stokstad
HERA Research
M-A Stephens, R.M. Diamond
Nuclei Far From Stability
J. Cerny
OASIS
J.M. Nitschke
Heavy Element Research
D.C. Hoffman
Operations
C.M. Lyneis(acting)
Mechanical Engineering
S. Lundgren
Electrical Engineering
(Vacant)
User Liaison
R.J. McDonald
Accelerator Physics
D.J. Clark
STAR Experiment at RHIC
J.W. Harris
EOS Spectrometer
H.G. Ritter/H. Wieman
CERN NA35 & NA35*
J.W. Harris
CERN NA36
D.E. Greiner
CERN WA80
A.M. Poskanzer
AGS Program
P.J. Lindstrom
Dense Matter
N.K. Glendenning
Relativistic Collisions
M. Gyulassy
Nuclear Dynamics
J. Randrup
Macroscopic Properties
W.J. Swiatecki
Chaos Project
W.J. Swiatecki
Data Evaluation
E. Browne-Moreno
Table of Isotopes
R. Firestone
4 June 1991

Introduction

T.J.M. Symons

This report describes the activities of the LBL Nuclear Science Division from October 1, 1988 to December 31, 1990. This has been a period of great change in our field which has provided an emotional roller coaster ride for anyone charged with assessing the future prospects of the Division! An early setback was the decision not to proceed with the Bevalac Upgrade, taken by the DOE in late 1988. With this decision came the realization that LBL is facing a future without a major nuclear physics accelerator facility on site. A series of planning meetings was held in the fall of 1989 to assess our situation resulting in decisions to concentrate on some key areas of research in the coming years:

The 88-Inch Cyclotron, which came through a competitive review in fine style in 1990, is now the focus of our low energy research program. Technical progress in the form of an Advanced ECR source, a revitalized program in heavy element research, and the recent decision to site the Gammasphere at the Cyclotron, are three factors which give us confidence in the productivity of the facility for many years to come.

The relativistic heavy ion groups are directing their efforts towards an experiment at the Relativistic Heavy Ion Collider (RHIC) which is being constructed at Brookhaven National Laboratory and is scheduled to operate in 1997. Considerable consolidation of these groups is taking place since we plan to have a major role at RHIC. However, there remains much enthusiasm for the program at CERN, where we will concentrate on contributing to NA35 and its lead beam extension. The last few years of the Bevalac are also expected to be very productive ones with the EOS 4π detector coming into operation in late 1991.

The third major direction for our program is in nuclear astrophysics and fundamental interactions. NSD has a growing involvement in this field and has joined the Sudbury Neutrino Observatory collaboration. We are taking on a major responsibility in the construction of this detector which will detect solar neutrinos (and hopefully supernova neutrinos also) starting in 1995.

As the Division evolves in these new directions, some changes to the ongoing activities are inevitable. These include the loss of some programs for which we have inadequate human or fiscal resources, and shifts in the organizational structure of the Division. The present organization is shown in the chart on the facing page.

Turning from these long range plans to a more personal level, we note with sadness the passing of Howel Pugh in November 1989. In his ten years with the Division, Howel provided leadership and intellectual depth to the

relativistic heavy ion program. Howel is sorely missed, but as one who looked resolutely to the future rather than the past, I believe that he would be profoundly excited by the opportunities ahead of the Division.

The Nuclear Science Division is well placed to exploit the opportunities of the coming decade. However, any success in the future will be based on the enthusiasm and dedication of our staff and visitors. The many contributions in this report provide strong evidence for their continuing productivity.

Finally, two points must be made concerning the production of this document. The period covered is twice as long as usual and, furthermore, this is the first Nuclear Science Division Annual Report which has been prepared by submission of camera-ready copy. Either one of these circumstances might have daunted a lesser editorial committee, but Art Poskanzer and his colleagues have assembled an outstanding report in record time. They deserve our hearty thanks.

Low-Energy Research Program

R.G. Stokstad

The Nuclear Science Division's efforts in the broad area of low-energy nuclear physics include studies of nuclear structure, chemistry, astrophysics, and heavy-ion reaction mechanisms. Main themes are the effects of high angular momentum, extremes in isospin and nuclear charge (the heaviest elements) and exotic modes of decay. Following an overview of the highlights of this research, recent developments at the 88-Inch Cyclotron, where a significant portion of this work has been carried out, are mentioned.

The focus of studies in high-spin nuclear structure continues to be on superdeformed nuclei. Many superdeformed bands (about 17 to date) have been seen first (or simultaneously) with the multi-Ge-detector array HERA. A collaboration of groups from LBL, LLNL, Rutgers U., U.C. Davis, and Iowa State U. has found a number of cases in which the energies of the transitions within some superdeformed bands in different mercury, thallium, and lead nuclei are astonishingly identical. An explanation of this phenomenon in terms of pseudo-spin symmetry has been proposed but many questions about this behavior remain unanswered. The Diamond/Stephens group, which built HERA, has also investigated superdeformation in other mass regions, notably in ^{135}Nd, ^{148}Gd, and ^{150}Tb nuclei.

The study of the transuranic elements has three aspects - the reaction mechanisms by which they are produced, the chemistry of the short-lived atoms, and the properties of their nuclear decay. A special, rare mode of decay, electron capture delayed fission (ECDF), has been of recent interest. Hoffman and collaborators have demonstrated unequivocally the existence of this decay mode by observing the fission fragments in coincidence with the x-rays that accompany the preceding electron capture and have gone on to study a number of cases of ECDF in the isotopes of Pu, Np and Bk. The chemistry of high-Z atoms is influenced by the effects of relativity on the valence electrons. A large international collaboration of chemists from Germany, Switzerland, the USSR, and the US recently made a series of experiments on the aqueous phase chemistry of ^{262}Ha (element number 105, $t_{1/2}$= 34 s). Their results show that Ha is more similar to the pseudo group V element Pa than the regular group V elements Nb and Ta. Radiochemical techniques were essential to the discovery of the two new isotopes, ^{253}Md and ^{263}Ha. The ability to work with radioactive targets underlies all of this research on the very heavy elements.

The mechanisms by which heavy ions react is a subject of broad interest that is approached in many different ways at the Cyclotron and by using other accelerators as well. Heavy-ion beams such as ^{31}P, ^{40}Ar, and ^{44,48}Ca are used in conjunction with radioactive targets for production of actinides by means of

nucleon transfer, whereas lighter beams (^{13}C, ^{18}O, and ^{22}Ne) are used in fusion reactions. Beams of ^{63}Cu at 12.6 MeV/nucleon have been used in reverse kinematics with light targets of C and Al to investigate the conditional barriers for fission and the production of complex fragments. These studies (by the Moretto/Wozniak group) are also carried out at the Bevalac using beams of La at higher bombarding energies. Fragmentation of the target has been studied using radiochemical techniques and a wide range of bombarding energies at the Cyclotron and at several other accelerators by the Loveland and Seaborg groups. The Stokstad/Chan group has used much lighter projectiles, such as ^{12}C, ^{14}N, ^{16}O and ^{20}Ne at 32 MeV/nucleon to produce projectile-like nuclei with excitation energies up to about 5 MeV/nucleon and to observe their decay into as many as five fragments. An array of 48 phoswich detectors is used in this work. At the other extreme of bombarding energy and reaction mechanism, this group has used beams from ^{3}He to ^{12}C to study angular momentum distributions in subbarrier fusion.

The spectroscopy of nuclei far from stability begins with the production and identification of a new nuclide, proceeds to the measurement of its mass and decay properties, and ultimately to the study of its (or its daughter's) level structure. The new isotopes ^{253}Md and ^{263}Ha mentioned above were observed recently at the 88-Inch Cyclotron. At the SuperHILAC, the OASIS group has studied neutron-deficient nuclei in the region Z=54-71 using their on-line isotope separator. Their investigations range from systematic studies of exotic decay modes to locations of single-particle states near N=82. The addition of a total-energy spectrometer (a large NaI well-detector in conjunction with x- and b-ray spectrometers) has enabled them to obtain new results on beta strength functions. Lighter and shorter-lived proton-rich nuclei are studied at the 88-Inch Cyclotron by the Cerny group. They have made a spectroscopic study of the nucleus ^{67}As and conducted searches for ground-state proton radioactivity from $^{64,65}As$, $^{68,69}Br$, ^{73}Rb, and ^{77}Y.

An experimental result that has aroused very wide interest has been the Norman group's study of the beta-decay spectrum of ^{14}C. This was measured with a Ge detector that had been doped with ^{14}C. At the upper end of the spectrum, in the region around 140 keV, the spectrum deviates from the standard prediction in a manner that is consistent with the emission of a neutrino of mass (17±2 keV) with a probability of (1.4±0.4)%. This result supports the earlier work of J.J. Simpson on the decay of ^{3}H, which was the first suggestion of the existence of such a massive neutrino.

The Nuclear Science Division is involved in two major construction projects in low-energy nuclear physics. The Sudbury Neutrino Observatory is a heavy-water neutrino detector to be located more than a mile underground in a mine in Sudbury, Ontario. The US is providing a portion of the funding for this project and the NSD is building the structure to support the approximately ten thousand phototubes that will record Cherenkov light from neutrino-induced

reactions. The second major project is Gammasphere, which will be built and initially operated at the 88-Inch Cyclotron for the international nuclear-structure community. Gammasphere will consist of 110 Compton-suppressed Ge detectors and will be the major new detector facility for the low-energy community.

The 88-Inch Cyclotron is a national facility and experiments in nuclear science are allocated beam time on the basis of recommendations made by a Program Advisory Committee. Although a separate and more complete overview of the operation of this facility is contained in this report, several significant developments will be mentioned here. The continued technical development of the Cyclotron is essential to the future of the low-energy research program of the Division. The significant developments in this area are three-fold. The development of high-temperature ovens for the ECR source has expanded the range of metallic ion beams. The introduction of an electron gun as a supplementary source of electrons for the ECR source is new and shows promise for improving both performance and operation. The successful testing of the Advanced ECR source indicates it will provide heavier beams at significantly higher energies.

The DOE commissioned a major review of the Cyclotron and two other comparable facilities by the Nuclear Science Advisory Committee with the unenviable charge to select one for closure. Thus began a difficult period for the community, NSAC, and the DOE. Because of its strong scientific program, to which all users of the Cyclotron contributed, closure of the 88-Inch Cyclotron was deemed "unacceptable" by NSAC. We look forward to the 88-Inch Cyclotron continuing to serve its users well, far into the future.

Nuclear Science Division Personnel and Collaborators in Low-Energy Nuclear Research

Many of the experiments described in the following one-page contributions to this annual report involve collaborations among NSD personnel and scientists from other institutions. The nature and extent of these collaborations varies widely - from single experiments to programs that have continued for decades. Although the following list containing NSD personnel and collaborating scientists and their institutions cannot convey this variety, it will give recognition to the important role of collaborative work in low-energy nuclear science. The membership of the large collaborations, which are now constructing Gammasphere and the Sudbury Neutrino Observatory, has not been included. Also, the work of groups using the low-energy national facilities without collaboration from NSD scientists has not been covered in this annual report.

Graduate students and undergraduate students are indicated by an asterisk and double asterisks, respectively. Leaders of the NSD groups are indicated in **bold face**. The period covered is approximately 1988- 1990.

High Energy Resolution Array

R.M. Diamond, F.S. Stephens, F. Azaiez, C.W. Beausang, J. Burde, M.A. Deleplanque, W. Korten, A.O. Macchiavelli

J.A. Becker[1], M.J. Brinkman*[2], A. Cizewski[2], J.E. Draper[3], E.A. Henry[1], J.C. Hill[4], H. Hubel[5], W.H. Kelly[4], A. Kuhnert[1], N. Roy[1], E. Rubel*[3], S.W. Yates[1], T.F. Wang[1], F.K. Wohn[4]

1. Lawrence Livermore National Laboratory, Livermore, CA, USA
2. Rutgers University, New Brunswick, NJ, USA
3. University of California, Davis, CA, USA
4. Iowa State University, Ames, CA, USA
5. Bonn University, Germany

Heavy Element Nuclear and Radiochemistry

D.C. Hoffman, G.T. Seaborg, B. Brady**, R.B. Chadwick*, K.R. Czerwinski*, A. Ghiorso, K.E. Gregorich, T.M. Hamilton*, N.J. Hannick*, G. Haynes**, J.E. Hudson**, C.D. Kacher**,*, B.A. Kadhodayan*, S.A. Kreek*, M.R. Lane**, D.M. Lee, M.P. Neu*, M. Nurmia, G. Simpson,

K. Aleklett[1], U. Baltensperger[2], H. Barth*[3], D.A. Bennett*[4], W. Brüchle[5], J.J. Cantley[6], R .M. Chasteler*[7], K.B. Chen*[8], H.W. Gäggeler[2], C.M. Gannett[9], M. Gober*[10], H.L. Hall*[11], M. Hecht*[3], R.A. Henderson*[12], D.T. Jost[2], J. Kovacs[2], J. Kratz[10], J.D. Leyba*[13], C. Lienart*[14], W.D. Loveland[15], Y. Nai-Qi*[2], M. Schädel[5], U.W. Scherer[10], E. Schimpf[2], A. Türler[14], A. Weber[2], Y.W. Yu[8], P. Zimmerman*[10], I. Zvara[16]

1. Studsvik Science Research Laboratory
2. Paul Scherrer Institut, Villigen, Switzerland
3. Phillips Universität, Marburg, Germany
4. Alamar Biosciences Laboratory, Sacramento, CA
5. GSI, Darmstadt, Germany
6. Craig Co. High School, Newcastle, VA
7. Duke University
8. National Tsing-Hua University, Taiwan
9. Orange Co. Sheriff's Dept., Santa Ana, CA
10. Institut für Kernchemie, Univ. Mainz, Germany
11. Lawrence Livermore National Laboratory, Livermore, CA
12. EG&G Rocky Flats, Inc., Golden, CO
13. Westinghouse Savannah River Co., Aiken, SC
14. University Bern, Switzerland
15. Oregon State University
16. Joint Institute for Nuclear Research, Dubna, USSR

OASIS

J.M. Nitschke, R.M. Chasteler, R.B. Firestone, P.A. Wilmarth

Y.A. Akovali[1], F.T. Avignone III[2], J. Bennett[3], J. Bergman[4], J.L. Feng[5], R. Ghanadan[6], J. Gilat[7], A.L. Goodman[8], M.O. Kortelahti[9], M.J. McNulty[10], P. Möller[11], C.M. Skluzacek[12], A.A. Shihab-Eldin[13], D.C. Sousa[14], K.S. Toth[1], K.S. Vierinen[15]

1. ORNL, Oak Ridge, TN, USA
2. University of South Carolina, SC, USA
3. Vanderbilt University, Nashville TN, USA
4. San Francisco State University, San Francisco, CA, USA
5. Harvard College, Cambridge MA, USA
6. University of Maryland, College Park, MD, USA
7. Soreq Nuclear Research Center, Yavne, Israel
8. Tulane University, New Orleans, LA, USA
9. University of Jyväskylä, Jyväskylä, Finland
10. East Greenwitch High School, East Greenwitch, RI, USA
11. Lund University, Lund, Sweden
12. Carleton College, Northfield MN, USA
13. Kuwait Institute for Scientific Research, Kuwait
14. Eastern Kentucky University, Richmond KY, USA
15. University of Helsinki, Helsinki, Finland

Exotic Nuclei: RAMA

J. Cerny, J.C. Batchelder*, D.M. Moltz, T.J. Ognibene*, M. Rowe*

P.E. Haustein[1], P.L. Reeder[2]

1. Brookhaven National Laboratory, Upton, New York
2. Pacific Northwest Laboratories, Richland, Washington

Heavy-Ion Reactions at Low and Intermediate Energies

Y. Chan, R.G. Stokstad, D.E. DiGregorio, B.A. Harmon, J.P. Pouliot, J.A. Scarpaci

S.J. Bennett[1], A. Dacal[2], G. Dai[3], B.R. Fulton[1], N.S. Jarvis[4], R. Knop[5], X. Liu[3], C. Moisan[6], J.T. Murgatroyd[1], M.E. Ortiz[2], J. Suro Perez[2], L. Potvin[6], Y. Qi[3], W. Rae[7], C. Riou[6], R. Roy [6], C. St.-Piere[6], D.L Watson[4], J. Zheng[3]

1. University of Birmingham, England
2. Instituto de Física, UNAM, México
3. Institute of Modern Physics, Lanzhou, PRC
4. York University, England
5. Harvey Mudd College

6. Laval University, Québec, Canada
7. Oxford University, England

Nuclear Astrophysics and Fundamental Symmetries

E.B. Norman, T. Ho**, R.M. Larimer, K.T. Lesko, B. Sur, E. Browne, J.T. Witort**

A. Champagne[1], M.M. Hindi[2], C. Jackson**[3], K. Wedding**[4], P. Englert[5], R. Paul[5]

1. Princeton University
2. Tennessee Technological University
3. Haverford College
4. Carleton College
5. San Jose State University

Bevalac Research Program

L.S. Schroeder

The Bevalac continues its unique role in the U.S. heavy ion program by providing beams spanning the periodic table from protons to uranium over a range of energies as low as 30 MeV/nucleon up to relativistic energies of 1-2 GeV/nucleon. A broad research program of nuclear science, atomic physics and cosmic-rays, as well as biology and medicine, is carried out under one roof. Utilizing unique experimental facilities, the planned Bevalac program will both complement and compete with the research now being carried out at GSI using SIS 18 into the period of the mid-1990's. Emphasis is placed on the most decisive experiments that can be conducted during this period.

The Bevalac's research community continues to be drawn from universities and laboratories throughout the world, including groups from France, Germany, Italy and Japan. The research environment provides an excellent training ground for research students over a wide spectrum of disciplines. Over 250 scientists are presently engaged in research in the physical sciences at the Bevalac and about 85 graduate students have received their Ph.D.'s from Bevalac-related work. Currently, about 40 graduate students are active in Bevalac experiments.

Central to the Bevalac's nuclear science research program is the production and study of extreme conditions in nuclear matter. Early Bevalac experiments by the Plastic Ball and Streamer Chamber demonstrated that nuclear systems at high temperatures (50-100 MeV) and densities (2-4 times normal) are created in the central collision of two nuclei and provided the first evidence for "collective flow" in nuclear matter. From such studies, thermodynamic and transport properties (hence an equation of state (EOS)) for nuclear matter can be deduced. This is of fundamental importance in nuclear physics and is of particular relevance to our understanding of the extreme conditions which can exist in the interior of neutron stars. The EOS TPC (time projection chamber), now under construction, will be used to extend our studies of the equation of state in the period of the 1990's. This next generation 4π device will expand upon existing measurements and provide new capabilities for complete event analysis of central collisions between the heaviest nuclei yielding new insights into the baryon-rich environment present at Bevalac energies. Improved measurements of the dynamics of nuclear matter produced in central nucleus-nucleus collisions, such as collective flow and pion interferometry, will be essential elements of the EOS program.

Dileptons (electron-positron pairs) continue to be studied as a fundamental probe of extreme conditions. Due to their relatively weak interaction with matter, they can be used to probe the hot, dense stage of the collision process.

Recent theoretical calculations suggest that dilepton production may be a sensitive probe of pionic annihilation in nuclear matter, thereby providing an important new tool for studying the role of pions in hot nuclear matter. Substantial currents of light nuclei (e.g., over 10^{10} Si/pulse) have been exploited to study subthreshold kaon and antiproton production. Subthreshold particle studies play an important role in our understanding of cooperative mechanisms in nuclear collisions.

The availability of substantial currents of heavy ion beams (A>100) in the 30-150 MeV/nucleon energy range has lead to an active research program studying nuclear matter at intermediate temperatures, but at below-normal densities (near the liquid-gas phase transition). These studies focus on the question of how much excitation energy can be contained in a nuclear system before dissembly occurs. Central to this is the study of the process of multifragmentation and its dependence on energy. The heavy beam capability of the Bevalac plays an especially important role in these studies and continues to provide experimentalists with fresh challenges.

Distant or grazing collisions between nuclei provide enormous opportunities for creating nuclear fragments with extreme numbers of neutrons and protons. The combination of Bevalac beams, energy variability and unique experimental facilities allow studies of nuclear species out to the proton and neutron driplines. The production of radioactive beams and measurements of their ground-state properties was pioneered at the Bevalac by several groups from Japan. Their recent work identifying ^{11}Li as being a nucleus with a "neutron halo" surrounding a ^{9}Li core is being extended to investigate the electromagnetic dissociation of the parent ^{11}Li to provide new insights into the nuclear structure of these apparently delicate nuclear species.

A variety of experiments in other disciplines continue to be performed at the Bevalac. Cosmic-ray scientists from around the world use Bevalac beams to calibrate their detectors for flights on high altitude balloons and satellites. Virtually all of the heavy-ion detectors which have flown on satellites over the last decade have been calibrated at the Bevalac. The availability of all nuclear species over a wide range of energies makes the Bevalac a unique national resource for this work. In addition, fragmentation cross sections, crucial to understanding the propagation of cosmic rays, are also measured. Atomic physicists study the extreme conditions of 1- and 2-electron uranium atoms to test the limits of quantum electrodynamics (QED). For example, precise measurements of the Lamb shift in uranium test the dependence of QED calculations on the nuclear charge (Z). Many of the atomic physics measurements made at the Bevalac have application to heavy ion physics at higher energies (e.g., Brookhaven AGS and the future RHIC).

Following are the named collaborations in which the Nuclear Science Divisions participates. The spokespersons are indicated in **bold face**.

DLS Collaboration

S. Beedoe[1], M. Bougteb[2], J. Cailiu, J. Carroll[1], T. Hallman[3], H.Z. Huang, G. Igo[1], P. Kirk[4], G. Krebs, A. Letessier-Selvon, B. Luttrell, L. Madansky[3], F. Manso[2], H.S. Matis, D. Miller[5], J. Miller, C. Naudet, J. Panetta, G. Roche[2], **L. Schroeder**, P.A. Seidl, Z.F. Wang[4], R. Welsh[3], A. Yegneswaran[6]

1. University of California at Los Angeles, Los Angeles, CA, USA
2. Université de Clermont II, Aubière, France
3. The Johns Hopkins University, Baltimore, MD, USA
4. Louisiana State University, Baton Rouge, LA, USA
5. Northwestern University, Evanston, IL, USA
6. CEBAF, Newport News, VA, USA

EOS Collaboration

F. Bieser, F. P. Brady[1], D. Carmony[2], D. Cebra, A. D. Chacon[3], J. Chance, Y. Choi[2], M. Gilkes[2], A. Hirsch[2], E. Hjort[2], **D. Keane[4]**, H. S. Matis, C. McParland, G. Odyniec, D. L. Olson, M. D. Partlan[1], N. Porile[2], G. Rai, J. Rasmussen, **H. G. Ritter**, J. L. Romero[1], **R. Scharenberg[2]**, A. Scott[4], Y. Shao[4], B. Srivastava[2], T.J.M. Symons, P. Warren[2], **H. H. Wieman**, K. Wolf[3]

1. U.C. Davis, Davis, CA, USA
2. Purdue University, West Lafayette, IN, USA
3. Texas A&M University, College Station, TX, USA
4. Kent State University, Kent, OH, USA

Intermediate Energy Collaboration

L. G. Moretto, G. J. Wozniak, N. Colonna, M. Justice, D. N. Delis, K. Hanold, K. Tso, A. C. Mignerey[1], B. Libby[1], P. Roussel-Chomaz[2], Y. Blumenfeld[3], Q. C. Sui[4], M. Colonna[5], M. Di. Toro[5], A. Pantaleo[6], G. Guarino[6], L. Fiore[6], M. A. McMahan, D. Bowman[7], G. Peaslee[7], K. Gelbke[7], W. Lynch[7], B. Tsang[7], R. de Sousa[7]

1. University of Maryland, College Park, MD, USA
2. Saclay, 91191 GIF-sur-YVETTE, Cedex France
3. Institut de Physique Nucleaire, Orsay, Cedex France
4. Institute of Atomic Energy, Beijing
5. INFN-LNS, Catania, Italy
6. INFN, Bari, Italy
7. Michigan State University, East Lansing, MI, USA

Janus Collaboration

K. Crowe, J. Rasmussen, J. Bistirlich, R. Bossingham, T. Case, M. Stoyer, Y. Dardennes[1], K. Wolf[2], A. D. Chacon[2]

1. Michigan State University, East Lansing, MI, USA
2. Texas A&M University, College Station, TX, USA

Secondary Radioactive Beams Collaboration

K. Matsuta, J. R. Alonso, G. F. Krebs, K. Sugimoto[2], T.J.M. Symons, O. Hashimoto[1], Y. Shida[1], M. Izumi[2], **T. Minamisono**[2], Y. Nojiri[2], N. Takahashi[2], K. Takeyama[2], **I. Tanihata**[3], E. Ekuni[4],K. Yoshida[3], T. Suzuki[3], T. Kobayashi[5], S. Shimoura[6], O. Testard[7],L. Greiner, W. Christie, D. L. Olson, H. Wieman, A. Ozawa, M. Fukuda[2], A. Kitagawa[2],S. Momota[2], T. Ohtsubo[2], Y. Matsuo[2], H. Takechi[2], S. Fukuda[2], I. Minami[2], K. Omata[1]

1. INS, University of Tokyo, Japan
2. Laboratory of Nuclear Studies, Osaka University, Japan
3. RIKEN, Wako, Saitama, Japan
4. Kyoto University, Kyoto, Japan
5. KEK, Tsukuba, Ibaraki 305, Japan
6. University of Tokyo, Hongo, Tokyo 113, Japan
7. Saclay, 91191 GIF-sur-YVETTE, Cedex, France

Subthreshold Kaons and Antiproton Collaboration

V. Perez-Mendez, S. N. Kaplan, J. Drewery, **A. Shor**[1], J. Tserruya[1], S. Trentalang[2], G. Igo[2], P. Kirk[3], Z. Wang[3]

1. Weizmann Institute of Science, Rehovot, Israel
2. University of California Los Angeles, Los Angeles, CA, USA
3. Louisiana State University, Baton Rouge, LA, USA

Nuclear & Astrophysics Collaboration

P.J. Lindstrom, **H.J. Crawford**[1], J. Engelage[1], I. Flores[1], L. Greiner[1], S. Costa[2],R. Potenza[2], C. Chen[3], C. Tull[3], C. Knott[4], J. Waddington[4], W.R. Webber[5], O. Testard[6], A. Soutoul[6], U. Lynen[7], W. Mueller[7]

1. UCSSL, Berkeley, CA, USA
2. INFN-LNS, Catania, Italy
3. Louisiana State University, Baton Rouge, LA, USA
4. University of Minnesota, Minneapolis, MN, USA
5. New Mexico State University, Albuquerque, NM, USA
6. Saclay, 91191 GIF-sur-YVETTE, Cedex France
7. GSI, Darmstadt, Germany

Ultrarelativistic Research Program

A.M. Poskanzer

At the Brookhaven AGS the Nuclear Science Division is participating with the UC Space Sciences Laboratory in a search for rare negative particle production in Si + Au collisions. The main purpose is to study the space-time evolution of the reaction through coalescence yields. The 1990 run provided the first measurement of antideuteron production by heavy ions. In other AGS experiments, the fractional charge search produced the most sensitive limit for stable fraction charge in heavy-ion collisions and the plastic track detectors measured the unusual reaction in which the Si projectile picked up one charge in passing through the target.

At the CERN SPS the emphasis of the present program of 60 and 200 GeV/nucleon ^{16}O- and ^{32}S-induced reactions is to explore the possibilities of producing a phase transition from hadronic matter to a baryon-rich quark-gluon plasma in central collisions of heavy ions at these energies. The Nuclear Science Division has been involved in several experiments at the CERN SPS: 1) NA35 Streamer Chamber, 2) NA36 Time Projection Chamber, 3) WA80 Plastic Ball, 4) EMU01 emulsion experiment, 5) plastic track detector experiment, and 6) free quark search experiment. NA36 finished their data taking in the August 1990 ^{32}S run and they are now in the analysis phase of the experiment looking for lambdas and kaons. The spokesman has switched from C.R. Gruhn to D.E. Greiner, both of whom are from LBL. WA80 removed the Plastic Ball from the experiment in 1990 and is concentrating on photon detection with Pb-glass detectors. The LBL contingent of WA80 is switching to NA35 but is continuing to analyze WA80 data through 1991. LBL has withdrawn from EMU01 and closed down its emulsion scanning effort. The plastic track detector and quark search experiments are on hold waiting for the Pb beam in 1994. Thus, LBL has effected a consolidation so that it is participating in only one data-taking active CERN experiment: NA35. This collaboration installed a TPC in 1990 and successfully took data. This TPC is the first such detector to operate in a magnetic field free region with pad readout only. In 1991 LBL will build and install 5000 additional channels of modern EOS-style electronics. This is a step on the way to an expected much larger contribution from LBL of integrated electronics for the 1994 NA35* Pb-beams experiment. There has been a letter of intent for this experiment and the full proposal will be submitted in the Spring of 1991. LBL's contribution will be another step in the development of fully integrated electronics for RHIC in 1997.

The Nuclear Science Division at LBL has played a seminal role in defining the forefront of relativistic heavy ion physics since the field's inception and continues to maintain its leadership role. An important step for the Division in adjusting to the evolution of the field to higher energies and larger experiments was a consolidation to provide a focus for RHIC activities. Thus the

Relativistic Nuclear Collisions Group was formed from the AGS group, the Bevalac EOS-TPC group, and CERN NA35, NA36, WA80 and EMU01 groups. With a plan to have thirty physicists and technicians from the Division eventually working on this experiment, the group has taken the lead role in developing a concept for a major RHIC experiment. In June 1990 a workshop was held at LBL to develope this concept. A collaboration resulted consisting of 75 physicists from 14 institutions which calls itself STAR (Solenoidal Tarcker At RHIC). They submitted a letter of intent in September 1990 for an experiment to study particle production and high transverse momentum jet production at midrapidity to identify the phase transition from normal nuclear matter to quark matter. Since hard-scattered partons, the precursors of jets, are predicted to be sensitive to the medium through which they propagate and since hard-scattering and the production of jets at high p_t is directly calculable in quantum chromodynamics, the study of high p_t jets as a function of energy and mass of the colliding system may be a very attractive experimental approach to identifying the presence of quark matter. Furthermore, a measurement of the produced particles at midrapidity provides the opportunity to select on events with extreme values of temperature (particle spectrum), flavor (strangeness content), shape (particle momenta) and size (two-particle correlations). The experiment will contain a Time Projection Chamber (TPC) located inside a superconducting solenoidal magnet for tracking, momentum analysis and particle identification. Segmented calorimeters will be implemented in an azimuthally symmetric geometry outside the magnetic field for jet identification and triggering. Time-of-flight detectors surrounding the TPC will extend particle identification to higher momenta and a silicon vertex tracker near the interaction region will distinguish primary and secondary vertices, and improve the tracking and momentum resolutions of the experiment. A detector R&D program is currently underway to provide the detector and data acquisition developments required to support such a RHIC experiment.

Following are the named collaborations in which the Nuclear Science Divisions participates. The spokespersons are indicated in **bold face**.

WA80 Collaboration

R. Albrecht[1], T.C. Awes[2], C. Baktash[2], P. Beckmann[3], F. Berger[3], M. Bloomer, R. Bock[1], G. Claesson[4], G. Clewing[3], L. Dragon[3], R.L. Ferguson[2], A. Franz[2], S.I.A. Garpman[4], R. Glasow[3], H.A. Gustaffsson[4], **H.H. Gutbrod**[1], J. Idh[4], P. Jacobs, K.-H. Kampert[3], B.W. Kolb[1], P. Kristiansson[4], I.Y. Lee[2], H. Löhner[3], I. Lund[1], F.E. Obenshain[2], A. Oskarsson[4], I. Otterlund[4], T. Peitzmann[3], S. Persson[4], F. Plasil[2], A.M. Poskanzer, M. Purschke[3], H.G. Ritter, S. Saini[2], R. Santo[3], H.R. Schmidt[1], T. Siemiarczuk[1], S.P. Sorensen[2], E. Stenlund[4], and G.R. Young[2]

1. Gesellschaft für Schwerionenforschung, Darmstadt, Germany
2. Oak Ridge National Laboratory, Oak Ridge TN, USA

3. University of Münster, Germany
4. University of Lund, Lund, Sweden

NA35 Collaboration

J. Bächler[7], J. Bartke[4], H. Bialkowska[11], R. Bock[5], R. Brockmann[5], P. Buncic[12], S.I. Chase, I. Derado[9], V. Eckardt[9], J. Eschke[6], C. Favuzzi[2], D. Ferenc[12], B. Fleischmann[5], P. Foka[5], M. Fuchs[5], M. Gazdzicki[10], H.J. Gebauer[9], E. Gladysz[4], C. Guerra[5], J.W. Harris, W. Heck[6], M. Hoffmann[7], T. Humanic[5,a], S. Kabana[6], K. Kadija[12], A. Karabarbounis[1], R. Keidel[8], J. Kosiec[6], M. Kowalski[9], A. Kühmichel[6], M. Lahanas[6], J.Y. Lee[6], M. LeVine[6,13], A. Ljubicic, Jr.[12], S. Margetis[6], E. Nappi[2], G. Odyniec, G. Paic[5,12], A.D. Panagiotou[1], A. Petridis[1], J. Pfennig[3], A. Piper[8], F. Posa[2], H.G. Pugh[c], F. Pühlhofer[8], G. Rai, W. Rauch[9], R. Renfordt[6], D. Röhrich[6], G. Roland[6], H. Rothard[6], K. Runge[7], A. Sandoval[5], E. Schmidt[6], N. Schmitz[9], E. Schmoetten[7], I. Schneider[6], L.S. Schroeder, P. Seyboth[11], J. Seyerlein[9], E. Skrzypczak[10], P. Spinelli[2], **R. Stock**[6], H. Ströbele[6], L. Teitelbaum, A. Thomas[6], S. Tonse, G. Vasileiadis[1], G. Vesztergombi[9,b], D. Vranic[12], S. Wenig[7]

1. Department of Physics, University of Athens, Athens, Greece
2. Dipartimento di Fisica, Università di Bari and INFN Bari, Bari, Italy
3. CERN, Geneva, Switzerland
4. Institute of Nuclear Physics, Cracow, Poland
5. Gesellschaft für Schwerionenforschung (GSI), Darmstadt, Germany
6. Fachbereich Physik der Universität, Frankfurt, Germany
7. Fakultät für Physik der Universität Freiburg, Germany
8. Fachbereich Physik der Universität, Marburg, Germany
9. Max-Planck-Institut für Physik u. Astrophysik, München, Germany
10. Institute for Experimental Physics, University of Warsaw, Warsaw, Poland
11. Institute for Nuclear Studies, Warsaw, Poland
12. Rudjer Boskovic Institute, Zagreb, Yugoslavia
13. Department of Physics, Brookhaven National Laboratory, Upton, NY, USA

a. Now at Physics Department, University of Pittsburg, Pittsburg, PA, USA
b. On leave from Central Research Institute of Physics, Budapest, Hungary
c. Deceased

NA36 Collaboration

E. Andersen[1], P.D. Barnes[7], R. Blaes[9], H. Braun[9], J.M. Brom[9], B. Castaño[8,c], M. Cherney[6], M. Cohler[11], B. de la Cruz[5], G.E. Diebold[7], C. Fernández[8], G. Franklin[7], C. Garabatos[8], J.A. Garzón[8], W.M. Geist[9], **D. Greiner, C. Gruhn**, M. Hafidouni[10], M. Heiden[b], J. Hrubec[10], D. Huss[9], J.L. Jacquot[9], P.G. Jones[2], J.P.M. Kuipers[3,11], P. Ladrón de Guevara[5], D. Liko[10], S. Lopez-Ponte[8],

G. Lovhoiden[1], J. MacNaughton[10], A. Michalon[9], M.E. Michalon-Mentzer[9], J. Mosquera[8], Z. Natkaniec[4], J.M. Nelson[2], G. Neuhofer[10], C.Perez de los Heros[5], M. Pló[8], P. Porth[10], B. Powell[3], B. Quinn[7], A. Ramil[8], J.L. Riester[9], H. Rohringer[10], I. Sakrejda, R. Schumacher[7], T. Thorsteinsen[1], J. Traxler[10], C. Voltolini[9], Y. Xia[7,a], A. Yañez[8], P. Yepes[8,d] and R. Zybert[2].

1. University of Bergen, Department of Physics, Bergen, Norway
2. University of Birmingham, Department of Physics, Birmingham, UK
3. European Organization for Nuclear Research (CERN), Genève, Switzerland
4. Instytut Fizyki Jadrowej, Krakow, Poland
5. CIEMAT, Div. de Física de Partículas, Madrid, Spain
6. Creighton University, Department of Physics, Omaha, NE, USA
7. Carnegie-Mellon University, Department of Physics, Pittsburgh, PA, USA
8. Universidad de Santiago, Dpto. Física de Partículas, Santiago de Compostela, Spain
9. Centre de Recherches Nucléaires, Strasbourg, France
10. Institut für Hochenergiephysik (HEPHY), Wien, Austria
11. University of York, Department of Physics, York , UK

a. Presently at Michican State University, MI, USA
b. Presently at Digital Equipment Corporation, Kaufbeuren, Germany
c. Presently at I.B. San Sebastian de los Reyes II, Madrid, Spain
d. Presently at McGill University, Montréal, Canada

STAR ★ Collaboration

B.D. Anderson[2], F. Bieser, M.A. Bloomer, F.P. Brady[6], W.J. Braithwaite[9], A. Breskin[12], P. Buncic[13], D.D. Carmony[3], J. Carroll[7], D.A. Cebra, A.D. Chacon, S.I. Chase, R. Chechik[12], M.G. Cherney[1], Y. Choi[3], W. Christie, J.G. Cramer[9], W. Dominik[10], J.E. Draper[6], D. Ferenc[13], Z. Fraenkel[12], E. Friedlander, M. Gazdzicki[10], V. Ghazikhanian[7], D. Greiner, C. Gruhn, E. Gulmez[7], T.J. Hallman[5], J.W. Harris, W. Heck[8], A.S. Hirsch[3], E. Hjort[3], H. Huang, G.J. Igo[7], P.M. Jacobs, K. Kadija[13], D. Keane[2], P.J. Lindstrom, A. Ljubicic[13], Jr., L. Madansky[5], R. Madey[2], H. Matis, C. McParland, C.J. Naudet, D.R. Nygren, G. Odyniec, D.L. Olson, G. Paic[13], M.D. Partlan[6], T. Pawlak[11], W. Peryt[11], J. Pluta[11], N.T. Porile[3], A.M. Poskanzer, D. Prindle[9], G. Rai, J. Rasmussen, R.E. Renfordt[8], H.-G. Ritter, D. Roehrich[8], J.L. Romero[6], J. Schambach, R.P. Scharenberg[3], L.S. Schroeder, P.A. Seidl, Y.P. Shao[2], A. Shor[12], B. Srivastava[3], R. Stock[8], H. Stroebele[8], T.J.M. Symons, M.L. Tincknell[3], S.R. Tonse, T.A. Trainor[9], S. Trentalange[7], I. Tserruya[12], D.Vranic[13], J.W. Watson[2], R.C. Welsh[5], S. Wenig[8], C. Whitten, Jr.[7], H. Wieman, K.L. Wolf[4]

1. Creighton University, Omaha, NE, USA
2. Kent State University, Kent, OH, USA
3. Purdue University, West Lafayette, IN, USA
4. Texas A & M University, College Station, TX, USA
5. The Johns Hopkins University, Baltimore, MD, USA

6. U.C. Davis, Davis, CA, USA
7. U. C. Los Angeles, Los Angeles, CA, USA
8. University of Frankfurt, Frankfurt, Germany
9. University of Washington, Seattle, WA, USA
10. Warsaw University, Warsaw, Poland
11. Warsaw University of Technology, Warsaw, Poland
12. Weizmann Institute of Science, Rehovot, Israel
13. Zagreb-Boskovic Institute, Zagreb, Yugoslavia

Nuclear Theory Program

J. Randrup

The nuclear theory program covers many of the major topics in modern nuclear physics, partly reflecting but also extending the rather broad range of the experimental program. The areas include the following broad categories: nuclear collisions at ultrarelativistic energies, reaction signatures, stopping power; high-energy lepton-nucleus reactions; effective field theories; nuclear dynamics at intermediate energies, transport theory, microscopic simulation, pre-equilibrium phenomena, dissipative processes; general nuclear properties, macroscopic models, nuclear structure and stability, exotic nuclei; nuclear astrophysics; matter at high energy density, nuclear equation of state; order-to-chaos transitions in nuclei.

The field of high-energy nuclear collisions continues to be of high priority, as is appropriate with the recent decision to construct a Relativistic Heavy-Ion Collider in this country. The chaos topic was recently taken up as a new initiative, funded initially by seed money from the Director's Program Development Fund, and it has developed into a vigorous component of our program.

Nuclear Data Evaluation Program

J. Randrup, E. Browne, and R.B. Firestone

The Isotopes Project compiles, evaluates, and disseminates nuclear structure and radioactive-decay data for basic and applied research, and for diverse technical applications. Since 1979, the project has coordinatedits efforts with the national and the international nuclear data networks, and is responsible for the evaluation of properties of nuclei with mass numbers A=167 to 194. This responsibility includes preparing data in computerized form for entry into the Evaluated Nuclear Structure Data File (ENSDF).

Spectroscopic data from radioactive decay and nuclear reactions -- after verification of completeness, correctness, and self-consistency -- serve as input data for determining recommended adopted values of specific nuclear properties. These "best values", deduced with the aid of statistical procedures, the application of systematics, and the use of nuclear models, constitute the main scientific contribution of the data evaluation effort. The project's data and corresponding bibliographic references are both computer retrievable and available in published form.

Comprehensive evaluations, produced from ENSDF, are subsequently published in the journal Nuclear Data Sheets. Concurrent with evaluation of data, the Isotopes Project develops methods and computer codes for data analysis. These include minimization procedures for deducing best values from various sets of data, and data-verification codes for assuring correctness and uniformity. The project has a continuing interest in methods for propagation of the experimental uncertainties reported for nuclear properties. Their application in nuclear data evaluation leads to uniform and rigorous interpretation of the data, and results in consistently reliable recommended values.

The Isotopes Project produced seven editions of the Table of Isotopes from 1940 to 1978, the sixth and seventh in book form. Each edition provided a comprehensive and critical evaluation of the known nuclear properties deduced from radioactive decay and reaction data. The project is also responsible for the production of the Table of Radioactive Isotopes, first published in 1986. This book provides a concise source of recommended data derived from ENSDF, and is tailored to the needs of applied users in industry, biology, medicine, and other fields. It has also proved itself as an indispensable reference for nuclear physicists and chemists in basic research.

The Isotopes Project serves a broad user community, and plays an active role in promoting the science of nuclear data evaluation. It has developed, and makes available, an extensive computerized database of nuclear structure and radioactive decay information (LBL/ENSDF) based on ENSDF.

88-Inch Cyclotron Operations

C. M. Lyneis, R. G. Stokstad, D. J. Clark, D. J. Deutscher, G. L. Low, R.M.Larimer, S. A. Lundgren, R.J. McDonald, and Z. Xie

The 88-Inch Cyclotron is operated by the Nuclear Science Division as a national facility in support of U.S. Department of Energy programs in basic nuclear science. Written proposals for experiments in nuclear science are evaluated by a Program Advisory Committee on the basis of the science proposed. Current members are C.D. Goodman (IUCF), R. Janssens (ANL), R.W. Hoff (LLNL), and R.L. McGrath (SUNY, chairman), and L. Sobotka (Wash. U.). Other PAC members during the period covered by this report were L. Riedinger (U. Tenn) and M. Blann (LLNL). The current membership of the Users' Executive Committee is J.M. Alexander (SUNY), J.A. Becker (LLNL), K.E. Gregorich (LBL), W.D. Loveland (Oregon State University, chairman) and H.R. Weller (Duke University).

Research at the Cyclotron is conducted by scientists from many institutions in addition to those from LBL and the University of California at Berkeley. During FY90, the Cyclotron was used by 137 scientists from 33 institutions. About 40% of the total beam time was used by scientists from institutions other than LBL and UCB. It also plays an important role in the education and training of young scientists at the undergraduate, graduate, and postdoctoral stages of their careers.

The central component of the facility is a sector-focused, variable-energy that has been upgraded by the addition of an Electron Cyclotron Resonance (ECR) high-charge-state ion source. [1-5] This versatile combination produces heavy ion beams from helium to oxygen with energies up to 32 MeV/nucleon. For heavier ions the maximum energy per nucleon decreases with increasing mass. Typical ions and maximum energy (MeV/nucleon) are argon (20), krypton (8), and xenon (5). Most metallic ions and all other gaseous ions up to xenon either have been accelerated or can be developed as needed. Light ions — p, d, ^{3}He and ^{4}He — are produced up to total energies of 55, 65, 135, and 130 MeV, respectively, with either the ECR or an internal filament source. Polarized proton and deuteron beams at intensities of up to 0.5 microampere are also available. Beams directly from the ECR source at up to 10 keV per charge state can be delivered by a transport system on the vault roof to any one of three target stations for atomic physics research.[6]

Accelerator Use

In FY91 the Cyclotron is operating 14.5 eight-hour shifts per week for research and one shift for routine maintenance each week. (The reduction from 17.5 shifts per week in FY90 is for budgetary reasons.) The Cyclotron operating

efficiency continues to benefit from the ECR source. There are long periods of steady operation, and only one operator per shift is required. The range of ions available from the ECR source has continued to expand. Table 1 summarizes the time distribution for FY90. The Accelerator Operation Summary shows that Cyclotron reliability was very high, with only 2% of the operating time being lost to unscheduled maintenance.

Ions and Energies

The Cyclotron fed by the ECR source provides a wide range of ions, energies, and intensities in support of the the experimental program. With the operation of the high temperature oven in the LBL ECR most elements can be accelerated. However, a few refractory materials such as tungsten and tantalum are not available. A partial list of beams, energies, and intensities is given in Table 2. In addition to those listed, many isotopic beams such as ^{26}Mg, ^{29}Si, ^{30}Si, ^{34}S, ^{37}Cl, and ^{65}Cu can be produced from natural feed material. Other isotopes such as ^{13}C, ^{15}N, ^{22}Ne, ^{44}Ca, and ^{48}Ca can be run economically from enriched isotopes because of the high efficiency of the ECR source. The beams listed in Table 2 were developed as needed for experiments proposed by the users of the 88-Inch Cyclotron. Heavy element radiochemistry experiments require several eμA of beams up to mass 48 at 6–8 MeV/nucleon. The study of ß-delayed proton emission and of light proton-rich nuclei requires a few eμA of ^{3}He at 40–110 MeV, and carbon, silicon, and sulfur at 6–7 MeV/nucleon. The nuclear astrophysics group typically uses beams of protons, deuterons, ^{3}He and ^{4}He at energies of 8–25 MeV/nucleon. A wide range of ion species, particularly of neutron-rich isotopes, is used for the study of high spin states using the HERA detector array. Groups studying heavy ion reaction mechanisms and complex fragmentation of highly excited nuclei use higher energy beams such as nitrogen and oxygen at 32 MeV/nucleon, neon (26), silicon (22), argon (20), copper (13), and U at 1.3 MeV/nucleon.

ECR Ion Source Development

Two types of ovens are used to produce beams from solid materials in the LBL ECR source.[7] The ovens are located outside the plasma, so their vapor feed rates depend only on their temperatures. This is an advantage over wire or rod feed. At the 1 eμA level at the source, the charge states from the oven beams are similar to those from gases in the same mass range, indicating that the oven feed systems have been well optimized. In the present configuration two ovens can be loaded at one time so that rapid changes between beams can be made during an experiment. The low temperature oven operates up to 700 ^{o}C and produces beams of lithium, phosphorus, magnesium, potassium, calcium, titanium and bismuth. The high temperature oven has a resistance-heated tantalum crucible, operating up to 2000 ^{o}C. Beams produced with this oven include beryllium, boron, germanium, scandium, iron, nickel, copper, silver, lanthanum and terbium. The long term stability of the ovens is excellent.

The Advanced Electron Cyclotron Resonance (AECR) source will provide new Cyclotron capabilities in the fall of 1991. Phase II of this AIP project is nearing completion. The AECR operates at 14.5 GHz and produces beams of greater intensity and higher charge states than are now available using the LBL ECR. During FY90 construction of a new horizontal beam line which connects the AECR to the Cyclotron was completed. The first AECR beams were injected into the Cyclotron in June of 1990 and since then a variety of ion species from the AECR have been accelerated. The Cyclotron recently accelerated bismuth to 954 MeV using a Bi^{38+} beam from the AECR. An electron gun, which injects 10 to 150 eV electrons into the plasma chamber has been developed to increase the production of high charge state ions.

Studies have been done on a design for a future superconducting ECR, the GECR. [8]

88-Inch Cyclotron User Support

The liaison scientists of the 88Users' Group provide information, assistance, and coordination to all users of the 88-Inch Cyclotron. These scientists are also the main contact between the Cyclotron operations staff and outside users. Presently, the outside user community includes both industrial users who purchase beam time for their own proprietary use and scientific users.

The 88Users' Group is also responsible for the development and maintenance of experimental facilities at the Cyclotron and for making these facilities attractive to a diverse group of users from around the world. The 88Users' Group supports the Users Association and its Executive Committee which conveys users' needs to the 88-Inch Cyclotron management via monthly telephone conference calls. 88Users, through the Users Association, sponsors an annual users meeting and the liaison scientist publishes a users newsletter.

During FY90, the HERA facility began operation as an 88-Inch Cyclotron facility, independent of the research group that built it. A dedicated liaison scientist was hired to help outside users on this facility. Within the first six months of its independent operation, four outside groups from four different institutions have used it.

88-Inch Cyclotron Computer Support

The low-energy computer support effort is aimed at developing and maintaining general software for experimental data acquisition and on-line diagnostics at the 88-Inch Cyclotron. The goal is to provide high-level, interactive software for the general use of all groups, and to support the daily operation of the computer hardware, providing a level of maintenance which will ensure the availability of the systems whenever needed. The VAX/780 at

the 88-Inch Cyclotron was replaced by a VAX/3300, providing users with increased computing power, more disk space, and at the same time reducing power, air conditioning, and maintenance costs.

The remaining Modcomp computers were retired, leaving a homogeneous environment of VAX computers, all interconnected via Ethernet, using the VMS operating system. The common login and distributed file system make it possible for experimenters to use any available computer without spending time learning the details of an unfamiliar system.

Applied Research

The 88-Inch Cyclotron provides a crucial service to organizations involved in the engineering and development of advanced systems for the U.S. space program. It is a major source of heavy-ion beams for the testing of computer chips and other solid-state components such as charge-coupled devices (CCD's). As such, it fulfills important national and regional needs. Because of the ability to change from one beam to another quite different one in a matter of minutes (e.g., from nitrogen to argon to krypton) it is possible to establish quickly the energy deposition level at which a single event upset (SEU) will occur. The availability of proton beams (used for studying radiation effects on CCD's) has further increased the demand for this use of the Cyclotron.

Some examples of the programs in which the use of the Cyclotron has had major importance are: i) the space projects Galileo (to Jupiter), Magellan (Venus radar mapping), and Mars Orbiter; ii) the CRRES research satellite program (Combined Radiation Release Effects Satellite); and iii) satellites for earth monitoring and national defense (DNA, DARPA, and the USAF).

The Aerospace Corporation and the Jet Propulsion Laboratory each have installed specially instrumented scattering chambers on dedicated beam lines. Their investment in these testing facilities is substantial. Future advances in device technology such as smaller size and greater complexity will result in ever greater sensitivity to SEU phenomena. This continuing trend in technology indicates a long-term need for access to the 88-Inch Cyclotron by more organizations involved in national and international space programs. Accelerator time used for the above purposes is charged to the industrial and government users on a cost recovery basis.

Reviews and Future Plans

The research programs at the Cyclotron underwent a major review at the end of FY90. This review was carried out by a subcommittee of the Nuclear Science Advisory Committee and covered the research programs of both local and outside users. After receiving in July a written description of the facility, its

users, graduate training, recent results from the research programs, and a list of publications covering the last three years, the review panel visited the 88-Inch Cyclotron on August 8-9, 1990. On November 29, NSAC endorsed the report of the subcommittee, which recommended continued operation of the 88-Inch Cyclotron in all cases.

A major effort also went into the preparation of the Facility for the January-February 1991 DOE Tiger Team site inspection. This advance preparation included the suspension of normal operations in December (to redirect staff effort toward bringing the Facility into closer compliance with DOE orders) and a reexamination of radiation protection and other safety procedures. Although there were a number of "findings" at the Cyclotron, they were in the category of least significance (Category III) and the 88-Inch Cyclotron has continued to operate throughout the Tiger Team inspection.

In January, 1991 it was decided by DOE that Gammasphere would be constructed and operated initially at the 88-Inch Cyclotron. Additional funding has been requested to increase the operating level of the Cyclotron to accommodate the increased demands for beam time associated with early implementation of Gammasphere.

The Laboratory decided to construct an addition to Building 88 using General Plant Projects funds. This will provide about twenty new offices and a much-needed seminar room. Design of the addition is underway with an expected completion date in the spring of 1993.

References

1. C. M. Lyneis, Journal de Physique, Tome 50, Coll. C1, Suppl. No. 1, Jan 1989, pp. C1-689-694.
2. D. J. Clark and C. M. Lyneis, Proc. 12th Int'l Conf. on Cyclotrons and Their Applications, Berlin, FRG, May 1989, LBL-26401.
3. T.A. Antaya and C.M. Lyneis, Proc. Int'l Symposium on Electron Beam Ion Sources and their Applications, Brookhaven National Laboratory, Nov 1988. and MSUCP-57 (1989).
4. C.M. Lyneis and Yves Jongen, Electron Cyclotron Resonance Ion Sources, The Physics and Technology of Ion Sources, pp 207-228, Ian Brown, Editor, John Wiley & Sons, 1989.
5. C.M. Lyneis and T.A. Antaya, Proc. Int'l Conf. on Ion Sources, Berkeley, July 1989, Rev. Sci. Instr. 61, 1, Pt. II, 221 (1990).
6. D.J. Clark, C.M. Lyneis, M.H. Prior, R.G. Stokstad, S. Chantrenne, and P.O. Egan, Nucl. Instr. & Meth. in Physics Research B40/41, 6 (1989).
7. D.J. Clark and C.M. Lyneis, Journal de Physique, Tome 50, Coll. C1, Suppl. No. 1, Jan 1989, pp. C1-759-766.
8. P.J. Countryman, C.M. Lyneis, R.C. Wolgast, Proc. 1989 Particle Accelerator Conference, IEEE Cat. No. 89CH2669 0, 325 (1989).

Table 1. FY 90

Accelerator Operation Summary

Machine Operation (Hours)	
Research	4953
Tuning	772
Machine Studies	171
Unscheduled Shutdowns	117
Scheduled Shutdowns	2747
Electrical Energy Consumption (GWH)	7.6

Experiment Summary

Beam Utilization for Research (Hours)	
Nuclear Research	4382
Biology and Medicine	29
Radiation Effects on Semiconductors	542
Total	4953
Number of Nuclear Science Experiments	71
Number of Scientists Participating in Research	137
Institutions Represented	
Universities	17
Other DOE National Laboratories	1
Industrial and Other Organizations	15
Percentage of Beam Time	
In-House Staff	59
Universities	14
DOE National Laboratories	15
Other Institutions	12
Total	100

Table 2. 88-Inch Cyclotron Beam List

Ion	Charge State	External Beam (eμA)	E/A Range or Max (MeV/u)
p	1	100-5	.2-55
p (pol.)	1	.7-.4	6-50
d	1	100-5	.3-32
d (pol.)	1	.7-.4	5-32
^{3}He	2	100-5	1-47
^{4}He	2	100-5	1-32
^{7}Li	2	.5	11
	3	.03	26
^{9}Be	2	.5	7
	3	.3	15
	4	.2	28
^{12}C	4	10	6
	4	5.0	16
	5	.1	24
	6	.01	32
^{14}N	5	5.0	18
	6	.15	26
	7	.01	32
^{16}O	5	10	9
	5	5	14
	6	3.0	20
	7	.1	27
	8	.03	32
^{19}F	6	2	9
	6	1	14
	7	.6	19
^{20}Ne	6	5	8
	6	2.0	13
	7	.4	17
	8	.1	22
	9	.02	28
^{24}Mg	6	1.5	9
	7	.7	12
	8	.2	16
	9	.1	20
	10	.03	24
^{28}Si	6	2.0	6
	7	1.0	9
	8	.7	11
	9	.5	14
	10	.2	18
	11	.05	22
^{31}P	8	.5	9
	10	.1	15
^{32}S	7	3.5	7
	8	2.0	9
	9	1.0	11
	10	.4	14
	11	.1	17
	12	.02	20
	13	.003	23
^{35}Cl	9	.4	9
	10	.1	11
	11	.02	14
	12	.005	16
^{39}K	9	4	7
	10	2	9
	11	1	11
	12	.02	13
^{40}Ar	9	3.0	7
	10	1.5	9
	11	.6	11
	12	.4	13
	13	.09	15
	14	.015	17
^{40}Ca	9	1.5	7
	10	1.0	9
	11	.8	11
	12	.4	13
	13	.06	15
	14	.006	17
^{63}Cu	15	.1	8
	19	.03	13
^{84}Kr	17	.2	6
	19	.08	7
	20	.04	8
^{129}Xe	23	.01	4
	27	.01	6
^{159}Tb	30	.005	5
^{238}U	21	.010	.7
	30	.001	2.2

The listed currents are based on natural isotopic source feed, except for ^{3}He. Beam intensity on target will vary according to beam line optics, collimation and energy resolution requirements. Other ions run include ^{11}B, ^{23}Na, ^{27}Al, ^{45}Sc, ^{48}Ti, ^{52}Cr, ^{56}Fe, ^{58}Ni, ^{107}Ag, ^{127}I, ^{139}La, ^{209}Bi and ^{238}U. Isotopes ^{44}Ca, ^{48}Ca and ^{235}U have also been run. These and other ions have energies and intensities similar to those in the table in the same mass range. Beam energies down to below 0.3 MeV/u are available.

Group Lists

Group Lists

Following are the lists of people in the Nuclear Science Division groups. The lists were not produced in any systematic way and their accuracy is not guaranteed.
At the end of each list are the long-term visitors with their home institutions in parenthesis.
*graduate student.
**undergraduate student.
group leader in bold face.

Administrative Staff
Austria, Olivia
Davis, Linda J.
Hines, Linda
Hodges, Robyn E.
Mann, Frances
Pouncey, Tonya S
Smith-Burnett, Wanda J.
Stenvold, Lynn
Sterling, Catherine J.
For Glenn T. Seaborg ,
Associate Director at Large:
Jackson, June D.
Ludwig, Janice L.
Whyte, Sherrill L.

Exotic Nuclei: RAMA
J.C. Batchelder*
J. Cerny
D.M. Moltz
T.J. Ognibene*
M. Rowe*

OASIS
R.M. Chasteler*
R.B. Firestone
J. M. Nitschke
P.A.Wilmarth

High-Spin Studies
F. Azaiez
C.W. Beausang
M.A. Deleplanque
R.M. Diamond
W. Korten
F.S. Stephens
J.E. Draper (UC, Davis)
W.H. Kelly (Iowa State University)
E. Rubel* (UC, Davis)

Heavy-Ion Reactions at Low and Intermediate Energies
Y. Chan
D.E. DiGregorio
B.A. Harmon
J.P. Pouliot
J.A. Scarpacci
R.G. Stokstad
A. Dacal (Instituto de Física, UNAM, México)
G. Dai (Insitute of Modern Physics, Lanzhou, PRC)
R. Knop** (Harvey Mudd College)
M.E. Ortiz (Instituto de Física, UNAM, México)
J. Suro Perez* (Instituto de Física, UNAM, México)

Nuclear Astrophysics and Fundamental Symmetries
T. Ho**
R.M. Larimer
K.T. Lesko
E.B. Norman
B. Sur
J.T. Witort**
A. Champagne (PrincetonUniversity)
M.M. Hindi (Tennessee Technological University)
C. Jackson** (Haverford College)
K. Wedding** (Carleton College)

Nuclear Astrophysics/Radioisotope Detection
S. Carlson
F. Crawford
H. Marvin*
R.A. Muller
C. Pennypacker
S. Perlmutter
C. Smith*
L. Wang*

Heavy Element Nuclear and Radiochemistry

B. Brady**
R.B. Chadwick*
K.R. Czerwinski*
A. Ghiorso
K.E. Gregorich
T.M. Hamilton*
N.J. Hannink*
G. Haynes**
D.C. Hoffman
J.E. Hudson**
C.D. Kacher**,*
B.A. Kadkhodayan*
S.A. Kreek*
M.R. Lane**
D.M. Lee
M.P. Neu*
M. Nurmia
G.T. Seaborg
G. Simpson**
H. Barth* (Phillips Universität, Marburg, Germany)
D.A. Bennett* (Alamar Biosciences Laboratory, Sacramento, CA)
W. Brüchle (GSI, Darmstadt, Germany)
J.J. Cantley (Craig Co. High School, Newcastle, VA)
R.M. Chasteler* (Duke University)
H. W. Gäggeler (Paul Scherrer Institut, Villigen, Switzerland)
C.M. Gannett* (Orange Co. Sheriff's Dept., Santa Ana, CA)
M. Gober* (Institut für Kernchemie, Univ. Mainz, Germany)
H.L. Hall* (Lawrence Livermore National Laboratory,Livermore, CA)
M. Hecht* (Phillips Universität, Marburg, Germany)
R.A. Henderson* (EG&G Rocky Flats, Inc., Golden, CO)
D. T. Jost (Paul Scherrer Institut, Villigen, Switzerland)
J. Kovacs (Paul Scherrer Institut, Villigen, Switzerland)
J. Kratz (Institut für Kernchemie, Univ. Mainz, Germany)
J.D. Leyba* (Westinghouse Savannah River Co., Aiken, SC)
C Lienert* (University Bern, Switzerland)
W.D. Loveland (Oregon State University)
Y. Nai-Qi* (Paul Scherrer Institut, Villigen, Switzerland)
M. Schädel (GSI, Darmstadt, Germany)
U. W. Scherer (Institut für Kernchemie, Univ. Mainz, Germany)
E. Schimpf (Paul Scherrer Institut, Villigen, Switzerland)
A. Türler (University of Bern, Switzerland)
A. Weber (Paul Scherrer Institut, Villigen, Switzerland)
Y.W. Yu (National Tsing-Hua University, Taiwan)
P. Zimmerman* (Institut für Kernchemie, Univ. Mainz, Germany)
I. Zvara (Joint Institute for Nuclear Research, Dubna, USSR)

Isotopes Project

E. Browne
R.B. Firestone
A.O. Macchiavelli
V.S. Shirley
C.M. Baglin (Morgan Hill, CA)
B. Singh (McMaster University, Canada)
C.A. Stone (San Jose State University)

Intermediate Energy

Y. Blumenfeld
D. Bowman
M. Colonna
N. Colonna
D. N. Delis*
K. Hanold*
M. Justice*
L. G. Moretto
G. Peaslee
P. Roussel-Chomaz
Q. C. Sui
K. Tso
G. J. Wozniak
B. Libby* (University of Maryland)

Bevalac Computers

R.A. Belshe
C. McParland
W.H. Rathbun
R. Wright
E. Yee

DLS

H. Z. Huang
A. Letessier-Selvon
H. S. Matis
J. Miller
C. Naudet
L.S. Schroeder
P. A. Seidl

S. Beedoe* (UCLA)
J. Carroll (UCLA)
G. Roche (Université de Clermont II, France)

Janus
J. Bistirlich
R. Bossingham
T. Case*
A. D. Chacon
K. Crowe
J.O. Rasmussen
M. Stoyer*
Y. Dardennes* (Michigan State University)

Transfer Reactions and Rotational Inelastic Scattering
J.O. Rasmussen
M. Stoyer*
L. Canto (Brazil)
R. Donagelo (Brazil)
A. Shihab-Eldin (Kuwait)

Plastic Track Detectors
S.W. Barwick
Y.D. He
D.M. Lowder
P.B. Price
D. Snowden-Ifft
A. Westphal
W.T. Williams
G. Jing (Institute High-Energy Physics, Beijing)
K. Kinoshita (Harvard)

Secondary Radioactive Beams
K. Matsuta
A. Ozawa*
K. Yoshida

Subthreshold Kaons and Antiprotons
J. Drewery
S.N. Kaplan
V. Perez-Mendez

Nuclear and Astrophysics
C. Chen (LSU)
S. Costa (Catania, Italy)
H.J. Crawford (UCSSL)
J. Engelage (UCSSL)
I. Flores (UCSSL)
L. Greiner (UCSSL)
C. Knott (University of Minnesota)
R. Potenza (Catania, Italy)
C. Tull (LSU)

Relativistic Nuclear Collisions
Peter Barnes*
Fred Bieser
Matt Bloomer
Dan Cebra
Scott Chase*
Santa Chatterji
Bill Christie
Achim Franz
Erwin Friedlander
Walter Geist
Doug Greiner
Chuck Gruhn
John Harris
Harry Heckman
Peter Jacobs
Jos Kuipers
Pete Lindstrom
Howard Matis
Zbigniew Natkaniec
Grazyna Odyniec
Doug Olson
Art Poskanzer
Howel Pugh (deceased)
Gulshan Rai
Wolfgang Rauch
Hans-Georg Ritter
Jo Schambach
Iwona Sakrejda
Rainer Schicker
Doug Shy**
Larry Teitelbaum*
Lois Tinay
Shaheen Tonse
Jean Marie Walker
Howard Wieman
John Wolf
Eugene Yee
Hester Yee
A. Dean Chacon (Texas A&M)
Eric Hjort (Purdue)
Martin Partlan* (UC Davis)
Fred Pottag (Marburg)
Yiping Shao* (Kent State)

Theory
G. Batko
S. Chapman*
M. Feingold
S. Gavin
N.K. Glendenning
T. Guhr
M. Gyulassy

Low Energy Experiments

Low-Energy Nuclear Fission and Our Understanding of the Nucleus*

H. L. Hall† and D. C. Hoffman

We review how experimental studies of low-energy and spontaneous fission have affected our theoretical understanding of the nucleus. The idea that a heavy nucleus could fission when bombarded with neutrons was so unexpected in 1934 that Fermi believed he was producing transuranium isotopes in bombardments of uranium with neutrons. Even at the end of 1938 Hahn and Strassmann were fearful of reporting their painstaking chemical studies proving that barium isotopes, not transuranics, were formed. During December, 1938 Lise Meitner and her nephew, Otto Frisch, discussed the surprising results of Hahn and Strassmann and came up with the idea of division of the uranium nucleus into two large fragments, a process which they called fission.

The interactions since then between experimental discoveries in low-energy nuclear fission and our theoretical understanding of the structure of the nucleus are reviewed. This synergistic relationship of experiment and theory began with the discovery of fission, led to the development of the liquid-drop model and the experimental evidence for magic numbers, continued through the development of the shell model, the experimental discovery of shape isomerism, Strutinsky's theory of double-humped fission barriers resulting from shell corrections to the liquid-drop model, the resolution of the spontaneous fission half-life disaster, the discovery of symmetric mass division in spontaneous fission and theoretical treatments based on different paths to scission. Current studies in low-energy fission include continuing attempts to understand and predict fission half-lives, measurement of the fission properties of the transfermium isotopes, and efforts to understand and exploit delayed fission as a probe of the nucleus.

The future relationship between low-energy fission (of which spontaneous fission is a subset) and our understanding of the atomic nucleus is bound to be varied and complex. As in the case of shape isomers, our understanding of the nucleus can be rapidly transformed by totally unexpected experimental results and the subsequent theoretical explanations - or vice-versa. However, it is possible to identify broad areas of fission science that warrant considerable effort in the future. These areas are not easily separated into either theory or experiment since, as we have shown in this review, theory and experiment interact in a synergistic manner - with the results of their interaction being greater than the sum of their individual parts. One such area is the continued investigation of mass-yield and kinetic-energy distributions from low-energy fission. Measurements have been performed on a number of fissioning systems, and in some regions theoretical predictions match the experimental results reasonably well. But the challenge of creating a physically realistic model which can predict the dynamic evolution of the fissioning system, taking account of the structure of both the fissioning nucleus and the fission fragments, and can correctly predict these distributions over the entire range of low-energy fission, still remains. Meeting this challenge will require both new theoretical approaches and experimental innovation in order to be able to perform measurements on as many fissioning systems as possible.

Another, somewhat related, area is the problem of SF half-lives. Experimental searches for new nuclides and elements are critically dependent on an ability to predict their half-lives; however, this rather rudimentary quantity has proven highly difficult to model because of its extreme sensitivity to even small changes in the fission barriers. Changes in the barriers as small as 0.1 MeV can lead to changes in SF half-lives on the order of 10^5. Thus, meaningful half-life calculations require a remarkably complete understanding of nuclear structure, the effect of odd nucleons, and details of the path to scission.

Many experiments and theories will fall into these broad areas, but many others undoubtedly will not. Such is the nature of scientific research and progress. However, one can be rather sure that the continued interplay of theory and experiment will provide many intriguing new results and will give new insights into our understanding of matter on the subatomic scale.

Footnotes and References

*Condensed from an invited review published in the *Journal of Radioanalytical and Nuclear Chemistry* 142, 53 (1990).

†Lawrence Livermore National Laboratory.

Spontaneous Fission Properties of 2.9-s ^{256}No*

D. C. Hoffman, D. M. Lee, K. E. Gregorich, M. J. Nurmia, R. B. Chadwick, K. B. Chen, K . R. Czerwinski, C. M. Gannett, H. L. Hall, R. A. Henderson, B. Kadkhodayan, S. A. Kreek, and J. D. Leyba

We have measured the mass and kinetic-energy distributions of 346 pairs of coincident fragments from the spontaneous fission (SF) of ^{256}No produced via the ^{248}Cm(^{12}C, 4n) reaction. The production cross section for 71-MeV ^{12}C projectiles was found to be 250 nb. The total kinetic energy (TKE) for SF of ^{256}No is 196±3 MeV. It is well fit by a single Gaussian and there is no evidence for a second component. The mass distribution is very broad (full-width at half-maximum of about 50 mass units) with no appreciable decrease in yield for symmetric mass division. ^{256}No seems to be the transition nucleus between the asymmetric mass division observed for SF of the lighter No isotopes and the symmetric mass division observed for the heavier No isotopes. Its properties are similar to those of ^{257}Fm, the isotope at which this transition occurs in the Fm isotopes, but the ^{256}No mass distribution is broader than that for ^{257}Fm, and its average TKE for symmetric mass division is about 15 MeV lower. Contour diagrams for fission yield as a function of pre-neutron-emission TKE and mass fraction for ^{256}No and ^{257}Fm are shown in Fig. 1. The average TKE as a function of mass fraction is also shown.

We determined the half-life of ^{256}No to be 2.91±0.05 s by measuring its alpha decay. The partial half-life for SF was measured to be 550 s. An energy of 8.448±0.006 MeV was measured for the alpha-particle decay to the ground state of ^{252}Fm, allowing us to calculate the mass excess for ^{256}No as 87820±8 keV. The energy of the 2^+ rotational level in the ^{252}Fm daughter is 47±5 keV, and the intensity of the 8.402-MeV alpha group populating this level is (13±2)%.

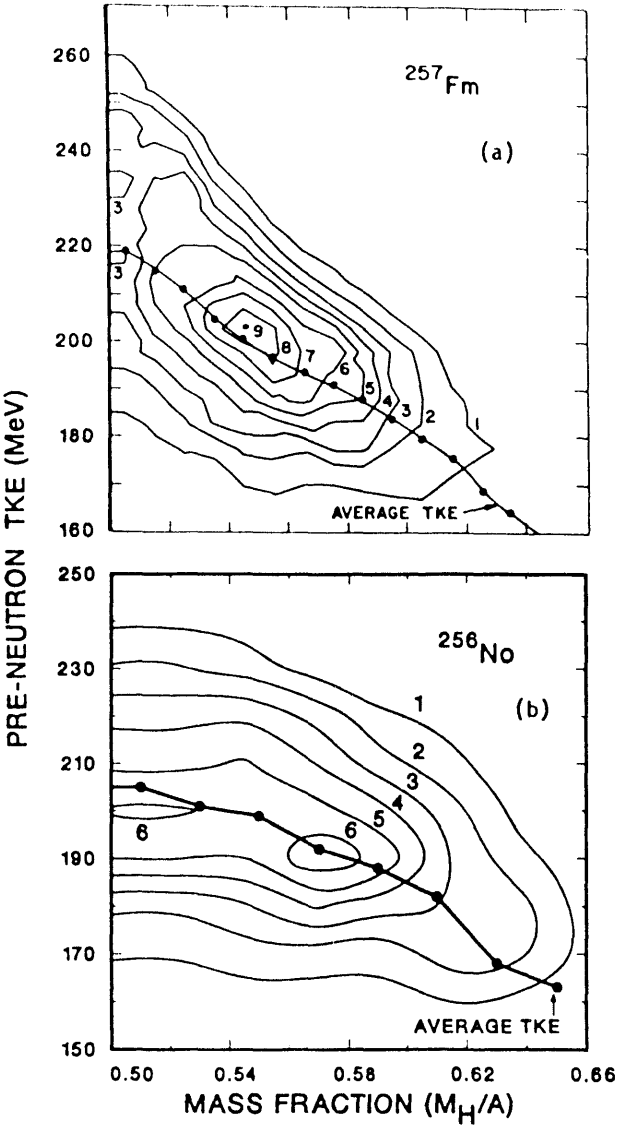

Fig. 1. Contour diagrams for fission yield as a function of pre-neutron emission TKE and mass fraction: a) ^{257}Fm (Ref. 1). Contours are lines of relative numbers of events based on data groupings 5 MeV x 0.04 units of mass fraction; b) ^{256}No. The contours indicate equal numbers of events based on data groupings 20 MeV x 0.04 units of mass fraction. Contours labeled 1-6 represent 10 through 60 events, respectively.

Footnotes and References

*Condensed from Hoffman et al., Phys. Rev. C, 41, 631 (1990).

1. J. P. Balagna, G. P. Ford, D. C. Hoffman, and J. D. Knight, Phys. Rev. Lett. 26, 145 (1971).

Delayed Fission Studies - An Overview

H. L. Hall, S. A. Kreek, and D. C. Hoffman*

Delayed fission (DF) is an exotic nuclear decay process that can occur when a nucleus decaying by β decay leaves its daughter in a highly excited state. If the excitation energy of the daughter nucleus is comparable to its fission barrier (B_f), the daughter can undergo fission as well as γ decay. This process is illustrated in Fig. 1. In the limiting case of high Q-values, delayed fission may be the dominant decay mode. Indeed, β-delayed

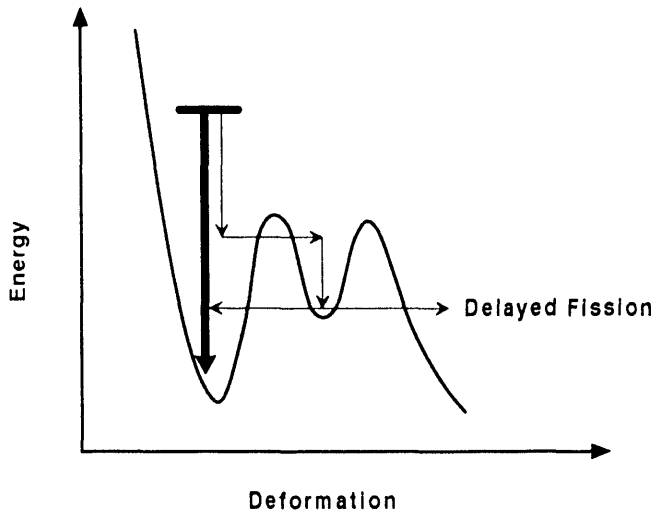

Fig. 1. Schematic illustration of delayed fission.

fission is believed to deplete the yields of the extremely neutron-rich heavy mass chains formed in the astrophysical r-process (rapid multiple neutron capture in explosive supernovae).[1] βDF also may affect the production of heavy elements in terrestrial nuclear explosions, although the complete role of βDF in these explosions is not well understood.[2]

The probability (or branching ratio) of DF (P_{DF}) is defined as

$$P_{DF} = \frac{N_f}{N_i}$$

where N_f is the number of delayed fissions arising out of N_i β (or EC) decays. In the energy regime where the Q-value is approximately equal to B_f, P_{DF} is highly dependent on the nuclear structure of the daughter as well as the energy available.[3] The β-strength function and the daughter's fission barrier strongly influence the competition between decay and fission.[4] The β-strength function governs the population of excited levels in the daughter nucleus, while the fission barrier determines the fission width at any given energy. In principle, the DF probability is a highly sensitive probe of these structure effects, but experimental difficulties hinder such studies.

Our program has concentrated primarily on electron-capture delayed fission. This type of delayed fission is analogous to β⁻-delayed fission, and is much more amenable to study than isotopes produced in nuclear explosions. Nuclei which display this decay mode can be produced at the LBL 88-Inch Cyclotron and studied by rapid radiochemical and spectroscopic techniques. Rapid measurements are necessary since the high Q-values for EC decay reduce the half-lives of the parents to minutes or less.

In recent work,[3,5-7] we have obtained the first unequivocal proof that ECDF is the correct explanation for the observed fissions by measuring the time-correlation between EC and the subsequent fission. We have used ECDF to measure the low-energy fission properties of ^{232}Pu and ^{234}Pu. Our experimental observation of βDF in ^{256}Es^{m} is the only case in which the actual level from which fission proceeds has been identified. We also have initial results for the ECDF of ^{228}Np and ^{238}Bk, which are presented in this annual report.

Of the ten nuclei we have studied ($^{228\text{-}230}$Np, ^{230,232,234,236}Am, ^{238,240}Bk, and ^{256}Es^{m}), four can be produced in sufficient quantities to observe 1-2 delayed fissions per minute. Much of the basic data such as half-life and fission properties have now been measured for these four nuclei. To further our understanding of the delayed fission process, we must now study the subtle effects of the daughter's nuclear structure on this decay mode. In particular, we expect the effects of the β-strength function and the level structure of the shape isomer to be significant factors governing delayed fission.

Footnotes and References

*Lawrence Livermore National Laboratory.

1. B. S. Meyer et al., *Phys. Rev. C* **39** 1876 (1989).
2. R. W. Hoff, *Inst. Phys. Conf. Ser. No. 88 / J. Phys. G: Nucl. Phys.* **27**, 475 (1986).
3. H. L. Hall et al., *Phys. Rev. C* **41**, 618 (1990).
4. H. V. Klapdor et al., *Z. Phys. A* **292**, 249 (1979).
5. H. L. Hall et al., *Phys. Rev. C* **39**, 1866 (1989).
6. H. L. Hall et al., *Phys. Rev. Lett.* **63**, 2548 (1989).
7. H. L. Hall et al., *Phys. Rev. C* **42**, 1480 (1990).

Direct Proof of Electron-Capture-Delayed-Fission Process*

H. L. Hall,† K. E. Gregorich, R. A. Henderson, C. M. Gannett, R. B. Chadwick, J. D. Leyba, K. R. Czerwinski, B. Kadkhodayan, S. A. Kreek, D. M. Lee, M. J. Nurmia, and D. C. Hoffman

Experimental observations of fission tracks from electron-capture delayed fission (ECDF) were reported in the light americium and neptunium isotopes as early as 1966.[1,2] However, all reports of ECDF have assigned the observed fissions to this decay mode by inference using fission half-life systematics. We sought to study a presumed delayed-fissile nucleus in sufficient detail to verify directly the ECDF hypothesis. Direct proof would come from the measurement of the time-correlation between the electron-capture decay and the subsequent fission.

^{234}Am was chosen for this study, and produced by the irradiation of twelve thin ^{237}Np targets with 70-MeV α particles from the LBL 88-Inch Cyclotron. From on-line data taken with our rotating-wheel system and from radiochemical data, we measured the fission properties of ^{234}Am ECDF.[3] The use of multiple targets allowed the production of a large number of fission events, permitting us to measure the time-correlation between the Pu x-rays from K capture in ^{234}Am and the subsequent fission of the ^{234}Pu.

The time-correlation between EC and fission was measured using activity collected directly from the target system without any chemical separation. At preset intervals, the sample was placed before a transmission mounted charged-particle detector which was sandwiched between two germanium γ detectors.

Approximately 1000 samples were collected and analyzed in this way in a 40-h irradiation. The background rate in the γ detectors was approximately 10^3 counts per second, and the probability of observing random correlations was on the order of 0.1% per fission. By narrowing the time gate in software later, the random correlation rate was reduced even further, to 0.01% per fission. Fig. 1 shows the photons observed in prompt coincidence with fission fragments, and Table I gives the expected and observed x-ray intensities.

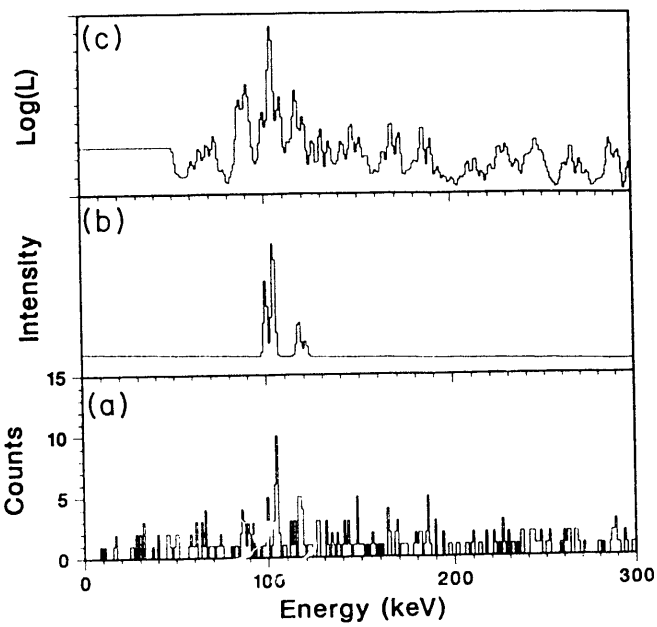

Fig. 1. X-ray - fission correlation results. (a) X rays in coincidence with fission fragments. (b) Idealized Pu K x-ray spectrum. (c) The likelihood function,[3] L, for the position of the ideal spectrum in the data. The likelihood is plotted as a function of $K_{\alpha 1}$ position of the ideal spectrum. The highest likelihood occurs at 103.6±0.5 keV.

Table I. Observed and expected x-ray intensities from the correlated x-ray - fission data.

Pu x-ray	E (keV)	I_{theo}	N_{obs} [a]	I_{obs}
$K_{\alpha 2}$	99.55	0.299	4	0.15±0.08
$K_{\alpha 1}$	103.76	0.479	14	0.54±0.18
$K_{\beta 1'}$	116.9	0.162	7	0.27±0.11
$K_{\beta 2'}$	120.6	0.06	1	0.04±0.04

[a]Approximately 6±3 of these events are attributable to the continuum of prompt γ rays from fission

This measurement of x-ray - fission correlations in the decay of ^{234}Am unequivocally proves that this decay mode is indeed EC followed by delayed fission. This is the first ECDF process for which direct proof has been obtained. The timing data also allowed us to set limits on the half-life of the shape isomer state in ^{234}Pu of 10^{-8} ns < $t_{1/2}$ < 25 ns.

Footnotes and References

*Condensed from *Physical Review Letters* 63, 2548 (1989).

†Lawrence Livermore National Laboratory.

1. V. I. Kuznetsov et al., *Yad. Fiz.* 4, 279 (1966) [*Sov. J. Nucl. Phys.* 4, 202 (1967)].
2. V. I. Kuznetsov et al., *Yad. Fiz.* 5, 271 (1966) [*Sov. J. Nucl. Phys.* 5, 191 (1967)].
3. H. L. Hall et al., *Phys. Rev. C* 41, 618 (1990).

Electron-Capture Delayed Fission Properties of $^{234}Am^{*}$

H. L. Hall,† K. E. Gregorich, R. A. Henderson, C. M. Gannett, R. B. Chadwick, J. D. Leyba, K. R. Czerwinski, B. Kadkhodayan, S. A. Kreek, D. M. Lee, M. J. Nurmia, D. C. Hoffman, C. E. A. Palmer,† and P. A. Baisden,†

Delayed fission following the electron-capture decay of ^{234}Am was studied. The $^{237}Np(\alpha, 7n)$ reaction with twelve thin ^{237}Np targets was used to produce ^{234}Am. The fission properties of the daughter (^{234}Pu) and the half-life of ^{234}Am were measured using a rotating-wheel system. The half-life of ^{234}Am, shown in Figure 1, was determined to be 2.32 ± 0.08 min from measurements of the fission activity. A highly asymmetric mass-yield distribution was observed for the fission activity, and the average total kinetic energy of the fission fragments was found to be 173 ± 5 MeV. The fission data is presented graphically in Fig. 2.

Radiochemical separations confirmed the elemental assignment of the fissioning species to americium or fission from short-lived states in its EC daughter, plutonium. The cross section for ^{234}Am produced in this reaction and decaying by electron capture was determined to be 5.4 ± 1.3 μb by measuring the intensities of the daughter plutonium K x-rays in radiochemically separated americium samples.

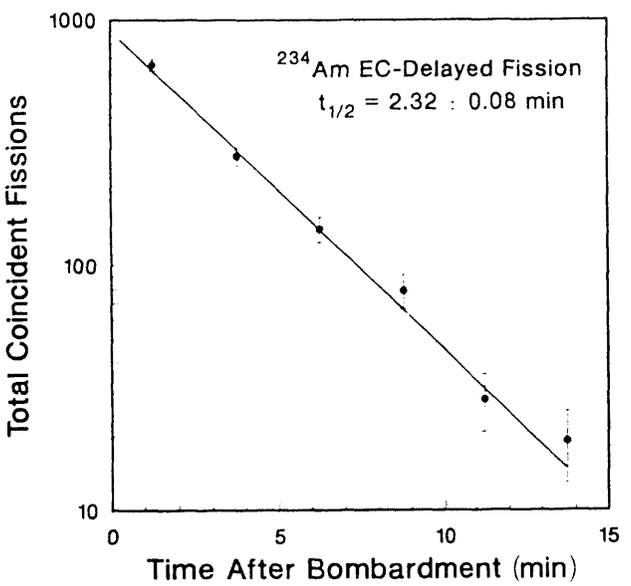

Figure 1. Decay of ^{234}Am ECDF activity.

The branching ratio of the 6.46-MeV α peak of ^{234}Am was found to be $(3.9 \pm 1.2) \times 10^{-4}$ in on-line measurements. The delayed-fission probability was determined to be $(6.6 \pm 1.8) \times 10^{-5}$ from the measured ratio of fissions to plutonium K x-rays. The observed fissions were unambiguously assigned to an EC-delayed fission process by measuring fissions coincident with K-capture x-rays.

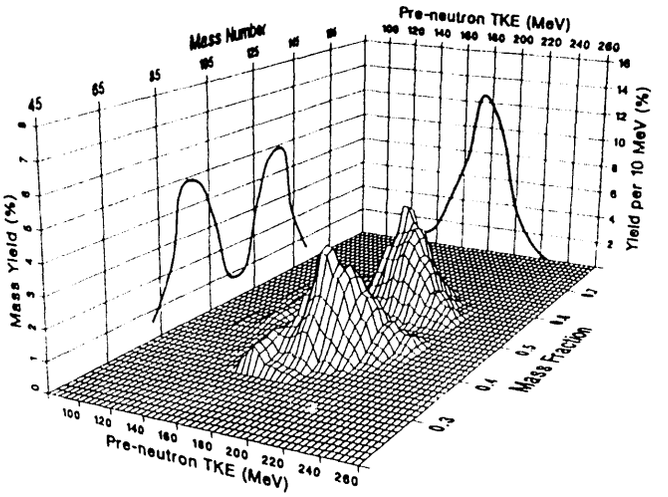

Figure 2. Fission properties of ^{234}Pu determined from ^{234}Am ECDF.

Footnotes and References

*Condensed from *Physical Review C* 41, 618 (1990).
†Lawrence Livermore National Laboratory.

Delayed Fission of ^{228}Np

H. L. Hall, P. A. Baisden,* C. E. A. Palmer,* K. E. Gregorich, S. A. Kreek, R. A. Henderson, J. D. Leyba, K. R. Czerwinski, B. Kadkhodayan, N. J. Hannink, D. M. Lee, M. J. Nurmia, and D. C. Hoffman*

Delayed fission (DF) is an exotic nuclear decay process believed to deplete the yields of the extremely neutron-rich heavy mass chains formed in the astrophysical r-process[1] and in terrestrial nuclear explosions, although the complete role of βDF is not well understood.[2]

Due to the inherent experimental difficulties of studying individual isotopes in supernovae and nuclear explosions, we have chosen to study the decay mode analogous to βDF, electron-capture delayed fission (ECDF). We report here initial results on the ECDF of ^{228}Np, produced via ^{233}U(p, 6n) at the LBL 88-Inch Cyclotron.

The half-life of ^{228}Np was observed to 64.2 ± 1.8 s as determined by the ECDF rate. Due to the complexity of the α spectra obtained in the irradiations to make ^{228}Np, it was not possible to measure the DF probability directly. Based on cross-section systematics, this probability is estimated to be approximately 10^{-4}.

A total of 2283 coincident fission fragments was observed. Analysis of the coincident fission fragments allowed determination of the low-energy fission properties of ^{228}U, shown in Fig. 2. Fission of ^{228}U was was highly asymmetric, with a single component in its total kinetic energy (TKE) distribution.

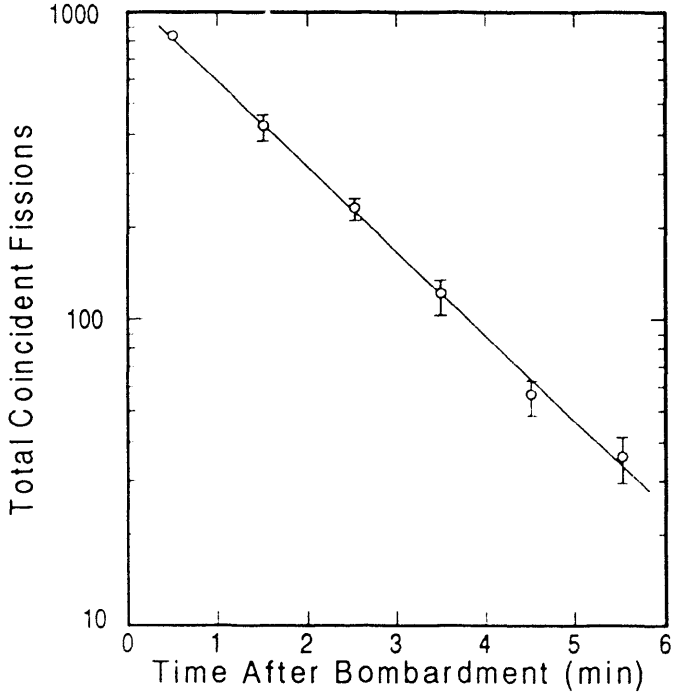

Figure 1. Decay of ^{228}Np ECDF activity.

With this study, there are now four isotopes which can be produced in sufficient quantities to observe 1-2 delayed fissions per minute (the others are ^{232,234}Am and ^{238}Bk).[3-7] To further our understanding of the delayed fission process, we must now begin to measure the effects of the daughter's nuclear structure on this decay mode. In particular, the effects of the β-strength function and the level structure of the shape isomer are expected to be significant factors in governing delayed fission.

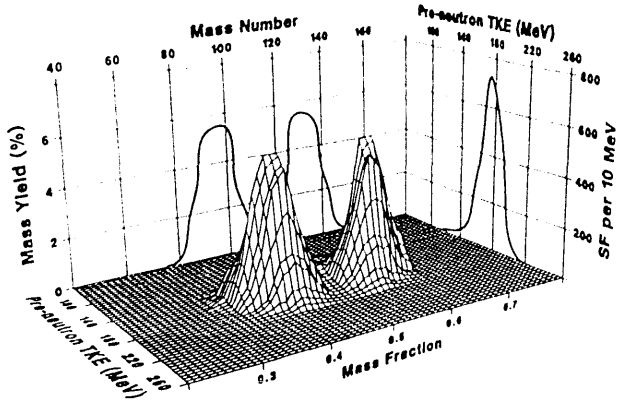

Fig. 2. Fission properties of ^{228}U determined from ^{228}Np ECDF.

Footnotes and References

*Lawrence Livermore National Laboratory.

1. B. S. Meyer et al., *Phys. Rev. C* 39, 1876 (1989).
2. R. W. Hoff, *Inst. Phys. Conf. Ser. No. 88 / J. Phys. G: Nucl. Phys.* 27, 475 (1986).
3. H. L. Hall et al., *Phys. Rev. C* 41, 618 (1990).
4. H. L. Hall et al., *Phys. Rev. C* 39, 1866 (1989).
5. H. L. Hall et al., *Phys. Rev. Lett.* 63, 2548 (1989).
6. H. L. Hall et al., *Phys. Rev. C* 42, 1480 (1990).
7. S. A. Kreek et al., This Report.

Electron-Capture Delayed Fission in ^{238}Bk

S.A. Kreek, K.E. Gregorich, H.L. Hall [†], R.A. Henderson [††], J.D. Leyba [†††], K.R. Czerwinski, B. Kadkhodayan, N.J. Hannink, C.D. Kacher, T.M. Hamilton, M. Neu, M.J. Nurmia, D.M. Lee, and D.C. Hoffman

We have extended our studies of electron-capture delayed fission (ECDF) from neutron deficient Np and Am isotopes [1,2] (Z = 93 and 95, respectively) to Bk isotopes (Z = 97) using the ^{241}Am(^{4}He,xn) reaction. It is expected that the delayed fission probability will be larger in this region because of the decreased fission barrier.

Our rotating-wheel system was used to detect fissions arising from the interactions of 75-MeV ^{4}He on ten ^{241}Am targets. These fissions are presumably from the ECDF of ^{238}Bk. Shown in Fig. 1. is the decay curve for ^{238}Bk. This yielded a half-life of 144 ±5.8 seconds.

Fig. 2 shows the data obtained from an x-ray/fission coincidence experiment. This critical information verifies that electron-capture (EC) is being followed by fission. Although the data here have very poor statistics, the presence of K-capture x-ray peaks in the curium region (the nucleus which fissions) shows that the process is indeed ECDF.

More experimental work is required to improve the x-ray/fission statistics. Additional fission data are needed to obtain good total kinetic-energy and mass-yield distributions. Radiochemistry will be performed to verify the mass and atomic number of this new isotope as well as to determine the EC branching ratio.

Footnotes and References

[†]Lawrence Livermore National Laboratory, Livermore, CA.

[††]EG&G Rocky Flats, Golden CO.

[†††]Westinghouse Savannah River Site, Aiken, S.C.

1. H.L. Hall, Ph.D. Thesis, LBL Report 27878 (1989).
2. H.L. Hall et al., This Report.

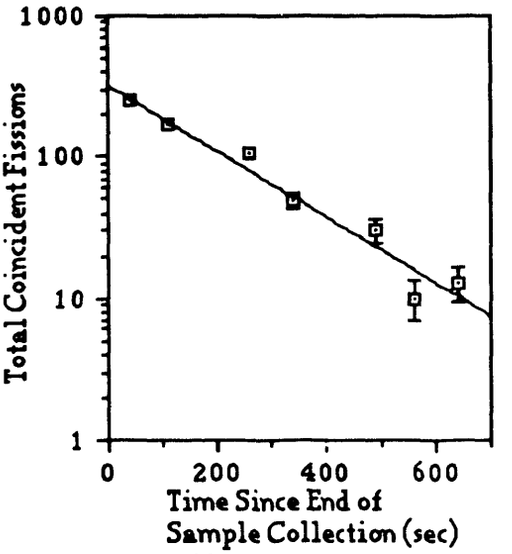

Fig. 1. ^{238}Bk decay curve.

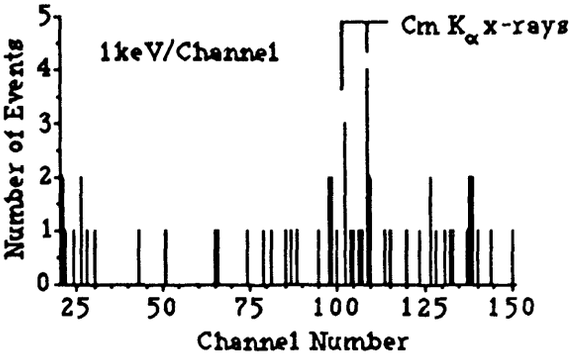

Fig. 2. X-rays observed in coincidence with fission.

Calculation of Cross Sections for Binary Reactions between Heavy Ion Projectiles and Heavy Actinide Targets*

D. C. Hoffman and M. M. Hoffman

Cross section values for the production of specific nuclei in heavy ion reactions with heavy actinide targets such as ^{248}Cm, ^{249}Cf, and ^{254}Es have been obtained from radiochemical analyses. Data for reactions with projectile kinetic energies very close to the Coulomb barrier show that nuclei with mass and charge near the values of the target nuclei are formed with large cross sections, of the order of thousands of microbarns. These large production cross sections have led to the conclusion that the heavy products are formed by binary transfer reactions rather than by compound nucleus formation. Based on a simple binary transfer mechanism, we showed earlier that many of the reactions producing neutron-rich target-like products have rather small excitation energies thus reducing the probability for losses due to prompt fission and particle emission. The cross sections have been found to decreases rapidly with the total number of nucleons transferred.

A simple model and computer program, PWAVED5, for calculating cross sections for nucleon transfer reactions in low energy heavy ion reactions has been developed in order to reproduce the experimental cross sections and to develop a predictive capability. Our calculation differs from several other partial wave calculations of heavy-ion reaction cross sections in two ways. First, it is designed specifically to calculate cross sections for nucleon exchange interactions and to exclude fusion reactions. Second, a statistical distribution is used to assign the total interaction cross section to the individual final mass states. In order to eliminate fusion events, only trajectories having radial kinetic energies in a small interval above the Coulomb barrier are allowed. The desired trajectories are selected by using the Rutherford formula to find the point of closest approach of the two ions

The calculated geometric cross section is distributed among the transfer of 1 to 12 nucleons with a Gaussian probability centered on a mean value proportional to the amount of nuclear overlap for each case. Cross sections were calculated for products with Z larger than that of the target, assuming a binary transfer mechanism. Yields for the heavy products as a function of the number of nucleons transferred and the kinetic energy of the projectile are given.

After correction of the experimental cross sections for multiplicity (the number of ways of transferring x nucleons where the probability for transferring protons, p_p, was taken to be either 0.5 or 0.39, the fraction of protons in the compound system), the results of PWAVED5 reproduce the general features of the experimental data rather well. An example is shown in Fig. 1 for interactions of ^{248}Cm with ^{18}O ions. Details of the calculation and a program listing are given in the report.

Footnotes

*Condensed from D. C. Hoffman and M. M. Hoffman, Lawrence Berkeley Laboratory Report LBL-29502, UC-413, November 1990.

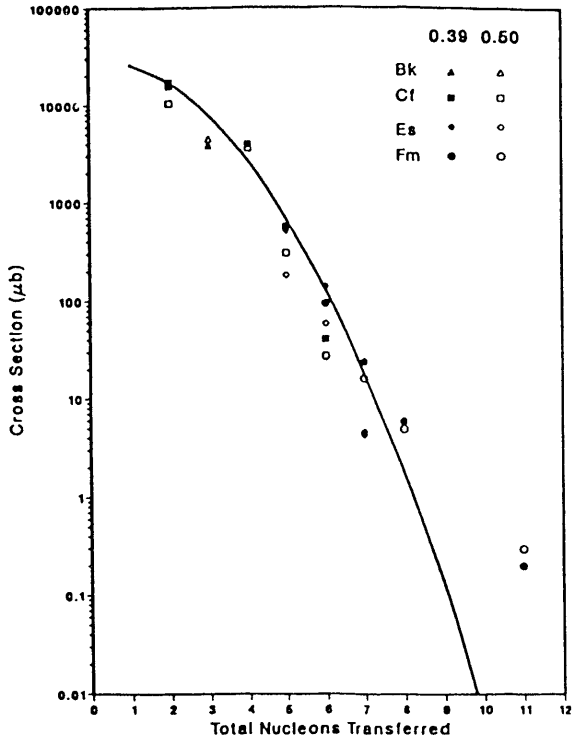

Fig. 1. Experimental data for ^{248}Cm + ^{18}O corrected for multiplicity with p_p=0.5 (solid symbols) and 0.39 (open symbols). The solid line represents the calculated cross sections.

A Systematic Study of Actinide Production from the Interactions of Heavy Ions with ^{248}Cm*

J. D. Leyba+

Production cross sections for heavy actinides produced from the interactions of ^{12}C, ^{31}P, ^{40}Ar, and ^{44}Ca ions with ^{248}Cm were measured at energies ranging from 0.98 to 1.35 X Coulomb barrier.[1] The recoiling reaction products were collected in copper or gold catcher foils located near the ^{248}Cm target. Separate fractions of Bk, Cf, Es, Fm, and Md were obtained from a radiochemical separation procedure. For the ^{12}C system, a He/KCl jet was used to transport the recoiling No activities of interest to a rotating wheel system. The isotopic distributions of the actinide products were found to be essentially symmetric about the maximum with full-widths at half-maximum of approximately 2.5 mass units. Isotopic distributions of the ^{12}C, ^{31}P, ^{40}Ar, and ^{44}Ca systems were found to be very similar to the $^{40,48}Ca$ systems studied previously. The maxima of the isotopic distributions generally occurred for those reaction channels which involved the exchange of the fewest number of nucleons between the target and projectile for which the calculated excitation energy was a positive quantity. Additionally, the maxima of the excitation functions occurred at those projectile energies which were consistent with the calculated reaction barriers based upon a binary reaction mechanism. The experimental data from the four systems investigated were compared to several models of heavy ion interactions including a damped reaction mechanism, compound nucleus formation and subsequent particle evaporation, and classical partial wave calculations for binary systems.

A model based upon heavy ion damped reactions was used to calculate the final isotopic distributions of the above target actinide products. This model does an inadequate job of reproducing the Bk, Cf, and Es experimental isotopic distributions of the ^{31}P, ^{40}Ar and ^{44}Ca systems. The model, however does a good job reproducing the Fm experimental isotopic distributions. In most cases, the experimental peak centroids of the isotopic distributions lie on the neutron-rich side of the calculated peak centroids, indicating that N/Z equilibration is not being achieved in these reactions. The damped reaction model consistently gives cross sections which are too low for many of the above target actinide reaction products, especially for isotopes of Bk, Cf, and Es. Since the cross sections for isotopes of Bk, Cf, and Es from the ^{12}C, ^{31}P, ^{40}Ar, and ^{44}Ca systems do not appreciably decrease over the energy range investigated, one can conclude that these products are being formed with little or no excitation energy. A quasi-elastic mechanism is thus probably responsible for the production of isotopes of Bk, Cf, Es, and perhaps some Fm.

The computer code ALICE, based upon compound nucleus formation and subsequent particle evaporation, was used to calculate actinide production cross sections for the ^{12}C system. ALICE does a very poor job of reproducing the isotopic distributions of the above target products, thus indicating that a compound nucleus mechanism is not involved in the production of these nuclides.

Hoffman and Hoffman[2] developed a model utilizing a classical geometric cross section calculation for binary reactions. The calculated isotopic distributions based upon this model agree quite well with the experimental isotopic distributions. This model, however, does show some discrepancies with the experimental isotopic distributions from the ^{12}C system.

Footnotes and References

* Condensed from Ph.D. dissertation, LBL-29540, September 1990.

+ Savannah River Laboratory, Westinghouse Savannah River Company, Aiken SC 29808.

1. J. D. Leyba, Ph.D. thesis, University of California, 1990.

2. D. C. Hoffman and M. M. Hoffman, "Calculations of Cross Sections for Binary Reactions", LBL-29502, UC-413, November 1990.

Excitation Functions for Actinides Produced in the Interactions of ^{31}P with ^{248}Cm

J. D. Leyba[*], *R. A. Henderson*[+], *H. L. Hall*[**], *K. R. Czerwinski, B. A. Kadkhodayan, S. A. Kreek, N. J. Hannink, E. K. Brady*[++], *K. E. Gregorich, D. M. Lee, M. J. Nurmia, and D. C. Hoffman*

Transfer reactions provide a potential route to the production of new neutron-rich actinide nuclei. The binary nature of these peripheral reactions makes the production of "cold," neutron-rich actinides possible. The Q values for particular reaction channels in many cases are endoergic by 5 MeV or greater.[1] The negative Q values decrease the excitation energy of the target-like products and thus increase their probability of surviving fission and/or neutron emission. Transfer reaction studies in the past involving ^{248}Cm as a target have only involved projectiles with even numbers of protons. The odd Z projectile ^{31}P (Z=15) was chosen for this study in order to ascertain any effects on the final isotopic distributions of the heavy actinide transfer products because of the odd proton. Since the odd proton would be unpaired in the ^{31}P nucleus, the probability of transferring an unpaired proton from this odd Z nucleus to the target should be greater than the probability of transferring one proton from an even Z nucleus.

Production cross sections for various isotopes of Bk, Cf, Es, and Fm were measured at energies ranging from 0.98 to 1.35 X Coulomb barrier. The maxima of the excitation functions occur at those projectile energies which are consistent with the calculated reaction barriers based upon a binary reaction mechanism.[2]

The isotopic distributions were found to be symmetric with full-widths at half-maximum of 2.5, 2.5, and 2.25 mass units for Bk, Cf, and Fm respectively (see Fig. 1). These values are similar to results obtained from the ^{40}Ar-^{248}Cm and ^{44}Ca-^{248}Cm systems.[3,4]

From the results of this study, it appears that the odd proton in ^{31}P does not enhance the yield of the odd Z products. A possible exception could be $^{248}Bk^{m}$, which has a maximum production cross section about a factor of two higher than the maximum production cross sections for $^{248}Bk^{m}$ from even Z projectiles interacting with ^{248}Cm.[1]

Footnotes and References

* Westinghouse Savannah River Company, 773-A, B-141, Aiken SC 29808.

+ EGG Rocky Flats, Rocky Flats Plant, P.O. Box 464, Golden CO 80402-0464.

**Nuclear Chemistry Division, L-396, Lawrence Livermore National Laboratory, Livermore CA 94550.

++Department of Chemistry, Beloit College, Beloit WI 53511.

1. J. D. Leyba *et al.*, submitted to Phys. Rev. C.
2. D. C. Hoffman and M. M. Hoffman, Los Alamos National Laboratory Report LA-UR-82-824, 1982.
3. J. D. Leyba *et al.*, Phys. Rev. C41, 2092 (1990).
4. J. D. Leyba, Ph.D. thesis, U.C. Berkeley, 1990.

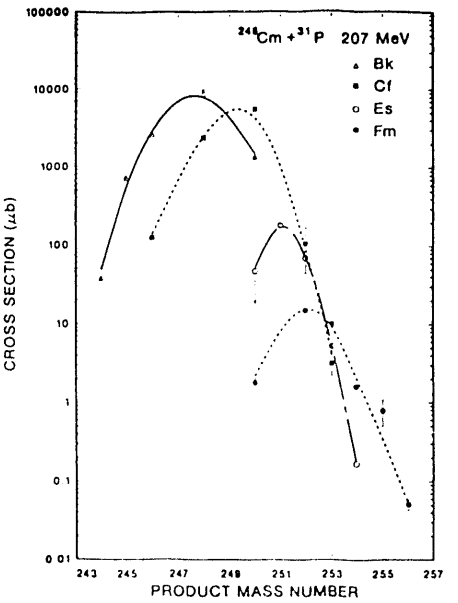

Fig. 1. Isotopic distributions for Bk, Cf, Es, and Fm from the reactions of 207-MeV (1.17 X Coulomb barrier) ^{31}P ions with ^{248}Cm. Taken from Ref. 3.

Heavy Actinide Production from the Interactions of ^{40}Ar with ^{248}Cm

J. D. Leyba, R. A. Henderson+, H. L. Hall**, C. M. Gannett++, R. B. Chadwick, K. R. Czerwinski, B. A. Kadkhodayan, S. A. Kreek, G. R. Haynes***, K. E. Gregorich, D. M. Lee, M. J. Nurmia, and D. C. Hoffman*

Transfer reactions continue to be of interest to our group because of their potential usefulness in the production of new neutron-rich actinides. Complete fusion does not take place since these reactions occur at rather large impact parameters.[1] The projectile-like fragment can carry off a large fraction of the kinetic energy and angular momentum, leaving the target-like product "cold." This present work is part of our continuing effort to obtain a better understanding of binary transfer reactions by systematically studying actinide production cross sections from the interactions of heavy ions with actinide targets.[2,3,4,5,6]

Excitation functions were measured for isotopes of Bk, Cf, Es, and Fm produced from the interactions of 207- to 286-MeV ^{40}Ar ions with ^{248}Cm. The shapes of the excitation functions were found to be consistent with their calculated excitation energies.[7] The cross sections generally decrease as the number of nucleons transferred increases. The isotopic distributions (see Fig. 1) were found to be essentially symmetric with full-widths at half-maximum between 2.0 and 3.5 mass units. Like the ^{44}Ca-^{248}Cm system,[1] the maxima of the isotopic distributions from the ^{40}Ar-^{248}Cm system generally occur for those reaction channels with involve the apparent exchange of the fewest number of nucleons for which the calculated excitation energy is a positive quantity. It appears that most of the data can be explained by a binary-type transfer mechanism in which the projectile transfers relatively little excitation energy to the target-like product.

Footnotes and References

* Westinghouse Savannah River Company, 773-A, B-141, Aiken SC 29808.

+ EGG Rocky Flats, Rocky Flats Plant, P.O. Box 464, Golden CO 80402-0464.

**Nuclear Chemistry Division, L-396, Lawrence Livermore National Laboratory, Livermore CA 94550.

++Forensics Division, Orange County Sheriff's Department, 601 North Ross, Santa Ana CA 92701.

***University of Illinois, Urbana IL 61801.

1. J. D. Leyba *et al.*, Phys. Rev. C41, 2092 (1990).
2. D. Lee *et al.*, Phys. Rev. C25, 286 (1982).
3. D. C. Hoffman *et al.*, Phys. Rev. C31, 1763 (1986).
4. A. Türler, Ph.D. thesis, University of Bern, 1989.
5. J. D. Leyba, Ph.D. thesis, University of California, 1990.
6. R. Welch *et al.*, Phys. Rev. C35, 204 (1987).
7. D. C. Hoffman and M. M. Hoffman, Los Alamos National Laboratory Report LA-UR-82-824, 1982.

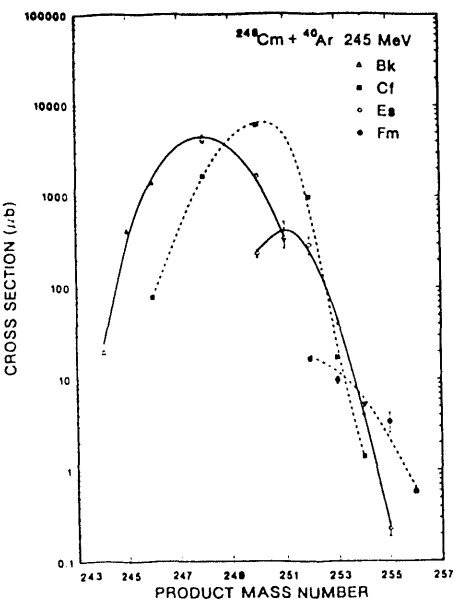

Fig. 1. Isotopic distributions for Bk, Cf, Es, and Fm from the interactions of 245-MeV (1.16 X Coulomb barrier) ^{40}Ar ions with ^{248}Cm. Taken from Ref. 5.

Maximum Likelihood Decay Curve Fits by the Simplex Method

K.E. Gregorich

A multicomponent decay curve analysis technique has been developed and incorporated into the decay curve fitting computer code MLDS[1] (Maximum Likelihood Decay by the Simplex method). The fitting criteria are based on the maximum likelihood technique for decay curves made up of time-binned events. The decay equations used to fit the decay curves are for the activities integrated over a set of time intervals to give numbers of counts expected in each interval. This avoids problems associated with using instantaneous decay rates at some time within the time intervals. The probabilities used in the likelihood functions are based on the Poisson distribution, so inaccuracies, encountered in other curve fitting programs, from applying normal statistics to small numbers of events, are avoided. Since the Poisson distribution is used, time bins which contain zero events are weighted correctly.

The search for the maximum in the multidimensional likelihood function for multicomponent fits is performed by the simplex method[2], which makes the success of the iterative fits extremely insensitive to the initial values of the fit parameters and eliminates problems of divergence. The simplex method avoids difficulties of programming the partial derivatives of the decay rates with respect to all variable parameters, which makes implementation for almost any type of curve straightforward. Any of the curve parameters can be fixed or allowed to vary. Asymmetric error limits for each free parameter, which do not consider the covariance effects of the other free parameters, are determined. A description of different types of asymmetric error limits and a procedure for the determination of these asymmetric error limits, which include the covariance effects, is also presented[1].

The correct treatment of time intervals containing zero events allows the use of discrete event times rather than time-binned data. This is accomplished by putting the discrete event times into narrow time bins (with time widths equal to the timing resolution of the acquisition system) and using intervals containing zero events for the time intervals between the decay times.

An example of a MLDS fit to a decay curve consisting of 52 events distributed among six time intervals is presented in Fig. 1. These data are for the SF of the new isotope, ^{263}Ha, produced in ^{249}Bk(^{18}O,4n) reactions[3] at the 88-Inch Cyclotron.

Footnotes and References

1. K.E. Gregorich, LBL-29306, Nucl. Instr. Meth. A (in press)
2. M.S. Caceci, W.P. Cacheris, Byte (May, 1984) p. 340
3. J.V. Kratz et al., (submitted to Phys. Rev. C)

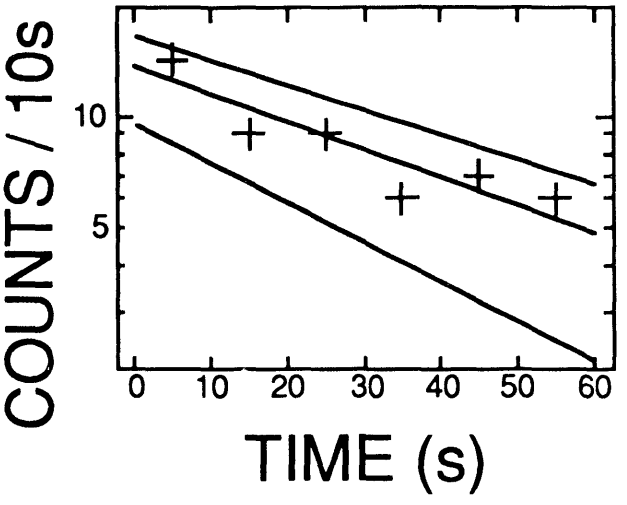

Fig. 1. Decay curve for the new isotope ^{263}Ha. The crosses represent the numbers of SF events detected in each of six 10-s intervals. The center line is the most probable single-component fit to the data. The upper and lower lines encompass 68% of the probability in a Poisson distribution about the most probable value for the number of events in each time interval.

^{261}Lr and ^{262}Lr Studies

R.A. Henderson[*], *K.E. Gregorich, H.L. Hall*[†], *J.D. Leyba*[✈], *K.R. Czerwinski, B. Kadkhodayan, S. A. Kreek, N.J.Hannink, M.J. Nurmia, D.M. Lee, and D.C. Hoffman*

^{261}Lr and ^{262}Lr were discovered by Lougheed et. al.[1] in reactions of ^{22}Ne + ^{254}Es. The half lives determined in these experiments were 39±12 min and 3.6 hours, respectively. Fission properties of the longer lived ^{262}Lr were determined after all of the ^{261}Lr had decayed from many chemically separated Lr samples. No detailed information was determined about the fission properties of ^{261}Lr.

We have obtained preliminary information on the fission properties of ^{261}Lr produced via ^{248}Cm(^{18}O,5n)^{261}Rf reactions at the LBL 88-Inch Cyclotron. The ^{261}Rf could decay by electron capture (EC) to produce ^{261} Lr. ^{261}Rf is known to be a 65±10 s α emitter[2], with no known EC branch. Radiochemical separations involving elution of actinides from cation exchange resin columns with ammonium α-hydroxyisobutyrate were performed to separate the Lr fraction. All separations were performed using ACCESS[3].

Over 100 separations were performed for the ^{261}Lr experiments. From a decay curve of 62 observed fission events, the half-life of ^{261}Lr was determined to be 44^{+17}_{-11} min, which agrees quite well with the reported half-life. A plot of the observed fission fragment kinetic energies is shown in Fig. 1, along with the ^{252}Cf calibration spectrum. From the appearance of this spectrum we are able to draw some preliminary conclusions about the properties of the fissioning species. It is not clear whether ground state fission is being observed from ^{261}Lr, or from fission following EC to ^{261}No. Regardless of what the species is, it shows a rather symmetric mass yield division with an average TKE of about 210±15 MeV. In order to help establish the production method of ^{261}Lr, a series of experiments was performed to look at the contribution of compound nucleus, pxn reactions in this region by looking at the production of ^{262}Lr from this same ^{248}Cm + ^{18}O reaction. A series of 6.5-hour bombardments was used to determine the production cross section for this 3.6 hour isotope; 80 fission events were observed.

The production cross sections for ^{261}Lr and ^{262}Lr were determined to be 700±70 pb and 240±24 pb, respectively. Cross section comparisons between ^{261}Lr (p,4n) and ^{261}Rf (5n), which has a 5 nb production cross section, set an upper limit of 14±1.4 % on the EC branch in ^{261}Rf. The systematics for these reactions seem comparable to the p4n and p3n out reactions, as the same number of nucleons are being ejected from the compound nucleus.

Footnotes and References

[*]EG&G Rocky Flats, Inc., Rocky Flats Plant.

[†]Department of Chemistry & Material Science, Lawrence Livermore National Laboratory.

[✈]Westinghouse Savannah River Co., Savannah River Laboratory.

1. R.W. Lougheed et. al., LLNL Annual Report, UCAR 10062, (1987).

2. A. Ghiorso et. al., Phys. Lett., 32B, 95 (1970).

3. C.E.A. Palmer et. al., LLNL, Report AR-88-448.2, (1988).

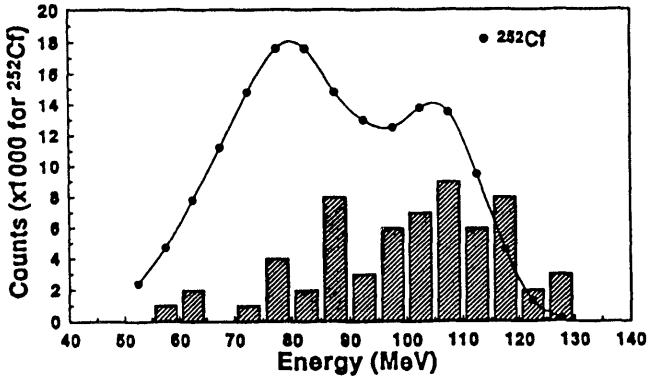

Fig. 1. Energy histogram of ^{261}Lr fission events.

^{259}Lr SF Branch and Confirmation of ^{258}Lr and ^{259}Lr Mass Assignments

K.E. Gregorich, H.L. Hall†,R.A. Henderson, J.D. Leyba§, K.R. Czerwinski, S.A. Kreek, B. Kadkhodayan, M.J. Nurmia, D.M. Lee, D.C. Hoffman*

The mass assignments of a 4.3-s 8.45- to 8.67-MeV α-activity[1] to the decay of ^{258}Lr and a 5.4-s 8.45-MeV α-activity[1] to ^{259}Lr have been confirmed, and a 23% fission branch has been measured for ^{259}Lr. The Lr activities were produced at the 88-Inch Cyclotron in ^{248}Cm(^{15}N,xn) reactions with an 80-MeV ^{15}N beam. Activities recoiling from the target were transported to our rotating wheel system with our gas-jet transport system. The experimental arrangement in the rotating wheel system is shown in Fig. 1. The activities were collected on 40-μg/cm^2 polypropylene foils at the periphery of an 80-position wheel which was stepped at 5.4-s intervals to successively position the sources through six detector stations. The α- and SF-activities from the sources were detected, after passing through the polypropylene foils, in ion-implanted detectors located below the wheel at each detector station. Above the wheel, each detector station contained an Al foil which was used to collect the recoiling daughters of α-decays. After the iradiations, these Al foils were removed and the Fm granddaughter activities were measured with a second set of ion implanted detectors. In this way, the distribution of granddaughter atoms among the Al foils is indicative of the Lr parent half-life. The decays of the Lr activities and their daughter and granddaughter activities are depicted in Fig. 2.

In the on-line measurements, we found the ^{258}Lr half-life to be $3.93^{+0.35}_{-0.31}$ s and the ^{259}Lr half-life to be $6.35^{+0.46}_{-0.42}$ s. In addition, we observed a 23±2% SF branch in the decay of ^{259}Lr. The single fragment kinetic-energies indicated a broadly symmetric mass-yield distribution and an average total kinetic energy of 200±10 MeV. In the off-line measurements, the ^{254}Fm and ^{255}Fm grand-daughters decayed with their well-known half-lives and their distributions among the Al foils were consistent with recoil from parents with 3.93-s and 6.35-s half-lives, respectively, confirming the mass assignments.

Footnotes and References

†Dept. Chem. Mat. Sci., L-310, LLNL, Livermore, CA
*EG&G Rocky Flats, P.O. Box 464, Golden, CO
§Savannah River Laboratory, Bldg 77 3-A, Aiken, SC

1. K. Eskola et al., Phys. Rev. C 4, 632 (1971)

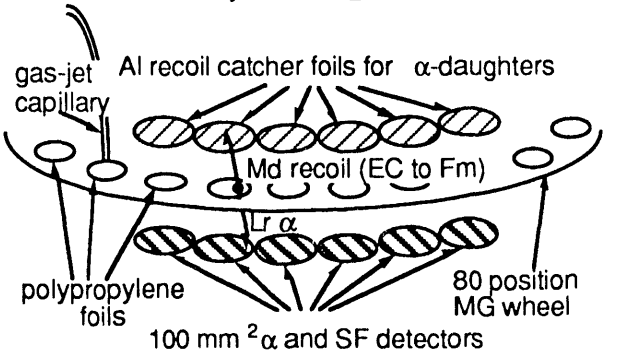

Fig. 1. Schematic of on-line detection system.

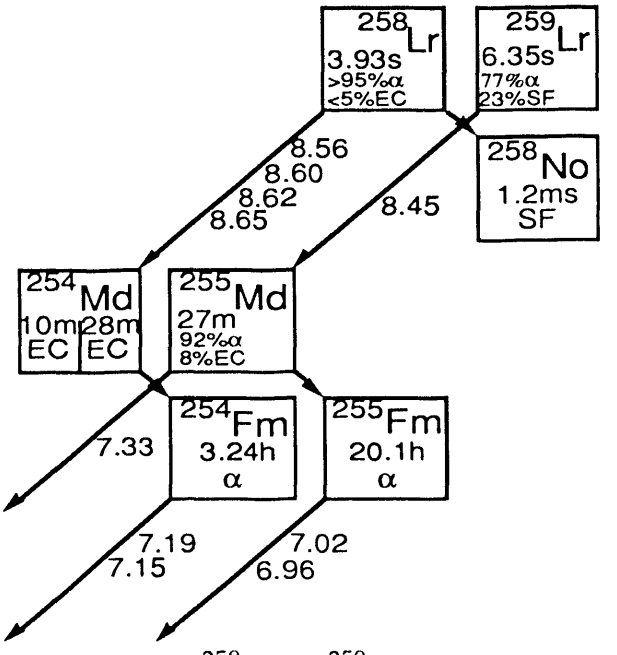

Fig. 2. Decay of ^{258}Lr and ^{259}Lr and their daughter and granddaughter activities.

New Isotope ^{263}Ha

K.E. Gregorich, A. Türler, K.R. Czerwinski, B. Kadkhodayan, N.J. Hannink, D.M. Lee, M.J. Nurmia, S.A. Kreek, C.D. Kacher, D.C. Hoffman, H.P. Zimmermann, J.V. Kratz*, M.K. Gober*, M. Schädel†, W. Brüchle†, E. Schimpf†, H. Gäggeler§, D. Jost§, J. Kovacs§, U.W. Scherer§, A. Weber§*

In our studies of the chemical properties of element 105 (hahnium, Ha), we developed an especially efficient procedure for the chemical separation of Ha. Ha^{5+} ions were separated from fission products and actinides by eluting from cation exchange resin columns with 0.05M α-hydroxyisobutyrate (α-HIB). Under these conditons, only the cations with a charge of 5+ are complexed to an extent sufficient for removal from the cation exchange resin.

This separation was tested with 34-s ^{262}Ha produced in the ^{249}Bk(^{18}O,5n) reaction[1] at the LBL 88-Inch Cyclotron with a 99-Mev ^{18}O beam. After transport of the activity by our He/KCl gas-jet transport system, the Automated Rapid Chemistry Apparatus (ARCA II)[2] was used to perform separations every 60 seconds. Several hundred separations were performed and the α-particles and SFs due to the decay of ^{262}Ha and its 3.9-s daughter, ^{258}Lr, were observed in the 5+ fractions from the column. We also observed the α-α correlations due to α-decay of ^{262}Ha followed by α-decay of the ^{259}Lr daughter. The separation proved to be extremely clean from interfering activities. The only other alpha-activities observed were due to small amounts of Bi^{5+} isotopes and a small amount of ^{249}Cf from the target which was not dissolved in the 0.05 M α-HIB and passed through the column.

Similar conditions were used in the search for the unknown isotope ^{263}Ha. The ^{18}O beam energy was lowered to 93 MeV to optimize production of ^{263}Ha by the ^{249}Bk(^{18}O,4n) reaction. Several hundred separation and counting cycles were performed. We observed 18 SFs and 9 α-particles which were attributed to the decay of ^{263}Ha and its 6.4-s daughter, ^{259}Lr. The absence of α-particles with energies above 8.5 MeV indicated that ^{262}Ha and its daughter, ^{258}Lr were not present at this bombarding energy. Five of the α-particles were assigned to the decay of ^{263}Ha, giving an α-energy of 8.355±27 MeV. The remaining four α-particles were assigned to the decay of the ^{259}Lr daughter. Two of the SF events were preceded in time (by 6.00 s and 8.58 s) by 8.36-MeV α-particles, indicating α-decay of ^{263}Ha followed by SF of the ^{259}Lr daughter. (In separate experiments[3], ^{259}Lr was found to have a 23% SF branch). There were no events in which we detected the α-decay of ^{263}Ha followed by the α-decay of ^{259}Lr. Taking the numbers of different types of events and parent-daughter correlations observed, we find the SF branch in ^{263}Ha to be 57^{+13}_{-15}%. This is an upper limit because we may not have been sensitive to an electron-capture branch in ^{263}Ha. The overall half-life of ^{263}Ha was found to be 27^{+10}_{-7} s. The single fragment energy distriution for the 18 fission events indicated that ^{263}Ha fissions symmetrically with an average total kinetic energy of about 210 MeV. The partial SF half-life gives a fission hindrance factor of 10^3 which is consistent with that observed for other odd-Z isotopes. The partial alpha half-life gives an alpha decay hindrance factor of 1.3, which is consistent with systematics in the region.[4] The production cross section of 13±8 nb is consistent with the cross section calculated for the ^{249}Bk(^{18}O,4n)^{263}Ha reaction using a compound-nucleus neutron evaporation code.

Footnotes and References

*Institut für Kernchemie, Univ. Mainz, Germany
†Gesellschaft für Schwerionenforschung, Germany
§Paul Scherrer Institut, Villigen, Switzerland

1. K.E. Gregorich et al., Radiochim. Acta, 43, 223 (1989)
2. M. Schädel et al., Radiochim. Acta, 48, 171 (1989)
3. K. E. Gregorich, submitted to Phys. Rev. C (1991)
4. Y. Hatsukawa et al., Phys Rev C 42, 674 1991)

Discovery of ^{253}Md

B. Kadkhodayan, R.A. Henderson[*], *H.L. Hall*[⇧], *J.D. Leyba*[✈], *K.R. Czerwinski, S.A. Kreek, N.J. Hannink, K.E. Gregorich, D.M. Lee, M.J. Nurmia, and D.C. Hoffman*

We have measured the half-life and production cross section of the new isotope ^{253}Md, produced via the ^{243}Am(^{13}C,3n) reaction at the LBL 88-Inch Cyclotron. Isolation of Md from other activities was accomplished using radiochemical separations involving elution with ammonium α-hydroxyisobutyrate from a cation exchange resin column. All separations were performed using ACCESS[1]. A chemistry flow chart is presented in Fig. 1. Experiments were performed with different irradiation time intervals, but the chemical separation always began and ended at exactly the same length of time after the end of irradiation. All separations with the same irradiation lengths were combined and analyzed for growth and decay of the 3.0-d ^{253}Fm daughter and 20.47-d ^{253}Es granddaughter of ^{253}Md. The amount of ^{253}Es in each fraction depends on the length of each irradiation and the ^{253}Md half-life. An increase in the length of irradiation will cause a corresponding increase in the amount of the new isotope ^{253}Md and, hence, in the amount of ^{253}Es produced, provided the lengths of irradiations are not very long compared to the half-life of ^{253}Md. Irradiation lengths of 5, 10, and 20 min were used. The number of Md atoms for each of the three irradiation time lengths was calculated. Fig. 2 shows the growth curve constructed by use of these numbers. A half-life of 6.4^{+12}_{-4} minutes and a production cross section of 46^{+243}_{-31} nb has been calculated for ^{253}Md. The error limits calculated are the approximate 68% confidence limits.

Now that we have found the half-life of ^{253}Md to be about 6 min, a future experiment in which several irradiation intervals both shorter and longer than the half-life should be performed in order to arrive at a better value. For more information about this discovery please see LBL report #30260.

Footnotes and References

[*]EG&G Rocky Flats, Inc., Rocky Flats Plant.

[⇧]Department of Chemistry & Material Science, Lawrence Livermore National Laboratory.

[✈]Westinghouse Savannah River Co., Savannah River Laboratory.

1. C.E.A. Palmer et. al., LLNL, Report AR-88-448.2, (1988).

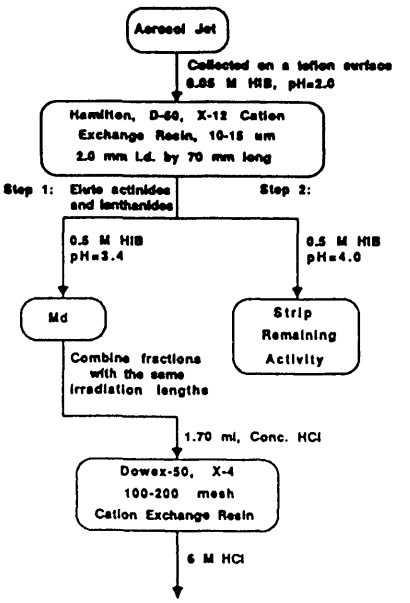

Fig. 1. Flowchart of the chemical separations.

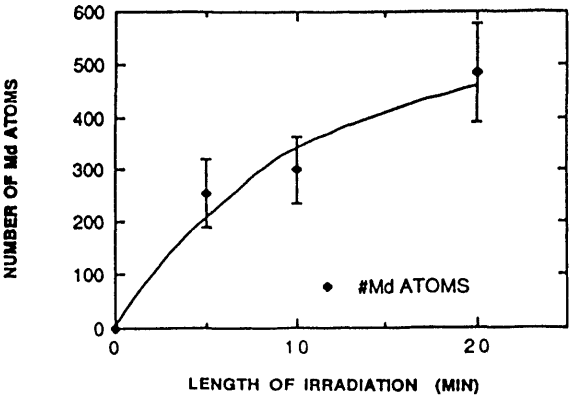

Fig. 2. Growth curve for ^{253}Md.

Separation Studies of Selected Actinide Ions with 4-Benzoyl-5-methyl-2-phenyl-pyrazol-3-thione and Tri-n-octylphosphine Oxide

Nancy J. Hannink, Darleane C. Hoffman, and Barbara F. Smith°

Separations involving lanthanides and actinides are especially difficult to achieve because the chemistry of the lanthanides and the trivalent heavy actinides is very similar since the 4f and 5f electron shells are being filled, respectively. A group separation for actinides from lanthanides would be most helpful.

Of the many separation methods used, solvent extraction is one of the fastest and simplest to perform. Ligands for use in solvent-extraction techniques involving the actinides and lanthanides ordinarily do not have sulfur atoms at binding sites since these trivalent cations exhibit "hard acid" properties; therefore, they will interact with "hard" ligand bonding sites like oxygen more extensively than with "soft" ligand bonding sites like sulfur.[1]

Recently, several papers have been published on a synergistic solvent extraction system using 4-benzoyl-5-methyl-2-phenyl-pyrazol-3-thione (BMPPT) and tri-n-octylphosphine oxide (TOPO).[2-5] The unusual aspect of BMPPT is that it has one oxygen and one sulfur bonding site so it has both "hard" and "soft" ligand sites. The previous studies [2-5]have focused on stochiometry of extracted complex and a systematic study of the lanthanides. In order to compare the work previously done with the lanthanides[5] and with Cf and Am by our group, the five actinides, Am, Bk, Cf, Es, and Fm have been studied. We used the following radioactive isotopes (their half-lives are in parentheses); ^{152}Eu (13.4 years); ^{241}Am (432 years); ^{250}Bk (3.22 hours); ^{249}Cf (351 years); ^{254}Es (276 days; and ^{253}Fm (3.00 days). The research can be done here because LBL is one of the few places where the production and handling facilities for short-lived actinide isotopes such as ^{253}Fm and ^{250}Bk exist.

My results for extraction of Am as a function of BMPPT concentration reproduce those of Smith et al.[3] Einsteinium does not extract as well as Am for the higher BMPPT concentrations studied. Our results for the extraction of Eu as a function of pH are similar to the results of Nekimken et al.[5]. Our studies for the extraction of the actinides (shown in Fig. 1) compared with those of Nekimken et al.[5] for the lanthanides suggest that the larger distribution coefficients for the actinides are because of stronger covalent bonding between the actinide metal ion and the sulfur in the ligand.

Footnotes and References

° Analytical Chemistry Group, Los Alamos National Laboratory, Los Alamos NM 87545

1. G.R. Choppin, Radiochim. Acta, 32, 43-53 (1983)
2. D.D. Ensor, G.D. Jarvinen, and B.F. Smith, Solvent Extr. Ion Exch., 6, 439-445 (1988).
3. B.F. Smith, G.D. Jarvinen, G.G. Miller, R.R. Ryan, and E.J. Peterson, Solvent Extr. Ion Exch., 5, 895-908 (1987).
4. B.F. Smith, G.D. Jarvinen, M.M. Jones, and P.J. Hay, Solvent Extr. Ion Exch., 7(5), 749-765 (1989).
5. H.L. Nekimken, B.F. Smith, G.D. Jarvinen, and C.S. Bartholdi, submitted for publication.

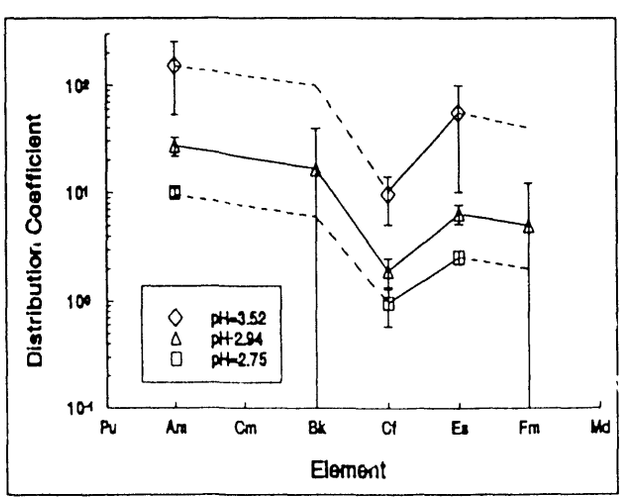

Fig. 1. Distribution coefficients for the actinides at three different pH's.

Extraction of Rf and its Homologs with TBP

K.R. Czerwinski, K. Gregorich, T. Hamilton, N.J. Hannink, C.D. Kacher, B.A. Kadkhodayan, S.A. Kreek, D. Lee, M. Nurmia, A. Türler, and D.C. Hoffman

The extraction of tetravalent Rf (element 104), Hf, Th and Pu by tributylphosphate (TBP) in benzene from acidic chloride solutions has been studied using 65-s ^{261}Rf produced at the LBL 88-Inch Cyclotron via the ^{248}Cm(^{18}O, 5n)^{261}Rf reaction. The ^{169}Hf was produced via reaction of ^{18}O with a natural Gd target. Tracer ^{238}Pu and ^{228}Th were used. The HCl, Cl^- and H^+ concentrations were varied between 8 and 12 molar; the TBP concentration was 0.25 M for Rf, Th and Hf and 1.0 M for Pu.

Studies of Rf extraction as a function of [H^+], with [Cl^-] constant at 12 molar, are presented in Fig. 1. The extraction of Rf increased sharply with [H^+], a behavior not exhibited by the other group 4 elements. Extraction for Pu was nearly constant as a function of HCl concentration (Fig. 2), but generally increased for the other nuclides.

The studies as a function of chloride concentration, with [H^+] held constant at 8 molar showed that Rf behaves differently than Hf and Th, and most like Pu (Fig. 3). The Rf extraction reached a maximum around 10 M [Cl^-], while the extraction for Hf and Th continued to increase. The extraction of Pu decreased above 10 M [Cl^-]. These results indicate that Rf forms anionic chloride species (which do not extract), similar to those of Pu at higher Cl^- concentrations while Hf and Th do not.

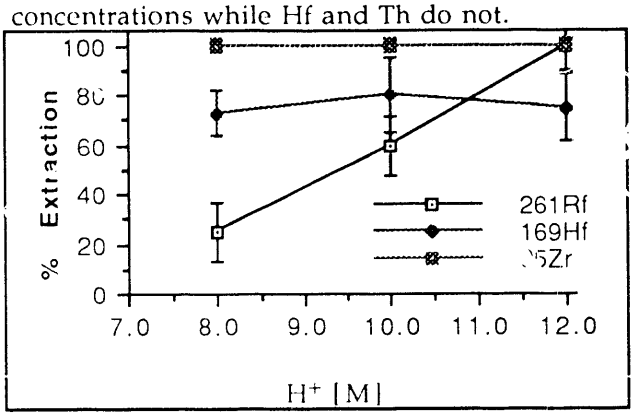

Fig.1. Extraction by TBP vs. [H^+]; [Cl^-] at 12 M.

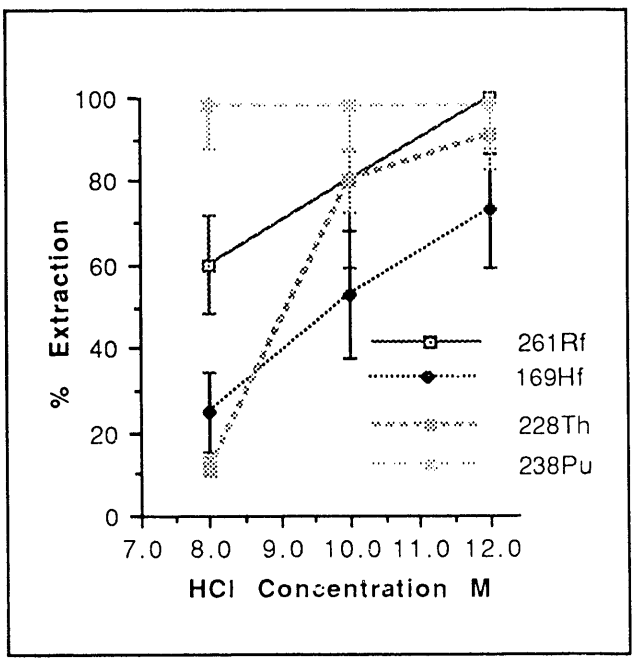

Fig. 2. Extraction into TBP vs [HCl]

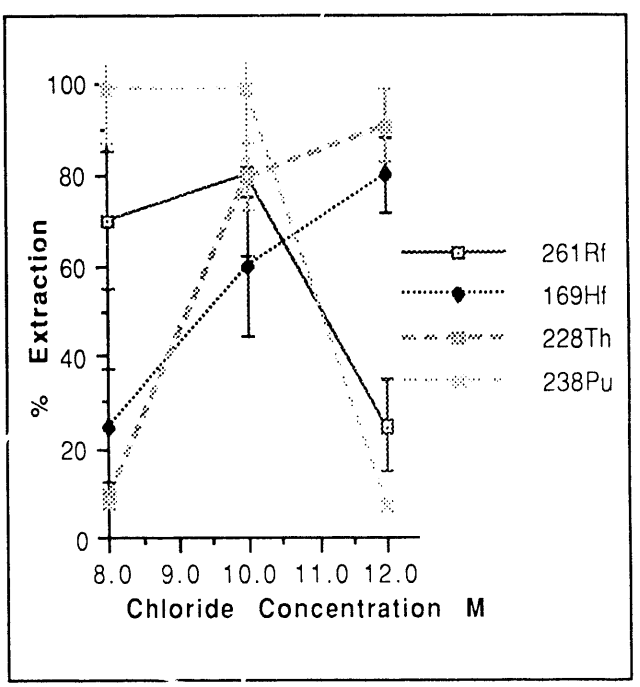

Fig. 3. Extraction into TBP vs. [Cl^-]; [H^+] at 8 M

Extraction of Zirconium with TBP

K.R, Czerwinski, C.D. Kacher, and D.C. Hoffman

Zirconium is being studied so that comparisons can be made to its heavier homolog, Rf (element 104). The liquid-liquid extraction of radioactive ^{95}Zr tracer into tri-n-butyl phosphate (TBP)from aqueous solutions were studied. TBP is a powerful extractant because of the phosphoryl group which allows the oxygen atom to form bonds with metal cations (M) : $(C_4H_9O)_3P{=}O$ --> M.

Experiments were conducted with an organic phase of 1 M TBP in benzene. The concentrations of HCl, H^+, and Cl^- in the aqueous phase were varied to examine the effects on extraction of ^{95}Zr, then the distribution coefficients (K_d) were calculated. The aqueous and organic phases contained equal volumes of 500 µL each.

Fig. 1 shows the effects of $[H^+]$ on ^{95}Zr extraction. The $[H^+]$ was varied from 2 M to 6 M while the $[Cl^-]$ was kept constant at 6 M. Extraction increased as the $[H^+]$ increase due to formation of Zr chloride species. The [HCl] was varied from 2 M to 12 M as shown in Fig. 2. The K_d for Zr increased with [HCl] up to 10 M HCl with a similar value for 12 M HCl.

Dependence of K_d on variations in $[Cl^-]$ is shown in Fig. 3. The $[Cl^-]$ was varied between 6 M and 10 M and $[H^+]$ was kept constant at 6 M. There was a large increase in K_d with concentration for Zr.

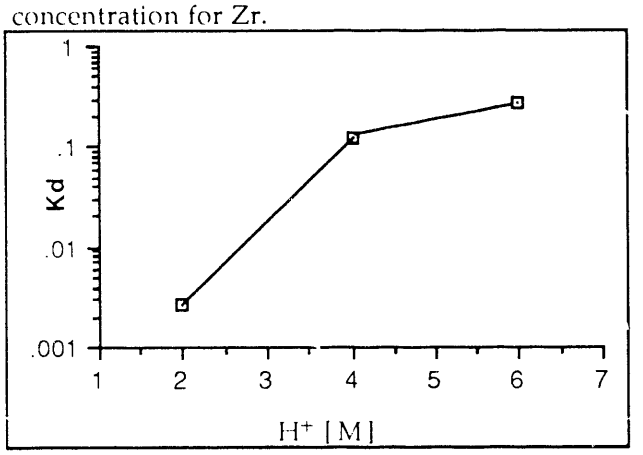

Fig.1 Effect of $[H^+]$M on Zr Extraction

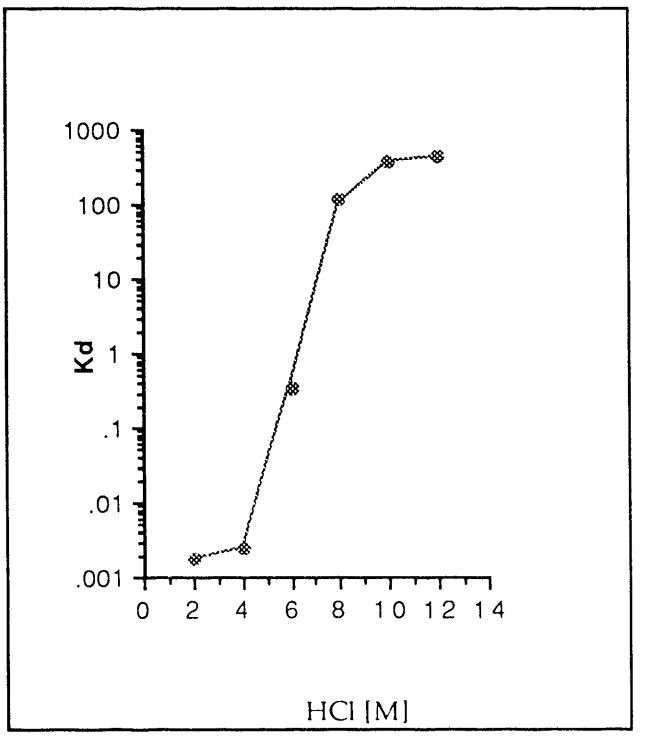

Fig. 2. Effect of [HCl] on Zr Extraction

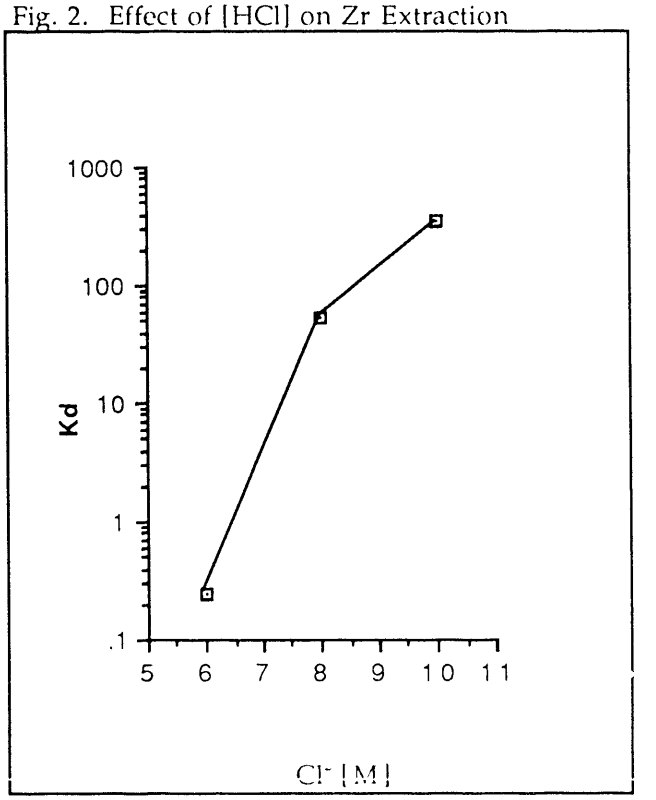

Fig. 3 Effect of $[Cl^-]$ on Zr Extraction

Extraction of Element 105 into Diisobutylcarbinol

K.E. Gregorich, A. Türler, K.R. Czerwinski, B. Kadkhodayan, N.J. Hannink, D.M. Lee, M.J. Nurmia, S.A. Kreek, C.D. Kacher, D.C. Hoffman, H.P. Zimmermann, J.V. Kratz*, M.K. Gober*, M. Schädel†, W. Brüchle†, E. Schimpf†, H. Gäggeler§, D. Jost§, J. Kovacs§, U.W. Scherer§, A. Weber§*

In our studies of the extraction of element 105 (hahnium, Ha) from HCl/HF solutions into the anion exchanger, triisooctyl amine (TIOA)[1], we found a similarity between the behavior of anionic halide complexes of Ha and Pa. In order to investigate this further, we performed a study of their extraction into the secondary alcohol, diisobutylcarbinol (DIBC). DIBC is known to be a very specific extractant for protactinium halide complexes[2]. In contrast to TIOA, which extracts all negatively charged species, DIBC extracts only complexes with a net charge of 1-. As shown in Fig.1, the extraction of Pa is nearly quantitative in conncetrated HBr or HCl, while the extraction of Nb is less complete at high concentrations of HCl or HBr due to the formation of polynegative complexes. This is especially evident in the extractions from strong HCl solutions.

A 99-MeV ^{18}O beam was used to produce 34-s ^{262}Ha by the $^{249}Bk(^{18}O,5n)$ reaction at the LBL 88-Inch Cyclotron. The products of the reaction were transported to the Automated Rapid Chemistry Apparatus (ARCA II)[3] with a He/KCl gas-jet transport system. ARCA II was outfitted with columns consisting of DIBC on an inert support material. An elution curve from a typical set of chemical separation conditions is presented in Fig.2. Here, the activities were loaded onto the DIBC column in concentrated HBr. A Nb fraction was removed with 6M HCl/0.0002M HF, and the remaining activities were stripped from the column with 0.5M HCl. Alpha- and SF-decay of ^{262}Ha and its daughter, ^{258}Lr, were observed in the fractions indicated by the horizontal bar in Fig.2.

In these experiments, Pa was adsorbed on the DIBC column from concentrated HBr with a high yield. The yield for Nb was 85%, and the yield for ^{262}Ha was about 50%. This shows that the tendency to form polynegative anionic bromide species (which are not adsorbed on the column) increases in the sequence: Pa < Nb < Ha.

Footnotes and References

*Institut für Kernchemie, Univ. Mainz, Germany
†Gesellschaft für Schwerionenforschung, Germany
§Paul Scherrer Institut, Villigen, Switzerland

1. J.V. Kratz et al., Radiochim. Acta, 48, 121 (1989)
2. N. Trautmann et al., Radiochim. Acta, 11, 168 (1969)
3. M. Schädel et al., Radiochim. Acta, 48, 171 (1989)

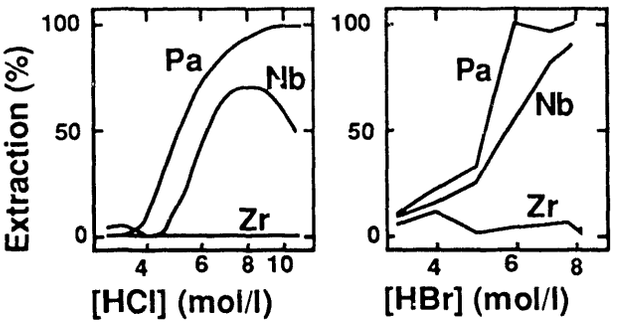

Fig. 1. Extraction of Zr, Nb, and Pa into DIBC from HCl and HBr solutions in batch experiments.

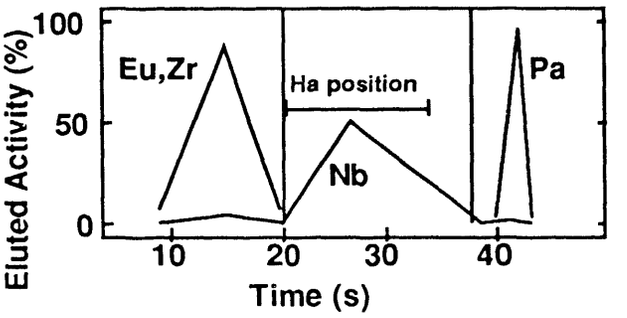

Fig. 1. Separation of Eu, Zr, Nb, and Pa on the DIBC columns in ARCA II. The conditions are the same as for the Ha separations, and the elution position of the ^{262}Ha events is indicated by the horizontal line.

Extraction of Element 105 into Triisooctyl Amine

K.E. Gregorich, A. Türler, K.R. Czerwinski, B. Kadkhodayan, N.J. Hannink, D.M. Lee, M.J. Nurmia, S.A. Kreek, C.D. Kacher, D.C. Hoffman, H.P. Zimmermann, J.V. Kratz*, M.K. Gober*, M. Schädel†, W. Brüchle†, E. Schimpf†, H. Gäggeler§, D. Jost§, J. Kovacs§, U.W. Scherer§, A. Weber§*

In 1988, we performed anion exchange separations of element 105 (hahnium or Ha) between HCl and HCl/HF solutions and Triisooctyl Amine (TIOA)[1]. We used the 34-s ^{262}Ha produced in the ^{249}Bk(^{18}O,5n) reacion at the LBL 88-Inch Cyclotron. The separations were performed with the miniaturized version of the Automated Rapid Chemistry Apparatus (ARCA II)[2]. Using ARCA II, we performed chemical separations every 40 to 60 s, and were able to detect the α- or SF-decay of a few atoms of ^{262}Ha or its ^{258}Lr daughter every hour. ^{262}Ha was shown to be adsorbed on the TIOA column from either 10M HCl or 12M HCl/0.02M HF, like its homologs, Nb, Ta, and Pa. We found that the Ha was removed from the columns along with Nb and Pa in 4M HCl/0.02M HF, rather than with Ta in 6M HNO_3/0.015M HF. To distinguish between Nb-like and Pa-like behavior, we performed elutions with 10M HCl/0.025M HF (Pa fraction) followed by 6M HNO_3/0.015M HF (stripping of Nb). The ^{262}Ha was found to be equally distributed between these two fractions.

In 1990, we extended the study of extraction of Ha into TIOA to lower HCl concentrations. A 99-MeV ^{18}O beam was used to produce 34-s ^{262}Ha by the ^{249}Bk(^{18}O,5n) reaction at the LBL 88-Inch Cyclotron. The products of the reaction were transported to the ARCA II with a He/KCl gas-jet transport system. As in the 1988 experiments, 12M HCl/0.02M HF was used to form negatively charged complexes of Nb, Pa, and Ta and adsorb them on a TIOA column. In nearly 600 individual separations, we found that ^{262}Ha was removed from the column with 0.5M HCl/0.01M HF, indicating that the negatively charged complexes are broken up at this low acid concentration. The elution positions of the hahnium in these experiments can be transformed into percent retained in the organic phase, as shown in Fig. 1. The extraction of Ha follows that for Nb or Pa, whereas, from a simple extrapolation of periodic table trends, one would expect Ha extraction to be similar to that for Ta. This non-tantalum like behavior is indicative of the formation of oxyhalide or hydroxyhalide complexes like $[NbOCl_4]^-$, $[PaOCl_4]^-$, or $[Pa(OH)_2Cl_4]^-$, in contrast to pure halide complexes like $[TaCl_6]^-$.

Footnotes and References

*Institut für Kernchemie, Univ. Mainz, Germany
†Gesellschaft für Schwerionenforschung, Germany
§Paul Scherrer Institut, Villigen, Switzerland

1. J.V. Kratz et al., Radiochim. Acta, 48, 121 (1989)
2. M. Schädel et al., Radiochim. Acta, 48, 171 (1989)

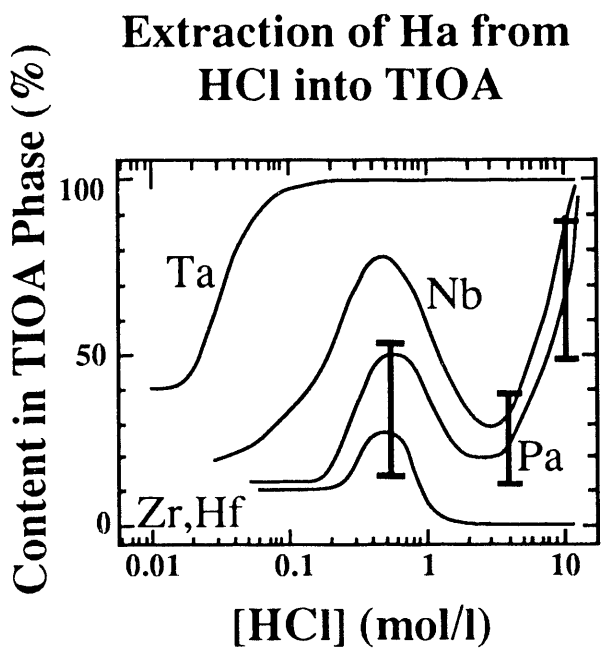

Fig. 1. Fraction of various elements extracted into TIOA vs. HCl concentration. The vertical bars represent the behavior of element 105.

Volatile Halides of Group 4 Elements Hf and Rf

A. Türler, H. Barth#, H.W. Gäggeler, K.R. Czerwinski, K.E. Gregorich, N.J. Hannink, R.A. Henderson, D.C. Hoffman, C.D. Kacher, B. Kadkhodayan, S.A. Kreek, D.M. Lee, J.D. Leyba, M.J. Nurmia,*

The chemistry of the transactinide elements has gained renewed interest from both experimental and theoretical chemists,[1] since relativistic alterations of the electronic structure might modify the chemical properties of these elements compared to their lighter homologs. As early as 1966 researchers from Dubna (USSR) claimed the discovery and the first chemical identification of element 104, based on the high volatility of its chlorides, which has also been observed for its lighter homologs Hf and Zr.[2] They named the new element Kurchatovium (Ku); however, the presented evidence was regarded as not sufficient for the discovery of a new element, because only SF decays were measured. Shortly thereafter, the isotope $^{257}104$ was unambiguously identified at LBL and the name Rutherfordium (Rf) has been proposed.[2] Until now no other than the group in Dubna has attempted volatility studies of element 104 halides.

OLGA II, the On-Line Gas chemistry Apparatus,[3] was used to investigate the volatility of Hf and Rf tetra-bromides and chlorides, by isothermal gas chromatography in empty quartz columns. 41 s ^{162}Hf and 65 s ^{261}Rf were produced in fusion reactions of 120 MeV ^{20}Ne + ^{147}Sm and 94 MeV ^{18}O + ^{248}Cm, respectively, at the 88-Inch Cyclotron. Reaction products, transported by a He/KCl gas jet, were continuously collected on a quartz wool plug inside the quartz column. The bromides and chlorides of Hf and Rf were formed by adding 100 ml/min HBr or HCl gas. Behind the quartz column, the molecules were reattached on new KCl particles, and transported through a capillary to the counting system. In experiments with ^{261}Rf, α-activities were detected with the MG system. Products were collected on thin polypropylene foils (40 μg/cm^2) and subsequently stepped through 6 pairs of PIPS (Passivated Ion implanted Planar Silicon) detectors. The measured α-spectrum is shown in Fig.1. In addition to the activities of ^{261}Rf and its daughter ^{257}Lr, lines due to Po and Fr isotopes are visible, which were produced from lead impurities in the ^{248}Cm target. The activity behind the quartz column was measured as a function of the temperature in the chromatography section. The temperature at the site of the quartz wool plug was kept constant at 900 °C. Fig. 2 depicts the relative chemical yields of Hf and Rf bromides, respectively. ^{162}Hf was identified via its γ-lines and ^{261}Rf by its α-decay and half-life. The volatility of Rf bromides is higher than that of the homologous Hf compounds. Both, Rf and Hf chlorides (not shown), are very volatile.

Footnotes and References

* Paul Scherrer Institut, Villigen, Switzerland

\# Phillips Universität Marburg, Germany

[1]B.L. Zhuikov et al., Radioanal. Nucl. Chem. 143, 103 (1990)

[2]E.K. Hyde et al., Radiochim. Acta 42, 57 (1987)

[3]W. Brüchle et al., J. Less Comm. Metals 122, 425 (1986)

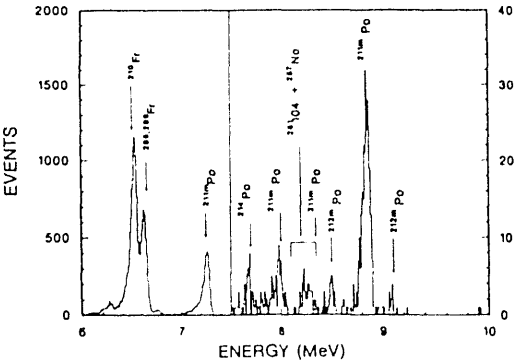

Fig. 1 α-particle spectrum of $RfCl_4$

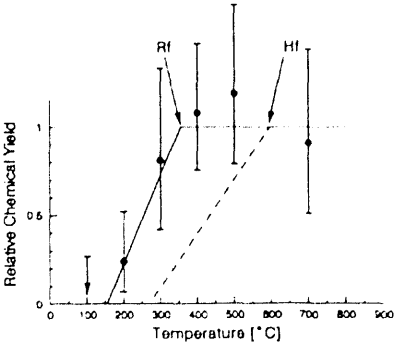

Fig. 2 Relative yields of Hf and Rf bromides as a function of the temperature in the isothermal section.

Gas Chemistry Experiments with Bromides of Nb, Ta and Ha

H.W. Gäggeler, H. Barth#, W. Brüchle♦, K.R. Czerwinski, K.E. Gregorich, M.K. Gober◊, N.J. Hannink, R.A. Henderson, D.C. Hoffman, D.T. Jost*, C.D. Kacher, B. Kadkhodayan, J. Kovacs*, J.V. Kratz◊, S.A. Kreek, D.M. Lee, J.D. Leyba, M.J. Nurmia, M. Schädel♦, U.W. Scherer*, E. Schimpf♦, A. Türler, D. Vermeulen*, A. Weber*, H.P. Zimmermann◊, I. Zvara°*

Recently, there has been considerable interest in the study of the chemistry of the transactinide elements (Z > 103) by both experimental and theoretical chemists.[1,2,3] Relativistic effects may affect the configuration of valence electrons to such an extent that the chemical properties of these elements may no longer be extrapolated from their lighter homologs in the periodic table.

OLGA II, the **O**n-**L**ine **G**as chemistry **A**pparatus[4] (Fig. 1) was used to investigate the volatility of the group 5 penta-bromides $NbBr_5$, $TaBr_5$, and $HaBr_5$, by isothermal gas chromatography in empty quartz columns. 15 s ^{99}Nbg, 35 s ^{166}Ta, and 34 s ^{262}Ha were produced[5] at the reactor SAPHIR at PSI, and in fusion reactions of 143 MeV ^{20}Ne + ^{nat}Eu and 98 MeV ^{18}O + ^{249}Bk, respectively, at the 88-Inch Cyclotron. Reaction products, transported by a He/KCl gas jet, were continously collected on a quartz wool plug inside the quartz column. The bromides of Nb and Ha were formed by adding 100 ml/min HBr gas; Ta bromides were formed only when the HBr gas was saturated with BBr_3 vapor. Behind the quartz column, the molecules were reattached on new KCl particles and transported through a capillary to the counting system. In experiments with ^{262}Ha α and SF-activities were detected in a 2π geometry with a magnetic tape station. Products were collected on the surface of a tape and subsequently stepped through 6 counting chambers equipped with PIPS (**P**assivated **I**on implanted **P**lanar **S**ilicon) detectors. The activity behind the quartz column was measured as a function of the temperature of the chromatography section. The temperature at the site of the quartz wool plug was kept constant at 900 °C. Fig. 2 depicts the relative chemical yields of bromides formed with Nb, Ta, and Ha respectively. ^{99}Nbg and ^{166}Ta were detected via their γ-lines and ^{262}Ha by its SF-decay and its half-life. The volatilities of Nb and Ta bromides are similar. Ha bromide has a significantly lower volatility. Saturating the HBr gas with the stronger brominating agent BBr_3 did not shift the yield curve of Ha.

Footnotes and References

* Paul Scherrer Institut, Villigen, Switzerland
# Phillips Universität Marburg, Germany
♦ GSI, Darmstadt, Germany
◊ Institut für Kernchemie, Univ. Mainz, Germany
° Joint Institue for Nuclear Research, Dubna, USSR

1V.A. Glebov et al., Radiochim. Acta 46, 117 (1989)
2B.L. Zhuikov et al., Radioanal. Nucl. Chem. 143, 103 (1990)
3E. Johnson et al., J. Chem. Phys., in press
4W. Brüchle et al., J. Less Comm. Metals 122, 425 (1986)
5Ya Nai-Qi et al., Radiochim. Acta 47, 1 (1989)

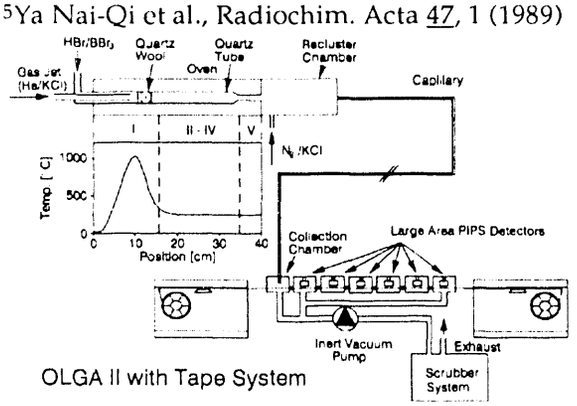

Fig. 1 Schematic of OLGA II with tape system.

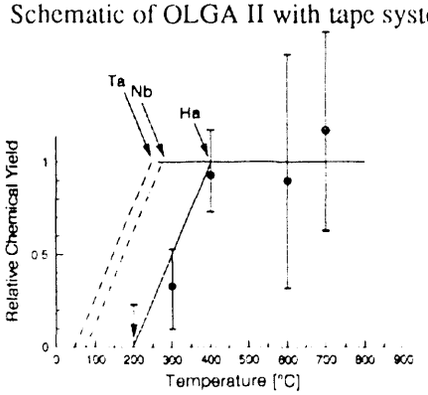

Fig. 2 Relative yields of Nb, Ta and Ha bromides as a function of the temperature in the isothermal section.

An Automatic Injection System for ACCESS

S.A. Kreek, M.J. Nurmia, B. Kadkhodayan, H.L. Hall†, and D.C. Hoffman

Fig. 1 is a schematic of the Automated Injection System (AIS) to be interfaced with our Automated Chemical Chromatographic Element Separation System (ACCESS)[1]. The reaction products from bombardments at the 88-Inch Cyclotron are transported out of our target system by KCl aerosols carried in He. The jet deposits the activity laden aerosols in one of two small depressions drilled into the surface of the Delrin bar (see Fig. 1). After a designated collection time, the Delrin bar is pneumatically positioned so that the aerosol deposit is in line with one of the solvent lines leading to ACCESS. The aerosol deposit is dissolved in the solvent and transported into ACCESS. The Delrin bar is pneumatically secured by two plungers at the bottom so that solvent leakage is avoided. Our rapid chemical separations can now be completely automated.

An advantage of this system is that while chemistry is being performed on one sample another is being collected. This maximizes the use of accelerator time and allows for the collection of as much data as possible during the course of one experiment.

The AIS has been successfully interfaced with ACCESS and experiments will be performed to determine chemical yield through the system.

Footnotes and References

†Lawrence Livermore National Laboratory, Livermore, CA.

1. H.L. Hall et al., LBL Annual Report #25295 (1986-1987).

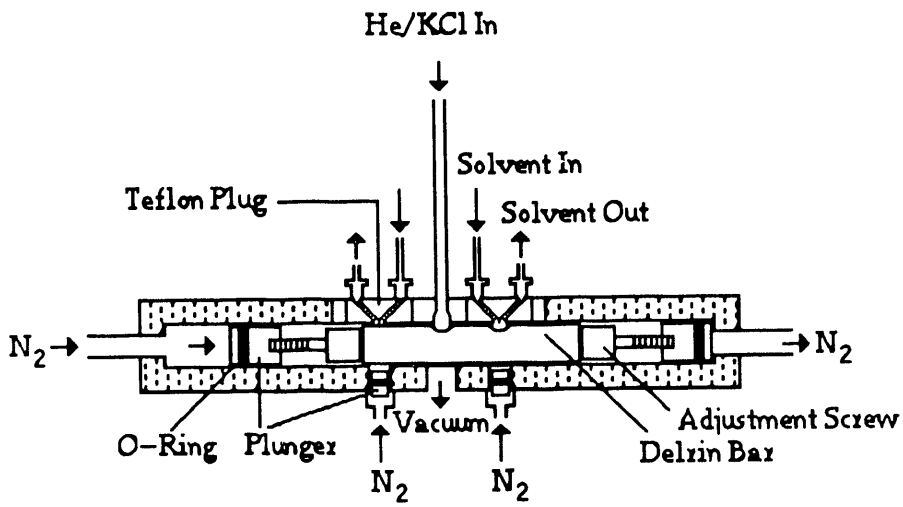

Fig. 1. Schematic of AIS.

Heavy Element Fission Tracker (HEFT)

*A. Türler, D.M. Lee, K.E Gregorich, D.C. Hoffman, M.J. Nurmia, Yuen-Dat Chan, M.M. Fowler**

At present it is impossible to identify the mass and the atomic number of heavy, short-lived nuclides, which decay by spontaneous fission. This creates enormous problems in the heavy element region, where fission sometimes is the only decay mode. These exotic nuclides can be produced with small cross sections in relatively unspecific nucleon transfer or fusion reactions, where large amounts of contaminating fission activities are generated. The HEFT-Detector system aims at the goal of identifying simultaneously the mass, charge and kinetic energy of both fission fragments in order to reconstruct the mass, charge and kinetic energy of the originally fissioning nuclide.

Two modules of the former PAGODA system[1] are setup in a test stand facing each other. These modules consist of a sandwich of four components. A first Multi-Wire Proportional Counter (MWPC) (8 x 16 cm) starts the Time-Of-Flight signal (TOF) and registers the x- and y-coordinate of each fragment with high accuracy. In a drift chamber filled with 2.5 Torr isobutane, the energy loss, dE/dx, of the fragment is measured. A second larger MWPC (16 x 16 cm) records the stop signal and provides a second determination of the x- and y-coordinate of the flight path. A reconstruction of the flight paths of coincident fragments allows the determination of the origin of the decay with very good resolution. The front window of the MWPC consists of a very thin (50 $\mu g/cm^2$) polypropylene foil. The MWPC's are inverted Breskin counters with 200 $\mu g/cm^2$ aluminized mylar foils which operate at 2.5 Torr isobutane. The remaining kinetic energy of the fragments is determined in the adjacent Ion Chamber (IC) kept at 25 Torr of freon (CF_4). At present, an aluminized mylar foil (400 $\mu g/cm^2$) separates the ion chamber from the drift region. First test measurements were performed with a ^{252}Cf source. However, to determine the resolution of the detectors and to determine optimum operation conditions, a calibration of the modules with a variety of beams from the 88-Inch Cyclotron will be performed.

The resolution of the detectors could be substantially increased by reducing the thickness of the various foils. We are currently investigating possibilities for producing large area polypropylene foils as thin as 10 $\mu g/cm^2$

A rotating wheel system, which will collect short-lived fission activities on thin polypropylene foils and subsequently step them between two HEFT modules is currently under construction. The modules will register coincident fission fragments from three of the 80 positions on the wheel. With the ability to determine the exact location of the origin of the decay, a limited half-life analysis will be possible. In a future first experiment we intend to investigate the exact fission properties of the symmetrically fissioning isotope ^{259}Fm.

Footnotes and References

* Los Alamos National Laboratory

[1] M.M. Fowler et al., NIM A281 517, (1989)

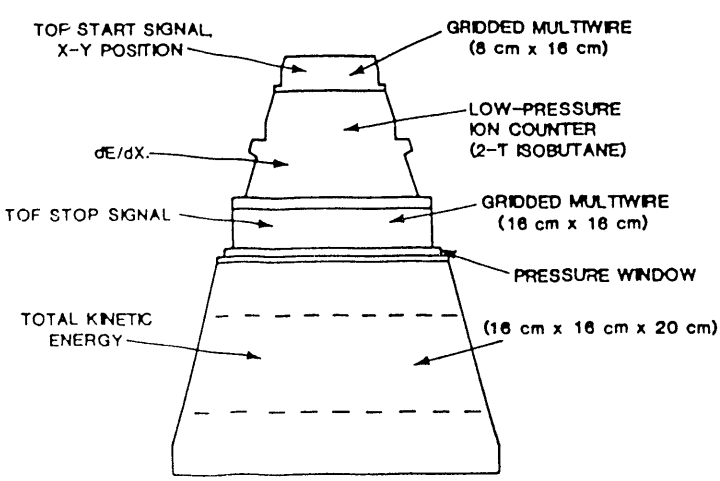

Fig. 1 Schematic of the composite detector system HEFT.

Changes in target fragmentation mechanisms with increasing projectile energy in intermediate energy nuclear collisions

W. Loveland, K. Aleklett,† L. Sihver,† Z. Xu,* C. Casey,* D. J. Morrissey,‡ J. O. Liljenzin,§ M. de Saint-Simon,** and G. T. Seaborg††*

We have measured the target fragment production cross sections and angular distributions for the interaction of 16 MeV/nucleon ^{32}S, 32 MeV/nucleon ^{40}Ar and 44 MeV/nucleon ^{40}Ar with ^{197}Au. We have deduced the fragment isobaric yield distributions and moving frame angular distributions from these data. The fission cross sections decrease with increasing projectile energy and the heavy residue cross sections (which are much larger than previous counter measurements) increase. Heavy residue production is the dominant reaction channel above 35 MeV/A (Fig. 1). There is an unusual change in the fragment isobaric yield distributions in the reactions induced by 32 MeV/N ^{40}Ar and 44 MeV/N ^{40}Ar. We have used the symmetry properties of the moving frame distributions to show the relative time scale of the reaction mechanisms involved. The fission fragments associated with the peripheral collision peak in the folding angle distribution originate in a normal, slow fission process in which statistical equilibrium has been established. At the two lowest projectile energies, the fission fragments associated with the central collision peak in the folding angle distribution originate in part in fast, non-equilibrium processes. At the highest projectile energies, there are no fission fragments associated with high momentum transfer events. The intermediate mass fragments originate primarily in events in which statistical equilibrium has not been established.

Footnotes and References

*Oregon State University
† Studsvik Neutron Research Laboratory
‡Michigan State University
§University of Oslo
**Laboratoire Rene Bernas
††Lawrence Berkeley Laboratory

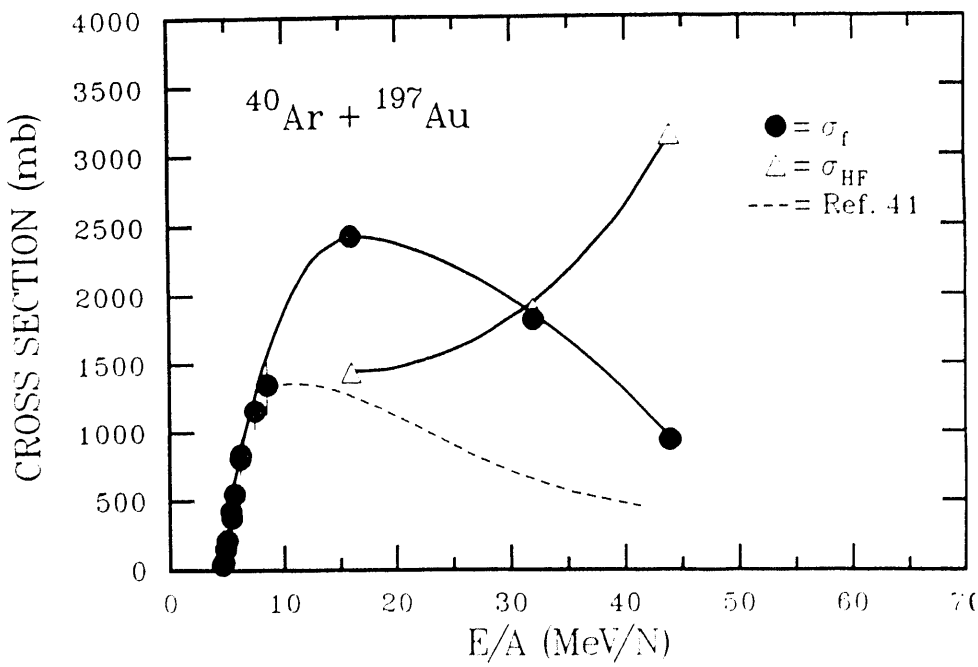

Fig. 1. Excitation functions for fission and heavy residue production for the $^{40}Ar + ^{197}Au$ reaction. The cross sections from the $^{32}S + ^{197}Au$ reaction have been scaled to the $^{40}Ar + ^{197}Au$ reaction by the ratio of the reaction cross sections.

Heavy residue linear momenta in intermediate energy krypton-gold collisions

K. Aleklett, W. Loveland,† M. de Saint-Simon,‡ L. Sihver,* J. O. Liljenzin,§ and G. T. Seaborg,***

ABSTRACT: We have measured the heavy residue energies and velocities for the interaction of 35 and 43 MeV/nucleon krypton with gold. The ratio $v_{||}/v_{cn}$ increases approximately linearly with mass removed from the target for small values of ΔA, agreeing with the kinematics of peripheral reactions (Fig. 1). For large values of ΔA, the maximum momentum transfer in the Kr-induced reactions is substantially less than that expected from the LMT systematics, possibly due to limitations on the maximum excitation energy a composite nucleus can sustain.

Footnotes and References

*Studsvik Neutron Research Laboratory
† Oregon State University
‡Laboratoire Rene Bernas
§Chalmers University of Technology
**Lawrence Berkeley Laboratory

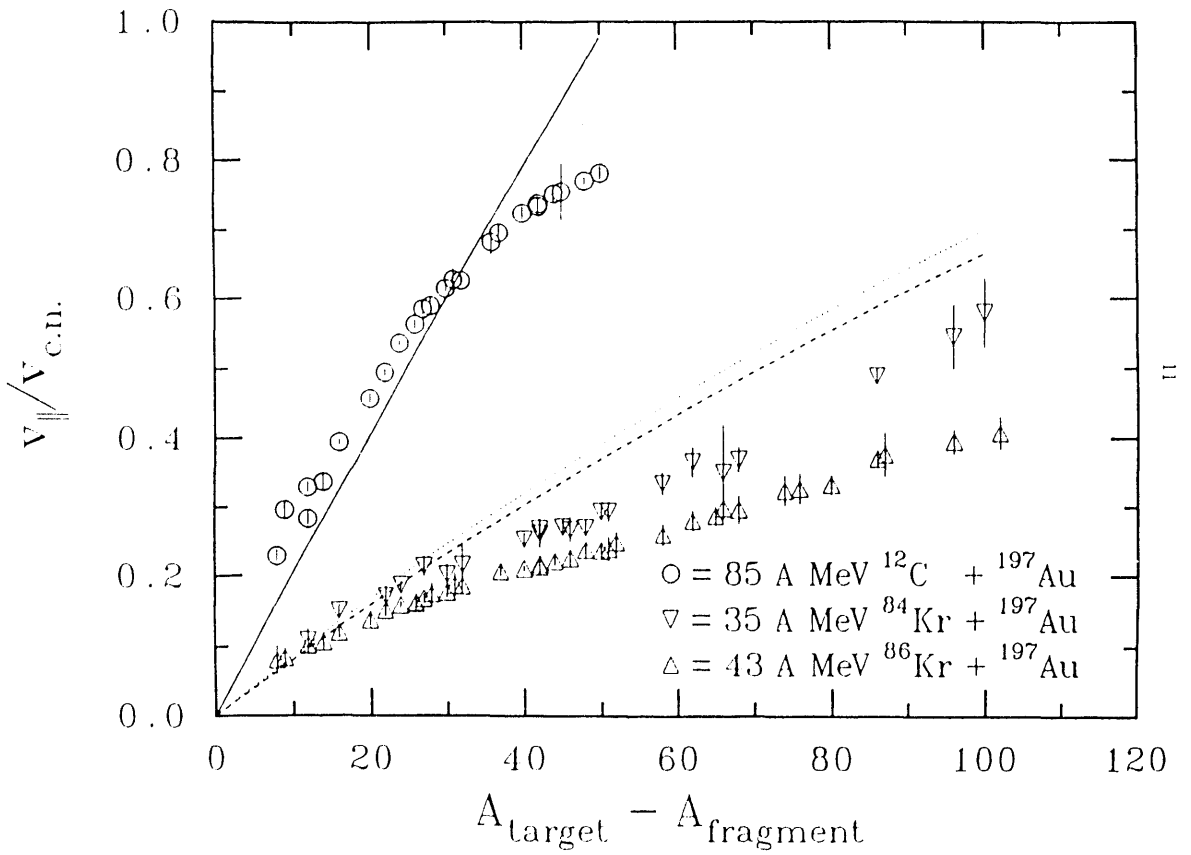

Fig. 1. The variation of $\langle v_{||}/v_{cn} \rangle$ for the heavy residues with mass loss from the target nucleus, ΔA. The lines are the predictions of a simple kinematic model for 85 MeV/N ^{12}C + ^{197}Au (solid line), 35 MeV/N ^{84}Kr + ^{197}Au (dotted line) and 43 MeV/N ^{86}Kr + ^{197}Au (dashed line).

Total projectile kinetic energy scaling in energetic nucleus-nucleus collisions

W. Loveland, Z. Xu,* C. Casey,* K. Aleklett,† J. O. Liljenzin,‡ D. Lee,§ and G. T. Seaborg§*

The target fragment production cross sections have been measured for the reaction of 150 MeV/nucleon ^{139}La with ^{197}Au. From these cross sections, the fragment isobaric yields were deduced. The resulting isobaric yield distribution is very similar to that observed for reactions in which limiting fragmentation is occurring (such as the reaction of 8 GeV ^{20}Ne with ^{197}Au) and unlike that observed with projectiles of similar velocity. This apparent extreme example of total projectile kinetic energy scaling is predicted by the intranuclear cascade model. Total projectile kinetic energy scaling is due to a combination of two effects that approximately cancel one another. For collisions of two different projectiles of the same total kinetic energy with a given target nucleus at a given impact parameter, the collision of the larger projectile with the target nucleus leads to: (a) more projectile nucleons being transferred to the target nucleus (due to the greater overlap volume between projectile and target nuclei) and (b) a lower excitation energy per transferred nucleon (due to the lower energy/nucleon of the larger projectile). Effects (a) and (b) appear to cancel each other.

Footnotes and References

*Oregon State University
† Studsvik Neutron Research Laboratory
‡University of Oslo
§Lawrence Berkeley Laboratory

Heavy-residue spectra in the interaction of 85 A MeV ^{12}C with ^{197}Au

K. Aleklett, M. Johansson,* L. Sihver,* W. Loveland,† H. Groening,† P. L. McGaughey,‡ and G. T. Seaborg‡*

ABSTRACT: We have measured the heavy-residue differential range distributions in the interaction of 85 MeV/nucleon ^{12}C with ^{197}Au. The range distributions were converted to energy spectra using known range-energy relationships. The average residue energies are very low, ranging from 15 keV/nucleon (A = 189) to 314 keV/nucleon (A = 131) (Fig. 1). The implications of these mean energies and spectral shapes for measurements of the heavy residues have been discussed with examples of the dangers inherent in typical low velocity cutoffs in time-of-flight spectrometers. Longitudinal momenta of the heavy residues have been deduced. The essential physics of heavy residue production is given by statistical models. The mean residue energies are apparently described by a simple model due to Bondorf *et al.* while description of the heavy-residue spectral shape is given correctly by a VUU calculation.

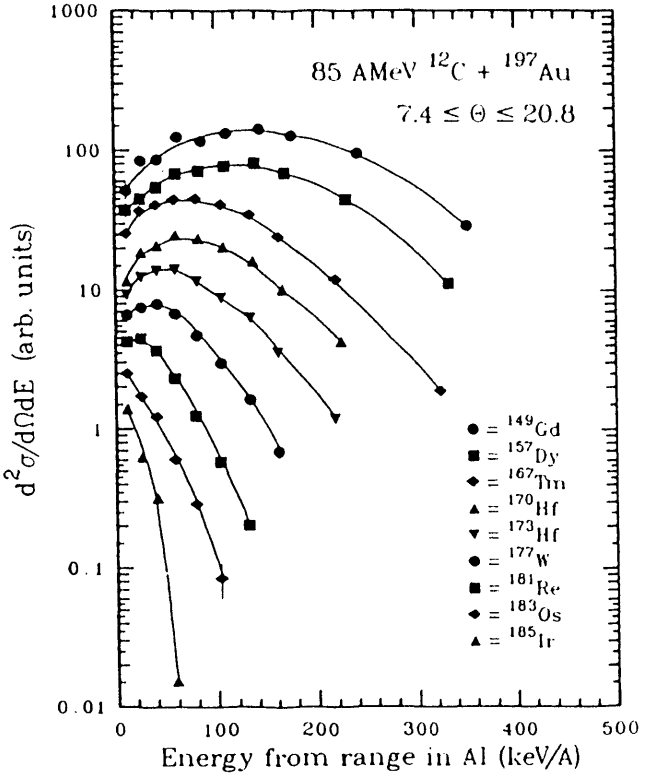

Fig. 1. Heavy-residue energy spectra deduced from the aluminum differential range distributions.

Footnotes and References

*University of Uppsala
† Oregon State University
‡Lawrence Berkeley Laboratory

Non-equilibrium fission and heavy residue production in the interaction of 12–16 MeV/Nucleon ^{32}S with ^{165}Ho

C. Casey, W. Loveland,* Z. Xu,* L. Sihver,† K. Aleklett,† and G. T. Seaborg‡*

The target fragment production cross sections, angular distributions, and range distributions have been measured for the interaction of 12–16 MeV/nucleon ^{32}S with ^{165}Ho. The fragment isobaric yield distribution and the fragment moving frame angular distributions have been deduced from the data. Symmetry properties of the moving frame angular distributions have been used to establish a relative time scale for the reaction mechanism(s). No fission fragment moving frame angular distribution is symmetric about 90°, suggesting that these products are produced, in part, by a fast, non-equilibrium process. The range distributions are used to deduce energy spectra, which suggest that the heavy residues are the result of complete or incomplete fusion and also of an inelastic process such as deep inelastic scattering.

Footnotes and References

*Oregon State University
† Studsvik Neutron Research Laboratory
‡Lawrence Berkeley Laboratory

Non-equilibrium fission processes in intermediate energy nuclear collisions

C. Casey, W. Loveland,* Z. Xu,* K. Aleklett,† L. Sihver,† and G. T. Seaborg‡*

We have measured the target fragment yields, angular and energy distributions for the interaction of 12–16 MeV/A ^{32}S with ^{165}Ho and ^{197}Au and for the interaction of 32 and 44 MeV/A ^{40}Ar with ^{197}Au. The Au fission fragments associated with the peripheral collision peak in the folding angle distribution originate in a normal, "slow" fission process in which statistical equilibrium has been established. At the two lowest projectile energies, the Au fission fragments associated with the central collision peak in the folding angle distribution originate in part from "fast" ($t \sim 10^{-23}$ s), non-equilibrium processes. Most of the Ho fission fragments originate in non-equilibrium processes. The fast, non-equilibrium process giving rise to these fragments has many of the characteristics of "fast fission," but the cross sections associated with these fragments are larger than one would expect from current theories of "fast fission."

Footnotes and References

*Oregon State University

† Studsvik Neutron Research Laboratory

‡Lawrence Berkeley Laboratory

Decay properties and synthesis of the heaviest nuclei

W. Loveland and G. T. Seaborg†*

The measured and predicted radioactive decay properties for nuclei with $93 \leq Z \leq 120$ have been compiled utilizing the best available data and prescriptions. No superheavy "island" is found but rather a "gently sloping peninsula" from the region of known nuclei out to Z ~118 is expected (Fig. 1). Spontaneous fission is the stability limiting mode of decay for the products of most attempts at laboratory synthesis of the heaviest nuclei. Estimates are made for the best approaches to new nuclei by complete fusion with or without radioactive beams and multi nucleon transfer reactions.

Footnotes and References

*Oregon State University

† Lawrence Berkeley Laboratory

Line Shapes and Lifetimes in the ^{135}Nd Superdeformed Band*

*R.M.Diamond, C.W.Beausang, A.O.Macchiavelli,† J.C.Bacelar,‡ J.Burde,§ M.A.Deleplanque, J.E.Draper,** C.Duyar,** R.J.McDonald, and F.S.Stephens*

Following the observation of a superdeformed band in ^{135}Nd (1), we carried out an experiment to confirm the large deformation indicated by the large moment of inertia derived from the transition energies.

The band in ^{135}Nd was populated by the reaction ^{100}Mo(^{40}Ar,5n) at 175MeV. The beam was provided by the 88-Inch Cyclotron and the target was 1.06mg/cm^2 of ^{100}Mo on 11mg/cm^2 Au backing. Twenty Compton-suppressed Ge detectors of the HERA array were used to obtain triple- and higher-coincidence events. The results were sorted into γ–γ matrices for forward and backward detectors. From the centroids of the Doppler-shifted lines and the angles of the detectors, an average v/c for the different transitions was determined. Values ranged from near the initial recoil velocity of 0.0272c at the top of the band to fully stopped for the 546-keV transition at the bottom. A Monte Carlo program was used to simulate the slowing down of the recoiling ^{135}Nd nuclei in the target and gold backing and an associated program calculated the multiple-step-cascade decay for a chosen value of the band transition quadrupole moment, Q_t. By comparing with the experimental centroids a value of Q_t=5.4 b was obtained. This small value was a surprise when compared to that found in ^{132}Ce (2), 8.8 b, since their moments of inertia are very similar.

However, the Monte Carlo method can provide a more stringent test, namely direct comparison of line shapes. The calculation for a single band with Qt=5.4 b did not reproduce the experimental results. The intensity of the transitions increased from top to bottom of the band thus suggesting side feeding at each level. The inclusion of slow side feeding then gave rather good agreement (Fig. 1), with a value of Q_t=7.4 ±0.5 b for the SD band and a side feeding about 4 times slower than the main band.

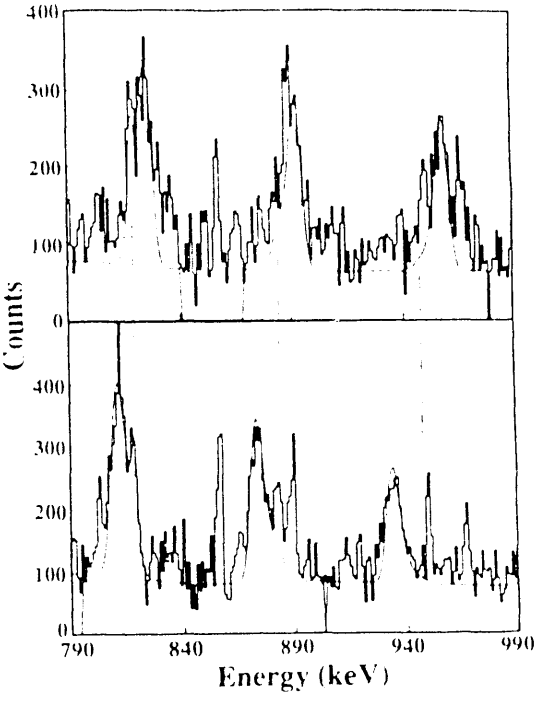

Fig. 1. Line shapes of 818-, 883-, and 946-keV transitions for forward (top) and backward (bottom) detectors; experimental shapes (heavy histogram) and those calculated with Q_t=7.4 b and side feeding cascades whose transition moments decrease from 4.0 to 3.3 b down the band. Dashed lines indicate the position of stopped peaks.

Footnotes and References

*Condensed from Phys. Rev. C41 (1990)R1327.

† Permanent Address: Comision Nacional de Energia Atomica, Buenos Aires , Argentina

‡Permanent Address: KVI, University of Groningen, Groningen, The Netherlands

§Permanent Address: Racah Institute of Physics, The Hebrew University, Jerusalem, Israel.

**Permanent Address: University of California , Davis, Ca 95611.

1. E.M.Beck et al., Phys.Rev.Lett. 58(1987)2182.

2. A.J.Kirwan et al., Phys.Rev.Lett.58(1987)467.

Superdeformation in the Odd-Odd Nucleus ^{150}Tb*

M.A. Deleplanque, C.W. Beausang, J. Burde†, R.M. Diamond, F.S. Stephens, R.J. McDonald, and J.E. Draper‡

A superdeformed (SD) band was found in the nucleus ^{150}Tb following the reaction ^{31}P+^{124}Sn at 160 MeV. This is the first odd-odd nucleus in the mass 150 region where such a band has been found. Since there was no clean gate in this band, the best spectrum (Fig. 1) was obtained by adding triple-coincidence spectra from any combination of two out of the ten strongest SD lines.

The properties of this SD band are not significantly different from those of other nuclei in that region. Using the seven known SD nuclei of that mass region, we subtracted the dynamic moments of inertia $J^{(2)}$ from adjacent nuclei to determine the contribution to the moment of inertia of the last particle and tried to identify it with a particular configuration (orbit). We found that the variations with frequency for a given nucleon number are consistent, at least in trend, for different mass numbers. These trends for the neutron numbers N=85,86 are consistent with the theoretical expectations[1]. For the neutron number N=86, the occupied orbital is predicted to be the second $j_{15/2}$ orbital, whereas for the N=85 neutron number, the first $j_{15/2}$ orbital or a low-j orbital are both consistent with the observed trend. The contribution to the moment of inertia of the Z=66 proton orbital increases with frequency, as the theoretical one does for the fourth $i_{13/2}$ proton orbit and is consistent with that assignment. For the proton orbital Z=65, however, the experimental trend does not follow the simple theoretical one.

Footnotes and References

*Condensed from Phys. Rev. C39, 1651 (1989)

†Racah Institute of Physics, The Hebrew University, 91904 Jerusalem, Israel

‡Physics Department, University of California, Davis, CA 95616

1. S.Aberg et al., Proceedings of the Twenty-Sixth International Winter Meeting on Nuclear Physics, Bormio, Italy, 1988.

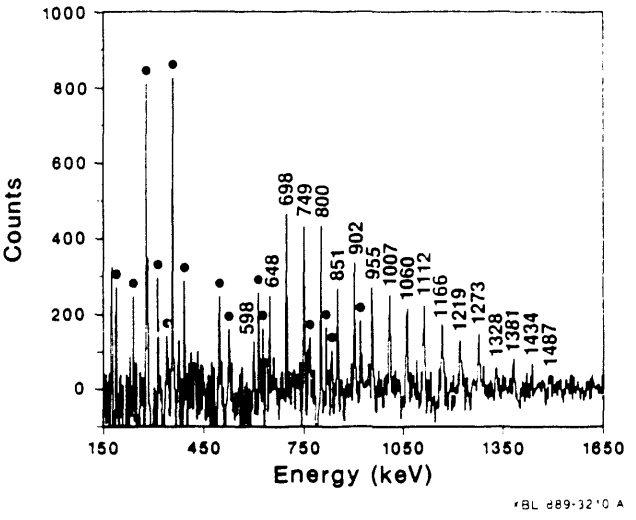

Fig. 1. Triple coincidence spectrum summed for all double-gate combinations of ten SD lines (698-1166 keV) in ^{150}Tb. The full dots indicate known lines of ^{150}Tb in coincidence with the SD band.

Observation of Superdeformation in ^{192}Hg*

J. A. Becker,† N. Roy,† E. A. Henry,† M. A. Deleplanque, C. W. Beausang, R. M. Diamond, J. E. Draper, F. S. Stephens, J. A. Cizewski,‡ and M. J. Brinkman‡

A γ-ray cascade in ^{192}Hg consisting of 17 members has been found found. The cascade is characteristic of superdeformation (SD), with lowest and highest transition energies of 214.6 keV, and 793.4 keV, respectively. The energy spacing (ΔE_γ) between transitions decreases from 43 to 30 keV with increasing transition energy. Fig. 1 illustrates a triple coincidence spectrum of the SD band. Analysis of γ-ray directional correlations shows that these bands are consistent with L=2. The SD band depopulates suddenly, linking transitions between the SD band and yrast transitions in ^{192}Hg were not observed, however transitions of the SD band were observed in prompt time coincidence with yrast transitions. The average spin of the yrast transition populated was $8\hbar$.

The band was populated with ^{176}Yb(^{22}Ne,6n)^{192}Hg at E(^{22}Ne) = 122 MeV. Resulting γ-radiation was detected with an array of 21 Compton suppressed Ge detectors, HERA. The ^{22}Ne reaction populated the band with an intensity estimated at 2% of the ^{192}Hg $2_1^+ \rightarrow 0^+$ transition. The observed cascade energies increase monotonically with increasing E_γ, the band includes low-energy transitions, there is no evidence of irregular behavior at low transition energy, and the nucleus is even-even: these conditions suggest a rotational model analysis will produce a reliable level spin assignment.

Least-squares fits to the expression for $\mathfrak{I}^{(2)}$ expanded in even-powers of $\hbar\omega$ result in a $10\rightarrow 8$ assignment for the 215 keV transition. This assignment is consistent with the average spin of the yrast levels populated in decay of the SD band to class I states. Comparison with rotational model expressions is proposed as a reliable procedure for spin determination of SD bands.

This is the second instance of superdeformation found in this mass region Ye, et al.[1] reported observation of this band simultaneously. Application of the rotational model formulae to extract level spin of SD nuclei was done here for the first time.

Footnotes and References

*Condensed from Phys. Rev. C 41, R9 (1990).

†Lawrence Livermore National Laboratory, Livermore, CA 94550.

‡Rutgers University, New Brunswick, NJ 08903.

1. D. Ye, et al., Phys. Rev. C 41, R13 (1990).

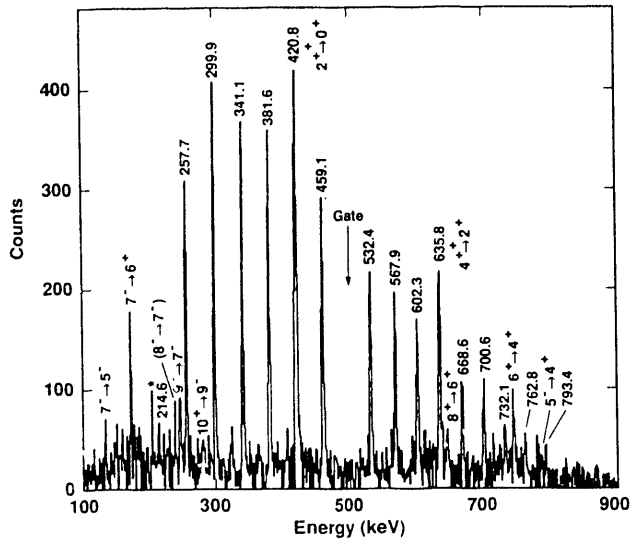

Fig. 1. Spectrum in coincidence with the transition E_γ = 496 keV and the sum of all other band members (except for the 215-and 732-keV members). Members of the SD band are labeled by transition energy. Known ^{192}Hg low-lying transitions are identified by $I_i \rightarrow I_f$, and transitions in ^{193}Hg are labeled by *.

Observation of Superdeformed Bands in ^{194}Hg*

C. W. Beausang,† E. A. Henry,† J. A. Becker,† N. Roy,† S. W. Yates,† M. A. Deleplanque, R. M. Diamond, F. S. Stephens, J. E. Draper, W. H. Kelly, J. Burde, R. J. McDonald, E. Rubel, M. J. Brinkman,‡ J. A. Cizewski,‡ and Y. A. Akovali§

Two superdeformed (SD) bands were observed in the ^{150}Nd(^{48}Ca,4n)^{194}Hg reaction. The ^{48}Ca beam was produced at the LBL 88-Inch Cyclotron, and incident bombarding energies were 195, 200, 205, and 210 MeV. Resulting γ-radiations were detected in HERA, an array of 20 or more Compton suppressed detectors. HERA now includes 40 element bismuth germanate inner ball. The two bands have different intensities. The strong band consists of 18 transitions with Eγ between 254 and 841 keV. The weak band consists of 16 transitions with E_γ between 201 and 742 keV. Transition energies for both bands decrease from ~40 keV to ~30 keV with increasing E_γ, while $\mathfrak{I}^{(2)}$ increases from ~96 to 135$\hbar^{(2)}$/MeV. This behavior is very similar to ^{191}Hg and ^{192}Hg, two other examples of superdeformation near A=194. The assignment of these bands to ^{194}Hg was made on the basis of excitation function results.

The bands exhibit very regular behavior and include low-energy transitions where the fractional change in E_γ is most sensitive to level spin. Reliable spin assignments were determined from comparison to rotational model formulae. We found that the strong-band transition of 254 keV corresponds to $I_i \rightarrow I_f$ = 12→10, while the weak band transition 201 keV corresponds to a 10→8 transition. $\mathfrak{I}^{(2)}$ for SD bands in this mass region are strikingly similar. Fig. 1 illustrates $\mathfrak{I}^{(1)}$ and $\mathfrak{I}^{(2)}$ for ^{191}Hg, ^{192}Hg, and ^{194}Hg. The unexpected similarity in $\mathfrak{I}^{(2)}$ is not presently understood.

Footnotes and References

*Condensed from Z. Phys. A 335, 325 (1990).

§Oak Ridge National Laboratory, Oak Ridge, TN 37831.

†Lawrence Livermore National Laboratory, Livermore, CA 94550.

‡Rutgers University, New Brunswick, NJ 08903.

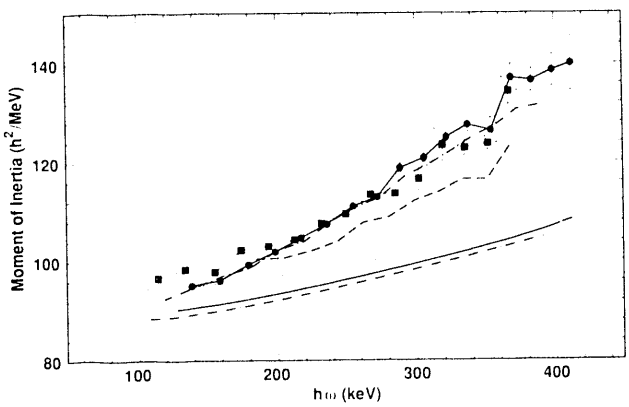

Fig. 1. Kinematic $\mathfrak{I}^{(1)}$ and dynamic $\mathfrak{I}^{(2)}$ moments of inertia for SD bands in Hg isotopes. The $\mathfrak{I}^{(1)}$ values (lower three curves) are represented by smooth identification lines drawn through the data. The lines are solid, dotted, and dot-dashed for ^{194}Hg strong band, ^{194}Hg weak band, and ^{192}Hg, respectively. $\mathfrak{I}^{(2)}$ data for the ^{194}Hg strong and weak bands are indicated by circles and squares, respectively, while $\mathfrak{I}^{(2)}$ values for ^{191}Hg and ^{192}Hg are indicated by the dashed and dot-dashed lines, respectively.

Superdeformed Bands in ^{193}Hg and ^{194}Hg*

E.A. Henry,† M. J. Brinkman,‡ C. W. Beausang, J. A. Becker,† N. J. Roy, † S. W. Yates,† J. A. Cizewski,‡ R. M. Diamond, M. A. Deleplanque, F. S. Stephens, J. E. Draper, W. H. Kelly, R. J. McDonald, J. Burde, A. Kuhnert,† W. Korten, E. Rubel, and Y. A. Akovali§

Three new superdeformed cascades have been observed. Two of these appear to be signature partners, and are assigned to ^{193}Hg. The third band is in ^{194}Hg. The nuclei were populated in the reactions ^{176}Yb(^{22}Ne, xn), at E(^{22}Ne) = 116 MeV, and in ^{150}Nd(^{48}Ca,xn), at E(^{48}Ca) = 195, 200, 205, and 210 MeV. Gamma-radiation was detected in HERA, an array of 21 Compton supressed Ge detectors. The mass assignment of the bands is based on cross-bombardment and excitation function data. There are 12 transitions in the strong band in ^{193}Hg with E_γ increasing from 293.3 keV to 694 keV, while ΔE_γ decreases from ~40 to ~32 keV. Transition energies in the weak band in ^{193}Hg are half-way between the strong band energies, and therefore this weak band is interpreted as a signature partner.

The band reported in ^{194}Hg is the third band in that nucleus. It was first reported by Riley, et al.[1] We find a cascade of 15 γ-rays populated with ~30% of the intensity of the strong ^{194}Hg band. The lowest energy transition connects levels of spin 13 and 11. These three new bands continue the general behavior of SD bands already known in this region: approximately the upper half of the band members show increasing population with decreasing spin until a maximum intensity is reached, and then at the lowest spins the band depopulates within 1-2 transitions, near $10\hbar$. The dynamic moment of inertia, $\Im^{(2)}$, increases from 100 to ~130$\hbar^2$/MeV as $\hbar\omega$ increases from 150 to 350 keV. An interesting feature of the new band in ^{194}Hg is that above $\hbar\omega$ = 180 keV, $E_\gamma[^{194}\text{Hg}(3)] \approx E_\gamma[^{192}\text{Hg}]$.

Footnotes and References

*Condensed from Z. Phys. A 335, 361 (1990).

§Oak Ridge National Laboratory, Oak Ridge, TN 37831.

†Lawrence Livermore National Laboratory, Livermore, CA 94550.

‡Rutgers University, New Brunswick, NJ 08903.

1. M. A. Riley, reported at the Symposium on the Nucleus at High Spin, Copenhagen, Denmark, 1989.

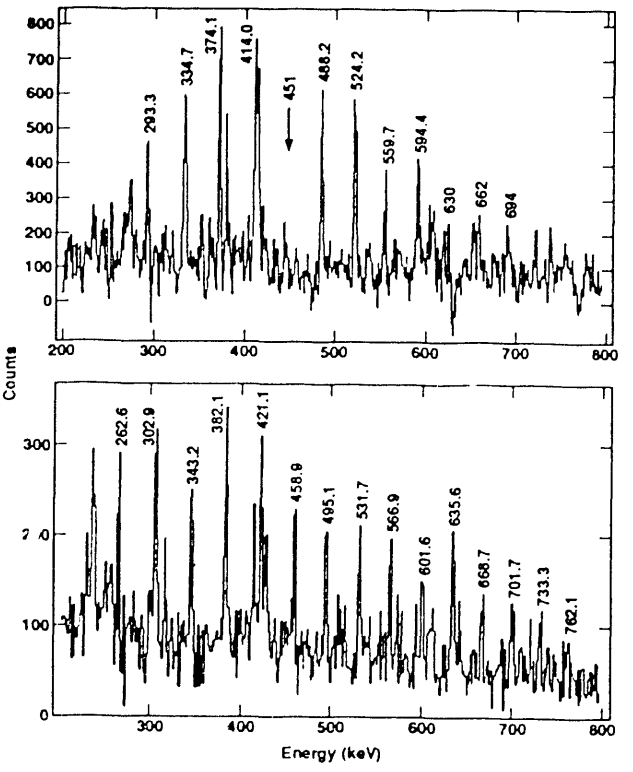

Fig. 1. (a) Spectrum of the strongly populated ^{193}Hg band produced in ^{22}Ne +^{176}Yb obtained by gating two-fold coincidence data by the 451-keV γ-ray. (b) Spectrum of the third ^{194}Hg SD band populated by the ^{48}Ca+^{150}Nd reaction, obtained by gating the three-fold coincidence data with the 263-, 303-, 382, 421-, 459-, 532-, and 567-keV γ-rays in combination with all band γ-rays with energies up to and including the 733-keV γ-ray.

Superdeformation in Lead Nuclei*

M. J. Brinkman†, A. Kuhnert‡, E. A. Henry‡, J. A. Becker‡, S. W. Yates‡, R. M. Diamond, M. A. Deleplanque, F. S. Stephens, W. Korten, W. H. Kelly, J. E. Draper, C. W. Beausang, E. Rubel, J. A. Cizewski†

Two rotational cascades with energy spacings characteristic of superdeformation have been discovered and assigned to the ^{194}Pb and ^{196}Pb nuclei, respectively. The ^{196}Pb band consists of eleven γ-rays, while the ^{194}Pb band is composed of twelve transitions. These were the first reported instances of superdeformation in the A ≈ 190 mass region beyond the mercury nuclides. The ^{194}Pb band was independently codiscovered by a collaboration composed of the HMI and Bonn[1].

These newly discovered bands share the characteristics of other superdeformed bands previously discovered in the A ≈ 190 mass region[2]. Their dynamic moments of inertia smoothly increases by ~ 20% with increasing transition energy. These bands extend to low spin and suddenly depopulate within one to two transitions.

The ^{194}Pb band has two features of special interest: 1) The lowest energy transition is the $8 \rightarrow 6$ transition[2], which is the lowest spin seen to date for superdeformation in this region and 2) The band has transitions identical within ~ 2 keV to the transitions in the superdeformed ^{192}Hg band[3,4]. The fact that superdeformed bands in distinct nuclei have identical energies was first pointed out by Henry and coworkers[5] and has been systematically studied by F. S. Stephens and coworkers[6]. This is, however, the only known instance in this mass region where nuclei with different atomic numbers have identical energies.

Footnotes and References

*Condensed from Z. Phys. A336, 115 (1990).
† Rutgers University, New Brunswick, NJ 08903
‡Lawrence Livermore National Laboratory, Livermore, California 94550.
1. K. Theine et al., Z Phys. A336, 113 (1990)
2. J. A. Becker et al., Nucl. Phys. A520, 187 (1990), and references therein.
3. J. A. Becker et al., Phys. Rev. C 41, R9 (1990)
4. D. Ye et al., Phys. Rev. C 41, R13 (1990).
5. E. A. Henry et al., Z. Phys. A335, 361 (1990).
6. F. S. Stephens et al., Phys. Rev. Lett. 64, 2623 (1990); Phys. Rev. Lett. 65, 301 (1990).

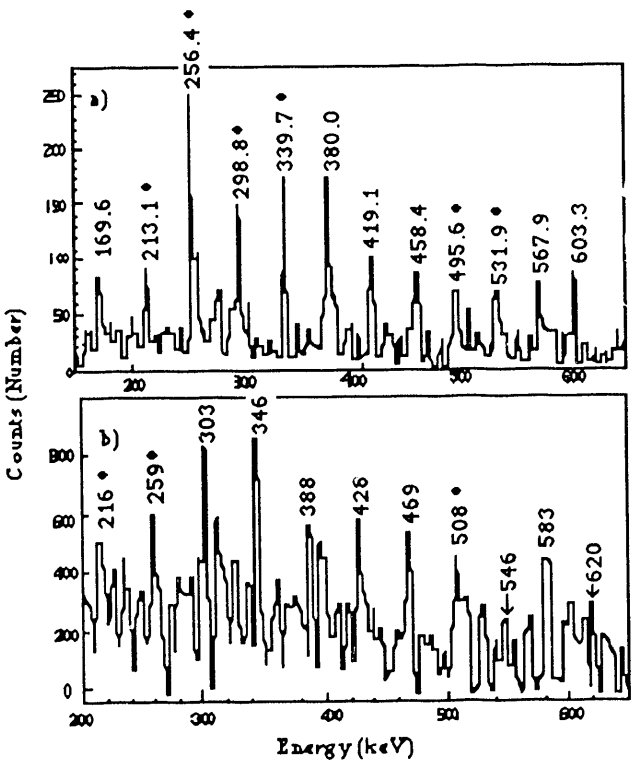

Fig. 1. (a) The ^{194}Pb superdeformed band from all three- and higher-fold events created by gating on all double combinations of the transitions marked by •. (b) The ^{196}Pb superdeformed band created by summing the transitions denoted by • from the $E_\gamma E_\gamma$ matrix.

The systematics of Superdeformation in ^{194,195}Tl*

*F. Azaiez,† W.H. Kelly,+ W. Korten, F.S. Stephens, M.A. Deleplanque, A.O. Macchiavelli, R. M. Diamond, J.E. Draper,‡ E.C. Rubel,‡ C.W. Beausang, § J.A. Becker,** E.A. Henry,** M. J. Brinkman,†† A. Kuhnert,** A. Cizewski,†† T. F. Wang,** S. W. Yates,& J. de Boer,*** and M. Rohn****

Three experiments were carried out at the 88-Inch Cyclotron to attempt to identify superdeformed bands (SD) in the thallium isotopes. The following fusion-evaporation reactions were used :

1. ^{23}Na + ^{176}Yb at 116 and 122 MeV
2. ^{18}O + ^{181}Ta at 95, 100 and 104 MeV
3. ^{15}N+ ^{186}W at 90 and 95 MeV

The gamma rays following the evaporation of 4, 5 and 6 neutrons in these reactions were detected in the 20 Compton-suppressed Ge detectors of the HERA array and the 40 BGO detectors of its central ball. The first reaction revealed the first two SD bands in the thallium isotopes. They have been assigned to the ^{194}Tl nucleus.The second reaction populated the same compound nucleus but with higher angular momentum. Including the two SD bands already mentioned, a total of 10 SD bands were observed in the ^{18}O data. Six of them were observed with different intensities at the three beam energies.Their assignment to ^{194}Tl was based on their intensity variation over the three beam energies. The two SD bands[1] in ^{193}Tl, already reported by the Argonne Group, were identified at the highest beam energy. In both the lowest ^{18}O beam energy and the highest ^{15}N beam energy, two SD bands were observed and assigned to ^{195}Tl. As in the mercury isotopes where a majority of SD bands exhibited identical or equivalent transition energies, all the SD bands in the thallium isotopes have this property. This can be interpreted in terms of constant alignment of a group of SD bands relative to a reference SD band[2]. The alignments, relative to the corresponding band in ^{193}Tl, of all known SD bands in the thallium isotopes are displayed in the figure. All alignments , for frequencies higher than 0.2 MeV, are integral with the value 0 or 1h. The pseudo-spin formalism gives clues to explaining these features, but problems remain. Perhaps some new basic physics is involved, that is, some new symmetries.

Footnotes and References

*Condensed from Phys. Rev. Lett. 66,1030 (1991),, Z. Phys. A336,243 (1990) and Z. Phys. A in Press.

† CEN-BG (Bordeaux-Gradignan) , IN2P3, France
+Iowa State University, Ames, IA 50011
‡University of California, Davis, CA 95616
§University of Liverpool, L69 3BX, United Kingdom
**LLNL, Livermore, CA 94550
††Rutgers University, New Brunswick, NJ 0890
&University of Kentucky, Lexington, KY 40506
***Universitat Munchen, Germany

1. P. B. Fernandez et al., Nucl. Phys. A 517, 386 (1990)
2. F. S. Stephens et al.,Phys. Rev. Lett. 65, 301 (1990)

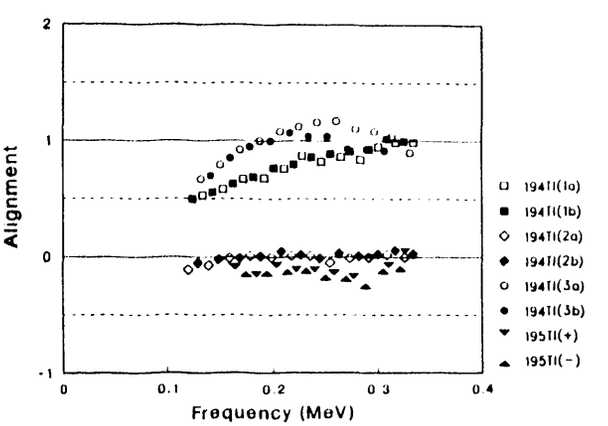

Fig. Alignment of all SD bands in ^{194}Tl and ^{195}Tl relative to the corresponding SD band in ^{193}Tl

Spins in Superdeformed Bands in the Mass 190 Region*

J.E. Draper, F.S. Stephens, M.A. Deleplanque, W. Korten, R.M. Diamond, W.H. Kelly,† F. Azaiez,‡ A.O. Macchiavelli, C.W. Beausang,§ E.C. Rubel,* J.A. Becker,‡‡ N. Roy,‡‡ E.A. Henry,‡‡ M.J.Brinkman,** A. Kuhnert,‡‡ and S.W. Yates****

Such spins are deduced with good accuracy by fitting experimntal values of the moment of inertia $J^{(2)}=4/\Delta E_\gamma$ to an expansion in even powers of the semiclassical frequency $\omega \equiv E_\gamma/2$, as $J(2)=A+B\omega^2+C\omega^4$. For most fits the lowest observed transition spin is ~10ħ, giving a statistical uncertainty $\sigma_I \sim 0.03\hbar$ for $\sigma_\gamma = 0.1$ keV error in E_γ when fitting the six lowest experimental transitions (0.16ħ for 0.4 keV). Figure 1 shows ^{192}Hg, a major reference band[1]. Such spin determinations have been important in our work on nonzero quantized spin alignment[1] in this region.

In this region the plots of $J^{(2)}$ *vs* ω^2 are nearly linear. Of major importance in the spin determinations is the question whether $J^{(2)}$ also has the same shape (A,B,C) for the transitions below those observed, since the spin is obtained from integrating the extrapolated $J^{(2)}=dI/d\omega$ from $\omega=0$ to the lowest observed ω. It is crucial to plot $J^{(2)}$ vs ω^2 as part of the fitting process to evaluate the validity of this extrapolation.

It is shown* how similar numerical results can be obtained from fitting an expansion[2] of spin I in odd powers of ω, while requiring that I increase by 2ħ at each transition. The spin uncertainties (statistical) are essentially the same[3] by both methods, but the important validation of the extrapolation is less clear in the spin-expansion method.

Footnotes and References

*University of California, Davis, CA 95616

†Iowa State University, Ames, IA 5011

‡Centre d'Etudes Nucleaires de Bordeaux-Gradignan, Institut National de Physique Nucleaire et de Physique des Particules, Le haut-vigneau 33170, Gradignan, France.

§ University of Liverpool, Liverpool, L69 3BX, United Kingdom

‡‡ Lawrence Livermore National Laboratory, Livermore, CA 94550

**Rutgers University, New Brunswick, NJ 08903

*** University of Kentucky, Lexington, KY 40506

* Condensed from Phys. Rev. C42, R1791 (1990)

1. F.S. Stephens et al, Phys. Rev. Lett. 65, 301 (1990)

2. J.A. Becker et al, Oak Ridge Conference on Nuclear Structure in the Nineties, April, 1990, and Nucl. Phys. A, to be published.

3. Spin errors for the $J^{(2)}$ method in Ref. * are based on quadrature of two E_γ errors for each $J^{(2)}$; this is shown by Monte Carlo runs to be too conservative for this application., since an error in an E_γ pushes one $J^{(2)}$ up (down) and its partner down (up).

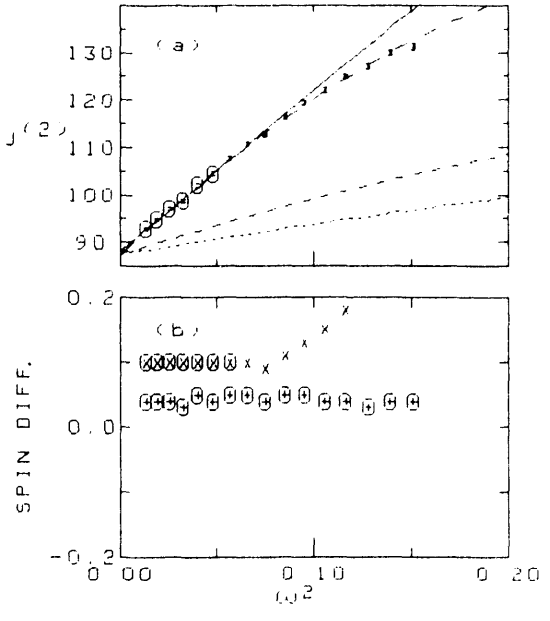

Fig. 1 (a) Solid curve is ^{192}Hg reference band fitted to circled $J^{(2)}$'s, with C=0. Long-dashed curve uses A, B and C fitting to the first 15 $J^{(2)}$'s. (b) Differences between fitted central spins and 9.0ħ, 10.0ħ,... for the two fits to $J^{(2)}$ in (a).

Spin Alignment in Superdeformed Hg Nuclei*

*F. S. Stephens, M. A. Deleplanque, J. E. Draper†, R. M. Diamond, C. W. Beausang‡, W. Korten, W. H. Kelly**, and F. Azaiez††, J. A. Becker#, E. A. Henry#, N. Roy#, M. J. Brinkman***, J. A. Cizewski***, S. W. Yates†††, and A. Kuhnert#*

One of the most remarkable properties so far discovered of rotational bands in superdeformed nuclei is the extremely close coincidence in the energies of the de-exciting gamma-ray transitions (or rotational frequencies) between certain pairs of bands in different nuclei. In the example reported here, the transitions of an excited band in ^{194}Hg are within about one keV of those of the yrast band of ^{192}Hg over a spin range of 20ħ. This is an equivalence of the frequencies to within about 0.1%, which is much smaller than the kind of similarities we could expect, or hope to calculate, using present models of rotating nuclei. This seems so unlikely that, as an isolated case, one might think it is accidental, but the two cases very recently reported in the mass 150 superdeformed region suggest this may be a relatively common feature of superdeformed nuclei. These near degeneracies in the frequencies of different bands suggest there may be some underlying symmetry, which is not well understood.

The similarity of the transition energies in the bands (both odd and even spin members are present and are treated as separate bands here) in ^{194}Hg to the band in ^{192}Hg is illustrated in Fig. 1, where the differences in transition energy between the bands in the two nuclei are plotted against the rotational frequency (1/2 the transition energy). The average agreement of the last 10 transitions in both bands with those of ^{192}Hg is less than 0.5 keV - incredibly small. This region of close similarity occurs after relatively large differences in the lower-frequency region of the bands. Such behavior implies an alignment of spin in the bands of ^{194}Hg relative to ^{192}Hg of 1ħ. This alignment provides a strong clue as to the cause of the similarities.

Footnotes and References

* Condensed from Phys. Rev. Lett. 64, 2623 (1990)

† Permanent address: University of California, Davis, CA 95616

‡ Present address: University of Liverpool, Liverpool, L693BX, United Kingdom

** Permanent address: Iowa State University, Ames, IA 50011

†† Permanent address: Centre d'Etudes Nucleaires de Bordeaux-Gradignan, Institut National de Physique Nucleaire et de Physique des Particules, Le Haut-Vigneau 33170, Gradignan, France

Lawrence Livermore National Laboratory, Livermore, CA 94550

*** Permanent address: Rutgers University, Piscataway, NJ 08903

††† Permanent address: University of Kentucky, Lexington, KY 40506

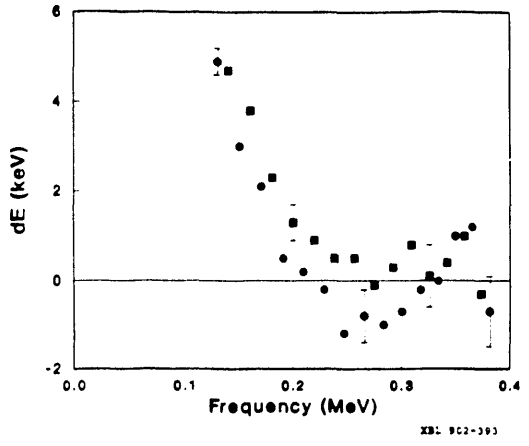

Fig. 1. The difference in the energy of the transitions in the odd-spin band of ^{194}Hg (dots) from those of the band in ^{192}Hg is plotted against the rotational frequency. The squares are the differences of the even-spin band from the midpoints of the ^{192}Hg energies. The error bars indicate experimental uncertainties.

Pseudospin Symmetry and Quantized Alignment in Nuclei*

*F. S. Stephens, M. A. Deleplanque, J. E. Draper†, R. M. Diamond, A. O. Macchiavelli, C. W. Beausang‡, W. Korten, W. H. Kelly**, and F. Azaiez††, J. A. Becker#, E. A. Henry#, S. W. Yates †††, N. Roy#, M. J. Brinkman***, J. A. Cizewski***, and A. Kuhnert#*

Rotational bands in different superdeformed nuclei have been found that have identical (or equivalent) transition energies within one or two keV -- some 10 to 100 times more similar than might have been expected. Since the transition energy (these are E2 transitions with $\Delta I = 2$) is very nearly twice the rotational frequency (dE/dI), this means that the rotational frequencies of the two bands are very similar and also implies equal moments of inertia, apart from (non-collective) angular-momentum alignment with the rotation axis, which does not affect the transition energies.

It appears that for many, but not all, of these superdeformed rotational bands the aligned angular momenta tend to be quantized in units of 1/2 or 1ħ. Nothing except pseudo-spin alignment has been thought of to account for this. Further, it appears that in the mass-190 region the aligned quantum may often be 1ħ, as shown in Fig. 1, rather than the expected 1/2ħ. This suggests that pairs of pseudo-spin-aligned particles might be involved and raises the question of whether these states might be low-lying collective states with alignment one that occur because of the rather good pseudo-spin symmetry (i.e. some kind of triplet pairing state). This is an interesting possibility, but one should remember that, even if true, it does not answer all the questions about these superdeformed bands. We still need to understand why the pseudo-spin symmetry is so good, and why other effects, like deformation changes, orbital alignment changes, pairing changes, and/or size and shape changes, do not affect the energy levels and mask the pseudo-spin effects that seem to be there. We have suggested that this aspect may involve systematic cancelations that occur in the contributions to the moment of inertia for systems having approximate SU(3) symmetry.

Footnotes and References

** Condensed from Phys. Rev. Lett. 645, 301 (1990)

† Permanent address: University of California, Davis, CA 95616

‡ Present address: University of Liverpool, Liverpool, L693BX, United Kingdom

** Permanent address: Iowa State University, Ames, IA 50011

†† Permanent address: Centre d'Etudes Nucleaires de Bordeaux-Gradignan, Institut National de Physique Nucleaire et de Physique des Particules, Le Haut-Vigneau 33170, Gradignan, France

Lawrence Livermore National Laboratory, Livermore, CA 94550

*** Permanent address: Rutgers University, Piscataway, NJ 08903

††† Permanent address: University of Kentucky, Lexington, KY 40506

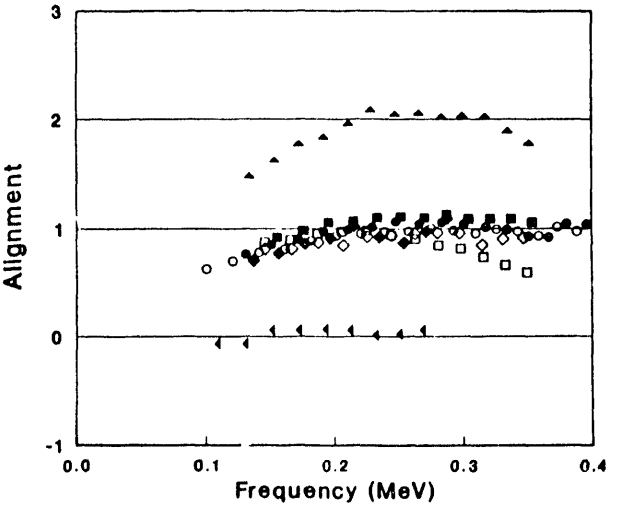

Fig. 1. Aligned angular momentum as a function of rotational frequency for eight bands in the mass-190 region relative to ^{192}Hg.

Level Spin and Moments of Inertia in Superdeformed Nuclei Near A = 194*

J. A. Becker,† N. Roy,† E. A. Henry†, S. W. Yates,† A. Kuhnert,† J. E. Draper, W. Korten, C. W. Beausang, M. A. Deleplanque, R. M. Diamond, F. S. Stephens, W. H. Kelly, F. Azaiez, J. A. Cizewski‡ and M. J. Brinkman‡

Transition energies of the SD cascades near A=194 have a general trend: within a band they vary from ~ 200 to 850 keV, and the difference in transition energy decreases smoothly from ~ 40 to 30 keV with increasing energy. The more intense SD transitions produced in the reaction are consistent with multipolarity L=2. These elongated nuclei are well deformed and are expected to obey the strong coupling scheme, i.e., the single particle angular momenta are coupled to the nuclear symmetry axis, and the energy spectrum is given by $E = \hbar^2/2\Im \cdot (I(I+1) - K^2)$. The Coriolis-interaction matrix elements are small compared to the level splitting of the single-particle energies for different Ω since the splitting of the Nilsson levels increases linearly with β, while the quantity $\hbar^2/2\Im$, which multiplies the Coriolis matrix elements, decreases as β increases.

The expansion for level spin as a function of ω is

$$J = 2\alpha\omega + \frac{4}{3}\beta\omega^3 \qquad (1)$$

(where $\hbar = 1$). In these equations α, β, and γ are expansion parameters with evident inertial interpretations, $J = \sqrt{(I+1)}$ is the intermediate nuclear spin, and $\hbar\omega \approx E_\gamma/2$. The corresponding expansion for $\Im^{(2)}$ is

$$\Im^{(2)} = 2\alpha + 4\beta\omega^2. \qquad (2)$$

For each band, the E_γ were least-squares fit to Eq. 1 assuming all γ-ray transitions to be L = 2. Thus I_f, α, and β are the fitting parameters in Eq.1. where I_f is the baseline spin. Frequency independent alignment (such as might arise for $\Omega = 1/2$ bands) is included in I_f. For strongly coupled nuclei, the nuclear alignment $i \to 0$ as $\hbar\omega \to 0$. Results of one fit are presented in Fig. 1 for ^{194}Hg[2]. The values of I_f deduced from the present data set are (half) integer for 13 of 16 cases within probable experimental error. Since alignment is not quantized, it is unlikely that the cases presented here, which include even-even, odd-A, and odd-odd nuclei, would have the fitting parameter I_f an (half) integer unless the frequency independent alignment = 0. These results suggest that we are determining directly the nuclear spin of the final state observed in the cascade.

Footnotes and References

*Condensed from Nucl. Phys. A 520, 187c (1990).

†Lawrence Livermore National Laboratory, Livermore, CA 94550.

‡Rutgers University, New Brunswick, NJ 08903.

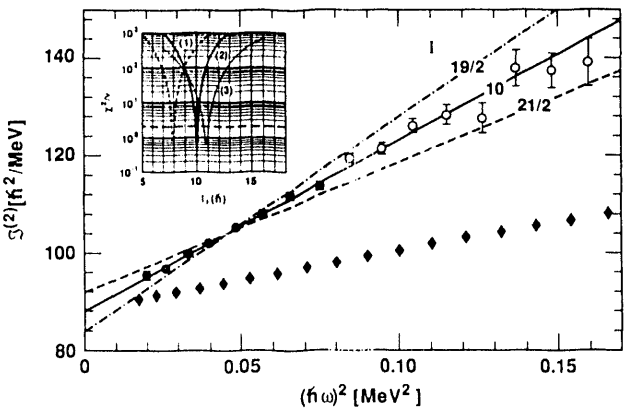

Fig. 1. $\Im^{(2)}$(o) and $\Im^{(1)}$(◊) for ^{194}Hg(2). Data represented by filled circles correspond to the 9 γ-ray transitions used in the least-squares fit. The solid line drawn through the data points represents $\Im^{(2)}$ calculated with Eq. 2. For comparison, the dot-dash and dash lines represent $\Im^{(2)}$ calculated with $I_f(min) \pm 1/2$.

High-Spin Structures in ^{137}Sm

R. Ma[†], E. S. Paul[†], W. F. Piel[†], N. Xu[†], D. B. Fossan[†], S. Shi[‡], J. Burde[§], C. W. Beausang, M. A. Deleplanque, R. M. Diamond, A. O. Macchiavelli, and F. S. Stephens

Collective bands were studied in the neutron-deficient ^{137}Sm by the ^{104}Pd(^{37}Cl,p3n)^{137}Sm reaction at 170 MeV. The study of odd-mass nuclei in this region is interesting because they are apparently "soft", in that occupation of a particular high-j orbital can change their shape and deformation. Multiparticle structures involving one or more $i_{13/2}$ neutrons appear to have an enhanced prolate deformation, and, in fact, the first superdeformed band (but with an axis ratio of only ~1.5) was found in this region.

Four rotational bands were seen in this study. The ground-state and two of the side bands are strongly coupled bands. The $\nu h_{11/2}$ ground band appears to be triaxial, most likely because of the shape-driving effect of the high-Ω, $h_{11/2}$ neutron, and the triaxiality gives rise to a large signature splitting of ~100 keV. A second result of the triaxial shape is the relatively high crossing frequency of $\hbar\omega_c \sim 0.29$ MeV for the crossing with the band containing two aligned low-Ω protons from the $h_{11/2}$ sub-shell. This three-quasiparticle band observed above the crossing has strong M1 transitions and shows a much reduced signature splitting. The latter feature is consistent with a change to near-prolate shape, for which cranked-shell-model calculations indeed predict a small signature splitting. The two aligned $h_{11/2}$ protons are able to overcome the effect of the $h_{11/2}$ neutron and drive the nucleus to a nearly axially symmetric prolate shape.

But the most interesting band is a decoupled one built on an $i_{13/2}$ single-quasineutron state. This band has a large moment-of-inertia indicative of a significantly enhanced quadrupole deformation; this was driven by the occupation of the $\nu i_{13/2}$ [660]1/2$^+$ orbital. Total-routhian surface calculations predict a quadrupole deformation of $\beta \sim 0.35$ for this state, and it probably is related to the several-quasiparticle states observed as superdeformed bands in the neighboring nuclei. But in the latter examples, the connecting transitions into the ground band have not been seen (except for the one case of ^{135}Nd), and it is not obvious why they should decay by so many weak transitions as to miss observation.

Footnotes and References

*Condensed from Phys. Rev. C40, 156(1989)

†State University of New York, Stony Brook, NY 11794

‡Institute of Nuclear Research, Shanghai, China

§The Hebrew University of Jerusalem, Israel

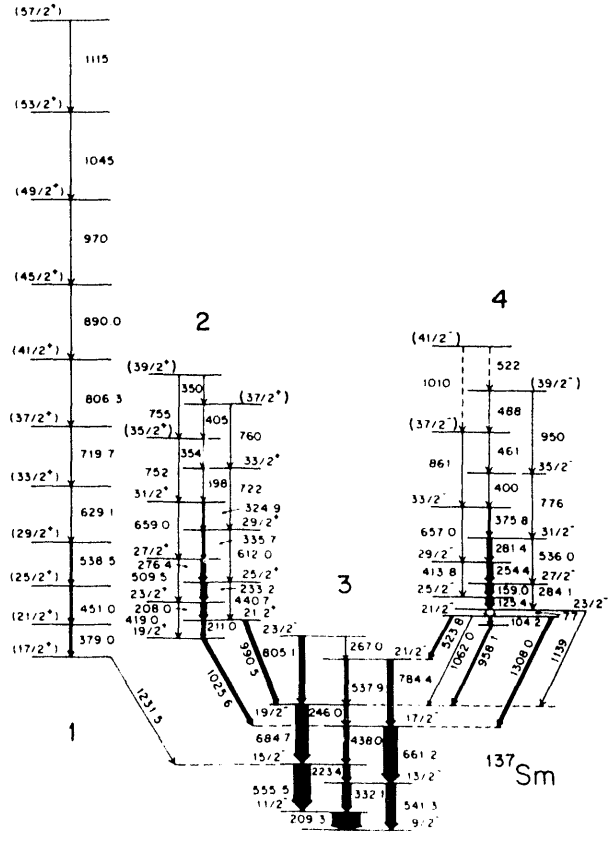

Fig. 1. Level scheme from this work. Transition energies are given in keV. The 9/2$^-$ ground-state assignment is from systematics.

Parallel Proton- and Neutron-core Breaking in ^{154}Er*

C. Schuck†, M.A. Deleplanque, R.M. Diamond, F.S. Stephens and J. Dudek‡

High-spin states of ^{154}Er have been studied using the 21 Compton-suppressed Ge detector array HERA following the ^{118}Sn(^{40}Ar,4n) reaction at 180 MeV. Triple coincidences were widely used in extending the complex level scheme up to 42ħ.

The level scheme evolves from a weakly collective rotational structure at the lower spins to a typical non-collective one including a few characteristic multiplet sequences: $(f_{7/2}^2)6,4,2,0$ and $(h_{11/2}^4)16,14,12,10$. At spin 36, the maximum angular momentum possible from alignment of the valence particles is attained, and at higher spins, the excitations must involve the breaking of the Z=64, N=82 core.

At these higher spins, the most striking feature seems to be the existence of two parallel unconnected paths involving the separate breaking of the neutron and proton cores. The configurations were identified using the cranked deformed Woods-Saxon model.

Footnotes and References

*Condensed from Nucl. Phys. **A496**, 385 (1989)

†C.S.N.S.M., F-91405 Orsay, France

‡Centre de Recherche Nucleaires et Universite Louis Pasteur, F-67037 Strasbourg, France

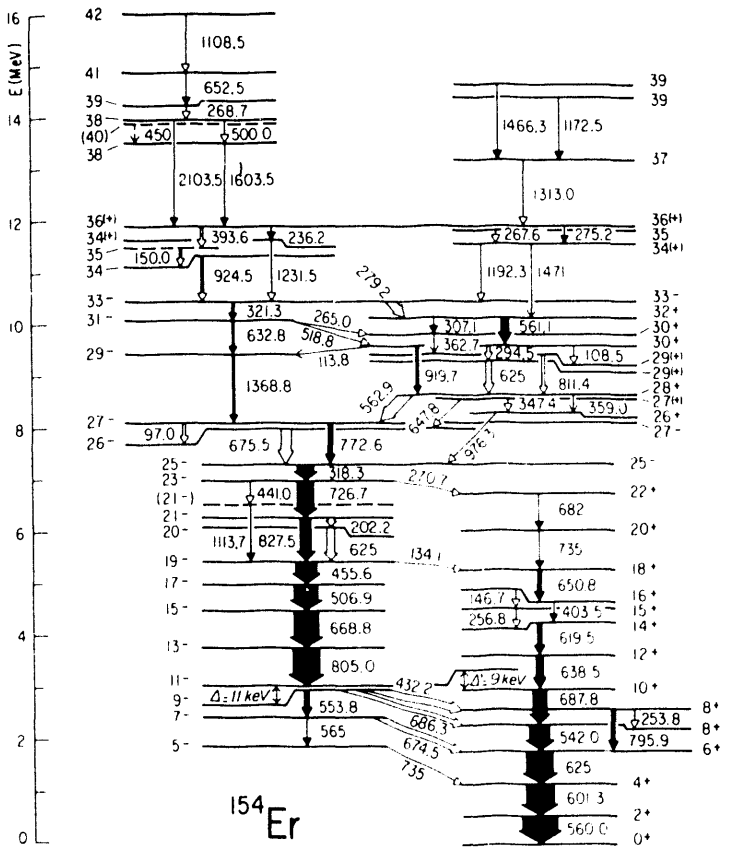

Fig. 1. Level scheme of ^{154}Er. The black arrows correspond to quadrupole transitions and the white arrows to dipole transitions.

Band Structure in ^{180,181}Pt*

M.J.A. de Voigt,† H.J. Riezebos,† R.F. Noorman,† J.C. Bacelar,† R. Kaczarowski,‡ M.A. Deleplanque, R.M. Diamond, F.S. Stephens, J. Sauvage,§ B. Roussiere§

The ^{144}Nd(^{40}Ar,xn)$^{181-x}$Pt reactions have been used to study collective and quasiparticle excitations in ^{180,181}Pt, mainly by gamma spectroscopic methods. The interest in the light Pt isotopes is that they involve both collective and single-particle excitations and show shape changes and co-existence even at low spins and excitation energies. Calculations indicate that different orbitals can favor different deformations, so that the location of these orbitals, as deduced from the present study of ^{181}Pt, can indicate the expected changes in deformation for the bands in ^{180}Pt determined, for example, by lifetime measurements. The backbending systematics in this region is also of interest, as here the rotational frequency at which two $i_{13/2}$ neutrons align is approximately the same at which two $h_{9/2}$ protons align. For this reason it is useful to study neighboring isotopes to observe the effect of blocking.

Before these studies only a few low-spin states were known in either nucleus; now four bands have been observed in ^{181}Pt to spins ranging from 31/2 to 55/2, and eight bands have been seen in ^{180}Pt to spins in the mid twenties.

The four bands in ^{181}Pt are the $1/2^-[521]$ ground-state band, and the $5/2^-[512]$, $7/2^-[514]$, $9/2^+[624]$ Nilsson orbitals. The systematics and the lifetimes, intensities, and multipolarities, where determined, support these assignments. Some anomalous behavior occurs which has not been completely explained. In the $7/2^-[514]$ and $1/2^-[521]$ bands the intensity of the in-band transitions suddenly decrease above spin ~33/2. There likely is a bandcrossing here involving two aligned $i_{13/2}$ neutrons or $h_{9/2}$ protons, but that in itself does not explain the sudden two-fold drop in intensity. In the weak continuation seen above the [514] band, an irregular structure exists which appears to have exceptionally large M1 strengths. These cannot be explained by a simple coupling scheme of two aligned neutrons or protons together with that odd neutron.

The eight bands seen in ^{180}Pt include the ground-state band and a band crossing it at spin 16-18 which, from blocking arguments based on the behavior of bands in ^{181}Pt, involves two aligned $i_{13/2}$ neutrons. The interaction strength between these two bands is determined to be ~34 keV from a two-level mixing calculation; this is equal to that in ^{180}Pt and slightly larger than in the isotone ^{178}Os. Two other bands in ^{180}Pt also show a backbend at about the same frequency. Four members of an excited band starting at 478 keV were found and can be interpreted as a beta-vibrational band, although an alternative description as a somewhat oblately deformed band cannot be excluded. It does fit into the energy systematics of the light Pt isotopes, as do two of the four other side bands. These two are probably negative-parity bands of a two quasiparticle nature, but with an admixture of octupole vibrational character.

Footnotes and References

*Condensed from Nucl. Phys. **A507**, 447 (1990) and **A507**, 472 (1990)

†K.V.I., 9747 AA Groningen, The Netherlands
‡Institute for Nuclear Studies, 05-400 Swierk, Poland
§Institut de Physique Nucleaires, 91406 Orsay, France

Correlated Two-Photon Lines from U+Th,U+U, and Th+Th Collisions*

K. Danzmann [†],W. E. Meyerhof[†], E. C. Montenegro[†] , E. Dillard[†] , H. P. Hulskotter[†] , N. Guardala[†] ,D.W. Spooner[†] , B. Kolinski[‡] , D. Cline[‡] , A. Kavka[‡], C. W. Beausang[§] , J. Burde[§] , M. A. Deleplanque[§] , R. M. Diamond[§] , R. J. McDonald[§] , A. O. Macchiavelli[§] , B. S. Rude[§] , F. S. Stephens[§] , and J. D. Molitoris[**]

Results with the EPOS spectrometer at GSI have revealed correlated equal-energy e^+ e^- lines at 615, 750, and 810 keV sum-energy in U+Th collisions between 5.8 and 5.9 MeV/u, and in U+Ta collisions between 5.9 and 6.4 MeV/u. The Orange spectrometer group has investigated the momentum correlation of coincident e^+ e^- pairs in U+U and U+Pb collisions at 5.9 MeV/u and found evidence for 180° correlation for lines at 810 keV and possibly at 630 keV, but not at 750 keV. It has been hypothesized that these results might be explained by the formation and decay of a new light neutral system which has two or three different states of excitation near 1640, 1772, and 1832 keV. These states might also decay into two or three photons, depending on their spin and parity.

Recently, we have reported[1] the observation of a narrow line (width 3.4 keV) at 1062 keV in the summed-energy, 180°-correlated two-photon spectrum from 5.95 MeV/u U+Th collisions. This could be interpreted as the two-photon decay of yet another state of the hypothesized neutral system moving with the center-of-mass velocity of the collision partners.

We have extended our measurements to the collision system U+U and Th+Th and have considerably improved the statistics for U+Th. We find that the narrow-peak structure at 1062 keV (Fig. 1) in U+Th can be explained by a cascade of Coulomb-excited transitions starting at high spin (32^+) in ^{238}U projectiles. The summed-energy line attains a narrow width because Coulomb excitation of the very-highest-spin states requires nearly head-on collisions which result in much lower average velocities than one would naively expect. Nevertheless, the velocities are high enough to wash out any structure in the singles spectrum. No structure corresponding to the GSI e^+ e^- peaks is visible in our data.

Footnotes and References

*Condensed from Phys. Rev. Lett. **62**, 2353 (1989)

† Stanford University, Stanford CA 94305

‡University of Rochester, Rochester NY 14627

§Lawrence Berkeley Lab, Berkeley CA 94720

**Lawrence Livermorre Lab, Livermore CA 94550

1. K. Danzmann et al., Phys. Rev. Lett. **59**, 1885 (1987)

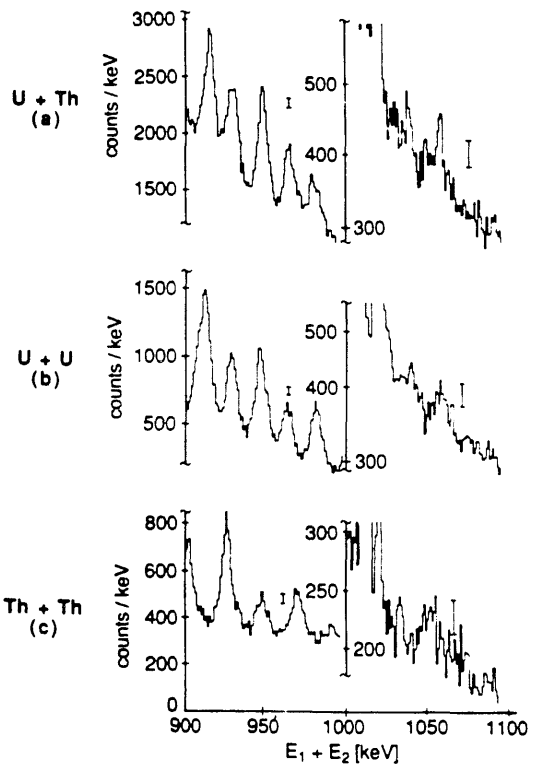

Fig. 1. 180°-correlated summed-energy spectra for the collision systems (a) U+Th, (b) U+U, and (c) Th+Th.

In-Beam Studies of High-Spin States of Actinide Nuclei*

M.A. Stoyer†

High-spin states in the actinides have been studied using Coulomb-excitation, inelastic excitation reactions, and one-neutron transfer reactions. Experimental data are presented for states in ^{232}U, ^{233}U, ^{234}U, ^{235}U, ^{238}Pu and ^{239}Pu from a variety of reactions. Figure 1 presents the Ge γ-ray spectrum observed in coincidence with known ^{238}Pu γ-rays as an example of the data. Energy levels, moments-of-inertia, aligned angular momentum, Routhians, gamma-ray intensities, and cross-sections are presented for most cases. Additional spectroscopic information (magnetic moments, $\frac{M1}{E2}$ mixing ratios, and g-factors) are presented for ^{233}U. One- and two-neutron transfer reaction mechanisms and the possibility of band crossings (backbending) are discussed. A discussion of odd-A band fitting and Cranking calculations is presented to aid in the interpretation of rotational energy levels and alignment. In addition, several theoretical calculations of rotational populations for inelastic excitation and neutron transfer are compared to the data. Figure 2 presents a comparison of the best theoretical calculation of the rotational population patterns in ^{238}Pu from one-neutron transfer with experimental data. Intra-theory comparisons between the Sudden Approximation, Semi- Classical, and Alder-Winther-DeBoer methods are made. In connection with the theory development, the possible signature for the nuclear SQUID effect is discussed.

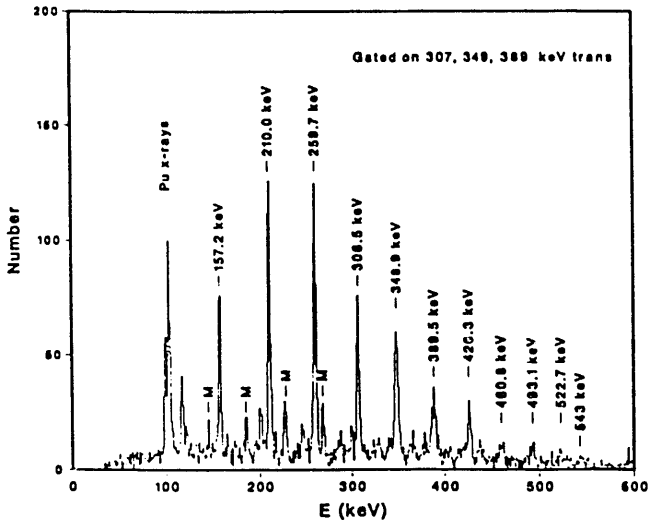

Figure 1: The γ-ray spectrum gated on three known ^{238}Pu transitions, the 307-keV $12^+ \rightarrow 10^+$, 349-keV $14^+ \rightarrow 12^+$ and 389-keV $16^+ \rightarrow 14^+$ transitions, for the one-neutron transfer reaction. The ^{238}Pu transitions are marked with energies. A "mystery" band was observed and is labelled with M's.

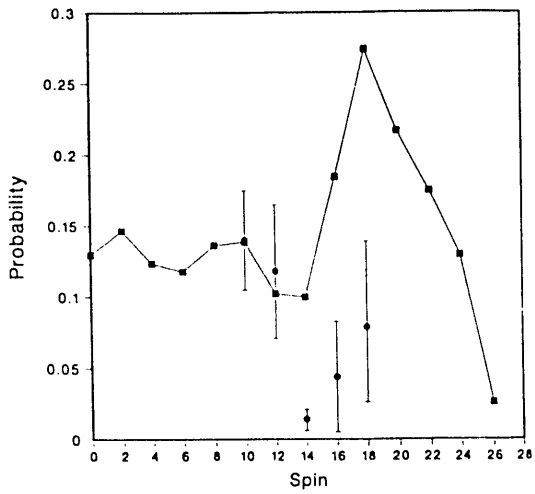

Figure 2: Comparison of rotational population patterns of ^{238}Pu between theory (solid squares–full line) and experimental data (solid circles–error bars) for one-neutron transfer.

Footnotes and References

*Ph.D. Thesis, November, 1990; LBL Report No. 29357.

†Dr. John O. Rasmussen, thesis advisor

Rotational Population Patterns and Searches for the Nuclear SQUID Effect *

L.F. Canto[†], *R. Donangelo*[†], *A.R. Farhan*[‡], *M.W. Guidry*[§], *J.O. Rasmussen and M.A. Stoyer*

This paper presents new theoretical results for rotational population patterns signalling the nuclear SQUID effect [1]. The SQUID effect is an interesting new twist to an old quest to understand Coriolis anti-pairing (CAP) effects in nuclear rotational bands at high spins. Two-neutron transfer reaction cross sections among high-spin states have long been proposed [2] as more specific CAP probes than other nuclear properties provide. Heavy projectiles like Pb generally are recommended to pump the deformed collision partner to as high a spin as possible at the point of closest approach, where the 2n transfer takes place. The interference and sign reversal of 2n transfer amplitudes at high spin, as predicted in the SQUID effect imposes the difficult requirement of Coulomb pumping to near back-bending spins at closest approach. Calculations show this can be attained in barrier-energy collisions of Pb with rare earths.

The hopeful result of our new calculations is that for such systems the departure from sudden approximation is so great that the SQUID alterations of spin population appear not at twice the backbending spin, as in the sudden approximation, but at spins as low as 10, comparable to or below the backbending spins (see Figure). A comparison between a calculation with no SQUID effects (dashed line labelled no A_{sp}) and a calculation containing SQUID effects (solid line labelled A_{sp}) clearly shows a difference in the rotational population pattern around spin 10 for the reaction indicated.

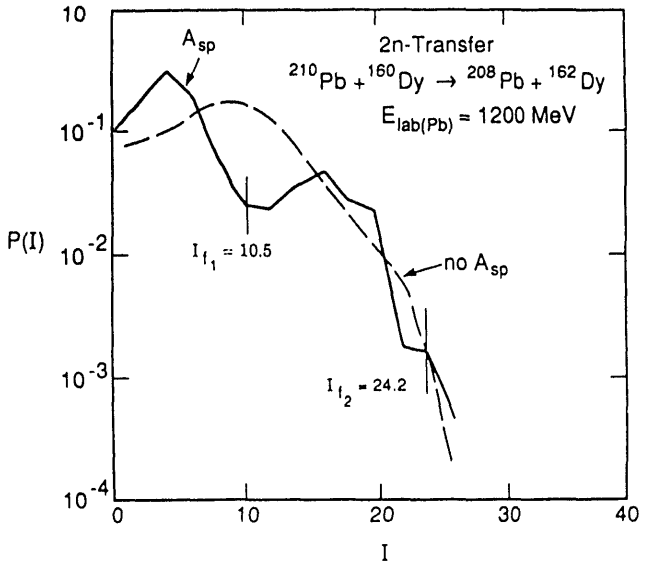

Figure 1: Calculated yrast rotational transfer population patterns for ^{210}Pb on ^{160}Dy at 1200 MeV. The dashed line is a traditional calculation and the solid line is the SQUID effect calculation using SQUID spectroscopic factors. Note the suppression of the population around spin $10\hbar$.

Footnotes and References

*Invited paper presented at the Symposium on Exotic Nuclear Spectroscopy, A.C.S. Meeting, Miami Beach, FL, Sept. 1989; to appear in Proceedings, W. McHarris, ed.; LBL report 27893; also with some enhancements Phys. Lett. **B248** (1990) 295.

[†]Instituto de Fisica, Universidade Federal do Rio de Janeiro, Cx. Postal 68.528, 21945 Rio de Janeiro, RJ, Brazil.

[‡]Physics Department, Kuwait University, Kuwait.

[§]Department of Physics and Astronomy, University of Tennessee, Knoxville, TN 37996.

[1] R.S. Nikam, P. Ring, and L.F. Canto, Zeits. f. Physik **324** (1986) 241; P. Ring, Proc. Workshop on Microscopic Models in Nuclear Structure Physics, Oak Ridge, TN, Oct. 1988, M.W. Guidry, J.H. Hamilton, D.H. Feng, N.R. Johnson, and J.B. McGrory, eds., World Scientific Press, Singapore, 1989.

[2] M.W. Guidry, T.L. Nichols, R.E. Neese, J.O. Rasmussen, L.F. Oliveira, and R. Donangelo, Nucl. Phys. **KAK361** (1981) 274.

Development of Low-Energy Proton Detectors

D. M. Moltz, J. D. Robertson, J.E. Reiff, J. C. Batchelder and Joseph Cerny

For many years delayed proton measurements have been hampered by the inability to directly identify protons whose energies were < 800 keV. Techniques that were used had serious drawbacks when either searching for a very small number of events, for two-proton coincidence measurements or for utilizing reactions which produce large amounts of particle decay background. Since many of our proposed measurements involved searching for very small branches of beta-delayed two-proton decays, ground state proton decays and ground state two-proton decay (as of now, unobserved), it became clear that a detection method was needed which clearly identified low-energy particles on an event-by event basis.

The approach used was the development of gas differential energy (ΔE) detectors in conjunction with standard silicon E detectors. To separate protons from alpha particles and the ubiquitous betas required operating the detectors as proportional counters. Additionally, they needed to operate near very intense cyclotron beams and at temperatures approaching -40 C and have electron collection times not that different from silicon. Of course, the gas had to give a large signal at low pressure (to reduce the proton threshold). The final design incorporated the best possible compromise; this included the use of CF_4 gas at 12 Torr (6 mm thick) ,a 30 μg/cm^2 polypropylene window and a very thin (67-100 μg/cm ^{2}) Ni signal collection foil.

A single telescope version and two six-telescope arrays suitable for use with our fast rotating wheel have been constructed. These detectors are capable of observing and identifying protons with energies down to 250 keV. The energy signal is taken only from the silicon counter; the gas counter is used only for identification. Their exist two major difficulties with the operation of these detectors: 1) although special electronics has been developed for these gas detectors, the system saturates to such an extreme when operated next to intense beams , that the baseline does not return to zero during the beam-off counting cycle, and 2) the large gas signal variance due to ion-electron recombination does not permit the complete separation of betas and low-energy protons.

The latter problem has been solved in a more direct manner. Only about 1% of all betas trigger the gas detector at all. Approximately 1: 10^5 betas give signals which overlap those of the low-energy protons. Our rudimentary solution was to incorporate a second gas detector to create the two-ΔE system shown schematically in Figure 1.

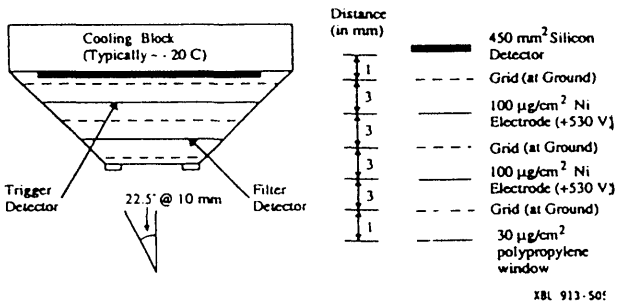

Fig. 1. Schematic diagram of our two-gas triples telescope system.

This triples telescope system has succeeded in reducing the beta contamination another 2 or 3 orders of magnitude as can be seen in Fig. 2.

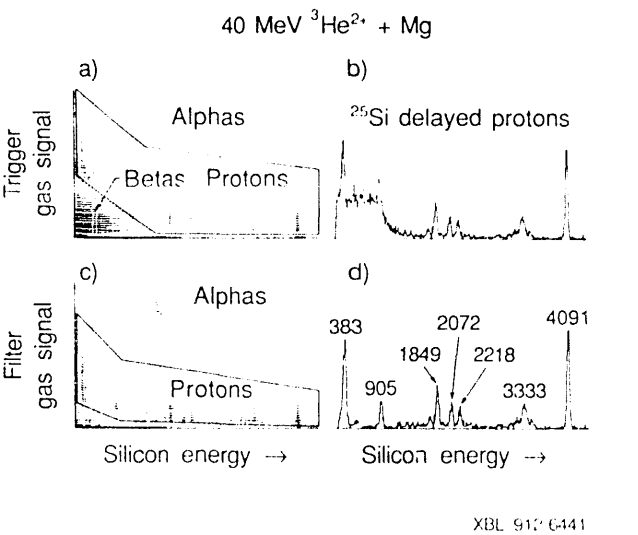

Fig. 2 ^{25}Si delayed-proton spectra-see text.

The Search for Proton Emission from ^{73}Rb, ^{77}Y, ^{64}As, and ^{68}Br

J. C. Batchelder, T. F. Lang, D. M. Moltz, T. J. Ognibene, and Joseph Cerny

In a recent series of experiments we have unsuccessfully searched for what was predicted to be the lightest members of the A=4n+1, Tz=-1/2 series that will proton decay from the ground state (^{65}As and ^{69}Br).[1] The results of these searches have led us to believe that all normally reliable mass predictions are seriously underestimating the nuclear binding energies at the drip line in this region. The next two higher mass members of this series, ^{73}Rb and ^{77}Y, therefore may exhibit observable ground state proton decay. ^{73}Rb and ^{77}Y are predicted by the Kelson-Garvey mass formula to be unstable towards proton decay by 790 and 780 keV respectively.

This search was conducted using our rapidly rotating wheel setup. In this setup, recoils from the target are stopped on Al catcher foils located on a rapidly rotating wheel, which rotates the activity between two arrays of six detectors each. An 180 MeV ^{40}Ca beam was used to bombard a 1.96 mg/cm^2 ^{nat}Ca target to produce ^{73}Rb and ^{77}Y via the ^{40}Ca(^{40}Ca,αp2n) and ^{40}Ca(^{40}Ca,p2n) reactions. The nuclear evaporation code ALICE predicts cross-sections of 45 and 65 μb, respectively.

Bombardments were carried out at wheel speeds of 2500 and 5000 rpm, which would allow us to observe activities down to 100 μs. These bombardments revealed no new proton groups that could be assigned to either of these two isotopes.

We have also searched for the next lightest isotopes of As and Br. If ^{65}As and ^{69}Br only positron decay, then the extra binding energy observed compared with theoretical predictions make ^{64}As and ^{68}Br candidates for proton emission. These are predicted to be unbound to proton emission by ~250 and ~600 keV, respectively. This search was also conducted using our rapidly rotating wheel, and an 180 MeV ^{32}S beam impinging on a 1.96 mg/cm^2 ^{nat}Ca target. Predicted cross-sections by ALICE are 70 and 65 μb, respectively. This search also revealed no new proton groups.

We conclude from all of this data that ^{73}Rb ^{77}Y , ^{64}As and ^{68}Br must either decay predominantly by beta decay, decay by proton emission with half-lives shorter than 100 μs, or have cross-sections much lower than predicted by ALICE.

1. J. D. Robetson, et al. 1989-1990 LBL Annual Report

The Search For ^{65}As and ^{69}Br*

J.D. Robertson, J.E. Reiff, T. F. Lang,D.M. Moltz, and Joseph Cerny

There has been a general interest in nuclei which decay by direct ground state proton emission. The lightest example to date is ^{109}I. We undertook a search for the ground state proton decays of ^{65}As and ^{69}Br, which are the lightest members of the Tz=-1/2, A=4n+1 series that are most likely to be unstable to ground state proton decay. Five of the seven mass models in Table 1 predict that ^{69}Br is unbound to proton decay, and four of seven predict that ^{65}As is proton unstable.

We conducted this search using our rapidly rotating wheel setup, which allows us to observe radioactivities with half-lives ranging from 100 μs (5000 rpm, the fastest wheel speed) to 100 ms (where beta decay will predominate). A 1.75 mg/cm^2 ^{nat}Ca target was bombarded with a 200 MeV ^{32}S beam from the 88 Inch Cyclotron to create ^{65}As and ^{69}Br via the $^{40}Ca(^{32}S,\alpha p2n)$ and $^{40}Ca(^{32}S,p2n)$ reactions. At this energy, the statistical model evaporation code ALICE predicts that the cross-sections will be 150 and 110 μb respectively. Bombardments were carried out at wheel speeds of 5000 rpm and 1250 rpm, with total integrated currents of 3.4 and 4.8 mC, respectively.

These bombardments revealed no new proton groups in any telescope that could be assigned to either ^{65}As or ^{69}Br. For the calibrated efficiency of the overall system, the number of counts that would have been seen given an accurate cross-section and observable half-life can be estimated. This is shown in figure 1 as a dashed peak centered at 350 keV.

We conclude from our search that ^{65}As and ^{69}Br must either decay predominantly by beta decay, decay by proton emission with half-lives shorter than 100 μs, or have cross-sections much lower than predicted by ALICE. Further, since mass predictions indicate that for ^{65}As the maximum proton separation energy is 321 keV, this predicts a minimum half-life of 100μs. This strongly suggests that ^{65}As decays primarily by beta emission. A similar conclusion cannot be drawn for ^{69}Br.

* Condensed from J. D. Robertson, J. E. Reiff, T. F. Lang, D. M. Moltz, and Joseph Cerny, Phys. Rev. C 42, 1922 (1990)

** P. E. Haustein, Atomic Data and Nuclear tables, Vol. 39, July 1988

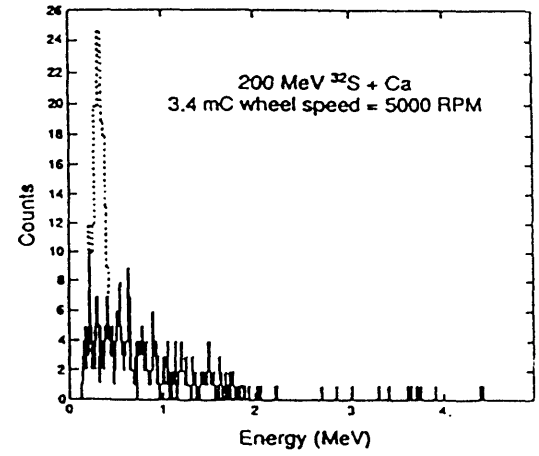

Fig. 1. The single telescope spectrum obtained from the ^{32}S+Ca bombardment at a wheel speed of 5000 rpm. The dashed peak illustrates the minimum requirement for an observable proton peak.

Table 1 **

Nuclide	Experimental	Moller, Nix	Moller *et al.*	Comay, Kelson, Zidon	Tachibana *et al.*	Janecke, Masson	Masson, Janecke	Wapstra, Audi, Hoekstra,
^{113}Cs	−0.967±0.004	−0.971	−0.891	−0.781	−0.871	−0.801	−0.741	−0.961
^{109}I	−0.819±0.005	−1.251	−0.981	−0.571	−0.461	−0.691	−0.611	−0.821
^{69}Br		−0.111	−0.131	−0.531	0.029	−0.661	−0.631	0.009
^{65}As		0.039	0.079	−0.181	−0.011	−0.261	−0.321	0.369
^{61}Ga		−0.001	0.009	0.299	0.449	0.269	0.339	0.644
^{57}Cu		0.738	0.429	0.429	0.889	0.819	0.789	1.289

Identification of the $\pi g_{9/2}$ Band in 67As*

T. F. Lang, D. M. Moltz, J. E. Reiff, J. C. Batchelder, Joseph Cerny, J. D. Robertson and C. W. Beausang

N~Z nuclei in the A=60–80 region show many interesting structural features, including strong ground state deformations, as well as, rapid variation in shape as a function of both spin and particle number. Total potential energy surface calculations with both deformed Woods–Saxon and folded–Yukawa potentials have described these properties in terms of competing gaps in the oblate and prolate Nilsson level sequences. Such calculations, which successfully describe the experimentally established properties of this region, have placed the oblate shell gap at nucleon numbers 35 and 36 and the prolate gap near nucleon number 38. At nucleon numbers between the oblate and prolate minima, competition between the two shapes results in the shape coexistence observed in the light Se and Kr isotopes. The same potential energy calculations which describe the interplay between quadrupole-deformed shapes have indicated that correlations between the octupole-active $1g_{9/2}$ and $2p_{3/2}$ orbitals may stabilize octupole shapes at moderate to high spins in nuclei with N~Z~34.

The 88" Cyclotron accelerated ^{32}S and ^{33}S beams to 95–110 MeV, impinging on a 1 mg/cm^2 natural Ca target evaporated onto a 50 mg/cm^2 Pb foil. ^{67}As was produced via $^{40}Ca(^{32}S,\alpha p)$ and $^{40}Ca(^{33}S,\alpha pn)$ reactions, representing ~2% and ~3% of the total reaction cross section, respectively. A 250 μm, 300 mm^2 Si counter was placed 5 mm behind the target assembly to provide discrimination between protons and alpha particles based on their differential energy losses in Silicon. The target assembly and the Si counter were located inside HERA, a spherical γ-ray detection system consisting of 21 Compton suppressed high-purity Ge detectors surrounding an inner array of 45 bismuth germanate scintillator elements. For these experiments, the 0° Ge detector was replaced by a 80 cm^2 x 10 cm liquid scintillation counter for detection of neutrons.

By gating on the α-region of the charged particle spectrum and the neutron peak in the scintillation counter TAC spectrum, it was possible to enhance coincident γ-rays over those from the dominant 3p and 4p evaporation channels. The ^{67}As level scheme shown in Fig. 1 was established on the basis of γ–γ, α–γ–γ and n–γ–γ coincidences, intensity balance and energy summing relationships.

The proposed structure of ^{67}As appears consistent with the systematics in this region. The energies of ^{67}As positive-parity states correspond to those in ^{67}Ge and to the vibrational ground state band in ^{66}Ge. This suggests that the odd proton in ^{67}As forms the positive-parity band by coupling to the vibrations of the even-even ^{66}Ge core. Thus it appears that the region of deformation seen to extend down to the lightest Se isotopes, disappears in the odd N~Z As isotopes.

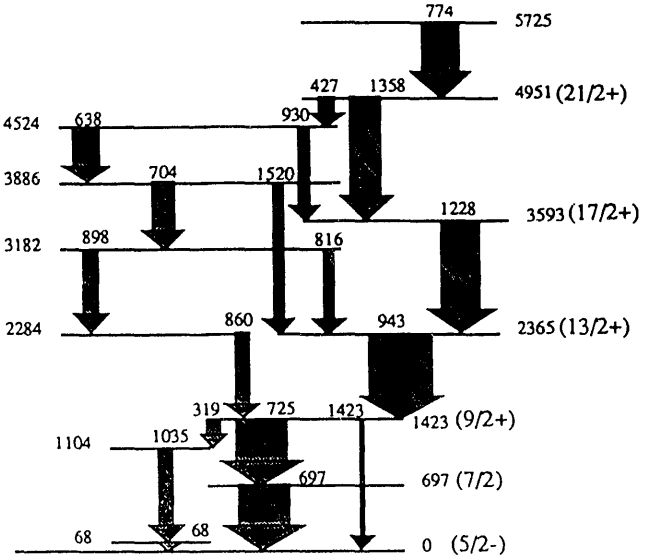

Figure 1. Proposed level scheme for ^{67}As.

* *Condensed from T.F. Lang, et. al., Phys. Rev. C42, 1175, (1990).*

8th Edition of the Table of Isotopes

R.B. Firestone

The 7th edition of the *Table of Isotopes*[1] was published in 1978, and the Isotopes Project published the *Table of Radioactive Isotopes*,[2] which concentrated on radioactive decay data, in 1986. In response to a request from the National Academy of Sciences Panel on Basic Nuclear Data Compilations and the additional encouragement of many nuclear scientists we are beginning preparation of a new edition of the *Table of Isotopes*. This version will emphasize nuclear structure data to a greater extent than previous editions, and it will continue to present radioactive decay data and decay scheme drawings. The principal source of information for the book will be the Evaluated Nuclear Structure Data File (ENSDF) with selective updating from the literature.

Several computer codes have been written to generate the drawings and tabular data for the 8th edition of the *Table of Isotopes*. The computer code ACHILLES prepares the skeleton mass chain decay scheme drawing for each mass chain. ACHILLES scans the mass chain for isotope and isomer half-lives, energies, J^π, decay modes, Q-values, and neutron or proton separation energies. ACHILLES generates a POSTSCRIPT format file for generation of the drawing on a laser printer or on a computer terminal which supports DISPLAY POSTSCRIPT.

The computer code LSTOI produces level scheme drawings in several formats including radioactive decay schemes, rotational band drawings, and level ladder diagrams. The program accepts the ENSDF format input data, and a separate command file controls plot scaling and style options. The output file is written in POSTSCRIPT. LSTOI will be used to generate combined decay scheme drawings for the 8th edition, similar to those in the previous edition, where decays from all parents to a given daughter nucleus are presented together. In addition, the 8th edition will contain conventional rotational band drawings which were not included in previous editions.

A third computer code TOITABLE was written to generate tables of levels and γ-rays for the *Table of Isotopes*. The first table for each nucleus is an energy ordered level table containing the level properties (J^π, half-life, decay branching intensities and moments), and a list of the γ-rays deexciting each level and their properties (branching intensity, multipolarity, and mixing ratio). Following the level table will be additional tables of radiations following the radioactive decays of the ground-state and isomers. TOITABLE creates a UNIX TROFF format file for table preparation which is readily converted by the UNIX PSROFF utility into a POSTSCRIPT file.

The 8th edition of the *Table of Isotopes* will initially become available electronically as a POSTSCRIPT computer file, suitable for printing on many laserprinters. Later, a single-volume of comparable size to the 7th edition will be published. We intend to regularly update the electronic version in the future so that the most current evaluated data is available. A first draft of the new *Table of Isotopes* is now available and will be widely distributed for comment.

Footnotes and References

[1] *Table of Isotopes*, the edition, editors: C.M. Lederer and V.S Shirley, authors: E. Browne, J.M. Dairiki, R.E. Doebler, A.A. Shihab-Eldin, L.J. Jardine, J.K. Tuli, and A.B. Buryn, John Wiley, New York (1978).

[2] *Table of Radioactive Isotopes*, E. Browne and R.B. Firestone, edited by V.S. Shirley, John Wiley, New York (1986).

The IsoSpin Laboratory

J. Michael Nitschke

In 1989 - as part of the Long Range Planning process for Nuclear Science - the author outlined a plan to build a National High Intensity Radioactive Nuclear Beam Facility. This concept was subsequently presented at several workshops and town meetings and incorporated in the Long Range Plan[1] (published in December 1989) which states:.

...It is becoming increasingly apparent that a facility producing beams of radioactive nuclei with extreme neutron to proton ratios is of high scientific interest and technically feasible. It would allow the study of nuclear structure and astrophysical reactions very far from the line of stable nuclei, and could provide new possibilities of reaching the long-sought island of stability of superheavy nuclei...

In October 1989, LBL hosted the First International Conference on Radioactive Nuclear Beams[2] in Berkeley; followed in April 1990 by a Workshop on the Science of Intense Radioactive Nuclear Beams[3] at Los Alamos. The 2nd International Conference on Radioactive Nuclear Beams will be held in Louvain, Belgium in August of 1991. In June 1990, a National Steering Committee was formed with members from BNL, LBL, TRIUMF, LANL, ANL, ORNL, MSU, Louisiana State, and Notre Dame to promote the planning for such a facility. In addition, an International Advisory Committee, an International Group of Technical Experts, and a Technical Advisory Panel were established. It was decided to name the new facility IsoSpin Laboratory (ISL). An ISL USER group was formed that presently has ~200 members. Several Experimental Working Groups that give scientific and technical support to the Steering Committee have been established. By the end of 1991, the Committee is planning to produce a White Paper that will contain the basic scientific justification for ISL and the accelerator and beam specifications. The White Paper will also outline the technical feasibility of the ISL in the form of a Bench Mark Facility based on "known" technologies. The main purpose of the White Paper is to invite the major laboratories in North America to submit a proposal to the Steering Committee, to NSAC, and to DOE that outlines how they would realize the ISL at their institution, given the specifications in the White Paper. The wide support that the project has received in the nuclear physics community makes it likely that several laboratories will attempt to attract this new initiative to their site.

As there are five projectile fragmentation facilities in operation that produce *high-energy* radioactive beams, the ISOL/Post-acceleration concept was chosen for the ISL. In this method, an intense high energy beam of light ions (p, ^{2}H, or ^{3}He) impinges on a thick target, kept at an elevated temperature, forming radioactive isotopes that diffuse out into an ion source. Subsequently, these radioactive ions are purified and post-accelerated to energies sufficient for experiments in nuclear and astrophysics.

References

1. Nuclei, Nucleons, Quarks, Nuclear Science in the 1990's, A Long Range Plan by the DOE/NSF Nuclear Science Advisory Committee, December 1989, U.S. DoE and NSF.

2. *Proceedings of the First International Conference on Radioactive Nuclear Beams*, October 16 18, 1989, Berkeley, California, W. D. Myers, J.M. Nitschke, and E.B. Norman, Eds. (World Scientific, Singapore, 1990).

3. *Proceedings of the Workshop on the Science of Intense Radioactive Beams*, Los Alamos National Laboratory, April 10 12, 1990, Los Alamos, New Mexico, LA-11964-C and UC-413.

Expected Beam Intensities for the IsoSpin Laboratory

J. Michael Nitschke

One of the most important characteristics of the IsoSpin Laboratory (ISL) is the expected distribution of radioactive beams intensities. Presently, cross sections calculations for spallation, fragmentation, fission, and peripheral reactions are carried out, and theoretical production yields have been obtained by multiplying these cross sections with the expected ISL luminosity of 4×10^{38} $cm^{-2}s^{-1}$. A comparison shows that there can be discrepancies of several orders of magnitude between calculated yields and yields measured at on-line isotope separators, depending mainly on the element, the target matrix, the target temperature, the half-life of the radioactive isotope, and the ionization efficiency. The first three factors affect, specifically, diffusion and surface desorption rates.

In an attempt to obtain some initial realistic estimates of the radioactive beams obtainable in a future ISL facility the *experimentally* observed beam intensities at the ISOLDE facility[1] at CERN were scaled up linearly to a planned primary proton beam intensity of 100 μA (at 600 MeV). It was assumed that the radioactive beams would be analyzed in an isotope/isobar separator and post-accelerated to energies of up to ~10 MeV/u in a "conventional" heavy ion linac similar to ATLAS at ANL. Transmission and stripping losses were taken into account and the expected intensities of *the most abundant isotopes* for each element are shown in the figure below. Further from stability lower beam intensities are anticipated. It should be emphasised that in many cases the production yields for specific elements have not been optimized. New target matrixes will have to be developed for the ISL. A comparison with calculated yields shows that for many isotopes increases of several orders of magnitude can be expected. Within an isotopic chain of a given element, isotopes with different isospins and half-lives may require different targets to optimize their production via spallation, fission, fragmentation, or peripheral reactions. Future developments in ion source technology, in particular ECR sources, will also significantly affect the yields of several elements.

Reference

1. ISOLDE Users Guide, H.-J. Kluge (ed.), CERN 86-05, 18 July, 1986 and later references.

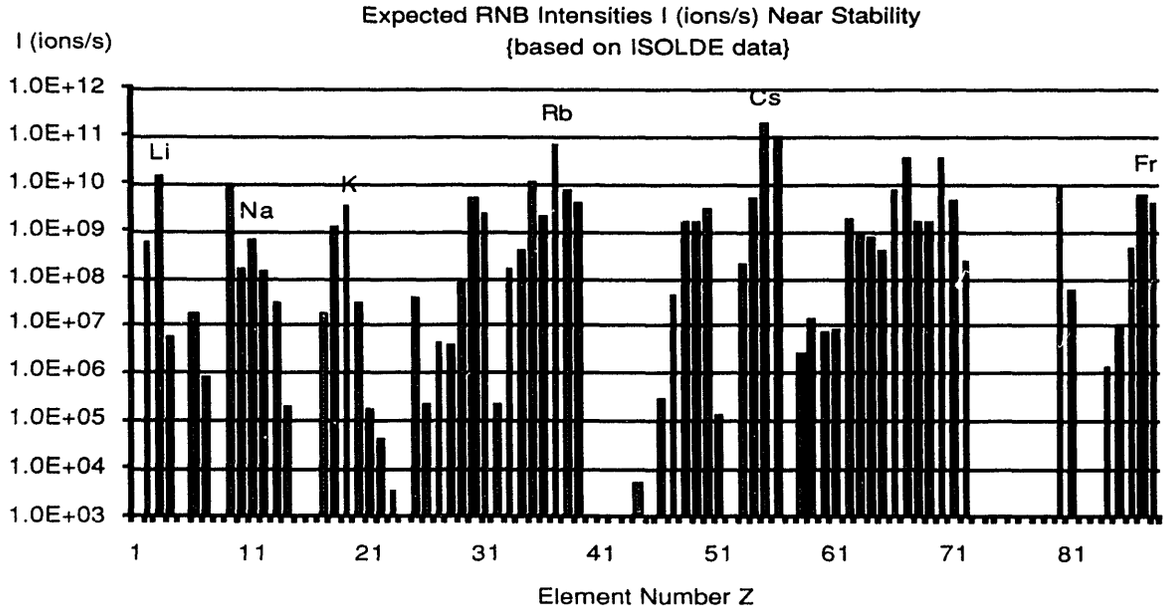

Mass and Beta-Strength Measurements on Proton-Rich Nuclei

J. M. Nitschke, P.A. Wilmarth, and R.B. Firestone

The measurement of masses of nuclei far from stability is of fundamental importance for many branches of nuclear physics—theoretical and experimental. While masses refer to nuclear ground states, β-strength functions (S_β) probe the squares of the overlap integrals between two sets of nuclear wave functions—one set, in general, characterizing a nucleus in an excited state. Far from stability, the excitation energies can exceed 10 MeV with correspondingly large level densities. Our previous investigations of β-delayed proton decay[1], which is strongly dependent on S_β, and new developments in the calculation of these functions[2] have enticed us to build a Total Absorption Spectrometer (TAS).

It consists of a large NaI(Tl) well detector and allows the measurement both of decay energies and S_β. The decay energy measurements are based on the end points of γ-ray spectra, and are valid for nuclei that have significant β strength near their Q value. S_β is deduced from the unfolding of the total absorption γ-ray spectra. Another, independent, measurement of the decay energy is obtained from the end point of the β spectrum measured in coincidence with a total γ-ray energy deposited in the NaI crystal equal to the annihilation energy of an e^+-e^- pair. This selects β transitions to the daughter ground state (g.s.) only, and also yields the g.s. to g.s. β transition probability that is, in general, difficult to determine by other techniques. In this method, there is no EC and no coincident x ray and, hence, no Z selectivity; therefore, several β spectra may be superimposed.

TAS is coupled via a fast tape system to the on-line isotope separator OASIS at the SuperHILAC, where neutron deficient nuclei can be produced in heavy ion reactions. The spectrometer is gain stabilized, by a computer, with reference to a light pulser, which, in turn, is stabilized with reference to the 2.50 MeV sum line of ^{60}Co. An important feature of TAS is an integral, cryogenically cooled, x-ray detector inside the 4π NaI(Tl) crystal which measures the K x rays following electron capture (EC). Together with the mass information from the isotope separator, this uniquely identifies A and Z of the β^+-decaying nuclei and allows the determination of the EC-decay intensity distribution from which S_β is calculated. In addition, a particle telescope can be added to the detector array in the well to study β-delayed and g.s. α and β emission in coincidence with the total γ-ray energy release, electrons, and x-rays. In general several isobars can be measured simultaneously and separated off-line by gating on characteristic x-ray lines.

Another feature of TAS is a small "plug" detector that is used to measure the γ-ray singles deexcitation spectra as a function of excitation energy which help avoid ambiguities in the unfolding of the sum spectra due to unknown γ-ray multiplicities.

The response matrix of TAS to monoenergetic γ-rays has been calculated up to 6 MeV for 120 energies with a Monte Carlo program (c.f. separate contribution). Using this response matrix, excellent agreement between calculated and measured spectra of several calibration sources has been obtained, off-line.

The first on-line runs were carried out with ^{28}Si beams on $^{92\text{-}100}$Mo targets producing proton-rich nuclei of Ba, Cs, and Xe as discussed in a separate contribution.

References

1. J.M. Nitschke, P.A. Wilmarth, J. Gilat, P. Möller, and K.S. Toth, *Proc. Fifth Intl. Conf. Nuclei Far from Stability, Rosseau Lake, Ontario, Canada,* 1987, ed. I.S. Townes (AIP Conf. Proc., New York, 1988), p. 697.
2. P. Möller and J. Randrup, Nucl. Phys. **A514,** 1 (1990).

Total Absorption Spectrometer: Response Function and Unfolding

P.A. Wilmarth, K.S. Vierinen, and J.M. Nitschke*

The Total Absorption Spectrometer (TAS) at the on-line isotope separator OASIS was designed to extract β-strength functions and decay energies from the sum energies of γ rays emitted following β decay. This would be trivial if TAS had an ideal response function (RF), i.e. if a γ ray always deposited its full energy in the detector. Unfortunately, it is impossible to build such a detector. The actual RF of TAS must, therefore, be empirically determined and used to "unfold" the *true* sum spectrum from the *measured* sum spectrum.

The traditional approach to RF determinations is to use mono-energetic γ-ray sources that cover the energy range of interest. Since there is no set of sources that can adequately span the energy range up to 10 MeV, we have simulated the TAS RF using the EGS4 Monte Carlo simulation software.[1] The NaI(Tl) well and plug detectors, Ge x-ray detector, detector housings, etc. were represented by 54 simple geometric shapes and the RF of the detector to mono-energetic γ rays was calculated.

The quality of the simulation was tested for ^{88}Y decay and compared to the measured spectrum (Fig. 1). There is excellent agreement

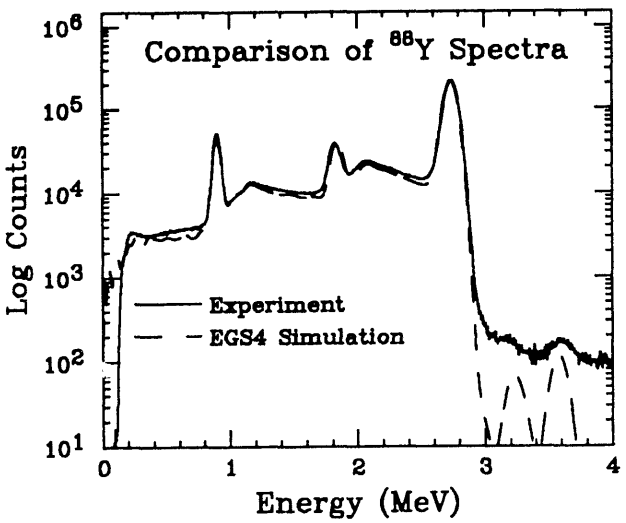

Fig. 1. Comparison between the calculated response and the measured TAS spectrum for ^{88}Y.

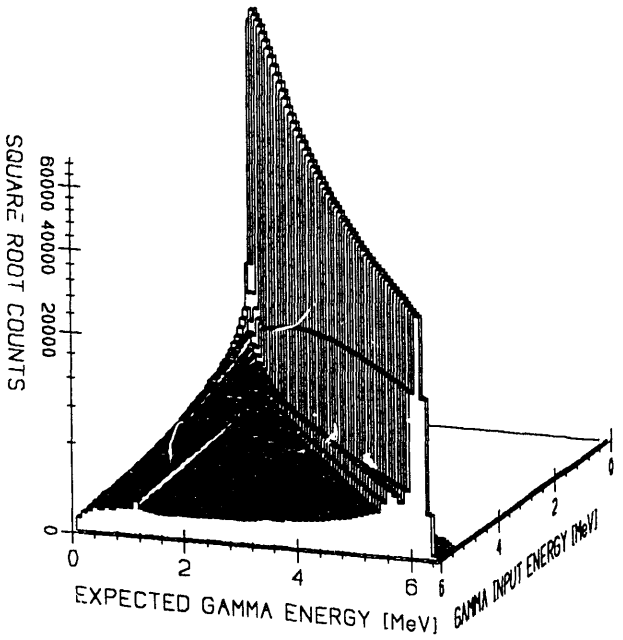

Fig. 2. Calculated response matrix of TAS to mono-energetic γ rays from 0.05 to 6.0 MeV.

and calculations of the TAS response to mono-energetic γ rays from 0.05 to 6.0 MeV, in steps of 0.05 MeV, have been completed and are shown in Fig. 2. Even though TAS is 4-10 times larger than detectors employed in past total absorption measurements, significant, multiplicity-dependant corrections must be applied to the measured γ-ray sum spectra. For example, the photopeak efficiency (PE) for a single 4-MeV γ ray is 57% in contrast to a PE of only 37% for a cascade of four 1-MeV γ rays (even though a 1-MeV γ ray has a 78% PE). We are developing unfolding techniques using the calculated RF to extract the known β-strengths of standard sources. These techniques can then be used to deduce β-strength functions and decay energies in nuclei far from stability.

Footnotes and References

*Present address: University of Helsinki, SF-00170 Helsinki, Finland.

[1] W.R. Nelson, H. Hirayama, and D.O. Rogers, "The EGS4 Code System", SLAC Report No. 265 (1985).

Total Absorption Spectrometer: First On-Line Results

J.M. Nitschke, P.A. Wilmarth, and R.B. Firestone

The two main objectives of the Total Absorption Spectrometer (TAS) are the determination of β-strength functions and the measurement of decay energies. In a first experiment with TAS, coupled to the on-line isotope separator OASIS, a series of neutron deficient Ba, Cs, and Xe isotopes was produced using a beam of ^{28}Si from the SuperHILAC on targets of ^{92,95,96,98,100}Mo. Only a very small subset of the results will be presented here. The mass-separated samples from OASIS were collected on a fast cycling tape and transported within 0.5 s into the center of the well in TAS. There, the following decay parameters were recorded: the total γ–ray decay energy E_{total} in the well plus the plug, the x-ray energy, the electron energy and energy loss, and time spectra between all detectors. In the case of EC decays, the x ray information together with the mass selection in the separator resulted in an unambiguous isotope identification. In some cases [i.e. ^{122}Cs(8-,1+), cf. fig 1(b)] it was possible to separate the isomer from the ground state, based on half-life differences (4.4 min versus 21 s, respectively), by choosing the appropriate tape cycle period.

Decay energies were determined from positron spectra recorded in coincidence with E_{total} under the condition that E_{total} =1022 keV, as shown for ^{122}Cs in fig. 1(a).

Total absorption γ-ray spectra were measured in the mass range 116≤A≤124. An example is shown for the ^{122}Cs isomers in fig. 1(b). The spectra are, in general, characterized by narrow structures which correspond to discrete states at energies below ~2 MeV, and broader resonances up to the Q-value (~7.0 MeV for ^{122}Cs). The end-points correspond to the Q_{EC}-values. Selecting different gates in the coincident x ray spectra allows a clean separation of the total absorption spectra for different elements. A preliminary calculation of the associated approximate β-strength functions (S_β) is obtained by dividing the measured E_{total} spectra by the Fermi function for EC decay [cf. fig. 1(c)], assuming an ideal detector response. More realistic unfolding techniques that make use of the information from the plug detector and the calculated response matrix are under development (cf. separate contribution to this report). It is evident from fig. 1(c) that the majority of the β-strength is observed above the region previously known from β/γ studies. In the case of ^{122}Cs, and several other isotopes, the published β feedings and log *ft* values will have to be corrected. Comparisons with calculated β-strength functions are in progress.

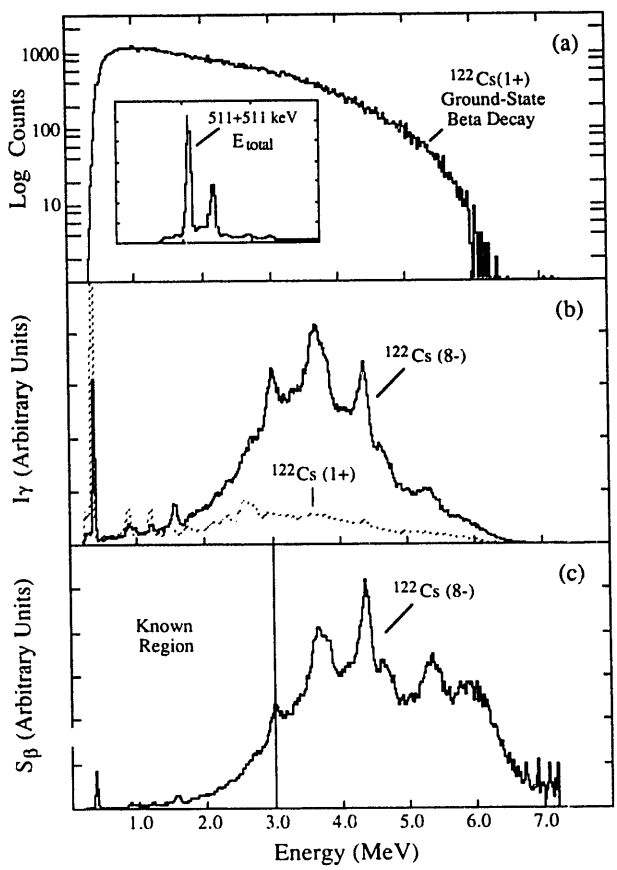

Fig.1. Results of ^{122}Cs decay: positron spectrum (a), E_{total} spectrum (b), and β-strength (c).

Single-Particle States near the Proton Drip Line

K. S. Toth, D. C. Sousa,† J. M. Nitschke, K. S. Vierinen,‡ and P. A. Wilmarth*

With the use of the OASIS separator facility on-line at the Lawrence Berkeley Laboratory SuperHILAC, we have investigated the decay properties of numerous short-lived neutron-deficient rare earth nuclei with $65 \leq Z \leq 71$. Part of the overall investigation has dealt with the study of low-lying states in isotopes near the 82-neutron shell. These levels are relatively pure single-particle states; as such, their properties can be compared with predictions of various shell-model calculations. Earlier we presented[1] systematics of protons in odd-Z, N = 82 nuclei and of neutron states in even-Z, N = 81 nuclei, together with results of spherical Hartree-Fock-Bogoliubov calculations. We have now extended this structure information to nuclei with higher atomic and lower neutron numbers.

In Fig. 1, we show systematics for the $s_{1/2}$, $d_{3/2}$, and $h_{11/2}$ neutron-hole states in Sm, Gd, Dy, and Er nuclei with N = 77, 79, and 81. (Excitation energies for the $d_{3/2}$ levels in ^{145}Dy and ^{147}Er and the $h_{11/2}$ level in ^{145}Dy were determined in our investigation of the ^{145}Ho and ^{147}Tm β−decay schemes.) The dramatic minimum for the $h_{11/2}$ level energy at N = 79 may signal a change in deformation near this neutron number. We should also add that the HFB calculations[1] do not reproduce the excitation energies of the $h_{11/2}$ level for N = 81 nuclei. This energy, which is 242 keV in ^{131}Sn, increases to a value of 754 keV in ^{139}Ce, and then remains the same in isotopes with higher Z values. The calculations, on the other hand, predict a steady drop in excitation energy as Z increases after the maximum is reached in ^{139}Ce.

We have also obtained information concerning the $s_{1/2}$, $d_{3/2}$, $d_{5/2}$, $g_{7/2}$, and $h_{11/2}$ proton states in ^{145}Tb, ^{147}Ho, ^{151}Tm, ^{151}Ho, and ^{153}Tm. These new results show that the single-proton level energies continue to follow the established trend,[1] i.e., as the atomic number increases the gap between the $d_{5/2}$ and $d_{3/2}$ orbitals increases while the one separating the $d_{3/2}$ and $s_{1/2}$ orbitals decreases. Also, while the $s_{1/2}$ level is the ground state in Tb nuclei, the $h_{11/2}$ level, which is isomeric for $Z \leq 65$, becomes the ground state in Ho and Tm isotopes.

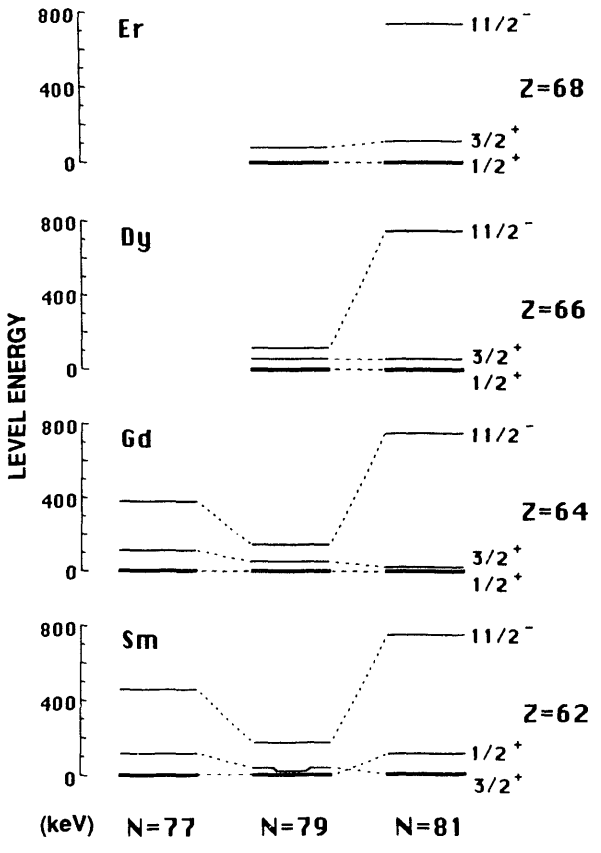

Fig. 1. Neutron-hole states in nuclei with N = 77, 79, and 81.

Footnotes and References

*Oak Ridge National Laboratory, Oak Ridge, TN 37831.

†Eastern Kentucky University, Richmond, KY 40475.

‡Present address: University of Helsinki, SF-00170 Helsinki, Finland.

[1] K.S. Toth *et al.*, Phys. Rev. C **32**, 342 (1985).

Decay Studies of Neutron Deficient Nuclei near the Z = 64 Subshell: ^{142}Dy, ^{140,142}Tb, ^{140,142}Gd, ^{140,142}Eu, ^{142}Sm, and ^{142}Pm *

R.B. Firestone, J. Gilat† , J.M. Nitschke, P.A. Wilmarth, and K.S. Vierinen‡

The EC/β^+ and delayed proton decays of A=142 isotopes with $61 \leq Z \leq 66$ and A=140 isotopes with $63 \leq Z \leq 65$ were investigated with the OASIS facility on-line at the LBL SuperHILAC. Electron capture and positron decay emission probabilities have been determined for ^{142}Pm and ^{142}Sm decays, and extensive decay schemes have been constructed for ^{142}Eu^g (2.34±0.12 s), ^{142}Gd (70.2±0.6 s), ^{140}Eu (1.51±0.02 s), and ^{140}Gd (15.8±0.4 s). Decay schemes for the new isotopes ^{142}Tb^g (597±17 ms), ^{142}Tb^m (303±17 ms), ^{142}Dy (2.3±0.3 s), ^{140}Eu^m (125±2 ms), and ^{140}Tb (2.4±0.2 s) are also presented. We have assigned γ rays to these isotopes on the basis of $\gamma\gamma$ and xγ coincidences, and from half-life determinations. Electron capture and β^+ decay branchings were measured for each decay, and β-delayed proton branchings were determined for ^{142}Dy, ^{142}Tb and ^{140}Tb decays. Q_{EC} values, derived from the measured EC/β^+ branchings and the level schemes, are compared with those from the Wapstra and Audi[1] and the Liran and Zeldes[2] mass calculation. The systematics of the N=77 isomer decays are discussed, and the intense $0^+ \rightarrow 1^+$ and $1^+ \rightarrow 0^+$ ground state beta decays are compared in fig. 1a and fig.2 with the shell model predictions for simple spin-flip transitions (fig. 1b). The logft values follow the expected shell model trends but are hindered by nearly two orders of magnitude. For N=80 and N=81 the blocking of the $\nu d_{3/2}$ orbital in the daughter is observed.

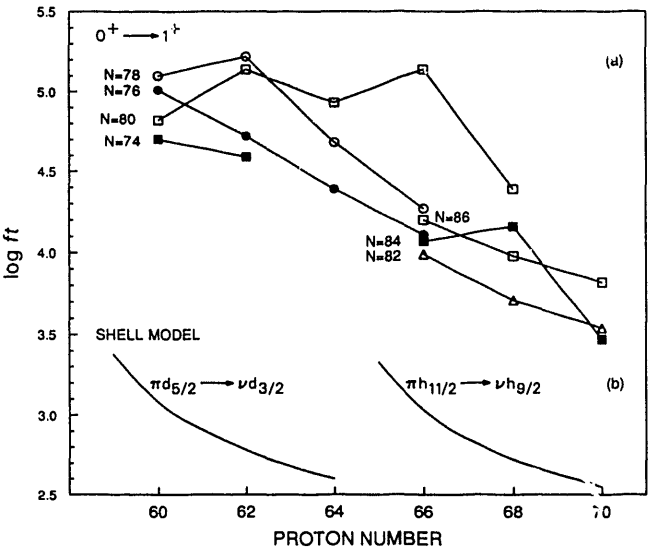

Figure 1: $0^+ \rightarrow 1^+$ transitions

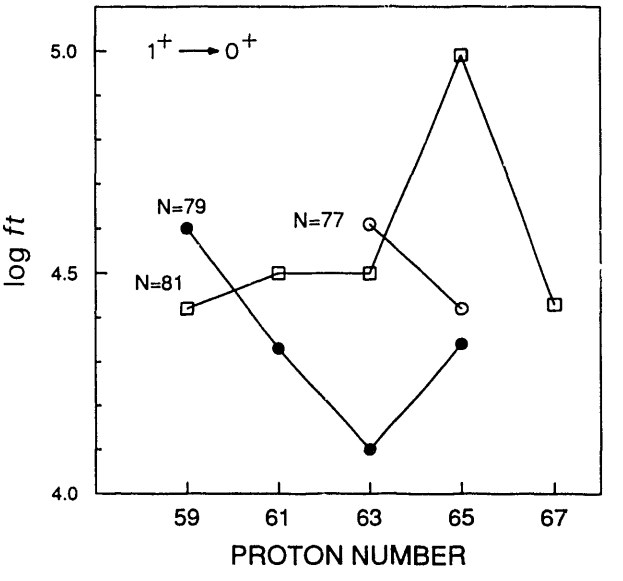

Figure 2: $1^+ \rightarrow 0^+$ transitions

Footnotes and References

*Condensed from Phys. Rev. C43, in press

†Soreq Nuclear Research Center, Yavne 70600, Israel

‡University of Helsinki, SF-00170, Helsinki, Finland

[1]A.H. Wapstra and G. Audi, Nucl. Phys. **A432**, 140 (1985)

[2]At. Data Nucl. Data Tables **17**, 431 (1976)

Beta-Delayed Particle Emission from ^{154}Lu Decay

A.A. Shihab-Eldin, P.A. Wilmarth, K.S. Vierinen,† J.M. Nitschke, R.M. Chasteler,‡ R.B. Firestone, and K.S. Toth§*

Previously, we reported on the β-decay properties of ^{154}Lu produced at the OASIS facility on-line via the ^{94,92}Mo(^{64}Zn,*pxn*) reactions. In addition to constructing a decay scheme for ^{154}Lu, we also reported the observation of fifteen proton events (3.2–5.7 MeV) and eight α events (8.5–11.5 MeV). Both activities were tentatively assigned to the decay of excited states of ^{154}Yb following β decay of ^{154}Lu.

In an attempt to confirm the identification of the precursor to these two decay modes, we have recently carried out additional experiments to produce ^{154}Lu at a higher yield. In a first experiment, we attempted to produce ^{154}Lu activity in higher yield via the ^{94}Mo(^{64}Zn,*p3n*) reaction at E_{lab}=285 MeV, but no measurable yield was observed. In a second experiment, we produced ~3 times the statistics from our earlier experiment over a 36 hour period using the ^{92}Mo(^{64}Zn,*pn*) reaction at E_{lab}=265 MeV.

The new measurements yielded forty-one proton events with energies of 2.6–5.5 MeV and seventeen α events with energies of 6.8–12.4 MeV. Maximum likelihood analysis of the time data of these events resulted in a $T_{1/2}=1.2^{+0.7}_{-0.4}$ s for the proton group and $T_{1/2}=1.3^{+1.5}_{-0.6}$ s for the α group, while a least square fit of the proton data yielded a $T_{1/2}$=1.2±0.5 s, all consistent with the previously reported 1.16 s ^{154}Lu half-life.[1] In addition, the observation of Lu *K* x rays in coincidence with the proton events confirms the identification of the proton activity with ^{154}Lu β-decay (fig. 1). The few *K* x rays observed in coincidence with the α events were inconclusive.

The β-delayed proton and α-particle decay properties of ^{154}Lu were analyzed within the framework of the Statistical Model[1] (SM). By choosing a β-strength function with concentrations of strength in the energy region of observed proton emission (7–8 MeV) and of α and γ emission (2–4 MeV) together with other reasonable model parameters, it was possible to reproduce the measured delayed proton branch and the experimental EC/β^+ ratio. However, the SM underestimated the delayed α branch by more than two orders of magnitude. This can be attributed, among other things, to the fact that the SM is known to be strictly valid only at high excitation energies in the intermediate nucleus where level densities are sufficiently high. In particular, the reduced α-decay level widths may be substantially larger than those calculated with the SM. We note for example that the ground state reduced α width of ^{154}Yb is more than a factor of 100 larger than typical values used in our model.

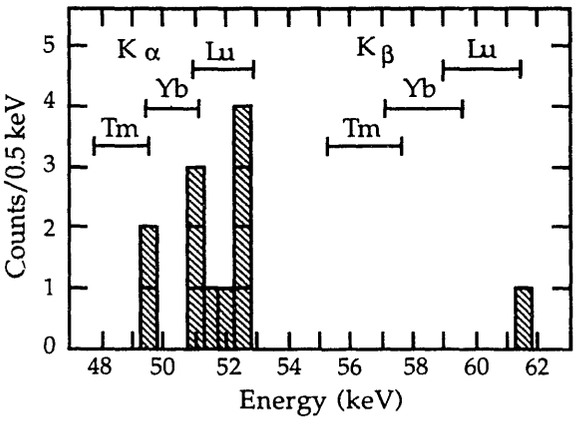

Fig. 1. Proton coincident K x rays. Parent Z x-ray energy ranges are also shown.

Footnotes and References

*On leave from Kuwait Institute for Scientific Research, Kuwait.

†Present address: University of Helsinki, SF-00170 Helsinki, Finland.

‡Present address: Duke University and TUNL, Durham, NC 27706.

§Oak Ridge National Laboratory, Oak Ridge, TN 37831

[1] K.S. Vierinen, *et al.*, Phys. Rev. C **38**, 1509 (1988).

Decay Studies of the Neutron-Rich Isotopes ^{168}Dy and ^{168}Ho^{g} and the Identification of the New Isomer ^{168}Ho^{m} *

R. M. Chasteler,† J. M. Nitschke, R. B. Firestone, K. S. Vierinen,‡ and P. A. Wilmarth

Multi-nucleon transfer reactions between ^{170}Er ions and ^{nat}W targets with on-line mass separation at the OASIS[1] facility were used to produce neutron-rich A=168 isotopes. Beta and gamma spectroscopy was used to study the decay of these activities. A new isomer, ^{168}Ho^{m}, was identified to decay by an isomeric transition with a half-life of 132(4) s. A decay scheme for the most neutron-rich A=168 isotope, 8.8(3)-m ^{168}Dy,[2] was determined and is shown in Fig. 1. The validity of the spin and parity assignments in the ^{168}Ho daughter are supported by comparison with microscopic theoretical calculations of the quasi-particle structure of corresponding states in ^{166}Ho.[3] Also, a new Q_{β}-value of 2.93(3) MeV for the decay of 3.0-m ^{168}Ho^{g} was obtained (Fig. 2).

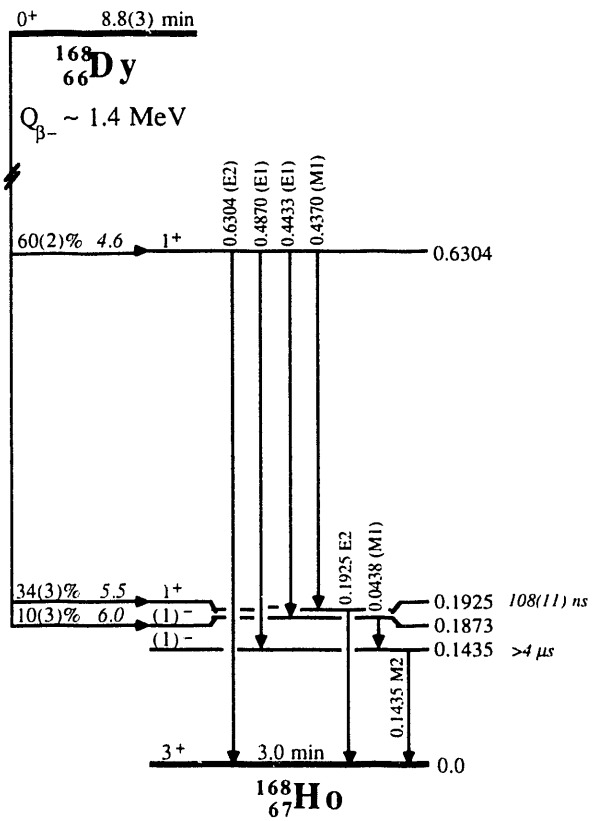

Fig. 1. Proposed decay scheme for 8.8-m ^{168}Dy. Energies are in MeV. Log *ft*'s are in italics.

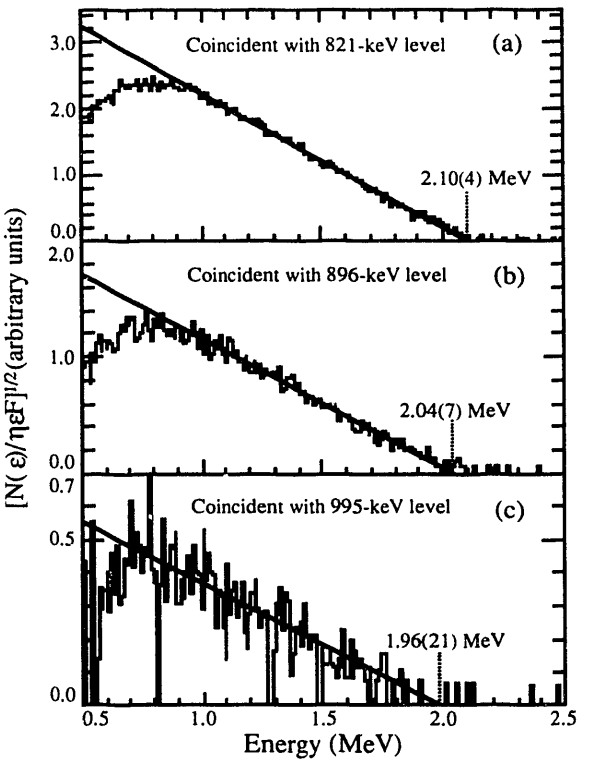

Fig. 2. Fermi-Kurie plots of γ-gated, background-subtracted beta particle spectra for ^{168}Ho^{g} β^{-} decays to levels in ^{168}Er; (a) 821-keV level, (b) 896-keV level, and (c) 995-keV level. The fitting intervals used in the least-squares analysis were (a) 1.0–2.0 MeV, (b) 1.0–1.9 MeV, and (c) 0.8–1.5 MeV.

Footnotes and References

*Condensed from Phys. Rev. C **42**, 1796 (1990).

†Present address: Duke University and TUNL, Durham, NC 27706.

‡Present address: University of Helsinki, Department of Physics, SF-00170, Helsinki 17, Finland.

[1] J.M. Nitschke, Nucl. Instr. & Meth. **206**, 341 (1983).

[2] R.J. Gehrke, R.C. Greenwood, J.D. Baker, and D.H. Meikrantz, Z. Phys. A **306**, 363 (1982).

[3] R.K. Sheline, J. Kvasil, and P.C. Sood, "*Configurational Assignments in ^{168}Ho and Comparison with ^{166}Ho*", submitted to Phys. Rev. C and private communication.

Decay of the Neutron-Rich Isotope ^{171}Ho and the Identification of ^{169}Dy *

R. M. Chasteler,† J. M. Nitschke, R. B. Firestone, K. S. Vierinen,‡ and P. A. Wilmarth

Neutron-rich rare-earth isotopes were produced in multi-nucleon transfer reactions between ^{170}Er ions and ^{nat}W targets. On-line mass separation at the OASIS[1] facility was used together with β and γ-ray spectroscopy in these studies. At mass A=169, the heaviest known dysprosium isotope, ^{169}Dy, was identified (see fig. 1) with a half-life of 39(8) s. It was observed to β^- decay to the ground state of ^{169}Ho and to a level at 1578 keV, as shown in Fig. 2. In the A=171 mass chain, a partial decay scheme for 55(3)-s ^{171}Ho[2,3] was determined and is shown in Fig. 3.

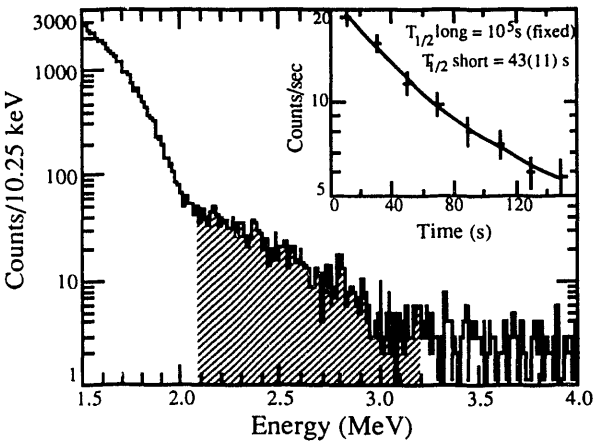

Fig. 1. β-particle spectrum measured in the β telescope for A=169. The inset shows the two-component decay of the β's between 2.1 and 3.2 MeV (shaded portion of the spectrum).

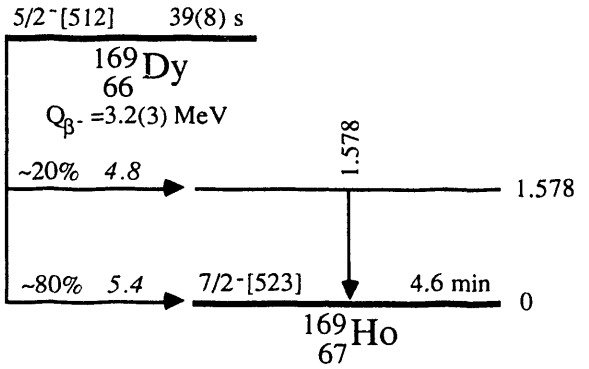

Fig. 2. Partial decay scheme proposed for ^{169}Dy.

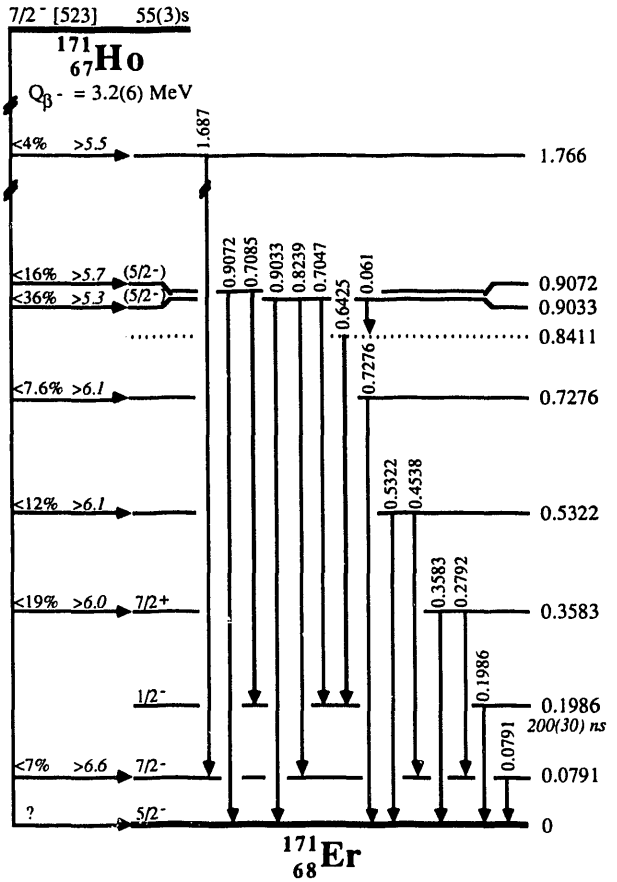

Fig. 3. Proposed decay scheme for ^{171}Ho. Energies are in MeV. The Q_β value is from this experiment. β branches and log *ft* limits (in italics) were calculated assuming no ground-state β branch.

Footnotes and References

*Condensed from Phys. Rev. C **42**, 1171 (1990).

†Present address: Duke University and TUNL, Durham, NC 27706.

‡Present address: University of Helsinki, Department of Physics, SF-00170, Helsinki 17, Finland

[1] J.M. Nitschke, Nucl. Instr. & Meth. **206**, 341 (1983).

[2] K. Rykaczewski, *et al.*, Nucl. Phys. **A499**, 529 (1989).

[3] R.M. Chasteler, *et al.*, Z. Phys. A **332**, 239 (1989).

Null Result for the Weight Change of a Spinning Gyroscope*

J. M. Nitschke and P. A. Wilmarth

In a recent Physical Review Letter,[1] the anomalous weight reduction of several gyroscopes is reported. The authors concluded from their experiments that the weight changes for rotations around the vertical axis were completely asymmetrical: no weight change was observed for left rotations, while right rotations caused weight reductions of up to 10 mg for rotational frequencies on the order of 10^4 rpm. Two subsequent experiments[2,3] have found no evidence for weight reductions. We have carried out experiments under similar conditions to those reported in Ref. 1 and also found no such weight changes.

Our gyroscope had a brass rotor with a radius of 1.92 cm and a mass of 142.4 g. It was enclosed, together with its frame, in an evacuated container (at a pressure of 1 to 3 Pa) and operated at rotational frequencies up to 2.2×10^4 rpm. The weight of the entire assembly was 242.4 g. All weights were determined using a Mettler HE20 balance with a capacity of 260 g and an electronic range of ±1 g with 0.1 mg readability.

Measurements were carried out with the gyroscope axis in the normal vertical, inverted vertical, and horizontal positions under left and right rotations. After the gyroscope was spun up to $(2.2\pm0.03)\times10^4$ rpm, several weight measurements were made until the rotor stopped. The relationship between rotational frequency and elapsed spin-down time was measured in a separate experiment using a photocell and an electronic counter.

Fig. 1 shows the differences in weight changes for left and right rotations versus rotational frequency. No weight change for our gyroscope in the rotational frequency range of 0 to 2.2×10^4 rpm was observed.

The results of our experiment and the results from References 2 and 3 are summarized in Table I. There is no apparent weight reduction, within experimental limits, for right-rotating gyroscopes in any of these experiments.

We wish to thank L. Archambault for his assistance during these experiments.

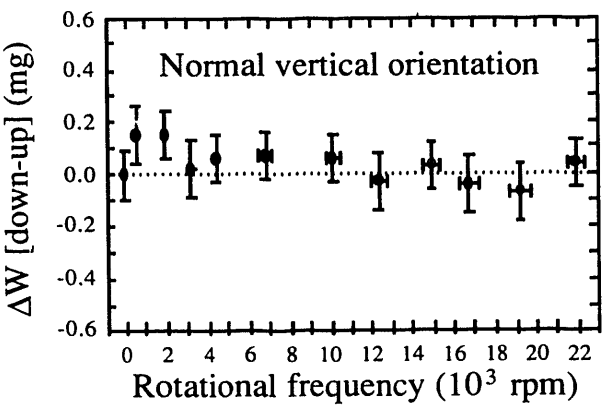

Fig. 1. Differences in the weight changes (expressed in mg) for the up and down spin vector directions as a function of rotational frequency for the normal vertical gyroscope orientation.

Table I. Summary of experiments attempting to confirm the results reported in Ref. 1. (Weight changes ΔW are expressed in mg.)

Experiment	Limit for ΔW (mg)	Predicted ΔW (mg)
Ref. 2	<0.4	-10.2[a]
Ref. 3	<0.06	-8.0[a]
This Work	<0.07	-10.2[b]

[a] Result from Ref. 1 scaled by both mass and equivalent radius.

[b] Assuming $r_{eff} = r_{eq}$.

Footnotes and References

*Condensed from Phys. Rev. Lett. **64**, 2115 (1990).

[1] H. Hayasaka and S. Takeuchi, Phys. Rev. Lett. **63**, 2701 (1989).

[2] J. E. Faller, W. J. Hollander, P. G. Nelson, and M. P. McHugh, Phys. Rev. Lett. **64**, 825 (1990).

[3] T. J. Quinn and A. Picard, Nature **343**, 732 (1990).

High-Statistics Study of Cluster Radioactivity from ^{233}U*

P. B. Price, K.J. Moody‡, E..K. Hulet‡, R. Bonetti§ and C. Migliorini§

Using a track-recording phosphate glass detector with a standard deviation σ_Z = 0.24 charge unit, we have collected ~103 tracks of energetic Ne clusters emitted from ^{233}U and have obtained a branching ratio B(Ne/α) = (7.2 + 0.5 + 0.7) x 10^{-13}. This is consistent with the previous value of (7.5 + 2.5) x 10^{-13} which was based on 16 events. The larger of our two errors is that estimated to be due to uncertainty in absorption in our source. The figure shows the measured distribution of charges of the emitted clusters. No candidate for ^{28}Mg emission survived our energy and angle cuts, from which we infer a branching ratio B(Mg/Ne) < 0.0018 (90% C.L.). The smallness of the Mg branch is inconsistent with predictions of the quantitatively most successful models of cluster emission heretofore used. The inconsistency is removed if the cluster emission models are modified by taking into account the Nilsson states of the parent and daughter nuclei for the two decay modes.

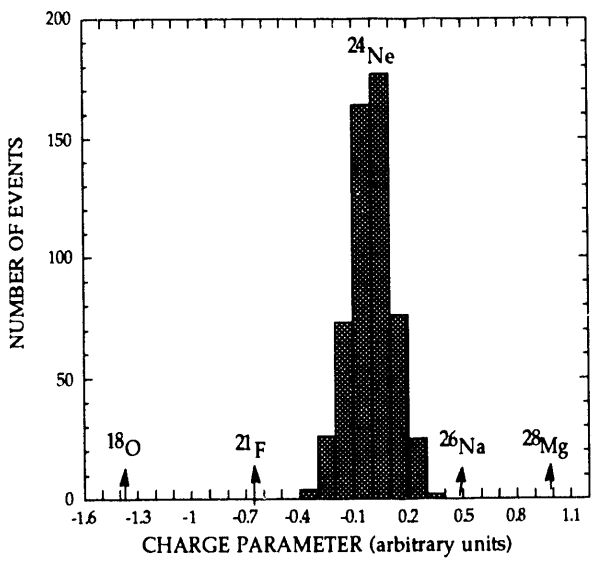

Fig. 1. Charge distribution of events with range > 14 μm and zenith angle 20° < θ < 50°.

Footnotes and References

‡Nuclear Chemistry Division, University of California, Lawrence Livermore National Laboratory, Livermore, California
§Istituto di Fisica Generale Applicata, Universita degli Studi di Milano, and Instituto Nazionale di Fisica Nucleare, Sezione di Milano, Italy
*Condensed from LBL-30300 and Phy. Rev. C (in press)

Antarctic Muon and Neutrino Detector Array (AMANDA)*

D. Lowder, S. Barwick‡, F. Halzen§, T. Miller, R. Morse§, P.B. Price, and A. Westphal

Observation of the small fluxes of neutrinos expected at energies above 1 TeV requires much larger neutrino telescopes than exist today. An instrument of such large dimension (~ 1 km^2) requires a large naturally occurring detector medium, so that only photodetectors and electronics have to be built. One such medium is Antarctic ice. A neutrino telescope could be built by drilling holes in the ice and lowering strings of photomultiplier tubes (PMTs) to a depth of ~ 1 km. Neutrinos would be detected via the Cerenkov light emitted by upward-moving neutrino-induced muons. At these high energies, the direction of the muon produced is within 1 degree of the direction of the parent neutrino, so neutrino source observation is possible. Such a detector would have many advantages over other proposed neutrino telescopes. Although the technique's feasibility depends on the optical clarity of the ice, the transparency of South Polar ice should be good, as the ice cap has been shown to be bubble free at large depths (~ 1 km), and is known to be quite free of impurities in the interior of the continent. We have begun the AMANDA project to test the feasibility of this idea and ultimately to build such a large-scale detector at the South Pole. During 13-16 August 1990, we conducted an initial investigation of the quality of *in situ* polar ice as a Cerenkov radiator at the GISP-II site in Greenland (72° N. 38° W.). We lowered a string of three 12 cm diameter hemispherical PMTs down a 15 cm diameter borehole to a depth of 217 meters. By comparing the observed muon rate, which depends upon the attenuation length of the ice, to Monte Carlo predictions, we determined the peak attenuation length of the polar ice to be at least 18 meters. This result is very encouraging, and we are planning more extensive experiments at the South Pole during November, 1991 to January, 1992, including the construction and operation of a string of 20 cm diameter PMTs at a depth of ~1 km. Over the following two austral summers, we plan to construct a prototype array of three strings of twenty PMTs, which would have a total effective area of ~5000 m^2 (10 x area of the IMB detector).

Footnotes and References

‡Department of Physics, University of California, Irvine, CA 92717, USA

§Department of Physics, University of Wisconsin, Madison, WI 53706, USA

*Condensed version of a preprint being submitted to *Nature*.

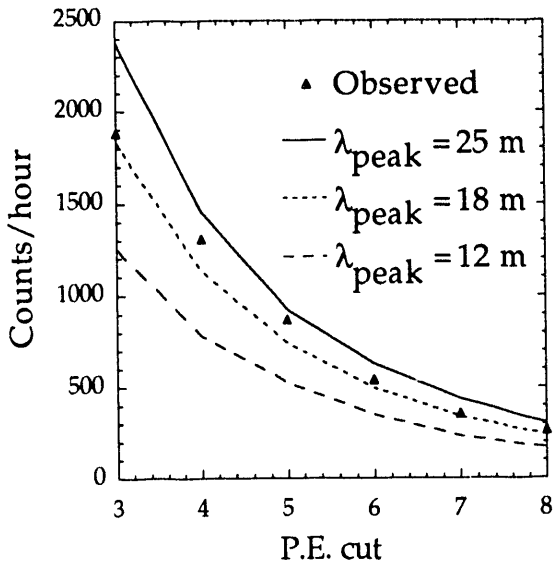

Fig. 1. Measured attenuation length of polar ice at 217 m depth at GISP-II site. The lines are Monte Carlo predictions at different peak attenuation lengths.

Sudbury Neutrino Observatory

Y.D. Chan, K. T. Lesko, E.B. Norman, R.G. Stokstad, B. Sur[†] , R. Fulton[‡] ,Y. Kajiyama[‡] , G. Koehler[‡] , S. Lundgren[‡] , A.R. Smith[‡], P. Purgalis[‡] , and the Sudbury Neutrino Observatory Collaboration

The Sudbury Neutrino Observatory (SNO) will be a world class observatory for neutrino astrophysics. It will contribute to both astrophysics by clarifying the basic energy generating processes in the Sun and to nuclear and particle physics by determining fundamental properties of the neutrinos themselves.

The SNO detector is a large cherenkov detector designed to detect neutrinos in it's 1000 tonnes of D_2O. This detector will have sensitivity both to the total flux of neutrinos, regardless of family (e,μ,τ), and to the electron type neutrino flux by separating the elastic scattering, charged-current, and neutral-current signals. The D_2O target is contained in a thin acrylic sphere which is, itself, suspended in a cavity filled with ultrapure light water 6800 feet below sea level in the Creighton Mine near Sudbury, Ont, Canada. The mine is an active nickel mine operated by INCO Limited.

Lawrence Berkeley Laboratory is designing the Photo-Multiplier Tube (PMT) Support Structure which will hold the approximately 10,000 PMTs which record the cherenkov light produced by neutrino events in the water. Design factors which influence the PMT Support Structure include the demands for very low radioactivity contents of all materials within the cavity, providing high PMT coverage, providing a maintenance-free structure for the projected ten year experiment life-time in the harsh environment of ultra-pure water, allowing for installation within an operating mine with limited access, and the need for essentially a clean-room environment within the cavity during the installation of the PMT Support Structure and the acrylic vessel. Present schedules call for installation of the PMT Support Structure beginning in January, 1993 with data taking beginning in 1994.

Footnotes and References

† Present address: Department of Physics, Queen's University, Kingston, Ont K7L 9N6, Canada.

‡ Engineering Division, Lawrence Berkeley Laboratory

Evidence for the Emission of Massive Neutrino in Nuclear Beta Decay

*Eric B. Norman, Bhaskar Sur *, K. T. Lesko , M. M. Hindi †, Ruth-Mary Larimer , Teressa R. Ho‡ , Jon T. Witort‡, Paul N. Luke §, William L. Hansen §, and Eugene E. Haller §***

Over the past two years, our group has conducted experiments searching for evidence of a massive neutrino (i.e. m_ν = 17 keV) emitted in the β-decay of ^{14}C and the radiative electron-capture decay (inner bremsstrahlung) of ^{55}Fe. The ^{14}C experiment utilizes a unique detector produced by LBL's detector laboratory: a planar germanium detector with ^{14}C grown into the crystal.[1] This provides a total energy spectrometer with a nearly perfect response function for electrons. We have taken four months worth of ^{14}C data using this crystal and 2 months of background using an undoped germanium crystal. This experiment is being performed in LBL's Low Background Counting Facility in Bldg. 72. The analysis of the ^{14}C data we have to date supports the claim by Simpson[2] that a neutrino with a mass of 17-keV is emitted with about a 1% probability in β-decay. Analysis of the data we have collected to date shows a 3-σ effect. We find $m_\nu = 17 \pm 2$ keV, and its emission probability is $(1.4 \pm 0.40)\%$ in the β decay of ^{14}C.

We have also studied the inner bremsstrahlung spectrum emitted in the electron capture decay of ^{55}Fe using a 10 mCi source of ^{55}Fe and a conventional planar germanium detector. The results of fitting the last 50 keV of the ^{55}Fe IB spectrum yield $m_\nu = 21 \pm 2$ keV and c = $(0.85 \pm 0.45)\%$ (all uncertainties are 1σ). These results indicate that there is a *kink* in the ^{55}Fe IB spectrum, but corresponding to a slightly different m_ν value than that found in the study of ^{14}C decay. Also, the overall χ^2 values obtained here are not as good as those found in the analysis of the ^{14}C data. We believe both of these effects are due to our lack of precise knowledge of the detector response function. Fits performed in which we varied the energy dependence of the detector efficiency showed that the position of the *kink* could be moved. Thus, these results are suggestive that there is a feature ~17 keV below the endpoint of the ^{55}Fe IB spectrum, but further study of this system is clearly necessary.

Footnotes and References

*Present address: Department of Physics, Queen's University, Kingston, Ont K7L 9N6, Canada.

† Tennessee Technological University, Cookeville, TN 38505

‡Physics Department, University of California, Berkeley, CA 94720

§Engineering Division, Lawrence Berkeley Laboratory

**Department of Materials Science and Mineral Engineering, University of California, Berkeley, CA 94720

1. E. E. Haller, W. L. Hansen, P. Luke, R. McMurray, and B. Jarrett, IEEE Trans. Nucl. Sci. Vol. NS-29, No. 1, 745 (1982).

2. J. J. Simpson, Phys. Rev. Lett. **54**, 1891 (1985).

Reinvestigations of ^{56}Ni decay*

Bhaskar Sur†, Eric B. Norman, K.T. Lesko, Edgardo Browne, and Ruth-Mary Larimer

The doubly magic nucleus ^{56}Ni decays via an allowed electron capture (EC) transition to the 1720-keV level in ^{56}Co with an approximate 100% branch and a half-life of 6.0 days. Although the decay of ^{56}Ni has been previously studied, we have reexamined its decay scheme specifically to search for two interesting, but rare decay modes. The first mode is β^+ decay, which would be the dominant channel for decay for fully ionized ^{56}Ni nuclei as relativistic cosmic rays. The second mode is the isospin forbidden EC transition to the 1451-keV level in ^{56}Co, which if found, could be used to calculate the isospin mixing in the ground state of ^{56}Ni.

The sample of ^{56}Ni was produced at LBL's 88-Inch Cyclotron using the ^{56}Fe(^{3}He,3n) reaction and the Ni fraction purified using standard radio-chemical techniques. This sample was then counted in a variety of different experimental set-ups which used a NaI annular detector, several high purity germanium detectors and addition NaI detectors in different arrangements.

To search for the β^+ transitions, we sought for 511 keV annihilation photons in coincidence with nuclear γ-rays. The multi-parameter data were then sorted off-line requiring various conditions. The absolute EC decay branchings to excited levels in ^{56}Co were also deduced from examining the γ-ray intensity balances. The half-life of ^{56}Ni was measured by following the time history of the decay rate of the 269- and 480-keV γ rays from ^{56}Ni decay, normalized to that of the 320-keV γ ray from ^{51}Cr decay.

We sought for the EC decay from the 0^+ ^{56}Ni ground state to the 0^+ 1451-keV state in ^{56}Co by observing the triple-sum coincidence peak in a germanium detector vetoed by the annular NaI detector.

We establish an upper limit of 5.8×10^{-7} for the branching ratio of the second forbidden unique β^+ decay to the 158-keV level in ^{56}Co, leading to a lower limit of 2.9×10^4 yr for the half-life of fully ionized ^{56}Ni nuclei in cosmic rays. We also establish an upper limit of 5.0×10^{-3} for the branching ratio of the isospin forbidden Fermi EC transition to the 1451-keV level in ^{56}Co, which in turn leads to an upper limit of 124-keV for the isospin mixing Coulomb matrix element of the ^{56}Ni ground state. We have, in addition, confirmed the previously reported decay scheme and half-life of ^{56}Ni.

Footnotes and References

*Condensed from Phys. Rev. C 42, 573 (1990)

† Present address: Department of Physics, Queen's University, Kingston, Ont K7L 9N6, Canada.

Study of γ Radiation from ^{100}Pd Decay*

*B. Singh† , H.W. Taylor‡ , E. Browne, H.L. Hall** , E.B. Norman, R.M. Larimer, A.O. Macchiavelli††, K.T. Lesko, and B. Sur.*

The electron capture decay of ^{100}Pd provides information on the nuclear levels of ^{100}Rh, serving to illustrate the coupling of unpaired protons and neutrons for the A=80-100 mass region. Also, ^{100}Pd has potential applications in nuclear medicine[1] because of its desirable half life and appropriate γ-ray energies and intensities. A recent review[2] of A=100, however, shows significant disagreement in the γ-ray data reported by various authors. This situation prompted our study of the γ-ray singles and γγ coincidence spectra of ^{100}Pd. Fig. 1 shows our decay scheme, with levels at 86-, 136-, and 154 keV, seen for the first time in the electron capture decay of ^{100}Pd. Our measured emission probability of 53 (4)% for the 84-keV γ ray, and the relative K x-ray intensities are consistent with the decay scheme, confirming the quality of the data.

Footnotes and References

*Condensed from a paper submitted for publication in Z. Phys.

†Tandem Accelerator Laboratory, McMaster University, Hamilton, Ontario, Canada, L8S 4K1.

‡Physics Department, University of Toronto, Toronto, Ontario, Canada, M5S 1A1.

**Nuclear Chemistry Division, Lawrence Livermore National Laboratory, Livermore, CA 94551, U.S.A.

††On leave from Departamento de Fisica, Comision Nacional de Energia Atomica, Buenos Aires, Argentina.

1. M.C. Lagunas-Solar, M.J. Avila, and P.C. Johnson, Int. J. Appl. Radiat. Isotope 35, 743 (1984); ibid 38, 151 (1987).

2. B. Singh and J.A. Szucs, Nuclear Data Sheets 60, 1 (1990).

Fig. 1. ^{100}Pd decay scheme. Photon intensities are relative to 100 for the 84-kev γ ray.

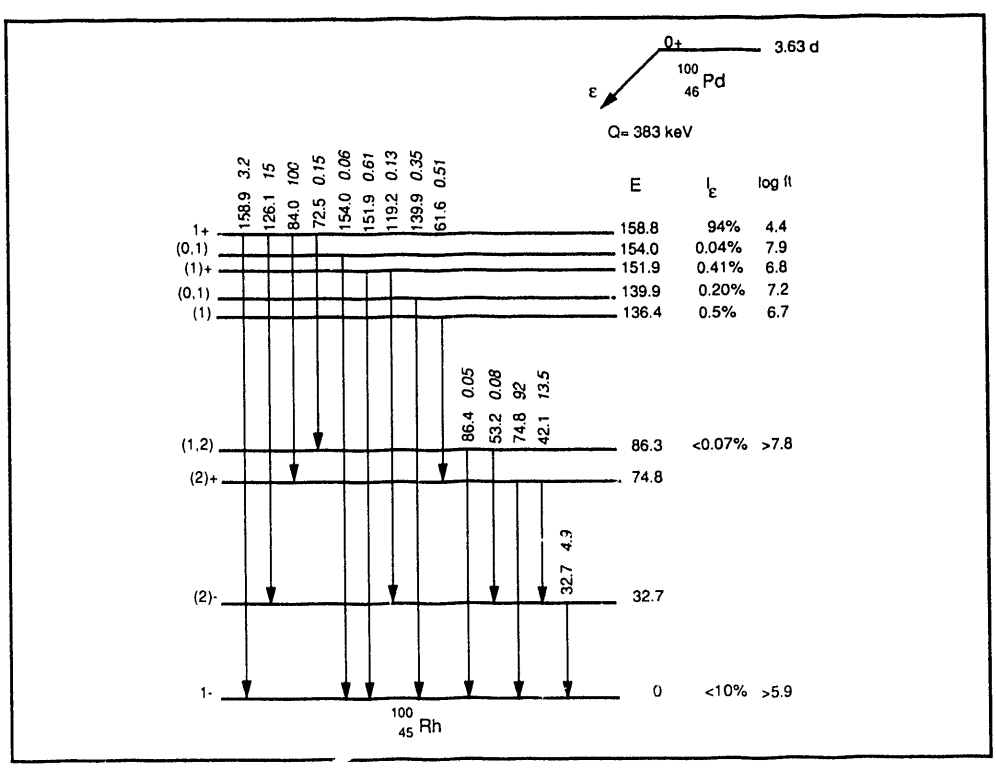

^{176}Lu: An Unreliable s-Process Chronometer*

K.T. Lesko, E.B. Norman, R.-M. Larimer, and B. Sur†

^{176}Lu can only be produced via the slow neutron capture process (s process). The stable isobars ^{176}Yb and ^{176}Hf shield this nucleus from rapid neutron capture and proton capture contributions. Due to the long half-life of the ground state (7^-, 4.08×10^{10} y), ^{176}Lu^g, it has been suggested that ^{176}Lu would be a candidate for a s-process chronometer[1,2]. However, there exists a much shorter lived isomer at 122.9 keV, (1^-, 3.7 hr). The large spin difference between these two levels prevents decays from the isomer to the ground state; the isomer decays to ^{176}Hf. The presence of this isomer could affect the decay of ^{176}Lu in astrophysical environments, providing a method of communication between the two levels exists. This communication could be mediated by the presence of a higher lying level with significant decay branches to both the ground state and the isomer. Such a level and the resulting equilibration path would severely compromise the usefulness of ^{176}Lu as an s-process chronometer due to the effective decay constant being temperature sensitive. The existence of such a mediating level between 662- and 1332-keV can be inferred from photoexcitation work[3].

We sought to determine the level scheme of ^{176}Lu up to approximately 1 MeV of excitation energy and to search for levels which could serve as a mediating level between the ground state and the isomer. Using LBL's 88-Inch Cyclotron and the HERA array of germanium detectors we collected coincidence γ ray data.

Using these data and previously published particle transfer data we have established 170 γ-ray transitions between 85 levels. A level at 838.5 keV ($J^\pi=5^-, t_{1/2}<10$ns) decays with substantial strength to the ground state and the 122.9 keV isomer. The presence of this level guarantees the thermal equilibration of ^{176}Lu^{g,m} for temperatures > 3×10^8 K and, therefore, during the s-process. The resulting extreme temperature sensitivity of its effective half-life rules out its use as an s-process chronometer.

Footnotes and References

*Submitted to Phys. Rev. C.

† Present address: Department of Physics, Queen's University, Kingston, Ont K7L 9N6, Canada.

1. M. Arnould, Astron. Astrophys. **22**, 311 (1973).

2. J. Audouze, W.A. Fowler, and D.N. Schramm, Nature, **238**, 8, (1972).

3. E.B. Norman, T. Bertram, S.E. Kellogg, S. Gill and P. Wong, Astrophys. J. **291**, 834 (1985).

Half-life of ^{56}Co*

K.T. Lesko, E.B. Norman, B. Sur†, and R.-M. Larimer

The wealth of new data provided by observations of supernova SN1987A has done much to suggest that our understanding of the final stages of stellar evolution and nucleosynthesis are basically correct. In particular, the observation of γ-ray lines and the optical light curve support the idea that large amounts of radioactive ^{56}Co and ^{56}Ni were produced in the core of the supernova. In fact, observations of the light curve were used to deduce the half-life of ^{56}Co. Pinto and Woosley[1] find a value of 77.1 ±(1%)days, whereas values in the literature cluster around two values, 78.75±0.12 days[2] and 77.7±0.5 days[3].

We have reinvestigated the half-life of ^{56}Co by measuring the time-dependent yields of several nuclear γ-ray lines over a period of 280 days. The sample of ^{56}Co was produced at LBL's 88-Inch Cyclotron by bombarding a stack of Fe metal foils with 13-MeV deuterons. The targets were dissolved and the cobalt fraction purified by standard radio-chemical techniques. The cobalt fraction was then mixed with similar strength sources of ^{137}Cs and ^{207}Bi. These two long-lived sources were used to normalize the decay of the cobalt nuclei and reduce our sensitivity to geometric and efficiency errors.

We deduced a value of 77.08 ±0.08 days by averaging results from the different γ-ray lines and using standard γ–ray calibration sources. We find good agreement between our result and several of the more recent values. This half-life is consistent with the observed light curve of SN1987A and further supports the idea that large amounts of ^{56}Co are produced in supernovæ.

Footnotes and References

*Condensed from Phys. Rev. C. **40**, 445 (1989)

† Present address: Department of Physics, Queen's University, Kingston, Ont K7L 9N6, Canada.

1. P.A. Pinto and S.E. Woosley, Nature **333**, 534 (1988)

2. C.M. Lederer and V.S. Shirley, *Table of Isotopes*, 7th ed. (Wiley, New York, 1978).

3. E. Browne and R.B. Firestone, *Table of Radioactive Isotopes* (Wiley, New York, 1986).

More Searches for Cold Fusion*

R.A. Henderson, K.R. Czerwinski, H.L. Hall, K.T. Lesko, E.B. Norman, B. Sur†, and D.C. Hoffman

Following the announcement of cold nuclear fusion being observed in electrochemical cells by Fleishmann and Pons[1] and by Jones *et al.*[2], we have searched for the characteristic radiations of the d+d and p+d fusion reactions in cells similar to those described by these references. No fusion product neutrons or γ rays have been observed from either palladium or titanium cathodes. From measured D/Pd ratios in the systems with the palladium cathodes, we set upper limits on the fusion rates for our systems: one sigma limits on cold fusion reactions $d(d,n)^3He$ and $d(d,\gamma)^4He$ of $\leq 2.1 \times 10^{-24}$ and $\leq 2.7 \times 10^{-24}$ reactions per deuteron per second, respectively. We conclude that if cold fusion is occurring under these conditions, it is below these limits. These limits are inconsistent with a nuclear mechanism for the generation of heat reported by Pons and Fleischmann. These limits are also about a factor of 10 below the rates reported by Jones *et al.*[2]

Footnotes and References

*Condensed from Journal of Fusion Energy, Vol 9, No. 4, 1990, page 475.

† Present address: Department of Physics, Queen's University, Kingston, Ont K7L 9N6, Canada.

1. M. Fleischmann, S. Pons, and M. Hawkins, J. Electroanal. Chem., **261**, 301 (1989).

2. S.E. Jones, *et al.*, Nature **388**, 737 (1989)

Cold Fusion: Effects of Possible Narrow Nuclear Resonance *

A.A. Shihab-Eldin †, *J.O. Rasmussen, M. Justice and M.A. Stoyer*

Following the reports of Fleischmann and Pons[1] and Jones *et al.* [2] we examined the influence of a possible and as yet undiscovered narrow resonance on the *d-d* fusion rate near threshold energy in the *d-d* channel (23.8 MeV in ^{4}He). Using a simple Breit-Wigner expression for the energy dependence of the fusion cross section and expressing the partial channel decay width as a product of three terms, a simple pentrability factor, frequency factor and a spectroscopic factor, it can be demonstrated that the *d-d* threshold fusion rate may vary by more than 10^8 going on and off resonance.

The problem of large heat generation relative to neutron and tritium production might be explained if the postulated narrow 0^+ resonance had a very small spectroscopic factor for the neutron and proton decay channels and primarily decayed by internal e^+ e^- pair formation either directly to ground or through the first excited $0^{+'}$ level at 20.2 MeV. The electrons would have at most an energy of 11.4 MeV. In water or other low-Z material such electrons will deposit most of their energy in the near surroundings as heat with but little escaping as bremsstrahlung.

If the resonance state is composed of excited proton structure and excited neutron structure, the n and p decay modes would both be suppressed. We denote the four basis configurations in terms of nucleon pair couplings that automatically take care of the Pauli principle, using the convention $\left\{\left\{\pi\, ^{2S+1}L_{J_p};\nu\, ^{2S+1}L_{J_n}\right\}_J;L\right\}_{I^\pi}$, as follows: $|\,0\rangle = \left\{\left\{\pi\, ^1S_0;\nu\, ^1S_0\right\}_0;0\right\}_{0^+}$,

$$|\,1\rangle = \left\{\left\{\pi\, ^3P_1;\nu\, ^1S_0\right\}_1;1\right\}_{0^+},$$

$$|\,2\rangle = \left\{\left\{\pi\, ^1S_0;\nu\, ^3P_1\right\}_1;1\right\}_{0^+} \text{ and}$$

$$|\,3\rangle = \left\{\left\{\pi\, ^3P_1;\nu\, ^3P_1\right\}_0;0\right\}_{0^+}.$$

We may note qualitatively several features. Admixture of the excited configurations $|\,1\rangle$, $|\,2\rangle$, and $|\,3\rangle$ into $|\,0\rangle$ will be small, as spin recouplings are involved. The mixing of configurations $|\,1\rangle$ and $|\,2\rangle$ with one another may be large, as their diagonal energies will be very similar by isobaric spin symmetry. Thus, we might suppose the first excited 0^+ level to be the positive linear combination $|\,0^{+'}\rangle \approx \frac{1}{\sqrt{2}}(|\,1\rangle + |\,2\rangle)$ and the possible resonance at d-d threshold to be the negative linear combination $|\,0^{+''}\rangle \approx \frac{1}{\sqrt{2}}(|\,1\rangle - |\,2\rangle)$.

The mixing between resonance and ground state dominant configurations will govern the E0 matrix element direct to ground. We can only set an upper limit of $\Gamma_{pair} < 3 \times 10^{-3}$ ev from a maximal mixing value $\rho^2 < 0.44$. In fact, the mixing is expected to be quite small since the subtractive linear combination constituting the resonance wave function would exactly cancel for charge-independent nucleon-nucleon forces.

The partial decay widths (and spectroscopic factors) for decay into the two particle emission channels will be proportional to the admixture of configuration $|\,0\rangle$ in the proposed resonance state. Since the particle-decay channels are over-barrier, their partial widths for unity spectroscopic factors will be several MeV.

In conclusion, it seems highly unlikely that the mixing could be so small as to suppress them by ten orders of magnitude necessary for internal pair emission to dominate. Hence, we have no reasonable way to explain the large ratio of fusions to neutrons implied by the Pons-Fleischmann calorimetric measurements.

Footnotes and References

*Modern Physics Letters **B3**, No.12(1989) 965

†On leave from Kuwait Institute for Scientific Research, Kuwait

[1] M. Fleischmann, S. Pons and M.J. Hawkins, J. Electroanal. Chem. **261** (1989) 310 and erratum, **263** (1989) 187

[2] S.E. Jones *et al.*, Nature **338** (1989) 737

Limits on Electromagnetic and Particle Emission from Palladium-D_2O Electrolytic Cells*

J.D. Porter, A. A. Shihab-Eldin†, H. Bossy, F.J. Echegaray, J.M. Nitschke, S.G. Prussin‡, J.O. Rasmussen and M.A. Stoyer

The reported claims by Fleischmann and Pons[1] (FP) and Jones *et al.* [2] of possible observation of cold fusion of deuterium in Pd and Ti cathodes have generated much interest. Shortly after these initial announcements were made, we initiated a series of experiments to test for "cold" fusion in similar electrochemical cells. We have chosen to follow the FP approach since they reported the largest energy, neutron and tritium production rates.

Initially we carried out a simple experiment with an electrochemical cell of a simple, undivided design, constructed with a thin Pd wire cathode. Neutrons were detected indirectly by measuring the 2224-keV γ-ray from the ^{1}H(n,γ) reaction in the surrounding water and paraffin, using a 20% intrinsic Ge detector.

Following this we designed a more thorough "blind" experiment equipped with a host of radiation detection systems for examining fusion reactions involving the emission of neutrons and/or radiations from fusion reactions not normally considered (e.g. high energy e^+e^- pair and conversion electrons). In this second experiment, two vacuum-cast Pd disks were the cathodes in "twin" cells, one with H_2O, and the other with D_2O. The two cells were shuttled every 24 hours between similar detector setups, equipped with neutron, γ- and X-ray detectors.

In addition, we designed a special cylindrical cell to measure production of protons (and other charged particles) from the d(d,p)t fusion reaction channel. In this third experiment, we used a Si surface barrier detector viewing the back of a 76 μm thick Pd foil cathode. A similar type of experiment is described in a recent publication by Ziegler *et al.*[3]

The cells in all these experiments were all operated as open systems. Furthermore, careful attention was paid to experimental design, especially with regard to control experiments and calibration of equipment. A matrix of four conditions was studied whenever possible and appropriate: 1) light water electrolysis, Pd cathode, 2) light water electrolysis, Pd anode, 3) heavy water electrolysis, Pd cathode, and 4) heavy water electrolysis, Pd anode. In order to minimize bias, a "single blind" protocol was adopted at every opportunity so that experimenters did not know the identity of the sample which was being measured or analyzed.

No statistically significant evidence of nuclear fusion has been obtained in any of these experiments, either in steady state operation or in transient response to a variety of perturbations. Upper bounds on the rate of various postulated fusion processes were set including $< 2 \times 10^{-23}$ neutrons (dd pair)$^{-1}$ s^{-1} for the d(d,n)^{3}He reaction and $< 6 \times 10^{-25}$ protons (dd pair)$^{-1}$ s^{-1} for the d(d,p)^{3}H reaction (2σ level). Chemical analysis of our "twin" Pd cylinder electrolyte solution revealed no measurable increase in tritium concentration, beyond the effects of electrolytic isotope enrichment during our experiment.

Footnotes and References

*Journal of Fusion Energy, **9** No. 3 (1990) 319

†On leave from Kuwait Institute for Scientific Research, Kuwait

‡Department of Nuclear Engineering, University of California, Berkeley, California

[1] M. Fleischmann, S. Pons, and M.J. Hawkins, J. Electroanal. Chem. **261** (1989) 301; **263** (1989) 187

[2] S.E. Jones, E.P. Palmer, J.B. Czirr, D.L. Decker, G.L. Jensen, J.M. Thorne, and S.F. Taylor, Nature **338** (1989) 737

[3] J.F. Ziegler, T.H. Zabel, J.J. Cuomo, V.A. Brusic, G.S. Cargill, III, E.J. O'Sullivan, and A.D. Marwick, Phys. Rev. Lett. **62** (1989) 2929

A Two Dimensional Barrier Penetration Study in Heavy Ion Collisions

A.A. Shihab-Eldin, W. H. Miller, J.O. Rasmussen, Q.Y. Shao†, L.F. Canto‡, R. Donangelo‡, and M. Hussein§*

We have investigated the use of semi-classical trajectory[1] methods to treat sub-barrier heavy ion transfer reactions. To incorporate the complication of a non-isotropic inertial tensor but nevertheless exactly expressible over most of the space, we have selected for study the case of collinear neutron-pair transferring between two ^{16}O nuclei. For the Hamiltonian of the system we have chosen an attractive Gaussian potential between the dineutron and the oxygen with a well depth V_o = 50 MeV and a width comparable to the oxygen nuclear radius, r_n. The nuclear interaction between the two oxygen nuclei was likewise chosen to be an attractive Gaussian with a depth V_1 = 200 MeV and a width parameter comparable to the sum of two oxygen nuclear radii. The Coulomb interaction is taken to be of a point-nucleus $1/r$ form.

It was convenient to solve the equations of motion in terms of the normal coordinates of the symmetric 3-body system, X for for the symmetric stretch, and Y for the asymmetric stretch. The tunneling process can thus be represented by vibrationally oscillating trajectory along the gently rising valley floor of the potential at 45° in the XY plane to near the classical turning point, then travelling vertically along the Y axis to near the opposite classical turning point whereupon it proceeds outward along the $-45°$ exit valley.

To keep the computation of this two-dimensional penetration simple with position coordinates remaining real, we must start our trajectories at rest from the classical turning contour, running in real time for connection to the initial condition and running in imaginary time across the barrier. We further make the approximation, equivalent to neglecting the recoil term, that the trajectory across the barrier moves vertically along the Y axis and comes to rest at a symmetrical turning point. From the real-time trajectories for various Y_i values along the classical turning contour we separate the translational energy from the vibrational energy at large separation and calculate the initial vibrational quantum number, n_i. Only integer n_i are allowed quantum mechanically, and for our system n_i has the value 2.

The neutron pair penetrability can then be calculated as $P = exp(-2S/\hbar)$, where S is the classical action integral across the barrier in imaginary time. For vey low collision energy, coherent enhancement resulting from several vibrational cycles within the collision time could be appreciable. For example, the penetrability at the classical turning point, P_o, was calculated to be 6.6 x 10^{-7} and 2.4 x 10^{-18}, corresponding to total system energies of -5 MeV and -8 MeV, respectively. The corresponding enhancement factors due to multiple collisions within the reaction zone are 7.4 and 30.6, respectively.

The fusion tunneling probability can similarly be calculated by considering the trajectory under the barrier along the relative motion coordinate, R, while keeping the appropriate dineutron-oxygen coordinate fixed. In addition, our simple method can be extended to calculate inelastic transition rates using analytic continuation techniques.

Footnotes and References

*On leave from Kuwait Institute for Scientific Research, Kuwait

†Present address: Physics Department, Fudan University, Shanghai, People's Republic of China

‡Instituto de Fisica, Universidade Federal do Rio de Janeiro, Rio de Janeiro, Brazil

§Instituto de Fisica, Universidade de Saõ Paulo, Saõ Paulo, Brazil

[1] W.H. Miller, Adv. Chem. Phys. **25** (1974) 69; **30** (1975) 77

Semiclassical Treatment of Nuclear Effects in Coulomb Excitation*

L.F. Canto †, *R. Donangelo* †, *J.O. Rasmussen, M.A.Stoyer and Peter Ring*‡

We introduce the effects of the nuclear potential in the semiclassical Alder-Winther-deBoer method of ref. [1], both in the coupling matrix elements and as corrections to the Rutherford orbit. We use the fully quantum mechanical, partial-wave, coupled-channel solutions of ref. [2], as our benchmark for comparison and then apply our codes to much heavier systems, such as ^{206}Pb on rare earths, both for rotational inelastic scattering and for neutron-transfer reactions.

We expand the deformed, complex optical potential in spherical harmonics up to order 6 (though only to order 2 for comparison with the benchmark work). The Rutherford trajectory is modified to correctly reproduce the turning radius and force at the turning point, by introducing an effective charge of the deformed partner and an effective beam energy. The Coulomb and real part of the optical potential are taken into account for equivalent spherical nuclei.

With these modifications the agreement with the benchmark coupled channel calculations is quite good. The Figure presents the rotational population patterns for (a) ^{40}Ar on ^{160}Gd at E_{lab} = 170 MeV and (b) ^{208}Pb on ^{160}Dy at E_{lab} = 1100 MeV. Results of the present work are compared to pure Coulomb excitation and (for (a) only) coupled-channel calculations of Rhoades-Brown et al.

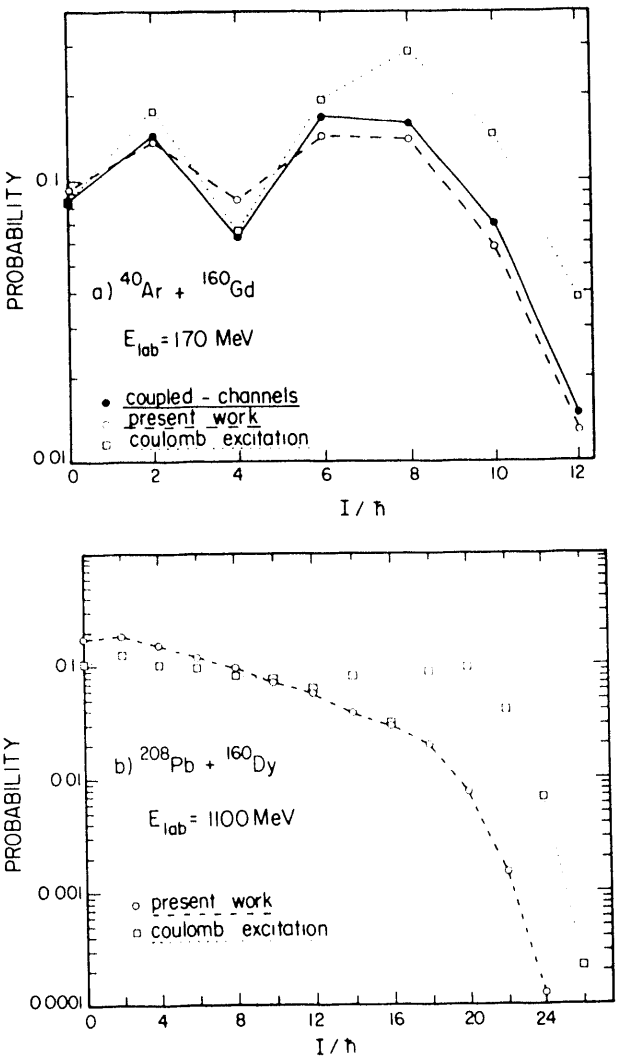

Figure 1: Rotational population patterns for the reactions (a) ^{40}Ar on ^{160}Gd at E_{lab} = 170 MeV and (b) ^{208}Pb on ^{160}Dy at E_{lab} = 1100 MeV. The present work (open circles–dashed lines) are compared to pure Coulomb excitation (open boxes–dotted lines) and coupled-channel calculations of Rhoades-Brown et al. (solid circles–full lines). Note that in the case (b) no coupled-channel calculations are available.

Footnotes and References

*Contributed papers to the symposium in honor of Akito Arima: **Nuclear Physics in the 1990's**; Physics Letters B 248 (1990) 10.

†Inst. de Fisica, Univ. Fed. do Rio de Janeiro, C.P. 68 528, 21945 Rio de Janeiro, Brazil.

‡Physik Department der Tech. Univ. Muenchen D-8046 Garching, Germany.

[1] A. Winther and J. deBoer, Caltech Report reprinted in K. Alder and A. Winther, Coulomb Excitation, Academic Press, N.Y. (1966)

[2] M.J. Rhoades-Brown, R. Donangelo, M.W. Guidry, and R.E. Neese, Phys. Rev. C 24 (1981) 2747

Excitation and Multiple Dissociation of ^{12}C, ^{14}N,and ^{16}O Projectiles in Peripheral Collisions at 32.5 MeV/nucleon

*J. Pouliot†, Y. Chan, D.E. DiGregorio‡, B.A. Harmon§, R. Knop** ,*

C. Moisan††, R. Roy† and R.G. Stokstad

Cross sections for the multiple breakup of ^{16}O, ^{14}N and ^{12}C projectiles into a large number of exit channels, some having as many as five charged particles, have been measured with an array of 34 plastic scintillators. This has enabled a more global examination of the breakup of the projectile than would be possible with two-particle coincidence experiments. Events resulting from the breakup of the primary projectile-like nuclei were selected in the off-line analysis by requiring that the sum of the identified charge be equal to the charge of the projectile. This, and the energy threshold for particle identification set by the 1 mm thick fast plastic, effectively eliminated any contributions of low energy particles (with $Z \leq 2$) evaporated by an excited target-like nucleus. The peripheral nature of the reaction was verified by observing that the velocities of all the detected fragments, including protons, were characteristic of the projectile and that the laboratory velocity, V_{pp}, of the center of mass system of the detected fragments was close to the beam velocity. The excitation spectrum of the primary projectile-like nucleus was reconstructed from the measured positions and kinetic energies of the individual fragments.

The relative yields of the different channels were observed to correlate approximately, over a range of 3 to 4 orders of magnitude, with the threshold energy for separation of the projectile into the detected fragments (see figure). The excitation spectrum of the primary projectile-like nucleus has a maximum at low excitation energies, but also extends to quite high excitation energies (5-6 MeV/nucleon). A Monte Carlo simulation of the B+He+H channel, which is produced by the decay of ^{16}O nuclei at excitation energies greater than 23 MeV, shows no evidence for final state interactions between fragments of the projectile and the Coulomb field of the target. The sharing of the excitation energy between the projectile-like nucleus and the target does not indicate any evidence for strong equilibration in the initial stage of the reaction and is thus consistent with a fast excitation process. The yields of the light particles are compared with the predictions of multiple sequential decay models. These models were found to underestimate the yields of the channels populated by the decay of the highest excitation energies in the projectile and the yields of protons at forward angles. With these exceptions, the statistical models, including the sphericity-coplanarity analysis presented in ref. 1, show good agreement for the multiple decay properties of the excited projectile-like nuclei studied in the present reactions.

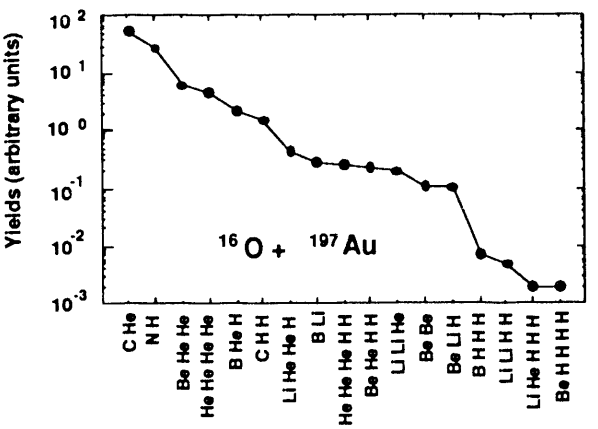

Footnotes and References

†Laboratoire de Physique Nucléaire, Université Laval, Québec, G1K7P4, Canada.

‡ Departamento de Fisica-TANDAR, CNEA 1429 Buenos Aires, Argentina and CONICET.

§ Space Science Laboratory, NASA, Marshall Space Flight Center, Huntville, AC 35812.

**Dept. of Physics, Caltech, Pasadena, Ca.

†† Univ. de Montréal, Mtl, Quebec H3C 3J7.

1. B.A. Harmon *et al.*, Phys. Lett. B235, 234(1990).

Kinematic Signatures of the Projectile Breakup Process at 32.5 MeV/nucleon*

*B. A. Harmon†, J. Pouliot‡, J. A. López§, J. Suro, R. Knop**, Y. Chan, D. E. DiGregorio††, and R. G. Stokstad*

In binary sequential decay there is sufficient time between the successive emission of particles to render them independent except for the constraints imposed by conservation laws. In multifragmentation the nucleus breaks up into three or more particles simultaneously and each particle can be influenced by the motion of the other particles through mutual Coulomb repulsion. López and Randrup have suggested the possibility of distinguishing between these two mechanisms on the basis of different kinematic signatures, and have developed a numerical model for each extreme[1].

We have studied projectile breakup reactions in the $^{16}O+^{197}Au$ system at 32.5 MeV/nucleon using an array of 34 phoswich detectors. The first kinematical correlation we examine is the distribution of relative angles between fragments, taken pairwise, in the rest frame of the primary nucleus. The simplest case is the mass-symmetric exit channel $^{16}O \Rightarrow$He-He-He-He. The figure shows the experimental distribution of relative angles for this channel. The calculations for sequential decay and multifragmentation, normalized by the ratio of calculated events to experimental events (after filtering through the experimental device), are also shown. It can be seen that the Monte Carlo calculation for sequential decay produces a shape very much like the experimental distribution.

A sphericity-coplanarity analysis[1] has also been performed to compare the experimental results with those of the two decay mechanisms. Multifragmentation tends to produce a more uniform distribution of fragment momenta (sphere-like), whereas a sequential decay yields a more elongated distribution (rod-like). A quantitative comparison of the two models with the experimental results is given in Table I for three exit channels. The average values before and after filtering are listed for each channel. The agreement between the filtered sequential decay calculation and the experiment is generally excellent.

Given this and the general agreement with the sequential decay calculations, we conclude that the present comparison of theory with experiment does not provide any evidence for multifragmentation of the projectile.

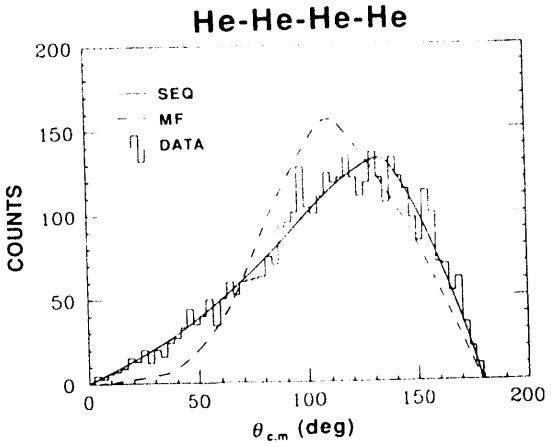

Footnotes and References

* Condensed from Phys. Lett. B235, 234(1990).

Present addresses:
† Space Science Laboratory, NASA, Marshall Space Flight Center, Huntville, AC 35812.
‡ Laboratoire de Physique Nucléaire, Université Laval, Québec, G1K7P4, Canada.
§ Dept. of Physics, Univ. of Texas at El Paso, Tx.
** Dept. of Physics, Caltech, Pasadena, Ca.
†† Departamento de Fisica-TANDAR, CNEA 1429 Buenos Aires, Argentina and CONICET.

1. J. Lopez and J. Randrup, Nucl .Phys. A491, 477 (1989).

	B-He-H		He-He-He-He		He-He-He-H-H	
	SPH	COP	SPH	COP	SPH	COP
MF	.138±.002	.068±.001	.291±.003	.140±.001	.231±.004	.094±.002
SEQ	.070±.002	.033±.001	.190±.003	.097±.002	.163±.005	.075±.003
DATA	.122±.003	.055±.001	.191±.004	.101±.002	.168±.006	.080±.003

Table I. Average Values of Sphericity-Coplanarity

Multiple Breakup of ^{20}Ne at 26.2 MeV/A in Peripheral Reactions

*J. Suro P., Y. Chan, D.E. DiGregoriott, A.B. Harmont, R. Knop§, J. A. López**, J. Pouliot‡, R.G. Stokstad, S. Houde‡, L. Potvin‡, R. Roy‡ and C. St. Pierre ‡.*

We have been studying the breakup of excited projectile-like nuclei resulting from peripheral reactions. The decay of ^{20}Ne at 26.2 MeV/A has been analyzed; this is the heaviest projectile we have studied, with a consequent higher number of possible decay channels. The detector array consisted of 48 plastic phoswiches that covered an area of 35°x35°, plus 6 position-sensitive phoswich strips covering an additional 15° at both sides of the main array.

Several peripheral channels have been investigated; in all of them the channel was selected by requiring the sum of charges be equal to the beam charge and the center of mass velocity be close to that of the beam.

We have focused on a comparison of the kinematical observables for channels of multiplicity 3, 4 and 5 with the corresponding calculations given by models for multifragmentation and sequential decay. In a first series of calculations, we used the model by López and Randrup[1]. As in the case of ^{16}O breakup[2], the comparison between ^{20}Ne breakup channels and the sequential counterpart in the calculation compared well for some channels and fair for others. Figure 1 shows a distribution of sphericity and coplanarity coordinates for the He+He+He+He+He events generated with the López code and the one obtained from the experiment. The qualitative comparison of the sequential calculation and experiment is quite favorable. The centroids of the three distributions are also indicated in the plots; the values of the centroids for sequential calculation and experiment are remarkably close.

Footnotes and References.

††Departamento de Física-TANDAR, CNEA 1429 Buenos Aires, Argentina and CONICET.

† Space Science Laboratory, NASA, Marshall Space Flight Center, Hunsville , AL 35812.

§Dept. of Physics, Caltech, Pasadena, CA.

**Dept. of Physics, Univ. of Texas at El Paso, TX.

‡Laboratorie de Physique Nucléaire, Université Laval, Québec, G1K7P4, Canada.

1. J.A. López and J. Randrup, Nucl. Phys. **A 491** (1989) 477.

2. B.A. Harmon et al. Phys. Lett. **B 235** (1990) 234.

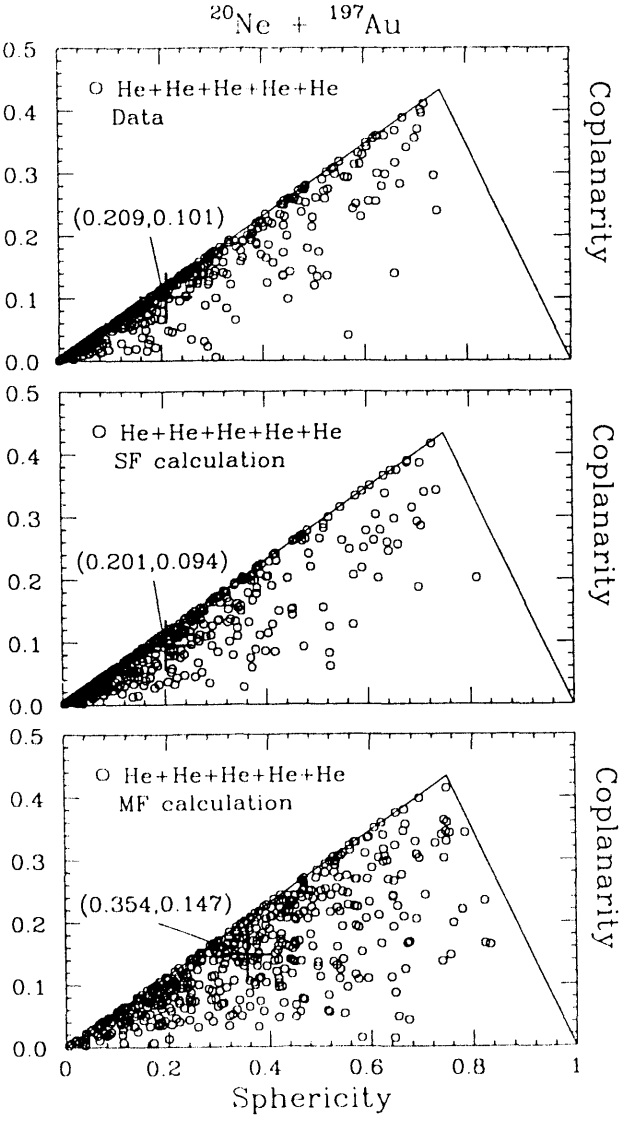

Fig. 1. Sphericity vs. Coplanarity plots. From top to bottom: experimental distribution, sequential fission calculation, and multifragmentation calculation. The calculations were obtained using López 'code (ref. 1)

^{15}N-Induced Charge Pickup Reactions on ^{27}Al and ^{208}Pb Targets at 28.3 MeV/nucleon

Y. Chan, D.E. DiGregorio††, A.B. Harmon†, R. Knop§, J. Pouliot‡, R.G. Stokstad, J. Suro, P. S. Houde‡, L. Potvin‡, R. Roy‡, and C. St. Pierre ‡

The cross section for charge pickup can be strongly influenced by the reaction Q-value, the nucleon density distribution at the surface of the nuclei, as well as by differences in the n-n, n-p, and p-p scattering cross sections. The interplay between these various factors at intermediate bombarding energies remains to be explored. It is also known that nucleon-pickup reactions can produce highly excited projectile-like fragments. Since primary fragments from a peripheral reaction can be characterized reliably via kinematic reconstruction techniques, the excitation and de-excitation of the fragments can be studied in detail. Due to the relatively high excitation energy resulting from the transferred mass, multi-particle exit channels are important and secondary particles have to be detected.

A plastic scintillator phoswich array of 48 elements has been used to study charge pickup reactions induced by ^{15}N projectiles on targets ranging from ^{27}Al to ^{209}Bi. Only charged particles were detected. The thickness of the scintillators has been optimized for beam velocity particles. ^{15}N was chosen as an acceptor nucleus because of its favorable Q-value for single proton pickup. The figure shows the observed yields for different decay channels resulting from a Z_{PLF}=9 fragment (picking up 2 charges from the ^{208}Pb target nucleus) as a function of the Q_{gg} values for the corresponding decay channels. Channels with charge multiplicties ranging from 2 to 6 are included. The data display an approximate exponential correlation with Q_{gg}, very similarly to those observed in inelastic scattering where the net charge gain is zero. Also shown in the figure are calculations performed with the sequential binary-decay code Brandex[1]. An exponential primary energy distribution, $p(E^*) \propto \exp(-E^*/E_0)$, and a high energy cut-off parameter, E_{cutoff}, have been used in the calculations. Curve 1, corresponding to E_0=40 MeV and E_{cutoff}=150 MeV, is a best fit to the data. The yields at large negative Q values are found to be very sensitive to the E_{cutoff} parameter used. Another calculation (curve 2), performed with parameters taken from inelastic scattering systematics with softer excitation energy distribution (E_0=10 MeV) and lower E_{cutoff} (=120 MeV) parameters, underpredicts the large negative Q_{gg} yields drastically. This is consistent with mass pickup as an efficient mechanism in generating internal excitation energy. Investigations of the possible dependence of the cross sections on structural properties of the target nuclei are in progress.

Footnotes and References

††Departamento de Física-TANDAR, CNEA 1429 Buenos Aires, Argentina and CONICET.
† Space Science Laboratory, NASA, Marshall Space Flight Center, Huntsville , AL 35812.
§Dept. of Physics, Caltech, Pasadena, CA.
‡Laboratorie de Physique Nucléaire, Université Laval, Québec, G1K7P4, Canada.

1. R. Knop and R.G. Stokstad, LBL-26439 (1988).

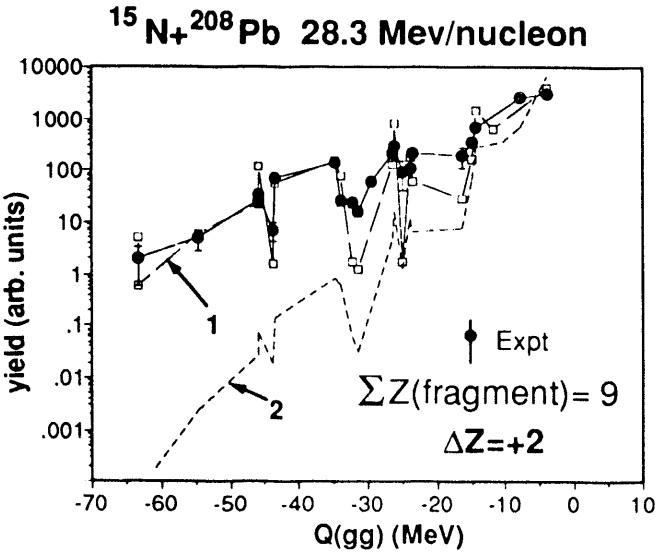

Multiple particle final states from the $^{16}O+^{12}C$ reaction at 32.5 MeV per nucleon.

J.A. Scarpaci, Y. Chan, D. DiGregorio†, B.A. Harmon‡, J. Pouliot§, R.G. Stokstad, and J. Suro

Our previous experiments(1) on the decay of the projectile in reactions such as $^{16}O+^{197}Au$ at 32.5 MeV per nucleon showed that the breakup process was in good agreement with sequential decay and did not reveal any evidence for prompt decay (multifragmentation). A new experiment concentrating on central collisions has been performed in which a minimum multiplicity of six particles per event was required. In this case many mechanisms can be involved even in a reaction between two such light nuclei. Disentangling these mechanisms in difficult, but the comparison with dynamical calculations can result in a better understanding of the reaction.

The experimental set up consisted of an array of 58 plastic phoswich detectors covering a total solid angle of 1 steradian at forward angles. The charge and energy of nuclei up to carbon were identified. The masses were taken to be those of the most tightly bound isotope.

The figure shows the laboratory velocity of the center of mass (CM) of the detected fragments in events for which the total detected charge (TDC) equals that of the projectile. Statistical model calculations (broken lines, code Gemini) are shown for the fusion of the projectile with portions of the target to form ^{20}Ne, ^{22}Na, ^{24}Mg and ^{28}Si. The events are then filtered through the detector. Undetected particles might have missed the array, had too low energy, or have been neutrons. The velocity and excitation energy of these nuclei correspond to incomplete fusion, with the target remnant at rest with no excitation energy. The normalisationin the figure is a best fit to the data. Because of the high multiplicity requirement, no significant decay of ^{16}O is seen. Most of the events arise from incomplete fusion.

Similar calculations have been fitted to CM velocity spectra of higher TDC. The normalisation factors are strikingly similar when comparing fits of different spectra up to TDC equal to 11. For higher TDC, however, fits are not as good. The data indicate a larger number of events at high CM velocity, suggesting that the emitting nucleus was moving faster than calculated. In order to produce faster nuclei with Z≥12, the projectile has to pick up less mass for the same amount of charge, giving rise to nuclei such as ^{22}Mg or ^{24}Si.

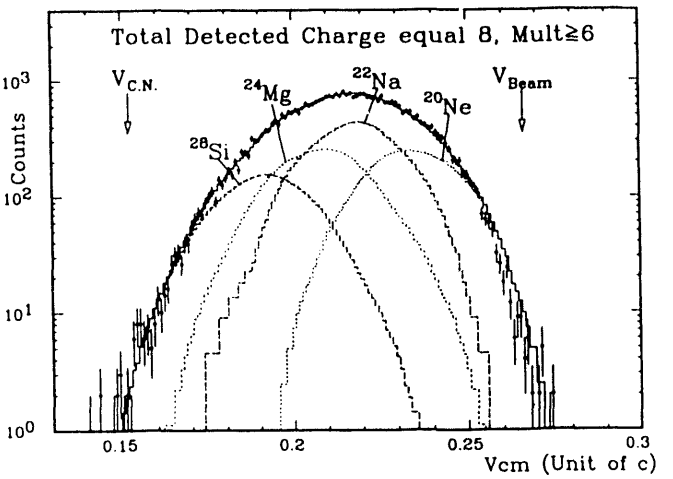

More work has to be done to confirm this trend. However, cross sections for different incomplete fusion channels can already be deduced from the fit of the lower TDC spectra. Furthermore, sphericity and coplanarity analyses(2) can be performed for all these events. Also, gates may now be set on the CM velocity in order to preferentially select the primary nuclei.

Present addresses:

† Departamento de Fisica-TANDAR, CNEA 1429 Buenos Aires, Argentina and CONICET.

‡ Space Science Laboratory, NASA, Marshall Space Flight Center, Huntville, AC 35812.

§ Laboratoire de Physique Nucléaire, Université Laval, Québec, G1K7P4, Canada.

References:

1. B.A.Harmon et al. Phys. Lett. B235, 234 (1990).

2. J. Lopez and J. Randrup, Nucl Phys. A491,477 (1989).

Cluster Structure in $^{24}Mg^*$

*J.T. Murgatroyd,† S.J. Bennett,† B.R. Fulton,† W. D. M. Rae,‡ N. S. Jarvis,§ D. L. Watson,§ J. A. Scarpaci, D.E. DiGregorio, J. Suro, Y.D. Chan, and R. G. Stokstad***

We are investigating cluster structure in the continuum of ^{24}Mg via the alpha-particle pickup reaction $^{12}C(^{20}Ne, ^{24}Mg^*)^8Be$ in which we detect the decay of $^{24}Mg^*$ to $^{12}C+^{12}C$. This reaction should select states in ^{24}Mg that have cluster components of both $\alpha + ^{20}Ne$ and $^{12}C + ^{12}C$. This study is motivated by the earlier observation of $^{12}C+^{12}C$ breakup following scattering with a ^{24}Mg beam in experiments at Berkeley and Daresbury.[1,2] Subsequent measurements have revealed that the breakup occurs from a series of states in ^{24}Mg which form a rotational sequence.[3] The moment of inertia of this band indicates a large moment of inertia and is consistent with isomeric states in highly deformed secondary minima in the ^{24}Mg potential energy surface at an axis ratio of 3:1.[4] The purpose of the present study is to determine whether the same states could be formed via alpha pickup.

The experimental arrangement consisted of six position sensitive (in X and Y) ΔE-E telescopes mounted in groups of three on opposite sides of the beam axis. The beam energy was 8 MeV/nucleon and the target was a carbon foil of 240 $\mu g/cm^2$. A measurement of the total energy of the two ^{12}C nuclei is sufficient to separate the events for which both ^{12}C nuclei and the ^8Be nucleus are in their ground state. After selecting these Q_{ggg} events, we calculate the relative energy of the two fragments, which gives directly the excitation energy in ^{24}Mg before it breaks up. This spectrum, shown in fig. 1, exhibits a series of narrow states in ^{24}Mg up to an excitation energy of 33 MeV. This extends well above the excitation region (20-23 MeV) where C+C states were seen following the breakup of a ^{24}Mg beam. The cross sections for producing these states in the present reaction is enhanced over that of projectile breakup. The large number of angle settings possible with the six telescopes yields data over a large angular range and it will be possible to make spin assignments for the angular correlation information. The bracketed assignments in fig. 1. are preliminary, but it is clear that the states have relatively high spin.

Footnotes and References

*Supported by the U. S. Dept. of Energy under Contract No. DE-AC03-76SF00098 and by a travel grant from NATO.

† Dept. of Physics, Univ. of Birmingham, UK.
‡Nuclear Physics Lab., Oxford Univ., UK.
§Dept. of Physics, Univ. of York, UK.

1. J. Wilczynski, et al., Phys. Lett. **181B,** 229 (1986).
2. B. R. Fulton, et al., Phys Lett. **181B,** 233 (1986).
3. M. Freer, et al., Proc. Workshop on Nucl. Struct and Heavy-ion React. Notre Dame, May, 1990.
4. G. Leander and S. Larsson, Nucl. Phys. **A239,** 93 (1975)

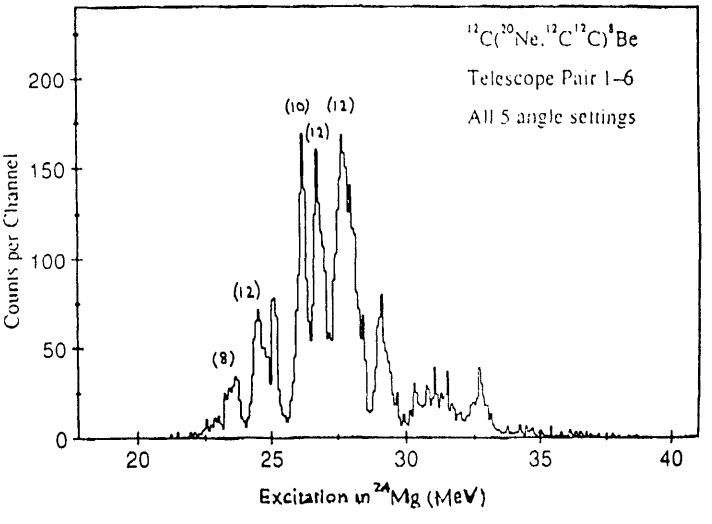

Fig. 1. Spectrum of excitation energy in ^{24}Mg for states decaying to $^{12}C+^{12}C$. Values in parenthesis are preliminary spin assignments.

Angular momentum in sub-barrier fusion: Experimental study using the isomer ratio $^{137}Ce^{m}/^{137}Ce^{g}$ *

D.E. DiGregorio,† K.T. Lesko, B.A. Harmon‡ E.B. Norman, J. Pouliot,§ B. Sur, Y. Chan, and R. G. Stokstad

We have measured the ratio of the yields for the isomer ($J^{\pi}=11/2^{-}$,$t_{1/2}$=34.4 h) and ground state ($3/2^{+}$, 9.0 h) of ^{137}Ce produced in the subbarrier fusion reactions ^{128}Te(^{12}C,3n), ^{133}Cs(^{7}Li,3n), and ^{136}Ba(^{3}He,2n) by observing the delayed x- and γ-rays emitted in the decay of these states. The isomer ratio, R, was determined by fitting the time dependence of these radiations and is shown in Fig. 1 as a function of bombarding energy relative to the Coulomb barrier. We deduce the average angular momentum, <J> from R with a statistical model[1]. The values of <J> exhibit the behavior predicted for the average angular momentum (solid lines) at low energies and the expected variation with the reduced mass of the entrance channel[2]. Fig. 2 shows the valuse of <J> as a function of excitation energy in the compound nucleus. These measurements are of interest because they demonstrate the existence of a finite average angular momentum at bombarding energies well below the barrier in contrast to the S-wave approximation, which is valid for neutrons. They are also relevant for a current problem in subbarrier fusion, namely that the angular momenta deduced from fission fragment anisotropies disagree with theory and are inconsistent with the slopes of the excitation functions. The isomer ratio method provides a third, and independent method (in addition to gamma-ray multiplicity and fission fragment angular correlations) for determining angular momenta. In the present case we have seen that the angular momenta and the excitation functions are consistent. These results are described in detail in ref 4.

Footnotes and References

*Supported by the U. S. Dept. of Energy under Contract No. DE-AC03-76SF00098

† Permanent address: TANDAR, CNEA, Buenos Aires, Argentina

‡Present address: NASA -Marshall SFC, Alabama

§Present address: Laval U. Montreal, Canada

1. R.G. Stokstad, *et al.*, Phys. Rev Lett. **62**, 399 (1989).

2. C. Dasso and S. Landowne, Phys. Rev. **C32**, 1094 (1985).

3. R. Vandenbosch, Proc. Symp., Legarno, Italy, June 1988, ed. by C. Signorini, et al., Lect. Notes in Phys. **317**, 157 (Springer Verlag, 1988).

4. D. Digregorio, *et al.*, Phys. Rev. **C42**, 2108 (1990).

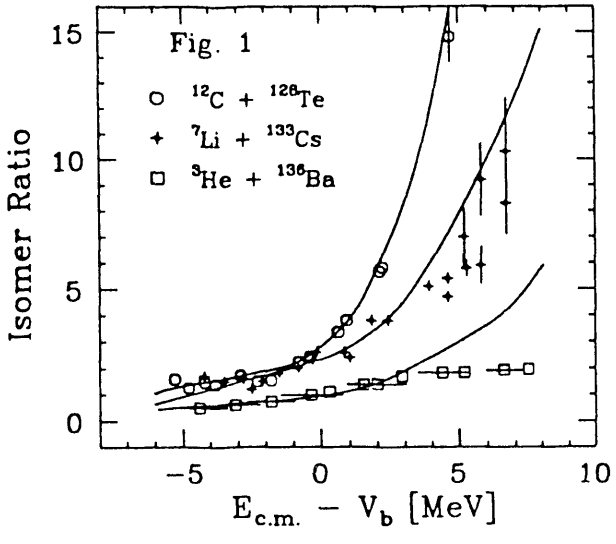

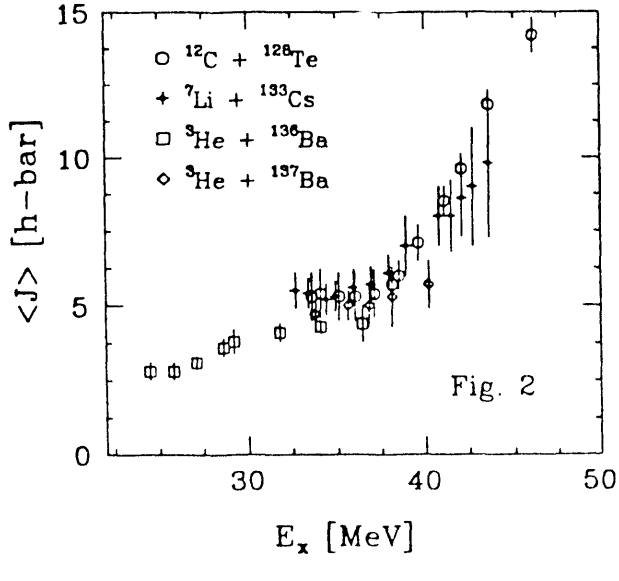

Fusion Cross Sections for $^{12}C + ^{128}Te$ and the Deduction of Absolute Average Angular Momenta*

D.E. DiGregorio,† Y. Chan, E. Chavez,‡ A. Dacal,‡ M.E. Ortiz,‡ J. Suro, and R.G. Stokstad

We have measured the fusion cross sections for $^{12}C + ^{128}Te$ at Ec.m. = 40.4 - 56.6 MeV by direct detection and identification of evaporation residues using a time-of-flight technique. Two position sensitive multiwire proportional counters (MWPC) were used in coincidence with each other and with the pulse structure of the beam (Fig.1). From the absolute cross sections well above the barrier we deduced the absolute angular momenta (Fig. 2) using the sharp cutoff approximation and, thereby, obtained an independent check of the isomer ratio method[1]. The present measurements, along with those reported in Ref. 1 also confirm that the energy dependence for both $\sigma_{fus}(E)$ and absolute values for <l> are self-consistent and well described by theoretical calculations. These results are presented in detail in Ref. 2.

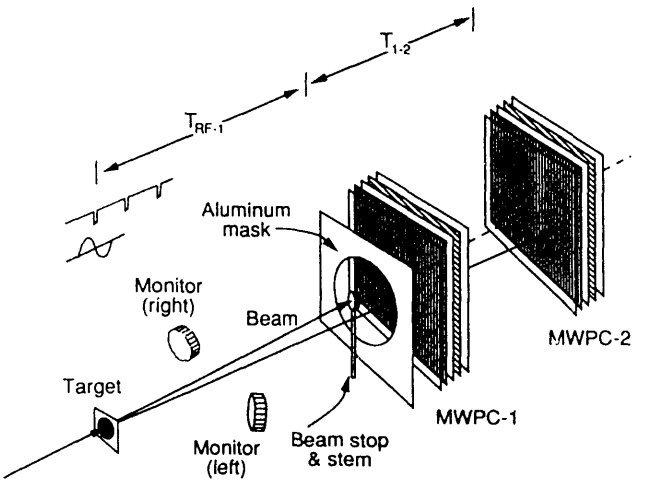

Fig. 1. Schematic of the experimental setup .

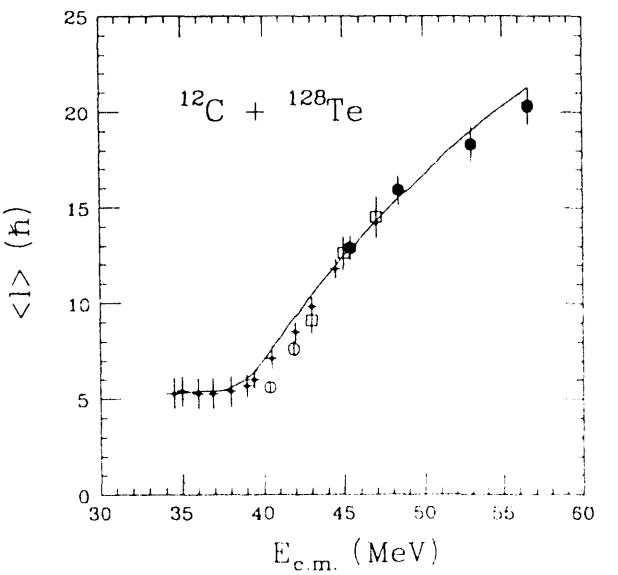

Fig. 2. Average angular momenta from present work (solid and open circles) and from isomer ratio measurements (Ref. 1).

Footnotes and References

*Supported by the U. S. Dept. of Energy under Contract No. DE-AC03-76SF00098

† Permanent address: TANDAR, CNEA, 1429 Buenos Aires, Argentina

‡ IFUNAM, Mexico D.F. 01000, Mexico.

1. R.G. Stokstad, *et al.*, Phys. Rev Lett. **62**, 399 (1989); D.E. Digregorio, *et al.*, Phys. Rev. **C42**, 2108 (1990).

2. D.E. DiGregorio, et al., Phys. Rev. **C43**, 687 (1991).

Systematic Analysis of Average Angular Momentum and Cross Sections in Subbarrier Fusion*

D.E. DiGregoriot and R.G. Stokstad

The moments of the angular momentum distributions leading to fusion have been studied by three different experimental techniques: γ-multiplicity, fission fragment angular distributions[1], and very recently by measurements of isomer ratios[2]. We present, following Ref. 1, all the available data on the first or second moments of the spin distributions leading to fusion and compare them with theory. All these calculations use the coupled channels code CCFUS[3]. In addition we analyze the corresponding experimental cross sections. We find that when theory underestimates cross section it usually enderestimates angular momentum, except for the fission fragments. This systematic overview suggests that the origin of the discrepancy in the latter case may lie in the deduction of the angular momentum from the measured fission fragment angular distribution. These results are described in detail in Ref. 4.

Footnotes and References

*Supported by the U. S. Dept. of Energy under Contract No. DE-AC03-76SF00098

† Permanent address: TANDAR, CNEA, Buenos Aires, Argentina

1. R. Vandenbosch, Proc. Symp., Legarno, Italy, June 1988, ed. by C. Signorini, et al., Lect. Notes in Phys. **317**, 157 (Springer Verlag, 1988).

2. R.G. Stokstad, *et al.*, Phys. Rev Lett. **62**, 399 (1989); D.E. DiGregorio, *et al.*, Phys. Rev. **C42**, 2108 (1990).

3. C. Dasso and S. Landowne, Comp. Phys. Comm. **B46**, 187 (1987).

4. D.E. Digregorio and R.G. Stokstad, Phys. Rev. **C43**, 265 (1991)

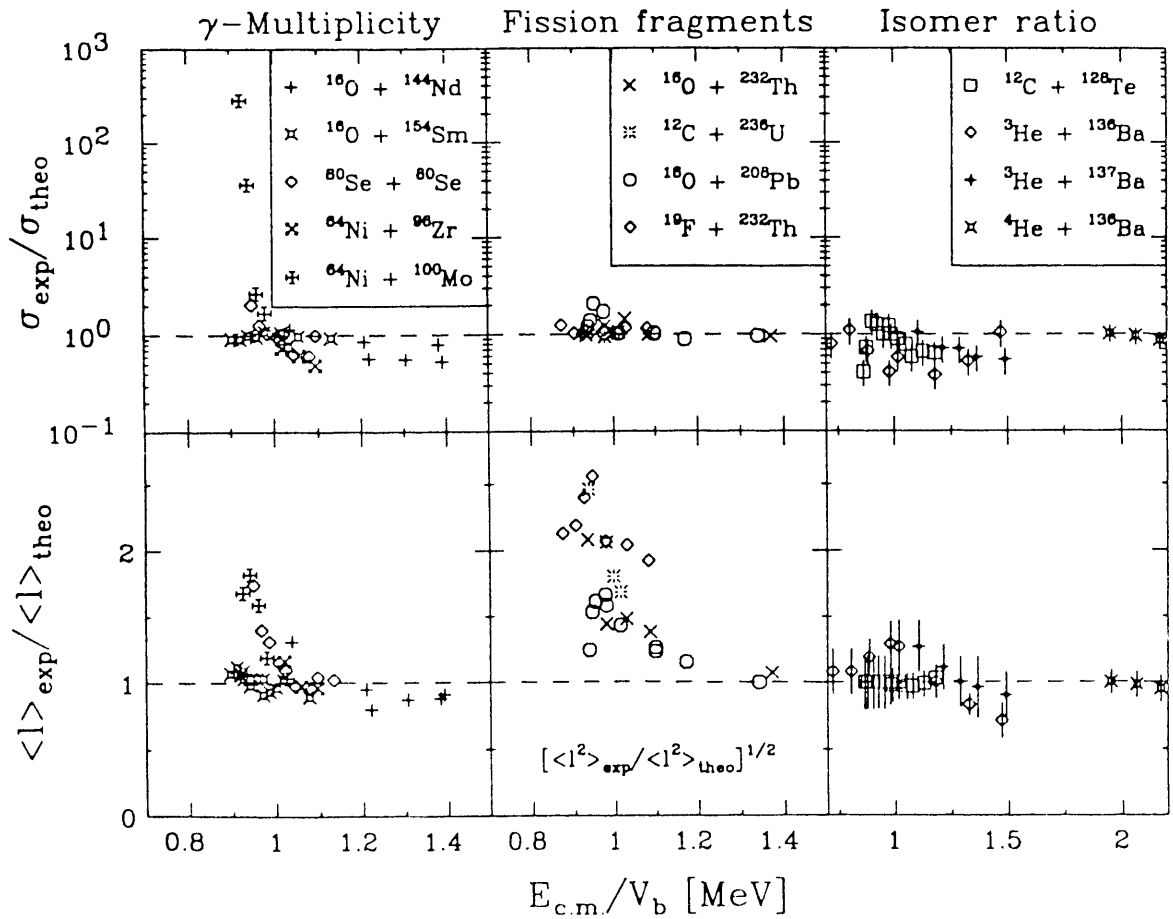

Angular Momentum Bearing Modes in Fission*

Luciano G. Moretto, Graham F. Peaslee[a] and Gordon J. Wozniak

The appreciation of the role of angular momentum in fission can be described as a punctuated evolution of ideas. The discovery of a critical stage in fission, involving the passage of the system through a deformed configuration (saddle point) by the negotiation of a barrier, brought to light the associated "rigid" rotational modes. The application of angular momentum to one such mode, through rotation about an axis perpendicular to the elongation axis, led to the conclusion that fission barriers would decrease and eventually vanish with increasing angular momentum.

The analogy of the axially symmetric nucleus at the saddle point with deformed ground state nuclei suggested a "rotational" spectroscopy in the saddle-point transition state. The assumption of conservation of the K quantum number from saddle to scission prompted attempts to study this spectroscopy by means of fission-fragment angular distributions. At higher excitation energies the introduction of the statistical distribution in K quantum numbers and the connection of its variance (K_0^2) to the nuclear temperature and the principal moments of inertia at the saddle point led to the classical theory of fission-fragment angular distributions.

The possibility that other intrinsic angular-momentum-bearing modes could be active in the fission process surfaced with the early observation of a sizeable amount of angular momentum in fission fragments from the spontaneous fission of ^{252}Cf. The magnitude of the fragment angular momentum ($7\hbar$ / fragment) despite the 0^+ ground state of the parent suggested a prescission origin and thus the involvement of non-rigid modes.

Deeply inelastic reactions showed that the entrance-channel orbital angular momentum could be dissipated in a continuous fashion all the way down to the rigid rotation limit. This implied the existence of an intrinsic mode coupling the orbital angular momentum to the spins of both fragments. The "wriggling" mode, described below, satisfies this requirement. Further studies of the magnitude of the fragment spins by means of γ-ray multiplicity measurements suggested that the fragments had angular momenta in excess of what was expected from rigid rotation. The explanation was found in the (diffusive or thermal) excitation of additional intrinsic angular-momentum-bearing modes.

A beautiful confirmation of the excitation of these modes came from the misalignment of the fragment spins. Misalignment was shown to arise from the coupling of the aligned angular momentum component associated with rigid rotation to that associated with the random fluctuations of those intrinsic modes, whose angular momentum is perpendicular to the rigid rotation component.

Finally, in recent times there has been a revisitation of the rigid rotation modes in the study of fission-fragment angular distributions associated with heavy-ion-induced fission. These studies have demonstrated that the K quantum number may not be frozen at the saddle point after all, but may be determined at scission, or somewhere in between. This opens up a problem that has never been truly solved, namely whether this and the other angular-momentum-bearing modes are thermally or dynamically excited, and, if they are thermally excited, whether the statistical equilibrium relevant for the description of the various observables is at the saddle or at the scission point. So, despite the large amount of work performed in the first half century of fission, there seems to be enough work left for a second half century.

Footnotes and References

*Condensed from Nucl. Phys. **A502** 453c (1989)

[a]NSCL, MSU, E. Lansing, MI 48824

Fission Throughout the Periodic Table*

Luciano G. Moretto and Gordon J. Wozniak

The answer to the simple question "What is fission?" is not unique but depends upon the space and time cross section of the scientists to whom the question is addressed. Before 1939, fission was still in imaginary space. It soon emerged into an altogether too real world by virtue of two chemists who dared thinking the unthinkable. Even today many of our physics colleagues think of fission as a peculiar reaction occurring around uranium, a somewhat embarassing process that gave and still gives us a bad reputation; then with nuclear bombs, now with nuclear energy.

Even among "experts," fission is typically associated with heavy elements. If its presence is acknowledged, as far down as the Lead region and even lower, its existence becomes progressively more evanescent as one moves farther down the periodic table and its cross section becomes lost in the abyss of nanobarns. Most emphatically, fission is believed to be a unique kind of compound nucleus (CN) reaction when compared with the more commonplace decays, like those involving the emission of protons, alphas and other "particles." Fission appeared so different from the other modes of CN decay that a separate theory was devised to calculate its decay width. As a result, we now have one theory for "evaporation" and another for fission.

Yet, a typical mass distribution of fission fragments while peaked, at times sharply, at masses near the symmetric splitting, is nonetheless a continuous distribution for which there are no firm boundaries other than those set by the total mass of the system. In all fairness, the search for ever lighter (and heavier) fission products was actively pursued by radiochemists, who were eventually stopped only by the abysmally small cross sections. So the belief was consolidated that fission fragments were confined to a rather narrow range of masses, despite the occasional disturbing detection of intermediate mass or complex fragments like Na, Si, etc. in higher energy reactions.

Complex fragments made their grand entrance with intermediate-energy heavy ion reactions. In these processes, the elegant simplicity of quasi and deep inelastic processes is substituted by a glorious mess of products that seem to bear no relationship to either of the entrance channel partners. Their glaringly abundant production, together with the turbid experimental environment prevailing in early studies, prompted a tumultuous development of theories, claims and counterclaims about their origin and manner of production.

Fortunately, in spite of the confusion, it did not escape some perceptive members of our community that most, if not all of the complex fragments were associated with essentially binary processes. Furthermore, after an allowance was made for target and projectile-like fragments, the remaining fragments appeared to originate from the binary decay of an isotropic source. Finally, the excitation functions of these fragments appeared to behave in accordance with CN branching ratios. The inescapable conclusion was that CN decay was responsible for the production of these fragments by a mechanism able to feed all the possible asymmetries. Such a mechanism without undue strain of the imagination could be well identified with a generalized fission process.

In fact, the observed modulation of the mass distribution is a most revealing signature of the underlying potential energy as a function of mass asymmetry and underscores the essential unity of these processes.

Footnotes and References

*Condensed from LBL-27144. Proc. of the ANS Conf. on Fifty Years with Nuclear Fission. Gaithersburg, MD, April 1989.

Conditional Fission Barriers for ^{75}Br

D.N. Delis, Y. Blumenfeld, D.R. Bowman**, N. Colonna, K. Hanold, K. Jing+, M. Justice, J.C. Meng+, G.F. Peaslee** G.J. Wozniak, and L.G. Moretto*

The main objective of the present work is to provide, for the first time, a complete set of experimental asymmetric fission barriers for a single nucleus, against which macroscopic models can be tested. A nearly complete experimental ridge line of conditional barriers was obtained at zero angular momentum for ^{75}Br by studying the reaction ^{63}Cu + ^{12}C at 5.0, 6.2, 6.9, 8.0, 10.2 and 12.7 MeV/N.

Fragments with atomic numbers covering nearly the entire range of the mass-asymmetry coordinate (4<Z<27) were observed at all energies. An isotropic equilibrium component of the cross section was identified for all Z-values at all energies and was attributed to compound nucleus decay following complete fusion[1]. Energy spectra and angular distributions show the presence of projectile and target-like components along with the isotropic component. This last component appears as a Coulomb ring in the invariant cross-section plots indicating the presence of a binary decay which is confirmed by the coincidence data.

Excitation functions were constructed for each Z value[2]. The complex fragment excitation functions were analyzed within the framework of the statistical model by a means of two parameter fits. One of these parameters was the fission barrier and the other the ratio of the level density parameters at the saddle point (a_z) and at equilibrium (a_n). Excellent agreement was obtained for all Z values. Figure 1 shows the conditional fission barriers and ratio of the level density parameters, extracted from fitting the excitation functions as a function of the fragment charge or asymmetry, Z/Z_{cn}. (Z/Z_{cn} = 0.5 corresponds to symmetric splitting.) Excellent agreement is obtained between the experimentally determined barriers and the finite range model predictions, thus justifying the need to include finite range and surface diffuseness refinements in the liquid drop model.

Footnotes and References

*Institut de Physique Nucl aire, Orsay, France
**NSCL, MSU, East Lansing, Michigan
+Institute of Atomic Energy, Beijing, China

1. H. Han et al., Nucl Phys. A492, 138 (1989)
2. D.N. Delis et al., accepted, Z. Phys. A (1991)

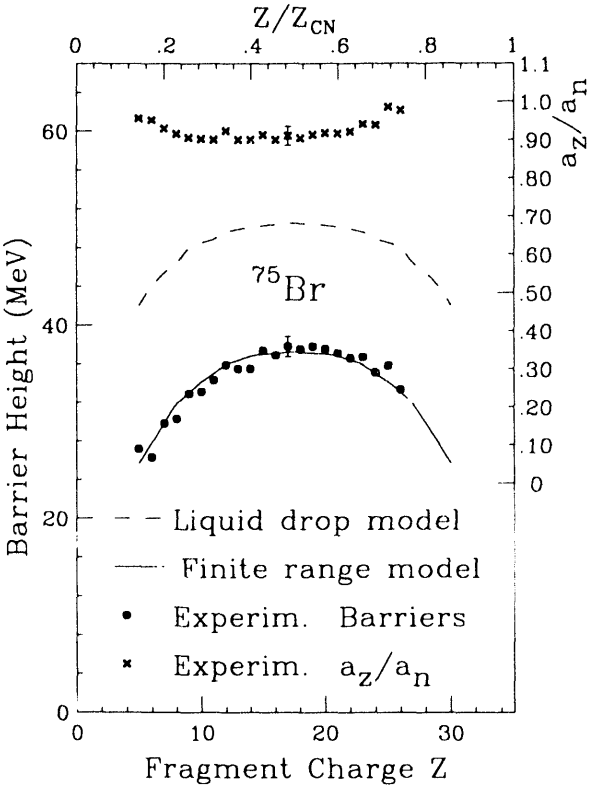

Fig. 1. The points are the extracted barriers and the errors arising from the $\chi 2$ of the fitting procedure are smaller than the size of the points. The single error bar shown is the overall uncertainty assigned to the barriers. The predicted values from the finite range model and the liquid drop model are shown by the solid line and dashed lines respectively.

Complex Fragment Emission in 12.6 MeV/u ^{63}Cu-Induced Reactions on ^{12}C and ^{27}Al Targets*

H. Y. Han[a], K. X. Jing[a], E. Plagnol[b], D. R. Bowman[c], R. J. Charity[d], L. Vinet[e], G. J. Wozniak, and L. G. Moretto

Complex fragments from the 12.6 MeV/u ^{63}Cu + ^{12}C, ^{27}Al reactions were investigated. In singles measurements a projectile-like and/or a target-like component was observed along with an isotropic component for both systems.

The coincidence data confirm the finding from the singles data that the process is essentially binary in nature. All the coincidence events lie in a narrow region of the Z_1 - Z_2 plane, quite close to the sum of the target and projectile Z values.

The $Z_1 + Z_2$ spectra for the two reactions are shown in Fig. 1. The relatively sharp peaks positioned near the total charge of the system indicate the binary nature of the reaction. Similar features are shown by the corresponding spectra calculated with the GEMINI code, although the experimental spectra are somewhat broader than the calculations. For ^{63}Cu + ^{12}C system, the peak of the $Z_1 + Z_2$ distribution is located at about 32.3, while the peak is at 36.7 for ^{63}Cu + ^{27}Al reaction. The atomic numbers of the corresponding compound nuclei are 35 and 42. The difference between the measured total charge and the compound nucleus atomic number can be attributed to light charged particle evaporation before and after the major binary decay. The charge lost is about 3 for the ^{63}Cu + ^{12}C reaction, whereas it is about 5 for the ^{63}Cu + ^{27}Al reaction.

Light particle evaporation strongly depends on the excitation energy of the compound system. The calculated excitation energies are about 132 MeV and 234 MeV for reactions using ^{12}C and ^{27}Al targets, respectively. The ratio of these excitation energies is quite close to the ratio of 5/3 for the charge lost in ^{63}Cu + ^{27}Al reaction to that in ^{63}Cu + ^{12}C reaction. Thus it appears that the charge lost is approximately proportional to the excitation energy as expected from statistical decay theory.

Footnotes and References

*Condensed from Nucl. Phys. A**492**, 138 (1989).

[a]Institute of Atomic Energy, Beijing, China
[b]GANIL, B.P. 5027-14021, Caen Cedex, France
[c]*NSCL, MSU, E. Lansing, MI 48824*
[d]Washington University, St. Louis, MO 63130
[e]CERN, Division EP, Ch-1211, Geneva 23, Switzerland

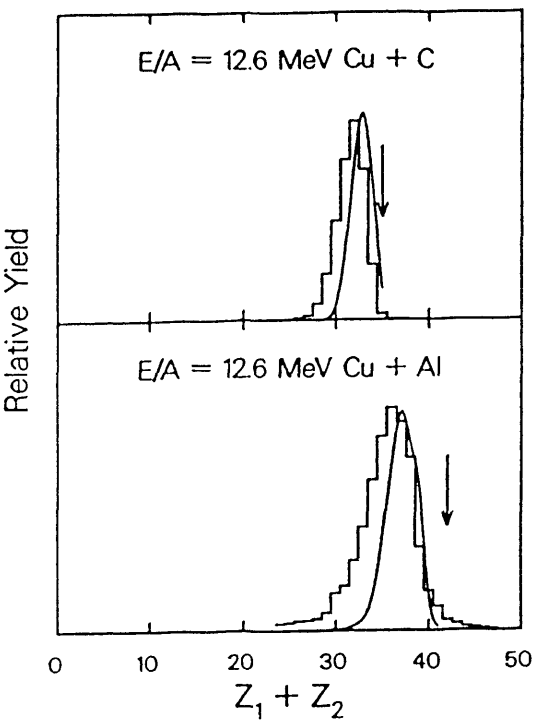

Fig. 1. The relative yield of coincidence events (histogram) plotted as a function of the sum of the atomic charges of the two coincident fragments. The solid curve was calculated with the evaporation code GEMINI. The vertical arrows indicate the atomic numbers of the compound nuclei.

Sources of Complex Fragment Emission in La-Induced Reactions at E/A = 14.7 and 18.0 MeV*

R. J. Charity[a], K. X. Jing[b], D. R. Bowman[c], M. A. McMahan, G. J. Wozniak, L. G. Moretto, N. Colonna, G. Guarino[d], A. Pantaleo[d], L. Fiore[d], A. Gobbi[e] and K. D. Hildenbrand[e]

Complex fragments with $4 \leq Z \leq 50$ have been detected in the reactions of $^{139}La + ^{12}C$ and ^{27}Al at E/A = 14.7 and 18.0 MeV. From the measured angular distributions, the cross sections for the isotropic, target-like and projectile-like components were extracted.

To address the question of the degree of equilibration of the intermediate systems, one needs to compare the experimental data to the predictions of the statistical model. To this end, statistical calculations were performed with the Monte Carlo computer code GEMINI[1]. This code simulates the decay of a compound nucleus via a series of binary decays. All possible binary divisions of the system from light particle emission to symmetric fission are allowed at each decay step. After each binary division, the decay of the resulting fragments is followed until all the available excitation energy is exhausted.

The calculated charge distributions are compared with the experimental data in Fig. 1. The experimental charge distributions are adequately reproduced by the statistical model. This is the strongest evidence for the formation of compound nuclei in these reactions. One should note that complex fragment emission is still a relatively rare occurrence. Most of the compound systems formed in these $^{139}La + ^{12}C$ reactions decay only by light particle emission. Thus, the majority of the predicted yield falls in the evaporation residue peak. This peak is associated predominantly with "classical evaporation residues", which result from systems that decay only via the evaporation of $Z \leq 2$ particles. The predicted cross sections for "classical evaporation residues" are indicated by the dashed histograms in Fig. 1 and the total cross section for these events accounts for 85% of the initial fusion cross section in the simulations. At the other extreme, the predicted cross section for ternary and higher order complex fragment events is very small < 1 mb at both bombarding energies. Apart from these very rare events, the simulated yield for $3 < Z < 50$ is associated with binary complex fragment events.

Footnotes and References

*Condensed from Nucl. Phys. **A511**, 59 (1990).

[a]Washington University, St. Louis, MO 63130
[b]Institute of Atomic Energy, Beijing, China
[c]NSCL, MSU, E. Lansing, MI 48824
[d]INFN, Bari 70126, Italy
[e]GSI, 6100 Darmstadt, Fed. Rep of Germany

1. R. J. Charity et al., Nucl. Phys. **A483** 371 (1988)

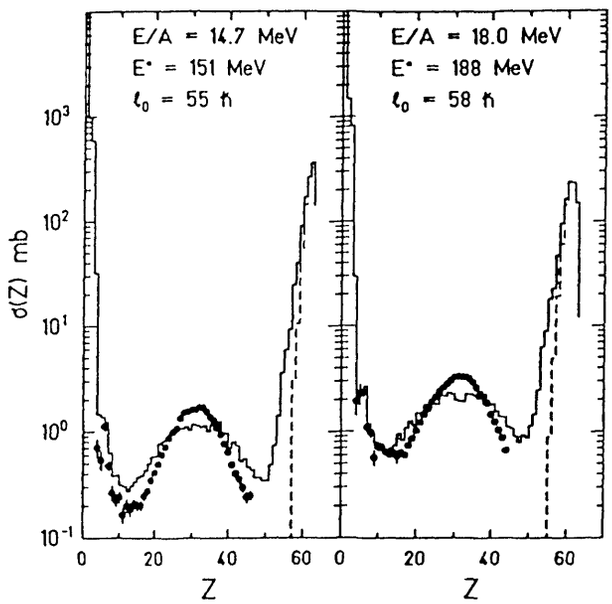

Fig. 1. Comparison between the experimental (data points) and predicted (histogram) charge distributions for the isotropic component of complex fragments emitted in the E/A = 14.7 and 18.0 MeV $^{139}La + ^{12}C$ reaction. The excitation energies and spin distribution parameters used in the GEMINI calculations are indicated.

Complex Fragments from Incomplete Fusion Processes*

N. Colonna, D. R. Bowman[a], R. J. Charity[b], L. Fiore[c], A. Gobbi[d], G. Guarino[c], K. Hildebrand[d], M. A. McMahan, L. Moretto, A. Pantaleo[c] and G.J. Wozniak

In very asymmetric target-projectile combinations the phenomenon of complex fragment emission has been associated with the binary decay of a single source with a well defined velocity, formed in complete [1] or incomplete [2] fusion processes. In such cases, a sharp isotropic Coulomb ring can be seen for all fragments, clearly indicating the compound nucleus origin of such fragments. This simple source pattern, though, disappears for more symmetric systems. We have studied the reaction ^{139}La + ^{64}Ni at 18 MeV/u to demonstrate that the only substantive change occurring in these more symmetric systems is the formation of a continuous range of sources associated with the full range of incomplete fusion processes.

Reaction products were detected with two position sensitive quad telescopes placed on either side of the beam, covering 20° in plane and 5° out of plane.

In Figure 1 the velocity spectrum of the centers of mass of the coincident fragments is shown for the ^{139}La + ^{64}Ni and, for comparison, ^{139}La + ^{12}C and ^{27}Al reactions. For these latter ones, the center-of-mass velocity spectra show a single sharp peak, corresponding to the center of mass of the entire system. For the ^{139}La + ^{64}Ni reaction one observes a similar peak, due to the complete fusion process, plus an additional shoulder that indicates the presence of a third body. This shoulder can be attributed to incomplete fusion processes extending over the entire impact parameter range.

By setting gates on the source velocity distribution for the ^{139}La + ^{64}Ni reaction, one can generate isotropic circular patterns similar to the Coulomb circles seen in the very asymmetric systems, but with their centers progressively shifted towards higher values of $v_{||}$. There is also a striking decrease in the radii of these Coulomb circles with increasing source velocity.

Even though the source velocity distribution is biased by the coincidence efficiency of the apparatus and broadened by the light-particle evaporation, it can be used to unravel the complexity of the ^{139}La + ^{64}Ni reaction, by selecting events with well defined source velocities.

Footnotes and References

*Condensed from Phys. Rev. Lett. 62, 1833 (1989)

[a]NSCL, MSU, E. Lansing, MI 48824
[b]Washington Univ., St. Louis, MO 63130
[c] INFN, 70126 Bari, Italy
[d]GSI, 6100 Darmstadt, West Germany

1. R. J. Charity et al., Nucl. Phys. A484, 371 (1988).
2. D. R. Bowman et al., Phys. Lett. B 189, 282 (1987).

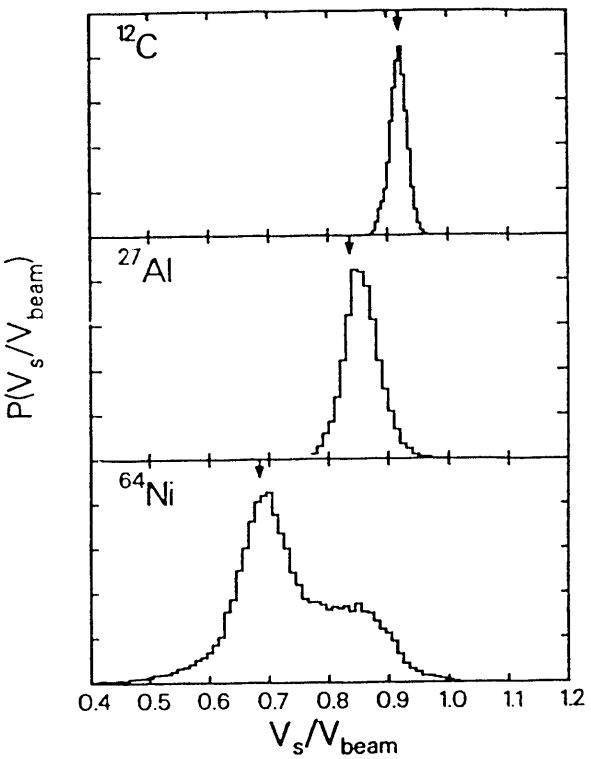

Fig. 1. Source velocity distributions for the 18 MeV/u ^{139}La + ^{12}C, ^{27}Al and ^{64}Ni reactions as extracted from the binary coincidences. The vertical arrows indicate the velocities corresponding to complete fusion for the three reactions.

Sputtering of Au, CsI, and $LiNbO_3$ by Multiply Charged Ar Ions*

D.L. Weathers,† T.A. Tombrello,‡ M.H. Prior,§ R.G. Stokstad, and R.A. Tribble **

The ionization potential energy carried by a slow, multiply charged ion can approach or even exceed its kinetic energy. The transfer of this potential energy to the atoms in a surface as the ion is neutralized may produce the same sorts of excitations in the target that give rise to electronic sputtering at higher projectile energies. Since the latter mechanism is known to exhibit a dependence on the charge state of the ion, it is of interest to establish whether the sputtering yield for highly charged ions at low kinetic energies exhibits similar effects.

The sputtering experiments were carried out in a cryopumped UHV chamber on a beam line at the ECR ion source associated with the 88-Inch Cyclotron. Argon ions with charge states of 4^+, 8^+, and 11^+ were accelerated to energies of 48 keV. The targets were mounted on an electrically isolated copper block and kept heated during and after an initial sputter cleaning. High purity Al foils mounted in a cylindrical geometry were used to catch the atoms sputtered from the surface. The number of incident ions was determined from the integrated charge. The total number of sputtered atoms was measured by Rutherford back-scattering of oxygen and chlorine ions (at the Caltech tandem accelerator) from the collector foils and by integrating the observed angular distribution.

The total sputtering yields, normalized to the yield for the 4^+ charge state, are shown in fig. 1. An indication of the reproducibility of the measurements is given by the two points for the 4^+ beam and the $LiNbO_3$ target. The absolute yields (atoms ejected per incident ion) were of the order of 0.5, 1250, and 9.7 for Nb, Cs, and Au, respectively, for the 4^+ charge state.

It is apparent from the results in the figure that no particularly dramatic dependence of the sputtering yields on charge state was observed. Even though the ionization potential energies varied from 144 to 578 to 2018 eV for the 4^+, 8^+, and 11^+ ions - the relative yields did not vary by more than about 15% and, in the case of Au, no change was observed at the level of 5% or less. (The latter result is consistent with earlier results.[1]) Given the velocities of the Ar ions ($5x10^7$cm/s) they are likely to be partially neutralized before penetrating the insulating targets. In this case it is difficult to ascribe the small effects seen here to a particular mechanism. See ref. 2 for a complete description of the present work.

Footnotes and References

*Work Supported by U.S. DOE Contracts No. DE-AC03-76SF00098 , DE-FG05-86ER40256, and the NSF [DMR86-15641].

† Now at University of North Texas , TX

‡Physics Division, Caltech, Pasadena, CA.

§MCSD, LBL

**Cyclotron Institute, Texas A&M Univ. , TX

1. A.J. Eccles, et al., Appl. Phys. Lett. **49,** 188 (1986).

2. D. L. Weathers, et al., Nucl. Inst. and Meth. in Phys. Research **B42,** 307 (1989).

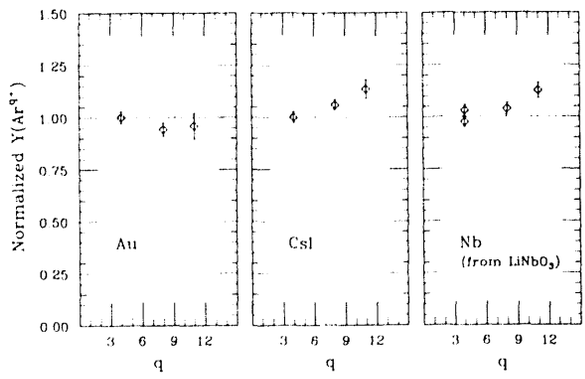

Fig. 1. Total Sputtering yield, scaled such that the Ar^{4+} yield is equal to 1, plotted as a function of projectile charge state q for all three targets.

Light Emission from Na Atoms Sputtered by Multiply-Charged Ar Ions*

R.E. Tribble,† M.H. Prior,‡ and R.G. Stokstad

This study reports, for the first time, the projectile charge dependence of the production of excited neutral atoms by heavy ions impacting upon a crystal surface. The yield of light following bombardment with heavy ions depends upon the sputtering yield and on the probability that a sputtered atom or ion will be excited as it leaves the surface. For an insulating surface, both of these processes can depend in principle on the charge state, and hence on the electronic potential energy, of the incident ion. The sputtering yield could be increased by a direct electronic ejection of a surface atom--a Coulomb "explosion" accompanying the passage and neutralization of an incident ion. The excitation and subsequent emission of light by atoms remaining in the surface may also depend on the charge state of the bombarding ion.

The optical spectrum emitted by atoms and ions sputtered from a NaCl crystal surface was observed normal to a beam of Ar^+ ions produced by the LBL ECR ion source at the 88-Inch Cyclotron. The experimental arrangement consisted of a NaCl crystal mounted on a target holder attached to a precision linear translator. The surface of the NaCl target was perpendicular to, and could be translated along, a line parallel to the ion beam direction. The light was analyzed by a Jarell-Ash 1/4 m grating spectrometer with the axis of the collimator system perpendicular to and intersecting the beam. In the figure we show the light yield in the Na-D lines as a function of the incident charge state for (a) light from the surface of the crystal (measured at the peak of the intensity curves) and (b) for light emitted by sputtered atoms well removed from the surface. The results indicate no significant change in the light yield from the sputtered atoms; however, there is a significant (25%) increase in the yield of light from the surface as the charge state is increased from 4 to 12.

This increase observed with increasing charge state is probably a result of the additional energy which is required to neutralize the incoming ion. The potential energy between the ion and surface increases from 144 eV for Ar^{4+} to 2636 eV for Ar^{12+}. Thus, neutralizing the 12^+ ions could cause a significant increase in surface excitation. This electronic excitation could be dissipated, at least in part, by excitation of the surface atoms, thus producing the increased light yield. This work is described in detail in Ref. 1

Footnotes and References

*Work supported by DOE contract No. DE-AC03-76SF00098

† Dept. Phys., Texas A&M Univ., College Station, TX

‡Materials and Chemical Sciences Division, LBL

1. R.E. Tribble, M.H. Prior, and R.G. Stokstad, Nucl. Inst. and Meth. in Phys. Res., **B44**, 412 (1990).

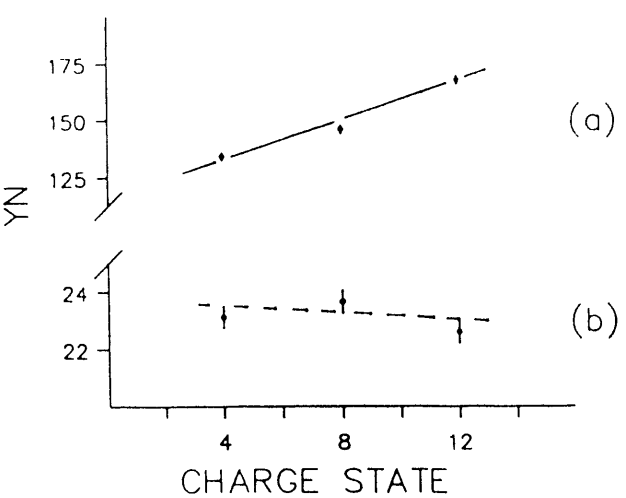

Fig. 1. Normalized light yield (YN) for the Na-D lines, versus incident charge state at 48 keV bombardment energy for (a) the light from the surface region, and (b) the light from sputtered atoms well beyond the surface.

Enhanced the ECR Ion Source Performance with an Electron Gun*

Z.Q. Xie, C.M. Lyneis, R.S. Lam and S.A. Lundgren

An electron gun for the Advanced ECR source, which operates at 14 GHz, has been developed to increase the production of high charge state ions. Fig. 1 shows the schematic view of the AECR source with the electron gun installed in the injection region. The electron gun is made from lanthanum hexaboride (LaB_6) because of its better electron emission, longer lifetime and lower evaporation compared to the tungsten material.[1] This electron gun injects up to 100 mA of 50 to 150 eV electrons axially into the plasma chamber of the AECR, which can provide electrons to the ECR plasma and may increase the electron density on axis and improve ion radial confinement, therefore significantly more intense high charge state ion beams can be extracted. With the electron gun the AECR has produced at 10 kV extraction voltage 131 eμA of O^{7+}, 13 eμA of O^{8+}, 17 eμA of Ar^{14+}, 1.4 eμA of Ar^{16+}, 2.2 eμA of Kr^{25+}, 1 eμA of Xe^{31+}, and 0.2 eμA of Bi^{38+}.

The AECR was also tested as a single stage source with a coating of SiO_2 on the plasma chamber walls.[2] This significantly improved its performance compared to no coating, but direct injection of electrons with the electron gun produced the best results. The enhancement of the source performance is a factor of 2 or higher for the high charge state ion beams. Fig. 2 shows the charge state distributions for oxygen and argon for the AECR running with the electron gun or with a SiO_2 coating.

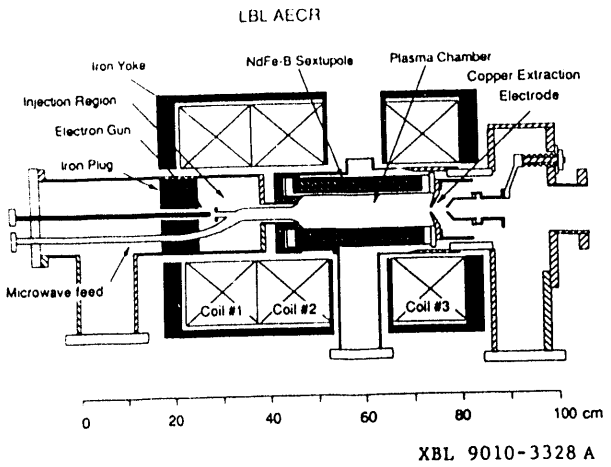

Fig. 1. Schematic drawing of the AECR. The axial magnetic field is produced by copper coils in an iron yoke. Electrons from a LaB_6 filament flow along the axial magnetic field lines into the plasma chamber.

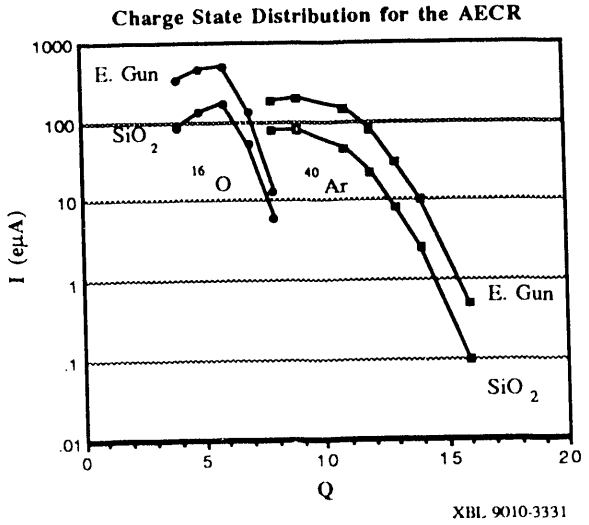

Fig. 2. Charge state distribution for oxygen and argon produced with the AECR for two cases: first, with SiO_2 on the plasma chamber walls and second, with the electron gun. For oxygen and argon the source was tuned to maximize O^{7+} and Ar^{11+}, respectively.

Footnotes and References

*Condensed from a paper submitted to Rev. Sci. Instrum., 1990.

1. K.N. Leung, P.A. Pincosy and K.W. Ehlers, Rev. Sci. Instrum. 55, 1064 (1984)

2. C.M. Lyneis, Proc. of the Int'l Conf. on ECR Ion Sources and their Appli., NSCL REPORT # MSUCP-47, E. Lansing, 1987.

The AECR Injecting the 88-Inch Cyclotron

D. J. Clark, R. S. Lam, S. A. Lundgren, C. M. Lyneis and Z. Xie

The new AECR, described in another contribution to this report, injects the cyclotron using a new section of horizontal beam line. This new line connects from the south with the vertical axial injection system of the cyclotron. The original LBL ECR source brings beam from the north to the vertical line. The AECR horizontal line contains a magnetic solenoid (Glaser) lens, a 17.5 degree vertical bending magnet, a magnetic quadrupole doublet lens, and a 72.5 degree vertical bending magnet to bring the beam to a vertical direction. The beam then passes through the vertical injection line used by both the AECR and the ECR sources.

In 1990 a series of injection tests was made to evaluate the efficiency of the transmission of the AECR through the new beam line, and to accelerate the higher charge states and energies available from the AECR source.[1] Table 1 shows the principal beams accelerated in these tests. The injection efficiency was similar to that with the LBL ECR, with about 10% transmission from source to external beam for a typical low mass first harmonic beam such as O^{6+}. For the heavier beams the transmission was reduced by charge exchange during aceleration in the cyclotron.

Table 1. Accelerated AECR Beams

Ion	Charge State	E (MeV)	BS (nA)
^{16}O	6	160	6200
^{16}O	8	520	200
^{20}Ne	10	650	90
^{40}Ar	14	686	320
^{40}Ar	16	896	30
^{86}Kr	23	861	60
^{86}Kr	25	1017	8
^{136}Xe	29	865	30
^{136}Xe	30	926	20
^{136}Xe	31	990	8
^{136}Xe	32	1054	3
^{209}Bi	35	809	1.4
^{209}Bi	36	856	1.1
^{209}Bi	37	904	0.3
^{209}Bi	38	954	0.1

Footnotes and References

1. C. M. Lyneis, Zuqi Xie, D. J. Clark, R. S. Lam and S. A. Lundgren, Proc. 10th Int'l Workshop on ECR Ion Sources, Knoxville, Tenn., Nov. 1990.

Fast Energy Changes with a Cyclotron[1]

D. J. Clark and G. J. Wozniak

Fast energy/ion switching of cyclotron beams is required for measurement of excitation functions and for economic and efficient operation of the accelerator. At the 88-Inch Cyclotron there are about 30 parameters for the ECR source and injection line, 40 for the cyclotron and another 10-20 for the external beam transport, that need to be reset for a change of energy. The tune-up time from source to target for a new beam is 2-4 hours. For constant magnetic field in the cyclotron, energy/mass is proportional to $(Q/A)^2$, so we can quickly change the energy of an isotope by switching from one charge state to another without changing the main cyclotron field. Since the cyclotron beam rigidity is constant, the magnetic fields of the transport magnets to the target need not be changed. The ion trajectories can also be constant in the injection line and cyclotron if all the magnetic fields are constant and all the voltages are scaled by Q/A of the ions. The voltages in the system are the ECR source accelerating voltage, the voltage on the electrostatic inflector in the cyclotron center region, the dee voltage and the voltages on the electrostatic deflector which extracts the cyclotron beam. The rf frequency must also be changed, and the trim coils are usually changed to maintain isochronism. In Fig. 1, examples are shown of experiments where energy changes were made by changing charge states, using ions ^{63}Cu, ^{235}U and ^{209}Bi.

Footnotes and References

1. D. J. Clark and G. J. Wozniak, Nucl. Instr. & Meth.,A295 (1990) p.34.

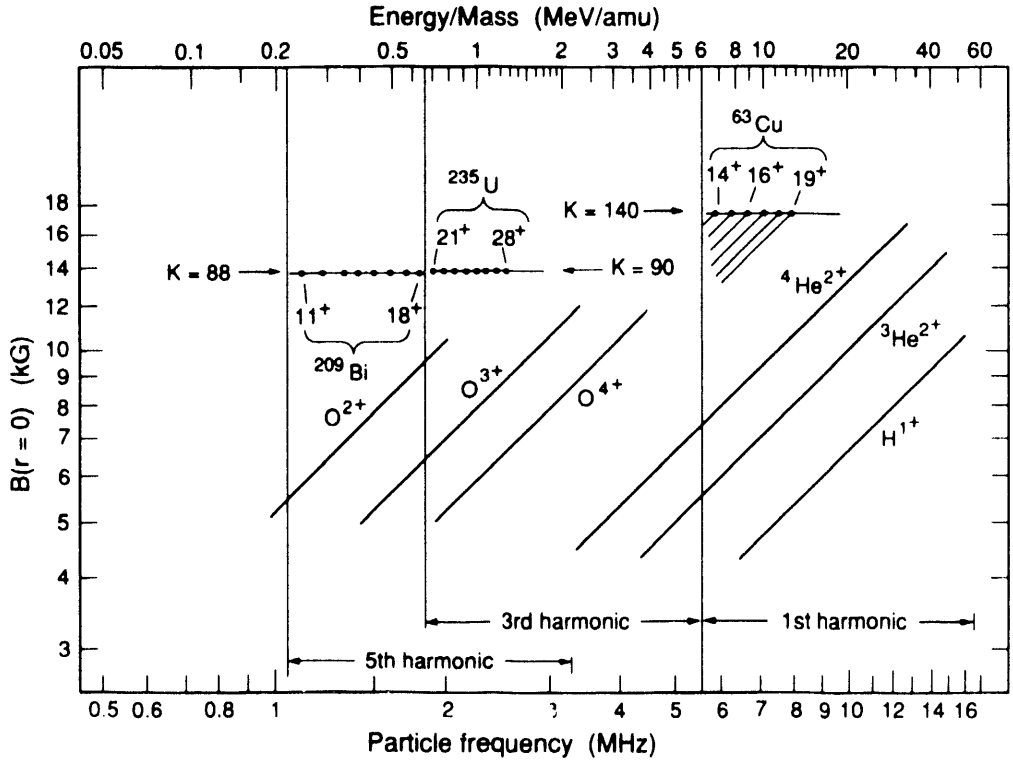

XBL 904-6739

Fig. 1. Resonance chart of cyclotron magnetic field and frequency.

Cyclotrons for the Production of Radioactive Beams[1]

D. J. Clark

The modern cyclotron is the third generation of cyclotrons. It has a magnetic field which increases with radius (and mass) and uses the sector focusing principle to provide enough axial focusing to overcome the defocusing of the average field. The radio-frequency is constant, like that of the classical cyclotron, giving 100% acceptance time from the ion source and high beam currents. The upper energy is limited by economics. Designs for booster cyclotrons of up to 1.3 and 2 GeV protons have been done at PSI, Zurich and up to 8 GeV protons at TRIUMF. Many of these cyclotrons have a wide range of energy variation made possible by rf systems tunable over a 2/1 or 3/1 range, which give energy ranges up to 100 to 1, by changing harmonic number. Trimming coils are used to shape the magnetic field for each energy. This also makes a wide range of particles available.

There are several major design choices to be made when building a cyclotron. One choice is between a magnet which has one single main coil around the pole and a magnet which has separate coils around each pole or "separate sectors". The single coil design has the advantage of compactness. The separate sector design requires an injector accelerator to inject beam radially through an empty valley. Space in the valleys can be used for high voltage accelerating cavities.

A second design choice is between the usual normal conducting coils providing average fields up to about 17 kG, and superconducting coils giving 50 kG. All the internal components of the superconducting designs are smaller in linear size by the ratio of the magnetic fields, about a factor of 3, for the same energy.

Radioactive beams can be produced when a high energy heavy ion beam of several hundred MeV/u is fragmented in a production target. Cyclotrons are good candidates for producing these beams because of their high intensities and energies, and well developed capabilities for multi-particle, variable energy operation. Both superconducting and separated sector cyclotrons can produce these beams.

Another application of the cyclotron is the acceleration of a high intensity primary light ion beam to bombard a target and produce many radioactive species at very low energy by spallation of the target nuclei. The separate sector cyclotron at PSI produces beams of 590 MeV protons at 200 μA, for example. To reduce beam loss damage the turns of the beam must be well separated at extraction radius by having a low average field and high energy gain per turn, as is done at PSI. An alternative is accelerating H^- and using stripping extraction, as at TRIUMF. In this case the cyclotron is large because a low magnetic field must be used to prevent v x B stripping of the weakly bound H^- ion during acceleration.

A third application of cyclotrons to radioactive beam production is the acceleration of beams from the spallation target system mentioned above. The radioactive atoms pass into an ion source. A cyclotron can then accelerate the beam to the MeV/u range for research in astrophysics or nuclear physics. Cyclotrons have 100% duty factor and can easily cover the energy range up to 100 MeV/u of interest for nuclear physics research. An important factor is whether the ion source can produce multiply charged ions at high efficiency and short transit time. The ECR source is a good candidate for R&D in this area.

Footnotes and References

1. D. J. Clark, Proc. The First Int'l Conf. on Radioactive Nuclear Beams, Berkeley, 1989, pg. 164, Ed. W. D. Myers, J. M. Nitschke and E. B. Norman, World Scientific.

Bevalac Experiments

The Decay of Hot Nuclei*

Luciano G. Moretto and Gordon J. Wozniak

The complexity of nuclear reactions at intermediate energies defies the scope of this short set of lectures. However, the title, in its deceptive simplicity actually defines our chosen subject quite precisely. The two key words are: "hot" and "decay". The word "hot" implies a thermalized source, namely some equilibrated intermediate structure that is created in the reactions under consideration. The word decay reminds us of radioactive or statistical decay. The two words together suggest naturally the the decay of a thermal source.

At low energies, the compound nucleus (CN) decay matches the words of the title very closely. This match is not accidental. To the contrary, we shall use the low energy CN decay as the paradigm against which to compare certain processes observed at higher energies. In order to clarify the kind of processes in which we are interested, we need to review briefly the reaction mechanisms prevailing both at low and at intermediate energies.

The classification of reaction mechanisms at low energies is rather simple. At one extreme, we have direct reactions, involving a narrow subset of nuclear modes, typically single particle degrees of freedom. In between, we have quasi-elastic and deep-inelastic reactions involving a much larger number of modes, both single particle and collective, and associated with a much more profound degree of relaxation. At the other extreme we have CN processes, in which there is full relaxation of all the modes, and which are characterized by a complete decoupling between entrance and exit channels.

At intermediate energies this simple picture seems to disappear, and the newly found complexity creates irresistible images of novel and exotic processes. For example, the variety and abundance of complex fragments produced in these reactions has suggested mechanisms like the shattering of glass-like nuclei,[1] or the condensation of droplets out of a saturated nuclear vapor,[2] or the somewhat equivalent picture of a nuclear soup curding simultaneously into many fragments.[3,4] The word "multifragmentation" has become very popular despite the perplexing lack of evidence for truly multi-fragment exit channels.

But complexity is not synonymous with novelty and caution should be used by verifying that the complexity of the reactions under study is not due to the proliferation and overlapping of conventional processes made possible by the large available energy. More than ever, it is necessary to assess the "background" of conventional processes before a new theory is declared proven, or a new mechanism prematurely discovered. In particular, one would be well advised to check how large is the CN contribution to the production of complex fragments, gamma rays and even pions. Specifically, it is important to assess the role of CN in the production of complex fragments even when more than two of them are present in the exit channel.

Footnotes and References

*Condensed from LBL-26207, Nov. 1988. Presented at the Brasov International Summer School, Recent Advances in Experimental Nuclear Physics, Poiana Brasov, Rumania Aug. 30 - Sept. 9, 1988.

[1] J. Aichelin and J. Hufner, Phys. Lett. **136B**, 15 (1984)

[2] J. E. Finn et al., Phys. Rev. Lett. **49**, 1321 (1982).

[3] D. H. E. Gross et al., Z. Phys. **A309**, 41 (1982)

[4] J. P. Bondorf et al., Nucl. Phys. **A443**, 321 (1985).

Very Hot Nuclear Systems and Their Binary and Multifragment Decay*

L. G. Moretto, Y. Blumenfeld[a], D. Delis and G. J. Wozniak

In its simplest version, the geometric model of incomplete fusion implies the fusion between the heavier partner with the geometrically occluded portion of the lighter partner. The resulting fusion product can be assigned a preevaporation mass and an excitation energy just from the determination of its velocity. In particular, this velocity can be determined from the binary, ternary, etc. coincidences of the decay products. If a given combination of target and projectile can give rise to incomplete fusion over a broad range of impact parameters, the resulting fusion products will have a correspondingly broad range of excitation energies.

The process of incomplete fusion depends not only upon the bombarding energy but, and perhaps just as strongly, upon the entrance channel mass asymmetry.

In Fig. 1 binary events contour plots in the source velocity - Z_{total} plane are shown for a series of targets and bombarding energies in Xe/La-induced reactions. In the case of light targets (C, Al), one observes essentially a single source, characterized by a well defined Z_{total} and bombarding energy. For the heavier targets (Ti, Cu/Ni), however, a broad distribution of sources is identifiable. Perhaps, the most impressive distributions are those at the lowest bombarding energy, where the source velocities are seen to decrease dramatically with an increase in total charge. This correlation, which can be taken as a rather vivid description of the incomplete fusion model, tends to disappear at higher bombarding energies. The reason may not be the failure of the model. Rather, at higher bombarding energies, the excitation energy brought in by the fusing portion of the target becomes so high that it is accompanied by a very large secondary evaporation of charged particles. Consequently, the correlation between source velocity and the total charge is lost.

Footnotes and References

*Condensed from LBL-29733. Proc. of the XXI Summer School on Nuclear Physics, Mikolajki, Poland, Sept 1990.

[a]INPN, Orsay, France

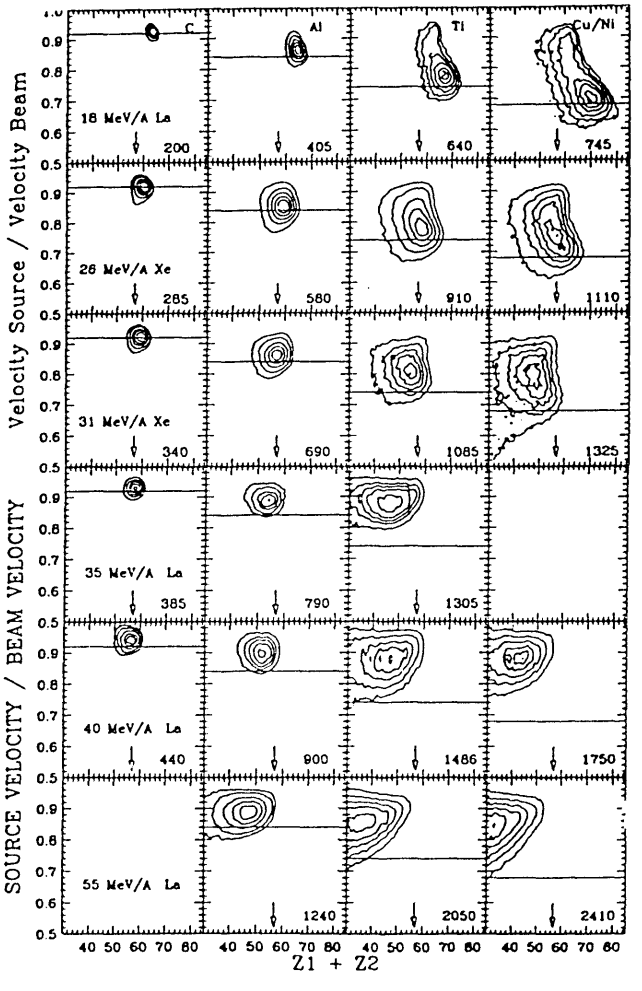

Fig. 1. Contours plots in the $V_{||}$ - Z_{1+2} plane for the reactions $^{139}La/^{129}Xe$ + ^{12}C, ^{27}Al, $^{48}Ti/^{51}V$, $^{64}Ni/^{nat}Cu$ at 18, 26, 31, 35, 40, and 55 MeV/A. The horizontal lines, vertical arrows and the number in the lower right hand corner indicate the complete fusion velocity, projectile charge and the available energy in the c.m., respectively.

Complex Fragment Production in 55 MeV/u ^{139}La + ^{27}Al, ^{51}V, ^{nat}Cu, ^{139}La Reactions

P. Roussel-Chomaz, Y. Blumenfeld+, N. Colonna, B.Libby**, S. Bradley$^{\tau}$, D.N. Delis, H.Madani**, A.Marchetti**, M.A. McMahan, A. Mignerey**, J.C. Meng, L.G. Moretto, G.F. Peaslee++, Q. Sui, and G.J.Wozniak*

In order to obtain a better understanding of the heavy-ion reaction mechanisms between 10 and 100 MeV/u, we have studied the production of complex fragments in the reactions ^{139}La + ^{12}C, ^{27}Al, ^{51}V, ^{nat}Cu, and ^{139}La between 18 and 100 MeV/u [1-3]. This report describes the data obtained at 55 MeV/u.

The figure presents the correlation observed between the total detected charge and the source velocity for the different targets and the different exit channels, these exit channels being classified according to the number of complex fragments (a n-fold event is defined as an event where n fragments of Z≥4 were detected). The first observation is that a large fraction of the coincidence events have a substantial multiplicity. We detect a significant number of events with four fragments in the final state. In the case of the heaviest targets, we could even observe some five-fold events.

The observed correlation is that a large detected charge has a high source velocity, whereas a small detected charge has a low source velocity, which is the opposite of what had been obtained at lower incident energies.

For a given target, the requirement of a larger multiplicity of complex fragments selects out events with lower source velocities which correspond to higher excitation energies in the incomplete fusion model.

The next step will be to try to understand these data by coupling a Boltzmann-Nordheim-Vlasov code describing the dynamical stage of the collision with a statistical binary decay code used to describe the deexcitation process.

Footnotes and References

* CEN Saclay, 91191 Gif sur Yvette Cedex France
+ IPN Orsay, 91406 Orsay Cedex France
** U. of Maryland, College Park, MD 20742
++ NSCL, Michigan State U., E.Lansing, MI 48824
τ Kaman Sc., 2560 Huntington Av, Alexandria, VA 22303

1. N. Colonna et al., Phys. Rev. Lett. 62, 1833, (1989)
2. D. Bowman et al., Nucl. Phys. A523, 386, (1991)
3. Y. Blumenfeld et al., Phys. Rev. Lett. 66, 576, (1991)

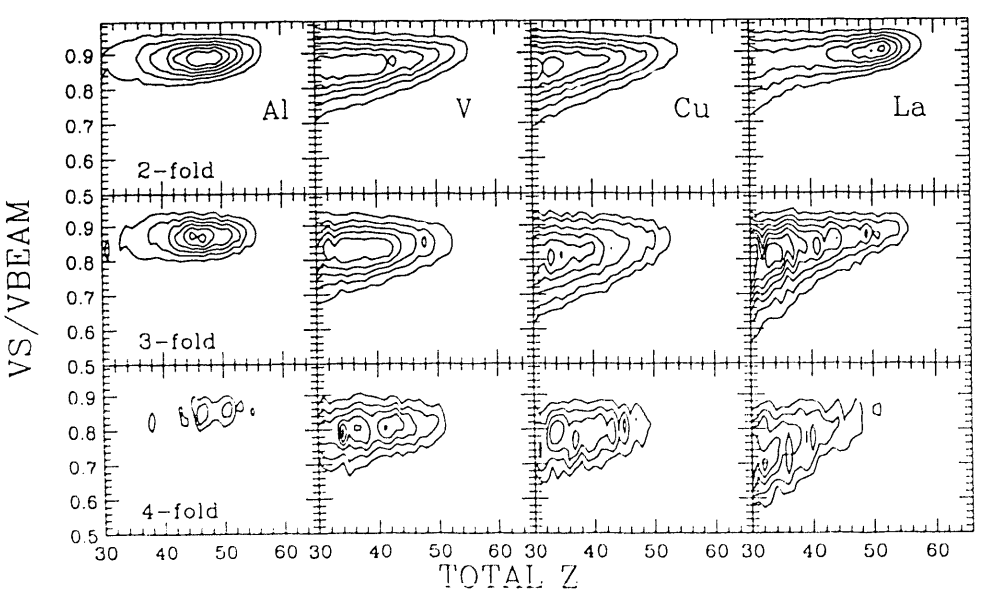

Binary and Multifragment Decay of Very Hot Nuclei*

L. G. Moretto, Y. Blumenfeld[a], R. J. Charity[b] and G. J. Wozniak

Heavy ion projectiles are able to impart to nuclear systems important amounts of excitation energy distributed over a large number of nucleons. Thus, heavy ion collisions allow one to study both the formation and decay of hot nuclei. At low energies, compound nucleus decay through binary complex fragment emission has been observed with a cross section which, although very small, is in excellent agreement with statistical model calculations using the transition state formalism. In order to approach the limits of stability of nuclei, higher beam energies must be used. This is not without complications, because the reaction mechanism become less clear-cut, and it is no longer straightforward to characterize the intermediate hot system under study.

Recently, it has been shown that the incomplete fusion mechanism persists up to rather high energies, producing a large range of nuclei with different masses and excitation energies. For the 18 MeV/u $^{139}La + ^{64}Ni$ reaction, a strong correlation was established between the degree of fusion (source velocity) and the mass and excitation energy of the product nucleus. By relating the center-of-mass velocity of binary events to the mass and excitation energy of the product nucleus, it was possible to study at one bombarding energy the decay properties of hot nuclei over an excitation energy range extending up to 4 MeV/u.

At even higher excitation energies, nuclei decay with a high probability of complex fragment emission. The sequential evaporation of several complex fragments gives to rise to multibody final states, and contributes to the measured cross sections. Figure 1 shows the relative proportions of evaporation residues, binary decays, and multifragment events predicted by code GEMINI[1] which treats the sequential statistical decay of a hot compound nucleus in the framework of the transition state formalism. A smooth increase of the multibody probability with excitation energy is observed, but binary decays dominate up to a least 1000 MeV excitation energy. Other models also indicate that above certain excitation energies prompt multifragmentation should begin to occur. Thus, experimental excitation functions for the various channels may provide the interpretative key to understanding the underlying decay mechanism.

In this talk we shall present evidence of binary compound nucleus decay at low energies leading to complex fragment production, and we shall show how, at higher energies, multifragment emission can be characterized in terms of excitation functions associated with binary, ternary and quaternary decay.

Footnotes and References

*Condensed from LBL-29090. Proc. of the Intern's Workshop on Nuclear Dynamics, Elba, Italy, April 1990.

[a]Institut de Physique Nucleaire, Orsay, France
[b]Washington University, St. Louis, MO 63130

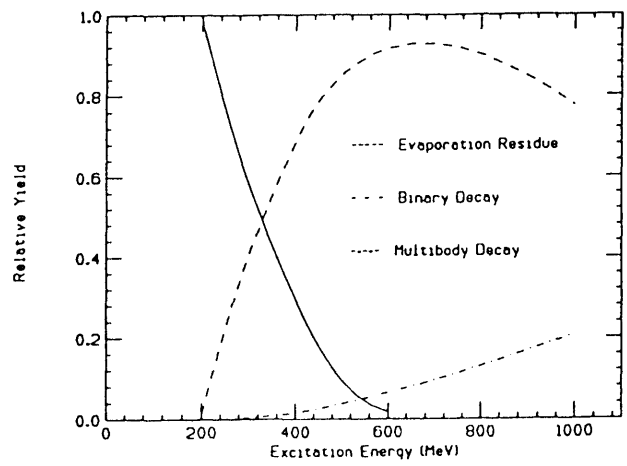

Fig. 1. Relative proportions of evaporation residues, binary decays and multibody decays calculated by the code GEMINI for a nucleus of mass A ~160 as a function of excitation energy.

Multifragment Decay of Hot Nuclei*

N. Colonna, Y. Blumenfeld[†], P. Roussel-Chomaz[††], D.N. Delis, G. Guarino, K. Hanold, I. Iori[†††], B. Libby[°], A. Mignerey[°], C. Meng, G.F. Peaslee, N. Santoruvo[†††], G.J. Wozniak and L.G. Moretto.

The branching ratios for 2, 3, 4 and 5 fragments decay channels as function of the excitation energy in the 35, 40, 45 and 55 MeV/u La + C, Al, Ca, V, Cu and La reactions have been determined in an attempt to gain some insight into the decay mechanism of very hot nuclei. The fragments were detected in two arrays of 9 Si-Si-plastic telescopes on either side of the beam, with unit charge resolution up to Z=57 for most telescopes.

In order to calculate the excitation energy of the decaying nucleus, the incomplete fusion model was assumed. For such a model, a strong correlation is expected between the velocity of the hot nucleus formed in the reaction and its mass and excitation energy [1]. If the fragments are emitted from a single source, its velocity is given by the following formula: $V_S = \Sigma_i m_i V_i / \Sigma_i m_i$. Here m_i and V_i are respectively the mass and the velocity of the detected fragments. The excitation energy is then given by: $E^* = E_b(1 - V_S / V_b)$, where E_b is the bombarding energy and V_b the beam velocity. In the analysis, the condition that the detected total charge be greater than 30 was required, in order to keep the contamination arising from incompletely detected events to an acceptable level.

In Figure 1 we plot the proportion of the n-fold events with respect to the total number of coincidence events as function of the excitation energy. Two remarkable features can be noted from the figure. First, the probabilities for 3, 4 and 5-fold events increase substantially with the excitation energy of the source up to the highest energy observed. Such a behavior would be expected from any statistical model and supports a strong relationship between source velocity and excitation energy over the entire source velocity range studied. Second, the relative proportion of multi-fold events for the heaviest targets and four bombarding energies are very similar, suggesting that the source produced in these reactions depend mainly on how much mass is picked up by the projectile from the target and relatively little on the nature of the target or the bombarding energy. This striking similarity of the excitation functions lends support to the idea of the formation of an intermediate nuclear system whose decay properties depend mainly on its excitation energy and angular momentum.

Footnotes and References

* Condensed from Phys. Rev. Lett. 66, 576 (1990)

† IPN Orsay, 91406 Orsay Cedex France

†† CEN, 91191 Saclay, Cedex France

††† Universita' di Milano, 20133 Milano, Italy

° U. of Maryland, College Park, MD 20742

[1] N. Colonna et al., Phys. Rev. Lett. 62, 1833 (1989).

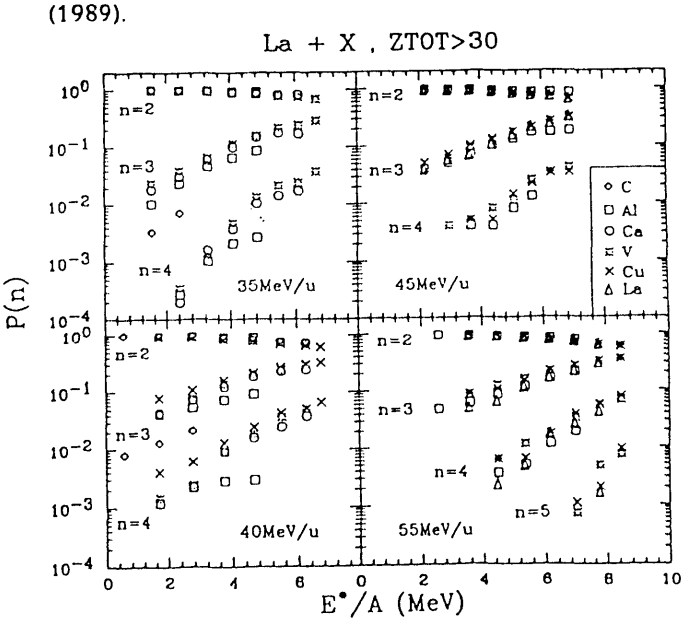

Fig. 1. Proportion of 2, 3 and 4 fragments events as a function of the excitation energy per nucleon of the decaying nuclei. Both the excitation energy and the mass of the hot nuclei are calculated according to the incomplete fusion model.

Dynamics-Statistics Coupling In Nuclear Fragmentation

M. Colonna, N. Colonna, P. Roussel-Chomaz†, M. Di Toro*, L.G. Moretto and G.J. Wozniak*

Complex fragment production represents a large part of the reaction cross section in medium energy heavy ion collisions. However quite different time scales maybe involved in the fragment emission and therefore a unique theoretical approach may not account for the final observed properties of fragment production. A dynamical stage is important to relate production yield and structure of primary fragments, at some freeze-out time, to the entrance channel. A statistical deexcitation stage is necessary to take into account all decay channels that require time scales not compatible with reliable dynamical evolution times. We solve the Boltzmann-Nordheim-Vlasov equation, mean field dynamics plus collision terms, in a test particle approach with a collision simulation based on the concept of mean free path of a nucleon in nuclear matter [1]. We use Skyrme forces and the free NN cross section, suitably parametrized to reproduce the experimental energy and angular behavior. Due to the test particle approach, the dynamical fluctuations from two-body collisions are strongly reduced. We follow such an average trajectory in phase space up to a freeze-out time, where all the properties of promptly produced fragments (mass, charge, c.m. velocity, emission angle, excitation energy and angular momentum) are extracted with a clustering procedure. All observables of the final fragments are then calculated from a statistical code, GEMINI [2], where all the decay channels, including intermediate mass fragment emission, are considered. Applications are considered for fragment data (inclusive cross sections, energy spectra and multiplicities) in reactions induced by La beam in the energy range 40-60 MeV/A. In Figure 1 we show a typical yield, in the case La + Al at 55 MeV/A, compared with experiment. We stress the points that without a sequential emission of complex nuclei it is not possible to reproduce the final yields of fragments with masses in between the projectile and target region, but that a dynamical stage is necessary to reproduce the non-equilibrium features of the lighter fragments (Z<15). The calculations have been done without any free parameters or normalizations.

Footnotes and References

* INFN-LNS Catania, Italy

† CEN, 91191 Sacaly, Cedex, France

[1] A. Bonasera, G.F. Burgio and M. Di Toro, Phys. Lett. B221 (1989) 233.

A. Bonasera, G. Russo and H.H. Wolter, Phys. Lett. B246 (1990) 337.

[2] R.J. Charity et al., Nucl. Phys. A551 (1990) 59.

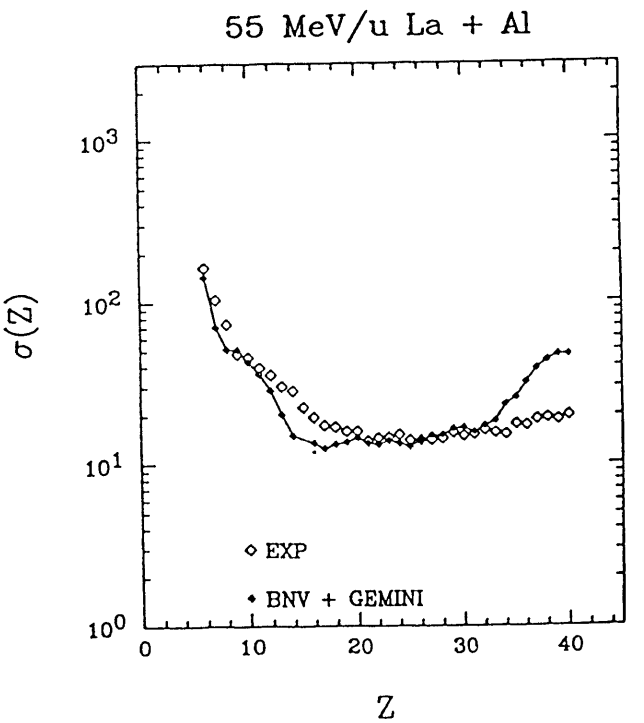

Fig. 1. Comparison between the experimental and predicted charge distribution in the 55 MeV/u La + Al reaction. The prediction is the result of the statistical decay of the primary products formed in the dynamical stage.

Equilibrium and Non-Equilibrium Complex Fragment Emission in 50-100 MeV/u $^{139}La + ^{12}C$ Reactions*

D. R. Bowman[a], G. F. Peaslee[a], N. Colonna, R. J. Charity[b], M. A. McMahan, D. Delis, H. Han[c], K. Jing[c], G. J. Wozniak, L. G. Moretto, W. L. Kehoe[d], B. Libby[e], A. C. Mignerey[e], A. Moroni[f], S. Angius[f], I. Iori[f], A. Pantaleo[g], and G. Guarino[g]

Complex fragment emission ($Z \geq 3$) has been studied in the reactions of 50, 80, and 100 MeV/u $^{139}La + ^{12}C$. Charge, angle, and energy distributions were measured inclusively and in coincidence with other complex fragments, and were used to extract the source rapidities, velocity distributions, and cross sections. The binary signature of the coincidence events and the sharpness of the velocity distributions illustrate the primarily 2-body nature of these reactions. The emission velocities, angular distributions, and absolute cross sections of fragments of $20 \leq Z \leq 35$ at 50 MeV/u, $19 \leq Z \leq 28$ at 80 MeV/u, and $17 \leq Z \leq 21$ at 100 MeV/u are consistent with the binary decay of compound nuclei formed in incomplete fusion reactions in which the ^{139}La projectile picks up about one-half of the ^{12}C target.

The angle-integrated cross sections for the $^{139}La + ^{12}C$ system at four bombarding energies are shown in Fig. 1 as a function of the fragment Z-value. The charge distribution for fragments at 18 Mev/u is consistent with statistical emission from a system above the Businaro-Gallone transition point[1]. There is a maximum in the yield at symmetry due to the minimum in the potential energy surface at this point. Between 18 and 50 MeV/u the charge distribution becomes flatter and the yields decrease. From 50 to 80 MeV/u the yields increase and the charge distribution becomes U-shaped and then flatter at the highest energy. The observed flattening of the charge distribution between 18 and 100 MeV/u can be explained by the increase in temperature of the system, which tends to make all of the decay channels more equally probable. The decrease in the yield for symmetric products is most likely due to the onset of incomplete fusion above 20 MeV/u.

Footnotes and References

*Condensed from Nucl. Phys. **A523**, 386 (1991).

[a]NSCL, MSU, E. Lansing, MI 48824
[b]Washington University, St. Louis, MO 63130
[c]Institute of Atomic Energy, Beijing, China
[d]MIT, Cambridge, MA 02139
[e]Univ. of Maryland, College Park, MD 20742
[f]INFN, Univ. of Milano, Milan, 20133 Italy
[g]INFN, Bari 70126, Italy

1. R. J. Charity et al., Nucl. Phys. **A511**, 59 (1990)

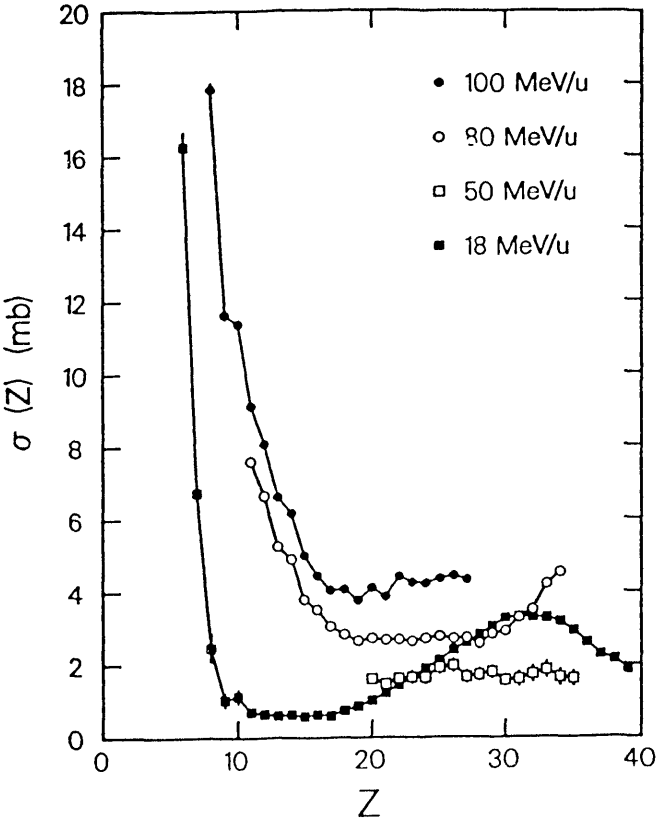

Fig. 1. Angle-integrated cross sections of products from the 18, 50, 80 and 100 MeV/u $^{139}La + ^{12}C$ reactions. The solid lines through each set of data are to guide the eye.

Complex Fragment Production in 50 MeV/A ^{197}Au + ^{12}C, ^{27}Al and ^{nat}Cu Reactions*

G. F. Peaslee[a], L. G. Moretto and G. J. Wozniak

Complex fragment (Z>6) production was studied in three reverse-kinematic reactions. Inclusive cross sections were measured as well as exclusive results for 2-, 3-, and higher-fold events. Reconstructing the source velocity of these fragments and using a simple incomplete fusion model gives a measure of the impact parameter and excitation energy of the reactions producing these fragments. A clear progression from peripheral (cold) events to more central (very hot) events is seen as a function of the source velocity.

The width of the source velocity is very narrow for the ^{12}C target implying that only a narrow range of impact parameters are available for this reaction. The mean value of the source velocity lies roughly halfway between the velocities of the projectile and of the compound nucleus formed from the complete fusion of the target and projectile. This means that roughly half of the ^{12}C target gets transferred to the gold projectile. For the ^{27}Al and ^{nat}Cu targets, there is a much broader source velocity distribution, which shows a strong correlation with the detected fragment charge between Z = 65 to 80.

In Fig. 1, the excitation energy of the emitter is extracted from the source velocity, and plotted against the percentage of n-fold events (as a fraction of the total n-fold events). Singles are not shown on this figure. It is remarkable that all targets show a smooth increase in multiplicity of the higher-fold events, even up to 5 MeV/A of excitation and beyond. This is very similar to statistical decay calculations of sequential multifragmentation, which also show a smooth increase in multiplicity as a function of excitation energy. This trend has also been seen[1], independent of target, for ^{139}La-induced reactions at 35, 40, 45 and 55 MeV/A.

Footnotes and References

*Condensed from LBL-29014. Proc. of the XIII Nucl. Phys. Symp., Oaxtepec, Mexico, Jan 1990.

[a]NSCL, MSU, E. Lansing, MI 48824

[1]Y. Blumenfeld et al., Phys. Rev. Lett. 66, 576 (1991).

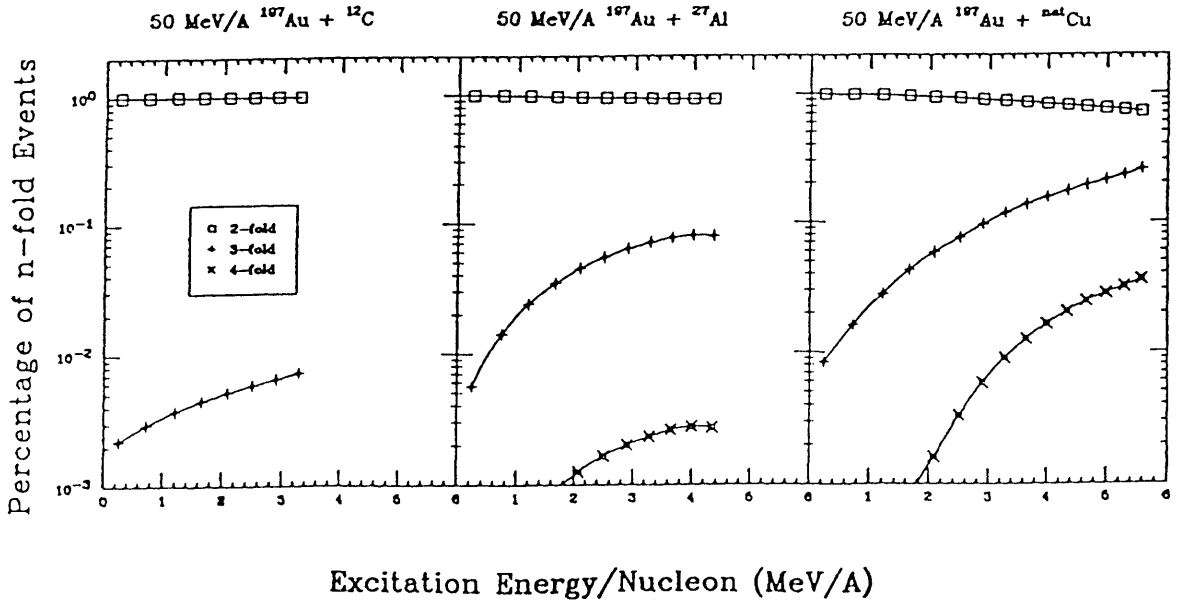

Response of a Prototype of a Neutron-Multiplicity Calorimeter*

A. Pantaleo[a], L. Fiore[a], G. Guarino[a], V. Paticchio, G. D'Erasmo[b], E. M. Fiore[b], N. Colonna, G. J. Wozniak and L. G. Moretto

A prototype module of a calorimeter[1] for the measurement of the neutron multiplicity associated with reverse-kinematic heavy-ion reactions, has been built with NE110 plastic scintillator block. The dimensions of each scintillator block is (50x25x60) cm^3 with the optical connection made through the (50x25) cm^2 face to a EMI 9823B photomultiplier by means of a lucite light guide. Total internal reflection of the scintillation light was obtained by preserving a plastic-air separation surface optically isolated from the environment.

The anode pulse rise time and the mean pulse duration were measured to be 2.5 and 15 ns, respectively. No significant gain variations were observed at counting rates up to $3 \times 10^5 s^{-1}$. The background from thermal tube noise and activation in the experimental area was found to contribute appreciably to the singles counting rate below 0.3 MeVee (MeV electron equivalent). The study of the contribution of low amplitude pulses to the calorimetric response was one of the goals of this work. To this end, the detection efficiency and response function of the module were studied with 14 MeV neutrons. The good reproduction of the experimental results with Monte Carlo (MC) calculations will enable us to accurately calculate the detector response at different neutron energies and to rely on the derived multiplicity calibration.

Finally a new n-γ discrimination technique was tested and upper limits were set for the signal-to-ratio.

Footnotes and References

*Condensed from Nucl. Instr & Meth. **A286**, 230 (1990)..

[a]INFN, Bari 70126, Italy

[b]Dipartimento di Fisica dell'Unversita di Bari, Italy

1. A. Pantaleo et al., Nucl. Instr. & Meth. **A5269** 580 (1988).

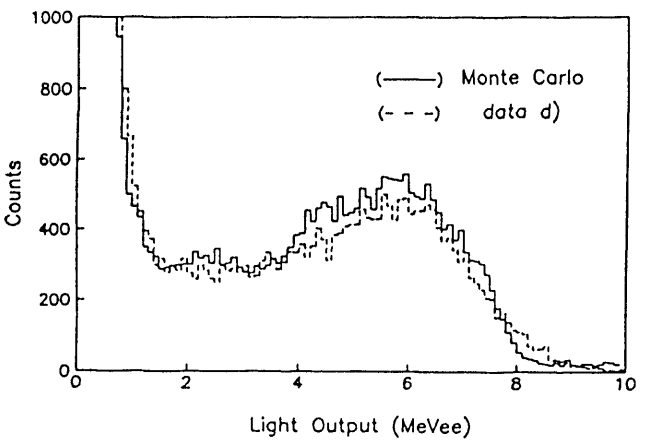

Fig. 1. Experimental and Monte Carlo simulated response functions of the prototype module to 14 MeV neutrons.

Interaction Cross Section of ^{11}Li + d Reaction

I. Taniahta, K. Yoshida,* T. Suzuki,* T. Kobayashi,† S. Shimoura,‡ K. Sugimoto,§ K. Matsuta, T. Minamisono,§ O. Testard,** L. Greiner, W. Christie, D.L. Olson, H. Wieman, and T.J.M. Symos*

The interaction cross section (σ_I) for ^{11}Li + d reaction at 790A MeV has been measured. The matter density distribution of ^{11}Li was determined from an analysis of present data combined with other σ_I data; σ_I at the same energy but with Be, C, and Al targets,[1] σ_I at 75A MeV, and σ_I at 40A MeV.[2]

A liquid deuteron target of 10 cm thickness was used at Bevalac. The σ_I was measured by a transmission method using HISS magnetic spectrometer system; the same system used for previous measurements.[1] The interaction cross section of ^{11}Li + d reaction has been determined to be (465 ± 5) mb.

Nuclear interaction radii determined from σ_I of reaction between neutron rich nuclei and nuclear targets (Be, C, and Al) show the separability of the interaction radii of a projectile and a target;

$$\sigma_I = \pi [R_I(P) + R_I(T)]^2 \qquad (1)$$

where $R_I(P)$ is the interaction radius of a projectile and $R_I(T)$ is that of a target. Observed σ_I of ^{11}Li + d reaction, however, is much smaller than the value expected from the equation (1) 567 mb. Thus the separability is broken in this reaction because the σ_I reflects the density at smaller radius. While, the σ_I of ^{11}Li at lower energy are sensitive to a density at larger radius because of the large nucleon-nucleon cross sections. Therefore if we combine all data we sample the density at different radius.

We used the Glauber type model of the σ_I with test density distributions with Gaussian and Yukawa tail. The Gaussian width, the slope coefficient of Yukawa distribution, and the amplitude of Yukawa part were the free parameter to fit all the cross sections. Fig. 1 shows the density distribution that gives the best fit for all σ_I. It clearly shows the long tail (halo). This density distribution has 1.4 nucleons in the region of r > 4 fm. The slope of the Yukawa distribution is consistent with the value expected by the separation energy of neutrons from ^{11}Li.

Footnotes and References

*RIKEN, Wako, Saitama 351-01, Japan
†KEK, Tsukuba, Ibaraki 305, Japan
‡Univ. of Tokyo, Hongo, Tokyo 113, Japan
§Osaka Univ., Toyonaka, Osaka 560, Japan
**Saclay, 91191 GIF-sur-YVETTE, Cedex, France

1. I.Tanihata et al., Phys. Rev. Lett. 55 (1985) 2676. ; I.Tanihata et al., Phys. Lett. B206 (1988) 592.
2. S. Shimoura et al., unpublished.

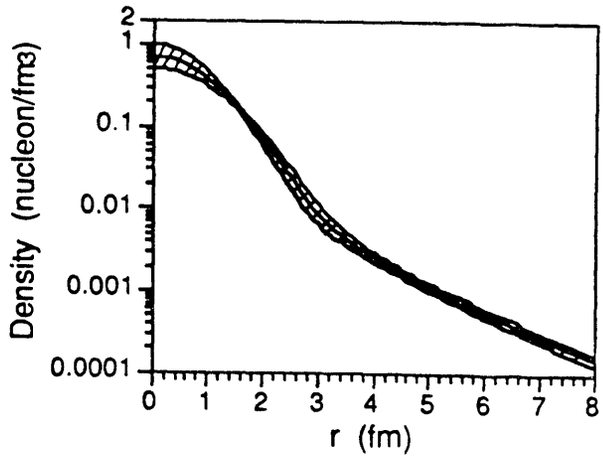

Fig. 1. ^{11}Li Density Distributions determined from interaction cross sections.

Spin Polarization of Projectile Fragments ^{39}Ca and ^{37}K

K. Matsuta, A. Ozawa, Y. Nojiri,† T. Minamisono,† M. Fukuda,† A. Kitagawa,†
S. Momota,† T. Ohtsubo,† Y. Matsuo,† H. Takechi,† S. Fukuda,† I. Minami,† K. Sugimoto,†
I. Tanihata,‡ K. Omata,§ J.R. Alonso, G.F. Krebs and T.J.M. Symons

Nuclear spin polarization of beta-emitting fragments ^{39}Ca($I^{\pi}=3/2^{+}$, $T_{1/2}$=0.86 sec) and ^{37}K($I^{\pi}=3/2^{+}$, $T_{1/2}$=1.23 sec) produced in the ^{40}Ca + Au collision has been measured at an effective energy of (106 ± 12) MeV/amu.

A 380 μm thick Au target was bombarded with a ^{40}Ca primary beam extracted from the Bevalac. Only the desired nuclides were selected and purified by the magnetic-rigidity and the energy-loss analyses using a fragment separator. The deflection angle of the fragments was defined by a collimator placed 0.6 m downstream of the target. The momentum was selected by a pair of horizontal slit jaws at the intermediate dispersive focus of the separator. Nuclear spin polarizations were measured by means of asymmetric distribution of beta rays.

Observed fragment polarization (P) was positive (parallel to the $\mathbf{k}_i \times \mathbf{k}_f$) for the momentum region higher than the projectile velocity, and was negative for the lower momentum region, for both ^{39}Ca and ^{37}K fragments as shown in the figure. The general trend in P is the same as that observed at the grazing angle around the quasi-elastic peak in low energy(around 10 MeV/amu) transfer reactions and that observed for a projectile-like fragment ^{12}B produced in the ^{14}N + Au collision at intermediate energy (40 MeV/amu)[1]. Thus, the fragment polarization showed persistently the same trend in the wide range of the projectile energy and mass, and the trend is independent of the number of nucleons removed from the projectile. The observed trend in P is accounted for quite well qualitatively by a simple projectile fragmentation model which is based on the idea that origin of the polarization is the orbital angular momentum held by the fragment part in the projectile before the collision takes place.

Footnotes and References

† Osaka Univ., Toyonaka, Osaka 560, Japan
‡ RIKEN, Wako, Saitama 351-01, Japan
§ INS, The Univ. of Tokyo, Tanashi, Tokyo 188, Japan

1. K. Asahi et al., Phys. Lett. 251B, 488(1990).

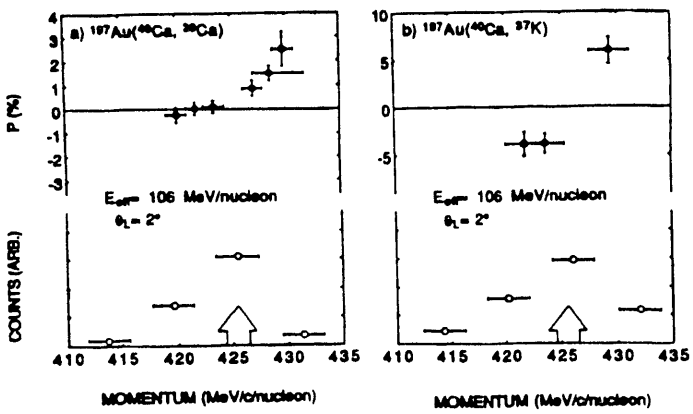

Fig. 1. Momentum dependence of the fragment polarization.

Closed circles are observed polarizations in %, and open circles are relative particle yields. The sign of polarization parallel to $\mathbf{k}_i \times \mathbf{k}_f$ is defined to be positive, where $\mathbf{k}_i$ and $\mathbf{k}_f$ are the wave vectors of incoming and out going particles. Momentum correspond to the beam velocity is also shown in the figure by the arrows.

Angler Distribution of Projectile Fragments from 106 MeV/amu ^{40}Ca on Au Collision

K. Matsuta, A. Ozawa, Y. Nojiri,† T. Minamisono,† M. Fukuda,† A. Kitagawa,† S. Momota,† T. Ohtsubo,† Y. Matsuo,† H. Takechi,† S. Fukuda,† I. Minami,† K. Sugimoto,† I. Tanihata,‡ K. Omata,§ J.R. Alonso, G.F. Krebs and T.J.M. Symons

Angular distributions of various projectile fragments produced in the ^{40}Ca + Au collision have been measured at an effective energy of (106 ± 12) MeV/amu.

A 380 μm thick Au target was bombarded with a ^{40}Ca primary beam extracted from the Bevalac to produce fragments. The deflection angle of the fragments was defined by a collimator placed 0.6 m downstream of the target. The atomic number(Z) and the mass(A) of the fragments were determined from the energy loss(dE/dx) in a 400 μm thick Si detector and the time of flight(TOF) for 8 m flight path, respectively.

Angular distributions of mirror nuclei were measured as shown in the figure. The window width was ± 0.6 degrees. The angular spread of the fragments was much wider than that predicted by the Goldhaber model[1] due to the Coulomb bounce off.

It was shown that the width of the spread is largest in the one nucleon stripped off case, i. e. ^{39}Ca, and becomes smaller as the larger number of nucleons are stripped off from the projectile. This trend in the angular distributions could be accounted for by the orbital deflection of the fragments discussed in ref. 2, but with the assumption of the positive deflection. In the ^{39}Ca case, main component is produced with relatively small overlapping with the target nucleus, i.e. with large impact parameter, and thus the trajectory of the projectile is close to the Coulomb trajectory. In the case that more nucleons are stripped off, overlapping region becomes larger and the fragment nucleus is less deflected because the relatively strong nuclear attractive force reducees the Coulomb force.

Footnotes and References

† Osaka Univ., Toyonaka, Osaka 560, Japan
‡ RIKEN, Wako, Saitama 351-01, Japan
§ INS, The Univ. of Tokyo, Tanashi, Tokyo 188, Japan

1. A.S. Goldhaber, Phy. Lett. **53B**, 306(1974).
2. K. Van Bibber et al., Phys. Rev. Lett. **43**, 840(1979).

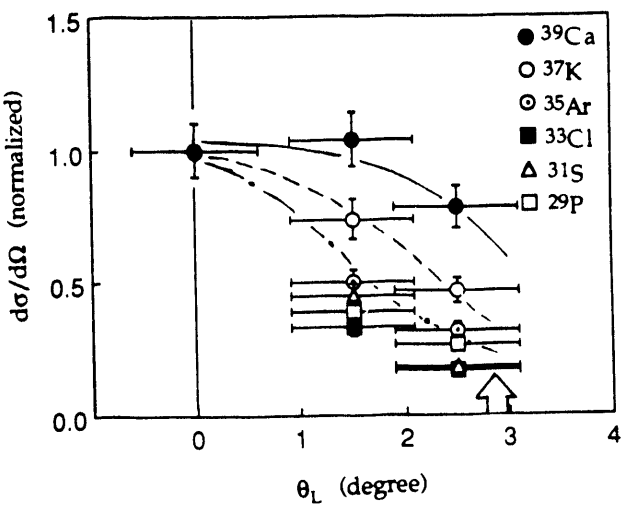

Fig. 1. Angular distributions of the fragments. Cross sections are normarized at 0 degree. Lines are guides for eyes. Error bars in abscissa show the window width. Classical grazing angle is also shown in the figure by the arrow.

Proton Emission in La+La Collisions at E/A=138 and 246 MeV*

G. Claesson, W. Benenson[†], J.-F. Gilot[‡], C. Hartnack[§], G. Krebs, G. Landaud[**], J. Miller, G. Roche, L. Schroeder, H. Stöcker[§], J. van der Plicht[†], J. Winfield[†]

We have measured the cross section for proton emission from La+La collisions at E/A = 138 and 246 MeV at several angles between 40 and 90 degrees in the center of mass. The associated multiplicity of charged particles was measured with a 110-element multiplicity array.

The inclusive cross sections (Fig. 1) are approximately isotropic over the limited angular range studied. The isotropy at E/A = 246 MeV is in contrast to the predictions of the Cugnon intranuclear cascade (INC) and the Quantum Molecular Dynamics (QMD) model. Furthermore, when we apply a cut on high associated multiplicity the data show a strong enhancement at 90 degrees in the CM compared to 40 degrees (Fig. 2), whereas the models are either still slightly forward-peaked (INC) or isotropic (QMD). Similar effects are observed when comparing the cross section at 65 and 90 degrees, at both E/A = 246 and 138 MeV.

We postulate that, while collective flow has heretofore been observed only in exclusive measurements, in the special case of collisions at very small impact parameter, the outward flow of nuclear matter normal to the beam axis is strong enough to be manifested in the multiplicity-selected inclusive cross section. If this is the case, then hydrodynamic effects at these intermediate beam energies may be sufficiently strong that semi-inclusive measurements can be used to probe the reaction dynamics.

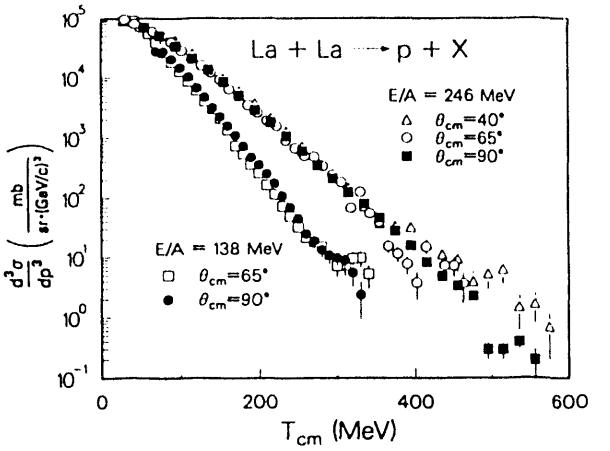

Figure 1: $d^3\sigma/dp^3$ as a function of T_{CM} for the reaction ^{139}La +^{139}La → p + X, E/A = 138 and 246 MeV and θ_{CM} = 40°, 65° and 90°.

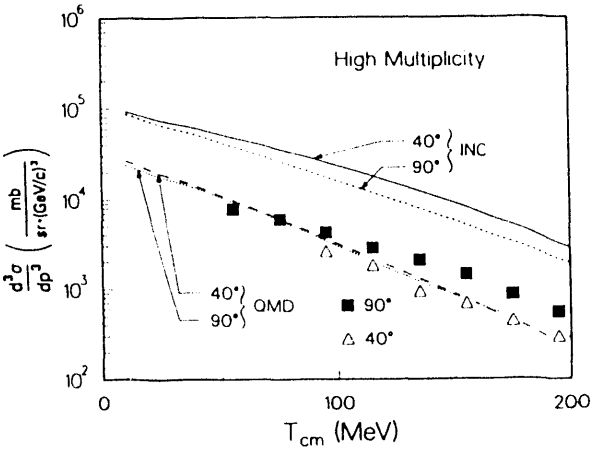

Figure 2: The cross section at E/A = 246 MeV and θ_{CM} = 40° and 90°, selected on high associated multiplicity. The curves represent the results of model calculations, as indicated.

Footnotes and References

*This work has been published in G. Claesson et al., Phys. Lett. B 251, 23 (1990).

[†]NSCL, Michigan State University, East Lansing, MI 48824

[‡]Department of Physics and Astronomy, Louisiana State University, Baton Rouge, LA 70803

[§]Institute of Theoretical Physics, Johann Wolfgang-Goethe Universität, W-6000 Frankfurt am Main, FRG

[**]Université de Clermont II-IN2P3, F63170 Aubière, France

Subthreshold Pion Production in Au+Au Collisions

J. Miller, W. Benenson , D. Cebra*, M. Cronqvist*, P. Kirk† , G. Krebs, T. Murakami‡ , J. Panetta, R. Pfaff*, T. Reposeur*, L. Schroeder, J. Stevenson*, T. Suzuki‡, I. Tanihata‡, A. Vandermolen*, Z.-F. Wang*, G. Westfall*, J. Winfield*, B. Young**

We have used the Beam 30-3 single arm spectrometer at the Bevalac to measure the inclusive cross section for subthreshold π^- production near mid-rapidity in ^{197}Au +^{197}Au, ^{139}La +^{139}La and ^{20}Ne + NaF collisions at E/A = 236 and 183 MeV. The pion-producing events were tagged according to associated multiplicity for charged particles, using a 110-element scintillator multiplicity array. The experimental apparatus and method are similar to those described in Refs. 1 and 2.

The results for Au+Au collisions, some of which are shown in Fig. 1, are the first measurements below threshold for that system, the heaviest from which subthreshold pion production has been measured.

Analysis of the full data set is proceeding, with the objective of studying how the pion yield scales with the mass and beam energy of the colliding system.

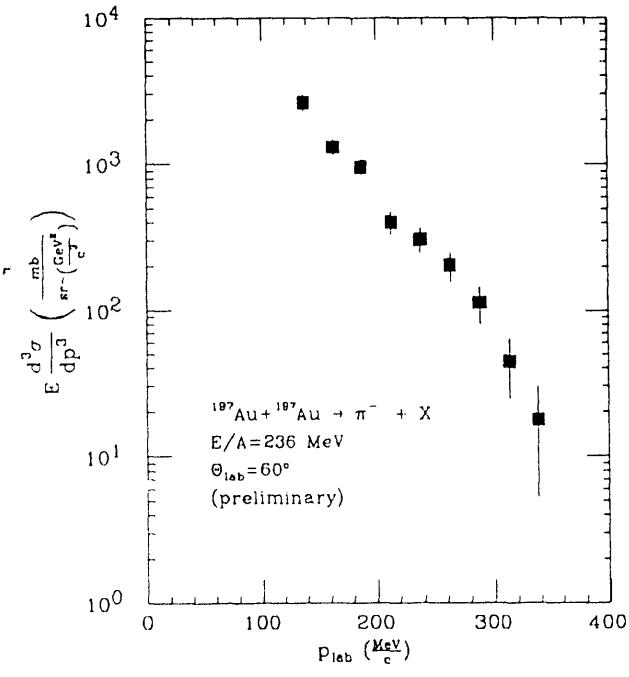

Figure 1: Invariant cross section, $E\mathrm{d}^3\sigma/\mathrm{d}p^3$ as a function of p_{lab} for the reaction ^{197}Au +^{197}Au $\rightarrow \pi^- + X$, E/A = 236 MeV at $\theta_{lab} = 60°$.

Footnotes and References

*NSCL, Michigan State University, East Lansing, MI 48824

†Department of Physics and Astronomy, Louisiana State University, Baton Rouge, LA 70803

‡RIKEN

[1] J. Miller et al., Phys. Rev. Lett. **58**, 2408 (1987) and **59** 519 (1987) (E)

[2] J. Miller, Ph.D. thesis, University of California, Lawrence Berkeley Laboratory Report LBL-24275 (1988).

Pion Production and Distribution in Grazing Relativistic Heavy-ion collisions: A Monte Carlo Method*

H.M.A. Radi †, *R.A. Mehrem*† *and J.O. Rasmussen*

Lorentz-invariant cross sections for the production of π^0, π^+, and π^- have been investigated, for the pion c.m. momentum range 0-0.5 Gev/c at angles $0° - 90°$ by Monte Carlo methods for grazing nuclear collisions of ^{207}Pb+^{207}Pb at 0.4 GeV/nucleon. Pions are considered to be produced isotropically at the center of mass at closest approach at random from a Gaussian momentum distribution. The relativistic equations of motion for the pion are solved including the electromagnetic effects due to the projectile and target ^{207}Pb nuclei.

The trajectory calculations differ from some earlier theoretical work in that pions are considered to scatter from the surface of, and propagate within, a spectator fragment. After surface scattering, the trajectory calculations continue but are weighted by the pion reflectivity. For that purpose, a model developed by Mehrem *et al.*[1], for the relativistic oblique incidence of pions on nuclear matter represented by a uniform complex nuclear potential, has been used to evaluate the pion reflectivity for the three type of pions.

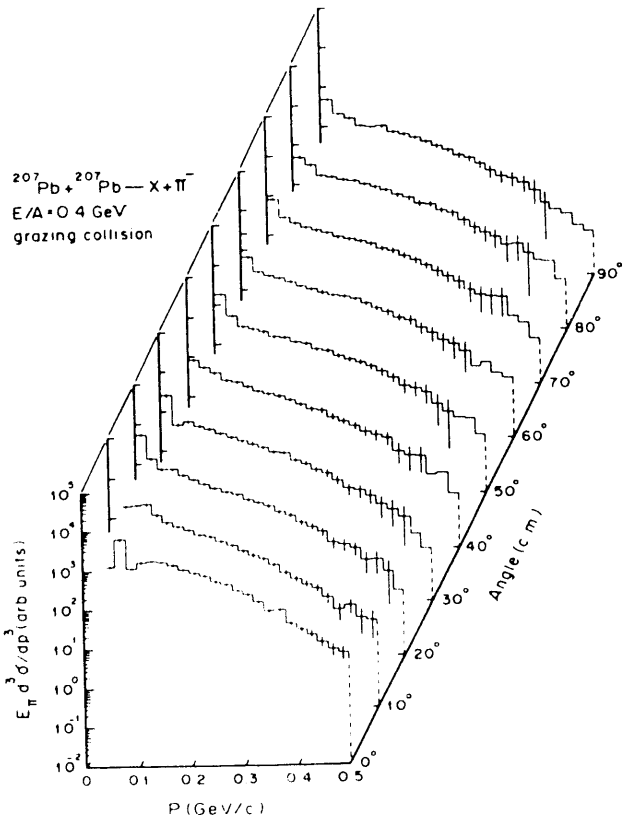

Figure 1: Differential cross sections for π^- resulting from a grazing collision of two ^{207}Pb nuclei in the center-of-mass frame. The cross section is given as a function of pion final momentum at the forward scattering angles 0°,10°,...90°.

Footnotes and References

*Phys. Rev. **C39** (1989) 1340

†Physics Department, Kuwait University, Kuwait

[1] R.A. Mehrem, H.M.A. Radi and J.O. Rasmussen, Phys. Rev. **C30** (1984) 301.

Pion-Nucleus Complex Refractive Index*

H.M.A. Radi†, J.O. Rasmussen and H.A. Halim†

A formal complex refractive index for pion-nucleus interaction is derived in terms of a full pion-nucleus optical potential operator including Lorentz-Lorenz effect and $\rho^2(r)$ terms. Two sets of optical potentials were used, the Stricker, Carr and McManus[1] (SCM), and the Carr McManus and Stricker[2] (CMS) potentials.

We have solved for wave functions and potentials using the eikonal approximation. The initial conditions are an inward moving wave at zero impact parameter. The solutions are equivalent to a left-moving plane wave on a slab of nuclear matter with diffuse boundaries and of a thickness equal to the lanthanum nuclear diameter. The proton and neutron densities are taken as Woods-Saxon form.

Numerical calculations are made for a radial propagation of a pion approaching a lanthanum (A=139, Z=57) with different energies (10-80 MeV). The real and imaginary refractive index (which are related to the complex pion wave number), the optical potential, and the absorption probability density are displayed as a function of r (Fig. 1).

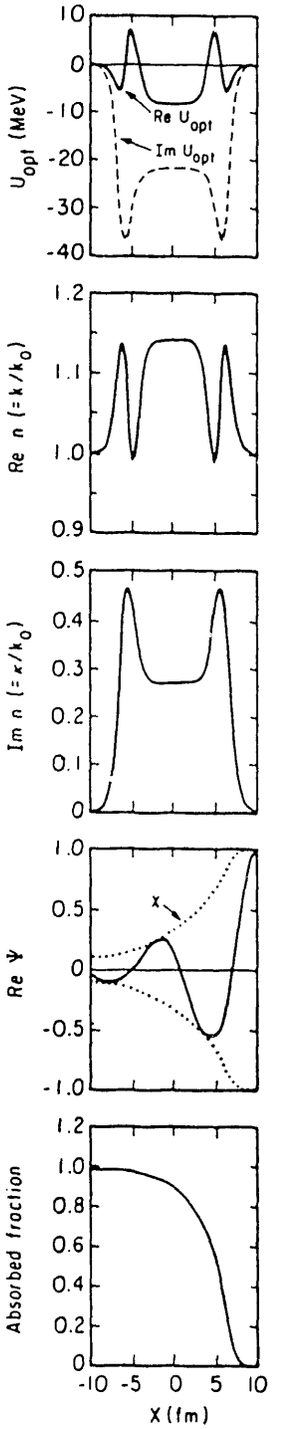

Figure 1: Radial propagation of π^0 in ^{139}La, E_{π^0} = 36 MeV.

Footnotes and References

*LBL Report 27893, Sept. 1988 (unpublished)

†Physics Department, Kuwait University, Kuwait

[1]K. Stricker, J.A. Carr and H. McManus, Phys. Rev. **C22** (1980) 2043.

[2]J.A. Carr, H. McManus and K. Stricker, Phys. Rev. **C25** (1982) 952.

Search for Bound States of Negative Pions and Neutrons*

*F.W.N. de Boer,† K.D. Wyatt, M. Justice, J.A. Bistirlich, R.R. Bossingham, A.D. Chacon, K.M. Crowe, R. van Dantzig,† C. Grab,‡ P. Kammel,§ S. Ljungfelt, C.A. Meyer, C.A. Petitjean,**J.O. Rasmussen, M.A. Stoyer, J.P. Sullivan,††and Y.W. Xu‡‡*

We have searched for bound systems of π^-'s and neutrons (pineuts) from relativistic heavy ion collisions at the Bevalac. The properties of such objects would constrain the short-range pion-nucleon interaction.[1] The mirror systems of π^+'s and protons have a lower chance of being bound than the pineuts due to Coulomb forces. The $(\pi^-)^2n^4$ system, a pseudo-alpha particle with Δ^-'s replacing the protons, was proposed[2] as a favored candidate. Collisions of relativistic, neutron-rich nuclei provide an optimal source for pineuts.

We looked for negatively charged particles with $Z \geq 2$ or $Z = 1$, $N \geq 3$ from collisions of 1.8 A·GeV ^{40}Ar and 1.3 A·GeV ^{139}La with a ^{238}U target. The JANUS spectrometer at Beam 30 was the detector; its relatively short, 3.4-m flight path is important in view of the short decay lengths expected. JANUS consists of two dipole magnets, four multiwire proportional chambers (MWPC's) and scintillation counters for triggering and time-of-flight/energy-loss data. Pion, muon, electron and proton detection was almost completely suppressed by lowering the MWPC voltages and raising the scintillator thresholds. Efficiencies and calibrations were deduced from π^+, p, d, t, ^{3}He and ^{4}He data.

In all, 6×10^6 events were recorded in the negative-particle mode. While 98% of the positive-particle data passed the analysis cuts, only 34 of the events from the negative setting survived, and only five traced back to the beam spot and had other parameters consistent with a pineut event. However, even these candidates are on the fringes of the reference distributions; because of this, we attribute them to background sources. A likelihood analysis was used to give 90% CL upper limits for pineut production.

Table 1 gives the limits on production of several pineut types from Ar + U, using a lifetime of 26 ns for $Z = 1$ and 13 ns for $Z = 2$ (assuming bound pions to have the free pion lifetime). Also listed are coalescence model estimates[3] which are two to six orders of magnitude higher. This result seems to rule out stability for the singly- and doubly-charged pineut types investigated.

TABLE 1. Pineut production per collision.

Type	Pineuts per collision	
	Experiment (upper limit, 90% CL)	Model
$(\pi^-)^1n^2$	$1.8 \cdot 10^{-6}$	1
$(\pi^-)^1n^3$	$1.2 \cdot 10^{-6}$	0.09
$(\pi^-)^1n^4$	$2.8 \cdot 10^{-6}$	0.006
$(\pi^-)^2n^2$	$2.8 \cdot 10^{-6}$	0.08
$(\pi^-)^2n^3$	$1.4 \cdot 10^{-6}$	0.008
$(\pi^-)^2n^4$	$2.0 \cdot 10^{-6}$	0.0005

Footnotes and References

*Phys. Rev. D (in press)

†NIKHEF, 1098-SJ Amsterdam, The Netherlands.
‡SLAC, Stanford, CA 94309.
§Austrian Academy of Science, A-1090 Vienna, Austria.
**Paul Scherrer Institute, CH-5232 Villigen, Switzerland.
††Texas A&M University, College Station, TX 77843.
‡‡Institute of Atomic Energy, Beijing, China.

[1] G. Kälbermann and J.M. Eisenberg, Phys. Lett. **B211**, 389 (1988); and H. Garcilazo and T. Mizatani, *πNN Systems*, World Scientific Press (1990).

[2] R. van Dantzig, F.W.N. de Boer and A. van der Schaaf, Czech. J. Phys. **B36**, 982 (1986) and R. van Dantzig, NIKHEF-K Internal Report PIMU 82-5, 1982 (unpublished).

[3] T. Kozlowski, in *Proceedings of the International Workshop on Properties of Nuclei and Nuclear Excitations*, Hirschegg, Austria, 1986, edited by H. Feldmeier (GSI, Darmstadt, 1986).

Squeeze-out of Nuclear Matter as a Function of Projectile Energy and Mass*

H.H. Gutbrod,† K.H.Kampert,‡ B. Kolb,† A.M. Poskanzer, H.G. Ritter, R. Schicker, and H.R. Schmidt†

Squeeze-out, a component of the collective flow of nuclear matter, is the preferential emission of particles out of the reaction plane. The sphericity method demonstrates it on data from the Plastic Ball detector at the Bevalac by showing a strong alignment of the medium length eigenvector in the out-of-plane direction. The sphericity squeeze-out ratio, which quantifies this effect, shows a maximum for semi-central collisions and increases with target-projectile mass. The effect peaks at surprisingly low beam energy as shown in Fig. 1, in contrast to the previously reported side-splash effect. This is disturbing because both effects describe the shape of the flow ellipsoid and one would think they would have the same energy dependence. However, side-splash is calculated from the first moment of the p_x distribution but squeeze-out may be thought of as the ratio of two second moments. As the beam energy increases, thermal smearing effects will wash out an effect in the second moments before the first moment is affected.

From the azimuthal distribution of the particles around the flow axis at mid-rapidity, the number squeeze-out ratios confirm the result from the above global sphericity analysis.

Finally, from a new method using the transverse momentum components of the particles, the $p_\perp$ squeeze-out ratio was investigated as a function of rapidity. It is clear that the effect is not jet-like, but appears at all rapidities.

Because, in a geometrical picture, squeeze-out particles escape from the hot and dense reaction zone unhindered by surrounding cold target or projectile matter, they provide a clean probe through which one can look directly at the compressed and hot fireball. It will be most interesting in the near future to see whether the successful microscopic models can consistently (using the same EOS and σ_{eff}) describe the $\langle p_x \rangle / A$, dN/dy, d/p, and squeeze-out ratios. Simultaneous description of all the exclusive experimental observables would be a large step forward in the ultimate goal of relativistic heavy-ion collisions, namely the determination of the bulk properties of nuclear matter.

Footnotes and References

*Condensed from Phys. Rev. C 42, 640 (1990).

†Gesellschaft für Schwerionenforschung, D-6100 Darmstadt, Germany

‡University of Münster, D-4400 Münster, Germany

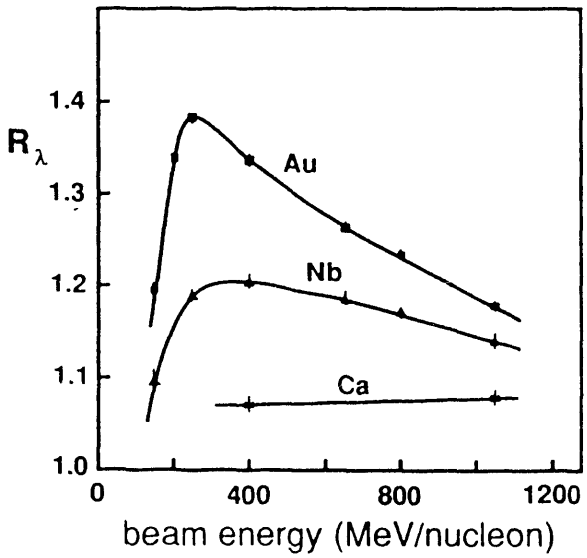

Fig. 1. The sphericity squeeze-out ratio in the three systems Au+Au, Nb+Nb and Ca+Ca. The values are shown for all the beam energies at which the systems were measured.

Pion Production in Au+Au Collisions at 1.15 GeV/N*

S.I.Chase, P.Barnes, J.W.Harris, J.Miller, G.Odyniec, W.Rauch, L.Teitelbaum, S.Tonse, R.E.Renfordt†, M.L.Tincknell‡

The LBL Streamer Chamber group and collaborators have studied pion production in central collisions of Au+Au at the highest available Bevalac enery for a Au Beam, 1.15 GeV/N. The purpose was to extend the study of pion production systematics to the heaviest system feasible with the streamer chamber. The chamber was imaged with 3 image-intensified megapixel charge-coupled-device (CCD) cameras.[1] The trigger selects approximately 5% of the total inelastic cross-section, corresponding to impact parameters $\leq$ 3 fm in a clean-cut geometrical model.

An estimate of the pion yield per participant, $< N_\pi/A >$, can be derived from measured multiplicities of negatives and total charged tracks. From the isospin excess of Au one can compute

$< N_\pi >= 2.64 < N_{\pi^-} >= 97. \pm 11.4,$

$< A >= 2.49 < N_{charge} >= 242. \pm 28.5,$

$< N_\pi > / < A >= .148 \pm .023.$

Now $< N_\pi > / < A >$ is not exactly $< N_\pi/A >$. With this caveat, the pion yield per participant is consistent with the published results on lighter systems[2] This preliminary estimate is consistent with previous results suggesting that pions are produced throughout the volume of the fireball, and not just at the surface. A complete analysis is forthcoming.

The preliminary π^- spectrum, Fig. 1, exhibits significant nonthermal behavior. No electron correction has been done, but it is expected to be less than 10% everywhere. Comparison with the La+La π^- spectrum [3] suggests that R1, the yield in the lower energy component of the spectrum, is of comparable magnitude, which reflects the systematics previously observed, given the heavier mass but lower energy of the Au+Au system. The solid curve in Fig. 1 is the VUU[4] model prediction. It is clearly concave, with R1 = 32.5%, and a very large second component. The La+La data of Ref. 3 has R1 = 42.9%.

The success of VUU in predicting the concave shape of the spectrum suggests the possibility that the mean field is responsible for the spectral shape, perhaps through the effect of the baryon flow on the pions. Baryons in the flow plane receive an extra boost from decompression. Pions produced from these baryons, or interacting with them through the Δ resonance, receive additional kinetic energy from the directed motion of the baryons.

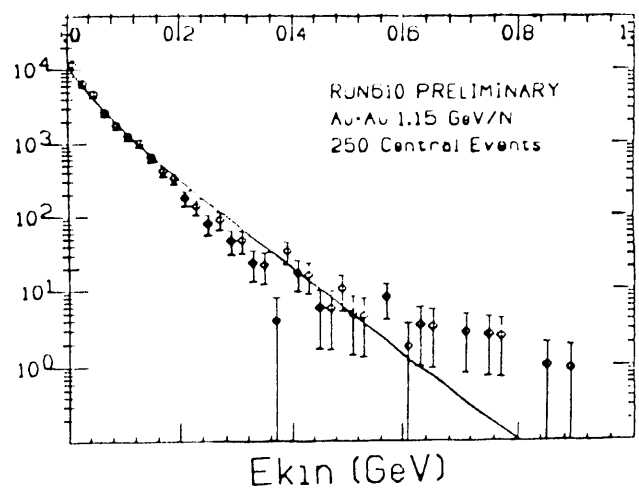

Fig.1 (1/pE)dN/dE vs. Kinetic Energy at 90 $\pm$ 30 degrees in the CM. Overlay is a VUU prediction.

Footnotes and References

*Workshop on Nuclear Dynamics VI (Jackson Hole, Wyoming 17-24 February 1990)

†Fachbereich Physik, Universität Frankfurt, D-6000 Frankfurt, Germany

‡Physics Div., Oak Ridge National Laboratory, Oak Ridge, TN 37830

[1] M.L.Tincknell *et al.*, Optical Engineering, 26, 1076 (1987).

[2] J.W. Harris *et al.*, Phys. Rev. Lett. 58, 463 (1987).

[3] G. Odyniec *et al., Proceedings of the 8th High Energy Heavy Ion Study*, Berkeley, CA 1987, p.215.

[4] J.J. Molitoris, H. Stöcker, and B.L. Winer, Phys. Rev. C 36, 220 (1987) and references therein.

Pion Correlations in Relativistic Heavy Ion Collisions for Three Symmetric Systems*

*A. D. Chacon, J. A. Bistirlich, R. R. Bossingham, H. Bossy, H. R. Bowman, C. W. Clawson, K. M. Crowe, T. J. Humanic, M. Justice, P. Kammel, J. M. Kurck, S. Ljungfelt, C. A. Meyer, C. Petitjean, J. O. Rasmussen, M. A. Stoyer, O. Hashimoto,† Wm. C. McHarris,‡ J. P. Sullivan,§ K. L. Wolf,§ and W. A. Zajc**

The method of two-pion interferometry was used to obtain size and lifetime parameters for the pion source in heavy ion collisions. Two acceptances (centered at approximately 0° and approximately 90° in the center-of-mass frame) were used for each of three systems, 1.70 GeV/nucleon ^{56}Fe + Fe, 1.82 GeV/nucleon ^{40}Ar + KCl, and 1.54 GeV/nucleon ^{93}Nb + Nb, allowing a search for dependences on nuclear mass and viewing angle. The correlation functions were calculated by comparing data samples to event-mixed reference samples. The effect of the particle correlations on the reference samples was corrected by weighting the events appropriately to remove the residual correlation effect.

The source parameters for the larger data samples are given in the tables. Sufficient data were available to allow separate parameters for the source size parallel to the beam ($R_{\|}$) and perpendicular to the beam ($R_{\perp}$), in addition to the lifetime (τ) and incoherence (λ). The parameters show an oblate source (i.e., $R_{\perp} > R_{\|}$) for the lighter systems and an approximately spherical source for the heaviest system. The dependence on nuclear mass shows that $R_{\perp}$ is essentially constant (under both viewing angles), whereas $R_{\|}$ for the 90° (cm) data increases with the nuclear mass. No evidence was found for a dependence of the source size on the pion momentum.

	Viewing Angle (cm)	
	90°	0°
$R_{\perp}$(fm)	4.5 ± 1.0	4.8 ± 0.3
$R_{\|}$(fm)	1.0 ± 1.0	4.2 ± 0.4
τ(fm/c)	$0.0^{+2.3}_{-0.0}$	$1.1^{+1.4}_{-1.1}$
λ	0.72 ± 0.10	0.81 ± 0.06
χ^2/NDF	138/156	581/537
Events	3300	12,900

Table 1: Parameters for the Ar data.

	Viewing angle (cm)	
	90°	0°
$R_{\perp}$(fm)	4.0 ± 0.65	4.8 ± 0.2
$R_{\|}$(fm)	$1.5^{+0.55}_{-0.9}$	2.7 ± 0.3
τ(fm/c)	1.7 ± 1.7	2.7 ± 0.6
λ	0.66 ± 0.06	0.88 ± 0.03
χ^2/NDF	381/403	939/729
Events	8400	32,000

Table 2: Parameters for the Fe data.

	Viewing Angle (cm)	
	90°	0°
$R_{\perp}$(fm)	4.8 ± 0.55	5.1 ± 0.2
$R_{\|}$(fm)	3.8 ± 0.2	4.1 ± 0.3
τ(fm/c)	4.8 ± 1.0	3.9 ± 0.4
λ	0.89 ± 0.035	1.11 ± 0.03
χ^2/NDF	846/795	1144/1087
Events	39,100	49,400

Table 3: Parameters for the Nb data.

Footnotes and References

*LBL report LBL-30084; Physical Review C (in press).

†Institute for Nuclear Study, University of Tokyo, Tanashi, Tokyo 188, Japan.

‡Michigan State University, East Lansing, Michigan 48824.

§Cyclotron Institute, Texas A & M University, College Station, Texas 77843.

**Columbia University, New York, New York 10027.

Pion Correlations in Relativistic Heavy Ion Collisions at the BEVALAC

W. Christie, D. Olson, T. Abbott, D. Beavis, P. Brady, S. Fung, J. Kang,
D. Keane, Y. Liu, W. Mueller, J. Romero, J. Symons, C. Tull, H. Wieman
UCD, UCR, LBL, BNL, Harbin Inst., Kent State

Presented here is a brief summary of the results of a pion correlation experiment[1] performed at HISS. The beams and targets used were 1.8 GeV/nucleon Argon on KCl and Lanthanum targets, and 1.2 GeV/nucleon Xenon on a Lanthanum target.

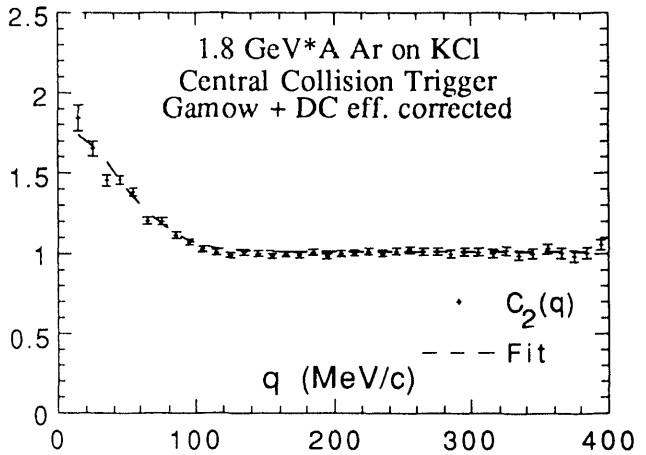

Fig. 1. $C_2(q)$ vs q.

The analysis technique used is commonly known as the Hanbury-Brown, Twiss (HBT) or Goldhaber, Goldhaber, Lee, and Pais (GGLP) method.

The acceptance for the π^-s was centered about 0° in the center of mass system. Central events were selected by triggering on events which had little ($Z \leq 2$) or no charge in the projectile fragment region. The trigger selected ≈ 26% of the geometric cross section for the Ar on KCL data, ≈ 40% for the Ar on La, and ≈ 37% for the Xe on La.

The experimental data was fit using the forms:

$$C_2(q,q_0) = N[1 + \lambda e^{(-q^2R^2/2 - q^2\ 0\tau^2/2)}],$$

$$C_2(q_\perp q_{//} q_0) = N[1 + \lambda * \exp(-q_\perp^2 R_\perp^2/2 - q_{//}^2 R_{//}^2/2 - q_0^2\tau^2/2)]$$

The quantities q, q_0, $q_\perp$ and $q_{//}$ refer to the relative three momentum, energy, perpendicular and parallel momentum relative to the beam direction, respectively. The fit parameters $R_\perp$ and $R_{//}$ are thus interpreted as measures of the source radius in these two directions. N is a normalization constant and λ, commonly referred to as the chaoticity parameter, allows for correlations due to effects other than the Bose Einstein (BE) statistics.

Table 1. Results with Systematic Corrections

Data Set	Ar on KCl 1.8 GeV*A	Ar on La 1.8 GeV*A	Xe on La 1.2 GeV*A
R (fm)	4.30± .14	3.88± .28	4.90± .75
τ (fm/c)	0.0	0.0± 1.0	$3.4^{1.9}_{3.4}$
λ	.78± .05	1.05± .13	.76± .17
$\frac{\chi 2}{NDF}$	$\frac{745.1}{726}$	$\frac{193.3}{178}$	$\frac{220.25}{158}$
$R_\perp$ (fm)	4.39± .15	4.63± .40	5.40± .65
$R_{//}$(fm)	3.48± .30	3.82± .50	7.70± 1.40
τ (fm/c)	$1.30^{+.90}_{-1.30}$	0.0± 2.0	0.0+ 3.60
λ	.77± .05	1.10± .14	.91± .18
$\frac{\chi 2}{NDF}$	$\frac{2088.3}{2081}$	$\frac{559.5}{548}$	$\frac{450.0}{394}$

As the dependence of the correlation function as described here does not show much dependence on q_0 one often sees its projection onto the q axis. This is shown in Fig. 1 for the Ar on KCl data.

The results of the fits are shown with systematic corrections applied for the Gamow Coulomb effects, the DC tracking efficiency, and for Background correlations. Where calculated, the one σ errors are given for the parameters. Also listed in the tables the reader will find the χ^2 and the number of independent degrees of freedom (NDF) for the fit.

Theoretical analyses show that, in the present case, $R_{//}$ and τ are correlated parameters, while $R_\perp$ is independent, and hence the most reliable parameter.

---

[1] W.B. Christie, Ph.D. Thesis, Lawrence Berkeley Laboratory Report # LBL - 28986, 1990.

Short Range Correlations and Nucleon Emission in Peripheral Relativistic Heavy Ion Collisions*

C.A. Bertulani†, L.F. Canto†, R. Donangelo† and J.O. Rasmussen

Following the pioneering work of Feshbach and Zabek [1], we have studied the effect of the short-range nucleon- nucleon correlations on the emission of one or two nucleons from a heavy target after a relativistic heavy-ion collision. The basic idea is that in a relativistic peripheral collision between two heavy nuclei a phonon of excitation may be generated by the field, such phonon carrying large energy (corresponding to the short Lorentz- contracted collision time) but low momentum (corresponding to the nuclear dimensions). Such a phonon, like stopped negative pion absorption, cannot be absorbed on a single nucleon but must be absorbed by a nucleon pair or cluster in order to conserve energy and momentum.

We have used Gaussian approximations for the nucleon-nucleus potential and for each nucleon-pair wave function. In this way we took into account absorption effects, which Feshbach and Zabek ignored. Thus, we were able to derive an analytical expression for the quadruple-differential cross section for the emission of two nucleons. This cross section is written as the product of several factors: a phonon spectrum, analogous to the one discussed by Feshbach and Zabek, a factor explicitly dependent on the correlation radius, and factors associated with momentum conservation in the absorption of a phonon by a correlated nucleon pair.

We have performed numerical calculations for the Ca + Ca and U + Ag systems at 14.5 GeV/u and 1 GeV/u, respectively. The calculated cross sections display a marked correlation between the energies and directions of the emitted nucleons. We have shown that these correlations predominantly arise from momentum exchange between the nucleon pair and the absorbed phonon. We suggest that such correlations can be used as a signature for short-range correlation effects in future exclusive experiments, since our estimate for the total cross section for this mechanism lies in the few tens of millibarns range. We have not attempted to compare these predictions with experiment, since such exclusive experimental data does not appear to be available at present.

Footnotes and References

*IF/UFRJ/88/29; Modern Physics Letters A4 (1989) 1315.

†Instituto de Fisica, Universidade Federal do Rio de Janeiro, Cx. Postal 68.528, 21945 Rio de Janeiro, RJ, Brazil.

[1] H. Feshbach and M. Zabek, Ann. of Phys. 107 (1977) 110; H. Feshbach, Prog. Part. Nucl. Phys. 4 (1980) 451.

Electron Pair Production in p-Be Collisions

C. Naudet, S. Beedoe , J. Carroll*, P. Force† , J. Gordon*, T. Hallman‡ , G. Igo*, P. Kirk§ , G. Krebs, A. Letessier-Selvon, L. Madansky‡, H.S. Matis, D. Miller**, J. Miller, G. Roche†, L. Schroeder, P. Seidl, Z. F. Wang§, R. Welsh‡, and A. Yegneswaran††*

The study of low-mass electron-positron pairs ($0.2 < M < 1.0$ GeV/c^2) in proton-nucleus collisions has been of considerable theoretical and experimental interest. Measurements in the early seventies showed that the low-mass dilepton and low-transverse momentum single lepton yeilds were not fully understood. In particular the dominate production mechanisms and the excitation function were unknown. The DLS collaboration performed a series of dielectron measurements from Dec 1986 until May 1989 in an effort to answer these and other questions.

The dielectron cross section for p-Be at three beam energies, 4.9, 2.1 and 1.0 GeV were measured. The total integrated e^+e^- production cross-section as a function of the available nucleon-nucleon center-of-mass energy Q is shown in Figure 1. A detailed dicussion of the kinematic dependences of the cross-section (invariant mass, p_t) maybe found in elsewhere.[1] A considerable amount of theoretical interest has been generated by the DLS data, in particular, Gy. Wolf's [2] calculations show that the $\Delta(1232)$ Dalitz-decay may well explain the high-mass dielectrons at the 1.0 GeV/c^2 beam energy.

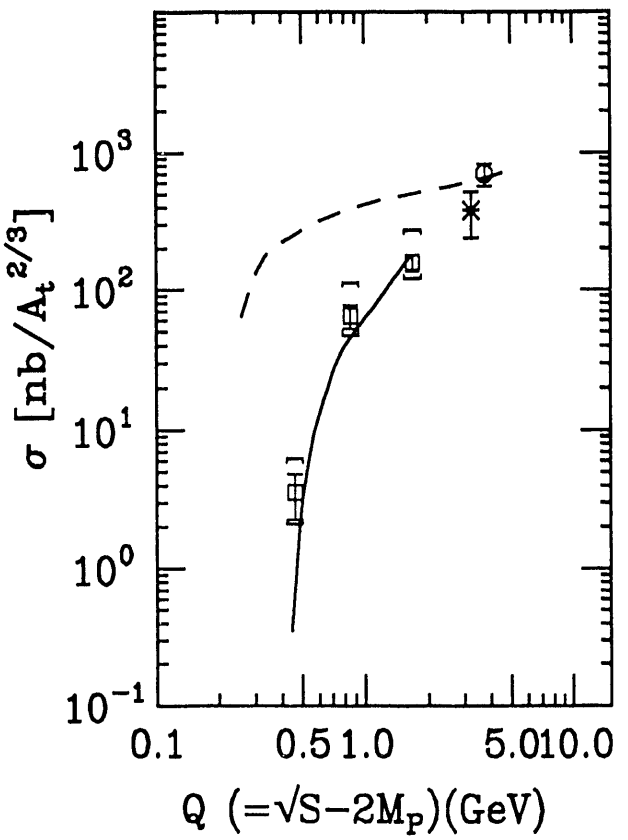

Figure 1: The total integrated e^+e^- production cross-section as a function of the avaiable nucleon-nucleon center-of-mass energy Q: squares, this experiment for ($0.2< M < 1.0$ GeV/c^2);circle and star, higher energy e^+e^- data. The inner error bar is statistical and the outer error brakets also includes in quadrature all systematic errors (DLS data). The solid and dashed curves show the $\pi^+\pi^-$ and π^0 production cross-sections, respectively, scaled by 1.33×10^{-5}.

Footnotes and References

*Department of Physics, University of California at Los Angeles, Los Angeles, CA 90024

†Université. de Clermont II, Aubière, France

‡Department of Physics, The Johns Hopkins University, Baltimore, MD 21218.

§Louisiana State University, Baton Rouge, LA 70803.

**Department of Physics, Northwestern University, Evanston IL 60201.

††CEBAF, Newport News, VA 23606.

[1] G. Roche. et. al. Phys. Rev. Lett. 61, 1069 (1988), C. Naudet et. al. Phys. Rev. Lett. 62, 2652 (1989).

[2] Gy. Wolf et. al. Proceedings of the 4'th Journees des Theoriciens at Saturne, Nov 22-23,1990.

Electron Pair Production in Ca+Ca Collisions

C. Naudet, S. Beedoe[*] , J. Carroll[*], P. Force[†] , J. Gordon[*], T. Hallman[‡] , G. Igo[*], P. Kirk[§] , G. Krebs, A. Letessier-Selvon, L. Madansky[‡], H.S. Matis, D. Miller[**], J. Miller, G. Roche[†], L. Schroeder, P. Seidl, Z. F. Wang[§], R. Welsh[‡], and A. Yegneswaran[††]

The Dilepton Spectrometer Collaboration (DLS) has undertaken a program of measuring electron-pair production in p-nucleus and nucleus-nucleus collisions at the Bevalac. In p-Be collisions at 1.0, 2.1 and 4.9 GeV beam kinetic energy the invariant mass and transverse-momentum spectra and the total cross sections have been studied in detail[1]. In nucleus-nucleus collisions, dileptons are expected to be a good probe of the hot and dense phase of the fireball. Recent calculations[2] applicable to the Bevalac energy domain have shown the possible interesting effects in the mass structure can be understood in terms of the pion dispersion relation in nuclear matter.

The existence of electron pairs in both p-Be and Ca-Ca has been clearly established down to 1.0 GeV/A. Shown in Fig. 1 is the cross-section per nucleon as a function of the invariant mass for Ca-Ca collisions at 1.0 GeV kinetic beam energy also shown is an estimate of the Dalitz background for Ca-Ca collisions. The Dalitz calculation includes the contributions of the π^0 and the $\Delta(1232)$, each dominating the background at low mass and high mass respectively. The Ca-Ca mass spectra is seen to much greater than the estimated Dalitz background indicating a large excess of electron-pairs (direct electron pairs). A comparison of the p-Be and Ca-Ca mass spectra shows the excess of higher mass dielectrons from the Ca-Ca reaction to be quite significant.

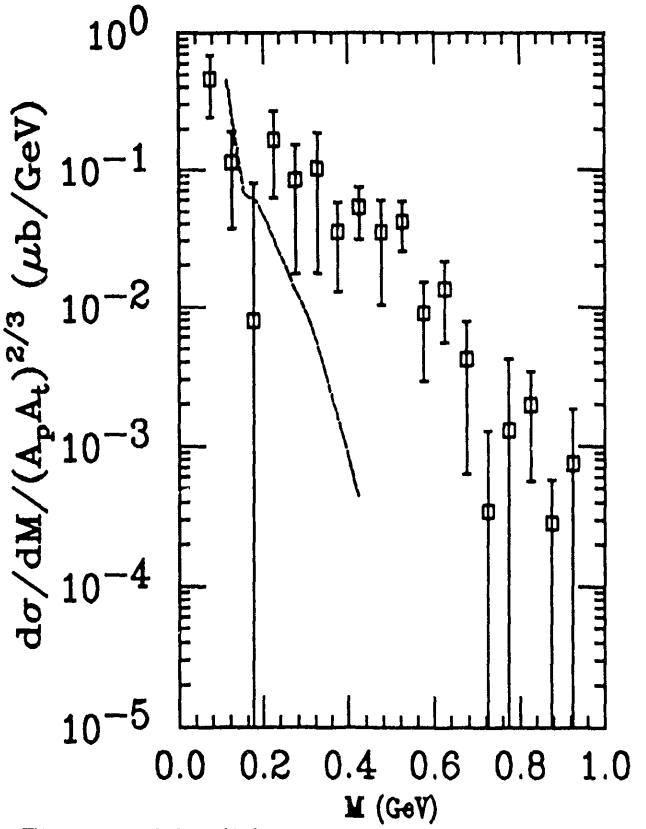

Figure 1: The dielectron invariant mass spectra for Ca+Ca at 1.0 GeV/c^2. Also shown is the estimated background contribution due to π^0 and $\Delta(1232)$ Dalitz-decay.

Footnotes and References

[*]Department of Physics, University of California at Los Angeles, Los Angeles, CA 90024
[†]Université. de Clermont II, Aubière, France
[‡]Department of Physics, The Johns Hopkins University, Baltimore, MD 21218
[§]Louisiana State University, Baton Rouge, LA 70803
[**]Department of Physics, Northwestern University, Evanston IL 60201
[††]CEBAF, Newport News, VA 23606

[1]G. Roche et al. Phys. Rev. Lett. **61**, 1069 (1988), C. Naudet et al., Phys. Rev. Lett. **62**, 2652 (1989)
[2]C. Gale and J. Kapusta Phys. Rev. C **35**, 2107 (1987).// L. H. Xia et al., Nucl. Phys. **A485**, 721 (1988).

Measurement of p+p Elastic Cross Sections with DLS Spectrometer

H.Z. Huang, S. Beedoe , M. Bougteb† , J. Cailiu, J. Carroll*, T. Hallman‡ , G. Igo*, P. Kirk§ , G. Krebs, A. Letessier-Selvon, B. Luttrell, F. Manso†, L. Madansky‡, H.S. Matis, D. Miller**, J. Miller, C. Naudet, G. Roche†, L. Schroeder, P. Seidl, Z. F. Wang§, R. Welsh‡, and A. Yegneswaran††*

In order to calibrate the DLS for the scale of momentum measurement, momentum resolution and for absolute normalization, the differential cross-section($\frac{d\sigma}{dt}$) for p+p elastic collisions at the incident proton kinetic energy of 1.03GeV has been measured with the DLS spectrometer system.

The p+p elastic data were taken during the September running of 1990, using di-hadron triggers which require at least one hit each on front and rear hodoscope arrays for both spectrometer arms. The momenta of both particles are measured from the reconstructed tracks using drift chambers and known magnetic field, and both particles are identified as protons using the time-of-flight(TOF) from the hodoscopes. Two magnetic field configurations, 1.5KGauss and 4.5KGauss, were used; however, only data at 1.5KGauss field are shown here since this field is relevant to our di-lepton measurements. Detailed information about the DLS spectrometer system can be found in Yegneswaran et al.[1]

Figs. 1a-1c show the sum of p_x, p_y and p_z distributions in the beam coordinate system for two protons from p+p elastic collisions. For an ideal case of p+p elastic kinematics the sums of p_x and p_y are zero and the sum of p_z is 1.73GeV/c. Fig.1d shows the differential cross-section, $\frac{d\sigma}{dt}$, in comparison with data from Jenkins et al.[2] at beam incident momentum of 1.896GeV/c. We conclude that the measured momentum from the DLS spectrometer system is correct within 6-7% uncertainties, that the momentum resolution($\frac{\sigma_p}{p}$) is about 13% for the p+p elastic sample with an average momentum about 0.8GeV/c, and that $\frac{d\sigma}{dt}$ agrees with the data from Jenkins et al. within 15%.

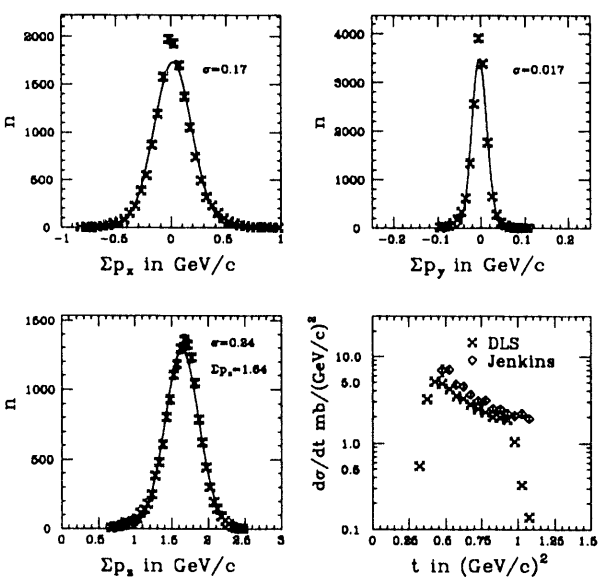

Figure 1: 1a-1c are distributions of Σp_x, Σp_y and Σp_z in GeV/c, the lines are gaussian fits. 1d shows the p+p elastic cross-sections $\frac{d\sigma}{dt}$ from DLS spectrometer in comparison with data from Jenkins at el.

Footnotes and References

*Department of Physics, University of California at Los Angeles, Los Angeles, CA 90024

†Université. de Clermont II, Aubière, France

‡Department of Physics, The Johns Hopkins University, Baltimore, MD 21218

§Louisiana State University, Baton Rouge, LA 70803

**Department of Physics, Northwestern University, Evanston IL 60201

††CEBAF, Newport News, VA 23606

[1] Yegneswaran et al. Nucl. Instr. and Meth. A290(1990), 61

[2] Jenkins et al. Phys. Rev. 21(1980), 2445

Liquid Hydrogen Target for DLS

J. Carroll, S. Beedoe*, M. Bougteb†, J. Cailiu, T. Hallman‡, H.Z. Huang, G. Igo*, P. Kirk§, G. Krebs, A. Letessier-Selvon, B. Luttrell, L. Madansky‡, F. Manso†, H.S. Matis, D. Miller**, J. Miller, C. Naudet, G. Roche†, L. Schroeder, P. Seidl, Z.F. Wang§, R. Welsh‡, and A. Yegneswaran††*

To interpret the electron-pair yield produced in nucleus-nucleus collisions , one needs to know the 'elementary' yields - those produced by p+p and p+n collisions. The DLS program to measure these elementary yields began in 1989.

Yields of electron pairs from p+p and p+d measurements made in 1989 had a very poor target (full/empty) ratio. Subsequent tests showed that the large target-empty yield was produced by interactions of a halo around the proton beam with the thick walls of the vacuum jacket in use at that time.

A new vacuum jacket was designed and constructed in which all of the metal components were more than 4" from the beam . A cylindrical flask of large diameter was constructed to remove the walls from the halo region. Tests of the new target assembly in a 4.9 GeV proton beam were made in May-June '90. These tests showed that the new assembly gives an adequate target full/empty ratio after geometric cuts are used to define tracks that originate near the flask. The residual background (not associated with the flask) is now negligible. Physics data taken during October, 1990 show (full/empty) ratios of ≥ 7 for p+p reactions and ≥ 15 for p+d reactions.

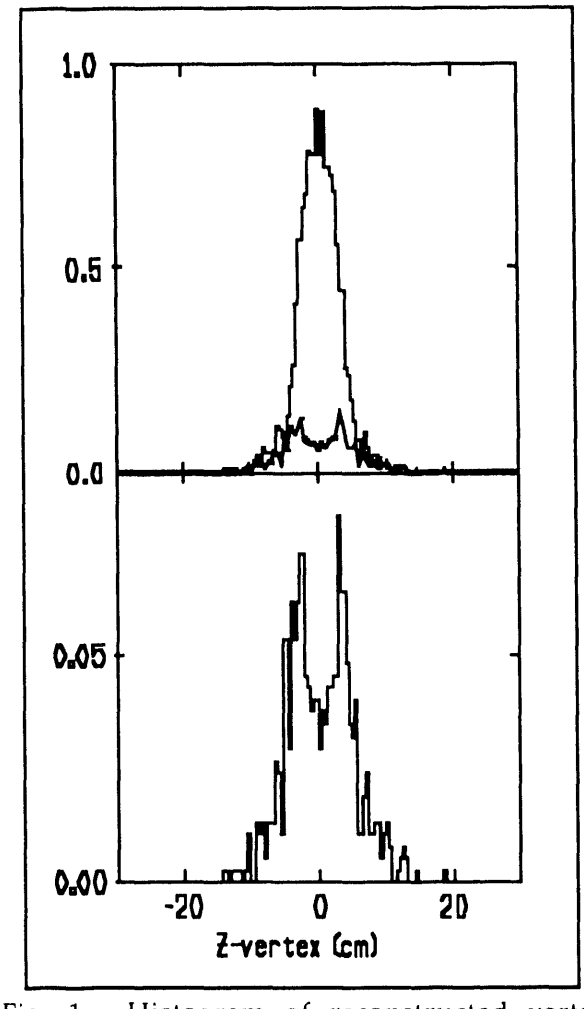

Fig. 1. Histogram of reconstructed vertex position along the beam line for detected electron pairs. The upper figure shows distributions normalized to incident flux for full target (liquid hydrogen) and 'empty' target (gaseous hydrogen). A vertically expanded 'empty' target distribution is shown in the bottom figure. The end caps of the kapton flask are visible in the 'empty target' spectrum, indicating that there is not much contribution from the cold gas.

Footnotes and References

*Physics Department, UCLA, Los Angeles, CA 90024

†Université de Clermont II - IN2P3, 63170 Aubière, France

‡Physics Department, The Johns Hopkins University, Baltimore, MD 21218

§Physics Department, Louisiana State University, Baton Rouge, LA 70803

**Physics Department, Northwestern University, Evanston, IL 60201

†† CEBAF, Newport News, VA 23606

The Multiplicity Array of the Dilepton Spectrometer

S. Beedoe , J. Carroll*, P. Force† , J. Gordon*, T. Hallman‡ , G. Igo*, P. Kirk§ , G. Krebs, A. Letessier-Selvon, L. Madansky‡, H.S. Matis, D. Miller**, C. Naudet, G. Roche†, L. Schroeder, P. Seidl, Z. F. Wang§, R. Welsh‡, and A. Yegneswaran††*

When the Dilepton Spectrometer (DLS) was upgraded for our May 89 experiment, a multiplicity array (MA) was implemented to measure the number of charged particles produced during the collision. The charged particle multiplicity provides knowledge about the centrality of the collision. Central collisions are important in nucleus-nucleus interactions since the study of dielectron production can serve as a probe of nuclear matter at high density and temperature.[1] In addition, each of the three drift chambers per arm was upgraded from 6 sense planes to 7. The added plane, measuring the x-position of a particle, improves the momentum resolution of the spectrometer.

The multiplicity array is composed of 96 (0.32 cm thick) plastic scintillator paddles, with 48 paddles covering the top half and 48 covering the bottom half of the conical-shaped scattering chamber. The target configuration is located at the base of the cone with its axis along the direction of the beam. The first half sector is referred to as up-stream multiplicity array, and the second half sector referred to as the down-stream multiplicity array. Particles enter the spectrometer through the side opening. The down-stream multiplicity array has an angular acceptance from about 13° to 51.7° in polar angle while the up-stream multiplicity array has an angular acceptance from 51.7° to 90° in polar angle. The top half extends from $\phi = 15°$ to $\phi = 165°$ in azimuthal angles, and the bottom half covers from 195° to 345°. The total angular acceptance subtended by the MA at the target is about 2.6 str. Each MA element has a scintillator and light guides which direct the scintillator light to the photo cathode, see Fig. 1. In Nb+Nb collisions, at beam kinetic energy of 1.05 GeV/nucleon, the average number of charged particle measured by the multiplicity array was about 27 for the dielectron trigger.

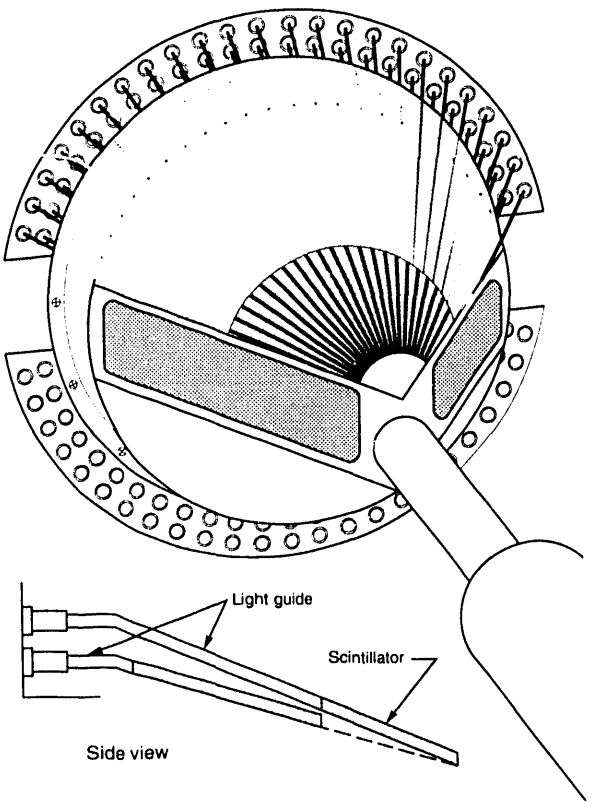

Figure 1: Diagram of the multiplicity array: 96 elements with 48 on top half and 48 on the bottom half of the conical scattering chamber.

Footnotes and References

*Department of Physics, University of California at Los Angeles, Los Angeles, CA 90024

†Université. de Clermont II, Aubière, France

‡Department of Physics, The Johns Hopkins University, Baltimore, MD 21218

§Louisiana State University, Baton Rouge, LA 70803

**Department of Physics, Northwestern University, Evanston IL 60201

††CEBAF, Newport News, VA 23606

[1] G. Roche, et al. Phys. Rev. Lett., B226, 228 (1989)

DLS Real Time Beam Monitoring System

H. S. Matis, J. Cailiu, S. Beedoe, M. Bougteb,† J. Carroll,* T. Hallman,‡ H. Z. Huang, G. Igo,* P. Kirk,§ G. Krebs, A. Letessier-Selvon, B. Luttrell, L. Madansky,‡ F. Manso,† D. Miller,** C. Naudet, G. Roche,† L. Schroeder, P. Seidl, Z. F. Wang,§ R. Welsh,‡ and A. Yegneswaran††*

The DLS has evolved from an experiment establishing the existence of a direct electron pair signal to a program searching for the detailed behavior of electron pair as a function of target and projectile mass.

This new program requires long running periods to make sure the detector efficiencies vary as little as possible. Consequently, we have improved the monitoring of systematic errors while data is taken.

Since we are searching for a relatively rare process, any change in the background can drastically reduce our signal to noise ratio. In particular, a small drift in the beam can cause a large increase in the flux of particles hitting our detector or else can produce a change in our normalization due to the beam missing the target.

As beam intensities vary from 10^7 to almost 10^9 ions per second, techniques which measure individual beam particles do not work very well. However we have found that by using the standard Bevatron wire chambers, the average position of the beam can be determined for each spill. Since the the Bevatron computer system does not talk to the DLS computer, we have connected the wire chambers directly to the DLS CAMAC crates.

Two wire chambers are placed downstream of our target. After each spill, the contents of the wire chambers are read, recorded on tape and a circular disk file, and then displayed both in the DLS and Bevatron control rooms. Any excursion from the nominal beam position, immediately produces an alert for an operator so that corrective action can be taken.

The disk file is continuously monitored by an analysis program which calculates the centroid of the beam distribution in both x and y. From these centroids, the program determines the extrapolated position of the beam at the target and displays the value on a CRT screen Fig. 1 shows a time plot of the extrapolated x position of the beam from one run. One can see that there was a drift of 1 cm near spill 100.

Experience has shown that this system works very well. Shifts in the beam position can be detected rapidly and a request for retuning of the beam can be quickly made. In addition, the beam position is recorded on tape so that triggers during the time of poor beam quality can be rejected.

Footnotes and References

*UCLA
†Université de Clermont II
‡The Johns Hopkins University
§Lousiana State University
**Northwestern University
††CEBAF

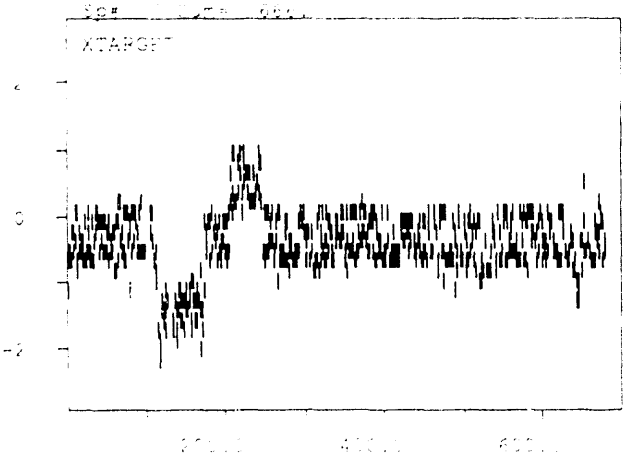

Fig. 1. A time profile for the x position of the beam at the DLS target. The horizontal axes shows the spill number of the beam while the vertical axes shows the x centroid position of the beam. Vertical scale is 1 cm. Times increases along the horizontal axis. There is one beam spill every 6 seconds.

Detector simulations for the Dilepton Spectrometer

P. A. Seidl, S. Beedoe , M. Bougteb† , J. Cailiu, J. Carroll*, T. Hallman‡ , H. Z. Huang, G. Igo*, P. Kirk§ , G. Krebs, A. Letessier-Selvon, B. Luttrell, L. Madansky‡, F. Manso†, H. S. Matis, D. Miller**, J. Miller, C. Naudet, J. Panetta, G. Roche†, L. Schroeder, Z. F. Wang§, R. Welsh‡, A. Yegneswaran††*

We have integrated our DLS GEANT[1] Monte Carlo output with our LISA[2] based analysis and reconstruction program. This has enabled us to address in detail issues such as resolution, and reconstruction algorithm efficiency.

The latter are particularly important for the interpretation of our heavy ion running, where the track multiplicity per arm is roughly five for $Nb+Nb$ and $Ca+Ca \rightarrow e^+e^-X$ at $T_{beam} = 1.0$ and $2.1GeV$, respectively (Fig. 1). We have studied electron misidentification probabilities and high multiplicity track matching by "mixing" Monte Carlo events from an intra-nuclear cascade model with Monte Carlo e^+e^- pairs.[3]

We have also compared our pp elastic scattering data[4] to Monte Carlo elastic scattering data, as this reaction provides a useful "line source" to quantify resolution effects.

To date, in the area of comparison of theory to experiment, we have folded some theoretical models with a resolution function of low dimensionality in order to include the effects of resolution in the model. However, this is only an approximation; our final state of interest, the e^+e^- pair, is characterized by six kinematic variables. Thus, we have recently begun to approach the task of comparing our measurements to models in such a manner so as to rigorously include uncertainties due to instrumental resolution for the model parameterizations. Thus Monte Carlo final states are generated according to the model parameterizations, processed with the GEANT model of our experiment, and reconstructed with our analysis program. This simulated data is then compared to our measurements, and will give a more accurate measure of the degree of aggreement with theory.

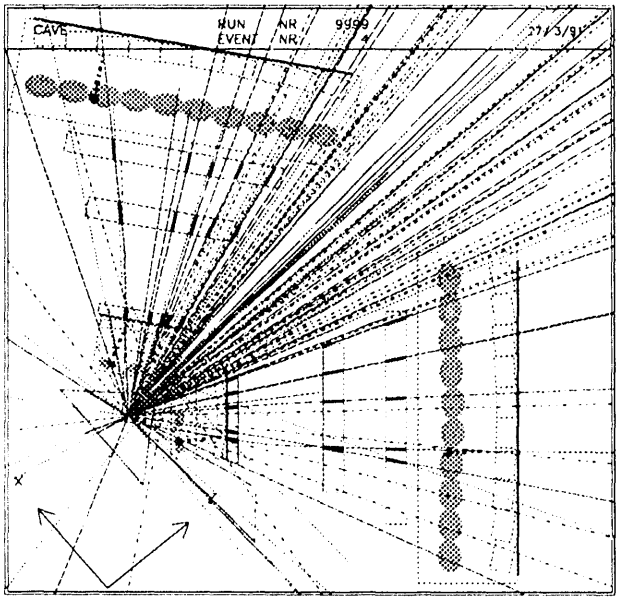

Figure 1: A $Ca + Ca$ ($T_{beam} = 2.1GeV$) central collision from the intra-nuclear cascade model is simulated with the DLS GEANT program.

Footnotes and References

*Physics dep't., University of California at Los Angeles, Los Angeles, CA 90024

†Université de Clermont II, IN2P3, 63170 Aubière, France

‡Physics dep't., The Johns Hopkins University, Baltimore, MD 21218

§Physics dep't., Louisiana State University, Baton Rouge, LA 70803

**Physics dep't., Northwestern University, Evanston IL 60201

††CEBAF, Newport News, VA 23606

[1] R. Brun et al., CERN DD/EE/84-1 (1987).

[2] Burkhard Kolb, GSI, Darmstadt, Germany; J. Liu and H. Matis LBL PUB-3071 (1988).

[3] A. Letessier-Selvon et al., Phys. Rev. **C40** (1989) 1513; K. Kinoshita, H. Satz, D. Schildknecht, Phys. Rev. **D17** 1978, 1834.

[4] see Huan Z. Huang et al., this volume.

EOS TPC Mechanical Construction

S. Abbott, A.A. Arthur, J. Bercovitz, C.W. Harnden and the EOS Collaboration

A time projection chamber (EOS TPC), now under construction at LBL, will be used to study relativistic heavy ion collisions at the Bevalac. The EOS TPC, sketched in Figure 1, is a single, rectangular box centered in the HISS dipole magnet and is designed to operate at one atmosphere pressure. Some design features of the detector are given in Table 1. The detector is configured as a drift volume enclosed with field cage panels on the sides and a single, proportional wire chamber - pad plane on the bottom. The active drift volume is 150 cm long in the beam direction, 96 cm wide in the bending direction and 75 cm high in the drift direction.

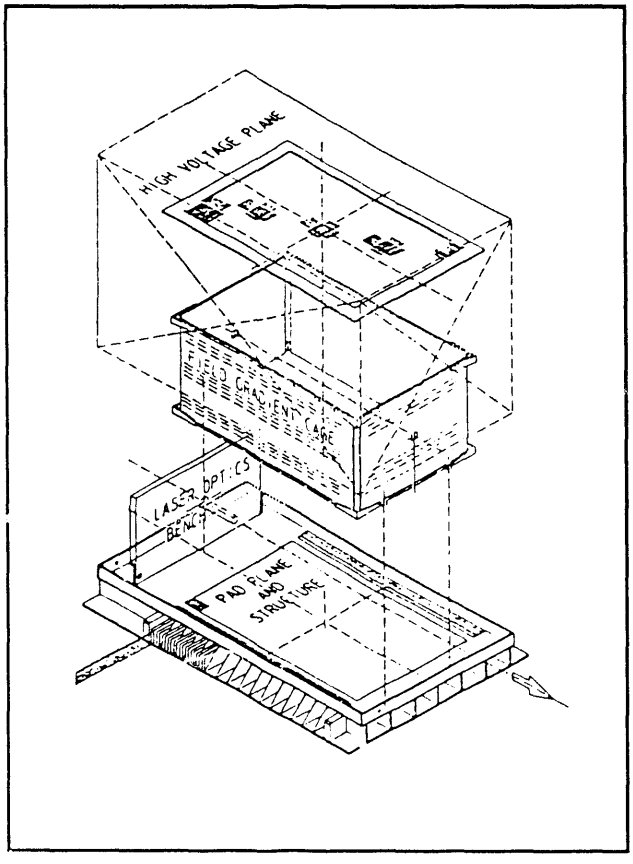

Fig. 1. Exploded view of EOS TPC

A 15 cm high, rigid I-beam box structure between the pad plane and the magnet pole tip maintains the pad plane uniformity and provides the support structure for the TPC. The front end electronics are located in the box structure and plug directly into the back side of the pad surface. The pad plane is a solid array of 1.2 cm X 0.8 cm pads (15,360 pads total). The wire planes over these pads will be essentially the same as in the PEP4, TOPAZ and ALEPH detectors. An optical platform located upstream of the active volume supplies laser beam tracks for spatial calibration. The detector is encased in a relatively lightweight skin for gas containment and thermal isolation. Multiple scattering is kept small so that the TPC can be operated in combination with other detectors.

EOS TPC Characteristics	
Pad Plane Area	1.5 m X 1.0 m
Number of Pads	15360 (120 X 128)
Pad Size	12 mm X 8 mm
Drift Distance	75 cm
Sampling Freq.	10 MHz
Shaping Time	250 ns
Electronic Noise	700 e
Gas Gain	3500
Gas Composition	90% Ar + 10% CH4
Pressure	1 Atmosphere
B Field	13 kG
E Field	120 V/cm
Drift Velocity	5 cm/μs
Event Rate	10-80 events/spill
dE/dx range	Z = 1-8, Λ, π, p, d, t, He, Li-O
Multiplicity Limit	~ 200

Tab. 1. EOS TPC Characteristics

EOS TPC Electronics

S. Abbott, A.A. Arthur, J. Bercovitz, C.W. Harnden, R. Jones, S. Kleinfelder, K. Lee, M. Nakamura, M. Wright, R. Wright, and the EOS Collaboration

The EOS Time Projection Chamber is designed to study relativistic heavy ion collisions at the Bevalac and to cope with the high multiplicity and high particle density environment typical for those reactions. The detector will provide particle identification and momentum measurements for most of the emitted charged particles.

The electronics requirements include low noise for good position resolution, large dynamic range for dE/dx identification of Z>1 particles, high density and low cost per channel. These are achieved with a design using custom integrated circuits and extensive signal multiplexing. Most of the electronics (schematically shown in Fig. 1) are located on the pad plane. A single motherboard services a row of pads (a total of 60 pads) across half the width of the chamber. The printed circuit boards are subdivided into 15 sections, each containing an integrated circuit, 4-channel preamplifier and four discrete shaper-amplifiers. The output of the shaper amplifiers are time sampled and stored in analog memory (switched capacitor arrays) at the end of the motherboard at a rate of 10 MHz. All 256 cells for 60 pad channels are multiplexed out of the switched capacitor arrays and digitized in a single ADC at a rate of 1 MHz. The digitized data from two boards are transmitted off the detector via a 100 Mbits/s optical link for further processing in the counting area. A complete prototype channel is currently operating and sending data to the analysis computers for use in testing and software development.

A 4-channel CMOS integrated preamplifier has been developed. The circuit design includes a selectable, on-chip pulser system to be used for diagnostics and absolute gain calibration. The chips have satisfied our requirements for linearity, rise time, and dynamic range. The measured noise at the input is 600 e rms. Production of the chips is completed and testing is underway.

A switched capacitor array for analog signal sampling and storage has been developed. This CMOS integrated circuit has 16 channels with 256 time samples per channel. The measured dynamic range of this device is 4000:1 at 1% nonlinearity. The main advantage of this chip over CCD's for our system is significantly reduced clock driving current and a factor of 8 improvement in channels per chip packing density. The chips have been produced and tested.

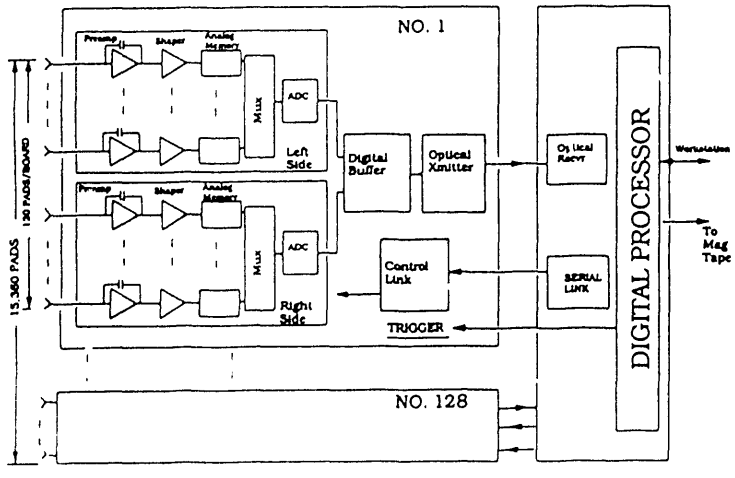

Fig. 1. Schematic view of the electronics.

EOS TPC Laser Calibration System

D. Cebra, H. Wieman, D. Harness, Y. Shao, M. Ingle, and the EOS Collaboration

Static distortions in the electron drift path due to the curving **B** field lines require a deconvolution procedure to extract spatial coordinants from the raw pad and time bucket information of the EOS TPC. This deconvolution routine must be checked against some set of positional references. The laser system will produce straight line ionization tracks through the active volume of the TPC. Use of the laser during the course of an experiment will make it possible to monitor time dependent distortions due to positive ion build up in the gas volume, and changes in ambient temperature and pressure.

The laser calibration system uses a Nd:YAG laser to produce the reference beams. The laser will be mounted seven meters upstream from the TPC. Within the laser housing, the frequency of the primary beam will be quadrupled to 266 nm (UV). The majority of the power from the primary beam will be dumped; the remaining intensity can be remotely controlled with a half-wave plate on a motorized rotation stage followed by a Glan polarizer. The radius of the beam is reduced with a two-lens focusing telescope. The precise position and angle of the outgoing beam is defined by two mirrors on remotely controlled kinematic mounts.

The laser beam is split into 18 calibration paths on an optics board that is mounted vertically on the upstream end of the TPC. A diagram of the distribution board is provided in Fig. 1. In addition to the 18 calibration paths, two paths are split off to allow for monitoring of the beam position with quadrant silicon detectors which serve as permanent reference points. Six of the calibration beams pass diagonally through the active region of the the TPC and intersect with the remaining beams which are parallel with the axis of the TPC. These intersections define additional reference points in three dimensions. Figure 2 illustrates the paths of the 18 calibration beams.

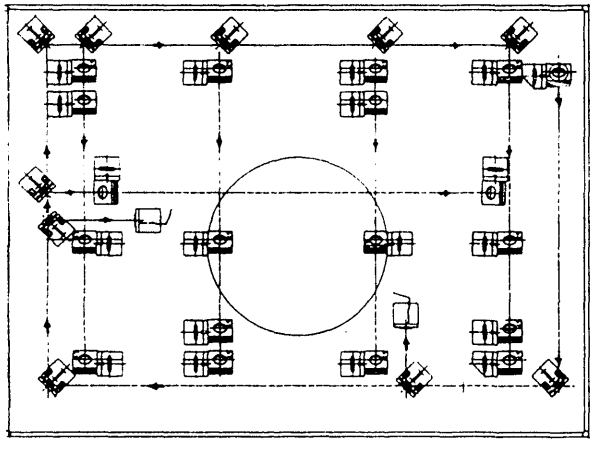

Fig. 1. A diagram of the laser distribution board. The mounts, beamsplitters , and mirrors are displayed for the 18 calibration paths and the two alignment paths. The primary beam enters at the top right hand corner and follows the dashed paths.

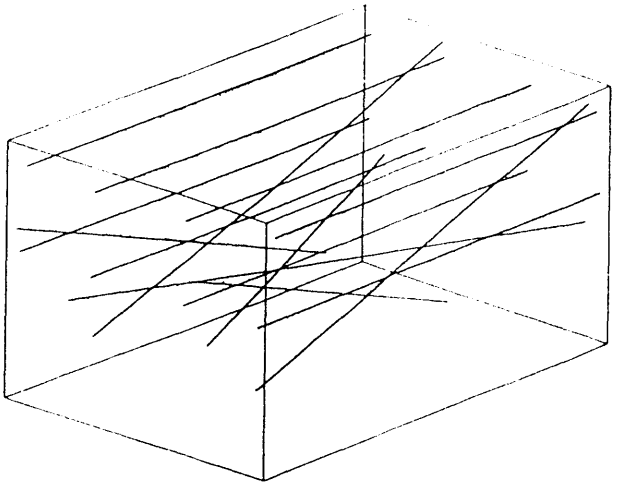

Fig. 2. The paths of the 18 calibration beams through the active region of the TPC.

Data Acquisition System for the EOS TPC

Charles McParland

The EOS TPC data acquisition system is responsible for interfacing to and acquiring data from the EOS TPC detector and its dedicated electronics. Acquisition system hardware consists of two sub-systems: one detector-mounted, the other located in a nearby counting area. Detector-mounted electronics consist of 128 assemblies. Each of these assemblies performs analog storage and pulse-shape digitization for signals on 120 TPC charge collection pads. These electronics assemblies are controlled, configured and tested by a network of embedded BITBUS processors. These processors, along with appropriate firmware, provide a low-cost, error-free control channels between the detector-mounted electronics and the VME-based acquisition system. Figure 1 gives a general overview of the hardware arrangement.

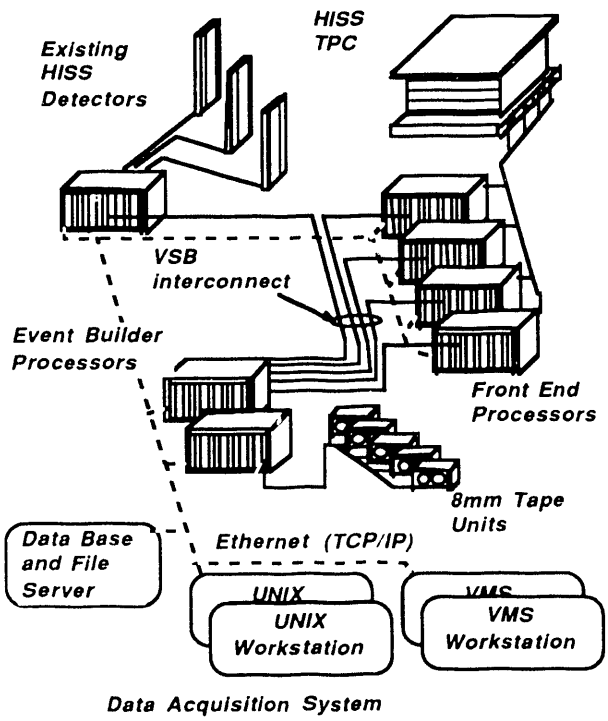

Figure 1: EOS TPC data acquisition system.

The data stream from each of these assemblies flows through a uni-directional, 70 Mbit/sec. optical data links to an array of 128 Motorola DSP56000 digital signal processors where compression algorithms reduce data volume by factors of up to 10. These processors, along with associated optical receivers, buffers and dual-ported memories, are designed into large-format VME boards that are packaged in four separate VME crates. A full-function DSP56000 simulation program has been implemented to aid in both hardware and software design of these boards.

The results of DSP processing are up to 128 compressed event fragments that must be assembled into a single coherent event stream. This is accomplished by writing event fragments from each of the four VME front-end crates into one of four dual-ported memories located in a fifth VME crate. These dual-ported memories allow access through both VME and VSB bus interfaces. A dedicated processor in each front-end crate is equipped with a differential VSB bus interface that provides a data path to the appropriate dual-ported memory within the event builder crate.

Within the event-builder VME crate, a dedicated processor collects event fragments into complete events. Using a dual-ported memory mechanism similar to that connecting the front-end VME crates to the event-builder crate, complete events are placed in taping queues that reside in dual-ported memory shared with a sixth VME crate. Processors within this sixth crate are responsible for de-queuing events and directing them to one of several (up to six) 8mm. tape drives. Processors in all six crates execute VxWorks kernel software and are connected, via ethernet, to both SUN and DEC workstations in the experimental area.

The EOS TPC Analysis Shell

D. L. Olson and the EOS Collaboration

The EOS TPC Analysis Shell (TAS) is a general purpose analysis program for event-based data processing. It is designed to handle many of the difficulties arising when doing analysis in a group environment. The major features contributing to this are:

- a specification for connecting analysis routines (analysis modules),
- a separation of the control and I/O functions from the analysis routines,
- a single point of input for specifying the data structures (tables),
- automatic initialization of the data structures,
- and a familiar user interface (KUIP/PAW[1]).

The specification for analysis modules along with the control and I/O functions being provided externally for these routines enables different analysis modules to be developed independently and then easily merged into a single analysis program. A single point of input for specifying the table data structures minimizes the chance for inconsistent definitions. The automatic initialization with default values, specified at the time the tables are defined, minimizes the need for file input simply to make the program run. Choosing a user interface which has many on-line help features, and that has become widely used, minimizes the time needed by most people to learn how to use this analysis shell.

A schematic diagram of TAS is given in Figure 1. There are three separable units in TAS, the user interface (UI), the processing manager (PM) and the event processor (EP). The user interface unit consists of KUIP command routines that format data structures for a message-response command distribution mechanism that communicates with the processing manager unit. The processing manager handles data I/O functions, event processing control, histogram booking and filling, and communication with the event processor. The event processor unit contains the experiment specific analysis modules that access data in the event-buffer tables.

The TAS tables are defined interactively by entering the descriptions of the variables into a database. Automatic database procedures are used to generate Fortran source files for defining the event buffer tables, various data I/O and initialization routines.

The specification of what output to save and histograms to fill is used by the EP to determine which analysis modules to call for processing a given event.

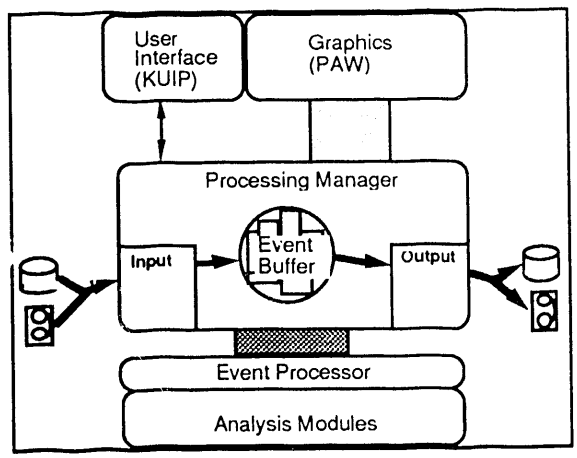

Figure 1. Diagram of TAS showing the user interface, processing manager, and event processor.

Footnotes and References

1. KUIP - Kit for an User Interface Package, CERN-DD I202, 1988,
PAW - Physics Analysis Workstation, CERN-DD, Q121, 1989.

Trackfinding in the EOS TPC

H. S. Matis and the EOS Collaboration

A TPC provides data that can be expressed as three dimensional space points. A pattern recognition program is needed to reduce the points to track information. The fact that a TPC can produce three dimensional data makes pattern recognition much simpler than streamer chambers, where two-dimensional pictures must be matched, and drift chambers, where projective geometry techniques are used. Therefore, TPC's are power tools to measure large track densities such as relativistic heavy-ion collisions.

The EOS TPC trackfinder was based on software developed by the E810 collaboration at BNL. E810, a fixed target experiment for heavy ions, uses a similar geometry as the EOS TPC. E810 adapted their code from the ALEPH experiment, a colliding beam experiment at LEP. Several routines developed for bubble chambers can be found in the code.

The method to find tracks from the space points can be called the "follow your nose method." The trackfinder first starts from the downstream end of the chamber and takes all combinations of points from the last and next-to-last row to produce a line. If it finds a nearby third hit close to this line, it has found a seed. Next, the trackfinder follows the seed track toward the target and looks for hits that are close to the track and includes those that are nearby. If sufficient hits are found, then the program has a candidate chain.

Once all the possible chains are found, they are checked to see if the points on each chain can be fit by a helix, the trajectory of a particle in the HISS magnetic field. At this stage, hits which deviate significantly from the others are removed. If a helix describes a good fit to the chain and there exists a significant number of acceptable points, then the chain is declared "good." The resulting good chains are then projected back to the target. Then, the lab momentum can be calculated and a preliminary vertex can be determined.

To test the trackfinder, events generated by the Freesco code are passed through Geant and space points are produced. Fig. 1 shows a simulated central Au-Au collision at 800 MeV/A. The lines indicate the trajectories found by the track finder. More than 98% of the tracks that the generated tracks were found. The only ones missed were very low momentum tracks that had a very large curvature. No extraneous tracks were found.

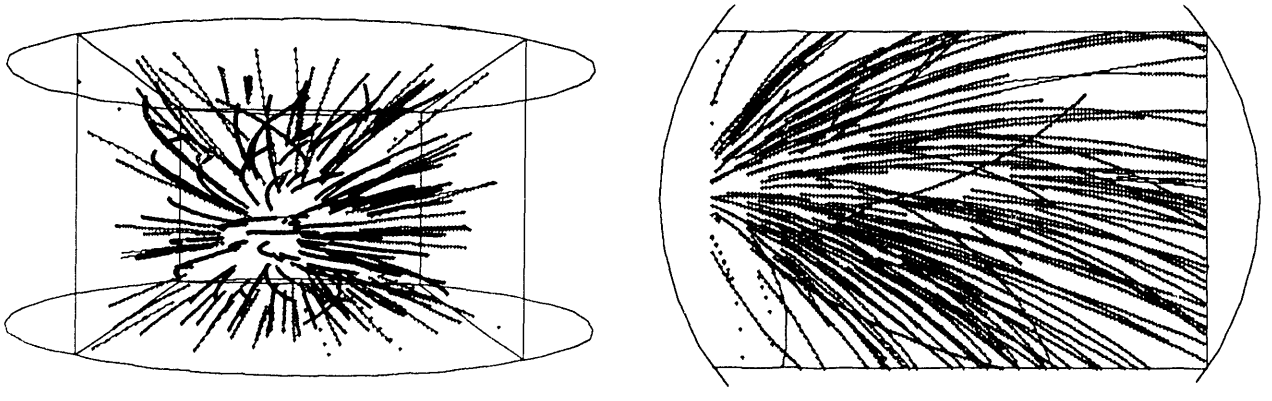

Fig. 1. Reconstructed event for a Au-Au central collision at 800 MeV/A. The figure on the left shows a three dimensional recontructed view of the event, while the figure on the right shows the projection in the bending plane of the magnet. Extraneous hits are added to simulate noise in the detector.

Simulation and Analysis software development for the EOS Time Projection Chamber

Gulshan Rai and the EOS Collaboration

A detailed computer simulation program has been developed for the EOS Time Projection Chamber (TPC). The software takes into consideration the physics processes pertinent to the TPC detector and the response of the entire front end readout electronics. Simulated data structures are produced in formats that represent the level of hardware processing.

The program starts by drifting primary electron clusters that are created in the wake of a charged particle trajectory in the TPC gas volume. The size and coordinate of each cluster is supplied by the CERN detector modeling package GEANT. The electrons are tracked until collected on a sense wire where they create an avalanche signal. The final current pulse is built up from a parameterization of the capacitive coupling that exists between a sense wire and the cathode pad plane. The drift velocity is calculated for a variety of gas mixtures as a function of temperature, pressure and the electric field. Also the affects of a non uniform magnetic field, the electrostatics of the wire-pad plane structure and the avalanche fluctuations at the sense wires have been included in the simulations.

We have extensively used the program to develop the necessary but often complicated software tools needed to work, monitor and control the TPC. The simulated data proved to be indispensible in writing the analysis and calibration programs.

The analysis program reduces the raw TPC data into three dimensional space points and energy loss values. It automatically performs peak finding, the deconvolution of over-lapping signals and clustering the pad hits. In a typical simulation, a Au+Au central collision at 1GeV/c produces on average 250 charged particles that pass through the TPC. The analysis program extracts ~ 10^4 space point coordinates from such an event in 38 cpu seconds on a SUN 4/90 SPARC workstation. A significant improvement in speed is, however, expected from the use of newer and more powerful workstations which are now becoming available. Figure 1 shows an event reconstructed by the analysis program.

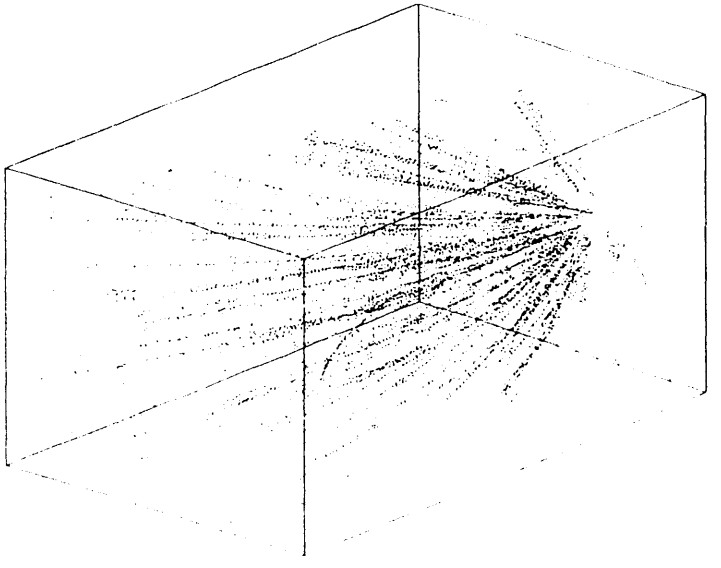

Figure 1. A perspective view of a reconstructed Au+Au event using simulated data

An Algorithm for Vertex Localization for Use with the EOS TPC

D. Cebra and the EOS Collaboration

A least squares algorithm has been developed for localizing the interaction vertex using simulated data from the EOS TPC. Precise knowledge of the location of the main vertex is necessary to improve the momentum resolution, to reject interaction, that occured outside of the central region of the target, to estimate the effect of energy loss within a thick target, and to identify the decay vertices of unstable neutral particles (i.e. K^0_S and Λ). These studies have used data from the event generator FREESCO[1]. GEANT[2] and a map of the HISS field were used to calculate the space points for the ionization tracks. These simulated data were run through a tracking routine to generate helix fits , which were then used for the determination of the vertex location.

The helices are characterized by six parameters (Ψ, λ, X_0,Y_0, Z_0, Q/ρ) where Ψ is the angle of a tangent line in the bend plane, λ is the pitch angle, X_0, Y_0, and Z_0 are the coordinants, Q is the charge, and ρ is the radius of curvature. For the purposes of this routine, the parameters are evaluated at $Z_0=Z_{target}$ or the point of closest approach. The optimization minimizes the sum of the perdendicular distances between the lines tangent to the helices at (X_0, Y_0, Z_{target}) and a point in space (which is taken as the vertex). The tracks are weighted based upon an estimate of the multiple Coulomb scattering and the uncertainty returned from the helix fitting routine.

Using the data from 100 simulated Au+Au central events, the resolution of the vertex locaization is 300 μm in the X direction, 100 μm in the Y direction (the non-bend direction), and 300 μm in the Z direction (the beam axis). Histograms of the deviation between the found and known coordinants are displayed in Fig. 1. The X-Y precision will allow effective rejection of beam halo events, while the Z resolution is sufficiently accurate to allow for energy corrections based upon the depth of the interaction within a thick target (thicknesses greater than 1 mm).

1. G. Fai and J. Randrup, Comp. Phys. Comm. 42 , 385, 1986.
2. GEANT manual, CERN DD/EE/84-1, 1987.

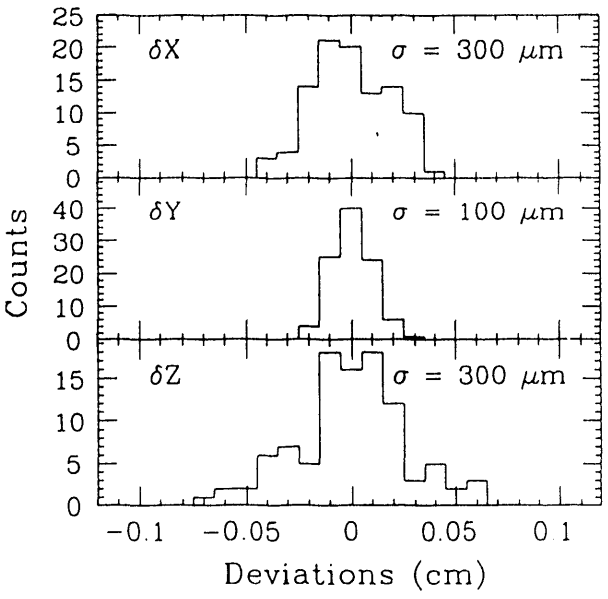

Fig. 1. Histograms of the deviations between the found and known vertex location in the X, Y (non-bend direction), and Z (beam axis) directions.

Energy Dependence of Cross Section for Charge Pickup of Relativistic Heavy Ions*

Jing Guiru[$], *W. T. Williams and P.B. Price*

We have measured the cross sections for charge pickup ($\Delta Z = +1$) reactions of ^{139}La nuclei at three energies in the interval 390 - 560 MeV/nucleon in a stack of VG-13 glass detectors ($\langle A \rangle = 26$). Our results strengthen the evidence by Binns *et al.* that the cross sections for charge pickup by heavy nuclei sharply increase as the energy decreases below ~600 MeV/nucleon.

Footnotes and References

*Condensed from LBL-29152 and Phys. Rev. C, vol 42, no. 2, pg. 769-770.

[$]Institute of High-Energy Physics, Academia Sinica, Beijing, China

Ultrarelativistic Experiments

Behavior of Nuclear Projectile Fragments Produced in Collisions of 14.5 A GeV ^{28}Si with Pb and Cu Targets*

P. B. Price and Y.D. He

Using CR-39 nuclear track detectors and an automated scanning system, we have studied the behavior of projectile fragments with charges $8 \leq Z_F \leq 13$ produced in interactions of 14.5 A GeV ^{28}Si nuclei with Pb and Cu targets. Both nuclear and electromagnetic spallation contribute to fragmentation of beam nuclei in Pb and Cu. As Fig. 1 shows, the total charge changing cross sections of nuclear projectile fragments with $8 \leq Z_F \leq 13$ interacting in Pb are found to be enhanced by 10 to 30% relative to charge changing cross sections of stable nuclides. The enhancement occurs primarily in interactions with large loss of charge. In Cu the charge changing cross sections of secondaries show no significant excess. As seen in Fig. 2, the mean free path of secondary fragments shows no dependence on the distance from the point of origin. This result rules out at 95% confidence level the production of nuclear fragments with interaction cross sections enhanced by a large factor as conjectured by some workers, but the result is consistent with a two-component model in which ~30% of secondary beams are off-stability isotopes with total cross sections enhanced by ~25%. Our measurements of angular distributions of projectile fragments showed that the transverse momentum distributions are similar to those measured at 1 to 2 A GeV. The charge pick-up cross section of 14.5 A GeV Si is measured to be 0.07 to 1.3 mb in Pb and $\leq$ 0.9 mb in Cu, which is of the same order of magnitude as that measured at ~1 A GeV.

Footnotes and References

*Condensed from LBL-29926 and Phys. Rev. Lett. C (in press).

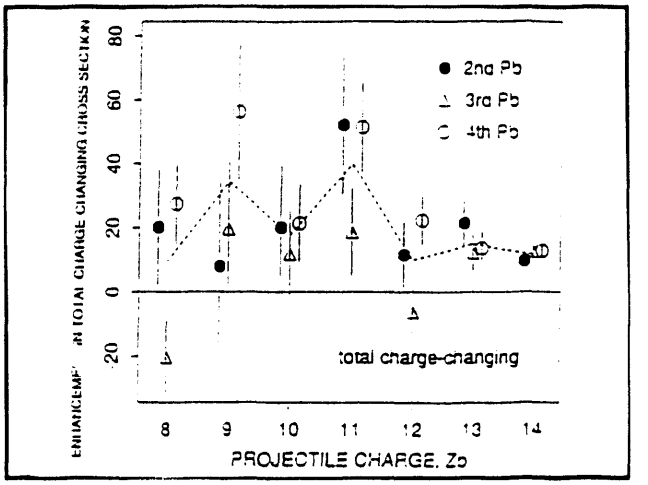

Fig. 1. Percentage enhancement in $\sigma_{\Delta Z \geq 1}$ of secondary beams over expected cross sections for primary beams in several successive thick Pb targets. Dashed line connects mean measured values in 3 Pt targets.

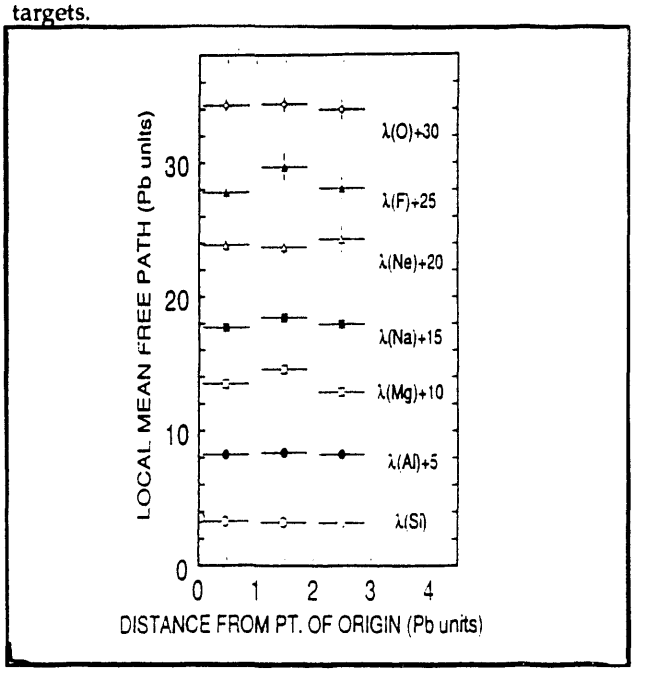

Fig. 2. The local mean free path as a function of distance downstream in Pb units from the point of creation (1 Pb unit = 1.6 cm of Pb + 0.22 cm of CR-39 plastic). To display all data for different nuclear fragments on the same graph, the measured λ (Z_p) have been displaced upward by the number of Pb units indicated.

Search for free quarks produced in ultra-relativistic collisions at BNL and CERN*

*H. S. Matis,† H. G. Pugh,† G. P. Alba,‡ R. W. Bland,‡ D. H. Calloway,‡ S. Dickson,‡ C. L. Hodges, T. L. Palmer,‡ D. A. Stricker,‡ R. T. Johnson,‡ G. L. Shaw,§ R. Slansky***

With the development of QCD, the concept of quark confinement or the statement the color is an exact symmetry of nature explains the non-observation of fractional charge or "free quarks". The fact that there is impressive evidence against the existence of free quarks supports that statement.

With the new ultra-relativistic machines at CERN and BNL, new experimental conditions can be reached. In particular, the conditions created in the hot dense region of ultra-relativistic collisions could liberate free quarks. Ultra-relativistic collisions can produce a large hot region is space which probes QCD over large distances, while elementary particle collisions probe QCD over point-like regions of space.

The quark collector for NA39 at CERN was a container, filled with Hg, that was placed downstream from the CERN NA38 target in the middle of the NA38 beam stop. The Hg target was designed to stop and capture quarks produced in interactions with the liquid target.

Two types of quark absorbers were used for the BNL experiment E801: four cylinders full of Hg and four liquid Ar tanks. Once a quark stopped in the liquid Ar tanks, it would be attracted to one of two oppositely charged wires which were immersed in the liquid. As the quark can never be neutralized with integer charges, it would always have a net charge and be attracted to one of the wires. After the quark reaches the wire, it will be trapped on the surface of the wire through its image charge.

A distillation apparatus was used to concentrate the Hg that was in the Hg tanks. Each of the wires from the Ar tanks were passed through a small bead of Hg enclosed in a glass tube. The wire was carefully checked to make sure all of the gold was dissolved.

The concentrated Hg was tested in a Millikan type apparatus. This detector measures the residual charge of a Hg drop with at resolution of about 0.03e. 118 μg of the CERN Hg sample, 142 μg from the BNL Hg, and 110 μg of the BNL liquid Ar sample were measured without any evidence for quark production. An estimate of the upper limit for quark production can be found in Table 1.

Footnotes and References

*extracted from LBL-29366

†Nuclear Science Division, Lawrence Berkeley Laboratory, Berkeley, CA 94720,

‡Physics Department, San Francisco State University, San Francisco, CA 94132

§Physics Department, University of California, Irvine, Irvine, CA 92717

**Los Alamos National Laboratory, Los Alamos, NM 87545

Beam Mom. (Gev/c)	Stopping Material	Beam	Integrated Intensity	Limit (90% cl)
14.5	LAr	O	6×10^{12}	1.0×10^{-9}
14.5	Hg	O	6×10^{12}	5.1×10^{-10}
14.5	Hg	Si	4×10^{11}	8.1×10^{-9}
60	Hg	O	1×10^{12}	1.7×10^{-6}
200	Hg	O	3×10^{12}	3.5×10^{-7}
200	Hg	S	1.5×10^{12}	1.3×10^{-6}

Table 1. Summary of beam conditions for each of the quark stopping materials. The limit is the 90% confidence value and is expressed in quarks per interacting ion.

Nuclear Stopping Power in 60 GeV/nucleon ^{16}O+Au Collisions using Proton and π^- Rapidity Distributions

S. Tonse, S.I. Chase, J.W. Harris, G. Odyniec, H.G. Pugh, G. Rai, J. Schambach, L. Teitelbaum, and the NA35 Collaboration*

Energy densities high enough to produce a quark-gluon plasma in relativistic heavy ion collisions require a beam-target system which can effectively convert the longitudinal motion of the projectile nucleus into excitation and transverse degrees of freedom. The degree to which this happens is referred to as the nuclear stopping power. We approach the topic of stopping by studying proton rapidity distributions from 60 GeV/n ^{16}O+Au collisions measured in the NA35 streamer chamber.[1]

The data consisted of 89 complete streamer chamber events, triggered by an electromagnetic calorimeter to select the most central collisions (4% of σ_{inel}). Monte Carlo comparisons show that all 16 of the projectile nucleons participate while the average number of target participant nucleons is approximately 50 + 8. The center of mass rapidity of this system is Y_{cm}=1.87. Only one streamer chamber camera view out of a possible three was used, yielding the longitudinal component of momentum along the beam and one transverse component of the momentum P_y. We calculate quasi-rapidity, compensating for the 2-dimensional projection by substitution $(\pi/2)p_y$ for p_T. Simulation studies show that the difference between rapidity and quasi-rapidity has a width of σ=0.09 units and that for our purposes they are identical.

The proton quasi-rapidity distribution was obtained by subtracting the quasi-rapidity distribution of negative from positive particles, both calculated using the proton mass. This assumes cancellation between the produced particles of opposite charges, leaving the original non-produced protons. Since the system is not isospin-symmetric some corrections were made.

The final quasi-rapidity distribution of the protons had an integrated content of 41.2 protons. The number of protons forward of Y_{cm} was 11.1 ± 0.7 protons, larger than the 8 protons initially forward of the mid-rapidity, but smaller than the 14 protons expected from calculations for a fully stopped projectile in a 16-on-50 collision.

Assuming that all of the projectile protons were still forward of mid-rapidity, we defined a longitudinal stopping variable S_L which compared the energy lost by the projectile protons to their maximum possible energy loss. This yielded a value S_L=0.82, lying between other estimates of stopping power that rely on calorimetric transverse energy measurements.

To extract information on the space-time dependence of the energy deposition, important for QGP calculations, it is necessary to compare theoretical model calculations to the data. With this in mind we chose several models that make predictions of stopping based on dynamical calculations at the nucleon or parton levels. We made comparisons to both the proton and π^- rapidity distributions from our data. The general shape of the proton quasi-rapidity distribution was well approximated by several of the models as shown in Fig. 1, although none of them could simultaneously agree with the π^- rapidity distribution.

Footnotes and References

1. For a more detailed description and references see LBL-29578

* Deceased

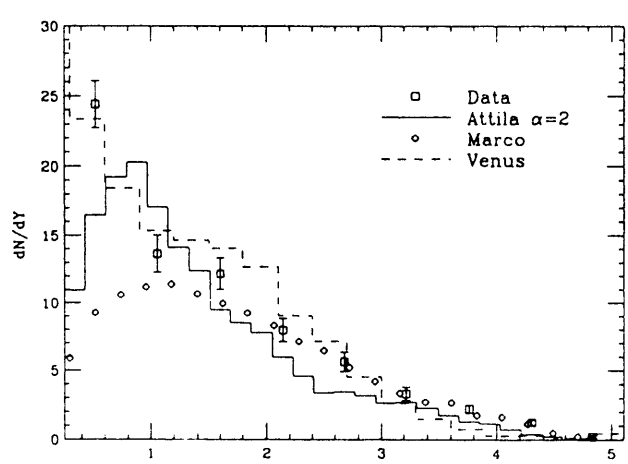

Fig. 1. Proton Rapidity Distributions

Energy Balance in 200 GeV/n Central $^{32}S + ^{32}S$ Collisions

The NA35 Collaboration

A complete study of the energetics of average central $^{32}S + ^{32}S$ collisions at 200 GeV/Nucleon can be undertaken using the Streamer Chamber detector in the NA35 experiment at CERN. This detector measures the charge-sign and momentum of all charged particles and the momentum of neutral strange particles via charged-particle decay modes over a large region in phase space. In addition, the $^{32}S + ^{32}S$ system has isospin zero which allows important conclusions concerning the participating nucleons and particle production. Thus, for the first time the energy deposited by the participating nucleons in the reaction volume of high energy heavy ion collisions and the repartition of this energy in produced particles can be determined.

The mean energy loss of the participating nucleons in the center-of-mass (cm) system, $<dE>^{cm}(N)$, can be extracted from the participant nucleon rapidity distribution using the formula

$$<dE>^{cm}(N) = \frac{1}{N} \cdot \Sigma(m \cdot \cosh(y_{cm}) - <m_T> \cdot \cosh(y_i)) \cdot \frac{dn}{dy_i} \quad (1)$$

where m denotes the nucleon mass, y_{cm} the rapidity of a projectile nucleon in the c.m. (y_{cm} = 3.0) and $m_T = \sqrt{(m^2 + p_T^2)}$ the transverse mass. The sum is over the rapidity distribution dn/dy and N is the integral over the distribution. From the measured rapidity distribution[2] one gets

$$<dE>^{cm}(N) = 5.8 \pm 0.3 \text{ GeV} \quad (2)$$

Together with the average number of participant nucleons, $<N_p> = 54 \pm 6$, obtained by integration over the distribution, one gets

$$<E> = 313 \pm 38 \text{ GeV} \quad (3)$$

for the average energy content <E> in the reaction volume. This energy is available for particle production. The energy E_p contained in the final state particles can be determined using the corresponding rapidity distribution with a formula similar to (1)

$$E_p = \Sigma (m_T) \cdot \cosh y_i \cdot dN/dy_i \quad (4)$$

The contribution of the various particle species are summarized in Table 1. Due to the isospin-scalar property of the ^{32}S-nucleus, measurement of the energy contained in the negative pions provides the energy contained in all directly produced pions. The contribution of all kaons and hyperons can be deduced by using isospin-symmetry from the measurement of K_s^o and $\bar{\Lambda}$-particles, respectively, performed in the same experiment.[2] The contribution of η-par-ticles, not decaying into ($\pi^+ \pi^- \pi^o$), was estimated from nucleon-nucleon interactions by assuming the same energy spectrum as for K_s^o particles. The estimate of the nucleon-antinucleon production implies that it is enhanced by the same factor as the $\bar{\Lambda}$-yield in central $^{32}S+^{32}S$ collisions.[2] The result for the total energy contained in produced particles (311± 30 GeV) shows very good agreement with the energy lost by the 54 participant nucleons (313 ± 38 GeV).

Footnotes and References

1. S. Wenig, GSI Report 20-23 (1990).
2. NA35 Collaboration, J. Bartke et. al., Z. Phys. C48 (1990) 191.

particle	⟨mT⟩ [GeV/c]	energy [GeV]
π^+, π^-, π^0	0.368	212 ± 20
$K, \bar{K}$	0.747	47 ± 5
hyperons	1.312	9 ± 3
η	0.747	6 ± 1
nucleons, antinucleons	1.148	37 ± 22
sum		311 ± 30

Table 1: Energy in produced particles for central $^{32}S + ^{32}S$ collisions

Neutral Strange Particle Production in Sulphur-Sulphur and Proton-Sulphur Collisions at 200 GeV/nucleon

S.I. Chase, J.W. Harris, G. Odyniec, H.G. Pugh [§] *, G. Rai, L. Teitelbaum, S. Tonse and the NA35 Collaboration*

At very high energy density a transient state of quark-gluon deconfinement which decays through a phase transistion to hadronic matter is expected to occur. Such conditions should be reached in central ultrarelativistic nucleus-nucleus collisions. One of the first predicted signatures of the existence of strongly interacting, deconfined matter is the enhancement of the strange and anti-strange quark content in the final state.

The production of Λ, anti-Λ and K^0_S has been studied in 200 GeV/nucleon p+S and S+S collisions in the streamer chamber of the NA35 experiment at the CERN SPS[†] . A significant enhancement of the multiplicities of all observed neutral strange particles relative to negative hadrons was observed in central S+S collisions compared to p+p and p+S collisions. The K^0_S/π^- ratio is about 0.11 extrapolated to 4π acceptance and 0.15 at midrapidity: a factor of two increase in the relative abundance. No simple scaling is found in comparing Λ, anti-Λ, K^0_S and mean ($<h^->$) multiplicities in p+S and central S+S collisions. The ratios along with the Lund Fritiof model predictions are shown in Figure 1. We deduce from recent QCD and hadronization calculations that our observation is consistent with the quark-gluon plasma formation except to which point we also offer several alternative explanations based on non-equilibrium arguments[†].

The p+S collisions show no overall (relative) strangeness enhancement over p+p, but the rapidity distributions and hadron multiplicities indicate some secondary cascading production of Λ particles in the p+S and p+Au collisions.

We have also analyzed the Λ polarization in central S+S collisions to test a different aspect of the collision dynamics: if S+S interactions were merely superpositions of nucleon-nucleon collisions we would expect the transverse polarization observed in p+p and p+Be collisions also to be present in S+S. However, we find the Λ polarization to be compatible with zero up to p_t = 2 GeV/c. This result is consistent with the secondary cascade picture in which a Λ produced by a leading projectile di-quark suffers considerable rescattering.

Footnotes and References

§ Deceased

† NA35 collaboration. Z. Phys. C - Particles and Fields 48, 191-200 (1990).

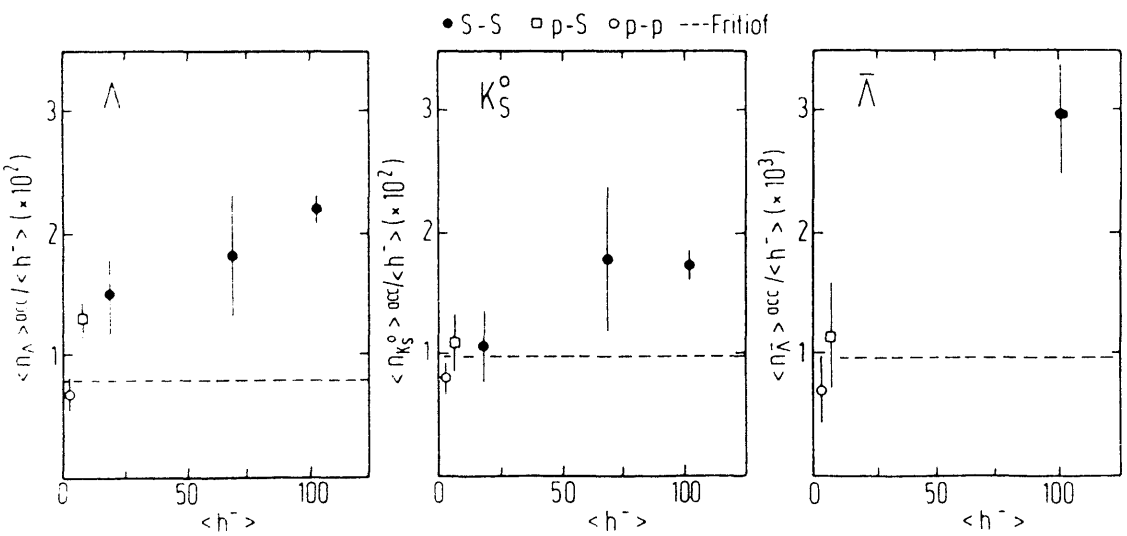

Figure 1. Ratio of the mean multiplicities of neutral strange particles observed in the NA35 streamer chamber acceptance region to negative hadron multiplicity in S+S, p+S and p+p collisions.

Charged Kaon Spectra in ^{32}S + S Collisions at 200 GeV/nucleon

S. I. Chase, J.W. Harris, G. Odyniec, H.G. Pugh, G. Rai, L.S. Schroeder, L. Teitelbaum, S.R. Tonse and the NA35 Collaboration*

The charged kaon production in $^{32}S+S$ collisions at 200 GeV/nucleon was studied using the NA35 Streamer Chamber at the CERN SPS.

The candidates for K+ and K- were identified by their two- and three-body decays. The measurements took place at the Max Planck Institut (Munich), Institut für Kernphysik (Frankfurt) and LBL (Berkeley). About 3200 two-body and 240 three-body decays were scanned and measured out of 13,400 interactions. The three-body decay of the kaon ($K^{+(-)} \rightarrow \pi^{+(-)} \pi^{+(-)} \pi^{-(+)}$) has no ambiguities but a small branching ratio (5.6%), whereas the two-body decay ($K^{\pm} \rightarrow \mu^{\pm} \nu$, $K^{\pm} \rightarrow \pi^{\pm} \pi^{0}$) with the branching ratio 84.68%, must be corrected for ambiguities ($\Sigma^{\pm}$, Ξ), contamination by π decays and losses in scanning due to small decay angles. Monte Carlo and stability studies were used to determine appropriate cuts in order to distinguish kaons from Σ and Ξ (a lifetime cut smaller than five times the kaon lifetime and a transverse momentum limit of 1.1 GeV/c). An angle-cut of 2 degrees rejects most of the pions. The phase space acceptance (in rapidity and p_t) of the NA35 streamer chamber for charged kaons is complementary to its acceptance for neutral kaons measured in the same experiment[1]. Yields of K+ and K-, after extrapolation to full phase space, were compared to VENUS 3.11 predictions[2]:

	Experiment	VENUS 3.11
<K + >	11.8 ± 0.8	10.08 ± 0.05
<K - >	6.6 ± 0.8	7.19 ± 0.04

The uncorrected K+ to K- ratio shows no significant dependence on p_t as shown in Fig. 1. The transverse mass distribution ($m_t = \sqrt{(p_t^2 + m_0^2)}$, where m_0 is the rest mass) of charged kaons after applying the acceptance correction in the common rapidity region, agrees with that of the neutral kaons[1], and extends the acceptance to low transverse masses.

Footnotes and References

1. J. Bartke et al., Z. Phys. C48, 191 (1990).
2. K. Werner, Phys. Lett. 208 B, 520 (1988)

* Deceased

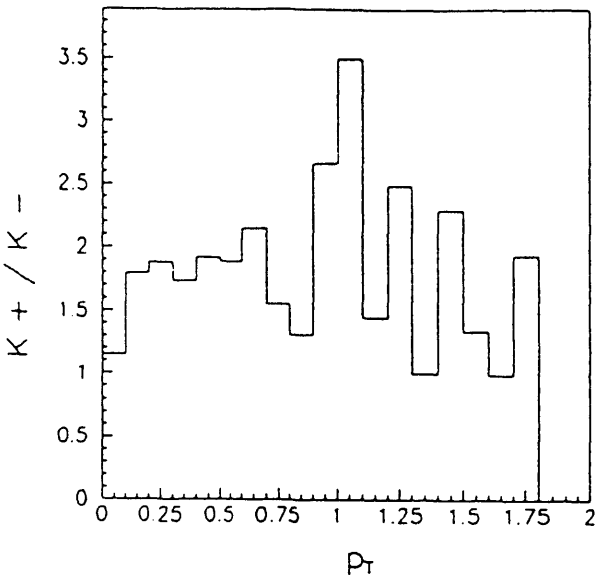

Fig. 1. Ratios of positive to negative kaons, measured in this experiment, plotted as a function of transverse momentum.

Study of Pion Interferometry with ^{16}O + Au Collisions at 60 GeV/N from the NA 35 Experiment

S. I. Chase, J.W. Harris, G. Odyniec, H.G. Pugh, G. Rai, L.S. Schroeder, L. Teitelbaum, S.R. Tonse and the NA35 Collaboration*

The most direct way to investigate the shape and size of a hadron source is to employ pion interferometry[1,2]. The basis of this method is that for the production of two identical bosons, there is a correlation in four-momentum space (Bose-Einstein effect) between the two particles, which has a width inversely related to the dimensions of the source in space-time. The method has been applied in numerous studies with a variety of energies, beams and targets[3-7]. We have studied the effective source in ^{16}O + Au central collisions at 200 GeV/nucleon[8] and find that there appears to be a central source at rest in the CM system having a large radius, freeze-out time and chaoticity[8].

Here, we report preliminary results from a pion interferometry analysis of 60 GeV/nucleon ^{16}O + Au collisions, which are presumably less affected by nuclear transparency than at 200 GeV/nucleon. Both a gaussian source and inside-outside cascade models were used to fit the experimental correlation function. the transverse and longitudinal shape parameters, freeze-out time parameter, and a chaoticity parameter for the pion-emitting source were extracted. We find a transverse source size consistent with the projectile radius except at the CM rapidity, where significantly larger transverse and longitudinal sizes were measured. Fig. 1 shows the correlation function projected onto the transverse momentum difference Q_t axis, for pairs with momentum difference parallel to the beam Q_l < 50 MeV/c, for the midrapidity interval 1.32 < y < 2.32. The source size from this fit is 4.46 ± 0.94 fm and the chaoticity parameter is 35.8 ± 9.9%. Further analysis is in progress.

Footnotes and References

1. G. Goldhaber et al., Phys. Rev. **120,** 300 (1960), G.I. Kopylov and M.I. Podgoretskii, Sov. J. Nucl. Phys. **15,** 219 (1972) ; **18,** 336 (1974) .
2. M. Gyulassy et al., Phys. Rev. **C20,** 2276 (1979).
3. W.A. Zajc et al., Phys. Rev. 2173 **C29,** (1984).
4. H. Aihara et al., Phys. Rev. **D31,** 966 (1985).
5. M. Arneodo et al., Z. Phys. **C32,** 1 (1986) .
6. C. De Marzo et al., Phys. Rev. **D29,** 363 (1984).
7. T. Akesson et al., Phys. Lett. **B187,** 420 (1987).
8. A. Bamberger et al., Phys. Lett. **Bf 203,** 320 (1988) .

* Deceased

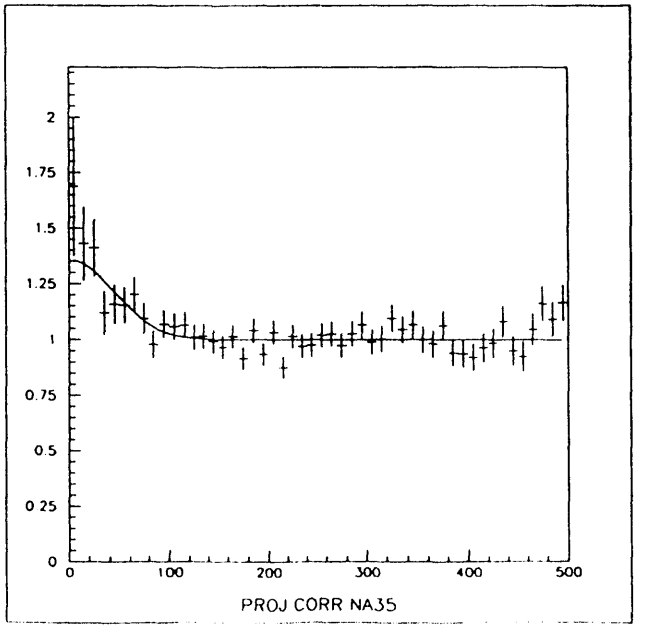

Fig. 1. Two pion correlation function at midrapidity in ^{16}O + Au collisions at 60 GeV/nucleon.

Addition of a New TPC to the CERN NA35 Experiment

The NA35 Collaboration

A Time Projection Chamber (TPC) has been installed in the NA35 experiment at CERN. It is located in the field-free region downstream from the superconducting Vertex Magnet, which houses the Streamer Chamber, as shown in Fig. 1. The purpose of the TPC is to measure the momenta of charged particles that are not resolved by the Streamer Chamber due to the high track density in the forward direction. Information on the energy loss of charged particles in the relativistic rise region will be used to identify particles. The present TPC will also allow evaluation of the suitability of a TPC for tracking and particle identification in experiments planned at CERN using collisions of 180 GeV/n Pb+Pb.

The TPC has a sensitive volume of dimensions 2.4 m x 1.0 m x 1.2 m. The readout plane is located on top (2.4 m x 1.2 m) and is subdivided into six identical readout modules 768 mm x 600 mm in size. Each readout module consists of 15 pad rows with 128 pads each (pad area 5.5 mm x 40 mm). Below the pad plane is the sense-wire plane, the cathode plane (Frisch grid) and the gating grid. A drift field is generated between the Frisch grid and the bottom plane at a potential of -13.5 kV. In order to determine the drift velocity, and possible field inhomogenities, three pairs of laser beams were installed and their positions in space determined.

There are 1920 pads per module. At present only half of the total number of pads are equipped with read-out electronics. The TPC was built at the Max Planck Institute (MPI) - Munich, using experience acquired by the MPI in constructing the ALEPH TPC for LEP at CERN.

Physics data were accumulated with a 200 GeV/n Sulphur beam on various targets at CERN in August 1990. The chamber gas used during most of the measurements was a mixture of Ar (91%) + CH_4 (9%). In some of the measurements a mixture of Ne (91%) + CH_4 (9%) was introduced, in order to reduce transverse diffusion.

The data using the Ar (91%) + CH_4 (9%) gas mixture was analyzed to determine TPC performance. A position accuracy of 243 microns was measured in the horizontal direction, which determines the momentum resolution. In the vertical drift direction an accuracy of 306 microns was measured after 50 cm drift. The two-track resolution was determined to be 1.8 cm.

During the August 1990 running period 75,000 Streamer Chamber events, 500,000 TPC events and 25,000 Ring Imaging Cerenkov events were recorded in 200 GeV/n S+Cu, S+Ag and S+Au reactions. First results are reported elsewhere in this annual report.

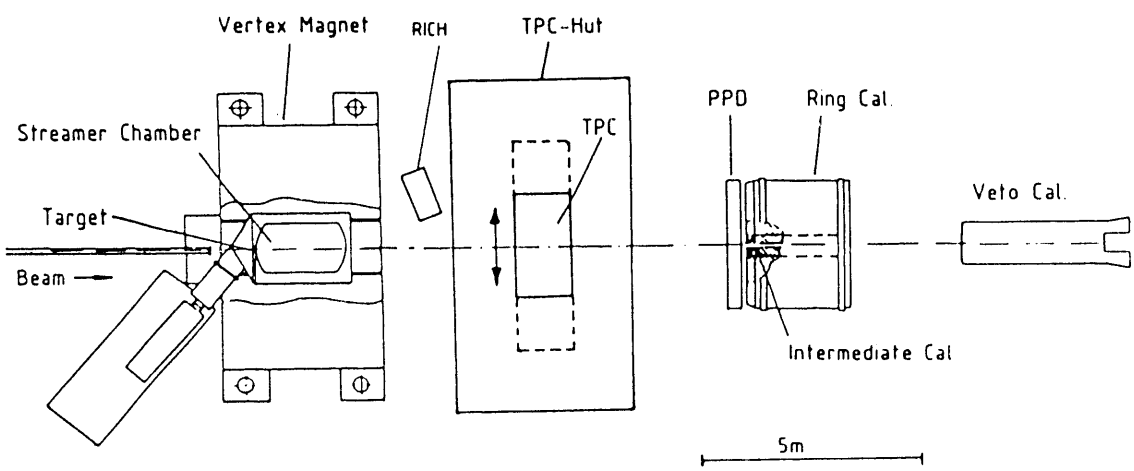

Fig. 1. Experimental setup of NA35

First Results on dE/dx Measurements in the NA35 TPC

The NA35 Collaboration

In order to study the dE/dx performance of the newly installed NA35 TPC, 8000 central $^{32}S+^{32}S$ events were analysed. These data were recorded in the TPC which was filled with an Argon (91%)-Methane (9%) gas mixture at atmospheric pressure. The TPC acceptance covered rapidities $y > 3$ for pions.

The data analysis was performed on a RISC-based Unix computer system. It consisted of a cluster detection algorithm operating in the padrow-time plane, a trackfinder combining clusters into straight lines (the TPC is operated without magnetic field) and momentum determination. The momentum determination was obtained by tracking in the TPC and projecting the fitted trajectories upstream through the 1.5 T field of the NA35 Vertex Magnet, while assuming that the particles originate from the interaction at the target. An average of 45 charged particles were detected in the TPC per event.

Due to the large inherent width of the energy loss distribution, the determination of the energy loss of relativistic particles required the measurement of many samples along each track.[1] The maximum number of samples for these tracks is 30, which corresponds to 15 padrows in each of two sectors deep.

The integral charge of the selected clusters in the padrow-time planes was used to measure the energy loss of the particles. The raw cluster charges were corrected for effects due to the absorption of free electrons by electronegative gases in the chamber. The distribution of cluster charges displays the typical Landau tail for high energy losses due to rare hard collisions. To eliminate effects of the tail a `truncated mean' was calculated for tracks consisting of more than 20 well-defined clusters, taking only the lowest 60% of the cluster charges into account. In the momentum region of 3 to 60 GeV the truncated mean exhibits the relativistic rise of the specific ionization, as displayed in Fig. 1.

The width of the peak in the distribution of average energy loss for 11 GeV/c particles corresponds to a dE/dx resolution of $\sigma(dE/dx)/(dE/dx) \approx 8.5\%$, compared to a difference in ionization of approximately 20% for protons and pions at this momentum. With an average number of samples per track of 23, this resolution is close to theoretical expectations.[1] The dE/dx resolution will be further improved by use of an online calibration system for the readout electronics and by implementation of more refined charge measuring algorithms. The latter will enhance the precision of the charge determination and allow the inclusion of partially overlapping clusters, thereby increasing the average number of samples and improving the dE/dx resolution.

Footnotes and References

1. I. Lehraus IEEE Trans. Nucl. Sci. 30 (1983) 50.

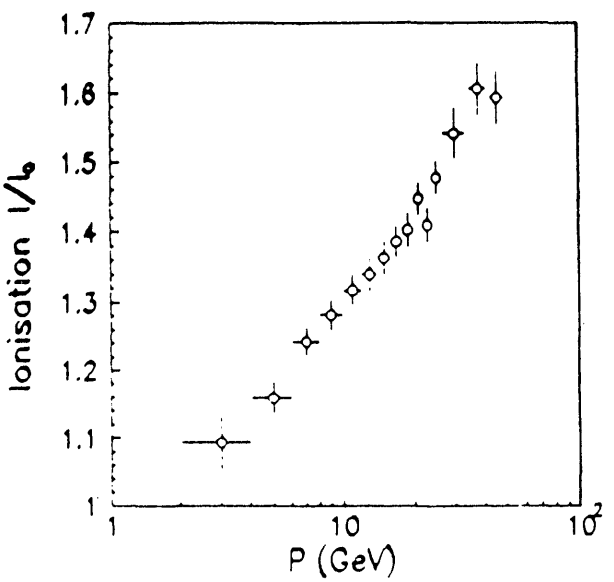

Fig. 1. The relativistic rise of the specific ionization measured for charged-particles in the NA35 TPC.

Target Dependence of $\pi^+\pi^+$-Correlations in 200 A GeV O + Nucleus Collisions

WA80 Collaboration

Pion interferometry allows one to study the space-time properties of the particle emitting source in high energy collisions. In ultra-relativistic heavy ion reactons the importance of rescattering of secondary particles in the target spectator matter has been emphasized[1]. It is therefore of interest to study pion correlations in the target fragmentation region to clarify both the general role of the target spectators and their influence on pion interferometry. In a previous report[2] first results on correlations of positive pions measured in the target fragmentation region of 200 A GeV O + Au reactions were presented. In this report the analysis is extended to other targets. In addition, the statistics for the reaction system O + Au was considerably increased.

Central reactions of 200 A GeV ^{16}O projectiles with C, Cu, Ag and Au targets were investigated. The pions were identified with the Plastic Ball detector for $\eta \leq 1.3$. The correlation functions were analyzed in terms of the absolute value of the four momentum difference:

$$Q \equiv \sqrt{-(p_1^u - p_2^u)^2}$$

For simplicity, Gaussian functions have been used:

$$C_2(Q) = 1 + \lambda_{inv} \cdot \exp\left(-\frac{1}{2} R_{inv}^2 Q^2\right)$$

Fig. 1 shows $\pi^+\pi^+$-correlation functions as a function of Q for central reactions of 200 A GeV ^{16}O with different targets in the rapidity region $-1 \leq y_{lab} \leq 1$. A clear enhancement for small values of Q is visible in all cases. A fit with a Gaussian parametrization is shown as a solid line. Counterintuitively the radii decrease with increasing target mass, and also the intercepts go down for the heavier systems. Fits with an exponential distribution show the same qualitative behavior. A premliminary analysis indicates[3] that rescattering of the pions in the target nucleus might be considered as a possible explanation for this observation.

Footnotes and References

1. R. Albrecht et al., Z. Phys. C-Particles and Fields 45, 529 (1990).
2. WA80 Collaboration, GSI Scientific Report 1989, p. 68.
3. T. Peitzmann, Ph.D. thesis, University of Münster, 1990.

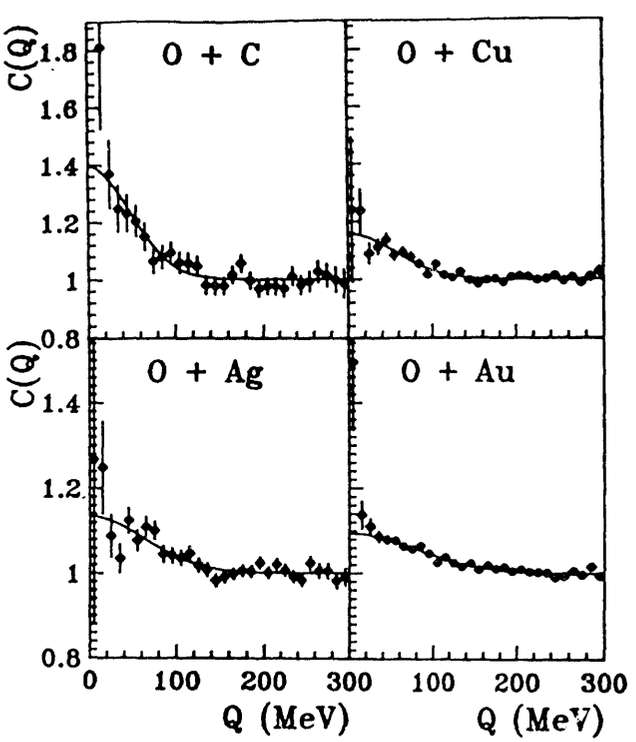

Fig. 1. $\pi^+\pi^+$-correlation functions (Gamow-corrected) for central ^{16}O + nucleus reactions as a function of Q for $-1 \leq y_{lab} \leq 1$.

Mass Dependence of the Target Fragmentation in Energetic Proton-Nucleus Collisions

WA80 Collaboration

Our knowledge on the fragmentation of the heavy target nucleus after the passage of a very energetic hadron is very limited[1]. We have thus studied systematically the target mass dependence of proton-like particle distributions in the target rapidity range. The data where taken with the Plastic Ball detector[2] employing the 200 GeV/c proton and π beams at the CERN SPS. The coverage is within $-1.7 \leq \eta \leq 1.3$.

The data are compared to VENUS 3.07 event simulations. VENUS 3.07 is a string model with cascading (rescattering) of secondary particles. In this approach strings are formed and break into string segments after typically one fm/c. If the strings, string segments (which may or may not be hadrons) or spectator nucleons come closer to each other than a certain distance, d_0, they interact.

Fig. 1a shows experimental pseudorapidity distributions $dN_p/d\eta$ of proton-like particles (N_p=p + d+ t + 2He) from the reactions p + Au, Ag, Cu, Al and C, while Fig. 1b shows the corresponding distributions from VENUS. The interaction distance, d_0, has been treated as a free parameter and is adjusted to reproduce the yield from p + Au. All other reactions were calculated with the same value. The VENUS events were subjected to experimental acceptance cuts which reduced the original proton yield by ≈70%. The experiment and simulation compare as follows:

- the position of the maximum of the experimental and simulated pseudorapidity distributions are in very good agreement

- there are deviations up to 50% between experiment and simulation at the very backward pseudorapidities; for the integrated yields the deviations are less than 10%, which is within the (systematical) uncertainty of the data.

- the A-dependence, expressed as the exponent α of $N_{proton} \propto A^{\alpha}$ is α=0.75 and 0.70 for the experimental data and for VENUS, respectively.

We compared the inverse slope parameters of the transverse momentum distributions of the protons by fitting them in the range $200 \leq p_{\perp} \leq 500$ GeV/c. The transverse momenta are essentially identical for the different targets. However, VENUS overestimates the average transverse momentum by about 50 MeV/c for $y < 0$. For $y > 0$ the data exhibit an increase of the inverse slopes of about 50%. A similar increase of the mean $p_{\perp}$ is not seen for the VENUS events.

Footnotes and References

1. W. Busza and R. Ledoux, Ann. Rev. Nucl. Part. Sci. **38**, 119 (1988).
2. H. Gutbrod, A.M. Poskanzer, and H.G. Ritter, Rep. Proc. Phys. **52**, 1267 (1989).

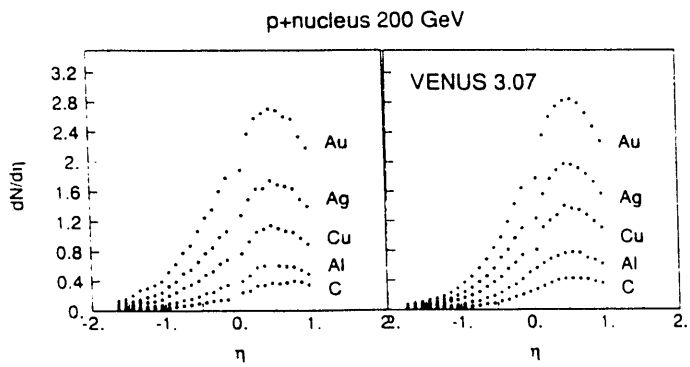

Fig. 1a) Experimental pseudorapidity distributions $dN_p/d\eta$ from p + nucleus collisions at 200 GeV; 1b) the same distributions from VENUS 3.07, filtered by the experimental acceptance.

Energy Dependence of the Target Fragmentation in Energetic Proton-Nucleus Collisions

WA80 Collaboration

From systematic studies carried out mainly by emulsion experiments[1] it is known that the charged particle yields depend on the bombarding energy like $\langle n_{ch} \rangle = a + b \cdot (\ln s) + c \cdot (\ln s)^2$. In the present study we investigate the proton yields in the target fragmentation region from proton-nucleus interactions at three different beam energies: 4.9, 60, and 200 GeV. The 4.9 GeV data were taken at the Berkeley Bevalac, the other data at the CERN-SPS. The detector was in all cases the Plastic Ball[2].

Our objective is to investigate whether the energy dependence of the yields of produced particles (mostly pions and kaons) influences the fragmentation mechanism of the target spectators due to rescattering processes of secondaries in the target matter.

As an experimental result (see Fig. 1) we find the yields of proton-like particles (p + d + t + 2He) from p + Au reactions being constant at all bombarding energies studied. The results from VENUS 3.07 simulations exhibit the same behavior.

In comparing the pion yields of 60 and 200 GeV p + Au reactions from VENUS, one finds that the pion yields in the target region $y_{lab} < 2$, are identical. Evidently, due to this purely kinematical effect slow pions cannot impose an energy dependence of the bayron yields in the target rapidity region.

However, one could naively expect that the pions produced with rapidities $y_{lab} > 2$ could impose a difference when they travel through the target matter. Assuming the validity of the string picture explains why this is *not* the case: due to a finite formation time τ_0, fast particles are formed at $\tau = \tau_0 \cosh(y_{lab})$, which exceeds the radius of the target for $y_{lab} > 2$. The faster particles are thus produced outside of the target nucleus, i.e. they cannot rescatter.

From the above arguments we conclude that the energy independence of the target fragmentation gives *experimental* evidence that particles are not instantaneously formed in a collision but require some "formation" time[3] until they exist and can reinteract.

Footnotes and References

1. W. Busza and R. Ledoux, Ann. Rev. Nucl. Part. Sci. **38**, 119 (1988).
2. H. Gutbrod, A.M. Poskanzer, and H.G. Ritter, Rep. Proc. Phys. **52**, 1267 (1989).
3. L.D. Landau and I. Pomeranchuk, Dokl. Akad. Nauk SSR **92**, 535, 734 (1953).

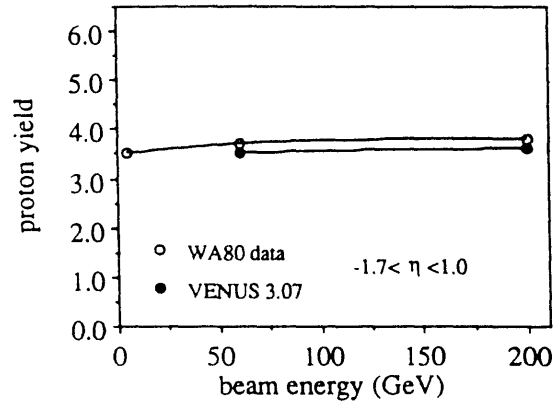

Fig. 1. Integrated yields of proton-like particles in the range $-1.7 < \eta < 1.0$ as a function of the beam energy for the reaction p + Au. The open circles are experimental results, the black are from VENUS 3.07 simulations

Intensified CCD Camera Optical Readout for Large Area Multiplicity Detectors

P. Jacobs, A. M. Poskanzer, and the WA80 Collaboration

The multiplicity distribution is one of the important observables in high energy nucleus–nucleus collisions. The multiplicity of a collision measured in a large pseudorapidity interval is directly related to the impact parameter of the collision, and at sufficiently high energy, the multiplicity density at mid–rapidity can be connected to the energy density of hot matter created in the collision. On the other hand, the fluctuations of the multiplicity distribution in very small pseudorapidity intervals are possibly related to features of the hadronization process, Bose–Einstein correlations, or more exotic phenomena.

The WA80 collaboration at CERN has studied multiplicity distributions using a large area, large acceptance, array of streamer tubes read out by capacitively coupled pads. WA80 decided for the future to develop highly efficient large area multiplicity counters based on two or three step parallel plate avalanche counters, filled typically with argon, methane and an organic vapour such as triethylamine (TEA). TEA emits UV light copiously in the presence of an electron avalanche– up to one photon per electron in the avalanche. If the detector is coupled to a wavelength shifter to shift the light to the visible region, the avalanches can be imaged by an intensified CCD camera. The advantage of this technique is that a large area can be imaged with fine granularity by a single intensified CCD camera (3x3 mm^2 pixels over an area of 1 m^2), giving true two dimensional readout at a much lower cost than that achievable using current electronics coupled to pads on gas detectors.

For the December 1989 calibration run at the CERN SPS, the WA80 collaboration built a test setup to investigate this technique. The LBL contribution was to assemble the optical readout chain and software. The camera, obtained from EEV Ltd., consists of a photocathode coupled through an electronic gating grid to a microchannel plate image intensifier having a gain of 10^3–10^4, which in turn is coupled to a phosphour mounted on the CCD itself. The CCD format is 288 x 385 pixels which is digitized at 8 bits, giving 110 kbytes per camera image. The camera was read out by an AC100 CAMAC module made by Data Design Corp.

Due to the large optical demagnification necessary to reduce the large area detector to the small area of the CCD (about 18x18 mm^2), the solid angle coverage is of order 10^{-4} and the intial 10^6 photons emitted in the avalanche are reduced to less than 10^2 incident on the photocathode. The finite photocathode efficiency reduces the number of imaged photons to about 20. Without the gating feature, the image would be dominated by ambient light and the small signal would not be observable. The background in the image with the gate operating is due to dark current in the CCD and to gas breakdown in the microchannel plate. The camera was clocked externally by the AC100, which also gated the image intensifier gate. Software was written to read out the AC100 over CAMAC and to analyse the images.

The camera and CAMAC readout were assembled and tested using pulsed LEDs and test images, and worked well. However, during the beam test the gas detectors did not produce sufficient light for avalanches to be imaged. Detector development is still underway by WA80, and further tests are planned.

Performance of the WA80 Streamer Tube Detector in a Test Beam

M.A. Bloomer, P. Jacobs, A.M. Poskanzer, H.G. Ritter, and the WA80 Collaboration

The WA80 charged particle multiplicity detector[1] is a large acceptance array of streamer tubes read out by ~40,000 capacitively-coupled pads. This fine segmentation makes it suitable for the study of multiplicity distributions and fluctuations in high energy heavy ion collisions at the CERN SPS.

In response to a streamer that develops after the passage of a charged particle, one or more pads will "fire" (i.e., exceed some threshold voltage). The response of the detector to individual charged particles was measured using data taken in December 1989 and April 1990 with a test setup in a 10 GeV e^- beam at the CERN SPS. The test setup consisted of a single plane of streamer tubes and pad read-out boards mounted on a moveable Al frame. Individual beam particles were tracked by upstream and downstream wire chambers with a position resolution of $\approx$1 mm. With this arrangement we measured 1) the probability of forming different cluster patterns, and 2) the position of a cluster with respect to the position of the particle. Differences in response between different boards and as a function of high voltage, threshold and angle of incidence were also measured.

The most important results of this analysis are shown in Fig. 1. Fig. 1a) is a plot of the probability (in per cent) of the eight most common cluster patterns for three different 160-pad boards. Even though each board has the same threshold, the probability of a given cluster can vary dramatically. These eight patterns account for over 90% of the patterns observed: the probability of all the remaining patterns is shown at the far right. Fig. 1b) is a plot of the standard deviation of the cluster position with respect to the projected wire chamber hit position (in the x-direction), for the same eight patterns. Despite the large differences in board response, the standard deviation in position for each board and each pattern is roughly the same, and considerably smaller than the cluster size. This is also true for the larger cluster patterns.

Analysis of the ^{32}S + S and Au data taken in August 1990 is currently underway.

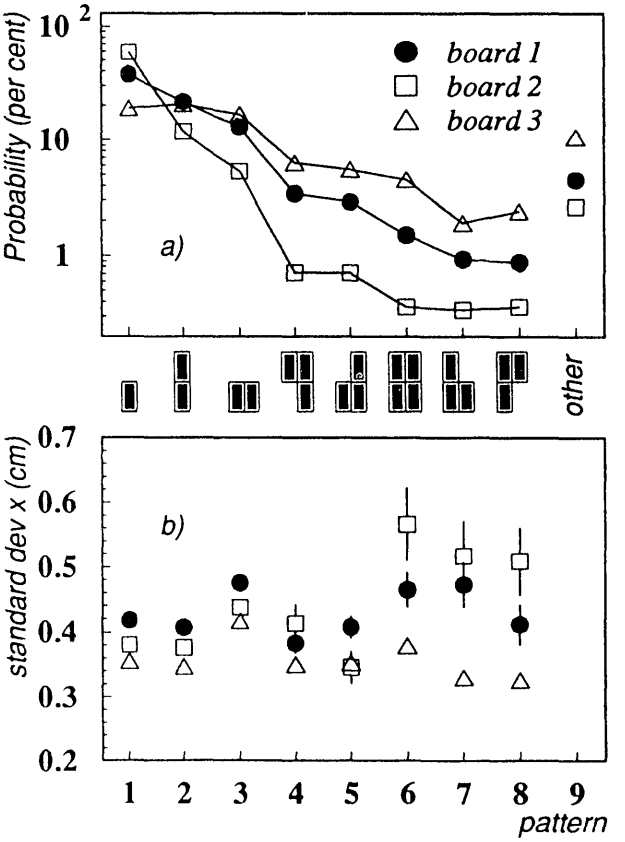

Figure 1: a) Probability of the eight most common cluster patterns (shown below the figure) for three different 160-pad boards at the same threshold. b) Standard deviation of the cluster position from the projected wire chamber hit position (x direction, in cm) for the same cluster patterns.

Footnotes and References

[1] R. Albrecht et al., *Nucl. Instr. and Meth.* **A276** (1989) 131.

CERN Experiment NA-36

D. E. Greiner, C. R. Gruhn and I. Sakrejda

The NA36 experiment at CERN was the only heavy ion experiment there which was lead by LBL personal from conception through the end of data taking. A TPC was used to measure the flux of neutral strange mesons and baryons produced in interactions of sulfur nuclei with various targets. There was data taking over the years 1986,1987,1989. Data taking in August-September of 1990 concluded the running for NA-36. In October of 1990 a new spokesman, Douglas Greiner of LBL, was elected.

The analysis phase of the experiment is proceeding at a rapid pace, track reconstruction codes have been perfected and pattern recognition production jobs are being run at centers in Switzerland, Great Britain and Norway. About 20% of the high quality data taken in 1990 has been analyzed. The detailed extraction of signal from background is proceeding at LBL, Birmingham, CERN and other institutions. Development of Monte Carlo codes to investigate combinatorial background and identification efficiency is centered at LBL.

At this time we can demonstrate clear detection of signal for the decay of lambda and neutral kaon particles. We present this evidence in the traditional form of the Podolanski-Armenteros plot.

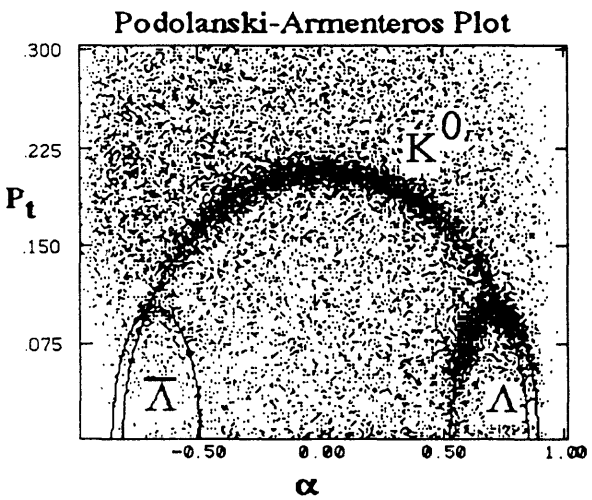

This plot was made with about 15% of the data collected in the 1990 run with a sulfur projectile incident on a lead target. The parabolic curves are the kinematically positions for decays of particles with the rest mass of neutral kaons and lambdas.The corresponding mass resolution plots for the kaons and lambdas are plotted below.

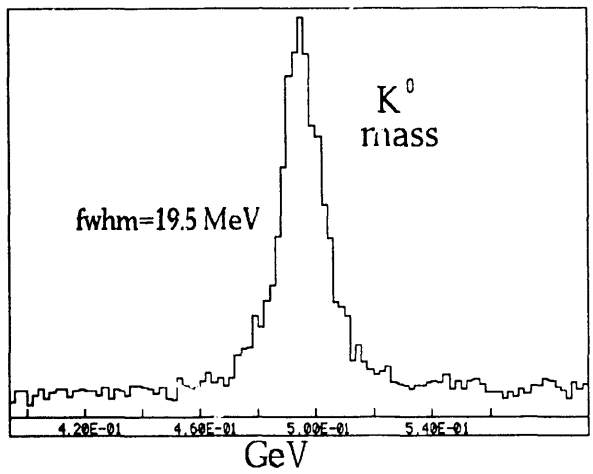

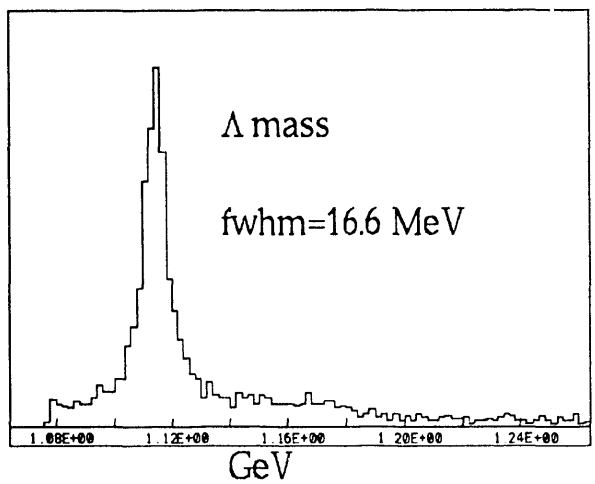

Since the signal is so strong, efficiency corrections and physics quantities will soon follow.

An Experiment on Particle and Jet Production at RHIC

STAR Collaboration

The aim of this experiment[1] is to search for signatures of Quark-Gluon Plasma (QGP) formation and investigate the behavior of strongly interacting matter at high energy density. Since there is no single accepted signature for the QGP, it is essential to use a flexible detection system at RHIC that can simultaneously measure many experimental observables. The proposed experiment will utilize two aspects of hadron production that are fundamentally new at RHIC: correlations between *global observables on an event-by-event basis* and the use of *hard scattering of partons* as a probe of the properties of high density nuclear matter. The event-by-event measurement of global observables - such as temperature, flavor composition, collision geometry, reaction dynamics, and energy or entropy density fluctuations - is possible because of the very high charged-particle densities, $dn_{ch}/d\eta \approx 1000$ - 1500 expected in nucleus-nucleus collisions at RHIC. Event-by-event fluctuations are expected in the vicinity of a phase change, so experiments must be sensitive to threshold-like features in experimental observables as a function of energy density. Full azimuthal coverage with good particle identification and continuous tracking is required to perform these measurements at momenta where the particle yields are maximal. Measurable jet yields at RHIC will allow investigations of hard QCD processes via both highly segmented calorimetry and high p_t single particle measurements in a tracking system. A systematic study of particle and jet production will be carried out over a range of colliding nuclei from p + p through Au + Au, over a range of impact parameters from peripheral to central, and over the range of energies available at RHIC. Correlations between observables will be made on an event-by-event basis to isolate potentially interesting event types. In particular, correlations of jet properties with full event reconstruction may lead to some surprising new physics.

Measurements will be made at midrapidity over a large pseudo-rapidity range ($|\eta| < 1$) with full azimuthal coverage ($\Delta\phi = 2\pi$) and azimuthal symmetry. The detection system will consist of a silicon vertex tracker (SVT) and time projection chamber (TPC) inside a superconducting solenoidal magnet for tracking, momentum analysis and low p_t particle identification via dE/dx; a time-of-flight system surrounding the TPC for particle identification at higher momenta; and electromagnetic and hadronic calorimetry outside the magnet to trigger on and measure jets, and to measure the transverse energy of events. The tracking and particle identification are needed mainly to study the soft physics, and the calorimetry to study the hard physics. Some of the details of the various detector systems have been worked out, while others require significant research and development before a final design can be established.

Footnotes and References

1. Letter of Intent, STAR Collaboration, Lawrence Berkeley Laboratory Report LBL-29651 (1990).

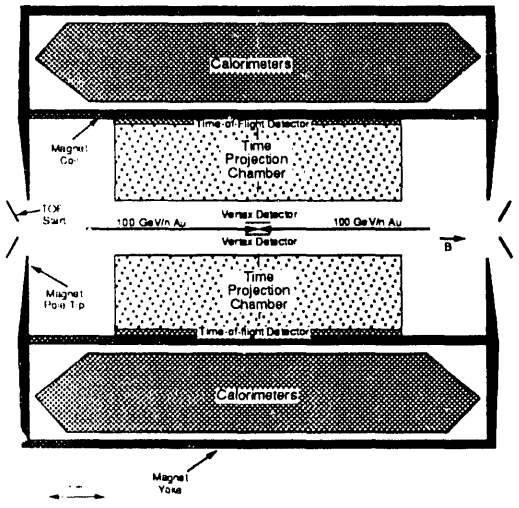

Fig. 1. Conceptual layout of the proposed experiment, with cylindrical symmetry around the beam axis.

RHIC TPC and Simulations

William Christie, Iwona Sakredja, Shaheen Tonse, Gulshan Rai, and the STAR Collaboration

The proposed TPC for RHIC is a cylinder with an inner radius of 50 cm and an outer radius of 200 cm. There is a thin cathode plane, perpendicular to the axis of the cylinder, which dissects the TPC into two halves. The ionization electrons in the TPC drift from the center of the cylinder to the anode structures on either end. The anode structure is divided into a twelve sided polygon as shown in figure 1. The TPC is placed in a solenoidal magnetic field whose direction is along the axis of the cylinder.

The general goal of our group is to use computer simulations to help guide the design and gauge the capabilities of the proposed LBL RHIC detector setup and experiment. Simulated data is also provided to groups investigating TPC tracking efficiency, vertex detector designs, calorimetry designs, high pseudo-rapidity multiplicity detector designs, and the effects of all such designs on the eventual physics analysis.

We are using the GEANT[1] software package from CERN for our simulation shell. GEANT allows one to define the geometry and material of the various detectors and structures in the proposed experimental setup. It then tracks the particles, taking into account the magnetic field and various physical processes which may affect the tracks such as: multiple coulomb scattering, energy loss, hadronic interactions, and particle decays with generation of secondaries.

To date we have been using the event generator code FRITIOF[2] exclusively to create the input events and particles for GEANT. We have recently added the capability to use the HIJING[3] code as an event generator.

At present we have all the geometry and detector component materials coded for the present design. We've installed an anode plane geometry. This allows us to generate space points for the tracks in the TPC which accurately represent the spatial distributions, including insensitive detector regions. These space points, for various pad plane geometries, will be input to the TPC tracking software to determine the tracking efficiency. Tracking will be accomplished using the space points and the ALEPH tracking code, modified for our application. We will then undertake detailed efficiency studies for the tracking in the TPC.

We aim to determine the performance for the proposed setup. This includes the tracking efficiency of the TPC in the large multiplicity density(~1000 charged particles per unit rapidity) environment expected at RHIC. Also to be investigated are the particle identification capabilities using dE/dx in the TPC and Time of Flight (TOF) information. The dependance of tracking efficiency on the number of space points, the position resolution of the points and the ratio of noise or lost points to real space points will be determined.

1. Geant Manual, Cern DD/EE/84-1, 1987.

2. B.Nilsson-Almquist, E. Stenlund, Comp. Phys. Com. 43,387,1987.

3. X.N.Wang, M. Gyulassy, LBL-29390, Sept. 1990.

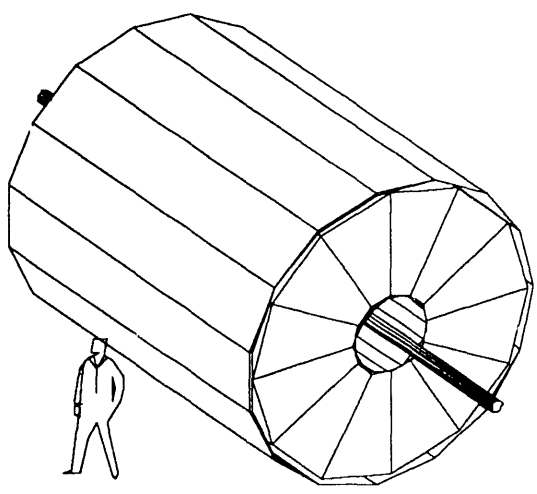

Figure 1. Perspective view of TPC.

Silicon Vertex Tracker for STAR at RHIC

W. Braithwaite†, D. Cebra, B. Christie, J. Cramer†, G. Odyniec , D. Prindle†, C. Naudet, L. Schroeder, T. Trainor† and the STAR Collaboration

Due to the physics motivations outlined in[1] and the expected complexity of events at RHIC, the experimental set-up requires a high precision tracking detector positioned close to the interaction point. Addition of a Silicon Vertex Tracker (SVT) to the apparatus will serve four purposes: 1. high-precision primary vertex determination (improving the primary vertex position accuracy by a factor ≈10 compared with that obtained from the TPC alone); 2. improvement of momentum determination of measured particles (addition of points from the SVT with an accuracy of 25μ to the track trajectory determined from the TPC with a 250μ accuracy) decreases uncertainties in the momen-tum determination on the average by a factor of ≈5); 3. determination of secondary vertices with high accuracy; 4. improvement of momentum determination for non-primary vertex tracks.

The SVT will be based on technology which has been proven to work in a physics experiment: Si strip detectors with capacitive charge division readout combined with LSI readout electronics allowing a high degree of multiplexing at the detectors. We envision a 2-3 year program devoted to exploring and understanding the most efficient design for application to the RHIC environment. Presently intensive simulations and Monte Carlo studies are underway to evaluate the tracking efficiency and its dependence on design parameters. Fig.1 shows the design presently envisioned, which consists of 2 individual cylinders of multilayer strip detectors made up of doublesided stereo layers. A list of specifications for the SVT is presented in Table 1. A comparison of the resolution of secondary vertices from the primary vertex using the TPC alone and with addition of the SVT will be undertaken. In addition, improvements in momentum measurements will be quantified.

Table 1. Silicon Vertex Tracker

Inner radius	10 cm
Outer radius	20 cm
Length	50 cm
Total thickness	600 μm
	~0.5% L_r
First layer of Strip Detector:	
Number of sections	8
Length of strips	6.25 cm
No. of strips per section	12,500
Pitch	50 μm
Stereo angle	5 mrad
Pixel dimensions	50 μm x 1 cm
Pixel area	0.5 mm^2
Cell occupancy	0.7 %
Double hit probability	2×10^{-5}

Table 1. Specifications for SVT.

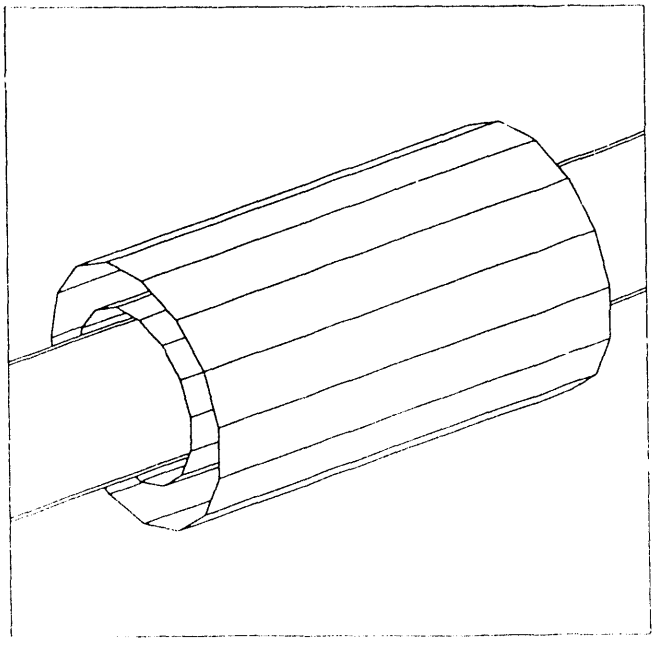

Fig.1. Possible design of SVT.

Footnotes and References

1. RHIC letter of intent, STAR Collaboration, Lawrence Berkeley Laboratory, Report LBL-29651.

† University of Washington

Jet Finding with Calorimetry at RHIC

M.A. Bloomer, D. Shy, J.W. Harris, P. Jacobs, and the STAR ⋆ Collaboration*

High $p_\perp$ jet production will occur with measurable rates at RHIC, and therefore is an important probe for studying high density matter[1]. However, the enormous background of particles produced from soft hadronic processes in the collision significantly impedes the detection and energy measurement of individual jets, and introduces "false" jet events with local fluctuations in the multiplicity and momenta of soft particles that mimic real jets.

Jet detection using EM and hadronic calorimetry was simulated. The detector covered a pseudorapidity width of $-1.5 \leq \eta \leq 1.5$, with cell sizes $\Delta\phi$=10 degrees and $\Delta\eta$=0.1. The calorimeter input consisted of particle energies from FRITIOF v1.7 central Au+Au events, mixed with ISAJET pp two-jet events. Charged particles were passed through a uniform solenoidal magnetic field of 0.5T, which imposed a minimum $p_\perp \simeq 300$ MeV/c on particles that reached the calorimeter. The CDF cluster-finding algorithm[2] was applied to the calorimeter cell energies to determine the jet direction and energy.

The results of this investigation are shown in Fig. 1. Fig. 1a) is the efficiency of finding at least one ($\epsilon_{1,2}$) or both jets (ϵ_2) of a pair, as a function of the jet energy E_t^{jet}. The efficiency increases with increasing E_t^{jet} because the cell with the largest E_t in a cluster must exceed a minimum value to be considered a jet, and this value was chosen to be quite high. The reconstructed jet energy is determined by summing the energy in a cone around the jet axis and subtracting the ambient soft particle energy. Fig. 1b) shows the standard deviation in the reconstructed jet azimuthal angle (ϕ), pseudorapidity (η), and energy (E_t^{jet}). On the average the full jet energy is recovered, but with large fluctuations from event to event. Similar values of these quantities for pp ISAJET events with $20 \leq E_t^{jet} \leq 50$ GeV are also displayed for comparison as open symbols.

This study demonstrates that conventional calorimeter-based jet finding algorithms can locate large E_t^{jet} jets in central Au+Au events at RHIC with good directional accuracy but poor energy resolution. In addition, it was found that these conventional algorithms do not efficiently discriminate between true and false jet events. Innovative algorithms for jet detection are now being investigated.

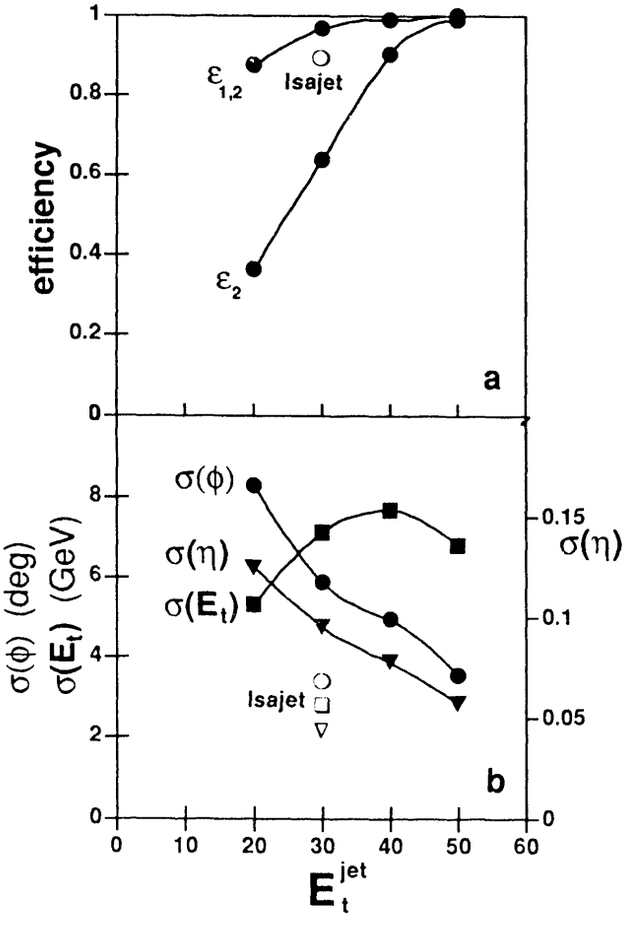

Figure 1: a) Efficiency for finding two-jet events as a function of E_t^{jet}. b) Standard deviations of the reconstructed jet ϕ, η and E_t^{jet}, as a function of E_t^{jet}.

Footnotes and References

*now at Physics Department, California Institute of Technology, Pasadena, CA.

[1]X.N. Wang and M. Gyulassy, *Fourth Workshop on Experiments and Detectors for RHIC*, Brookhaven National Laboratory, Upton, New York, 2-7 July 1990, BNL report 52262, p. 79.

[2]F. Abe et al., *Phys. Rev. Lett.* **62** (1989) 613.

Highly integrated electronics for a RHIC TPC detector

A.A. Arthur, F. Bieser, W. Hearn, S. Kleinfelder, K. Lee, J. Millaud, M. Nakamura, G. Rai, H.G. Ritter, H. Wieman, Y. Ye and the STAR Collaboration

It is the purpose of our work to develop a complete chain of highly integrated electronics for a RHIC TPC detector. Our long term goal is the production of an integrated circuit that contains several channels consisting of a preamplifier, a shaper and analog storage (switched capacitor array). We proceed by developing and optimizing the individual components separately, using the same process for all three elements so that the integration can be done later.

The RHIC R+D has been stimulated by our work on the EOS TPC electronics. For this detector we have developed a preamplifier and a switched capacitor array, components that will be integrated in the RHIC electronics. Presently, the work on the integrated shaper is the main focus of the RHIC effort.

The design of a shaper amplifier is complicated since discrete component circuit techniques are not directly applicable to IC design. It is difficult to achieve the precision and consistency for the resistors and capacitors needed for uniformity of the time constants in all channels. We have decided to solve the problem with the simple approach illustrated in Fig. 1: in parallel to the main capacitors we will use auxiliary capacitors that are switchable via a digital register. This will allow adjustment of individual time constants and to compensate for variations in the process parameters. A simple one stage wide band amplifier, schematically shown in Fig. 1, has been simulated, laid out and submitted to MOSIS. Once this principle works, we still have the choice to design a shaper with all the appropriate poles and zeros or to do only rudimentary shaping and to correct the pulse shape digitally.

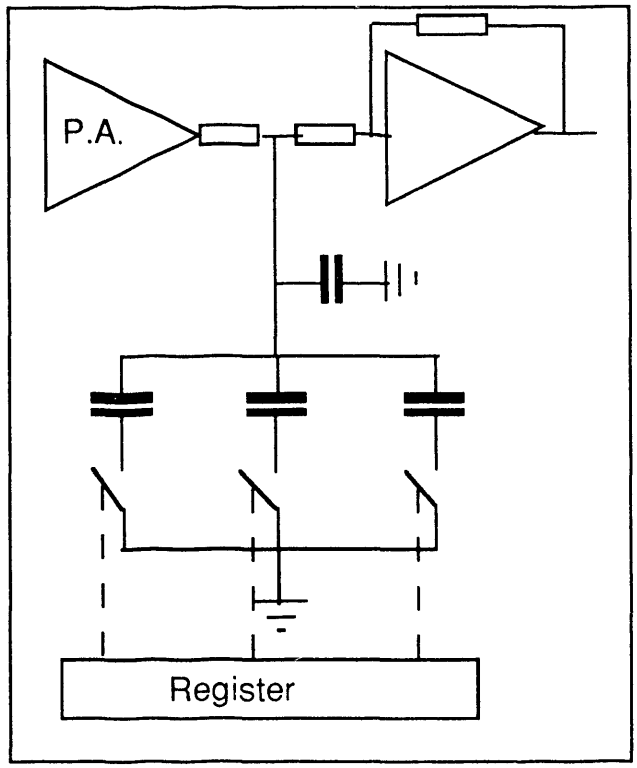

Fig. 1. Schematic representation of the correction capacitors

Footnotes and References

1. G. Rai, A.A. Arthur, F. Bieser, C.W. Harnden, R. Jones, S. A. Kleinfelder, K. Lee, H.S. Matis, M. Nakamura, C. McParland, D. Nesbitt, G. Odyniec, D. Olson, H.G, Oygh, H.G. Ritter, T.J.M. Symons, H. Wieman, M. Wright, and R. Wright, IEEE Trans. on Nucl. Sci. 37, 56 (1990).
2. S. A. Kleinfelder, IEEE Trans. on Nucl. Sci. 37, 1230-1236 (1990).

Theory

Fast Pulsars, Strange Stars: An Opportunity in Radio Astronomy* †

Norman K. Glendenning

There is presently no evidence to support the commonly held assumption, apparently anthropocentric, that the confined hadronic phase of individual nucleons and nuclei is the absolute ground state of the strong interaction. The fact that most of the mass in every object that we know to all the visible galaxies resides in nucleons and nuclei tells us for certain only that this is a possible phase of matter and that it is very long lived; not necessarily that it is the lowest energy one. How misleading the present composition is in revealing the nature of the ground state is immediately exposed by noting that the lowest energy state of the confined phase is Fe^{56} and there is very little of that in the universe. From the QCD energy scale it is quite plausible that the deconfined (3-flavor) strange-quark-matter phase is lower in energy and we show that the present upper limit on the abundance of strange nuggets in the earth's crust does not rule out this possibility. Indeed the universe would be almost identical in either case. We are only just now entering an era in which advances in technology may allow the detection of the *necessarily* subtle signals that might be present if the universe exists in a metastable phase, albeit long-lived, instead of the ground state. The most promising signals, both from the point of view of prospects for their existence as well as for their detection, are submillisecond pulsars. The shorter the period of rotation the more secure the conclusion that the universe is in a metastable phase of matter

Of course the assumption that the confined hadronic phase is the ground state cannot be realistically challenged by resort to specific models of the equation of state of dense nuclear matter, nor of quark matter, but rather by use of model independent limits, and when it is necessary to invoke models of matter, by exploration of the most general forms subject only to the minimal generally accepted constraints. Our approach within this framework is to exhibit the difficulties and contradiction encountered in trying to understand very rapid rotation of pulsars if they are assumed to be neutron stars. We then show how these are naturally resolved under the assumption that strange matter is the absolute ground state.

Our approach is therefore to carry out an exhaustive grided search over a flexible parameterization of the equation of state that is constrained only by (1) causality, (2) its smooth matching to the sub-nuclear equation of state and (3) the requirement that the maximum mass neutron star be at least $1.44 M_{\odot}$. The result of a search over more that 1400 models of the equation of state spanning a broad spectrum of behavior from soft to stiff at low density and independently at high, and including first or second order phase transitions representing pion or kaon condensates, for example, subject only to the above minimal constraints is that we find that no star bound only by gravity can have a period less than about 0.4 ms. This limit on rotation period is analogous to the mass constrant derived for neutron stars by Ruffini, In contrast to this lower limit on rotation period, stars that are self-bound with sufficiently large equilibrium energy can sustain shorter periods. If pulsars of such short periods are found the likely candidate is a strange quark star.

Footnotes and References

*Mod. Phys. Lett. A **5** (1990) 2197.

†Invited talk at Washington APS and Boston ACS spring meetings of 1990

Strange Quark Stars*

Norman K. Glendenning

Pulsars, of which some 400 are known, are thought to be neutron stars. Their rotation periods range from seconds down to milliseconds. The lower bound on the observations is due to observational bias associated with dispersion of the radio frequencies within the pulsed radiation. However the recent discovery that globular clusters are rich in fast pulsars offers the possibility, once one fast pulsar is found in a cluster, of determining the dispersive effects and thus achieving sensitivity to shorter periods, by applying the now known correction. Elsewhere we established a lower bound on the period of stars bound only by gravity (neutron stars). Here we examine the conditions that fast rotation imply for self-bound strange quark matter, under the hypothesis of Witten that it is the absolute ground state. In that case the macroscopic structure of a neutron star and that of a quark matter star are entirely different because they are bound by different forces, gravity in the case of the neutron star, confinement and gravity in the case of the quark star. This can be seen in the different behavior of radius as a function of mass of the star shown in Fig.1 where several neutron stars are compared with several quark matter stars. This difference *does not depend on the particular implementation of self-binding.* In that case we do not need an exact solution of QCD, but only a model of confinement to sketch, qualitatively, the properties of such stars. For this purpose we adopt a simple equation of state that embodies the hypothesis of self-binding, $\epsilon = 3p + \epsilon_b$ in which ϵ_b is the energy density at which self-binding occurs. Results are shown in Fig.1. It is seen that the quark stars with larger self-binding density, e_b, can withstand higher rotation. At the same time the star is more compact and the limiting mass is smaller. (We note that if the equation of state of quark matter is stiffer than in the MIT model, say $\epsilon = p/v^2 + \epsilon_b$, with $v^2 = 1$ instead of 1/3, then the maximum mass will be increased to $1.8M_\odot$ from 1.1. The limiting frequency remains high, since it is ϵ_b on which this depends most sensitively.) The curves marked .5 ms and 1.5 ms in Fig.1 represents the trajectory defined by the Kepler period and represent the upper bounds on stars that can withstand these rotation periods respectively. For equations of state for which the mass-radius relation lies below the curve, or those parts that do, the fast rotation can be supported. In a range of values of the self binding density, e_b , the window in baryon number ($A \sim M/m$) for which quark stars can sustain fast rotation is very broad, even encompasing the entire family of strange stars, whereas for neutron stars (albeit at unrealistic densities) the window is very narrow because of the mass-radius relation (Fig.1).

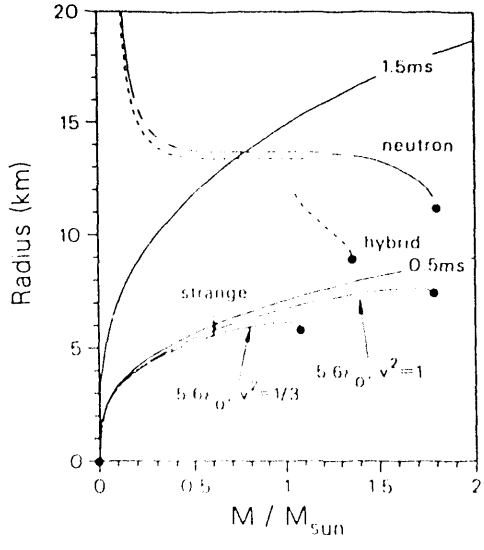

Figure 1: Radius vs mass for neutron and strange stars.

Footnotes and References

*Phys. Rev. Lett. **63** (1989) 2629; J. Phys. G. **15** (1989) L255.

Hadron to Quark-Gluon Phase Transition*

Norman K. Glendenning

The hadron to quark-gluon phase transition is studied in charge symmetric matter. Nuclear field theory describes the hadronic phase, including baryon resonances and thermal pions and kaons. The pion dispersion in medium is computed. The other phase is described as a gas of massless u and d quarks and gluons and massive s quarks, with or without gluon exchange. The Rankine-Hugoniot relation is employed to estimate the initial properties of matter produced in nuclear collisions as a function of energy. It is found that signals depending on pressure or entropy seem not so promising because the difference between the behavior of these in the hadron and mixed phases is not very different. In contrast the most dramatic differences between the hadronic phase and mixed phase occur in the temperature and density. Di-lepton and photon signals ought therefore to be good ones. It is shown that the analogy of "melting" of hadrons in the plasma is incorrect as concerns formation of a plasma in nuclear collisions in contrast to the adiabatic heating of matter. Neither the phase diagram nor the properties of matter on the shock trajectory depend very much on the nuclear equation of state within the uncertainties with which it can be defined in terms of conventional nuclear saturation properties, because the thermal energy dominates over these. The main dependences are on the hadron spectrum, the pion dispersion in medium, the bag constant and the QCD coupling constant. Within accepted uncertainties in the nuclear and plasma equations of state, the mixed phase could be formed in collisions with laboratory kinetic energy as low as 2.5 GeV.

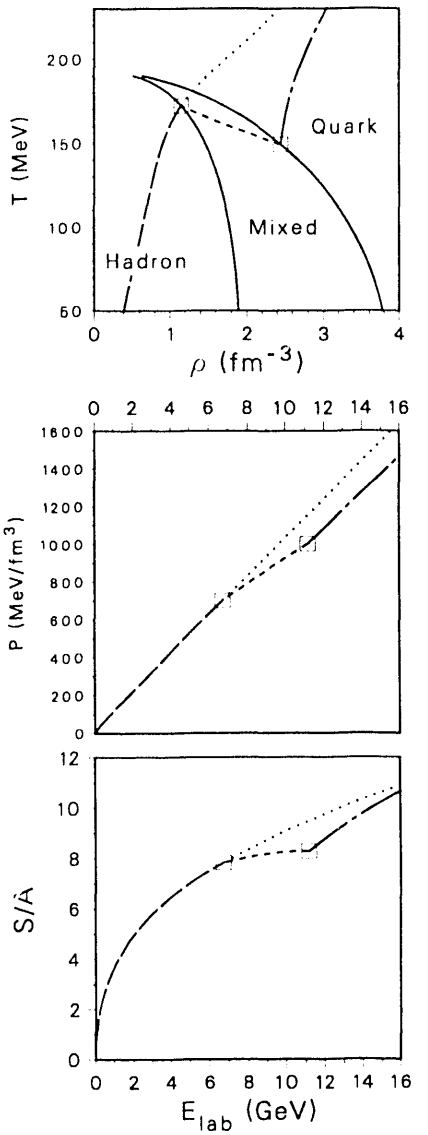

Figure 1: Sample Phase diagram, pressure and entropy

Footnotes and References

*Nucl. Phys. **A512** (1990) 737.

Modulation of Pulsar Signals by Star Deformation*

Norman K. Glendenning

The well known gross characteristics of pulsar signals are that the pulse profile, averaged over many pulses, and its frequency is very stable. Otherwise the individual pulses generally are different one from the other (1) Some pulsars produce signals within the average profile with apparently random structure compared to each other. (2) Still others produce successive pulse timings that vary systematically around the mean, the pulses drifting across the average profile and after a few pulses beginning at the other side and repeating a similar sequence of pulses. (3) The drift can occur in either direction. (4) Successive bunches of pulses constituting a cycle in the drift are not precisely the same in number or structure. (5) In some pulsar signals there are nulls, meaning the absence of pulses when they are otherwise expected from the period. (6) In others the average pulse profile switches between several patterns.

We accept the standard view that pulsars are rotating magnetized neutron stars and that the pulse is the manifestation of beamed radiation along the magnetic axis which is fixed in the star. In this paper we discuss the effects of a small deformation of a pulsar whose symmetry axis is not aligned with the rotation axis For simplicity we assume rigid-body motion. The two additional motions introduced by deformation, the precession of the symmetry axis about the angular momentum axis and the rotation of the body about its symmetry axis, will modulate the *intrinsic* radiation pattern produced by the emission mechanism that a fixed observer would see. As we show there is a rich variety in possible modulations, depending on the degree of eccentricity and the two angles between its axis, and the angular momentum axis and the magnetic axis, as well as the observers orientation.

Depending on the observer's orientation with respect to the angular momentum axis, and the parameters defining the pulsars motion, the modulation can manifest itself as drifting of individual pulses either in an advanced or retarded sense, with nulls or weaker pulses connecting the groups of drifting pulses. Under other circumstances the modulation can produce a group of pulses whose periods are nearly the same followed by nulls and then another group at a shifted timing, but again having nearly the same periods. The latter pattern resembles mode switching. Under certain circumstances an observer would see a sequence of pulses whose frequency is approximately sinusoidally modulated, and whose intensity varies, perhaps falling below the detection threshold so that a sequence of visible pulses is followed by nulls. In practice, the above cycles must be quasi-periodic because precise periodicity can occur only if the ratio of precession frequencies is a rational number; because of radiation damping this situation, though occasionally attained, cannot be maintained.

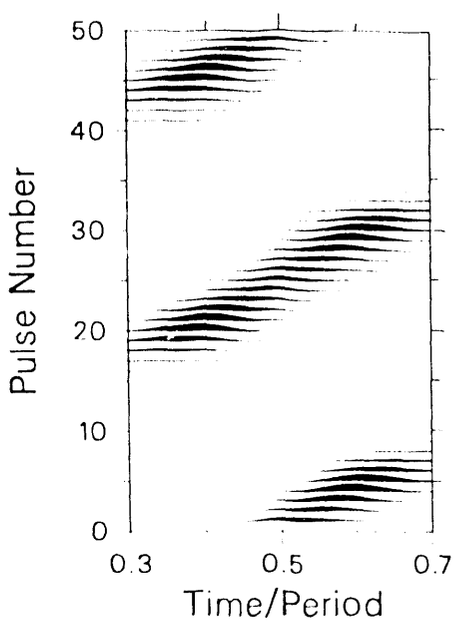

Footnotes and References

*Astrophys. J. **359** (1990) 186.

Cyclic Appearances of Pulsars*

Norman K. Glendenning

We discuss how a very small eccentricity whose symmetry axis is inclined at an angle to the angular momentum axis will slowly rotate a pulsar about the symmetry axis causing cyclic disappearance and reappearance of radiation beamed along a magnetic axis fixed in the star. Using the rate of change of the period, measured for most pulsars, as a constraint on the eccentricity, we can find a lower limit on the period of the cycle for disappearance and reappearance. Small asymmetric ellipticities could occur in puslars due to one or a combination of several factors: radiation-reaction torque of the magnetic dipole radiation, anisotropic pressure of charged fermions in the magnetic field, short-range component of the tensor interaction which preferentially aligns a strand of alternating neutrons protons and their spins, coupling of the magnetic moment of such an aligned structure to the magnetic field.

From the mechanics of a rigid body possessing an axis of symmetry that makes an angle β with the angular momentum axis which is fixed in space, the body will rotate about its own symmetry axis with an angular velocity of

$$n = \Omega \frac{e}{1+e} \cos\beta, \qquad e \equiv \frac{I_3}{I_1} - 1 \tag{1}$$

where $I_1 = I_2 \neq I_3$ are the principal moments of inertia and Ω is the precession frequency of the symmetry axis about the fixed direction of the angular momentum vector. From eq.(1) we have the inequality,

$$\left|\frac{n}{\Omega}\right| < \left|\frac{e}{1+e}\right| \tag{2}$$

The postulated eccentricity of a pulsar will cause it to radiate gravity waves, and accordingly cause a time rate of change of the period according to

$$\dot{P} = (2\pi)^4 \frac{64}{25} \frac{1}{P^3} M R^2 e^2 \tag{3}$$

in gravitational units ($G = c = 1$). This can be regarded as an upper limit on the eccentricity allowed by an observed value of period, P and its derivative. Combing the equations we have for the period of the cycle of appearrance and disappearance,

$$T > 7000 \left(\frac{\dot{P}}{10^{-15}} \frac{P}{\text{ms}} \right)^{-1/2} \text{ s} \tag{4}$$

Typical values of the rate of change of pulsar periods are in the range $10^{-13} > \dot{P} > 10^{-18}$. There are two observed pulsed sources that exhibit long time periodic variations, Hercules X-1 and Cygnus X-3 which are possible candidates for this phenomenon.

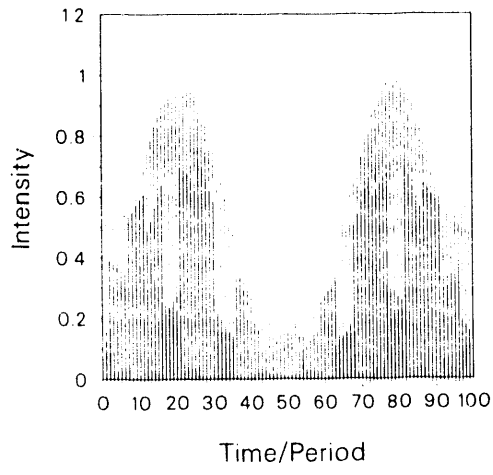

Figure 1: Intensity vs time for parameters that allow convenient display of signal variation due to precession.

Footnotes and References

*Phys. Rev. Lett. **63** (1989) 1443.

Limiting Angular Velocity of Realistic Relativistic Neutron Star Models *

F. Weber† *and N. K. Glendenning*

A fundamental problem encountered in the treatment of rotating neutron stars is the question of stability of these objects. An absolute upper bound on stable rotation is set by (1) the Keplerian frequency, Ω_K, which is defined by the balance between gravitational and centrifugal forces at the star's equator. Another type of instability has its origin in the (2) growth of non-axisymmetric instability modes that are driven by gravitational radiation-reaction [1]. The latter instability can be stabilized by viscosity [2].

In this investigation we concentrate on the problem of stable rotation of newly formed (and therefore hot, $T \approx 10^{10}$K) neutron stars as well as on estimating the critical angular velocity of rotating neutron stars that have been spun up by mass accretion from a companion and thereby reheated to $T \approx 10^8$K. We stress that the determination of viscosity of neutron star matter is a cumbersome and not yet completely solved problem [3]. Typical values of viscosity are $\nu(T) \approx 100$ cm^{2}s^{-1} for a temperature of $T \approx 10^9$K. The temperature of a newly formed neutron star is expected to be about 10^9K after the initial burst of neutrino emission. The cooling to about 10^9K may take place within the first two years. As the star cools, the viscosity increases rapidly like $\nu(T) \propto T^{-2}$.

We find for a neutron star of mass $M = 1.5 M_\odot$ for a collection of four equations of state (HV, $\Lambda^{00}_{\rm Bonn}$+HV, HFV, $\Lambda^{00}_{\rm HEA}$+HFV) the limiting rotation periods, P^ν_m, shown in Fig. 1. The index m refers to the order of the instability mode and has values of $3 \le m \le 6$. The superscript ν refers to viscosity and has values of $\approx 0, 1, 10, 100, 200,$ and 10^4 cm^{2}s^{-1} (from right to left). For all equations of state the $m = 5$ mode is largest (crosses) and hence is excited first. It turns out that the Kepler periods, P_K, are considerably smaller than P^ν_m. For neutron stars that have been spun up and reheated to temperatures $T \approx 10^8$K ($\nu \approx 10^4$cm^{2}s^{-1}) by accretion of mass from a companion, we find that the limit on stable rotation is set by the $m = 4$ and/or $m = 3$ instability modes. These stars can rotate at periods closer to the Kepler period.

The indication of this work is that gravitation radiation-reaction instabilities set a lower limit of a little more than 1 msec (1.27 msec for our models) on rotation periods of young neutron stars. This has very important implications for the nature of any pulsar that is found to have a shorter period. (The period of the fastest known pulsar, 1.56 msec, is shown in Fig. 1.)

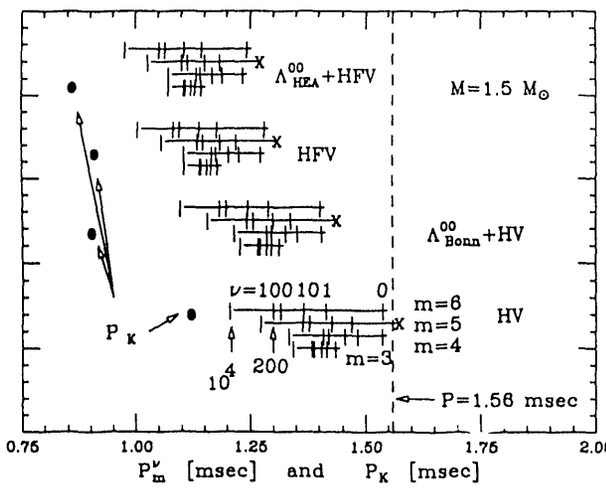

Figure 1: Limiting rotation periods P^ν_m and P_K for four equations of state (the vertical axis is without meaning).

Footnotes and References

*F. Weber and N. K. Glendenning, Limiting Angular Velocity of Realistic Relativistic Neutron Star Models, LBL-29141 (1990) (to appear in the Z. Phys.)

†Fellow of the Max Kade Foundation of New York

[1] J. L. Friedman, Comm. Math. Phys. 62 (1978) 247

[2] L. Lindblom, Ap. J. 303 (1986) 146; 317 (1987) 3[illegible]

[3] E. Flowers and N. Itoh, Ap. J. 206 (1976) 218; 230 (1979) 847

Models of General Relativistic Rotating Neutron Stars *

F. Weber† and N. K. Glendenning

The discovery of the first millisecond pulsar in 1982 [1] has stimulated considerable interest in the rotation of neutron stars. The realization that globular clusters are ideal environments for the formation of binaries including neutron star binaries in which accretion from the companion spins up the compact star, promises much more data [2]. Against this background we have reexamined Hartle's method of constructing rotating neutron star models in the framework of general relativity. We demonstrate that Hartle's method, which is limited to "slow" rotation rates, provides a practical tool for constructing models of rotating neutron stars. In particular we confirm its applicability down to periods $P \approx 0.5$ msec, a value which is by far smaller than the smallest yet observed pulsar period (1.6 msec).

Neutron star models are reported which are constructed from a collection of four different neutron star matter equations of state. Two of them have only recently been calculated by us for the relativistic ladder approximation to the two-particle scattering matrix in matter. For this purpose the HEA and Bonn meson-exchange potentials served as an input. The remaining two equations of state are calculated in the relativistic Hartree and Hartree-Fock approximation for electrically charge neutral many-baryon matter.

Considerable amount of work has been put toward the determination of the limiting angular velocity of rotating neutron star models. The Keplerian velocity, Ω_K (beyond which mass shedding at the equator sets in) determines an absolute upper bound on rotation (Fig. 1). However instability against gravitational radiation-reaction which is damped by virtue of viscosity, is known to set in at lower frequencies [3]. From a systematic study we find that the gravitational radiation instability sets in between 63-71% of the Keplerian value for young neutron stars. The limiting frequency of an old neutron star of mass $1.5M_\odot$ being spun up and reheated to temperatures of $T \approx 10^7$ K by mass accretion was found to lie in the range 77-92% of the Keplerian value.

This has important implications for the nature of any pulsar that is found to have a shorter period than $\approx$1 msec.

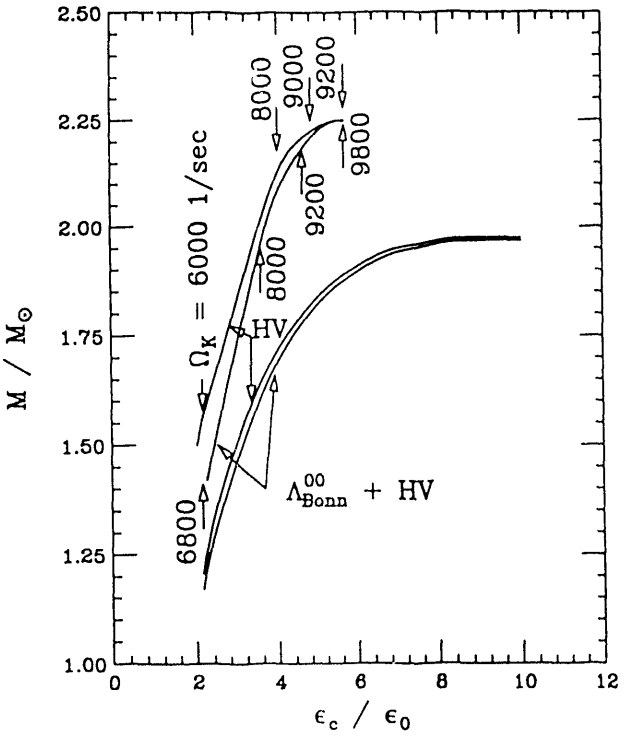

Figure 1: Rotation induced mass increase for rotation at Ω_K vs. central energy density ϵ_c.

Footnotes and References

*F. Weber and N. K. Glendenning, Structure and Stability of Rotating Relativistic Neutron Stars, LBL-28845 (1990) (to appear in the Astrophys. Journal)

†Fellow of the Max Kade Foundation of New York

[1] D. C. Backer et al., Nature 300 (1982) 615

[2] D. C. Backer and S. R. Kulkarni, Phys. Today 43 (1990) 26

[3] L. Lindblom, Ap. J. 303 (1986) 146

Semiclassical Expansion of the Nuclear Relativistic Hartree-Fock Theory*

M. K. Weigel and S. Haddad†,
F. Weber ‡

Since the pioneering work of Wigner [1], semiclassical approaches have been applied with great success in many fields of quantum physics. The advantage of semiclassical methods rests on the theoretical insight into the quantum structure as well as on simplifications as concerns their numerical treatments. One of the first calculations of nuclear properties on a large scale were performed by Myers and Swiatecki [2].

In recent years much interest has been put toward describing the nucleus as a relativistic system [3]. Calculations of nuclear systems within the relativistic quantum field approach have been performed by several groups, utilizing different many-body approximations. The simplest one is the Hartree approximation, which has later been extended to the more refined Hartree-Fock and Brueckner-type approximations.

However for finite systems the calculations within the Hartree-Fock or the Brueckner scheme turned out to be rather complicated. Semiclassical expansions in this field have been treated up to date (with the exception of an attempt to include higher-order contributions in the extended Thomas-Fermi approach) only for the Hartree approximation in first order of $\hbar$.

In this work we formulate in the first step the relativistic Hartree-Fock approximation in the Wigner (mixed position-momentum) representation utilizing the Green's function scheme. For the Lagrangian we use the standard boson-exchange model, where the nuclear forces are described by the exchange of σ, ω, ϱ and (pseudovector coupled) π mesons. The Coulomb interaction is taken into account too. The resulting set of coupled equtions between the one-particle Green's functions,

$$\begin{aligned}(i\hbar c\gamma^\lambda\partial_\lambda - m_N c^2 &+ \mu\gamma^0 + \frac{\nu}{2}\tau_3\gamma^0)_{12}G(2,1') \\ -\Sigma(1,2)G(2',1') &= \hbar c\delta(1,1'),\end{aligned}$$

$$\begin{aligned}G(1,2)(-i\hbar c\gamma^\lambda\partial_\lambda &- m_N c^2 + \mu\gamma^0 + \frac{\nu}{2}\tau_3\gamma^0)_{21'} \\ -G(1,2)\Sigma(2,1) &= \hbar c\delta(1,1'),\end{aligned}$$

and the mass operator,

$$\begin{aligned}\Sigma(1,2) = &- i\ \{< 13|v|24 > - < 13|v|42 >\} \\ &\times\ G(4,3^+)\end{aligned}$$

with

$$< 12|v|34 >= \sum_{i=\sigma,\omega,\varrho,\pi,e} < 12|v^{(i)}|34 > ,$$

permit a systematic so-called $\hbar$-expansion of the relativistic Hartree-Fock approximation.

In this paper the general structure of such an expansion is described, and the second-order self-consistency problem is formulated and discused in detail.

Footnotes and References

*M. K. Weigel, S. Haddad, and F.Weber, Semiclassical Expansion of the Nuclear Relativistic Hartee-Fock-Theory, Univ. Munich preprint (1990), to appear in the J. Phys. G.

†Sektion Physik of the Ludwig-Maximilians-University of Munich, Am Coulombwall 1, W-8046 Garching, Germany

‡Fellow of the Max Kade Foundation of New York

[1] E. Wigner, Phys. Rev. 40 (1932) 749

[2] D. Myers and W. J. Swiatecki, Ann. Phys. 55 (1969) 395; 84 (1979) 186

[3] L. S. Celenza and C. M. Shakin, Relativistic Nuclear Physics, World Scientific, Singapore (1986)

Deviations from the Single-Particle Propagation in Relativistic Many-Baryon Systems*

F. Weber† *and M. K. Weigel*‡

Due to the interest in the nuclear equation of state, needed for example for the understanding of heavy-ion reactions and the properties of neutron stars, the relativistic treatment of baryon matter has been investigated in many reports. In most cases one has applied the mean-field [1] theory, but extensions to more complicated approximations, as, for instance, the relativistic Hartree-Fock model [2] or the Brueckner-Hartree-Fock approximation [3] have been treated too. To the best of our knowledge however one has utilized a single-particle description for the baryon propagation in the nuclear medium. This implies in the Green's function scheme a δ-function structure for the spectral function, with a definite energy-momentum relation (see below). The Green's function of a baryon of type B, denoted by $G^B(p^\nu)$, is defined in terms of the spectral function, $\Xi^B(p^\nu)$, as

$$G^B(z,\mathbf{p}) = \int_{-\infty}^{+\infty} d\omega \, \frac{\Xi^B(\omega,\mathbf{p})}{\omega - z} \qquad (1)$$

with

$$\Xi^B(\omega,\mathbf{p}) = \frac{G^B(\omega+i\eta,\mathbf{p}) - G^B(\omega-i\eta,\mathbf{p})}{2\pi i} \, . \qquad (2)$$

The Green's function G^B is given as the solution of Dyson's equation:

$$[\gamma^\lambda p_\lambda - m_B - \Sigma^B(p)]\, G^B(p) = -\delta \, . \qquad (3)$$

A δ-function structure of Ξ^B of Eq. 2 demands a vanishing imaginary part of the self-energy, i.e. $\mathrm{Im}\,\Xi \to 0$. One arrives at

$$\Xi^B(\omega,\mathbf{p}) = \delta[\omega + \mu^B - \epsilon^B(\mathbf{p})]\, \Xi^B(\epsilon^B(\mathbf{p}),\mathbf{p}) \, , \qquad (4)$$

where $\epsilon^B(\mathbf{p})$ stands for the energy-momentum relation of a baryon propagating in matter. Only for vanishing imaginary parts of Ξ^B one gets

$$\epsilon^B(\mathbf{p}) = \Sigma_0^B(\mathbf{p}) + \sqrt{[m_B + \Sigma_S^B]^2 + [|\mathbf{p}| + \Sigma_V^B(\mathbf{p})]^2} \, . \qquad (5)$$

Complex self-energies are caused by a treatment which takes dynamical correlations into account [4] (like the so-called ladder approximations), or by the (explicit) inclusion of unstable particles (as, for instance, the Δ_{1232} resonance). For that reasons it is interesting to investigate the structure of the spectral function of Eq. 2 for complex self-energies and to derive an expression for Ξ^B in this more general case.

The deviations from the single-particle description, as expressed in Eqs. 4-5, are investigated in the present work. An expansion in powers of the imaginary part of Σ^B by maintaining an approximate single-particle description is performed.

Footnotes and References

*F. Weber and M. K. Weigel, Europhys. Lett. 12 (1990) 603

†Fellow of the Max Kade Foundation of New York

‡Sektion Physik of the Ludwig-Maximilians-University of Munich, Am Coulombwall 1, W-8046 Garching, Germany

[1] B.D. Serot and J. D. Walecka, Adv. Nucl. Phys. 16 (1986) 1

[2] F. Weber and M. K. Weigel, Nucl. Phys. A493 (1989); A505 (1989) 779

[3] B. Ter Haar and R. Malfliet, Phys. Rep. 149 (1987) 208

Footnotes and References

[4] P. Poschenrieder and M. K. Weigel, Phys. Rev. C38 (1988) 471

Aspects of the Relativistic Many-Body Theory of Baryonic Systems *

F. Weber[†] *and M. K. Weigel*[‡]

In the last decade there has been increasing interest in describing nuclear systems, like nuclear matter, neutron matter, and neutron star matter, in the framwork of a relativistic nuclear field theory (quantum hadron dynamics) [1]. Relativistic methods are advantageous in several respects. Among these are, for instance: The shift of the equilibrium density of nuclear matter from the so-called Coester line toward the equilibrium density of nuclear matter ($\varrho \approx 0.15$ fm^{-3}) via a new saturation mechanism, the relativistic analysis of scattering data, the description of finite systems, and the natural incorporation of the spin-orbit force [2]. Of great importance is also the access to the nuclear equation of state of high-density matter, encountered in the treatment of astrophysical problems (neutron stars and supernovae) and the analysis of heavy-ion reactions. Naturally there exists a great interest to explore the relativistic nuclear field approach in many respects in a more microscopic framework. To mention several are the consideration of consistency questions, predictive power and limitations of the method.

A useful tool for the description of many-body systems is the Green's function scheme. Here one has to solve, in the case of Brueckner-type approximations, the coupled system of the Dyson equation for the two-point Green's function (denoted by G) and the effective scattering matrix, T, in matter (G^0 denotes the free two-point function),

$$([G^0(1,2)]^{-1} - \Sigma(1,2))G(2,1') = \delta(1,1') \,, \quad (1)$$

$$\begin{aligned} < 12|T|1'2' > &= < 12|v|1'2' - 2'1' > \\ + \; i \; &< 12|v|34 > \Lambda(34,56) < 56|T|1'2' > \,, \end{aligned} \quad (2)$$

respectively. The self-energy, Σ, is given by

$$\Sigma(1,2) = -i < 14|T|52 > G(5,4) \,. \quad (3)$$

The Hartree and Hartree-Fock approximations result from Eqs. 1-3 by setting $T = v$ and $T = v - v^{ex}$. In the framework of these two approaches one has to adjust the coupling strenghts to the properties of nuclear matter at saturation [3]. The quantity v stands for the nucleon-nucleon interaction in free space. We have chosen the Ho2 and HEA meson-exchange models for the nucleon-nucleon interaction. In the case of the T matrix formalism one can choose for the intermediate particle-particle propagator either the Brueckner propagator or those of the so-called Λ treatment. These are given by $\Lambda^{00} \equiv iG^0G^0$, $\Lambda^{10} \equiv \frac{i}{2}(GG^0 + G^0G)$, and $\Lambda^{11} \equiv iG^1G^1$ and correspond to the so-called Λ^{00}, Λ^{10} and Λ^{11} approximations, respectively. We report results obtained from calculations performed for the Hartree-, Hartree-Fock-, Brueckner-, Λ^{00}-, and Λ^{10} approximation schemes.

Footnotes and References

*F. Weber and M. K. Weigel, Some Aspects of the Relativistic Many-Body Theory of Baryonic Systems, Conference Proceedings, to appear in Nucl. Phys. A, LBL preprint 28922 (1990)

[†]Fellow of the Max Kade Foundation of New York

[‡]Sektion Physik of the Ludwig-Maximilians-University of Munich, Am Coulombwall 1, W-8046 Garching, Germany

[1]B.D. Serot and J. D. Walecka, Adv. Nucl. Phys. 16 (1986) 1

[2]L. S. Celenza and C. M. Shakin, Relativistic Nuclear Physics, World Scientific (Singapore 1986);
B. Ter Haar and R. Malfliet, Phys. Rep. 149 (1987) 208;
P. Poschenrieder and M. K. Weigel, Phys. Rev. C38 (1988) 471

Footnotes and References

[3]J. Ramschütz, F. Weber, and M. K. Weigel, J. Phys. G16 (1990) 987;
M. Jetter, F. Weber, and M. K. Weigel, Determination of the effective Lagrangian in the Relativistic Hartree-Fock Theory, Univ. Munich preprint (1990) (to appear in the J. Phys G)

Energy Loss and Damping Rate of a High-Energy Quark in a Quark-Gluon Plasma*

Markus H. Thoma† *and Miklos Gyulassy*

Jets caused by high-energy quarks and gluons in ultrarelativistic heavy-ion collisions might provide a probe for the possible existence of a quark-gluon plasma (QGP) at RHIC and LHC. High-energy partons coming from initial hard collisions lose energy by propagating through the dense matter formed between the nuclei after collision. Therefore jet quenching is expected in AA collisions compared to pp or pA collisions.

Gyulassy and Plümer[1] suggested that jet quenching is suppressed if the dense matter consists of a QGP instead of hadrons. Their observation was based on an estimation of the energy loss of high-energy partons in a QGP by Bjorken[2] ($dE/dx \simeq 0.2$ GeV/fm for a 20 GeV quark), which turned out to be considerably smaller than in hadronic matter ($dE/dx \simeq 1$ GeV/fm). Bjorken considered the energy loss by elastic scattering on the quarks and gluons of the QGP using a tree level approximation. He encountered a logarithmic infrared singularity which he removed by a cutoff obtained from physical arguments.

We improved this estimation using plasma physics techniques. We calculated the energy loss of a high-energy quark considering the Lorentz force of the induced chromoelectric field on the quark. We included screening effects of the QGP and obtained an infrared finite result, which agrees on the 30% level with the one found by Bjorken. A comparison of Bjorken's dE/dx (dashed curve) and the plasma physics result (solid curve) is shown in figure 1, for which a temperature of 250 MeV and a strong coupling constant $\alpha = 0.2$, as indicated by lattice calculations, are assumed. In addition, the energy loss of a heavy quark (charm or bottom) was found to be significantly smaller than the one of a light quark.

Screening effects can also be taken into account using an effective perturbation theory developed by Braaten and Pisarski[3] in order to solve long-standing problems of high-temperature QCD. We applied this method for the computation of the damping rate of a high-energy quark in the QGP. The damping rate turned out to be logarithmically divergent since the dynamical screening of the long-range magnetic forces is not sufficient in this case in contrast to the energy loss.

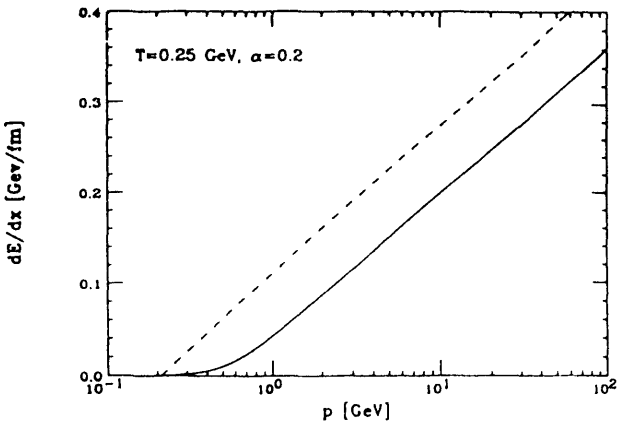

Figure 1: Comparison of Bjorken's (dashed line) and the plasma physics (solid line) energy loss of a light quark in the QGP versus the quark momentum.

Footnotes and References

*LBL-29276 (1990); Nucl. Phys. B351 (1991) 491

†Fellow of the Deutsche Forschungsgemeinschaft

[1] M. Gyulassy, M. Plümer, Phys. Lett. B243 (1990) 432

[2] J.D. Bjorken, Fermilab-Pub-82/59-THY (1982)

[3] E. Braaten, R.D. Pisarski, Nucl. Phys. B337 (1990) 569

Dynamical Properties and Flux Tubes of the Friedberg-Lee Model*

M. Grabiak† and M. Gyulassy

We believe that all strong interaction effects including particle properties of hadrons and heavy ion reactions could in principle be derived from quantum chromodynamics. However, the intricate nonlinear self-couplings of the gluons make this practically impossible. Thus, in order to understand the nonperturbative features of QCD it is useful to study phenomenological models. One simple model is the Friedberg-Lee model, where one neutral scalar field σ is introduced in order to describe the vacuum itself in a dynamical way. The Lagrangian of this model (without quarks) is given by

$$\mathcal{L} = -\frac{\kappa(\sigma)}{4} F^a_{\mu\nu} F^{\mu\nu}_a + \frac{1}{2}(\partial_\mu \sigma)^2 - U(\sigma) \quad .$$

The potential $U(\sigma)$ is chosen so that it has a global minimum at $\sigma = \sigma_V$, corresponding to the nonperturbative ground state, and a second minimum for $\sigma = 0$, corresponding to the perturbative vacuum. σ is coupled to the gluon field by introducing a σ-dependent dielectric constant κ. One assumes that the gluon self-couplings can be treated as a perturbation, with the nonperturbative effects being described by the field σ. The functional form of κ is chosen in such a way that $\kappa(0) = 1$ and $\kappa(\sigma_V) \geq 0$. The first condition ensures that in the perturbative vacuum the theory is reduced to ordinary Maxwell theory if one neglects the gluon self-couplings, whereas the second condition states that the dielectric constant of the nonperturbative vacuum is zero. In such a medium no electric charges can exist, because the corresponding energy would be infinitely high. Electric charges have to break the vacuum condensate, leading to bag-like structures and flux tubes. In this way this model yields a phenomenological description of confinement. It has been successfully applied to statical problems, describing hadrons as nontopological solitons and also describing flux tubes. However, we found that one encounters two major problems if one tries to apply this model to dynamical problems. In the nonperturbative vacuum it seems that the gluon field has no physical meaning at all, since the corresponding energy vanishes for $\kappa = 0$. Furthermore, one finds that an an axially symmetric flux tube is associated with a nonvanishing electric field in the whole universe, so one must really make sure that this field has no physical significance. However, we found that a gluon wave travelling into the nonperturbative vacuum $F^a_{\mu\nu}$ will blow up like $1/\kappa^{1/2}$, exactly compensating the factor κ in the energy. This means that there is no gluon confinement in this model. Another problem is that a nonvanishing $F^a_{\mu\nu} F^{\mu\nu}_a$ influences the mass and the self-couplings σ in the nonperturbative vacuum. We found that we can solve both problems by choosing κ so that all its derivatives vanish at $\sigma = \sigma_V$. This means that $\kappa(\sigma)$ has to be a non-analytical function. But since one generally also assumes $\kappa = 0$ for $\sigma > \sigma_V$ our model ensures that all derivatives are smooth at $\sigma = \sigma_V$, in contrast to any polynomial ansatz for κ at $\sigma < \sigma_V$.

We have used this model to study flux tube solutions. One interesting aspects of flux tubes in the Friedberg-Lee model is that they are always attractive and that the electric flux is strictly contrained to the interior of the flux tubes. In this respect they behave very much like flux tubes in type I superconductors.

Footnotes and References

*LBL 28516: accepted for publication in J. Phys. G

†Supported by the Alexander von Humboldt Stiftung

Nielsen-Olesen Vortices and Independent String Fragmentation*

M. Grabiak†, *J. Casado*‡, *M. Gyulassy*

We studied the Nielsen-Olesen model as a phenomenological model for QCD. Our motivation was to understand within this model why independent string fragmentation models such as Lund or DPM can work so well. The Nielsen-Olesen model is the relativistic version of a superconducting model. In the superconducting phase magnetic monopoles are confined. Thus it can be used to model the confinement of color electric charges in QCD if the roles of the electric and magnetic fields are exchanged and the superconducting phase is identified with the nonperturbative QCD vacuum.

In the Nielsen-Olesen model the electromagnetic field is coupled to a charged scalar Higgs field. The model contains three free parameters: The charge of the Higgs field, the photon mass m_A (which is the inverse of the London penetration length), the Higgs mass m_H (which is inversely proportional to the coherence length). Alternatively one can choose $\lambda = m_H^2/m_A^2$ as one parameter. $\lambda < 1$ means that the penetration length is small compared to the coherence length, corresponding to a type I superconductor, whereas $\lambda > 1$ corresponds to a type II superconductor. Since the electric charge of the Higgs particle corresponds to a magnetic charge in the QCD picture it can be related to the strong coupling constant α_s by the Dirac quantization condition. One more parameter can be fixed by fitting the string tension t of a flux tube solution to the charmonium potential. Finally λ can be used to adjust the vacuum energy ε_{vac}, i. e. the energy difference between the perturbative and the nonperturbative vacuum. Remarkably, for $\lambda = 1$ one gets exactly the same results for the string tension and the root mean square flux tube radius as in the MIT-bag model if one identifies ε_{vac} with the bag constant $B^{1/4}$. For example $\alpha_s = 0.385$ and $B^{1/4} = 235$ MeV, obtained from charmonium potential fits, yields $t = 1$ GeV/fm and $r_{rms} = 0.45$ fm. One of the possible explanations why flux tubes fragment independently is that this radius is rather small. Another remarkable feature of $\lambda = 1$ is that one can show that parallel flux tubes do not interact at all. Vortices with arbitrary relative orientations can interact in the region of closest approach, which can give rise to a string flip interaction. For $\lambda < 1$ parallel attract each other, whereas for $\lambda > 1$ they repel each other. However, as long as $\lambda \approx 1$ the interaction energy is only a few percent of the total energy, i. e. the strings interact only weekly. $\lambda > 1$ corresponds to higher ε_{vac}, in agreement with QCD sumrules, 229 MeV $< \varepsilon_{vac} <$ 271 MeV corresponding to $0.9 < \lambda < 2.0$. Due to the higher vacuum pressure $\lambda > 1$ also leads to thinner strings.

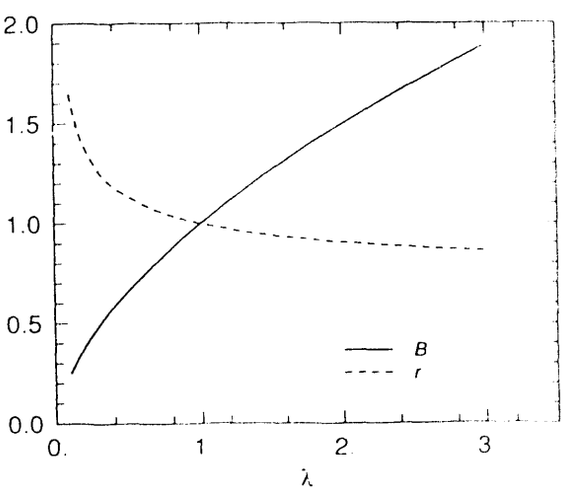

Figure 1: The volume energy $B = \varepsilon_{vac}^4$ and the flux tube radius r_{rms} normalized to the corresponding values in the MIT bag-model

Footnotes and References

*LBL 28857: accepted for publication in Z. Phys. C

†Supported by the Alexander von Humboldt Stiftung

‡On leave from Departamento de Física de Partículas, Universidade de Santiago de Compostela, Spain

Theoretical Issues in the Search for the Quark Gluon Plasma*

M. Gyulassy

Issues connected with independent string fragmentation, initial conditions, and hadronic transport in light ion reactions at AGS and SPS are discussed.

*Invited talk at IUPAP 1989 International Nuclear Physics Conference, Sao Paulo, Brazil, August 20-26, 1989; LBL-27881.

Non-Equilibrium Aspects of Ultrarelativistic Nuclear Collisions*

M. Gyulassy

This is a review of nuclear transport models from Bevalac to RHIC energies. Emphasis is on the non-equilibrium features and the space-time development of nuclear collisions.

*"Quark Gluon Plasma", World Scientific Advanced Series in "Directions in High Energy Physics," R. Hwa, Ed.,Vol. 6, Singapore, Republic of Singapore, p.223-270.

Workshop on Heavy Ion Physics at the AGS: Outlook*

M. Gyulassy

This report presents the closing talk of the workshop on AGS Heavy Ion program held at BNL March 5-7, 1990. The emphasis is on new questions posed by the new data presented at this meeting with emphasis on the pion-proton puzzle.

*Proceedings from the Workshop on AGS Heavy Ion Program, Upton, NY, Mar 5-7, 1990; LBL-29076.

Is Intermittency Caused by Bose-Einstein Interference?*

M. Gyulassy

Bose-Einstein interference leads naturally to enhanced fluctuations in narrow rapidity intervals on scales controlled by the widths of contributing resonances and may explain at least a part of the intermittency phenomenon observed recently in a variety of high energy reactions.

*in Multiparticle Dynamics, ed. A. Giovannini and W. Kittel, La Thiule, Italy, March, 1989 (World Scientific); LBL-26831.

Implications of Pion Interferometry for O+Au at 200 AGeV*

M. Gyulassy and S.S. Padula

Recent NA35 data on O+Au +X at 200 AGeV are shown to be consistent with both a hadronic resonance gas model and a quark-gluon plasma model for this reaction. We show, in addition, that much higher statistics data will be required to differentiate between these models even with the outward and sideward transverse projected correlation functions.

*Phys. Lett. B217 (1988) 181.

Interferometric Probes of Ultrarelativistic Nuclear Collisions

S.S. Padula and M. Gyulassy

We suggest that pion and kaon interferometry are complementary probes that help differentiate hadronic resonance gas from plasma dynamical models. We also discuss how interferometry could be used to test the presence of resonances at AGS energies. Finally, we study the A dependence of interferometry in the resonance model at 200 A GeV.

Analytic Approximations for Inside-Outside Interferometry*

S.S. Padula and M. Gyulassy

Analytical expressions for pion interferometry are derived illustrating the competing effects of various non-ideal aspects of inside-outside cascade dynamics at energies 200 AGeV.

*Nuclear Phys. B339 (1990) 378-392.

Pion Interferometric Tests of Transport Models*

S.S. Padula, M. Gyulassy and S. Gavin

In hadronic reactions, the usual space-time interpretation of pion interferometry often breaks down due to strong correlations between spatial and momentum coordinates. We derive a general interferometry formula based on the Wigner density formalism that allows for arbitrary phase space and multiparticle correlations.

Correction terms due to intermediate state pion cascading are derived using semiclassical hadronic transport theory. Finite wave packets are used to reveal the sensitivity of pion interference effects on the details of the production dynamics. The covariant generalization of the formula is shown to be equivalent to the formula derived via an alternate current ensemble formalism for minimal wave packets and reduces in the nonrelativistic limit to a formula derived by Pratt. The final expression is ideally suited for pion interferometric tests of Monte Carlo transport models. Examples involving gaussian and inside-outside phase space distributions are considered.

*Nucl. Phys. B329 (1990) 357-375.

Jet Quenching in Dense Matter*

M. Gyulassy and M. Plumer

The quenching of hard jets in ultrarelativistic nuclear collision is estimated emphasizing its sensitivity to possible change in the energy loss mechanism in a quark gluon plasma.

*Phys. Lett. B243 (1990) 432, 1-16.

Jet Quenching in Lepton Nucleus Scattering*

M. Gyulassy and M. Plumer

Two mechanisms for attenuation of produced hadrons in 10-100 GeV deep inelastic lepton-nucleus (A) reactions are contrasted to data: (1) independent quark fragmentation followed by final state intranuclear cascading and (2) string-flip fragmentation. We find that contrary to previous estimates, the observed suppression of low-momentum secondaries is substantially greater than can be accounted for by the first mechanisms. The second mechanism, which involves a strong nuclear modification of quark fragmentation up to jet energies ~10-20 GeV, appears to be more consistent with the available data.

*Nuc. Phys. B346 (1990) 1-16.

Antiproton Production as a Baryonometer in Ultrarelativistic Heavy Ion Collisions*

S. Gavin, M. Gyulassy, M. Plumer and R.Venugopalan

We propose that measurements of the antiproton and proton yields in ultrarelativistic nucleus-nucleus collisions can provide sensitive probe of the spacetime evolution in these reactions. We estimate the antiproton suppression expected due to annihilation processes for collisions in the energy range 10 - 200 AGeV.

*Phys. Lett. B234 (1990) 175.

Initial and Final State Interactions in J/ψ Production*

S. Gavin and M. Gyulassy

The systematics of J/ψ suppression in 200 AGeV O+U and S+U reported by NA 38 are interpreted as consequences of initial-state parton scattering and final-state inelastic scattering with comoving secondary particles.

*Nucl. Phys. A498 (1989) 477c-482c.

Jets in Relativistic Heavy-Ion Collisions*

Xin-Nian Wang and Miklos Gyulassy

The state of hot and dense matter which could consist of deconfined quarks and gluons has only been a theoretical topic for more than a decade until the notable experiments of relativistic heavy ion collisions at CERN and BNL, which at least give us some respectable feeling, if not understanding, of what is happening in these heavy ion interactions. With the results from these experiments and the accompanying controversy on whether quark gluon plasma (QGP) is created, we are now looking forward to the experiments at Relativistic Heavy Ion Collider (RHIC). At $\sqrt{s}$ = 200 GeV/n, one would expect that hard parton scattering or jet production becomes important, since it has already played a major role in every aspect of $p\bar{p}$ collisions at Sp$\bar{p}$S energies. However, in heavy ion collisions nuclear effect on the jets must also come in. First, due to the large number of binary collisions in heavy ion interactions, the number of jets produced will also be large. It is estimated[1] that half of the transverse energy in a central $U + U$ collision at RHIC comes from minijets. Second, the involvement of many nucleons and the particle production in the central rapidity region over a large transverse space will give rise to the effect of initial state and final state interations on the jets production, the former resulting in the Cronin effect and the latter causing jet quenching in hadronic matter.

Studies of jet production in pp and $p\bar{p}$ collision show that[2] multiple jets have important contribution to particle production. We use the same formula for the jet production per nucleon-nucleon interaction in heavy-ion collisions. Taking into account the nuclear effect, we developed the Monte Carlo program HIJING aiming at studying jets in high-energy nuclear collisions. A simple jet quenching in hadronic matter is incorporated in the program. Our results show that in heavy ion collisions jet production contributes to near half of the total particle production at $\sqrt{s}$ = 200 GeV. If parton shadowing in nuclear in taken into account, jet effect will be reduced but is still significant. The jet quenching effect in HIJING reduces the high p_T particles will could be obserable by comparing to pp result. We can motivate that a novel reduction of energy loss dE/dx for a jet in a dense matter near QCD phase transition T_c would result in an abnormal behavior of the jets and high p_T particle production rate. By studying the suppression factor of jets in heavy nucleus-nucleus collisions and its energy variation we could get some information about the state of the excited nuclear matter and hopefully to identify the formation of the quark-gluon plasma.

Footnotes and References

*LBL-29390, published in BNL-52262, proceedings of Fourth Workshop on Experiments and Detectors for a Relativistic Heavy Ion Collider, July 2-7, 1990, edited by M. Fatyga and B. Moskowitz.

[1]K.J. Eskola, K. Kajantie and J. Lindfors, Nucl. Phys. **B323**, 37 (1989).

[2]Xin-Nian Wang, Phys. Rev. **D43**, 104 (1991).

Role of Multiple Mini-jets in High-energy Hadronic Reaction*

Xin-nian Wang

In high-energy nucleon-nucleon collisions the production of mini-jets becomes increasingly important for the colliding energies beyond the ISR energy range[1]. Many model calculations indicate that mini-jets are responsible for the rapid growth of pp and $p\bar{p}$ cross sections, the violation of KNO scaling of multiplicity distributions and the increase of average transverse momentum with the charged multiplicity at high energies. In this paper we are going to show that production of multiple mini-jets with $P_T \sim$ few GeV are dominant in large multiplicity events.

We consider the problem in the impact-parameter representation of hadronic interaction where we can write down the inelastic cross section as

$$\sigma_{in} = \int d^2b \left[1 - e^{-2(\chi_s(b,s)+\chi_h(b,s))}\right], \quad (1)$$

and the probability for multiple jets production as

$$G_0 = \frac{1}{\sigma_{in}} \int d^2b \left[1 - e^{-2\chi_s(b,s)}\right] e^{-2\chi_h(b,s)}, \quad (2)$$

$$G_j = \frac{1}{\sigma_{in}} \int d^2b \frac{[2\chi_h(b,s)]^j}{j!} e^{-2\chi_h(b,s)}, \quad (3)$$

where $\chi_s(b,s)$, $\chi_h(b,s)$ are the eikonal functions associated with soft and hard QCD interactions which are directly related to corresponding inclusive cross sections σ_s and σ_h. We assume a constant value for σ_s and σ_h can be calculated by perturbative QCD. Eq. 1 can reproduce the interaction cross section and its energy dependence well up to very high energies.

With the known particle production from low energy hadronic interaction where no mini-jets are produced and the data from e^+e^- as the input for particle production from jets, we can calculate the multiplicity distribution at higher collider energies. The results agree with the experimental data at all available energies. As an example we show in Fig. 1 the calculated average multipicity and the data[2] as a function of energy.

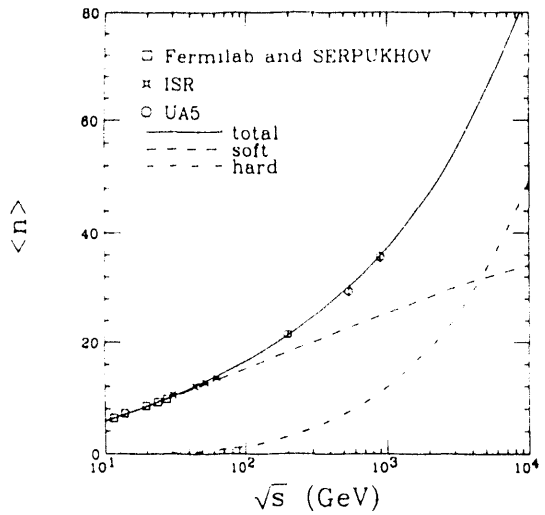

Figure 1: Calculated average charged multiplicities in pp and $p\bar{p}$ collisions comparing with the data.

Further investigations show that most of the jets with contribute to particle production have $2 \leq P_T \leq 4$ GeV. But in smaller rapidity windows higher P_T jets becomes important in large multiplicity events.

Footnotes and References

*LBL-28790, published in Phys. Rev. **D43**,104 (1991)

[1]C. Albajar,*et al.*, Nucl. Phys. **B309**, 405 (1988).

[2]M. Althof *et al.*,Z.Phys. C **22**, 307(1984); G. J. Alner *et al.*, Phys. Lett. **160B**,199(1985); R. E. Ansorge *et al.*,Z. Phys. C **43**, 357(1989).

Mini-Jets and Multiplicity Fluctuation in Small Rapidity Intervals*

Xin-Nian Wang

Since Białas and Peschanski[1] proposed a new way to analyse the particle density fluctuation in different rapidity intervals, experimentalists have found evidences of the so called intermittency, or the power-law behavior of the factorial moments as functions of the rapidity interval, in both hadron-hadron and nucleus-nucleus collisions[2]. On the other hand, when colliding energy is increased beyond the ISR energy range both experiments and theoretical estimations show that the hard or semi-hard collisions between point-like partons become important and are responsible for many phenomena which pertain to high-energy hadronic interactions. In this letter we explore the contribution to the intermittency from mini-jet production and its implications in high-energy hadron-hadron collisions.

If we know the multiplicity distribution $p_n(\overline{n}_{jet})$ in a rapidity window δy from a pair of jets with fixed P_T, y_1 and y_2, the multiplicity distribution in δy from an inclusive hard process in the nucleon-nucleon collisions is

$$P_n^{jet}(\delta y) = \int_{P_0^2}^{s/4} dP_T^2 dy_1 dy_2 \frac{p_n(\overline{n}_{jet})}{2\sigma_{jet}} \frac{d\sigma_{jet}}{dP_T^2 dy_1 dy_2}. \tag{1}$$

Note that $\overline{n}_{jet} \equiv \overline{n}_{jet}(y_1, y_2, \hat{s}, \delta y)$ depends on the rapidities and the center-of-mass enery $\hat{s} = x_1 x_2 s$ of the jet. We consider the particle production from a pair of jets is the same as in e^+e^-. From data we know that the multiplicity distribution follows a Poisson form and $\overline{n}_{jet}(y_1, y_2, \hat{s}, \delta y)$ can be obtained from the rapidity distribution. Thus $P_n^{jet}(\delta y)$ can be calculated from Eq. 1. The resultant distribution shows that contributions from jets with $2 \leq P_T \leq 4$ Gev are most dominant with higher P_T jets becoming important in a narrow rapidity window and with large multiplicities. We then calculate the normalized factorial moments of the multiplicity distribution $P_n^{jet}(\delta y)$,

$$F_i(\delta y) = \frac{\sum_{n=1}^{\infty} n(n-1)\cdots(n-i+1)P_n^{jet}(\delta y)}{\left[\sum_{n=1}^{\infty} nP_n^{jet}(\delta y)\right]^i}. \tag{2}$$

The calculation shows that $\ln F_i(\delta y)$ becomes linear in $\ln \delta y$ when $\delta y \leq 1$. Therefore a power-law behavior $F_i(\delta y) \propto \delta y^{-a_i}$ exists for all the mements for small rapidity intervals, where a_i which is the slope of the log-log plot is refered to as the index of the intermittency. Furthermore fluctuation from mini-jets increases with their P_T. Therefore one would expect the observed moments to increase with p_{Tcut} if only those particles with $p_T \geq p_{Tcut}$ are selected. Our study also shows that the fluctuation decreases with the number of mini-jets which contribute to the particle production. If one measures the fluctuation in different multiplicity intervals, the moments should decrease with the multiplicity. This is because that at higher energies the events with higher multiplicities are dominated by more mini-jets production and multiple mini-jets reduce the fluctuation from the mean in a small rapidity window.

Even though we can not make direct comparision with the data at this stage, we hope the investigation here can give some guidance to search for the effects of mini-jets in terms of intermittency. Most importantly, it provides a new source of multiplicity fluctuation in small rapidity intervals and the related power-law behavior.

Footnotes and References

*LBL-28789, published in Phys. Lett. **B248**, 447 (1990)

[1] A. Białas and R. Peschanski, Nucl. Phys. **B273**, 703 (1986).

[2] see papers in Leon van Hove Festschrift (World Scientific, Singapore, 1989).

Cluster Cascading in the Geometrical Branching Model*

Wei R. Chen[†], *Rudolph C. Hwa*[‡], *Xin-Nian Wang*[§]

Multiparticle production at low p_T in high-energy hadronic collisions has been described by a large number of models, all of which can reproduce the gross features very well[1]. The geomertrical branching model (GBM) is one among them, which combines the geometrical properties of hadronic collisions with the stochastic properties of particle production. After the suggestion by Białas and Peschanski to investigate intermittency in multiplicity fluctuations in various scales of resolution, experimental data on normalized factorial moments have revealed power-law behaviors in leptonic, hadronic and nuclear processes. Since random cascade processes can lead to intermittency, the GBM is well poised to account for the observed effect in small rapidity intervals. However, before a Monte Carlo code can be developed to demonstrate intermittency, there is one intermediate step that must be taken to render the GBM suitable for such considerations. That is, the branching process, which was summarized by the Furry distribution previously, must now be implemented by a specific scheme of successive branching. It is the aim of this paper to accomplish this limited objective.

Our starting point is the multiplicity distribution in GBM,

$$P_n = \frac{1}{\sigma_{in}} \int d^2b \sum_{\mu=1}^{\infty} \pi_\mu(b) F_n^{k(\mu)}, \qquad (1)$$

$$\pi_\mu(b) = \frac{1}{\mu!}[2\Omega(b,s)]^\mu e^{-2\Omega(b,s)}, \qquad (2)$$

where μ is the number of cut Pomeron in the interaction and $k(\mu)$ is a paramenter denoting the number of initial branching clusters. $F_n^{k(\mu)}$ is the Furry distribution function. Now we will replace $F_n^{k(\mu)}$ by actually performing massive cluster branching in a Monte Carlo program. Specifically, our procedure is the following. For each set of values of μ and E_i, $i = 1, ...\mu$ generated in our Monte Carlo simulation, we let the initial cluster in the ith cut Pomeron decay into two clusters whose masses m_1 and m_2 are determined randomly according to $\rho(m) \sim m^\alpha e^{-\beta m}$ Energy-momentum conservation then fixes their longitudinal momenta, their transverse momenta being neglected in this investigation. We then go to the rest frames of the daughter clusters and repeat the decay procedure, always using the same distribution to determine the subsequent cluster masses. The decay sequence is terminated when the mass reaches a value below $2m_\pi$. In this way we can determine the multiplicity distribution. Because we have not considered the charge and flavors of the produced hadrons, we take all the final particles to be pions and regard the number of charged pions as 2/3 of the total produced particles.

We have found that by choosing $\alpha = 0.1$ and $\beta = 0.01$ GeV^{-1} we obtain approximately Koba-Nielsen-Olesen(KNO) scaling for pp collision in the ISR region. The resultant multiplicity distribution agrees well with the data. The average multiplicity $<n>$ is also in good agreement with experminets. At higher energies minijet production must also be taken into consideration, so P_n is expected to get broader[2].

Footnotes and References

*LBL-29335, to be published in Phys. Rev. D**43** (1991).

[†]Oklahoma School of Science and Mathematics, 1515 North Lincoln Blvd., Oklahoma City, OK 73104 USA

[‡]Institute of Theoretical Science and Department of Physics, University of Oregon, Eugene OR 97403 USA

[§]Nuclear Science Division, Lawrence Berkeley Laboratory, University of California, Berkeley, CA 94720 USA

[1]Most of the models are described in review articles in *Hadronic Multiparticle Production*, edited by P. Carruthers (World Scientific,Singapore, 1988).

Footnotes and References

[2]Xin-Nian Wang, Phys. Rev. **D43**, 104 (1991).

String Models

*L.M. Robledo**

It is well known the success of all the phenomenological string models like the DPM, Lund, etc. in the description of all the relevant quantities (E_T, multiplicity distributions, dN/dy) describing the dynamics of heavy ion collisions at ultrarelativistic energies. However, one of the main assumptions of these models is a quite large string density $\rho_S \approx 2$ fm^{-2} which is in contradiction with the value obtained in the MIT bag model $\rho_S^{MIT} \approx 0.1$ fm^{-2}. This is a real problem because of the success of the MIT model in describing hadronic spectroscopy: depending on the type of phenomena one wants to describe, one is forced to choose between two contradictory models. On the other hand, it would be of great insight to have a more fundamental model for hadronic strings in order to be able to describe (instead of guessing) such fundamental issues as string-string interaction, stiffness of the string, etc which are of great relevance in any attempt to device a phenomenological string transport theory.

Inspired on the vortex solutions of the Abelian Higgs model [1], a model for finite strings was proposed [2]. The QCD vacuum in the model is represented by a charged scalar field ϕ and the quark (anitquark) at the ends of the string by a magnetic monopole (antimonopole). In analogy with superconductivity such magnetic monopoles produce a "color" magnetic Meissner effect which expels "color" magnetic field from the vacuum and at the same time create a hole in it. This would lead to confinement. In ref.[2] a variational calculation was carried out yielding to the typical linearly rising potential which reproduces quite well the Charmonium and Upsilon spectra in a nonrelativistic quantum mechanical calculation. Under the assumption of a small value for α_S and large value for the vacuum energy density $\Lambda^{1/4}$ (Hasenfratz parametrization[3]) the string transverse radius resulted to be $\Lambda \approx 0.4$ fm. This value leads to a string density of ≈ 2 fm^{-2}. The variational calculation in ref.[2] has, however, a serious flaw: we have repeated their calculation and, although we have found complete agreement with their results, the asymptotic behavior of the solutions is completely wrong. We have written the equations of motion in the form of integral equations and in this way we have been able to extract analytically the correct asymptotic behavior of the solutions. We are now using as variational functions a more extenive set of functions than the one used in ref.[2] and also incorporating the right asymptotic behavior. Numerical work along these lines is in progress.

Footnotes and References

*Permanent address: Madrid, Spain

[1] H.B. Nielsen and P. Olesen, Nucl. Phys. B61 (1973), 45

[2] J.W. Alcock et al, Nucl. Phys. B226 (1983), 299

[3] P. Hasenfratz et al, Phys. Lett. B95 (1980), 299

Subnuclear shadowing effect on the J/ψ production

*José A. Casado**

It was suggested[1] that the high density of colour charges in the QGP would cause a reduction in the number of J/ψ particles observed in the final state of a nucleus-nucleus collision. Shortly after, the NA38 Collaboration reported that a significant decrease of the ratio of the resonant $\mu^+\mu^-$ production cross section in the region of the J/ψ mass to the continuum of Drell - Yan $\mu^+\mu^-$ production in central AB collisions was observed[2]. Nonetheless, before we can assume that what NA38 has found is a signal of QGP formation, we must investigate all other possible sources of J/ψ suppression.

A generalization of the Glauber-Gribov model for nucleus-nucleus collisions to the case of J/ψ production in hadronic interactions has been studied[3]. It constitutes a simple and a consistent way of taking into account the requirement of unitarity and provides a framework in which energy constraints can be naturally accommodated. This model appears to be a useful tool to interpret the experimental results concerning J/ψ production in nuclear collisions.

One of the key elements of this work is the realization that energy constraints are relevant to the study of the J/ψ production at CERN ISR energies. A proper interpretation of the different functions and parameters of the model allowed us to discuss what is the influence of these constraints. This influence can be understood as follows: To generate a J/ψ particle it is necessary that at least one of the parton pairs formed in the collision has an energy above the J/ψ mass threshold. The number of these energetic pairs does not increase linearly with the atomic mass number of the nuclei due to the necessity of sharing the total energy among all the parton pairs. This is a point that so far has been generally disregarded.

The results can be classified according to two regimes: (1) The low-A regime is applied to the case of hA collisions and gives the right functional form for the A-dependence of the cross-section. This functional form presents a quadratic deviation from linearity. The order of magnitude of this deviation can be related to the double J/ψ production cross section in hadron nucleus collisions, which constitutes a consistency test of the model. Other phenomenological results also qualitatively agree with the known data. Of especial importance is the result concerning the x_F dependence of the J/ψ suppression: The model gives a qualitative explanation to the observed increase of the J/ψ suppression with x_F. Nevertheless, more experimental analysis would be desirable. For instance, the variation of k'/k^2 with the energy of the collision would constitute a test of the model.

(2) The large-AB regime is appropriate to study the nucleus-nucleus collisions case. The model implies that present experimental data on J/ψ suppression in central collisions can be understood with no need of the assumption that a QGP has been formed. A test of its major results, namely, the $(AB)^{2/3}$ limit and the absence of a large open charm enhancement, would be very interesting. In connection with this, it is important to remember that a large-x_F cut is essential. It is in this kinematical region that the $(AB)^{2/3}$ limit can be reached. This cut would also make contributions from other mechanisms of the J/ψ suppression less significant; it means that open charm production correlated with the J/ψ suppression shouldn't be observed.

Footnotes and References

*On leave from Departamento de Física de Partículas, Universidade de Santiago de Compostela, Spain

[1] T. Matsui and H. Satz, Phys. Lett. B 178 (1986) 416.

[2] NA38 Collab., M. C. Abreuet al., A. Bussiere, presented in *Quark Matter'87 Conf.* (Nordkirchen, Fed. Rep. Germany, August 1987), in: Proc. eds., H Satz and H. J. Specht, published in Z. Phys. C.

[3] J. A. Casado, LBL-29533

Systematics of J/ψ Production in Nuclear Collisions*

R. Vogt†, *S. J. Brodsky*‡, *and P. Hoyer*‡§

The dependence of J/ψ production on the longitudinal momentum fraction, x_f, and on the size of the nuclear target are in striking conflict with predictions of perturbative QCD. The strong absorptive component observed at high x_f is in complete disagreement with the parton-fusion model of J/ψ production. One would expect that large x_f J/ψ's have less probability of absorption than those produced at $x_f \sim 0$. The J/ψ distribution at large x_f is too hard to be accounted for by conventional mechanisms. Clearly another explanation is needed.

The A dependence is conventionally parameterized by a power law as

$$\sigma_{hA\to\psi} = \sigma_{hN\to\psi} A^{\alpha} , \qquad (1)$$

where $\sigma_{hN\to\psi}$ is the total J/ψ production cross section of hadron h on a nucleon. If J/ψ production were independent of nuclear effects, the production cross section would grow linearly with A. The exponent α decreases ~30% from $x_f = 0$ to $x_f \to 1$.

We study a two-component explanation of the x_f dependence. The first component, dominant at moderate values of x_f, is the parton-fusion model. This hard-scattering approach yields an approximately linear A dependence. Some absorption occurs, leading to a less than linear A dependence of J/ψ production by parton fusion. Effects contributing to the A dependence of parton fusion include final-state interactions with nucleons and comovers and nuclear shadowing of the target gluons and sea quarks. The second component of the x_f dependence is assumed to arise from an intrinsic heavy quark component of the projectile. Since the charm quark mass is large, these quarks carry a significant fraction of the longitudinal momentum and contribute to the large x_f portion of the cross section. The intrinsic $c\bar{c}$ state is small and passes through the target while the slower light quarks interact primarily on the nuclear surface, giving rise to a near $A^{2/3}$ dependence.

Our starting point is the J/ψ production data of NA3[1]. In their analysis, the x_f dependent data was divided into two different pieces so that

$$\frac{d\sigma(A)}{dx_f} = A^{\alpha'} \frac{d\sigma_h}{dx_f} + A^{\beta} \frac{d\sigma_d}{dx_f} . \qquad (2)$$

The 'hard' component, σ_h, is attributed to parton fusion. We associate the 'diffractive' component, σ_d, with intrinsic charm. Together these components give the effective α of eq. (1).

We examined J/ψ, ψ', and Υ production over a wide range of energies and made predictions for quarkonium production at RHIC under the assumption that no quark-gluon plasma is formed. All of the discussed effects contribute to an overall picture of the x_f, A, and E_T dependences of quarkonium production in hadron-nucleus and nucleus-nucleus collisions. The importance of each contribution depends on the kinematic regime studied. We believe that we have developed a plausible set of parameter values, but these should be systematically tuned in experiments that kinematically isolate each production component. These effects will be present in the 'background' of ultrarelativistic heavy-ion collisions. It is necessary to understand the systematics of J/ψ production to search for quark-gluon plasma production.

Footnotes and References

*UCRL-JC-106453 and SLAC-PUB-5421; Nucl. Phys. **B** (in press)

†Lawrence Livermore National Laboratory, P. O. Box 808, Livermore, California 94550

‡Stanford Linear Accelerator Center, Stanford University, Stanford, California 94309

§On leave from Department of High Energy Physics, University of Helsinki, SF-00170, Helsinki, Finland

Footnotes and References

[1] J. Badier *et al.*, Z. Phys. **C20** (1983) 101

J/ψ Suppression from Hadron–Nucleus to Nucleus–Nucleus Collisions*

Sean Gavin[†] *and Ramona Vogt*[‡]

Experiments with 200 AGeV oxygen and sulphur beams on a uranium target show a substantial suppression of J/ψ production in central relative to peripheral collisions. Matsui and Satz predicted that J/ψ suppression signals the formation of a quark–gluon plasma[1]. However, a similar suppression is already seen in hadron–nucleus reactions where quark–gluon plasma production is not expected.

We seek a common explanation of J/ψ production in hadron–nucleus and nucleus–nucleus collisions in terms of final–state interactions with both nucleons and comoving secondaries. A consistent, realistic spacetime description of ψ–N and ψ–comover interactions is formulated and applied to the available data. Our ultimate goal is to learn how future experiments can establish the J/ψ signal as a quantitative probe of the properties of high–density hadronic matter.

Evidence of J/ψ suppression in hadron–nucleus collisions is found in the A dependence of the inclusive cross section, conventionally expressed as a power law, $\sigma_{hA\to\psi} = \sigma_{hN\to\psi}A^{\alpha}$, where $\sigma_{hN\to\psi}$ is the J/ψ production cross section for hadron h on a nucleon. Semihard $c\bar{c}$ production should increase in proportion to the target mass A so that $\alpha < 1$ corresponds to a suppression.

Fermilab experiment E537 found results inconsistent with a power law. An anomalous A dependence may arise if the evolution of the $c\bar{c}$ pair into a J/ψ is taken into account. While the pair is small we expect its scattering cross section to be correspondingly reduced, introducing a path dependence in the effective J/ψ absorption cross section.

The NA38 collaboration studies J/ψ production in nucleus–nucleus collisions as a function of the hadronic transverse energy E_T. E_T is correlated with the impact parameter since central collisions produce more particles on average than peripheral collisions. In nucleus–nucleus collisions, we expect an increased density of secondaries in the central rapidity region. Since E_T is proportional to the final–state multiplicity and thus to the number of participants, no anomalous A dependence is expected from comover scattering.

We demonstrate that final–state interactions with comoving secondary particles as well as with nucleons provide a consistent description of hA and AB data. We show that comover scattering alone cannot explain the A dependence while a description of the NA38 E_T data requires comover scattering as well as nuclear absorption. We find that the presence of the comovers is indicated regardless of the description of $c\bar{c}$ hadronization. Our quantitative conclusions can be tested by demanding the consistency of the dynamical model over as wide a range of data as possible.

We also show how the measured A and beam–momentum dependences of the inclusive J/ψ cross section in hA collisions provide an exciting glimpse of $c\bar{c}$ hadronization. The effects of nuclear absorption were shown to be important at low energy while at high energy absorption is dominated by comover scattering. Measurements at higher energies are expected to further clarify the hadronization issue. We indicate that E_T–correlated experiments in hadron–nucleus and hadron–nucleon systems can provide important information on comover interactions.

Footnotes and References

*Nucl. Phys. **B345** (1990) 104.

[†]Research Institute for Theoretical Physics, Siltavuorenpenger 20C, Helsinki, Finland

[‡]Lawrence Livermore National Laboratory, P. O. Box 808, Livermore, California 94550

[1]T. Matsui and H. Satz, Phys. Lett. **178B** (1986) 416.

Mean Field Pion Interactions in a Hydrodynamic Model*

Ramona Vogt†

A relativistic, three-dimensional, one-fluid hydrodynamic model to simulate heavy-ion collisions has been developed at Livermore. One-fluid hydrodynamics is exactly solvable without recourse to assumptions about the initial conditions of the system, making it an ideal benchmark against which to compare experimental measurements, as well as other models. We begin with momentum-energy and baryon-number conservation. Scalar quantities are defined in the fluid rest frame. The equations of motion are solved numerically on a fixed spatial grid with the matter flowing through the grid. Mass and momentum conservation are strictly enforced, but the solution scheme does not explicitly conserve energy. However, energy is conserved to within a few percent. In one dimension, the model has been extensively checked for accuracy against analytical solutions of the equations of motion.

Hydrodynamics alone is not sufficient to describe the global properties of heavy-ion collisions. The hydrodynamic equations of motion do not allow particle production, yet many particles, mostly final-state pions are produced. A Monte Carlo scheme to approximate pion production and propagation was developed which couples the pions to the baryonic fluid via momentum and energy exchange, guaranteeing detailed balance of pion production and absorption but not requiring that the pions are in thermal equilibrium. The model follows the temporal and spatial evolution of each pion until freeze-out.

Previously, pions scattered elastically with nucleons as though they were free particles. The pion model has been modified to include the effects of the nuclear medium, which may influence the pion energy spectrum[1]. In medium, the pion exists partly as itself and partly as a nucleon-hole or delta particle-nucleon hole excitation. The energy of the pion, $\omega(k)$, is found from the poles of the pion propagator,

$$\mathcal{D}^{-1}(k,\omega) \equiv \omega(k)^2 - m_\pi^2 - k^2 - \Pi(k,\omega) = 0. \quad (1)$$

The proper polarization, $\Pi(k,\omega)$, includes the effects of the nucleon and delta states on the pion. We use the dominant contribution to the polarization, the delta-hole resonance, in symmetric nuclear matter. There are two solutions to the pion energy spectrum as a function of density ρ and momentum k. As $\rho \to 0$, neither solution describes the free pion dispersion at all k, switching behavior at k_0, the momentum at which the delta-hole energy equals that of the free pion. Below k_0, the lower root follows the free pion energy, but above k_0, this solution follows the delta-hole energy. Thus medium effects make pion production difficult to treat dynamically while still conserving energy and momentum.

The model solves the relativistic Boltzmann equation with pion production, absorption, and transport terms fully included. The inclusion of medium effects makes the Bose-Einstein distribution appear to be at a higher temperature, increasing pion production at high densities. The Bose-Einstein distribution of the free pion must be obtained in the limit $\rho \to 0$. The mean field now exerts a force on the pions as they move through the nuclear fluid, causing them to be accelerated. Scattering of pions off nucleons occurs through this acceleration, rather than through a collision integral. The pion model will be applied to nuclear collisions at Bevalac energies.

Footnotes and References

*in the proceedings of the Sixth Winter Workshop on Nuclear Dynamics, Jackson Hole, Wyoming, 1990

†Lawrence Livermore National Laboratory, P. O. Box 808, Livermore, California 94550

[1] B. Friedman, V. R. Pandharipande and Q. N. Usmani, Nucl. Phys. **A372** (1981) 483.

J/ψ Suppression: Catching up with the Comovers*

Ramona Vogt† *and Sean Gavin*‡

Measurements of J/ψ suppression by NA38 strongly suggest the formation of high energy density matter in the central rapidity region of light–ion collisions with a uranium target. Significantly, a similar suppression is evident from the A–dependence of J/ψ hadroproduction. In a previous work[1], we found that nuclear scattering dominates the suppression in hA collisions while a comparable contribution from scattering in the dense comover gas appears in the AB case. Here, we confront the preliminary E772 pA data at 800 GeV find that the comover contribution can become substantial in hA interactions at these considerably higher energies.

We consider midrapidity J/ψ production since the majority of J/ψ's are produced there, comover effects are strongest, and the $c\bar{c}$ production mechanism -- semihard gluon fusion -- is best understood. The pair is initially small, effectively reducing its absorption cross section. The cross section is assumed to reach its full hadronic value at the formation time τ_ψ, the time needed for the pair to separate to the J/ψ radius. The γ of the pair accounts for the Lorentz dilation of the formation time in the target frame and reduces the nuclear absorption of midrapidity J/ψ's with increasing beam energy.

If the $c\bar{c}$ pair escapes the nucleus, it may yet scatter with comovers, which form at a time $\tau_0 \sim 1 - 2$ fm characteristic of soft processes. The comover contribution to the survival probability is roughly depends on the rapidity density of comovers, expected to grow with center–of–mass energy $\sqrt{s}$ as $dN/dy \sim a + b\ln^2 s$ in the central re gion where a and b are empirical constants, amounting to a 30% multiplicity increase at E772 compared to E537. Comover scattering should thus increase with increasing beam energy while nuclear absorption is reduced. We expect comover scattering to become the dominant absorption mechanism in hA collisions for beam momenta exceeding $\sim$ 1 TeV, somewhat above the E772 energy.

The E772 collaboration has recently reported the A dependence of J/ψ, ψ', and Υ production. Preliminary results show that the J/ψ and ψ' appear to have similar A dependences while the Υ dependence is weaker. To calculate the J/ψ A dependence in 800 GeV pA collsions, we take the energy dependence into account and use the parameter values from our low energy fits. To calculate the ψ' and Υ A dependence we scale σ_0 and σ_{co} according to the meson sizes, taking $\sigma_{hN} = \sigma_{J/\psi N}\,(R_h/R_{J/\psi})^2$. The formation times of the resonances are determined from potential models. We find reasonable agreement with the data using our model.

Footnotes and References

*in the proceedings of Quark Matter '90, Menton, France, 1990, to be published in Nucl. Phys. **A**

†Lawrence Livermore National Laboratory P. O. Box 808, Livermore, California 94550

‡Research Institute for Theoretical Physics, Siltavuorenpenger 20C, Helsinki, Finland

[1]S. Gavin and R. Vogt, Nucl. Phys. **B345** (1990) 104

Rate Estimates for Vector Meson and Drell–Yan Production in Relativistic Heavy Ion Collisions*

R. Vogt†

The capabilities of the planned relativistic heavy-ion collider, RHIC, are such that a systematic study of vector-meson resonance production in hadron-nucleus, pA, and nucleus-nucleus, AB, collisions is possible. The variations in collider energy and beam allow a careful study of the A and $\sqrt{s}$ dependences of resonance production as well as the dependences on the kinematic variables, y and p_T.

We describe a calculation of the production cross section and the total rate as well as the rate binned as a function of y and p_T for the ϕ, J/ψ, ψ', and Υ resonances and the Drell-Yan continuum over the mass region $2 < M < 11$ GeV. We have used parameterizations of the production cross sections to obtain order of magnitude estimates.

It has been noted that hadroproduction of vector mesons scales as a universal function of $\tau = M_R/\sqrt{s}$, where M_R is the meson mass. A compilation of available data[1] shows that vector meson production in pp collisions obeys

$$B_R \frac{d\sigma}{dy}|_{y=0} = A_R \exp(-14.7\tau) \ , \qquad (1)$$

where B_R is the branching ratio of the meson decays to muon pairs and A_R is the normalization while the Drell-Yan continuum scales as

$$\frac{d^2\sigma}{dydM}|_{y=0} = \frac{A_{DY}}{M^3} \exp(-14.9\tau) \ . \qquad (2)$$

The differential production cross section has been parameterized as

$$E\frac{d\sigma}{d^3p} = A'(1-x_f)^c \exp(-bp_T) \ , \qquad (3)$$

which reproduces the broad features of the x_f and p_T dependences of the experimental data. The longitudinal momentum fraction, $x_f = 2p_{||}/\sqrt{s}$, is related to the center of mass rapidity by $x_f = \frac{2m_T}{\sqrt{s}} \sinh y$, where $m_T = \sqrt{M_R^2 + p_T^2}$ is the transverse mass.

To extrapolate to pA and AA collisions, we need to know the A dependence of resonance production. The growth of the production cross section with A is conventionally parameterized by $\sigma_{pA\to R} = \sigma_{pp\to R} A^\alpha$, where α depends on the resonance mass. In the Drell-Yan process, $\alpha_{DY} = 1.0 \pm 0.03$. Meson resonances have an α less than unity. We have $\alpha_\phi = 0.86 \pm 0.02$, $\alpha_{J/\psi} = \alpha_{\psi'} = 0.92$ and $\alpha_\Upsilon = 0.97$.

For resonance production, the cross section, $B_R\sigma$, integrated over all momentum space is

$$\begin{aligned} B_R\sigma &= A^{a\alpha} b^2 B_R \frac{d\sigma}{dy}|_{y=0} \int dy\, d^2p_T \exp(-bp_T) \\ &\quad \times (1 - \frac{2m_T}{\sqrt{s}} \sinh y)^c \\ &\quad \times \theta(1 - \frac{2m_T}{\sqrt{s}} \sinh y) \ , \end{aligned} \qquad (4)$$

where $a = 1$ for pA collisions and 2 for AA collisions. The θ-function excludes the region outside the kinematic limit. The total rate of resonance production expected in a RHIC year (3000 hours) is $N_R = 1.08 \times 10^7 L B_R \sigma$, where L is the beam luminosity. The Drell-Yan cross section $d\sigma/dM$ and the events per RHIC year may be obtained similarly.

The projected production rates are high enough to justify optimism. To maximize physics prospects, the entire energy range and all available beams should be used. Increasing the luminosity of nuclear beams would, however, improve the situation immensely.

Footnotes and References

*UCRL-JC-105057; submitted to Atomic Data and Nuclear Data Tables

†Lawrence Livermore National Laboratory, P. O. Box 808, Livermore, California 94550

[1] N. S. Craigie, Phys. Rep. **47** (1978) 1

Quasi-Classical Simulation of Nuclear Dynamics I: Phase Evolution of Disassembling Nuclei*

Claudio Dorso† *and Jørgen Randrup*

Heavy-ion induced reactions at intermediate energies produce unique physical scenarios and offer special opportunities for studying non-equilibrium effects in small many-body systems. Conversely, the interpretation of nuclear collision experiments relies heavily on our understanding of nuclear dynamics far from equilibrium. Significant progress has been made in recent years on developing dynamical models for nuclear collisions at intermediate energies.

We have recently developed a quasi-classical model which seeks to take approximate account of the exclusion principle by means of a repulsive Pauli potential depending on the separation between two nucleons in phase space.[1] When this Pauli potential is augmented with a suitable internucleon potential, it is possible to construct a model giving a fairly good reproduction of general thermostatic nuclear properties.[2] In the present work we make a first application of that model for dynamical studies, namely the evolution of a compressed and heated system containing 40 protons and 40 neutrons.

First, we have established general means for extracting thermodynamic quantities (density, temperature, and pressure) from many-body systems that are not in equilibrium, *e.g.*:

$$\text{Temparature}: \tau_{\rm eff} = \frac{1}{3A}\sum_{i=1}^{A} \mathbf{p}_i \cdot \mathbf{r}_i \ ,$$

$$\text{Pressure}: P_{\rm eff} = \rho_{\rm eff}\left(\tau_{\rm eff} + \frac{1}{3A}\sum_{i<j} r_{ij}F_{ij}\right)$$

where r_{ij} is the separation between two fragments and F_{ij} is the interfragment force. The effective density is determined from the *rms* extension q of the innermost 40 nucleons: $\rho_{\rm eff} = A/(\frac{4}{3}\pi R^3)$, with $q^2 = \frac{3}{5}R^2$.

On this basis, we have calculated the equation of state, *i.e.* the relationship between pressure density for fixed temperature, for finite nuclear systems.

Subsequently, we have calculated the dynamical evolution of disassembling nuclear systems. Specifically, we have discussed the temporal evolution of compressed and hot ^{80}Zr nuclei in terms of the effective density and pressure prevailing in their interior, mapping the trajectories of these thermodynamic variables onto the equation of state for a static ^{40}Ar nucleus, which provides a more instructive reference system than infinite nuclear matter.

We prepare the 80 nucleons as a spherical drop at twice normal density, with a specified kinetic temperature. A systematic change in the disassembly process is observed as the initial temperature is raised: at low temperatures the compressional energy is released by blowing off the outer layer of nucleons leaving a single liquid residue. As the temperature is raised, the size of the liquid residue shrinks, and at high temperatures, the system quickly turns into an expanding gas of nucleons and small clusters.

This explosive disassembly typically proceeds via filamentary structures, as is common in association with spinodal decomposition of ordinary liquids. This feature should manifest itself in observable multifragment correlations, since the final fragments should be clustered with respect to solid angle. Modern (existing and planned) multifragment detector systems might be able to test whether such dynamics actually occurs in nuclear disassembly.

Footnotes and References

*LBL-27075: Physics Letters 232B (1989) 29

†Departamento de Física FCEN-UBA, Buenos Aires, Argentina

[1] C. Dorso, S. Duarte, and J. Randrup, Phys. Lett. 188B (1987) 287

[2] C. Dorso and J. Randrup, Phys. Lett. 215B (1988) 611

Clustering in Nuclear Matter at Subsaturation Densities*

G. Peilert†, *J. Randrup*, *H. Stöcker* †, *and W. Greiner* †

In recent years, considerable progress has been made with regard to the modelling of nuclear systems within classical molecular dynamics. Such models have the advantage that they yield an explicit representation of the many-body state of the system and thus contain correlation effects to all orders. Therefore, they are especially suitable for studying the development of non-uniformities in nuclear matter. This class of models also has the conceptual advantage that it treats statics and dynamics on an equal footing.

On the basis of a quasi-classical many-body nuclear simulation model, we have shown that the nuclear cohesion causes the development of spatial non-uniformities in infinite matter at subsaturation densities, and thereby reduces the energy per nucleon by several MeV, for temperatures below ≈ 8 MeV. This significant effect can not easily be calculated with currently available more refined models, because of the irregular and varied appearance of the clustered system. Because of the significant lowering of the energy, it appears necessary to include the clustering in both statistical and dynamical treatment of nuclear disassembly, if quantitative reliability is to be achieved. Certainly, this phenomenon should be taken into account when seeking to determine the nuclear equation of state from data, and it may impact the search for the liquid-gas phase transition in heavy-ion reactions at intermediate energies.

In the present work we employ the Gaussian Pauli potential introduced by Dorso *et al.*[1], using different parameter values so that the total energy (rather than the kinetic energy E_{kin} alone) compares to the kinetic energy of the free Fermi gas. In addition, we use a Skyrme-type density-dependent nuclear interaction and a screened Coulomb potential (so that infinite systems can be addressed with the same model parameters).

The thermostatic properties of the system are obtained by averaging over several hundred statistically distributed manifestations of the system, sampled by means of the Metropolis procedure on the basis of the appropriate canonical weight. We have demonstrated that both infinite systems of noninteracting nucleons and finite droplets of interacting nucleons can be simulated rather satisfactorily.

We have studied periodic nuclear matter at densities below saturation. Near the saturation density, the system appears quite uniform in space and the energy follows closely that associated with a truly uniform system.

However, as the density is lowered well into the mechanically unstable regime, the effect of spatial rearrangement is significant, because the dilute system seeks to take advantage of the nuclear cohesion, and a significant amount of clustering occurs. For the lowest density considered ($\varrho = 0.1\,\varrho_0$) there is a pronounced condensation into distinct clusters, and the energy is considerably lower than that of the corresponding uniform gas. Indeed, for extremely low densities the system forms individual nuclei and the binding energy approaches that characteristic of finite nuclei, namely 6-8 MeV per nucleon.

Although the system is strongly clustered at $\rho \approx 0.1\,\rho_0$, the clusters do *not* appear as ordinary spherical ground-state nuclei, but seem to have a rather irregular appearance. This result calls into question the adequacy of approaches describing a disassembling nuclear source in terms of spherical fragments.

Footnotes and References

*UFTP preprint 247/1990; Physics Letters B (in press); supported by BMFT, GSI, and the Alexander von Humboldt Stiftung.

†Institüt für Theoretische Physik, Johann Wolfgang Goethe-Universität, D-6000 Frankfurt am Main, Germany

[1]C. Dorso, S. Duarte, and J. Randrup, Phys. Lett. 188B (1987) 287; C. Dorso and J. Randrup, Phys. Lett. 215B (1988) 611; Phys. Lett. 232B (1989) 29.

Time-Dependent Density-Matrix Theory II: Mass Dispersion in Damped Nuclear Reactions*

M. Gong†, *M. Tohyama*† *and J. Randrup*

A characteristic aspect of damped nuclear reactions is the broad distribution of the observables such as mass, charge, energy and angular momentum. In part I of this series of papers, [1] we developed a new, consistent method for calculating fluctuations in nuclear dynamical processes. This method, called the *time-dependent density-matrix* theory (*TDDM*), was derived from the time-dependent density-matrix formalism proposed by Wang and Cassing[2] which includes the effects of nucleon-nucleon collisions. *TDDM* determines the time evolution of the two-body density matrix in addition to that of the one-body density matrix. In ref.[1] we applied the *TDDM* to the damping of the isoscalar quadrupole motions of ^{16}O and ^{40}Ca and found that *TDDM* gives decay widths comparable to the experimental values.

In the present work we have applied the *TDDM* to the partition of mass between the two fragments in damped nuclear reactions. Since *TDDM* provides the two-body density matrix, in addition to the one-body density matrix, it is straightforward to calculate the fluctuations of one-body observables. The aim of the investigation is then to ascertain whether *TDDM* gives sufficiently large fluctuations in mass asymmetry to eliminate the qualitative failure of the time-dependent Hartree-Fock theory, which is so far the most fundamental theory applied to the problem, but which treats only the one-body density matrix.

We focus on the reaction $^{16}O + ^{16}O$ which is the largest system we can practically treat for the present. Since no experimental data are available on the mass dispersions in $^{16}O + ^{16}O$, we compare our results with those calculated in a transport theory called the *nucleon exchange transport* model (*NET*)[3], which has been successful in reproducing experiment data for various systems. Therefore, the results in *NET* for $^{16}O + ^{16}O$ are considered to be "empirical" values. In the comparison between *NET* and *TDDM*, basic macroscopic parameters in *NET* are obtained from quantities calculated in *TDDM*.

We studied the mass dispersions in damped reactions of $^{16}O + ^{16}O$ at E_{lab} = 185 MeV, based on the time-dependent density matrix theory. The advantage of the *TDDM* theory is that it provides the two-body density matrix determined consistently with the dynamics of a nuclear reaction. The fluctuations of one-body observables, such as fragment mass, were calculated with the two-body density matrix. It was found that the mass dispersions calculated in *TDDM* are considerably larger than those in *time-dependent Hartree-Fock* theory, by factors of 2.5–3. The *TDDM* results were also compared with the nucleon exchange transport model which reproduces experimental data for many reaction systems. The *TDDM* results were of the same order of magnitude as those of the *NET* model. We have also discussed the difference in the temporal behavior of the mass dispersion between *TDDM* and *NET* and it was noted that the *NET* assumption of quick internal relaxation is not satisfactory for an accurate description of the dynamics of these nuclear reaction processes.

Footnotes and References

*Z. Phys. A335 (1990) 331; supported in part by the National Science Foundation.

†NSCL and Physics Department, Michigan State University, East Lansing, Michigan 48824-1321

[1] M. Gong and M. Tohyama, Z. Phys. A355 (1990) 153

[2] S.J. Wang & W. Cassing, Ann. Phys. 159 (1985) 328

[3] J. Randrup, Nucl. Phys. A307 (1978) 319; A327 (1979) 490; A383 (1982) 468

Unsupervised Competitive Learning in Neural Networks*

Atilla E. Gunhan†, *László P. Csernai*†, *and Jørgen Randrup*

In the present work, we study numerically the learning ability of a schematic, one layer network that possesses some similarity with natural neurophysiological systems. The learning is associated with the plasticity of the synaptic couplings. The synapses can be excitatory or inhibitory. In biological networks the excitatory or inhibitory nature of a synaptic coupling do not change. We adopt this feature, and furthermore we fix the inhibitory connections (the lateral inhibitions) in our network. Only the excitatory connections are then modified by a Hebbian learning rule, which depends on the firings of the pre- and post-synaptic neurons only.

During the learning phase the network is subjected to a steady input stream, and the status of the network, as given by the excitatory coupling strengths, will converge to a final stationary state. Such final states act as attractors in the system and may be denoted as the *fix points* of the network, even though the randomness of the input causes the couplings to fluctuate around these values. The number of possible fix points is determined by the architecture of the net. Depending on its initial state, the system will converge towards one of these fix points. However, the positions of the fix points depend on the experience of the network, *i.e.* on the set of inputs presented to the network during the learning period, as we shall also show. Thus, our model calculation illustrates the importance of both the network architecture and the learning set.

Our study seeks to establish limits for the architecture producing networks capable of learning. The characteristics of the fix points are discussed and their dependence on the random training set of inputs is also analysed. The speed of convergence and its dependence on the network size are studied.

For this simple schematic neural network, we studied the dependence of the learning ability on the different external training conditions and on the strength of synaptic couplings. As stated above, the excitatory connections were changed during the training by a Hebbian-type learning rule, while the inhibitory connections were kept fixed. In a learning process these two components correspond to the outside experience and the inherited abilities, respectively. The importance of both processes was clearly demonstrated. Inadequate network architecture ("inherited anatomy"), such as degraded lateral inhibition, may result in loosing the perceptive learning ability or the ability to distinguish among different input patterns. At the same time, the learning experience is decisive in the development of the final learned state and the fix points are sensitive to the training sets.

We have shown that strong lateral inhibition is required if we want the network to discriminate between different inputs. Otherwise the network will not discriminate but generalize.

The lesson of this schematic study is that the network architecture (the "anatomy") should be adapted to the particular type of learning process, and for a balanced learning a wide and uniform experience is required. Networks of similar type but of essentially larger size can be used to classify certain sets of input patterns in situations where the information is available but no general classification or understanding has yet been achieved.

Although we have a particular biological system in mind, our model may be of much more general relevance. For example, the model may be of utility for problems in contemporary collision experiments involving high-energy beams.

Footnotes and References

*International Journal of Neural Systems 1 (1989) 177; supported in part by the National Science Foundation

†Department of Physics and Department of Information Science, University of Bergen, N-5007 Bergen, Norway

Theory of Nuclear Multifragmentation
I. Transition-State Treatment of the Breakup Process*

Jorge A. López and Jørgen Randrup

The transition-state treatment of ordinary binary fission has been generalized to describe statistical disassembly of a highly excited nucleus into multifragment channels. In this first part of the work, the focus is on deriving the general expressions for the transition widths into an assembly of specified prefragments. These are still interacting and may experience a significant post-transition evolution which must also be addressed (see part II).

The transition configurations are described in terms of a number of interacting prefragments, whose positions are constrained by a generalized disassembly degree of freedom q characterizing the overall spatial extension of the system and whose phase space is included in the statistical weight. Angular-momentum conservation is readily incorporated in the formulation.

The partial decay width for a transformation into a specified mass partition $A_1 \cdots A_N$ is expressed as the ratio between the outwards flow rate ν and the level density ρ of the compound nucleus A,

$$\Gamma_{A_1 \cdots A_N}(E) = h \frac{\nu_{A_1 \cdots A_N}(E)}{\rho(A, E)} \ . \qquad (1)$$

At low excitation, channels with only two fragments dominate and the formula for the decay width reduces to a form rather similar to the standard Bohr-Wheeler expression, but with an extra factor arising from the orbital motion of the binary complex. The dominant multiplicity increases with excitation and at high excitation the treatment acquires considerable formal similarity with standard statistical multifragmentation models, although certain notable differences are present. An important advantage of the treatment is that it automatically provides the constraint on the fragment positions so that a finite result is obtained; in this regard it is a significant advance relative to current statistical models in which the freeze-out volume must be prescribed separately.

This novel transition-state treatment of multifragmentation provides a well-defined means for calculating the partial widths for transition of the system into a number of interacting prefragments with specified masses and total energy. In order to obtain the actual final channel for a particular disassembly process, it is necessary to follow the further propagation of the system from the transition point towards asymptotia, since some prefragment pairs may find themselves inside the barrier of their respective two-body interaction potential and hence may recombine. We address this important question in a subsequent paper (see next contribution).

A major motivation for undertaking the present work has been the need for a model in which the evolution of the disassembly process from low to high excitation can be addressed. Having attractive limits, the developed model provides such a framework and its utility has been illustrated by calculations of the dependence of the (pre)fragment multiplicity on excitation energy. Though depending on Monte-Carlo sampling, the application of the model is not more computer-demanding than current statistical multifragmentation models, and a variety of instructive applications of the model are foreseen, at first primarily for the purpose of gaining theoretical insight. The application of the method to observable quantities must await the incorporation of the post-transition dynamics of the prefragment complex into well-separated fragments.

Footnotes and References

*LBL-26164: Nuclear Physics A503 (1989) 183

Theory of Nuclear Multifragmentation
II. Post-Transition Dynamics*

Jorge A. López and Jørgen Randrup

In previous work (see part I), expressions were derived for the rate at which a highly excited nucleus breaks up into several interacting prefragments. The present work treats the dynamical evolution of the system subsequent to such a transition.

The post-transition system is described as a number of distinct prefragments that experience both conservative and dissipative pairwise interactions, obtained by a suitable generalization of the dynamics governing damped nuclear reactions.

The post-transition dynamics has a significant effect on the disassembly process. Most importantly, some prefragments may fuse in the course of the evolution, thus reducing the heavy-fragment multiplicity. The nuclear dissipation enhances this effect, as illustrated in the figure below, where the upper curves are calculated without dissipation and the lower ones with the proximity friction included:

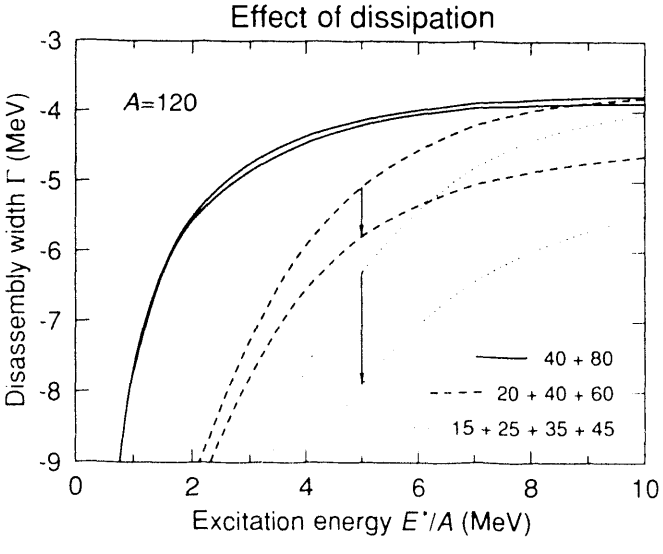

It is generally expected that the early stage of energetic nuclear collision leads to significant enhancements of the density. Such a compression may in turn produce an overall radial flow in the system at the subsequent disassembly stage. Our multifragmentation treatment can readily be employed to study the effect of such a feature, if it were indeed present. We have found that the survival probability of a specific mass partition is significantly increased when the source is endowed with an overall radial flow, characterized by the outwards directed collective kinetic energy per nucleon, $E_{\rm blast}/A$:

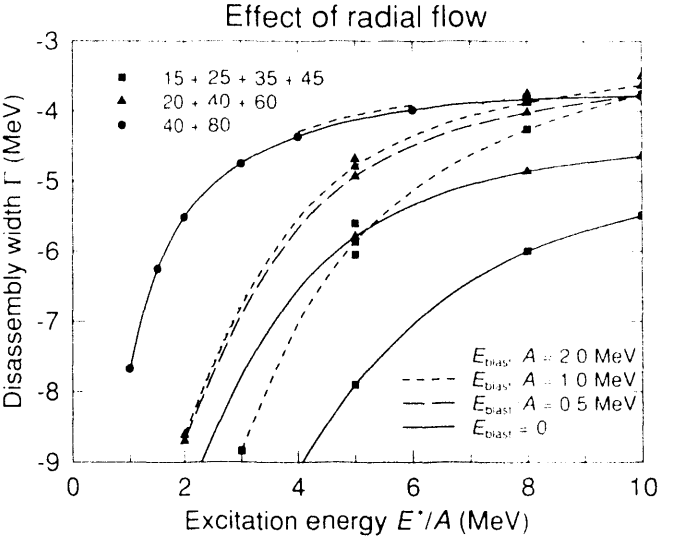

As the detector technology advances and powerful multifragment detector systems are being constructed, there are growing demands on theory to provide the tools necessary for making informative analysis of the data. The present theory, though yet incomplete, may prove useful for attempts to investigate the extent to which interesting properties of a produced source, such as a collective flow, are manifested in quantities amenable to experimental measurement.

Footnotes and References

*LBL-26810: Nuclear Physics A512 (1990) 345

Microcanonical Sampling of Momenta*

Jørgen Randrup

In numerical simulations of systems containing several "particles", it is often desirable to generate statistical samples of the particle momenta, under microcanonical contraints of the total energy and, possibly, the total linear, radial and/or angular momenta. We have presented a simple, efficient, and exact method for solving such tasks, within the realm of non-relativistic classical mechanics.

When only the energy is constrained, the calculational task is equivalent to picking a random point on a $3N$-dimensional unit sphere, a straightforward computational task.

It is apparently less recognized that this simple method can readily be extended to accommodate also conservation of the linear momentum. Furthermore, the method can be generalized to also incorporate the conservation of radial and/or angular momentum. This useful fact appears to have gone unnoticed and may in fact be a novel finding.

The main characteristic of the microcanonical momentum distributions is the energy constraint

$$\sum_{n=1}^{N} \frac{p_n^2}{2m_n} = E_0 \ . \qquad (1)$$

It is often of interest to incorporate additional constraints, in particular conservation of linear, radial, and/or angular momenta,

$$\sum_{n=1}^{N} \mathbf{p}_n = \mathbf{P}_0 \ \text{(linear)} \ ,$$

$$\frac{1}{q} \sum_{n=1}^{N} \mathbf{r}_n \cdot \mathbf{p}_n = p_0 \ \text{(radial)} \ ,$$

$$\sum_{n=1}^{N} \mathbf{r}_n \times \mathbf{p}_n = \mathbf{J}_0 \ \text{(angular)} \ ,$$

where q is the *rms* extension of the system, $m_0 q^2 = \sum_n m_n r_n^2$, with $m_0 = \sum_n m_n$, and $\mathbf{r}_n$ are the given positions of the particles.. These constraints can be included by relatively simple modification of the basic method pertaining to energy conservation alone. Furthermore, if the particles carry internal angular momenta $\mathbf{S}_n$, the situation is more complicated, but can be treated in a similar manner. It should be noted that the radial and angular momenta are only defined when the positions $\mathbf{r}_n$ of the particles are known.

The general procedure can be described in words as follows: Consider N particles for which the total energy E_0 has been specified, together with its total linear, radial, and angular momenta, $\mathbf{P}_0$, p_0, and $\mathbf{J}_0$, respectively. Start by picking a set of tentative momenta $\{\mathbf{p}_n\}$ and spins $\{\mathbf{S}_n\}$ from a canonical distribution, using an arbitrary temperature. First eliminate the overall linear, radial, and angular momenta by performing appropriate overall linear, radial, and angular boosts. Then renormalize the remaining momentum and spin vectors by a common factor, so as to match the specified available statistical energy, $E_{\rm stat} = E_0 - \mathbf{P}_0^2/2m_0 - p_0^2/2m_0 - \mathbf{J} \cdot (2\mathcal{I})^{-1} \cdot \mathbf{J}$, where $\mathcal{I}$ is the total moment of inertia. Finally boost the system up to achieve the desired total linear, radial, and angular momenta.

The developed general method offers a very useful tool for certain types of simulations of many-particle systems, such as nuclear multifragmentation. Not only do the described procedures yield exact samplings of the appropriate microcanonical momentum space, but they are also simple and efficient (hence fast), since all candidate sets are useable. The method presented may find application in a variety of physical contexts and should therefore be of interest to a broad community.

Footnotes and References

*LBL-28390: Comp. Phys. Comm. 59 (1990) 439; Nuclear Physics A522 (1990) 651; supported in part by the Alexander von Humboldt Stiftung.

New Developments in the Calculation of β–Strength Functions*

Peter Möller† *and Jørgen Randrup*

The need to model astrophysical processes and the desire to understand how nuclear structure variations influence β-decay properties, are challenges that have stimulated the development of theoretical models for Gamow-Teller β-strength functions. For astrophysical applications it is necessary to model properties of a large number of nuclei, which limits the complexity of the models that can be considered.

Earlier treatments were often statistical in nature and thus suited only for describing average properties of the β-strength function, and to account for its structure it is necessary to use a microscopic model of the nucleus as the starting point for constructing the wave functions and energy levels of the parent and daughter nuclei.

We have presented an improved model for the calculation of strength functions for Gamow-Teller β-decay. It incorporates many significant enhancements over the model for Gamow-Teller β-decay of deformed nuclei that was presented 6 years ago[1]. The most important are:

- In addition to the Nilsson modified-oscillator single-particle potential, we can now also use Woods-Saxon and folded-Yukawa potentials as starting points for determining the wave functions of the mother and daughter nuclei involved in the decay. This is particularly advantageous, since the latter model has been employed in a microscopic-macroscopic calculation of structure quantities such as masses, shapes, spins, levels, and pairing effects for 8979 nuclei from oxygen and up.
- The pairing part of the model has been improved. The pairing Δ_n and Δ_p values are determined in a microscopic model with the effect that the underlying level structure is reflected in the values obtained. We can use either a BCS pairing model or a Lipkin-Nogami model. The latter model avoids the collapses that occur in the BCS model. The strength G of the pairing interaction is determined by a method that is valid in any part of the nuclear chart.
- The perturbation treatment of $\Delta v = 0$ transitions in odd-even and odd-odd nuclei has been improved so that we now avoid the singularities that occurred in earlier treatments. Odd-odd nuclei are also treated.
- Decays from states where the unpaired odd particle is in an excited state can now be treated.
- Models for the calculation of half-lives with respect to β^- and β^+ decay and electron capture have been studied and incorporated into our computer codes.

The resulting model constitutes a unified model framework for the study of a large number of nuclear structure quantities within a single model and with a single, limited model parameter set. A detailed analysis of these results is now in progress. This analysis, together with more extensive studies of β-decay properties of known nuclei with the present model, now give us a better understanding of the properties of these nuclei and also the experience with the models that is required for extensive applications to regions far from stability.

Footnotes and References

*LBL-27504: Nuclear Physics A514 (1990) 1

†Theoretical Division, Los Alamos Scientific Laboratory, Los Alamos, New Mexico 87545.

[1] J. Krumlinde and P. Möller, Nuclear Physics A417 (1984) 419

Statistical Properties of Nuclear Systems at Finite Temperature*

Jørgen Randrup and Emil de Lima Medeiros†

In the laboratory, a large variety of physical environments can be created transiently by means of nuclear reactions at intermediate energies. Such collision experiments are often aimed at probing the nuclear equation of state and their interpretation depends critically on our understanding of the statistical properties of non-uniform nuclear matter at finite temperature.

We have developed a model that can be brought to bear on these problems. The model may also prove of some utility in connection with the supernova process, in which matter is compressed to densities near the saturation value and the temperature reaches several to many MeV, although we are not presently contemplating astrophysical applications.

The model uses the local Thomas-Fermi approximation in conjunction with an effective finite-range two-body interaction depending both on density and momentum. At zero temperature the model is similar to the generalized Seyler-Blanchard model recently considered by Myers and Swiatecki[1]. In this first part of the work, we have derived the central formalism, including expressions for the free energy $F[\rho]$ from which other quantities can be derived (*e.g.* the statistical weight and the pressure). These are *functionals* of the specified density distribution ρ, as well as functions of the temperature τ.

We have calculated the phase diagram for uniform isosymmetric matter and the associated equation of state; we find a limiting temperature of 12-13 MeV, while the critical temperature is around 16 MeV. These results agree well with more refined calculations.

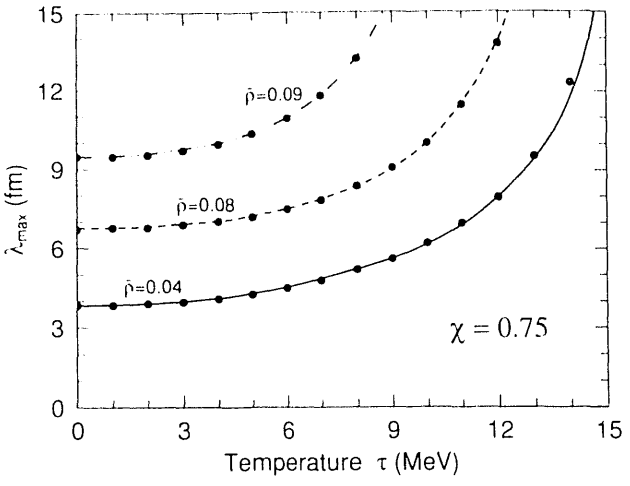

The figure shows the maximum wavelength λ_{max} for which matter is stable against ripples of finite amplitude. In nuclear multifragmentation the transformation of the source into an assembly of (pre)fragments may well be strongly influenced by such instabilities.

The developed model gives a consistent statistical description of nuclear systems with arbitrary density distributions, within the confines of semi-classical mean-field theory. The model combines three important features: 1) it is conceptually simple and computationally relatively easy; 2) it has a rather general applicability, namely to arbitrary density distributions held at a fixed temperature; and 3) it agrees quantitatively with general (average) nuclear properties, both as regards a broad spectrum of experimental data (binding, barriers, optical potential, *etc.*) and with respect to theoretical expectations based on more elaborate calculations.

The model can readily be subjected to Metropolis sampling and may thus form a basis for addressing scenarios with large fluctuations, thus helping elucidate the properties of hot nuclear systems far from equilibrium.

Footnotes and References

*LBL-28797; Nuclear Physics A (1991) in press

†Centro Brasileiro de Pesquisas Físicas - CBPF, Rio de Janeiro, Brazil; fellow of the Brazilian Conselho Nacional de Desenvolvimento Científico e Tecnológico.

[1]W.D. Myers and W.J. Swiatecki, Annals of Physics 204 (1990) 401

Relativistic Transport Theory for Hadronic Matter*

Shun-Jin Wang[†‡], *Bao-An Li* [‡], *Wolfgang Bauer* [‡], *and Jørgen Randrup*

In nuclear collisions of energy up to around one GeV per nucleon, nuclear matter at high density and high temperature can be formed transiently. In such systems baryon excitations and mesonic degrees of freedom play a significant role, whereas the pressure is well below what is required to dissolve the hadrons into deconfined quarks and gluons. Relativistic quantum hadrodynamics is the appropriate tool for describing these dynamical processes. Aspects of particular interest are both of microscopic nature, such as the in-medium hadron-hadron cross sections and the dispersion relation of the pion in hot matter, and macroscopic, such as the nuclear equation of state, the transport properties (*e.g.* viscosity and heat conductivity), and the collective motion during the decompression phase.

We have derived coupled equations of motion for the density matrices for nucleons, Δ resonances, and π mesons, as well as for the pion-baryon interaction vertex function, for the description of nuclear reactions at intermediate energies. These particles are the main constituents of the hadronic matter formed in relativistic nuclear collisions.

We start from an effective hadronic Lagrangian density containing free fields of nucleons, deltas, as well as σ-, ω- and π-mesons, and assume a minimal coupling between them. The associated equations of motion for the hadron fields can be obtained by means of the Euler-Lagrange equations. Moreover, by treating the mesons as contributing to the potentials only, and using the Green's function technique, the mesonic degrees of freedom can be eliminated. This reduces the dynamics to the baryonic level, and we derive closed equations of motion for the density matrix and the correlation functions for nucleons and deltas. The associated BBGKY hierarchy is truncated at the level of three-body correlations.

Subsequently, we extend the baryon dynamics to hadron dynamics by introducing an independent dynamical pion field, and we obtain equations of motion for the density matrix of nucleons, deltas, and pions, as well as the pion-baryon interaction vertex function. We then perform Wigner transformations of these equations, in order to obtain a set of transport equations for the phase-space distribution functions for baryons and pions. These equations contain a Vlasov term of the usual form and several collision terms, in analogy with the standard *BUU* equations, for interacting nucleons, deltas, and pions.

Our derivation is rather similar to the approach taken in ref. [1], but we go beyond that work by including both Δ resonances and dynamical pions, which are expected to be significant at relativistic energies.

The transport equations reflect the physics of relativistic nuclear collisions in an instructive manner. A special advantage of the formulation in term of phase-space densities is that these can be represented by test-particle distributions. The theory is then amenable to numerical solution by suitable extension of the powerful simulation techniques developed in recent years. In conjunction with the formal work, a practical method of solution has been developed and is being applied to problems of experimental interest.

Footnotes and References

*MSUCL-752 (1990); Annals of Physics (in press)

[†]Center of Theoretical Physics, CCAST (World Laboratory), Beijing, and Department of Modern Physics, Lanzhou University, Lanzhou 730001, P.R. China

[‡]National Superconducting Cyclotron Laboratory and Department of Physics and Astronomy, Michigan State University, East Lansing, Michigan 48824-1321, USA

Footnotes and References

[1] W. Cassing and S.J. Wang, Z. Phys. A337 (1990) 1; S.J. Wang and W. Cassing, Nucl. Phys. A495 (1989) 371c

Fluctuations in One-Body Dynamics*

Jørgen Randrup and Bernard Remaud†

With a view towards nuclear dynamics at intermediate energies, we have developed a transport treatment for systems whose reduced one-body phase-space density exhibits a markovian time evolution. Performing a moment expansion of the corresponding Fokker-Planck equation, we have derived closed equations for the temporal evolution of the ensemble average of the phase-space occupancy and its correlation function. The general properties of the associated relaxation processes were illustrated and the utility of the formulation for studies of nuclear collisions was discussed.

We have adapted standard techniques from transport theory for the derivation of closed equations for the first and second moments of the one-body phase-space distribution. This approach is motivated by the observation that although the full treatment of the fluctuations of the one-body density are too complex to allow practical calculations, most problems of actual interest can be addressed without such degree of detail. While the equation derived for the first moment corresponds to the *BUU* treatment, the equations for the second moments are novel and give access to the variances and covariances of one-body observables within a one-body treatment.

In the absense of residual interactions, the evolution of the f is governed by the Vlasov equation. The individual nucleons then move in a common one-body field, described by an effective Hamiltonian which is determined self-consistently from the instantaneous one-body density matrix or prescribed in some other manner. The inclusion of direct two-body collisions subjects the individual nucleons to irregular forces which in turn produces random changes in one-body the phase-space density f. Consequently, the dynamical evolution exhibits a continual branching and the temporal trajectory of f is no longer a single trajectory but an ever widening bundle of trajectories. We treat this diffusive behavior within the framework of transport theory.

The derivation of the equations of motion for the correlation function is somewhat similar to approaches developed in classical fluid dynamics. Within the context of nuclear dynamics, the incorporation of the second moments is an important advance and extends the utility of nuclear one-body models.

The developed equations of motion for the variances and covariances of the one-body phase-space density may be used to elucidate the character of the relaxation processes occuring in nuclear dynamics. Our present studies indicate that the fluctuations relax rather rapidly, within less than 10^{-22} s, towards the equilibrium distribution associated with the instantaneous mean occupancy. This finding may provide the basis for significant simplifications in the analytical treatment of fluid-dynamical fluctuations.

Our formal developments establish a solid basis for implementing numerical simulations of stochastic one-body dynamics. In particular, the formulation gives firm guidance with regard to how the Pauli-blocked two-body scattering should be treated, thus eliminating the need for relying on intuition. Thus, we have established the necessary formal tools for extending nuclear one-body simulation models from their current confines of mean trajectories to the practically more useful realm of dynamical branchings. Not only is such an advance of theoretical interest, but it also allows more direct contact with experimental data on nuclear collision processes.

Footnotes and References

*LBL-25852: Nuclear Physics A514 (1990) 339

†Laboratoire de Physique Nucléaire, IN2P3-CNRS Université de Nantes, F-44072 Nantes Cedex 03, France

Fluctuations of the single-particle density in nuclear dynamics

G.F. Burgio *, *Ph. Chomaz* †, *and J. Randrup*

In recent years semiclassical methods have been developed to study heavy-ion collisions in the framework of the Boltzmann-Uehling-Uhlenbeck theory, in which the collisionless mean field evolution has been augmented by a Pauli-blocked Nordheim collision term. Since these models describe the average dynamical trajectory, they cannot be applied to describe fluctuations of one-body observables, correlations in the emission of light particles and catastrophic processes like multifragmentation.

In refs.[1,2] we have developed a new method in order to include the stochastic part of the collision integral into BUU-type simulations of the nuclear dynamics. Since the collision term acts as a random Langevin-type force on the one-body distribution, the dynamical problem is then treated as Brownian motion and the system is represented by a distribution in the space of the one-body densities. Therefore the evolution of the system is studied by following an ensemble of trajectories, each characterized by one particular phase-space distribution. In order to implement such a scheme, it is necessary to simulate the basic stochastic process correctly. In our treatment we represent the one-particle distribution on a lattice of grid points in phase-space. Since the actual number of collisions is a random variable, it follows a Poisson distribution which demands that the variance of the number of transitions from two initial phase-space cells to two final ones be equal to its mean value. Consequently, the fluctuating part of the collision term can be produced by augmenting the mean number of collisions with a noise chosen randomly from a normal distribution with a variance equal to the mean value. We apply this method to a two-dimensional gas of fermions on a torus, considering two different initial conditions: a) a hollow Fermi sphere[1], and b) two tangential Fermi spheres[1,2]. Below we show the evolution of the variance in phase-space occupancy (thick histogram) for the disphere. The variance relaxes towards the quantum-statistical limit (dashed curve) and follows closely the instantaneous equilibrium value $\sigma^2 = f(1-f)$ (thin histogram), where f is the mean trajectory. It was shown that this relation presents a strong constraint on the fluctuations and must be satisfied dynamically in any transport treatment of fluctuations in one-body dynamics.

The breaking of the translational and spherical symmetry in our model permits the study of unstable situations in phase-space. The introduction of the non-linear one-body field will allow us to explore dynamical instabilities and bifurcations. Therefore the model can be appropriate for studying nuclear multifragmentation.

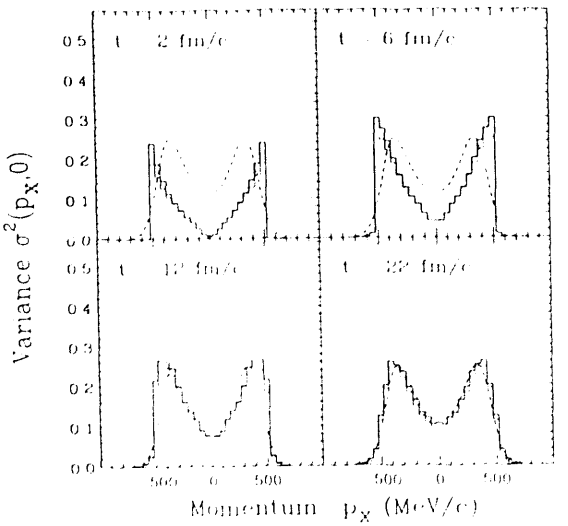

Footnotes and References

*INFN Sezione di Catania and LNS, I-95129 Catania, Italy

†Division de Physique Théorique, Institut de Physique Nucléaire, F-91406 Orsay Cedex, France

[1]LBL-29557: Ph. Chomaz, G.F. Burgio and J. Randrup, Phys. Lett. B254 (1991) 340

[2]LBL-29558: G.F. Burgio, Ph. Chomaz and J. Randrup, Nucl. Phys. A, in press

Research activities at LBL - Spring 1989

*H.S. Köhler**

I have during the last years developed a microscopic transport model for such collisions[1] In this model the scatterings between nucleons is separated into a mean-field part and a two-body collision part. It is in that respect similar to the semi-classical BUU (or VUU) models used by other investigators[2]. It differs from these models in that the scatterings with the mean field are quantum-mechanical and in that the two-body collisions are calculated in the relaxation-time approximation.

The physical content of the two models, the semi-classical and my quantum-mechanical time-relaxation model, is however very similar. A numerical comparison between the two methods was commenced last summer and completed during my stay at LBL. The BUU and relaxation time methods were compared numerically for collisions between two ^{16}O nuclei. Phase-space trajectories and double differential cross-sections for nucleon emission are compared. Results are pracically identical although the relaxation time method exhibits a slightly higher degree of stopping power.[3]

In another ongoing investigation, a microscopic study of the mean field and the two-body collision term has been initiated. The primary purpose of heavy-ion collisions is to explore the properties of hot nuclear matter; both static and dynamic. It is of particular interest to analyze these collisions in order to learn about nucleonic degrees of freedom. But before proceeding to introduce some model of these into a theory of hot nuclei it seems appropriate to investigate the consequence of incorporating important many-body effects in a "nucleons only" theory. This has not yet been done satisfactorily. A first step is to find the "effective" force Veff in hot nuclear matter from the known "free" N-N interaction. Most "microscopic" calculations have been done with forces that are fitted to zero temperature properties like binding and compressibility and depend on local density only but not on other variables of the medium. This might be adequate for low energies. It is however well known that the effective force in nuclear matter is momentum dependent (non-local). Collisions at higher energy result in strong deformations in momentum space. A force that depends on density only, gives an energy-functional that is independent of such deformations, while a momentum-dependent force leads to a dependence on this deformation. It follows that it may be necessary to incorporate the momentum dependence of the force especially in a theory of high energy H.I. collisions. Furthermore, the strength of the force depends not just on density but also on excitation; it is "temperature"-dependent. A related matter that has to be clarified is the validity of using 'Free' N-N cross-sections in the collision term.[4]

To address these problems I have used Brueckner methods to calculate "effective" force $V_{\rm eff}$ as well as the momentum and temperature dependent mean field for nucleons propagating through hot nuclear matter. The mean field is complex and the imaginary part is related to the "two-body" collisions, while the real part relates to "one-body" collisions. In these calculations I use a version of Brueckner theory that allows a calculation of the reaction matrix, (i.e., the "effective" force $V_{\rm eff}$) directly from the N-N phase-shifts).[5]

Footnotes and References

*Physics Department, University of Arizona, Tucson, Arizona 85721

[1]H.S. Köhler and B.S. Nilsson, Nucl. Phys. A477 (1988) 318; H.S. Köhler, Nucl. Phys. A (1989)

[2]W. Bauer, Nucl. Phys. A471 (1987) 604; G.F. Bertsch, H. Kruse, and S. Das Gupta, Phys. Rev. C29 (1984) 673

[3]H.S. Köhler and W. Bauer, LBL-27084; Phys. Rev. C

[4]H.S. Köhler, Nucl. Phys. A415 (1984) 37

[5]H.S. Köhler, In Proceedings "The Nuclear Equation of State, to be published and preprint LBL-27322

Dense Matter at Nuclear Subsaturation Densities *

C.S. Wang† *and W.D. Myers*

This paper concerns the equation of state of cold dense matter at densities that are below the saturation density of nuclear matter, which (for symmetric, $N = Z$ nuclear matter) corresponds to nuclear particle number densities $\rho \leq 0.15/\ \mathrm{fm}^3$. Uniform nuclear matter is unstable at a density somewhat below saturation, which (when defined as the density where the nuclear incompressibility becomes negative) is at a particle number density of about $0.1/\mathrm{fm}^3$ for symmetric nuclear matter and somewhat lower for asymmetric nuclear matter). The thermodynamically favored configuration is then a periodic structure of bulk matter immersed in a neutron gas and an electron gas which is required for overall electrical neutrality. At each density the equilibrium configuration can be determined by a minimization of the total energy at a fixed volume and a fixed number of nucleons.

Since this subsaturation density regime exists in a collapsing steller core during the formation of a supernova, it has been studied by many authors. The usual approach is to assume that the bulk matter consists of spherical neutron rich nuclei. At higher densities the role of the nuclear matter and the neurton gas are reversed and the dense matter is assumed to consist of neutron gas bubbles surrounded by neutron rich nuclear matter. A consistant treatment of the bulk matter, the neutron gas and the nuclear surface energy is essential for a macroscopic model of this dense matter system.

Figure 1 shows our result for the number of protons Z as a function of the matter density. The dotted curve is an early result of Baym, Bethe and Pethic[1] using a liquid drop model, the thin curve is the result of Mackie and Baym[2] using a compressible liquid drop model, the dashed curve is the result of Ravenhall, Bennett and Pethick[3] based on a Hartree-Fock model, and the dot-dashed curve is from Buchler and Barkat[4] using a Thomas-Fermi model. The crosses are from Negele and Vautherin[5] using a Hartree-Fock model for the complete unit cell. The heavy lines are our result.

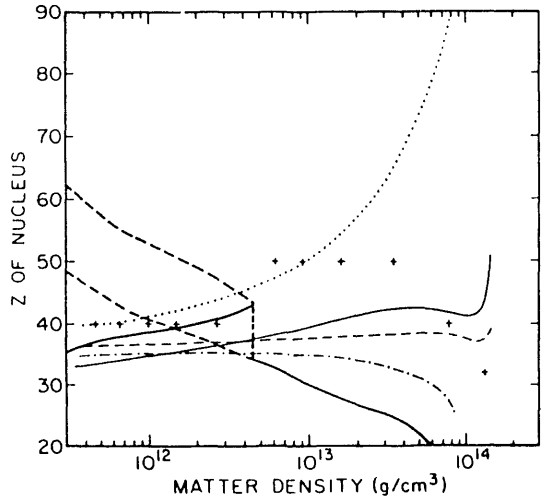

Figure 1: The charge number Z of a nucleus centered in a unit cell, as a function of the matter density. The thick curves (both solid and dashed) are our result.

Footnotes and References

*Nucl. Phys. **A514** (1990) 322

†Present address: Department of Technical Physics, Beijing University, Beijing 100871, China

[1]Nucl. Phys. **A175** (1971) 225

Footnotes and References

[2]Nucl. Phys. **A285** (1977) 332

[3]Phys. Rev. Lett. **28** (1972) 978

[4]Phys. Rev. Lett. **27** (1971) 48

[5]Nucl. Phys. **A207** (1973) 298

The Charge and Mass Dependence of Nuclear Interaction Cross Sections *

H.S. Chung† *and W.D. Myers*

As the first step in a major program of applying the Thomas-Fermi method to the prediction of macroscopic nuclear properties we have calculated interaction radii of exotic-isotopes for comparison with the values measured by Tanihata et al. The parameters of the force were chosen to reproduce nuclear binding energies and the charge distributions measured by electron scattering. The resulting density distributions for the isotopes of interest were calculated and interaction radii inferred using a simple Glauber theory approach and an effective nucleon-nucleon cross section.

Originally we thought that even the anomalously large interaction radii of ^{11}Li and ^{14}Be might be reproduced by the theory since the diffuseness of the density distribution increases as the drip-line (limit of stability against particle emission) is approached. The trend, while present, was not sufficient to explain the observed values of R_I. We hope that more measurements at the limit of stability will be made so it can be determined whether the sudden increase in size is associated with some macroscopic effect that has not yet been properly treated or whether it is associated with the discreteness of the system and the filling of specific shell model states.

In the Figure we have plotted the ratio of our interaction radii to the quantity 1.13 $A^{1/3}$ against mass number for the isotopes of carbon and neon. By and large it is clear that the nuclei are more compact the more stable they are, and that the relative size tends to increase as one moves in either direction toward the limits of stability.

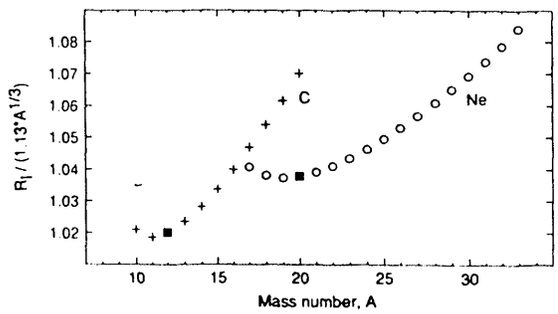

Figure 1: The ratio of our calculated interaction radii to the liquid drop model value of 1.13 $A^{1/3}$ is plotted versus mass number A for the isotopes of carbon and neon. In each case the most stable isotope is indicated by a solid square.

Footnotes and References

*Nucl. Phys. **A513** (1990) 283

†Present address: 1813 Windsong, Richardson, TX 75081

Aspects of Incompressibility*

W.D. Myers

The nuclear matter incompressibility K_∞ has been receiving an increasing amount of attention lately. Quite a spirited discussion is underway between groups who favor rather low values for use in simulations of supernova explosions, those who favor much higher values for the explaination of certain measurements in high-energy nuclear collisions, and many others who favor intermediate values for various nuclear structure reasons. The purpose of this paper is to present some preliminary results concerning the value of K_∞ arising from a statistical model of macroscopic nuclear properties that we are currently developing.

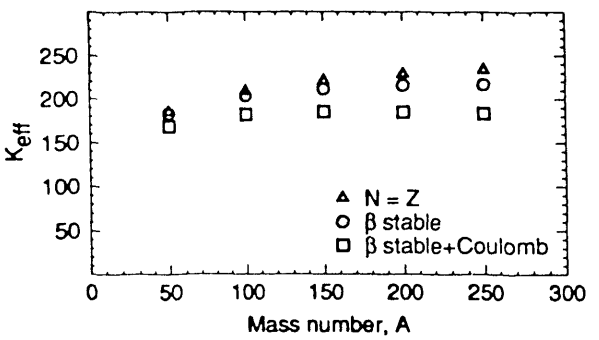

Figure 1: The effective value of the compressibility for a number of nuclei is plotted versus their mass number A. The triangles correspond to $N = Z$. The circles show the reduction that occurs when the N, Z ratio is changed to correspond to β stability. The effect of adding the Coulomb repulsion is indicated by the square symbols.

The surface energy and the compressibility are closely related since the surface energy arises in part from the fact that there is a loss of binding energy associated with reduced density, and the compressibility coefficient K_∞ is the quantity that governs this effect for small density deviations. In fact we find in our work that the value of K_∞ is determined by the requirement that the calculated surface energy and surface diffuseness agree with the measured values.

Even though K_∞ has been determined, the effective value of the compressibility $K_{\rm eff}$ for a finite nucleus can be quite a bit smaller because the resistance of the nucleus to changes in scale consists not only of a bulk effect but depends also on the surface, curvature and higher order effects. See Fig. 1.

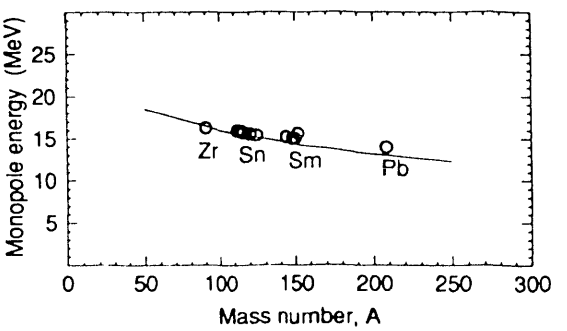

Figure 2: The solid line corresponds to our estimate of the energy of the Giant Monopole Resonance. The circles correspond to measured values.

In Fig. 2 we show our prediction for the energy of the Giant Monopole Resonance based on these values of $K_{\rm eff}$ and a simple hydrodynamical value for the inertial parameters.

Footnotes and References

*Proceedings of the Gross Properties of Nuclei & Nuclear Excitations International Workshop XVIII, Hirschegg, Kleinwalsertal, Austria, 15-20 January, 1990

Looking for Precursors of Neutron Matter Exotica *

W.D. Myers

If neutron matter were bound, nuclear physics would be enriched by amazing structures. These structures, with lifetimes limited only by beta decay, would include neutron balls of arbitrary size. Unfortunately, neutron matter is probably not bound. But how far is one from such an exotic generalization of nuclear physics?

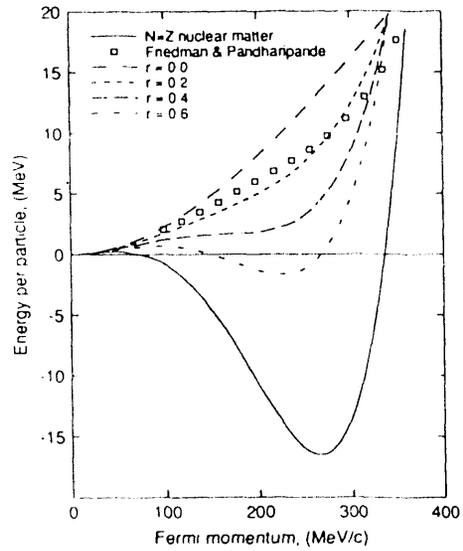

Figure 1: The energy per particle of $N = Z$ nuclear matter is plotted versus the Fermi momentum as the solid curve. The energy per particle for neutron matter is also shown various choices of the parameter r. The open squares correspond to the work of Friedman & Pandharipande.

If neutron matter is unbound the maximum neutron excess for a given Z is limited by neutron drip. Otherwise, (for a sufficiently large system) the neutron excess could grow indefinitely. In connection with questions like these, we have undertaken a series of self-consistent, Thomas-Fermi calculations using a phenomenological interaction.

We have solved the finite nucleus Euler equation with various choices for the parameter r for a broad range of nuclei. Along the line of beta-stability in the nuclide chart the value of r has little effect, but the limit of particle stability at the neutron drip line is strongly effected. Shown in Fig. 2 is a portion of the nuclide chart where the grey squares represent nuclei that have been observed or are thought to be particle stable on the basis of extrapolation. The heavy lines, labeled with r values from 0.0 to 0.4 correspond to a rough estimate of the corresponding location of the neutron drip line. Examination of this figure suggests that the Friedman & Pandharipande[1] value ($r = 0.16950$) is a little small. However, a value higher than 0.4 seems to be clearly excluded. This means that neutron matter is unlikely to be bound.

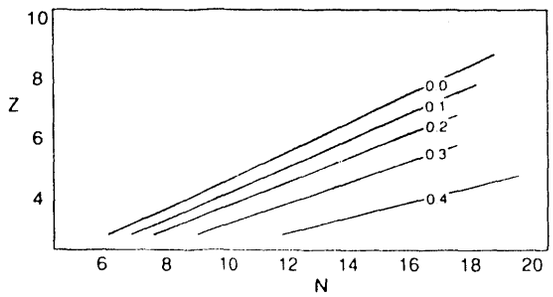

Figure 2: A portion of the nuclide chart showing as grey squares nuclei that are known (or thought to be) stable against particle emission. The solid lines correspond to the predicted limits of stability for different values of the parameter r.

Footnotes and References

*Proceedings of the First International Conference on Radioactive Nuclear Beams, 16-18 Oct.,1989, Berkeley, California

Footnotes and References

[1]B. Friedman and V.R. Pandharipande, Nucl. Phys. **A361** (1981) 502

A Thomas-Fermi Model of Nuclei
Part I: Formulation and First Results *

W.D. Myers and W.J. Swiatecki

We formulate a Thomas-Fermi model of average nuclear properties (i.e. of nuclear masses, deformation energies, density distributions, optical model potentials, etc.) by generalizing the momentum dependent Seyler-Blanchard effective nucleon-nucleon interaction. In addition to reproducing the binding energy, density, symmetry energy and surface energy of nuclear matter, the generalized model can be adjusted to reproduce the diffuseness of the nuclear density distribution, as well as theoretical estimates of the binding properties of neutron matter. The

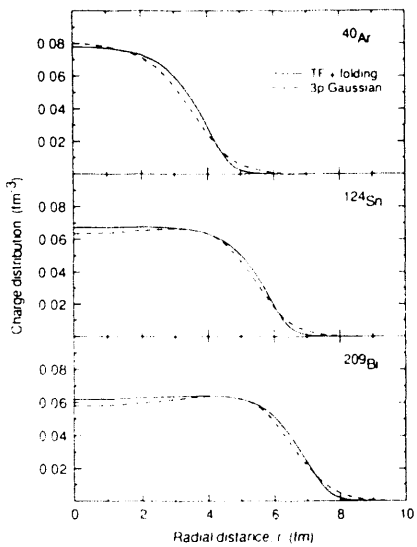

Figure 1: The calculated Thomas-Fermi charge distribution of three nuclei (after folding in the proton size) are compared with experimental distributions represented by a so-called 3-parameter Gaussian fit.

depth of the nuclear optical potential, including its energy and isospin dependences, can also be reproduced. The above properties of nuclei and of neutron matter determine quite firmly the seven adjustable parameters of the theory, yielding a model that, apart from shell effects and the discreteness of nucleons, is expected to be accurate for very small or very deformed systems, and to be reliable for extrapolating to extremely large hypothetical nuclei, including systems with arbitrary neutron excess and arbitrary geometries, such as those that sometimes arise in astrophysical applications. A preliminary set of the model's parameters has been determined, and one of the predictions of the theory is that the measured values of the nuclear surface energy and surface diffuseness, taken together, place a significant constraint on the value of the compressibility coefficient of standard nuclear matter.

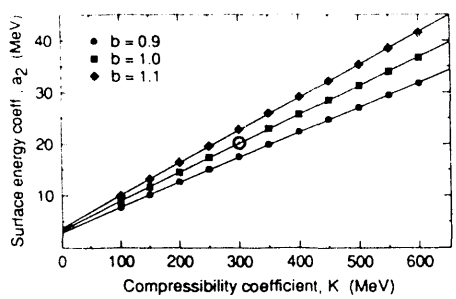

Figure 2: Each set of symbols represents the result of calculating the surface energy of semi-infinite nuclear matter using interaction parameters chosen so as to give the same volume energy per particle, the same equilibrium density and the same surface width b. The value of b deduced from measured charge distributions ($b \approx 1$ fm), together with the value of a_2 deduced from fits to measured binding energies ($a_2 \approx 20$ MeV), leads to an estimated value for K of about 300 MeV.

Footnotes and References

*Ann. of Phys. (N.Y.) **204** (1990) 401

A Thomas-Fermi Model of Nuclei
Part II: Fission Barriers and Charge Distributions *

W.D. Myers and W.J. Swiatecki

The Thomas-Fermi model of average nuclear properties described in Part I [1] is simplified further and then applied to the calculation of fission barriers and charge distributions. An extensive comparison with experimental data reveals a small but clear-cut barriers vs. size discrepancy: if the radius constant r_0 is chosen to be 1.13 fm so as to reproduce measured nuclear sizes, the calculated fission barriers are too high.

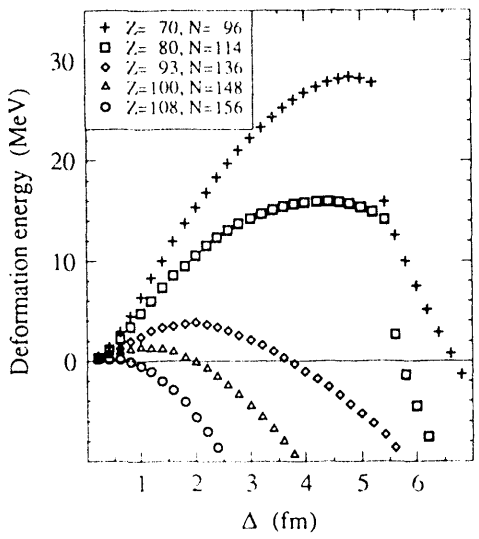

Figure 1: Calculated deformation energies of conditional equilibrium shapes for five nuclei. The constraint parameter Δ is half the distance between the centers of mass of the two halves of the nuclear shape, less its value for the spherical configuration. The maximum in each curve corresponds to the fission barrier height.

We have explored a number of additional parameter choices and hypotheses in order to test the firmness of the above conclusion, and we believe that, within the framework of the Thomas-Fermi approach, no adjustments of parameters can remove the discrepancy.

The identification of this missing piece of physics is an outstanding problem. We believe the answer may be along the following lines. The Thomas- Fermi treatment is a semi-classical approximation that works well in the bulk region of the nucleus but becomes less accurate in the surface and eventually fails completely in the sense that it allows no penetration of the particles into classically forbidden regions of space. Estimates show that even in heavy nuclei a significant fraction of the nuclear matter finds itself in the classically forbidden region, forming a quantal halo of material contributing positive density but negative kinetic energy density. One anticipated consequence of the presence of a fringe of negative kinetic energy in the outer layers of the surface is that such a surface should be relatively easier to bend, and the corresponding nucleus should be easier to deform. As a result, the calculated fission barriers should be lowered by the presence of the halo, possibly removing the abovementioned discrepancy. In more technical terms, the presence of the quantal halo should have the effect of reducing the curvature correction to the nuclear surface energy: a convexly curved surface has a relatively greater volume of space available for the energetically favourable quantal halo, and this reduces the opposite effect of curvature, that of decreasing the interaction energy (the result of the increased exposure of particles in the surface region). In a forthcoming paper we hope to examine the effect of the quantal halo on the size vs. barriers discrepancy uncovered in the present work.

Footnotes and References

*LBL-30395, submitted to Ann. of Phys. (N.Y.)

[1] W.D. Myers and W.J. Swiatecki, Ann. of Phys. (N.Y.) **204** (1990) 401

New Algebraic Representations of Quantum mechanics*

*Shun-Jin Wang***

Contrary to the usual view that quantum mechanics in configuration space has, in general, only one algebaic representation (the Heisenberg algebraic representation), we have proved that quantum mechanics in configuration space has, in general, alternative algebraic representations: (i) In a finite domain of configuration space, it can be expressed in terms of su(2) algebra; (ii) in an infinite domain of configuration space, it can be expressed in terms of su(1,1) algebra. The above results open a new possibility to reformulate quantum mechanics and provide more mathematical tools to solve diverse physical problems. Nonlinear relations of different Lie algebas may imply a unification of Lie algebras and their physical implications (the quantum motion modes) in a deeper nonlinear domain. This observation raises challenging mathematical and physical questions.

Footnotes and References

*Condensed from LBL-29467

**Center of Theoretical Physics, CCAST (World Lab.) Beijing, and Department of Modern Physics, Lanzhou University, Lanzhou 730001, PR China.

Non-Adiabatic Effect On Berry's Phase For Light Propagating In An Optical Fibre*

*Shun-Jin Wang***

A Schrödinger equation for a photon propagating in a helix has been derived from Maxwell's equations and their quantization. The exact solutions of this equation are employed to study the non-adiabatic effect on Berry's phase. It is shown that non-adiabaticity alters the time evolution ray and in turn changes its Berry's phase. A new expression for Berry's phase is given, which indicates a close link between Berry's phase and spin expectation value. For SU (2) dynamical group, non-adiabatic effect on Berry's phase manifests itself as spin-alignment (familiar in nuclear physics). Two kinds of experiments are suggested to measure non-adiabatic effect on Berry's phase.

Footnotes and References

*Condensed from LBL-29253

**Center of Theoretical Physics, CCAST (World Lab.) Beijing and Department of Modern Physics, Lanzhou University, Lanzhou 730001, PR China.

Nonadiabatic Berry's Phase for a Quantum System With a Dynamical Semi-simple Lie Group*

*Shun-Jin Wang***

The nonadiabatic Berry's phase is investigated for a quantum system with a dynamical semisimple Lie group within the framework of the generalized cranking approach. An expression for nonadiabatic Berry's phase is given, which indicates that the nonadiabatic Berry's phase is related to the expectation value of Cartan operators along the cranking direction in group space, and that it depends on (i) the geometry of the group space, (ii) the time evolution ray generated by the Hamiltonian (i.e., by the dynamics) in some irreducible representation Hilbert space, and (iii) the cranking rate. The expression also provides a simple algorithm for calculating the nonadiabatic Berry's phase. The general formalism is illustrated by examples of SU(2) dynamic group.

Footnotes and References

*Condensed from Phys. Rev. A42, 5103 (1990)

**Center of Theoretical Physics, Chinese Center of Advanced Science and Technology (CCAST) (World Laboratory) Beijing, People's Republic of China; and Department of Modern Physics, Lanzhou University, Lanzhou 730001, People's Republic of China.

Nonadiabatic Berry's Phase for a Spin Particle in a Rotating Magnetic Field*

*Shun-Jin Wang***

The time-dependent Schrödinger equation for a spin particle in a rotating magnetic field is solved analytically by the cranking method, and the exact solutions are employed to study the nonadiabatic Berry's phase. An alternative expression for Berry's phase is given, which shows that is related to the expectation value of spin along the rotation axis and gives Berry's phase a physical explanation besides its gauge geometric interpretation. This expression also presents a simple algorithm for calculating the nonadiabatic Berry's phase for Hamiltonians that are nonlinear functions of the SU(2) generators. It is shown that nonadiabaticity alters the time evolution ray and in turn changes its Berry's phase. For the SU(2) dynamical group, the nonadiabatic effect on Berry's phase manifests itself as spin alignment (a phenomenon in nuclear physics), and spin-alignment quantization (observed recently in high-spin nuclear physics) is related to Berry's phase quantization.

Footnotes and References

*Condensed from Phys. Rev. A42, 5107 (1990)

**Center of Theoretical Physics, Chinese Center of Advanced Science and Technology (World Laboratory), Beijing; and Department of Modern Physics, Lanzhou University Lanzhou 730001, People's Republic of China.

Spin Alignment Quantization, Berry' Phase Quantization, Stationary Condition and Twinned Superdeformed Bands*

*Shun-Jin Wang***

Striking regularities of the twinned superdeformed bands are discussed in terms of non-adiabatic Berry's phase quantization and stationary condition within the framework of cranking shell model. It is shown that the rotating deformed mean field will generate a Berry's phase for nucleons subjected to this potential. The non-adiabatic Berry's phase is related to spin alignment. The stationary condition of the rotational states requires Berry's phase quantization and in turn leads to spin alignment quantization. For nucleons which are weakly coupled to the deformed field, spin alignment quantization will take place as the rotational frequency reaches critical value. Those nucleons whose spin alignment is quantized and keeps constant do not contribute to the rotational energy and the moment of inertia. For nuclei at extreme conditions of large elongation and high spins, the normal parity states posses pseudo-SU(3) - pseudo-SU(2) dynamical symmetry which provides a weak pseudo spin-orbit coupling scheme. If the pseudo-angular momentum is stuck to the large deformation, the critical frequency for spin alignment quantization can be calculated to yield reasonable values. The main aspects of the regularities of the twinned superdeformed bands can thus be understood.

Footnotes and References

*Condensed from LBL-29543

**Center of Theoretical Physics, CCAST (World Lab.) Beijing, and Department of Modern Physics, Lanzhou University, Lanzhou 730001, PR China.

Elastic Tracking and Neural Network Algorithms for Complex Pattern Recognition*

M. Gyulassy and M. Harlander

A new Elastic Tracking (ET) algorithm is proposed for finding tracks in very high multiplicity and noisy environments. It is based on a dynamical reinterpretation and generalization of the Radon transform and is related to elastic net algorithms for geometrical optimization. ET performs an adaptive nonlinear fit to noisy data with a variable number of tracks and is more efficient numerically than the traditional Radon or Hough transform method because it avoids binning of phase space and the costly search for valid minima. Spurious local minima are avoided in ET by introducing an iteration time dependent effective potential. The method is shown to be very robust to noise and measurement error and extends tracking capabilities to much higher track densities than possible via local road finding or even the novel Denby-Peterson (DP) neural network tracking algorithms. A possible neural network implementation of ET is also discussed.

*LBL-29654 (1990).

Order, Chaos and Nuclear Dynamics. An Introduction*

W. J. Swiatecki

This is an introductory lecture illustrating by simple examples the anticipated effect on collective nuclear dynamics of a transition from order to chaos in the motions of nucleons inside an idealized nucleus. The destruction of order is paralleled by a transition from a rubber-like to a honey-like behavior of the independent-particle nuclear model.

Footnotes and References

*Condensed from LBL-29482

On the Universality Class Dependence of Period Doubling Indices*

Mario Feingold, Diego L. Gonzalez,‡ Marcelo O. Magnasco,† ‡ and Oreste Piro†‡§

The dependence on v of the period doubling scaling indices for unimodal maps with a critical point of the form $|x|^v$ is numerically investigated. To perform extensive computations of these indices a new symbolic dynamics based technique in configuration space is introduced. For $v \to 1$ it is shown that the Feigenbaum bifurcation rate converges to the theoretically exact value $\delta = 2$ limit only if $v - 1$ is exponentially small. On the other hand, the existence of an upper bound for $\delta(v \to \infty)$ is numerically verified. An accurate estimae of 29.8 is given for this limit. Moreover, the global functional form of $\delta(v)$ is shown to have an interesting symmetry.

Footnotes and References

*Condensed from LBL-28256

† The James Franck Institute, The University of Chicago, Chicago, IL

‡Departamento de Física, Universidad Nacional de La Plata, C.C. 67, (1900) La Plata, República Argentina

§Center for Nonlinear Studies, MB-S 258, Los Alamos National Laboratory, Los Alamos, NM

Phase-Space Localization: Topological Aspects of Quantum Chaos*

*P. Leboeuf,† J. Kurchan,‡ M. Feingold, and D.P. Arovas***

We study quantized classically chaotic maps on a toroidal two-dimensional phase space. A discrete, topological criterion for phase-space localization is presented. To each eigenfunction is associated an integer, analogous to a quantized Hall conductivity, which when nonzero reflects phase-space delocalization. A model system is studied, and a correspondence between delocalization and chaotic classical dynamics is discussed.

Footnotes and References

*Condensed from Phys. Rev.Lett., 65, 3076 (1990)

† Division de Physique Théorique, Institut de Physique Nucléaire, 91406 Orsay CEDEX, France

‡Nuclear Physics Department, Weizmann Institute of Science, Rehovot 76100, Israel

**Department of Physics, B-019, University of California at San Diego, La Jolla California 92093

Localisation and Spectral Statistics in a Banded Random Matrix Ensemble*

Michael Wilkinson,† Mario Feingold, and David M. Leitner§

We give a scaling analysis for the localisation of the eigenvectors of a banded random matrix ensemble, in which the diagonal matrix elements increase along the diagonal. We relate the results to a transition in the spectral statistics which is observed as a parameter is varied, and discuss the relevance of this model to the quantum mechanics of chaotic Hamiltonian systems.

Footnotes and References

*Condensed from LBL-29329

† Department of Physics and Applied Physics, John Anderson Building, University of Strathclyde, Glasgow, G4 ONG, Scotland, U.K.

§Department of Chemistry, Brown University,, Providence, RI 02912, USA

Semiclassical Structure of Hamiltonians*

Mario Feingold, David M. Leitner,‡ and Oreste Piroe§

The structure of few-body Hamiltonian matrices is studied in the semiclassical regime. Given $(\hat{A}_1(\hat{q},\hat{p}), \hat{A}_2(\hat{q},\hat{p}))$, a pair of operators, it can be shown that, under quite general conditions, $\hat{A}_2$ takes the form of a banded matrix in the ordered eigenrepresentation of $\hat{A}_1$. Moreover, the bandwidth depends only on $\hbar$ and certain generalized microcanonical averages. In particular, if $H=H0+\epsilon V$, this implies that the perturbed Hamiltonian is banded in the appropriately ordered unperturbed basis.

Footnotes and References

*Condensed from Physical Review A, Vol. 39, No. 12

‡The James Franck Institute, The University of Chicago, Chicago, IL and Departmentof Chemistry, The University of Chicago, Chicago, IL.

§The James Franck Institute, The University of Chicago, Chicago, IL and Physics Department, Brookhaven National Laboratory, Building 510A, Upton, NY

Scaling in Semiclassical Random Matrix Ensembles*

Mario Feingold, David M. Leitner,‡ and Michael Wilkinson§

A novel Random Matrix Ensemble is introduced which mimics the global structure inherent in the Hamiltonian matrices of autonomous, ergodic systems. Changes in its parameters induce a transition between a Poisson and a Wigner distribution for the level spacings, P(s). The intermediate distributions are uniquely determined by a single scaling variable. Semiclassical constraints force the ensemble to be in a regime with Wigner P(s) for systems with more than two freedoms.

Footnotes and References

*Condensed from LBL-29302

‡Department of Chemistry, Brown University, Providence, RI 02912

§Department of Physics and Applied Physics, University of Strathclyde, Glasgow G4 ONG, UK

Scars in Billiards: The Phase Space Approach*

Mario Feingold, Robert G. Littlejohn,† Stephani B. Solina,† S. Pehling,† and Oreste Piro‡

Although scars in the eigenfunctions of classically chaotic systems were originally observed in the configuration space representation, we show that these can be better visualized in phase space. On the quantitative side, a recent theory of scars is extended to billiards. For the stadium detailed agreement between theory and numerical experiment is found.

Footnotes and References

*Condensed from Phys. Letters A146, 199 (1990)

‡Physics Department, Building 510A, Brookhaven National Laboratory, Upton, NY 11973, USA

Scars and the Order to Chaos Transition*

Hans Frisk

A numerical investigation of the localization of eigenfunctions around periodic orbits is presented. The classical motion in the potential shows a generic order to chaos transition when the deformation is increased. Some eigenfunctions are found to be remarkably ordered even if the underlying classical motion is strongly chaotic.

Footnotes and References

*7th International Symposium on Capture Gamma-Ray Spectroscopy, Asilomar, California, 14-19 Oct. 1990

Seminars

Nuclear Science Division

Reinhard Stock University of Frankfurt	Ultrarelativistic Nucleus-Nucleus Collisions	Sept. 19, 1988
John Durell University of Manchester	Fission Fragment Gamma-Ray Spectroscopy	Sept. 20, 1988
Wolfram von Oertzen Hahn-Meitner Institute	Nucleon Transfer Between Very Heavy Nuclei at the Coulomb Barrier	Sept. 23, 1988
Peter M. Endt University of Utrecht	26Al: A Complete Nucleus	Sept. 28, 1988
John Sharpey-Schafer Univ. of Liverpool	Superdeformation, Shape Coexistence, and the Decline and Fall of Pairing all Between N=86 and N=92	Sept. 30, 1988
Wolfgang Norenberg GSI	Nuclear Elastoplasticity: A Phenomenon of a Transition from Ordered to Chaotic Motion	Oct. 3, 1988
Rainer Renfordt U. Frankfurt	Is There Evidence for Radial Flow in 200 GeV/n Nucleus-Nucleus Collisions?	Oct. 4, 1988
Marek Gazdzicki U. Frankfurt	Neutral Strange Particle Production in 200 GeV/n S + S Collisions	Oct. 4, 1988
Cary Davids Argonne National Lab.	Present Status and Future Plans of the Argonne Fragment Mass Analyzer	Nov. 10, 1988
Grazyna Odyniec LBL	Review of Strangeness Production in Relativistic Heavy Ion Collisions	Nov. 14, 1988
Shaheen Tonse LBL	Polarisation in Strange Particle Production	Nov. 30, 1988
Joseph Kapusta University of Minnesota	Single- and Multi-Particle Analysis of Nucleus-Nucleus Collisions at 14.6, 60, and 200 GeV/N	December 12, 1988
Yorick Blumenfeld Institut de Physique Nucleaire - Orsay	Heavy Ion Inelastic Scattering at GANIL: Collective Mode Excitations	January 9, 1989

Gerald Brown SUNY at Stony Brook	Stopping in Bevalac Heavy-Ion Collisions	Jan. 18, 1989
W. N. Catford Australian National Univ.	Exotic Nuclei and Equally Exotic Transfer Reactions	Jan. 23, 1989
Asher Shor Weizmann Institute/LBL	Subthreshold Particle Production (pi-, K, p-) Collisions	Jan. 25, 1989
Erwin Friedlander LBL	Multiplicity Fluctuations in Very High Energy Nuclear Collisions: I. The EMU01/CERN Experiment	Feb. 6, 1989
Dave Bowman LBL	La-Induced Reactions at 18-100 MeV/u; The Demise of the Incomplete Fusion Process	Feb. 8, 1989
Eugene Beier Univ. of Pennsylvania	Kamiokande II and SNO: Two Generations of Real-Time Solar Neutrino Experiments	Feb. 13, 1989
Erwin Friedlander LBL	Multiplicity Fluctuations in Very High Energy Nuclear Collisions: II. Intermittency vs. Quantum Statistical Correlations	Feb. 15, 1989
Frank Stephens LBL	GAMMASPHERE and EUROBALL, Gamma-Ray Detectors for the 90's	Feb. 27, 1989
Harry Heckman LBL	Production of He Projectile Fragments in 16O-Emulsion Interactions from E/A = 2 to 200 GeV	March 1, 1989
Guy Roche LBL	Results from the Dilepton Spectrometer on p + Be and Ca + Ca Collisions	March 6, 1989
Sandra Padula LBL	Implications of Pion Interferometry at CERN	March 8, 1989
E. J. Heller Univ. of Washington	Quantum Eigenstates of a Classically Chaotic System	March 13, 1989
George Bertsch MSU	Detecting the Quark-Gluon Plasma	March 20, 1989

Howel Pugh LBL	A New Time Projection Chamber for the NA35 Experiment at CERN	March 22, 1989
Bradley Filippone CalTech	High Energy Electron Scattering From Nuclei	March 27, 1989
Wolfgang Bauer MSU	New Adventures with the Nuclear Equation of State	April 10, 1989
Weiming Zhang Kent State University	Triple Differential Cross Sections as a Probe of the Equation of State	April 11, 1989
Hank Crawford SSL/LBL	Search for Anti-Nuclei and New Particles at the AGS	April 12, 1989
Nikolai Nikolaev Landau Inst. of Theor. Phys., USSR	Is Creation of a Quark-Gluon Plasma in Nuclear Collisions Feasible?	April 17, 1989
Joel Galin GANIL	Hot Nuclei Studied with a Four-Pi Neutron Detector	April 20, 1989
Heinz Homeyer Hahn-Meitner Institute	Dissipative Fragmentation in Heavy Ion Collisions	April 21, 1989
Robert Charity GSI	Multi-Fragment Production in Highly Dissipative Collisions	April 24, 1989
Craig Tull GSRA	Reduced Momentum Widths and Isotopic Production Cross Sections from 1.65 GeV/Nucleon Ar Fragmentation	April 26, 1989
Mark A. Stoyer GSRA	High-Spin Studies in the Actinide Region	April 26, 1989
Yuri Oganessian Dubna	The Heaviest Elements	May 1, 1989
Martin Sarabura MIT	Entropy Production in Nucleus-Nucleus Collisions at 15 GeV/n	May 3, 1989
Georgy Flerov Dubna	Soviet Research in Nuclear Fission Before 1941	May 3, 1989

Miklos Gyulassy LBL	Is Intermittency Caused by Bose-Einstein Interference?	May 3, 1989
V. Strutinsky Kiev	Macroscopic and Microscopic in Nuclear Physics and Elsewhere	May 5, 1989
Peter Vogel CalTech	Open Questions in Beta Decay	May 8, 1989
W. Haxton University of Washington	Double-Beta Decay, etc.	May 8, 1989
Y. Pomeau Ecole Normale Superiure	Chaos in Extended Systems	May 15, 1989
Dawn Meredith U. New Hampshire and ITP - Santa Barbara	Chaos in a Schematic Shell Model	May 25, 1989
P. B. Price UC/LBL	1. Electromagnetic Spallation at 200 GeV/Nucleon 2. Systematics of High-Energy Charge Pickup Reactions 3. Heavy-Particle Radioactivity 4. Cold Fusion Italian Style	June 5, 1989
Peter Lichard Dept. of Theor. Phys. Bratislava	Soft and Very Soft Electromagnetic Phenomena of Hadronic Origin	June 12, 1989
M. Sakai University of Tokyo	Electron Lines in e+ + Th and U Interactions and Their Correlation to the Positron Lines in Heavy Ion Collisions	June 21, 1989
Tom Lang GSRA	First Spectroscopy of Se67 and As66	June 28, 1989
Dimitri Delis GSRA	Complex Fragment Emission in 12.6, 10.2 and 8 MeV/n Cu-Induced Reactions on C	June 28, 1989
Matthew Bloomer MIT	Energy and Baryon Densities in AA Collisions at 15AGeV	July 12, 1989
Udo von Wimmersperg BNL	Observation of Resonant Structures in Positron Annihilation	July 17, 1989

Walter Greiner U. Frankfurt	QED of Strong Fields: Facts, Fiction and a Possible Explanation	July 24, 1989
Uri Karshon Weitzmann Institute/SLAC	New TASSO Results on Symmetric Three-Jet Events and Intermittency	July 26, 1989
Eberhard Klempt U. Mainz	Recent Results on Antiproton-Proton Annihilation at Rest from the Low Energy Antiproton Ring (LEAR) at CERN	July 31, 1989
Hiroyasu Egiri Osaka University	Spin-Polarization in Weak Decays of Hypernuclei	August 2, 1989
R. Weiner U. Marburg	Bose-Einstein Correlations: A Case of Collective Amnesia	August 14, 1989
Adam Kiss Eotvos University	Neutron Emission in Intermediate Energy Heavy-Ion Collisions	August 16, 1989
Hans A. Weidenmueller MPI-Heidelberg	Tests of Fundamental Symmetries in Compound Nucleus Reactions	August 28, 1989
Heinz Sorge U. Frankfurt	Stopping and Strangeness Production in Ultrarelativistic Heavy Ion Collisions	October 4, 1989
Daniel Ardouin GANIL	Decay Properties of an Evaporative System Using Two-Particle Correlations	October 9, 1989
Udo Ornik U. Marburg	Relativistic Hydrodynamics, Cosmology and Heavy Ion Reactions	October 16, 1989
Miklos Gyulassy LBL	Physics Objectives at RHIC	October 18, 1989
Barbara Jacak LANL	Hadron Distributions from Ultrarelativistic Heavy Ion Experiments at CERN	October 23, 1989
Norman Glendenning LBL	Fast Pulsar in SN-1987A: The Case for Strange Quark Matter Stars	November 6, 1989
Yeong E. Kim Purdue U.	Nuclear Theoretical Hypotheses for Cold Fusion	November 9, 1989

S. Frankel University of Pennsylvania	Time Evolution of Hadron Structure: Drell-Yan and Vector Meson Production in Nuclei	December 4, 1989
Chuck Parsons MIT	A-Dependence of Strange Particle Production in Nucleus-Nucleus Collisions at 15 GeV/n	December 11, 1989
Arthur Poskanzer LBL	Squeeze-out of Nuclear Matter	January 8, 1990
Huan Huang MIT	Multiparticle Production in p-A and Si-A Collisions at AGS Energies	January 9, 1990
Gerry Brown SUNY Stony Brook	Hot Baryons and Cool Pions	January 22, 1990
Mark Senko Vanderbuilt	Charmed Meson Production in 800 GeV pp Collisions	January 24, 1990
Jean-Pierre Alard U. Clermont-Ferrand	Recent Exclusive Experimental Results from Relativistic Ne and Ar Induced Reactions with the Diogene Facility at Saturne	January 29, 1990
A. Migdal Landau Inst. Moscow	Physics of QCD and Hadron Models	January 30, 1990
Dan Cebra MSU	Event Shape Analysis: Sequential vs. Simultaneous Multifragmentation	February 1, 1990
Mark Tincknell ORNL	Learning about Relativistic Nuclear Collisions from Calorimetry: Teaching an old Dog Some New Tricks	February 12, 1990
Bruce Denby FermiLab	Looking for Beauty with Neural Nets	February 26, 1990
Richard Hahn Brookhaven National Lab.	Gallium as a Radiochemical Detector of Solar Neutrinos	March 1, 1990
James Costales MIT	Anti-Proton Production and Baryon Distributions in p + A and Si + A Collisions at the AGS	March 12, 1990

Mirek Fatyga BNL	Studying Electromagnetic Phenomena with RHIC	March 12, 1990
Cheng Li Wu Univ. of Tennessee/ORNL	Fermion Dynamical Symmetry Model and Nuclear Structure	March 14, 1990
Peter Seidl LBL	Measurement of e+e- Pairs in the Mass Range 0.1 to 1.5 GeV at the Bevalac	March 19, 1990
Peter Jacobs LBL	Correlations in Multiparticle Distributions from High Energy Nuclear Collisions	March 26, 1990
Klaus Schiffer Australian National Univ.	Population of Superdeformed States	March 30, 1990
Shoji Nagamiya Columbia Univ.	Recent Relativistic Heavy-Ion Results from the AGS at Brookhaven	April 2, 1990
Timothy Chupp Harvard Univ.	The Structure of the Neutron	April 5, 1990
Robert Charity Washington University	Properties of Three and Four Fragment Events Produced in Symmetric Reactions at E/A = 20 MeV	April 9, 1990
Richard Seto Columbia University	Search for Neutrino Oscillations	April 12, 1990
Joel Moss LANL	A-Dependence of Dimuon Production with 800 GeV Protons	April 16, 1990
Marek Gazdzicki U. Warsaw	Strange Particle Production in 200 GeV/n S + S	April 23, 1990
Leon van Hove CERN	Particle Physics and Cosmology	April 24, 1990
Leon van Hove CERN	Recent Developments in Soft Multiparticle Production	April 25, 1990
Phillip Wilmarth LBL	Do Spinning Gyroscopes Really Weigh Less?	May 2, 1990

Joachim Schambach Kent State U.	Neutron Triple Differential Cross Sections from Central Au + Au Collisions	June 4, 1990
G. Montarou Univ. of Clermont-Ferrand	Collective Flow and Pion Production at Diogene	June 19, 1990
S. Gales IPN Orsay	AGOR Project: Superconducting Cyclotron for Light and Heavy Ions	July 2, 1990
Fred Pottag U. Marburg/LBL	Particle Distributions in the Hydrodynamical and Quantum Statistical Context and Their Implication for Future Colliders	July 9, 1990
Thomas Semkow SUNY at Albany	Radon Emanation at the Atomic Level	July 23, 1990
Kenneth Gregorich LBL	Chemistry of Elements 103 and 105	July 25, 1990
Howard Hall LLNL	Delayed Fission in the Heavy Elements	July 30, 1990
John D. Vergado Univ. of Ioannina	Neutrinoless Double Beta Decay - an interplay of particle and nuclear physics	August 1, 1990
Kenneth Wilson Michigan State Univ.	Azimuthal Distributions in Intermediate Energy Ar + V Collisions	August 3, 1990
Ivo Zvara JINR Dubna, USSR	Search for Relativistic Effects in the Chemical Properties of Element 104	August 13, 1990
Ivo Zvara JINR Dubna, USSR	Problems in Fast Thermochromotograhic Separartions of Chemical Elements	August 20, 1990
David Siebert Univ. of Minnesota	Correlation Studies in High Energy Heavy Ion Collisions	Sept. 10, 1990
Wolfgang Stoffl LLNL	Results from the LLNL Neutrino Experiment and Atomic Physics in Multiple Charged Ions	Sept. 17, 1990
Rainer Jahn Univ. of Bonn	Near Threshold One- and Two-Meson Production in Hadronic Fusion Reactions	Sept. 24 , 1990

Paul Reeder Battelle Pacific Northwest Lab.	Beta Delayed Neutron Emission from Light Mass Precursors: Li - Al	October 1, 1990
Magnus Harlander LBL	Neural Networks versus Dynamic Radon Transforms for Complex Pattern Recognition	October 3, 1990
Werner Joho Paul Scherrer Institute	Status and Upgrade Plans at the PSI Meson Factory at Zurich	October 8, 1990
Eric Norman LBL	Evidence of a Massive (i.e. 17 keV) Neutrino Emitted in Nuclear Beta Decay	October 15, 1990
Vladim Soloviev Dubna	Structure of Low-Lying Vibrational States in Deformed Nuclei	October 22, 1990
Grazyna Odyniec LBL	Strangeness Production in Nucleus-Nucleus Collisions: An Experimental Review	November 5, 1990
Betty Tsang Michigan State Univ.	Collective Effects in Intermediate Energy Heavy Ion Induced Reactions	Nov. 12, 1990
John Cramer University of Washington	Analysis of Multiparticle Bose-Einstein Correlations in Ultrarelativistic Heavy Ion Collisions	Nov. 26, 1990
Erwin Friedlander LBL	Evidence for "Fine Structure" of Multiplicity Distributions in High Energy Hadronic Multiparticle Production	December 3, 1990
Takeshi Kodama Univ. of Rio de Janeiro	Does the Nuclear Cross Section Stay Constant at Ultra-Relativistic Energies?	December 17, 1990

Nuclear Theory

Wolfgang Nörenberg GSI	Nuclear Elastoplasticity: A Phenomenon of a Transition from Ordered to Chaotic Motion	3 Oct 88
Klaus Werner Brookhaven	Space-Time Evolution of Heavy- Ion Collisions in the String Model VENUS	25 Oct 88
Luis Robledo Univ. Autonoma de Madrid	A Microscopic Study of the Octopule Degree of Freedom in the Light Actinide Region	29 Oct 88
Rudi Malfliet Groningen	Dirac-Brueckner Approach to Nuclear Matter	1 Nov 88
Mitsuru Tohyama Michigan State Univ.	Application of ETDHF to Heavy- Ion Reactions and Giant Resonances	15 Nov 88
Ramona Vogt SUNY, Stony Brook	J/ψ Suppression by Hadrons: The Stony Brook Version	23 Nov 88
Joseph Kapusta Univ. of Minnesota	Single- and Multi-Particle Analysis of Nucleus-Nucleus Collisions at 14.6, and 200 GeV/N	12 Dec 88
Karen Tang LBL	Superconductivity with a Possible Application to QCD Confinement	3 Dec 88
Joseph Kapusta Univ. of Minnesota	Dileptons from Nucleon- Nucleon and Nucleus-Nucleus Collisions	14 Dec 88
Joseph Kapusta Univ. of Minnesota	Finite-Latice-Size-Effect on QCD Thermodynamics	15 Dec 88
Qi-Ren Zhang Beijing University	Mesons and Quarks in Nuclei	11 Jan 89
Andrzej Bialas Crakow, Poland	Intermittency in Rapidity Distributions	17 Jan 89

Gerald Brown SUNY, Stony Brook	Stopping in Bevalac Heavy-Ion Collisions	18 Jan 89
Sven Bjohnholm Niels Bohr Inst.	Shells and Supershells in Pseudo-Nuclei	25 Jan 89
Xiangdong Ji CalTech	Relativistic Approach to Quasi-Elastic Scattering	30 Jan 89
Matthias Grabiak Frankfurt	Magnetic Resonances in QCD at E = 1.8 GeV	1 Feb 89
Sean Gavin LBL	Report on the paper: "Fluctuations and Coherence in Ultrarelativistic Heavy-Ion Collisions" by Baym	6 Feb 89
David A. Wassor. CalTech	Effect of Quantum Fluctuations on Solitons	7 Feb 89
Edward A. Remler College of William/Mary	A Method for Direct Numerical Solution of the Equation of Motion of the Q.M. Density Operator	8 Feb 89
Hank Crawford LBL	Production of Anti-Nuclei at AGS	10 Feb 89
Norman Glendenning LBL	A Simple Model of Irregularities in Pulsar Signals	13 Feb 89
Edward A. Remler College of William/Mary	Relativistic Collisions of Stringonic Matter	15 Feb 89
Matthias Grabiak Frankfurt	Mysteries in the Dirac Equation - New Solutions	16 Feb 89
Karen Tang LBL	Magnetic Dipole in a Superconductor	22 Feb 89
Edward A. Remler College of William/Mary	Relativistic Collisions of Stringonic Matter: A Continuation	22 Feb 89
Fumihiko Sakata	Breaking of Separability	23 Feb 89

INS, Univ. of Tokyo	Condition for Dynamical Collective Subspace -- Onset of Quantam Chaos in Large-Amplitude Collective Motion	
Jørgen Randrup LBL	Nuclear Colissions at 30-150 MeV/N: Which are the Important Observables?	1 Mar 89
Matthias Grabiak Frankfurt	Vortex Solutions of a Non-Linear Dielectric Model with Electric Confinement	10 Mar 89
Martin Gutzwiller IBM Yorktown/ITP	Invariant Multi-Fractal Sets in Hamiltonian Systems	16 Mar 89
George Bertsch Michigan State Univ.	Detecting the Quark-Gluon Plasma	20 Mar 89
Subal Das Gupta Montreal	Transverse Momenta · Nuclear Equation of State and Momentum Dependent Interactions	21 Mar 89
R. Shankar Yale Univ./ITP	Quantum Antiferromagnets for Field Theorists: Massless Fermions and the Non-Linear Sigma Model	3 Apr 89
Wolfgang Bauer MSU	New Adventures with the Nuclear Equation of State	10 Apr 89
Sigurd Kohler Tucson	Nuclear Dynamics and Heavy-Ion Collisions	11 Apr 89
Mario Feingold LBL	KAM Surfaces and Diffusion in Three-Dimensional Volume-Preserving Maps	12 Apr 89
Nikolai Nikolaev USSR	Is Creation of a Quark-Gluon Plasma in Nuclear Collisions Feasible?	17 Apr 89
T. Hans Hansson Univ. of Stockholm	Charged Vortices and the Many-Anyon Problems	25 Apr 89

Miklos Gyulassy LBL	Is Intermittency Caused by Bose-Einstein Interference?	3 May 89
Jitendra Parikh Ahmedabad, India	Classical QCD Plasmas	3 May 89
V. Strutinsky KIEV	Macroscopic and Microscopic in Nuclear Physics and Elsewhere	5 May 89
Wick Haxton Univ. of Washington	Double-Beta Decay	8 May 89
Peter Lichard Bratislava	Soft and Very Soft Electromagnetic Phenomena of Hadronic Origin	12 Jun 89
Dieter Hartman UC Santa Cruz	Gamma Ray Bursts from Neutron Stars	20 Jun 89
Hilmar Forkel SUNY, Stony Brook	Dense Skyrmion Matter: The Hypershere Approach	24 Jun 89
Pawel Danielewicz MSU	New Results in Non-Equilibrium Quantum Many-Body Theory	27 Jun 89
Philip J. Siemens Corvallis	Update on Dilepton Controversy	29 Jun 89
Raju Venugopalan SUNY, Stony Brook	Transverse Spectra in the Hydrodynamic Model	30 Jun 89
Per Arve Lund, Sweden	Is there a Controversy about the Nuclear Collective Mass Parameters	6 Jul 89
Yoram Alhassid Yale University	Landau Theory of Hot Rotating Nuclei	11 Jul 89
Bent Lauritzen NORDITA	Static Path Approximation in Deformed Nuclei	12 Jul 89
Miklos Gyulassy LBL	Neurodynamics: Differential Equations that Walk and Talk	13 Jul 89
Alan Goodman Tulane University	Shape Transitions at Finite Temperatures	14 Jul 89

Walter Greiner Univ. of Frankfurt	QED of Strong Fields; Facts, Fictions and a Possible Solution	19 Jul 89
Thomas Janka Astrophysics Inst. Munich	How Do Stars Explode: A Still Unresolved Problem	26 Jul 89
Jose Casado University of Santiago	Dual Parton Model: From Hadron-Hadron to Nucleus-Nucleus Collisions	31 Jul 89
Richard Chasman Argonne National Laboratory	Superdeformation	1 Aug 89
Luis Robledo Univ. Autonoma de Madrid	The Abelian Higgs Model with Monopoles: A Model for Quark Confinement	2 Aug 89
Jorn Knoll GSI	Pair Creation in Finite Dynamical System	3 Aug 89
Marcos Saraceno Buenos Aires, Argentina	Solution of the Schrödinger Equation in Time Dependent Cavities	4 Aug 89
Jorn Knoll GSI	Can We See the Quark-Gluon Plasma from Flavor Signals	4 Aug 89
Tamas Biro Giessen	Gluon Mass and Confinement	14 Aug 89
Michael Schaefer University Giessen	Photon and Dilepton Production in PN Collisions	22 Aug 89
Raju Venugopalan SUNY, Stony Brook	Anti-Protons as a Baryonometer?	23 Aug 89
Joseph Kapusta Univ. of Minnesota	Non-Perturbative Approach to Dilepton Production	24 Aug 89
Michael Wilkinson Univ. of Strathclyde	Random Matrix Theory and Spectral Rigidity	25 Aug 89
Hans Weidenmüller	Tests of Fundamental	28 Aug 89

Max-Planck Inst.	Symmetries in Compound Nucleus Reactions	
Yogiro Hama Univ. of So Paolo	Collective Transverse Motion Multiple Production	1 Sep 89
Emil Medeiros CBPF Rio de Janeiro	The Effect of the Nuclear Mean Field on Intranuclear Cascade Calculations of Pion Multiplicities	7 Sep 89
Matthias Grabiak Frankfurt/LBL	QCD Sum Rules	3 Oct 89
Fridolin Weber Munich, Germany	Dense Baryon Matter Calculations	1 Feb 90
Tetsuo Hatsuda SUNY, New York	Anomalous Gluon Content	7 Feb 90
Markus Thoma Munich, Germany	Gluon Dynamics	8 Feb 90
Paul Bonche Saclay, France	Superdeformed Bands in Hg Nuclei	9 Feb 90
Jean-Paul Blaizot Saclay, France	The J/ψ and the Nucleus	13 Feb 90
Phillipe Chomaz Orsay, France	Neutrinos in Supernovae	28 Feb 90
Jean-Paul Blaizot Saclay, France	The J/ψ and the Nucleus	13 Feb 90
Fiorella Burgio Catania, Italy	Non-Equilibrium Processes in Nuclear Dynamics	7 Mar 90
Stuart Pittel Delaware	Nuclear Structure Effects in Double Beta Decay	13 Mar 90
Cheng-Li Wu UTK/ORNL	Fermion Dynamical Symmetry Model	14 Mar 90
Alan Goodman New Orleans, LA	Thermal Shape Fluctuations: Constant-Energy versus Constant-Temperature Ensembles	15 Mar 90

Mike Guidry UTK/ORNL Peter Ring TU München	Two-Neutron Transfer Experiments and Theory	16 Mar 90
Jose Casado U. Santiago/LBL	Parton Shadowing Effect on the J/ψ Production	29 Mar 90
Osamu Miyamura Osaka, Japan	Charmonium Melting and Kinetic Balance in the Mixed Phase	30 Mar 90
Frans Klinkhamer Amsterdam	Sphalerons	4 Apr 90
Matthias Grabiak Frankfurt/LBL	Nielsen - Olesen vs. Friedberg-Lee vs. MIT bag- What is the right model?	5 Apr 90
Michael Wilkinson Univ. Strathclyde	Suppression of Dissipation	11 Apr 90
Scott Chapman UCB	Comparison of Fireball and String Models at AGS Energies	4 May 90
Weimin Zhang Univ. Washington	Chaos and Dynamical Symmetry Breaking in Quantum Systems	16 May 90
J. Treiner Orsay, France	Liquid Helium	8 May 90
Matthias Grabiak LBL	C for Fortran Programmers Part I of	22 May 90
Felix Izrailev Novosibirsk, USSR	Quantum Statistical Properties of Classically Chaotic Systems: Spectrum and Eigenfunctions	23 May 90
Matthias Grabiak LBL	C for Fortran Programmers Part II of	29 May 90
Matthias Grabiak LBL	C for Fortran Programmers Part III of	5 Jun 90

Sean Gavin Univ. of Helskini	Antimatter Probes in Nuclear	22 Jun 90
Helmut Hofmann TU Munchen	Nuclear Transport Theory	25 Jun 90
Jose` Gracia`-Bondia Univ. of Costa Rica	Recent Advances in the Theory of Wigner Functions	26 Jun 90
Madeleine Soyeur Saclay, France	In-Medium Behavior of Vector Mesons	3 Jul 90
Thomas Schönfeld Univ. of Frankfurt	Pair Creation in a Flux Tub	12 Jul 90
Georg Pielert		17 Jul 90
Fred Pottag Marburg, Germany	Multiplicity Distributions from Hydrodynamics and Quantum Statistics	3 Aug 90
Steve Moszkowski UCLA	Nuclear Equation of State	7 Aug 90
Bo Anderson LUND	On the Dipole Structure in QCD or How does QCD Work?	15 Aug 90
Shun-jin Wang Lanzhou Univ./LBL	Relativistic Transport Theory for Hadronic Matter	21 Aug 90
Bo Anderson LUND	YQCD?	24 Aug 90
Michaela Harlander Univ. Munchen	Direct CP Violation in the Standard Model	28 Aug 90
Jörg Hüfner Heidelberg	Multiplicity Distributions and Correlations in Nuclear Multifragmentation	29 Aug 90
Bishu Banerjee TATA Inst.	Primordial Nucleosynthesis and QCD Phase Transition	20 Sep 90
Antje Höring	Gamma Decay of Giant	10 Oct 90

Max-Planck Inst.	Resonances in Pre-Equilibrium Nuclear Reactions in a Statistical Approach	
Wolfgang Bauer NSCL/MSU	Decay of Ordered and Chaotic	15 Oct 90
Thomas Gühr Max-Planck Inst.	Isospin Mixing, Breaking of Quantum Numbers and Fluctuation Properties	17 Oct 90
Gyuri Wolf Univ. Giessen	Dilepton Production in Heavy-Ion Collisions	24 Oct 90
Markus Thoma Munich/LBL	Summary of the First Month of the Nuclear Theory Institute Fall '90	7 Nov 90
Thomas Hoch TH. Darmstadt	Study of Nuclear Ground State Properties in the Framework of a Relativistic Point Coupling Model	9 Nov 90
Matthias Grabiak LBL	Report on the Nuclear Theory Institute, November 1990	11 Dec 90

Order, Chaos and the Atomic Nucleus

Aurel Bulgac MSU	Berry's Phase, Effective Gauge Potentials and the Structure of Collective Hamiltonians	9 Mar 89
Erik J. Heller Univ. of Washington	Quantum Eignestates of a Classically Chaotic System	13 Mar 89
Martin C. Gutzwiller IBM, Yorktown	Invariant Multi-Fractal Sets in Hamiltonian Systems	16 Mar 89
Bruno Eckhardt KFA Julich	Organizing Quantum Chaos-Periodic Orbit Quantization that Works	23 Mar 89
Alfredo Ozorio de Almeida ITP Santa Barbara	Quantization of Homoclinic Chaos	2 May 89
Michael Baranger MIT/ITP Santa Barbara	If Poincare Came Back Today Periodic Trajectories in Classical and Quantum Systems	11 May 89
Marcos Saraceno Buenos Aires Argentina	Periodic Trajectories in the Quantum Baker Map	12 May 89
Yves Pomeau Ecole Normale Superieure/Univ. of AZ	Chaos in Extended Systems	15 May 89
Dawn Meredith ITP S. Barbara Univ. of N. Hampshire	Chaos in a Schematic Shell Model	25 May 89
Francois Brut Institute des Sciences Nucleaires, France	Semiclassical Quantization via the Adiabatic Switching Method	17 Jul 89
Yoram Alhassid	Statistical Fluctuations of	17 Jul 89

Yale University	Spectra and Matrix Elements: The Transition from Regular to Chaotic	
Michael Wilkinson Strathclyde University	Near Degeneracies in Generic Quantum Systems	18 Jul 89
S. Fishman Technion/ITP Santa Barbara	Quantum Localization in Chaotic Systems	18 Jul 89
Michael Nauenberg	Quantum Recurrence of Wave Packets in Kepler Elliptic Orbits	18 Jul 89
R. Littlejohn	Semi-Classical Structure of the Gutzwiller Trace Formula	19 Jul 89
Marcos Saraceno Buenos Aires Argentina	Classical Structures in the Quantum Baker Transformation	19 Jul 89
D. Lightner	Chaos in Van der Waals Clusters	20 Jul 89
Mario Feingold LBL	Scars in Billiards: The Phase Space Approach	20 Jul 89
A. Litchenberg	Diffusion in 2-dimensional Mappings	21 Jul 89

RHIC Planning

Miklos Gyulassy LBL	Physics Objectives at RHIC	October 18, 1989
Doug Greiner LBL	4π Tracking TPC	October 25, 1989
John Harris LBL	Tracking and Particle Identification at Midrapidity	October 31, 1989
Chuck Naudet LBL	Jets at FermiLab	October 31, 1989
Hans-Georg Ritter LBL	4π Calorimetry	November 8, 1989
Jim Carroll UCLA/LBL	Electron Pairs	November 15, 1989
Glenn Young ORNL	Muon Pairs	November 30, 1989
Lee Schroeder LBL	RHIC the Machine	January 10, 1990
Tom Ludlam BNL	Getting Started with RHIC Experiments	January 16, 1990
Chuck Gruhn LBL	RHIC Tracking Detectors, Compromises and Physics	January 31, 1990
Walter Geist LBL	High p_t Jets	February 7, 1990
Grazyna Odyniec LBL	Strangeness Production at RHIC	February 14, 1990
Richard Kadel LBL	The CDF Tracking Chamber	March 7, 1990

Author Index

Author Index

END

DATE FILMED

11/08/91